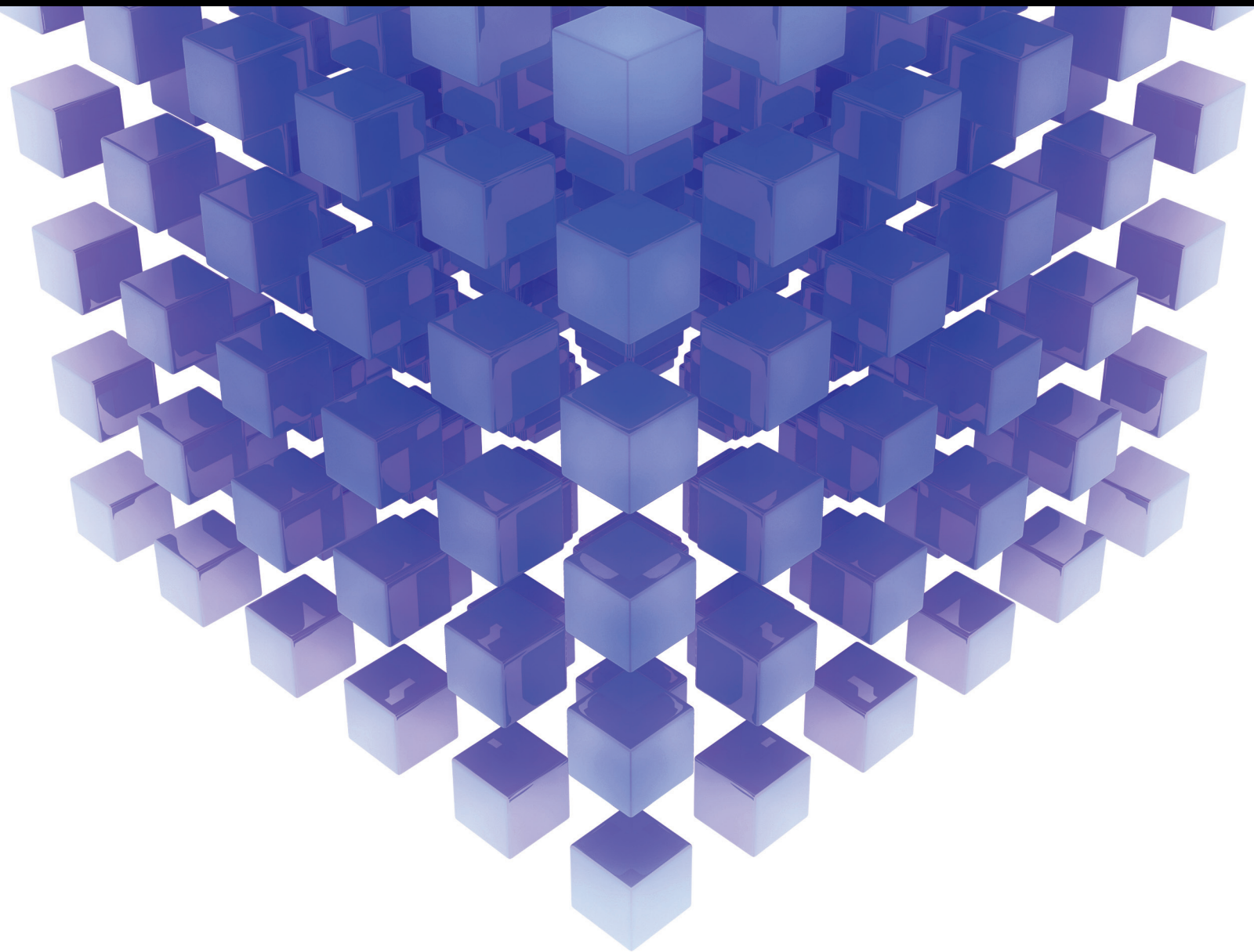


Time-Delay Systems: Modeling, Analysis, Estimation, Control, and Synchronization

Lead Guest Editor: Olfa Boubaker

Guest Editors: Valentina E. Balas, Abdellah Benzaouia, Mohamed Chaabane, Magdi S. Mahmoud, and Quanmin Zhu





Time-Delay Systems: Modeling, Analysis, Estimation, Control, and Synchronization

Mathematical Problems in Engineering

Time-Delay Systems: Modeling, Analysis, Estimation, Control, and Synchronization

Lead Guest Editor: Olfa Boubaker

Guest Editors: Valentina E. Balas, Abdellah Benzaouia,
Mohamed Chaabane, Magdi S. Mahmoud, and Quanmin Zhu



Copyright © 2017 Hindawi. All rights reserved.

This is a special issue published in “Mathematical Problems in Engineering.” All articles are open access articles distributed under the Creative Commons Attribution License, which permits unrestricted use, distribution, and reproduction in any medium, provided the original work is properly cited.

Editorial Board

Mohamed Abd El Aziz, Egypt
Farid Abed-Meraim, France
J. Ángel Acosta, Spain
Paolo Addresso, Italy
Claudia Adduce, Italy
Ramesh Agarwal, USA
Juan C. Agüero, Australia
R Aguilar-López, Mexico
Tarek Ahmed-Ali, France
Hamid Akbarzadeh, Canada
Muhammad N. Akram, Norway
Guido Ala, Italy
Mohammad-Reza Alam, USA
Salvatore Alfonzetti, Italy
Francisco Alhama, Spain
Mohammad D. Aliyu, Canada
Juan A. Almendral, Spain
Lionel Amodeo, France
Sebastian Anita, Romania
Renata Archetti, Italy
Felice Arena, Italy
Sabri Arik, Turkey
Alessandro Arsie, USA
Edoardo Artioli, Italy
Fumihiro Ashida, Japan
Hassan Askari, Canada
Mohsen Asle Zaeem, USA
Romain Aubry, USA
Matteo Aureli, USA
Viktor Avrutin, Germany
Francesco Aymerich, Italy
Seungik Baek, USA
Khaled Bahlali, France
Laurent Bako, France
Stefan Balint, Romania
Alfonso Banos, Spain
Roberto Baratti, Italy
Azeddine Beghdadi, France
Denis Benasciutti, Italy
Ivano Benedetti, Italy
Elena Benvenuti, Italy
Michele Betti, Italy
Jean-Charles Beugnot, France
Simone Bianco, Italy
Gennaro N. Bifulco, Italy

David Bigaud, France
Antonio Bilotta, Italy
Jonathan N. Blakely, USA
Paul Bogdan, USA
Alberto Borboni, Italy
Paolo Boscariol, Italy
Daniela Boso, Italy
Guillermo Botella-Juan, Spain
Abdel-Ouahab Boudraa, France
Fabio Bovenga, Italy
Francesco Braghin, Italy
Michael J. Brennan, UK
Maurizio Brocchini, Italy
Julien Bruchon, France
Matteo Bruggi, Italy
Michele Brun, Italy
Javier Buldu, Spain
Tito Busani, USA
R. Caballero-Águila, Spain
Filippo Cacace, Italy
Pierfrancesco Cacciola, UK
Salvatore Caddemi, Italy
Jose E. Capilla, Spain
F. Javier Cara, Spain
Ana Carpio, Spain
Federica Caselli, Italy
Carmen Castillo, Spain
Inmaculada T. Castro, Spain
Gabriele Cazzulani, Italy
Luis Cea, Spain
Miguel Cerrolaza, Venezuela
M. Chadli, France
Gregory Chagnon, France
Ludovic Chamoin, France
Ching-Ter Chang, Taiwan
Michael J. Chappell, UK
Kacem Chehdi, France
Peter N. Cheimets, USA
Xinkai Chen, Japan
Francisco Chicano, Spain
Hung-Yuan Chung, Taiwan
Simone Cinquemani, Italy
Joaquim Ciurana, Spain
John D. Clayton, USA
Giuseppina Colicchio, Italy

Mario Cools, Belgium
Sara Coppola, Italy
Jean-Pierre Corriou, France
J.-C. Cortés, Spain
Carlo Cosentino, Italy
Paolo Crippa, Italy
Andrea Crivellini, Italy
Erik Cuevas, Mexico
Peter Dabnichki, Australia
Luca D'Acerno, Italy
Weizhong Dai, USA
Andrea Dall'Asta, Italy
Purushothaman Damodaran, USA
Farhang Daneshmand, Canada
Fabio De Angelis, Italy
Pietro De Lellis, Italy
Stefano de Miranda, Italy
Filippo de Monte, Italy
M. do R. de Pinho, Portugal
Michael Defoort, France
Xavier Delorme, France
Angelo Di Egidio, Italy
Ramón I. Diego, Spain
Yannis Dimakopoulos, Greece
Zhengtao Ding, UK
M. Djemai, France
Alexandre B. Dolgui, France
Florent Duchaine, France
George S. Dulikravich, USA
Bogdan Dumitrescu, Romania
Horst Ecker, Austria
Ahmed El Hajjaji, France
Fouad Erchiqui, Canada
Anders Eriksson, Sweden
R. Emre Erkmen, Australia
Andrea L. Facci, Italy
Giovanni Falsone, Italy
Hua Fan, China
Yann Favennec, France
Fiorenzo A. Fazzolari, UK
Giuseppe Fedele, Italy
Roberto Fedele, Italy
Jose R. Fernandez, Spain
Jesus M. Fernandez Oro, Spain
Francesco Ferrise, Italy

Eric Feulvarch, France
Barak Fishbain, Israel
S. Douwe Flapper, Netherlands
Thierry Floquet, France
Eric Florentin, France
Jose M. Framinan, Spain
Francesco Franco, Italy
Elisa Francomano, Italy
Leonardo Freitas, UK
Tomonari Furukawa, USA
Mohamed Gadala, Canada
Matteo Gaeta, Italy
Mauro Gaggero, Italy
Zoran Gajic, Iraq
Erez Gal, Israel
Ugo Galvanetto, Italy
Akemi Gálvez, Spain
Rita Gamberini, Italy
Maria L. Gandarias, Spain
Arman Ganji, Canada
Xin-Lin Gao, USA
Zhong-Ke Gao, China
Giovanni Garcea, Italy
Fernando García, Spain
Jose M. Garcia-Aznar, Spain
Alessandro Gasparetto, Italy
Vincenzo Gattulli, Italy
Oleg V. Gendelman, Israel
Mergen H. Ghayesh, Australia
Agathoklis Giaralis, UK
Anna M. Gil-Lafuente, Spain
Ivan Giorgio, Italy
Alessio Gizzi, Italy
Hector Gómez, Spain
David González, Spain
Rama S. R. Gorla, USA
Oded Gottlieb, Israel
Nicolas Gourdain, France
Kannan Govindan, Denmark
Antoine Grall, France
Fabrizio Greco, Italy
Jason Gu, Canada
Federico Guarracino, Italy
José L. Guzmán, Spain
Quang Phuc Ha, Australia
Zhen-Lai Han, China
Thomas Hanne, Switzerland
Xiao-Qiao He, China


Sebastian Heidenreich, Germany
Luca Heltai, Italy
A. G. Hernández-Díaz, Spain
M.I. Herreros, Spain
Eckhard Hitzer, Japan
Paul Honeine, France
Jaromir Horacek, Czech Republic
Muneo Hori, Japan
András Horváth, Italy
Gordon Huang, Canada
Nicolas Hudon, Canada
Sajid Hussain, Canada
Asier Ibeas, Spain
Orest V. Iftime, Netherlands
Giacomo Innocenti, Italy
Emilio Insfran, Spain
Nazrul Islam, USA
Benoit Iung, France
Benjamin Ivorra, Spain
Payman Jalali, Finland
Reza Jazar, Australia
Khalide Jbilou, France
Linni Jian, China
Bin Jiang, China
Zhongping Jiang, USA
Ningde Jin, China
Grand R. Joldes, Australia
Dylan F. Jones, UK
Tamas Kalmar-Nagy, Hungary
Tomasz Kapitaniak, Poland
Julius Kaplunov, UK
Haranath Kar, India
K. Karamanos, Belgium
Jean-Pierre Kenne, Canada
C. M. Khaliq, South Africa
Do Wan Kim, Republic of Korea
Nam-Il Kim, Republic of Korea
Oleg Kirillov, Germany
Manfred Krafczyk, Germany
Frederic Kratz, France
Petr Krysl, USA
Jurgen Kurths, Germany
K. Kyamakya, Austria
Davide La Torre, Italy
Risto Lahdelma, Finland
Hak-Keung Lam, UK
Jimmy Lauber, France
Antonino Laudani, Italy

Aimé Lay-Ekuakille, Italy
Nicolas J. Leconte, France
Marek Lefik, Poland
Yaguo Lei, China
Stefano Lenci, Italy
Roman Lewandowski, Poland
Panos Liatsis, UAE
Anatoly Lisnianski, Israel
Peide Liu, China
Peter Liu, Taiwan
Wanquan Liu, Australia
Alessandro Lo Schiavo, Italy
Jean Jacques Loiseau, France
Paolo Lonetti, Italy
Sandro Longo, Italy
Sebastian López, Spain
Luis M. López-Ochoa, Spain
V. C. Loukopoulos, Greece
Valentin Lychagin, Norway
E. Jiménez Macías, Spain
Antonio Madeo, Italy
J. María Maestre, Spain
Fazal M. Mahomed, South Africa
Noureddine Manamanni, France
Didier Maquin, France
Giuseppe C. Marano, Italy
Damijan Markovic, France
F. Marotti de Sciarra, Italy
Rodrigo Martinez-Bejar, Spain
Benoit Marx, France
Franck Massa, France
Paolo Massioni, France
Alessandro Mauro, Italy
Michael Mazilu, UK
Driss Mehdi, France
Roderick Melnik, Canada
Pasquale Memmolo, Italy
Xiangyu Meng, Canada
Jose Merodio, Spain
Alessio Merola, Italy
Luciano Mescia, Italy
Laurent Mevel, France
Y. V. Mikhlin, Ukraine
Aki Mikkola, Finland
Hiroyuki Mino, Japan
Pablo Mira, Spain
Vito Mocella, Italy
Roberto Montanini, Italy

Gisele Mophou, France
Rafael Morales, Spain
Marco Morandini, Italy
Simone Morganti, Italy
Aziz Moukrim, France
Emiliano Mucchi, Italy
Josefa Mula, Spain
Domenico Mundo, Italy
Jose J. Muñoz, Spain
Giuseppe Muscolino, Italy
Marco Mussetta, Italy
Hakim Naceur, France
Hassane Naji, France
Keivan Navaie, UK
Dong Ngoduy, UK
Tatsushi Nishi, Japan
Xesús Nogueira, Spain
Ben T. Nohara, Japan
Mohammed Nouari, France
Mustapha Nourelfath, Canada
Roger Ohayon, France
Mitsuhiro Okayasu, Japan
Calogero Orlando, Italy
Javier Ortega-Garcia, Spain
A. Ortega-Moñux, Spain
Naohisa Otsuka, Japan
Erika Ottaviano, Italy
Arturo Pagano, Italy
Alkis S. Paipetis, Greece
Alessandro Palmeri, UK
Pasquale Palumbo, Italy
Elena Panteley, France
Achille Paolone, Italy
Xosé M. Pardo, Spain
Manuel Pastor, Spain
P. N. Pathirana, Australia
Francesco Pellicano, Italy
Marcello Pellicciari, Italy
Haipeng Peng, China
Mingshu Peng, China
Zhike Peng, China
Marzio Pennisi, Italy
Maria Patrizia Pera, Italy
Matjaz Perc, Slovenia
Francesco Pesavento, Italy
Dario Piga, Switzerland
Antonina Pirrotta, Italy
Marco Pizzarelli, Italy

Vicent Pla, Spain
Javier Plaza, Spain
Sébastien Poncet, Canada
Jean-Christophe Ponsart, France
Mauro Pontani, Italy
Stanislav Potapenko, Canada
Christopher Pretty, New Zealand
Carsten Proppe, Germany
Luca Pugi, Italy
Giuseppe Quaranta, Italy
Dane Quinn, USA
Vitomir Racic, Italy
Jose Ragot, France
K. R. Rajagopal, USA
Gianluca Ranzi, Australia
Alain Rassineux, France
S.S. Ravindran, USA
Alessandro Reali, Italy
Oscar Reinoso, Spain
Nidhal Rezg, France
Ricardo Riaza, Spain
Gerasimos Rigatos, Greece
Francesco Ripamonti, Italy
Eugenio Roanes-Lozano, Spain
Bruno G. M. Robert, France
José Rodellar, Spain
R. Rodríguez-López, Spain
Ignacio Rojas, Spain
Alessandra Romolo, Italy
Debasish Roy, India
Gianluigi Rozza, Italy
Rubén Ruiz García, Spain
Antonio Ruiz-Cortes, Spain
Ivan D. Rukhlenko, Australia
Mazen Saad, France
Kishin Sadarangani, Spain
Andrés Sáez, Spain
Mehrddad Saif, Canada
Salvatore Salamone, USA
Nunzio Salerno, Italy
Miguel A. Salido, Spain
Roque J. Saltarén, Spain
Francisco J. Salvador, Spain
Alessandro Salvini, Italy
Maura Sandri, Italy
Miguel A. F. Sanjuan, Spain
Juan F. San-Juan, Spain
Vittorio Sansalone, France

Roberta Santoro, Italy
Ilmar Ferreira Santos, Denmark
José A. Sanz-Herrera, Spain
Nickolas S. Sapidis, Greece
E. J. Sapountzakis, Greece
Andrey V. Savkin, Australia
Thomas Schuster, Germany
Mohammed Seaid, UK
Lotfi Senhadji, France
Joan Serra-Sagrasta, Spain
Gerardo Severino, Italy
Ruben Sevilla, UK
Leonid Shaikhet, Israel
Hassan M. Shanechi, USA
Bo Shen, Germany
Suzanne M. Shontz, USA
Babak Shotorban, USA
Zhan Shu, UK
Dan Simon, USA
Luciano Simoni, Italy
Christos H. Skiadas, Greece
Alba Sofi, Italy
Francesco Soldovieri, Italy
Raffaele Solimene, Italy
Jussi Sopanen, Finland
K. Sörensen, Belgium
Marco Spadini, Italy
Ruben Specogna, Italy
Sri Sridharan, USA
Ivanka Stamova, USA
Salvatore Strano, Italy
Yakov Strelniker, Israel
Sergey A. Suslov, Australia
Thomas Svensson, Sweden
Andrzej Swierniak, Poland
Yang Tang, Germany
Alessandro Tasora, Italy
Sergio Teggi, Italy
Alexander Timokha, Norway
Gisella Tomasini, Italy
Francesco Tornabene, Italy
Antonio Tornambe, Italy
Irina N. Trendafilova, UK
George Tsiatas, Greece
Antonios Tsourdos, UK
Emilio Turco, Italy
Vladimir Turetsky, Israel
Mustafa Tutar, Spain



Ilhan Tuzcu, USA
Efstratios Tzirtzilakis, Greece
Filippo Ubertini, Italy
Francesco Ubertini, Italy
Hassan Ugail, UK
Giuseppe Vairo, Italy
Kuppalapalle Vajravelu, USA
Robertt A. Valente, Portugal
Eusebio Valero, Spain
Pandian Vasant, Malaysia
Marcello Vasta, Italy
M. E. Vázquez-Méndez, Spain
Josep Vehi, Spain
K. C. Veluvolu, Republic of Korea
Fons J. Verbeek, Netherlands

Franck J. Vernerey, USA
Georgios Veronis, USA
Anna Vila, Spain
R.-J. Villanueva-Micó, Spain
Uchechukwu E. Vincent, UK
Mirko Viroli, Italy
Michael Vynnycky, Sweden
Shuming Wang, China
Yan-Wu Wang, China
Yongqi Wang, Germany
Roman Wendner, Austria
Desheng D. Wu, Sweden
Yuqiang Wu, China
Guangming Xie, China
Xuejun Xie, China

Gen Q. Xu, China
Hang Xu, China
Joseph J. Yame, France
Xinggang Yan, UK
Luis J. Yebra, Spain
Peng-Yeng Yin, Taiwan
Qin Yuming, China
Vittorio Zampoli, Italy
Ibrahim Zeid, USA
Huaguang Zhang, China
Qingling Zhang, China
Jian G. Zhou, UK
Quanxin Zhu, China
Mustapha Zidi, France

Contents

Time-Delay Systems: Modeling, Analysis, Estimation, Control, and Synchronization

Olfa Boubaker, Valentina E. Balas, Abdellah Benzaouia, Mohamed Chaabane, Magdi S. Mahmoud, and Quanmin Zhu

Volume 2017, Article ID 1398904, 3 pages

Recent Progress in Stability and Stabilization of Systems with Time-Delays

Magdi S. Mahmoud

Volume 2017, Article ID 7354654, 25 pages

Consensus Conditions for High-Order Multiagent Systems with Nonuniform Delays

Mengji Shi, Kaiyu Qin, Ping Li, and Jun Liu

Volume 2017, Article ID 7307834, 12 pages

Consensus Control for a Multiagent System with Time Delays

Yiran Cao, Toshiki Oguchi, Paul Verhoeckx, and Henk Nijmeijer

Volume 2017, Article ID 4063184, 11 pages

MIMO PI Controllers for LTI Systems with Multiple Time Delays Based on ILMIs and Sensitivity Functions

Wajdi Belhaj and Olfa Boubaker

Volume 2017, Article ID 1241545, 25 pages

Direct Yaw-Moment Control of All-Wheel-Independent-Drive Electric Vehicles with Network-Induced Delays through Parameter-Dependent Fuzzy SMC Approach

Wanke Cao, Zhiyin Liu, Yuhua Chang, and Antoni Szumanowski

Volume 2017, Article ID 5170492, 15 pages

Multiple Periodic Solutions for a Class of Second-Order Neutral Impulsive Functional Differential Equations

Jingli Xie, Zhiguo Luo, and Yuhua Zeng

Volume 2017, Article ID 5041783, 5 pages

Stabilization for Damping Multimachine Power System with Time-Varying Delays and Sector Saturating Actuator

Linlin Ma, Yanping Liang, and Jian Chen

Volume 2016, Article ID 9191073, 13 pages

High Precision Clock Bias Prediction Model in Clock Synchronization System

Zan Liu, Xihong Chen, Jin Liu, and Chenglong Li

Volume 2016, Article ID 1813403, 6 pages

Robust Quadratic Stabilizability and H_∞ Control of Uncertain Linear Discrete-Time Stochastic Systems with State Delay

Xiushan Jiang, Xuemin Tian, and Weihai Zhang

Volume 2016, Article ID 7843940, 11 pages

Robust Stability Criteria for T-S Fuzzy Systems with Time-Varying Delays via Nonquadratic Lyapunov-Krasovskii Functional Approach

Sung Hyun Kim

Volume 2016, Article ID 7547148, 10 pages

Fixed Points and Exponential Stability for Impulsive Time-Delays BAM Neural Networks via LMI Approach and Contraction Mapping Principle

Ruofeng Rao, Zhilin Pu, Shouming Zhong, and Xinggui Li

Volume 2016, Article ID 3154683, 8 pages

A Control Method to Balance the Efficiency and Reliability of a Time-Delayed Pump-Valve System

Zhounian Lai, Peng Wu, Shuai Yang, and Dazhuan Wu

Volume 2016, Article ID 5898209, 10 pages

A Decoupling Control Strategy for Multilayer Register System in Printed Electronic Equipment

Shanhui Liu, Bingzheng Yin, Li'e Ma, Hongwei Xu, and Geshun Zhu

Volume 2016, Article ID 7165163, 14 pages

Multiple Model-Based Synchronization Approaches for Time Delayed Slaving Data in a Space Launch Vehicle Tracking System

Haryong Song and Yongtae Choi

Volume 2016, Article ID 9319282, 12 pages

An Expert PI Controller with Dead Time Compensation of Monitor AGC in Hot Strip Mill

Fei Zhang, Shengyue Zong, Xiang Wang, and Xiaohuai Ren

Volume 2016, Article ID 3041538, 8 pages

Novel Robust Exponential Stability of Markovian Jumping Impulsive Delayed Neural Networks of Neutral-Type with Stochastic Perturbation

Yang Fang, Kelin Li, and Yunqi Yan

Volume 2016, Article ID 1492908, 20 pages

Editorial

Time-Delay Systems: Modeling, Analysis, Estimation, Control, and Synchronization

Olfa Boubaker,¹ Valentina E. Balas,² Abdellah Benzaouia,³ Mohamed Chaabane,⁴ Magdi S. Mahmoud,⁵ and Quanmin Zhu⁶

¹*National Institute of Applied Sciences and Technology, Tunis, Tunisia*

²*Aurel Vlaicu University, Arad, Romania*

³*Faculty of Sciences Semlalia, Université Cadi Ayyad, Marrakech, Morocco*

⁴*University of Sfax, Sfax, Tunisia*

⁵*King Fahd University of Petroleum & Minerals, Dhahran, Saudi Arabia*

⁶*Department of Engineering Design and Mathematics, University of the West of England, Bristol, UK*

Correspondence should be addressed to Olfa Boubaker; olfa.boubaker@insat.rnu.tn

Received 6 March 2017; Accepted 6 March 2017; Published 15 June 2017

Copyright © 2017 Olfa Boubaker et al. This is an open access article distributed under the Creative Commons Attribution License, which permits unrestricted use, distribution, and reproduction in any medium, provided the original work is properly cited.

The subject of time-delay systems is a rather old research topic dating back to the works of Euler-Bernoulli in the XVIII century. Effective results in this area were initiated in the late fifties of the twentieth century since the works of Krasovskii and Razumikhin on the Lyapunov functions. However the significant progression in this area has been made during the last decade where numerous books, research, and survey papers and special issues have been devoted.

Delay is not just a mathematical exercise but more importantly is rooted in many natural and man-made systems such as biology, processes industries, and mechatronic motions. In engineering applications, time-delays generally describe propagation phenomena, material or energy transfer in intercommoned systems, and data transmission in communication systems. They have been the main sources inducing oscillations, instability, and poor control performances. Stability analysis and robust control of such systems are then of theoretical and practical importance. Much effort in the analysis and synthesis of these systems has been dedicated to delay-dependent and delay-independent issues based both/either on Lyapunov methods and/or frequency domain techniques. However, it should be noted that there are still numerous challenging issues pending in many classes of time-delay systems.

The purpose of this special issue is to draw attention of the scientific community to some recent advances and possible applications in the analysis, control, and synchronization of time-delay systems remaining unresolved until now. The special issue includes several high-quality papers written by leading and emerging specialists in the field. Engineering applications, such as power systems, rolling mills, hydraulic systems, distillation columns, aircrafts, space launch vehicle, and automotive and robotic systems, are seriously considered in this special issue.

Over 77 submissions from 14 countries (Australia, Brazil, China, Egypt, Iran, Japan, Malaysia, Morocco, Mexico, Nigeria, Republic of Korea, Saudi Arabia, Netherlands, and Tunisia) had been received to reflect the increasing interest in the topic and the authority in organization of the special issue. Only 16 papers are published with an acceptance rate of 20%. The primary guideline has been the originality of the work, relevance to the topics, and presentation of the contents.

Among the papers of the special issue, a single survey paper and four research papers are devoted to the stabilization and robust control of time-delay systems using Lyapunov theory and LMI tools. Three papers discuss the PID control design problem. Three papers cover industrial and automotive applications using test-benches or simulators to validate

the proposed approaches. There are also two papers solving synchronization problems and two other papers focusing on control of multiagent systems. Finally, there is a single paper solving the crucial problem of finding solutions for functional differential delayed equations. A very short description of the addressed topics is presented as follows.

The survey paper “Recent Progress in Stability and Stabilization of Systems with Time-Delays,” by M. S. Mahmoud, gives an overview of research investigations in the field. All revised results are classified on delay-independent and delay-dependent LMI conditions obtained via Lyapunov-Krasovskii and Lyapunov-Razumikhin theories where complexity and conservatism of each approach are discussed.

In “Novel Robust Exponential Stability of Markovian Jumping Impulsive Delayed Neural Networks of Neutral-Type with Stochastic Perturbation,” by Y. Fang et al., some new delay-dependent stability conditions are established using Lyapunov-Krasovskii function, Jensen integral inequality, free-weight matrix method, and LMI tools.

In “Robust Stability Criteria for T-S Fuzzy Systems with Time-Varying Delays via Nonquadratic Lyapunov-Krasovskii Functional Approach,” by S. H. Kim, a less conservative relaxed condition based on the nonquadratic Lyapunov-Krasovskii functional is proposed and will be useful for high computational complexities.

In “Robust Quadratic Stabilizability and H_∞ Control of Uncertain Linear Discrete-Time Stochastic Systems with State Delay,” by X. Jiang et al., a sufficient condition for the existence of a desired robust H_∞ controller is obtained.

In “Fixed Points and Exponential Stability for Impulsive Time-Delays BAM Neural Networks via LMI Approach and Contraction Mapping Principle,” by R. Rao et al., the authors proposed new LMI-based exponential stability by formulating a contraction mapping in a product space.

In “MIMO PI Controllers for LTI Systems with Multiple Time Delays Based on LMIs and Sensitivity Functions,” by W. Belhaj and O. Boubaker, a temporal/frequency-based design procedure is proposed for synthesis and tuning of MIMO PI controllers for stable, unstable, and nonminimum phase linear systems with delays in state and input variables.

In “Stabilization for Damping Multimachine Power System with Time-Varying Delays and Sector Saturating Actuator,” by L. Ma et al., a MIMO PD controller is designed by transforming the problem of PD controller design to that of state feedback stabilizer design for a system in descriptor form. A new sufficient condition is derived based on the Lyapunov theory.

In “An Expert PI Controller with Dead Time Compensation of Monitor AGC in Hot Strip Mill,” by F. Zhang et al., the authors presented a monitor automatic gauge control based on hydraulic roll gap control system algorithm with Filtered Smith Predictor suitable for the control of processes with long dead time, simple to implement and tune and having the advantages of obtaining real-time information and improving robustness.

In “A Control Method to Balance the Efficiency and Reliability of a Time-Delayed Pump-Valve System,” by Z. Lai et al., a test bench is used to validate the efficiency and the reliability of a sliding mode controller applied to the MIMO

Pump-Valve System by using a Modified Smith Predictor to compensate time-delays of the system.

In “A Decoupling Control Strategy for Multilayer Register System in Printed Electronic Equipment,” by S. Liu et al., a control approach based on feedforward control and active disturbance rejection is proposed to solve the strong coupling and strong interference and time-delay problems of multilayer register system used for Printed Electronic Equipment.

In “Direct Yaw-Moment Control of All-Wheel-Independent-Drive Electric Vehicles with Network-Induced Delays through Parameter-Dependent Fuzzy SMC Approach,” by W. Cao et al., a robust parameter-dependent fuzzy sliding mode control method based on the real-time information of vehicle states and delays is proposed for all-wheel-independent-drive electric vehicles subject to network-induced delays where the effectiveness of the proposed controller is proved using Simulink and CarSim software.

In “Multiple Model-Based Synchronization Approaches for Time Delayed Slaving Data in a Space Launch Vehicle Tracking System,” by H. Song and Y. Choi, the authors give a solution to the serious network delays problem caused by the multiple heterogeneous sensors installed over widespread areas generally leading to the failure of the space launch vehicle tracking systems. They propose a slaving data synchronization approach for the range safety system based on multiple model estimators so that the mission control system can adaptively find an appropriate dynamic model at an arbitrary time index, where time-delays occur.

In “High Precision Clock Bias Prediction Model in Clock Synchronization System,” by Z. Liu et al., the authors solve the synchronization problem of the clocks exploited in a distributed system and generally caused by interference time signal transmission or equipment failures. They use the first-order grey model with one variable optimized using the particle swarm optimization.

In “Consensus Conditions for High-Order Multiagent Systems with Nonuniform Delays,” by M. Shi et al., the consensus control problem of third-order to sixth-order multiagent systems with multiple nonuniform time-delays is solved where necessary sufficient conditions are provided in the form of simple inequalities.

In “Consensus Control for a Multiagent System with Time-Delays,” by Y. Cao et al., the consensus control problem for a multiagent system of integrator dynamics with input and output time-delays is solved using a state predictor and a linear controller without any delay compensation.

Finally, in “Multiple Periodic Solutions for A Class of Second-Order Neutral Impulsive Functional Differential Equations,” by J. Xie et al., the existence solutions of such crucial but frequent problem in modeling many real processes and phenomena is solved by means of critical point theory and variational methods. A typical example is also given to illustrate the applicability of such results.

Acknowledgments

The editors would like to express their gratefulness to all authors of the special issue for their valuable contributions and to all reviewers for their helpful and professional efforts

to provide precious comments and feedback. We hope this special issue offers a wide-ranging and timely view of the area of time-delay systems, which will grant stimulation for further academic research and industrial applications.

Olfa Boubaker
Valentina E. Balas
Abdellah Benzaouia
Mohamed Chaabane
Magdi S. Mahmoud
Quanmin Zhu

Review Article

Recent Progress in Stability and Stabilization of Systems with Time-Delays

Magdi S. Mahmoud

Systems Engineering Department, KFUPM, P.O. Box 5067, Dhahran 31261, Saudi Arabia

Correspondence should be addressed to Magdi S. Mahmoud; msmahmoud@kfupm.edu.sa

Received 8 November 2016; Accepted 7 March 2017; Published 13 June 2017

Academic Editor: Sabri Arik

Copyright © 2017 Magdi S. Mahmoud. This is an open access article distributed under the Creative Commons Attribution License, which permits unrestricted use, distribution, and reproduction in any medium, provided the original work is properly cited.

This paper overviews the research investigations pertaining to stability and stabilization of control systems with time-delays. The prime focus is the fundamental results and recent progress in theory and applications. The overview sheds light on the contemporary development on the linear matrix inequality (LMI) techniques in deriving both delay-independent and delay-dependent stability results for time-delay systems. Particular emphases will be placed on issues concerned with the conservatism and the computational complexity of the results. Key technical bounding lemmas and slack variable introduction approaches will be presented. The results will be compared and connections of certain delay-dependent stability results are also discussed.

1. Introduction

The occurrence of time-delay phenomenon appears to present many real-world systems and engineering applications. This takes place in either the state, the control input side, or the measurements side. It turns out that delays are strongly involved in challenging areas of communication and information technologies including stabilization of networked controlled systems and high-speed communication networks. In many cases, time-delay is a source of instability. However, for some systems, the presence of delay can have a stabilizing effect. The stability analysis and robust control of time-delay systems (TDS) are, therefore, of theoretical and practical importance.

On the other hand, time-delay systems (TDS) are also termed systems with aftereffect or dead-time, hereditary systems, equations with deviating argument, or differential-difference equations [1]. As opposed to ordinary differential equations (ODE), TDS belong to the class of functional differential equations (FDE) which are infinite dimension [2, 3]. A wide variety of dynamical systems can be modeled as time-delay systems [4]. Loosely speaking, time-delay is usually a source of poor performance and instability of a control system. Alternatively, in some few cases, the presence of time-delay is helpful for the stabilization of some systems.

Therefore, stability analysis of time-delay systems is of both practical and theoretical importance [5–9].

A great deal of the basic results is reported in [10–16]. Broadly speaking, stability conditions for time-delay systems can be broadly classified into two categories. One is delay-independent stability conditions and the other is delay-dependent stability conditions. Much attention was paid to the study of delay-dependent stability conditions as they yield less conservative results. Recently much work was presented in [17–30] covering alternative issues pertaining to stability and stabilization of dynamical systems with time-delays.

The primary objective of this paper is to

- (i) familiarize wider readers with TDS,
- (ii) provide a systematic treatment of modern ideas and techniques for researchers.

The paper bridges the huge gap from some basic classical results to recent developments on Lyapunov-based analysis and design with applications to the attractive topics of network-based control and interconnected time-delay control systems. Essentially, it provides an overview on the progress of stability and stabilization of time-delay systems (TDS). Particular emphases will be placed on issues concerned with the conservatism and the computational

complexity of the results. For simplicity in exposition, the discussions are limited to linear or linearizable systems. Some methods and techniques used to derive stability conditions for time-delay systems are reviewed. Several future research directions on this topic are also discussed.

Notations. Let \mathbb{R}^n denote the n -dimensional Euclidean space equipped with the norm $\|\cdot\|$. We use W^t , W^{-1} , $\lambda_m(W)$, and $\lambda_M(W)$ to denote, respectively, the transpose, the inverse, the minimum eigenvalue, and the maximum eigenvalue of any square matrix W and $W > 0$ ($W < 0$) stands for a symmetrical and positive- (negative-) definite matrix W . I stands for unit matrix with appropriate dimension. $\|\alpha\|_2^2 = \sum_{k=0}^{\infty} \alpha^t(k)\alpha(k)$. δH denotes the first difference of H . We let \mathbb{R}^+ denote the set of nonnegative real numbers; $\mathbb{C}_n = \mathbb{C}([-h, 0], \mathbb{R}^n)$ denotes the Banach space of continuous functions $\varphi : [-h, 0] \rightarrow \mathbb{R}^n$, and for $\varphi \in \mathbb{C}_n$, the associated norm is $\|\varphi\|_c = \sup_{-h \leq s \leq 0} \|\varphi\|$. We let $\mathbf{N} = \{1, \dots, N\}$.

Matrices, if their dimensions are not explicitly stated, are assumed to be compatible for algebraic operations. In symmetric block matrices, we use the symbol \bullet to represent a term that is induced by symmetry. Sometimes, the arguments of a function will be omitted when no confusion can arise.

The following facts are provided in [6].

Fact 1. Let $\Sigma_1, \Sigma_2, \Sigma_3$, and $0 < R = R^t$ be real constant matrices of compatible dimensions and let $H(t)$ be a real matrix function satisfying $H^t(t)H(t) \leq I$. Then for any $\rho > 0$ satisfying $\rho \Sigma_2^t \Sigma_2 < R$, the following matrix inequality holds:

$$\begin{aligned} & (\Sigma_3 + \Sigma_1 H(t) \Sigma_2) R^{-1} (\Sigma_3 + \Sigma_2^t H^t(t) \Sigma_1^t) \\ & \leq \rho^{-1} \Sigma_1 \Sigma_1^t + \Sigma_3 (R - \rho \Sigma_2^t \Sigma_2)^{-1} \Sigma_3^t. \end{aligned} \quad (1)$$

Fact 2. For any real matrices Σ_1, Σ_2 , and Σ_3 with appropriate dimensions and $\Sigma_3^t \Sigma_3 \leq I$, it follows that

$$\Sigma_1 \Sigma_3 \Sigma_2 + \Sigma_2^t \Sigma_3^t \Sigma_1^t \leq \alpha^{-1} \Sigma_1 \Sigma_1^t + \alpha \Sigma_2^t \Sigma_2, \quad \forall \alpha > 0. \quad (2)$$

Lemma 1 (Finsler's lemma, [31]). *Let $X \in \mathbb{R}^n$, $P = P^t \in \mathbb{R}^{n \times n}$, and $H \in \mathbb{R}^{m \times n}$ such that $\text{rank}(H) = r < n$. The following statements are equivalent:*

- (i) $x^t P x < 0 \quad \forall Hx = 0, \quad x \neq 0$.
- (ii) $(H^\perp)^t P (H^\perp) < 0$.
- (iii) $\exists N \in \mathbb{R}^{n \times m} : P + NH + H^t N^t < 0$.
- (iv) $\exists \lambda \in \mathbb{R} : P - \lambda H^t H < 0$.

2. Overview

There are many applications where time-delay phenomena appear quite naturally. This includes, but not limited to, the following:

- (A) Automotive: combustion model (ignition delay); electromechanical brakes (actuator delay).
- (B) Heat exchanger: distributed delay due to conduction in a tube.

- (C) Hydraulic networks: the transport phenomenon of water which is modeled as a varying time-delay.
- (D) Electrical networks.
- (E) Intelligent building: time-delay due to wireless transmission of sensor data.
- (F) Marine robotics: transport delay due to sonar measurement of depth.
- (G) Population dynamics: predator-prey model based on Volterra model with predator (y) and prey (x) populations (t is the time-life of prey):

$$\begin{aligned} \dot{x}(t) &= rx \left(1 - \frac{x(t-\tau)}{K} \right) - \alpha xy, \\ \dot{y}(t) &= -cy + \beta xy. \end{aligned} \quad (3)$$

- (H) Manufacturing process: the metal cutting process on a lathe which can be described as

$$m\ddot{y}(t) + c\dot{y}(t) + ky(t) = -F_t [f + y(t) - y(t-\tau)]. \quad (4)$$

The study of this model is critical in understanding the regenerative chattering phenomenon.

- (I) Epidemics: understanding the dynamics of biological processes and epidemics which is a challenge for health workers engaged in managing treatment strategies. The underlying mechanisms can be revealed by considering epidemics and diseases as dynamical processes, for which the hematology dynamics can be modeled by

$$\dot{y}(t) = -\lambda y(t) + F[y(t-\tau)] \quad (5)$$

which formulates the circulating cell populations in one compartment, where y represents the circulating cell population, λ is the cell-loss rate, and the monotone function F (describing a feedback mechanism) denotes the flux of cells from the previous compartment. The delay τ represents the average length of time required to go through the compartment.

- (J) Glucose-insulin model: letting $G(t)$ and $I(t)$ represent the levels of plasma glycemia and insulinemia; then

$$\begin{aligned} \dot{G}(t) &= K_{xgi} G(t) I(t) + \frac{T_{gh}}{V_G}, \\ \dot{I}(t) &= -K_{xi} I(t) + \frac{T_{iG_{\max}}}{V_I} f[G(t-\tau_g)], \end{aligned} \quad (6)$$

where

- (i) K_{xgi} is rate of glucose uptake by tissues (insulin-dependent) per pM of plasma insulin concentration,
- (ii) T_{gh} is net balance between hepatic glucose output and insulin-independent zero-order glucose tissue uptake (mainly by the brain),

- (iii) V_G is apparent distribution volume for glucose,
- (iv) K_{xi} is apparent first-order disappearance rate constant for insulin,
- (v) $T_{iG_{\max}}$ is maximal rate of second-phase insulin release,
- (vi) V_I is apparent distribution volume for insulin,
- (vii) τ_g is apparent delay with which the pancreas varies secondary insulin release in response to varying plasma glucose concentrations,
- (viii) $f(\cdot)$ is nonlinear function that models the Insulin Delivery Rate.

(K) Neutral delay systems: arising, for instance, in the analysis of the coupling between transmission lines and population dynamics: evolution of forests. The model is based on a refinement of the delay-free logistic (or Pearl-Verhulst equation) where effects as soil depletion and erosion have been introduced

$$\dot{x}(t) = rx(t) \left[1 - \frac{x(t-\tau) + c\dot{x}(t-\tau)}{K} \right], \quad (7)$$

where x is the population, r is the intrinsic growth rate, and K is the environmental carrying capacity.

3. Models and Solutions

A general model of TDS can be expressed as

$$\begin{aligned} \dot{x}(t) &= f(x_t, t, u_t), \quad t \geq t_0 \\ y(t) &= g(x_t; t, u_t), \end{aligned} \quad (8)$$

where

$$\begin{aligned} x_t(\theta) &= x(t+\theta); \quad -h \leq \theta \leq 0, \\ u_t(\theta) &= u(t+\theta); \quad -h \leq \theta \leq 0, \\ x(\theta) &= \varphi(\theta); \quad t_0 - h \leq \theta \leq t_0. \end{aligned} \quad (9)$$

3.1. Retarded Systems. It is quite natural to consider, as state-space, the set $\mathbb{S} = \mathbb{S}([-h; 0]; \mathbb{R}^n)$ of continuous functions mapping the interval $[-h; 0] \rightarrow \mathbb{R}^n$, with the topology of uniform convergence. The initial condition $\varphi(\theta)$ must be prescribed as $\Phi : [-h; 0]; \mathbb{R}^n$. Observe that $\Phi \in \mathbb{C}$ or may involve bounded jumps at some discontinuity instants. The nature of the solution (and of its initial value) then distinguishes FDE from ODE.

Definition 2 (see [3]). A function x is said to be a solution on $[\sigma - h; \sigma + a]$ of the retarded functional differential equation (RDE)

$$\begin{aligned} \dot{x}(t) &= f(t, x_t), \\ f : \Omega \subset \mathbb{R} \times \mathbb{S} &\rightarrow \mathbb{R}^n, \end{aligned} \quad (10)$$

if there are $\sigma \in \mathbb{R}$ and $a > 0$ such that $x \in \mathbb{S}([\sigma - h; \sigma + h]; \mathbb{R}^n)$, $(t, x_t) \in \Omega$, and $x(t)$ satisfies (10) for $t \in [\sigma - h; \sigma + a]$. For

given $\sigma \in \mathbb{R}; \varphi \in \mathbb{S}$, we say that $x(\sigma; \varphi; f)$ is a solution of (10) with initial value φ at σ or simply a solution through $(\sigma; \varphi)$ if there is $a > 0$ such that $x(\sigma; \varphi; f)$ is a solution of (10) on $t \in [\sigma - h; \sigma + a]$ and $x_\sigma(\sigma; \varphi; f) = \varphi$.

Supposing that Ω is open and $f \in \mathbb{S}(\Omega, \mathbb{R}^n)$, then a function $x \in \mathbb{S}([\sigma - h - \alpha; \sigma]; \mathbb{R}^n)$, $\alpha > 0$, is referred to as a backward continuation of the solution through $(\sigma; \varphi)$ if $x_\sigma = \varphi$ and for any $\sigma_1 \in [\sigma - \alpha, \sigma]; (\sigma_1; x_{\sigma_1}) \in \Omega$ and x is a solution of (10) on $(\sigma_1 - h; \sigma)$ through $(\sigma_1; x_{\sigma_1})$.

The interested reader is referred to [3] for further useful discussions.

3.2. Neutral Systems. Neutral systems also are delay systems but involve the same highest derivation order for some components of $x(t)$ at both time t and past time(s) $t^o < t$, which implies an increased mathematical complexity. Neutral systems are represented by

$$\dot{x}(t) = f(x_t, t, \dot{x}_t, u_t) \quad (11)$$

or

$$\frac{dFx_t}{dt} = f(x_t, t, u_t), \quad (12)$$

where $F : \mathbb{S} \rightarrow \mathbb{R}^n$ is a regular operator with deviating argument in time, as, for instance, with D constant matrix

$$Fx_t = x(t) - Dx(t - \omega). \quad (13)$$

It is significant to observe that the solutions of retarded systems have their differentiability degree smoothed with increasing time, but this is no longer true for neutral systems due to the implied difference-equation involving $\dot{x}(t)$; the trajectory may replicate any irregularity of the initial condition $\varphi(t)$, even if f and F satisfy many smoothness properties.

3.3. Models for Linear Time-Invariant Systems. In the linear, time-invariant case (LTI), the corresponding general time-delay model is

$$\begin{aligned} \dot{x}(t) &= \sum_{\ell=1}^p D_\ell \dot{x}(t - \omega_\ell) \\ &+ \sum_{j=0}^q [A_j x(t - h_j) + B_j u(t - h_j)] \\ &+ \sum_{m=1}^r \int_{t-\tau_m}^t [G_m(\theta) x(\theta) + H_m(\theta) u(\theta)] d\theta, \\ y(t) &= \sum_{j=0}^q C_j x(t - h_j) + \sum_{m=1}^r \int_{t-\tau_m}^t N_m(\theta) x(\theta) d\theta, \end{aligned} \quad (14)$$

where

- (i) $h_0 = 0$ and A_0 is constant instantaneous matrix;
- (ii) constant matrices A_j ; $j > 0$ represent discrete-delay phenomena;

- (iii) the sum of integrals corresponds to distributed delay effects, weighted by G_m over the time intervals $[t - \tau_m; t]$;
- (iv) matrices D_ℓ account for the neutral part;
- (v) matrices B_j and $H_m(s)$ are input matrices;
- (vi) in brief, $h = \max_{j,m,\ell} \{h_j; \tau_m; \omega_\ell\}$.

Note that (15), $y(t) \in \mathbb{R}^p$, represents the output description, with discrete C_j and distributed $N_m(\theta)$ delayed parts as well. The special case of (14)-(15)

$$\dot{x}(t) = \sum_{j=0}^q \left[A_j x(t - h_j) + B_j u(t - h_j) \right], \quad (16)$$

$$h_0 = 0 < h_1 < \dots, h_{q-1} < h_q$$

has been investigated extensively in the literature.

4. Notion of Stability

As a starting point, we recall the following stability notion for time-delay system (3).

Definition 3. If, for any $t_0 \in \mathbb{R}$ and any $\varepsilon > 0$, there exists a $\delta = \delta(t_0, \varepsilon) > 0$ such that $\|x_{t_0}\|_c < \delta$ implies $\|x(t)\| < \varepsilon$ for all $t \geq t_0$, then the trivial solution of time-delay system (3) is stable.

The following properties are readily recognized.

- (i) If the trivial solution of time-delay system (3) is *stable* and if δ can be chosen independently of t_0 , then the trivial solution of time-delay system (3) is *uniformly stable*.
- (ii) If the trivial solution of time-delay system (3) is stable and if, for any $t_0 \in \mathbb{R}$ and any $\varepsilon > 0$, there exists $\delta_a = \delta_a(t_0, \varepsilon) > 0$ such that $\|x_{t_0}\|_c < \delta_a$ implies $\lim_{t \rightarrow \infty} x(t) = 0$, then the trivial solution of time-delay system (3) is *asymptotically stable*.
- (iii) If the trivial solution of time-delay system (3) is uniformly stable and there exists $\delta_a > 0$, such that $\|x_{t_0}\|_c < \delta_a$ implies $\|x(t)\| < \eta$ for $t \geq t_0 + T$ and $t_0 \in \mathbb{R}$, then the trivial solution of time-delay system (3) is *uniformly asymptotically stable*.
- (iv) If the trivial solution of time-delay system (3) is (uniformly) asymptotically stable and if δ_a can be arbitrarily large but finite number, then the trivial solution of time-delay system (3) is *globally (uniformly) asymptotically stable*.

5. Fundamental Stability Theorems

In the study of stability analysis of time-delay systems, the methods of Lyapunov functions and Lyapunov-Krasovskii functionals play important roles. There are two Lyapunov methods are often used:

- (A) *Lyapunov-Krasovskii functional (LKF) method*,
- (B) *Lyapunov-Razumikhin function (LRF) method*.

It is significant to observe that LKF method deals with functionals which essentially have scalar values whereas Lyapunov-Razumikhin function (LRF) method involves only functions rather than functionals.

In this section, these two methods are reviewed; see [6] for details.

Consider the following time-delay system described by

$$\dot{x}(t) = f(t, x_t), \quad t \geq t_0, \quad (17)$$

where

- (i) $x_t = x(t + \theta); -\theta_m \leq \theta \leq 0$,
- (ii) $f; \mathbb{R} \times \mathbb{C}_n \rightarrow \mathbb{R}^n$ is continuous and is Lipschitz in x_t ,
- (iii) $f(t, 0) = 0$.

In the sequel, we let $x_t(s, \varphi)$ be the solution of (17) at time t with initial condition $x_s = \varphi$. Let \mathbb{G} be a bounded subset of \mathbb{C}_n and let \mathbb{H} be a bounded subset of \mathbb{R}^n .

A statement of *Lyapunov-Krasovskii stability method* is provided by the following theorem.

Theorem 4. Suppose that f maps $\mathbb{R} \times \mathbb{G}$ into \mathbb{H} and $u, v, w : \mathbb{R}^+ \rightarrow \mathbb{R}^+$ are continuous, nondecreasing functions with $u(0) = v(0) = 0$ and $u(\beta) > 0$ and $v(\beta) > 0$, for $\beta > 0$. If there exists a continuous functional $\mathbb{V} : \mathbb{R} \times \mathbb{C}_n \rightarrow \mathbb{R}$ such that

- (1) $u(\|\varphi(0)\|) \leq \mathbb{V}(t, \varphi) \leq v(\|\varphi(0)\|)$,
- (2) $\dot{\mathbb{V}}(t, \varphi) \leq -w(\|\varphi(0)\|)$,

where

$$\dot{\mathbb{V}}(t, \varphi) = \lim_{\Delta t \rightarrow 0^+} \frac{1}{\Delta t} (\mathbb{V}(t + \Delta t, x_{t+\Delta t}(t, \varphi)) - \mathbb{V}(t, \varphi)), \quad (18)$$

then the trivial solution of time-delay system (3) is uniformly stable. If $w(\beta) > 0$, for $\beta > 0$, then the trivial solution of time-delay system (3) is uniformly asymptotically stable. Additionally, if $\lim_{\beta \rightarrow \infty} u(\beta) \rightarrow \infty$, then the trivial solution of time-delay system (3) is globally uniformly asymptotically stable.

In some cases, the LKF involving terms depending on the state derivatives \dot{x}_t are quite effective in the derivation of the stability conditions. This will in turn requires the modification of the conditions in Theorem 4. See [8] for details.

A statement of *Lyapunov-Razumikhin stability method* is provided by the following theorem.

Theorem 5. Suppose that f maps $\mathbb{R} \times \mathbb{G}$ into \mathbb{H} and $u, v, w : \mathbb{R}^+ \rightarrow \mathbb{R}^+$ are continuous, nondecreasing functions with $u(0) = v(0) = 0$ and $u(\beta) > 0$ and $v(\beta) > 0$, for $\beta > 0$, and v is strictly increasing. If there exists a continuous functional $\mathbb{V} : \mathbb{R} \times \mathbb{R}^n \rightarrow \mathbb{R}$ such that

- (1) $u(\|x\|) \leq \mathbb{V}(t, x) \leq v(\|x\|)$,
- (2) $\dot{\mathbb{V}}(t, \varphi) \leq -w(\|\varphi(0)\|)$, if

$$[\mathbb{V}(t + \theta, x(t + \theta)) \leq \mathbb{V}(t, x(t))], \quad \text{for } \theta \in [-h, 0], \quad (19)$$

where

$$\begin{aligned}\dot{\mathbb{V}}(t, x(t)) &= \frac{d}{dt}\mathbb{V}(t, x(t)) \\ &= \frac{\partial \mathbb{V}(t, x(t))}{\partial t} + \frac{\partial \mathbb{V}(t, x(t))}{\partial x} f(t, x_t),\end{aligned}\quad (20)$$

then the trivial solution of time-delay system (3) is uniformly stable. If $w(\beta) > 0$, for $\beta > 0$, there exists a continuous nondecreasing function $q(\beta) > 0$, for $\beta > 0$, and the foregoing condition (2) is strengthened to $\mathbb{V}(t, x(t)) \leq -w(\|x(t)\|)$, if

$$\begin{aligned}(\mathbb{V}(t + \theta, x(t + \theta)) &\leq q(\mathbb{V}(t, x(t))), \\ \text{for } \theta &\in [-h, 0],\end{aligned}\quad (21)$$

then the trivial solution of time-delay system (3) is uniformly asymptotically stable. Additionally, if $\lim_{\beta \rightarrow \infty} u(\beta) \rightarrow \infty$, then the trivial solution of time-delay system (3) is globally uniformly asymptotically stable.

The following Halanay result [7] also plays an important role in the stability analysis of time-delay systems.

Theorem 6. Suppose that constant scalars k_1 and k_2 satisfy $k_1 > 0$, $k_2 > 0$, and $y(t)$ is a nonnegative continuous function on $[t_0 - \tau, t_0]$ satisfying

$$\begin{aligned}\dot{y}(t) &\leq -k_1 y(t) + k_2 \bar{y}(t), \quad t \geq t_0, \\ \bar{y}(t) &= \sup_{t-\tau \leq s \leq t} \{y(s)\}, \quad \tau \geq 0.\end{aligned}\quad (22)$$

Then, for $t \geq t_0$, one has

$$y(t) \leq \bar{y}(t_0) \exp(-\kappa(t - t_0)), \quad (23)$$

where $\kappa > 0$ is the unique solution to the following equation:

$$\kappa = k_1 - k_2 \exp(-\kappa\tau). \quad (24)$$

Remark 7. Theorems 4 through 6 can be used to derive stability conditions for the case when the delay is time-varying, which is continuous but not necessarily differentiable.

Remark 8. In the sequel, stability conditions for time-delay systems can be broadly classified into two types:

- (1) Delay-independent stability (DIS) conditions which do not include information about the delay. Generally speaking, DIS conditions are simpler to apply.
- (2) Delay-dependent stability (DDS) conditions which involve information on the size and pattern of the delay. DDS conditions are less conservative especially in the case when the time-delay is small.

In the sequel, this paper focuses on the delay-dependent stability problem and the objective is twofold:

- (A) to develop delay-dependent conditions to provide a maximal allowable delay as large as possible,

- (B) to develop delay-dependent conditions by using as few as possible decision variables while keeping the same maximal allowable delay.

Alternatives approaches were proposed in the literature to obtain DDS conditions, among which the linear matrix inequality (LMI) approach is the most popular. The LMI approach has played a significant role due to the fact that family linear matrix inequalities can be readily converted into a convex optimization problem. The latter can be handled efficiently by resorting to recently developed numerical algorithms for solving LMIs [31]. Additional reason that makes LMI conditions appealing is their frequent readiness to solve the corresponding synthesis problems once the stability (or other performance) conditions are established, especially when state feedback is employed.

6. Stability Results for Linear Delay Systems

For the sake of simplicity, the following linear system with a single discrete delay is considered:

$$\dot{x}(t) = Ax(t) + A_d(t - \tau(t)), \quad t \geq t_0, \quad (25)$$

where $x(t) \in \mathbb{R}^n$ is the state vector, A and A_d are system matrices with appropriate dimensions, and $\tau(t)$ is the time-delay factors. There are several classes of time-delay patterns considered in the literature as follows:

Class A: constant delay,

$$\tau(t) = d, \quad \forall t. \quad (26)$$

Class B: unknown-but-bounded delay,

$$0 < \tau(t) \leq \tau_M, \quad \forall t. \quad (27)$$

Class C: bounded time-varying delay,

$$\tau_m \leq \tau(t) \leq \tau_M, \quad \forall t. \quad (28)$$

Class D: bounded time-varying delay with bounded derivative,

$$\begin{aligned}\tau_m &\leq \tau(t) \leq \tau_M, \quad \forall t \\ d_m &\leq \dot{\tau}(t) \leq d_M, \quad \forall t.\end{aligned}\quad (29)$$

6.1. Constant Delay. When the time-delay is constant, the system described by (30) can be rewritten as

$$\dot{x}(t) = A_0 x(t) + A_d x(t - d), \quad t \geq t_0. \quad (30)$$

Natural extensions of the quadratic Lyapunov functions can be particularly used to study in the framework of LTI delay systems (30) and the functional

$$\mathbb{V}_0(x_t) = x^t(t) \mathcal{P} x(t) + \int_{-d}^0 x^t(t + \theta) \mathcal{Q} x(t + \theta) d\theta. \quad (31)$$

One obtains sufficient conditions by the following theorem.

Theorem 9. *The time-delay system (30) is asymptotically stable for any $d \geq 0$ if there exist matrices $\mathcal{P} > 0$ and $\mathcal{Q} > 0$, \mathcal{R} verifying*

$$\mathcal{P}A_0 + A_0^t \mathcal{P} + \mathcal{P}A_d \mathcal{Q}^{-1} A_d^t \mathcal{P} + \mathcal{Q} + \mathcal{R} = 0 \quad (32)$$

or equivalently the LMI

$$\begin{bmatrix} \mathcal{P}A_0 + A_0^t \mathcal{P} + \mathcal{Q} & \mathcal{P}A_d \\ \bullet & -\mathcal{Q} \end{bmatrix} < 0. \quad (33)$$

It is significant to observe in the delay-free case, $A_d = 0$, that (33) provides the link with the Lyapunov equation for ODE. Nevertheless, in the delayed case $A_d \neq 0$, this sufficient condition is far from being necessary. From here, many generalizations were proposed, involving different alternative terms:

$$\mathbb{V}_1(x_t) = x^t(t) \mathcal{P}x(t),$$

$$\mathbb{V}_2(x_t) = x^t(t) \int_{-d_j}^0 \mathcal{Q}_j x(t+\theta) d\theta,$$

$$\mathbb{V}_3(x_t) = \int_{-d_j}^0 x^t(t+\theta) \mathcal{S}_j x(t+\theta) d\theta,$$

$$\mathbb{V}_4(x_t) = \int_{-\tau_j}^0 \int_{t+\theta}^0 x^t(\theta) \mathcal{R}_j x(\theta) d\theta ds,$$

$$\mathbb{V}_5(x_t) = x^t(t) \int_{-d_j}^0 \mathcal{P}_j(\eta) x(t+\eta) d\eta,$$

$$\mathbb{V}_6(x_t) = \int_{-d_j}^0 \int_{-d_j}^0 x^t(t+\eta) \mathcal{P}(\eta, \theta) x(t+\theta) d\eta d\theta. \quad (34)$$

The following points are noteworthy:

- (1) Loosely speaking, the terms $\mathbb{V}_2; \mathbb{V}_3$ are used for the delay-independent stability of discrete delays.
- (2) The term \mathbb{V}_4 is meant for distributed delays or discrete-delay dependent stability. On considering system (30) along with

$$\mathbb{V}(x_t) = \mathbb{V}_1(x(t)) + \mathbb{V}_4(x_t) + \mathbb{V}_4(x_{t-h}) \quad (35)$$

standard manipulation leads, with R_1 for $\mathbb{V}_4(x_t)$; R_2 for $\mathbb{V}_4(x_{t-h})$, to the following delay-dependent LMI condition:

$$\begin{bmatrix} \mathcal{P}(A_0 + A_d) + (A_0 + A_d)^t \mathcal{P} + d\mathcal{R}_1 + d\mathcal{R}_2 & d\mathcal{P}A_d A_0 & h\mathcal{P}A_d^2 \\ \bullet & -d\mathcal{R}_1 & 0 \\ \bullet & \bullet & -d\mathcal{R}_2 \end{bmatrix} < 0. \quad (36)$$

- (3) Although the terms \mathbb{V}_5 and \mathbb{V}_6 appear, in a general form, in necessary and sufficient schemes (see [10–12]), the general computation of the time-varying matrices is excessively burden. To avoid such computational limitations, a discretization scheme incorporating piecewise-constant functions $P_j(\cdot)$ was introduced in [15, 16].

6.2. Time-Varying Delay. In what follows, we will review the LMI techniques in deriving DDS results for the single-delay case. Extension to the multiple-delay case is a straightforward task. We consider the class of time-delay systems (class B) in which the delay factor is continuous but bounded.

$$\begin{aligned} \dot{x}(t) &= A_0 x(t) + A_d x(t - \tau(t)), \\ x(t) &= \varphi(t), \quad t \in [-\tau_M, 0]. \end{aligned} \quad (37)$$

Similar to (31), we consider the LKF of the form

$$\begin{aligned} \widehat{V}_0(x_t) &= x^t(t) \mathcal{P}x(t) \\ &+ \int_{t-\tau(t)}^t x^t(t+\theta) \mathcal{Q}x(t+\theta) d\theta. \end{aligned} \quad (38)$$

Since the time-varying delay $\tau(t)$ may not be differentiable, we introduce the following equalities for any matrices \mathcal{Y}, \mathcal{W} , and \mathcal{S} with appropriate dimensions:

$$\dot{x}^t(t) \mathcal{Y} [A_0 x(t) + A_d x(t - \tau(t)) - \dot{x}(t)] = 0,$$

$$x^t(t) \mathcal{W} [A_0 x(t) + A_d x(t - \tau(t)) - \dot{x}(t)] = 0, \quad (39)$$

$$x^t(t - \tau(t)) \mathcal{S} [A_0 x(t) + A_d x(t - \tau(t)) - \dot{x}(t)] = 0.$$

The following theorem summarized the main result.

Theorem 10. *The time-delay system (37) is asymptotically stable if there exist matrices $\mathcal{P} > 0$, \mathcal{Y}, \mathcal{W} , and \mathcal{S} such that*

$$\begin{bmatrix} \mathcal{W}A_0 + A_0^t \mathcal{W}^t & \mathcal{W}A_d + A_0^t \mathcal{S}^t & A_0^t \mathcal{Y}^t + \mathcal{P} - \mathcal{W} \\ \bullet & \mathcal{S}A_d + A_d^t \mathcal{S}^t & A_d^t \mathcal{Y}^t - \mathcal{S} \\ \bullet & \bullet & -\mathcal{Y} - \mathcal{Y}^t \end{bmatrix} < 0. \quad (40)$$

Consider the time-delay system

$$\dot{x}(t) = A_0 x(t) + A_d x(t - \tau(t)),$$

$$x(t) = \varphi(t), \quad t \in [-\tau_M, 0], \quad (41)$$

$$0 \leq \tau_m \leq \tau(t) \leq \tau_M,$$

$$\sigma \leq \dot{\tau}(t) \leq \mu. \quad (42)$$

According to the Lyapunov-Razumikhin stability method Theorem 5, the following stability condition can be obtained.

Theorem 11. *The time-delay system (41) is asymptotically stable if there exist matrix $\mathcal{P} > 0$ and a scalar $\sigma > 0$ such that*

$$\begin{bmatrix} \mathcal{P}A_0 + A_0^t \mathcal{P} + \sigma \mathcal{P} & \mathcal{P}A_d \\ \cdot & -\sigma \mathcal{P} \end{bmatrix} < 0. \quad (43)$$

On choosing the LKF (31), a delay-independent stability condition can be derived in the following form.

Theorem 12. *The time-delay system (41) is asymptotically stable if there exist matrices $\mathcal{P} > 0$ and $\mathcal{Q} > 0$ such that*

$$\begin{bmatrix} \mathcal{P}A_0 + A_0^t \mathcal{P} + \mathcal{Q} & \mathcal{P}A_d \\ \cdot & -(1 - \mu) \mathcal{Q} \end{bmatrix} < 0. \quad (44)$$

Remark 13. It should be noted that Theorem 12 is independent of the time-delay and therefore is very conservative especially when the time-delay is small. When the delay is constant, $\tau(t) \equiv d$, it follows from the Schur complements that (40) is equivalent to

$$\mathcal{P}A_0 + A_0^t \mathcal{P} + \mathcal{Q} + \mathcal{P}A_d \mathcal{Q}^{-1} A_d^t \mathcal{P} < 0. \quad (45)$$

In turn this implies that

$$\mathcal{P}(A_0 + A_d) + (A_0 + A_d)^t \mathcal{P} < 0 \quad (46)$$

which is a necessary and sufficient condition for the stability of system (41) with zero delay.

In the literature, the following Lyapunov functional is often used to derive delay-dependent results.

$$\begin{aligned} \mathbb{V}(t, x_t) &= x^t(t)^t \mathcal{P} x(t) + \int_{t-\tau(t)}^t x^t(s)^t \mathcal{Q} x(s) ds \\ &+ \int_{-\tau_M}^0 \int_{t+\theta}^t \dot{x}^t(s)^t \mathcal{Z} \dot{x}(s) ds d\theta. \end{aligned} \quad (47)$$

It was first introduced in [32, 33]. Using the free-weighting [34], the following DDS condition can be derived based on the LKF (47).

Theorem 14. *The time-delay system (41) is asymptotically stable if there exist matrices $\mathcal{P} > 0$, $\mathcal{Q} > 0$, $\mathcal{Z} > 0$, and*

$\begin{bmatrix} X_{11} & X_{12} \\ \cdot & X_{22} \end{bmatrix} \geq 0$, and any matrices M and N of appropriate dimensions such that

$$\begin{bmatrix} \mathbb{L}_{11} & \mathbb{L}_{12} & \tau_M A_0^t \mathcal{Z} \\ \cdot & \mathbb{L}_{22} & \tau_M A_d^t \mathcal{Z} \\ \cdot & \cdot & -\tau_M \mathcal{Z} \end{bmatrix} < 0, \quad (48)$$

$$\begin{bmatrix} X_{11} & X_{12} & M \\ \cdot & X_{22} & N \\ \cdot & \cdot & \mathcal{Z} \end{bmatrix} \geq 0,$$

where

$$\mathbb{L}_{11} = \mathcal{P}A_0 + A_0^t \mathcal{P} + M + M^t + \mathcal{Q} + \tau_M X_{11},$$

$$\mathbb{L}_{12} = \mathcal{P}A_d + M + N^t + \tau_M X_{12}, \quad (49)$$

$$\mathbb{L}_{22} = -N - N^t - (1 - \mu) \mathcal{Q} + \tau_M X_{22}.$$

6.3. Augmented Lyapunov Functional. Recalling that the first term in most LKFs is $x^t(t) P x(t)$ which involves the current state $x(t)$ only and does not reflect the delayed state. Hence, an augmented Lyapunov functional was proposed in [35] for system described by (30).

$$\begin{aligned} \mathbb{V}(t, x_t) &= \xi^t(t)^t \mathcal{P} \xi(t) + \int_{t-d}^t \varrho^t(s)^t \mathcal{Q} \varrho(s) ds \\ &+ \int_{-d}^0 \int_{t+\theta}^t \varrho^t(s)^t \mathcal{Z} \varrho(s) ds d\theta, \end{aligned} \quad (50)$$

$$\xi^t(t) = \begin{bmatrix} x^t(t) & x^t(t-d) & \int_{t-d}^t x^t(s) ds \end{bmatrix}, \quad (51)$$

$$\varrho^t(s) = \begin{bmatrix} x^t(s) & \dot{x}^t(s) \end{bmatrix}.$$

Remark 15. Compared with the Lyapunov functional (47), the augmented Lyapunov functional can lead to less conservative results. Additionally, it is also applicable for systems with time-varying delay, which can be seen in [36] and references therein.

6.4. Triple Integral Lyapunov Functional. On examining the LKFs (31) and (50), it can be seen that the Lyapunov functional often contains integral terms: single $\int_{t-\tau(t)}^t x^t(t + \theta) \mathcal{Q} x(t + \theta) d\theta$ and double $\int_{-d}^0 \int_{t+\theta}^t \varrho^t(s)^t \mathcal{Z} \varrho(s) ds d\theta$ in order to bring the effect of time-delays.

A natural question which arose is whether introducing triple integral terms in the Lyapunov functional would yield improvement in the stability behavior. This question

is addressed [37, 38] by extending the LKFs (50)-(51) and incorporating a triple integral term to yield the form

$$\begin{aligned} \mathbb{V}(t, x_t) = & \xi^t(t) \mathcal{P} \xi(t) + \int_{t-d}^t \varrho^t(s) \mathcal{Q} \varrho(s) ds \\ & + \int_{-d}^0 \int_{t+\theta}^t \varrho^t(s) \mathcal{L} \varrho(s) ds d\theta \\ & + \int_{-d}^0 \int_{\theta}^0 \int_{t+\beta}^t \dot{x}^t(s) \mathcal{R} \dot{x}(s) ds d\beta d\theta. \end{aligned} \quad (52)$$

Remark 16. It is reported in [37, 38] by simulation results that the Lyapunov functional containing triple integral terms is quite effective in reduction of the conservatism of the stability conditions.

6.5. Newton-Leibniz Formula. An alternative route can be pursued by using the Newton-Leibniz formula

$$\begin{aligned} x(t-d) &= x(t) - \int_{t-d}^t \dot{x}(\alpha) d\alpha \\ &= x(t) - \int_{t-d}^t [A_0 x(\alpha) + A_d x(\alpha-d)] d\alpha \end{aligned} \quad (53)$$

and recalling (30) to yield

$$\begin{aligned} \dot{x}(t) &= [A_0 + A_d] x(t) \\ &\quad - A_d \int_{t-d}^t [A_0 x(\alpha) + A_d x(\alpha-d)] d\alpha. \end{aligned} \quad (54)$$

Remark 17. It should be clear that the asymptotic stability of the time-delay system in (54) implies that of system (30).

Following [6], we proceed to study the DDS of system (54) using the following LKF candidate:

$$\begin{aligned} \mathbb{V}(t, x_t) = & x^t(t) \mathcal{P}^{-1} x(t) \\ & + \int_{-h}^0 \int_{t+\alpha}^t x^t(\theta) A_d^t \mathcal{Q}_1^{-1} A_d x(\theta) d\theta d\alpha \\ & + \int_{-h}^0 \int_{t-h+\alpha}^t x^t(\theta) A_d^t \mathcal{Q}_2^{-1} A_d x(\theta) d\theta d\alpha, \end{aligned} \quad (55)$$

$$\mathcal{P} > 0, \mathcal{Q}_1 > 0, \mathcal{Q}_2 > 0.$$

Define

$$\begin{aligned} \Gamma = & \mathcal{P} (A_0 + A_d) + (A_0 + A_d)^t \mathcal{P} \\ & + A_d (\mathcal{Q}_1 + \mathcal{Q}_2) A_d^t. \end{aligned} \quad (56)$$

The main stability result is established by the following theorem.

Theorem 18. *The time-delay system (54) is asymptotically stable for any delay satisfying $0 < d \leq d_M$ if there exist matrices $\mathcal{P} > 0$, \mathcal{Q}_1 , and \mathcal{Q}_2 such that*

$$\begin{bmatrix} \Gamma & d_M \mathcal{P} A_0^t & d_M \mathcal{P} A_d^t \\ \bullet & -\mathcal{Q}_1 & 0 \\ \bullet & \bullet & -\mathcal{Q}_2 \end{bmatrix} < 0. \quad (57)$$

Remark 19. The technique by using the Newton-Leibniz formula to transform the time-delay system to appropriate for DDS analysis is quite useful. However, still a different route of writing (54) would be

$$\begin{aligned} \dot{x}(t) &= [A_0 + A_d] x(t) - A_d \int_{t-d}^t \dot{x}(\alpha) d\alpha, \\ \frac{d}{dt} \left[x(t) + A_d \int_{t-d}^t x(\alpha) d\alpha \right] &= (A_0 + A_d) x(t). \end{aligned} \quad (58)$$

However, all the transformed time-delay systems by using the Newton-Leibniz formula introduce additional dynamics which may cause conservatism as the delay-dependent conditions derived based on the transformed systems.

6.6. Bounding Techniques. In studying delay-dependent stability for time-delay systems, it is desirable to find methods that yield stability conditions with reduced conservatism. A wide class of early methods rely on generating improved bounds on some weighted cross products arising in the analysis of the delay-dependent stability problem. This class of methods is obtained by using the well-known algebraic inequality

$$-2\alpha^t \beta \leq \alpha^t \Xi \alpha + \beta^t \Xi^{-1} \beta, \quad (59)$$

where the vectors $\alpha, \beta \in \mathbb{R}^n$ and matrix $\Xi \in \mathbb{R}^{n \times n}$. An integral bounding inequality is as follows.

Lemma 20 (see [39]). *Assume that $a(\alpha) \in \mathbb{R}^{n_a}$ and $b(\alpha) \in \mathbb{R}^{n_b}$ are given for $\alpha \in \Omega$. Then, for any $0 < X \in \mathbb{R}^{n_a \times n_a}$ and any matrix $M \in \mathbb{R}^{n_a \times n_b}$, one has*

$$\begin{aligned} - \int_{\Omega} a^t(\alpha) b(\alpha) d\alpha &\leq \int_{\Omega} \begin{bmatrix} a(\alpha) \\ b(\alpha) \end{bmatrix}^t \\ &\quad \cdot \begin{bmatrix} X & XM \\ \bullet & (M^t X + I) X^{-1} (M^t X + I)^t \end{bmatrix} \begin{bmatrix} a(\alpha) \\ b(\alpha) \end{bmatrix} d\alpha \end{aligned} \quad (60)$$

which when applied to time-delay systems of the type (30), it yields the following.

Theorem 21. *The time-delay system (30) is asymptotically stable for any delay satisfying $0 < h \leq h_M$ if there exist matrices $\mathcal{P} > 0$, \mathcal{Q} , \mathcal{V} , and \mathcal{W} such that*

$$\Phi = \begin{bmatrix} \Phi & -\mathcal{W}^t A_d^t & A_0^t A_d^t \mathcal{V} & h_M (\mathcal{P} + \mathcal{W}^t) \\ \bullet & -\mathcal{Q} & A_d^t A_d^t \mathcal{V} & 0 \\ \bullet & \bullet & -\mathcal{V} & 0 \\ \bullet & \bullet & \bullet & -\mathcal{V} \end{bmatrix} < 0 \quad (61)$$

$$\begin{aligned} \Phi &= \mathcal{P} (A_0 + A_d) + (A_0 + A_d)^t \mathcal{P} + \mathcal{W}^t A_d \\ &\quad + A_d^t \mathcal{W} + \mathcal{Q}. \end{aligned}$$

An improved version of Lemma 20 is expressed by the following.

Lemma 22 (see [40]). *Assume that $a(\alpha) \in \mathbb{R}^{n_a}$ and $b(\alpha) \in \mathbb{R}^{n_b}$ and $\mathcal{N}(\alpha) \in \mathbb{R}^{n_a \times n_b}$ are given for $\alpha \in \Omega$. Then, for any $0 < X \in \mathbb{R}^{n_a \times n_a}$ and any matrix $M \in \mathbb{R}^{n_a \times n_a}$, one has*

$$\begin{aligned} & - \int_{\Omega} a^t(\alpha) \mathcal{N}(\alpha) b(\alpha) d\alpha \\ & \leq \int_{\Omega} \begin{bmatrix} a(\alpha) \\ b(\alpha) \end{bmatrix}^t \begin{bmatrix} X & Y - \mathcal{N}(\alpha) \\ \bullet & Z \end{bmatrix} \begin{bmatrix} a(\alpha) \\ b(\alpha) \end{bmatrix} d\alpha, \end{aligned} \quad (62)$$

where

$$\begin{bmatrix} X & Y \\ \bullet & Z \end{bmatrix} \geq 0. \quad (63)$$

By considering the following LKF,

$$\begin{aligned} V(t, x_t) &= x^t(t) \mathcal{P} x(t) + \int_{t-d}^t x^t(\alpha) \mathcal{Q} x(\alpha) d\alpha \\ &\quad + \int_{-d}^0 \int_{t+\beta}^t \dot{x}^t(\alpha) Z \dot{x}(\alpha) d\alpha d\beta. \end{aligned} \quad (64)$$

Applying Lemma 22, we obtain the following delay-dependent stability theorem.

Theorem 23. *The time-delay system (30) is asymptotically stable for any delay satisfying $0 < d \leq d_M$ if there exist matrices $\mathcal{P} > 0$, \mathcal{Q} , X , Y , and Z such that*

$$\begin{aligned} & \begin{bmatrix} \Lambda & \mathcal{P} A_d - Y & d_M A_0^t Z \\ \bullet & -\mathcal{Q} & d_M A_d^t Z \\ \bullet & \bullet & -d_M Z \end{bmatrix} < 0, \\ & \begin{bmatrix} X & Y \\ \bullet & Z \end{bmatrix} \geq 0, \end{aligned} \quad (65)$$

Λ

$$\begin{aligned} \Lambda &= \mathcal{P} (A_0 + A_d) + (A_0 + A_d)^t \mathcal{P} + \mathcal{W}^t A_d \\ &\quad + A_d^t \mathcal{W} + \mathcal{Q}. \end{aligned}$$

On the other hand, deploying Lemma 1 together with Lemma 22, a different delay-dependent stability criterion is provided by the following theorem.

Theorem 24 (see [41]). *The time-delay system (30) is asymptotically stable for any delay satisfying $0 < d \leq d_M$ if there exist matrices $\mathcal{P}_1 > 0$, \mathcal{S} , P_2 , P_3 , P_4 , Y_1 , Y_2 , Z_1 , Z_2 , Z_3 and $R > 0$ such that the following LMIs hold:*

$$\begin{bmatrix} \Theta_1 & \Theta_2 & \Theta_3 \\ \bullet & \Theta_4 & \Theta_5 \\ \bullet & \bullet & \Theta_6 \end{bmatrix} < 0,$$

$$\begin{bmatrix} R & Y_1 & Y_2 \\ \bullet & Z_1 & Z_2 \\ \bullet & \bullet & Z_3 \end{bmatrix} \geq 0,$$

$$\begin{aligned} \Theta_1 &= A_0^t P_2 + P_2^t A_0 + Y_1 + Y_1^t + \mathcal{S} \\ &\quad + d_M Z_1, \end{aligned} \quad (66)$$

$$\Theta_2 = \mathcal{P}_1 - P_2^t + A_0^t P_3 + Y_2 + d_M Z_2,$$

$$\Theta_3 = P_2^t A_d - Y_1^t + A_0^t P_4,$$

$$\Theta_4 = d_M (R + Z_3) - P_3^t - P_3,$$

$$\Theta_5 = P_3^t A_d - Y_2^t - P_4,$$

$$\Theta_6 = A_d^t P_4 + P_4^t A_d - \mathcal{S}.$$

Remark 25. The inequality in Lemma 22 is more general than both inequalities (59) and (60) and for this reason, it was extensively used in dealing with various issues related to time-delay systems to obtain delay-dependent results.

Now, we present another important inequality, which is also effective in the derivation of DDS conditions.

Lemma 26 (see [42]). *For any constant matrix $0 < \mathcal{M} \in \mathbb{R}^{m \times m}$, scalars $b > a$, and vector function $\omega : [a, b] \rightarrow \mathbb{R}^m$ such that the integrations in the following are well-defined, then*

$$\begin{aligned} & (b - a) \int_a^b \omega^t(\alpha) \mathcal{M} \omega(\alpha) d\alpha \\ & \geq \int_a^b \left[\int_a^b \omega^t(\alpha) d\alpha \right]^t \mathcal{M} \left[\int_a^b \omega(\alpha) d\alpha \right]. \end{aligned} \quad (67)$$

Using Lemma 26 and selecting the LKF

$$\begin{aligned} V(t, x_t) &= x^t(t) \mathcal{P} x(t) + \int_{t-d}^t x^t(\theta) \mathcal{Q} x(\theta) d\theta \\ &\quad + d \int_{-d}^0 \int_{t+\alpha}^t \dot{x}^t(\theta) \mathcal{Z} \dot{x}(\theta) d\theta d\alpha, \end{aligned} \quad (68)$$

$$\mathcal{P} > 0, \quad \mathcal{Q} > 0, \quad \mathcal{Z} > 0,$$

we obtain the following stability result.

Theorem 27 (see [6]). *The time-delay system (30) is asymptotically stable for any delay satisfying $0 < d \leq d_M$ if there exist matrices $\mathcal{P} > 0$, $\mathcal{Q} > 0$ and $\mathcal{Z} > 0$ such that*

$$\begin{bmatrix} \mathcal{P}A_0 + A_0^t\mathcal{P} + \mathcal{Q} - \mathcal{Z} & \mathcal{P}A_d + \mathcal{Z} & d_M A_0^t \mathcal{Z} \\ \cdot & -\mathcal{Q} - \mathcal{P} & d_M A_d^t \mathcal{Z} \\ \cdot & \cdot & -\mathcal{Z} \end{bmatrix} < 0. \quad (69)$$

Alternatively, selecting the LKF

$$\begin{aligned} \mathbb{V}(t, x_t) &= x^t(t) \mathcal{P} x(t) \\ &+ \tau_M \int_{-\tau_M}^0 \int_{t+\alpha}^t \dot{x}^t(\theta) \mathcal{Z} \dot{x}(\theta) d\theta d\alpha, \end{aligned} \quad (70)$$

$$\mathcal{P} > 0, \mathcal{Z} > 0,$$

we obtain the following stability result.

Theorem 28 (see [6]). *The time-delay system (37) is asymptotically stable for all continuous delay $\tau(t)$ satisfying $0 < \tau(t) \leq \tau_M$ if there exist matrices $\mathcal{P} > 0$ and $\mathcal{Z} > 0$ such that*

$$\begin{bmatrix} \mathcal{P}A_0 + A_0^t\mathcal{P} - \mathcal{Z} & \mathcal{P}A_d + \mathcal{Z} & \tau_M A_0^t \mathcal{Z} \\ \cdot & -\mathcal{Z} - \mathcal{P} & \tau_M A_d^t \mathcal{Z} \\ \cdot & \cdot & -\mathcal{Z} \end{bmatrix} < 0. \quad (71)$$

A useful result is summarized by the following lemma.

Lemma 29 (the integral inequality [43]). *For any constant matrix $0 < \Sigma \in \mathbb{R}^{n \times n}$, scalar $\tau_* < \tau(t) < \tau^+$, and vector function $\dot{x} : [t - \tau^+, t - \tau_*] \rightarrow \mathbb{R}^n$ such that the following integration is well-defined, then it holds that*

$$\begin{aligned} & -(\tau^+ - \tau_*) \int_{t-\tau^+}^{t-\tau_*} \dot{x}^t(s) \Sigma \dot{x}(s) ds \\ & \leq -[x(t - \tau_*) - x(t - \tau^+)]^t \\ & \quad \cdot \Sigma [x(t - \tau_*) - x(t - \tau^+)]. \end{aligned} \quad (72)$$

Lemma 29 is frequently called the “integral inequality” and it is derived from Jensen’s inequality [44].

Remark 30. It is significant to observe that Theorem 27 establishes that the time-delay system (30) is asymptotically stable for any delay d satisfying $0 < d \leq d_M$ when the LMI (69) attains a feasible solution, which implies that, for d satisfying $0 < d \leq d_M/2$, the time-delay system (30) is asymptotically stable as well. Then, introducing the half delay into the time-delay system (30) will take more information on the system and thus may tend to reduce the conservatism in Theorem 27. For further elaboration on this argument, see [45].

6.7. Discrete-Time Systems. Less attention has been paid to discrete-time systems with a time-delay because a linear discrete-time system with a constant time-delay can be transformed into a delay-free system by means of a state-augmentation approach. However this approach is not suitable

for systems with either unknown or time-varying delays. For a small time-varying delays, the descriptor model transformation approach was employed [46].

Consider a class of discrete-time systems with state-delay is represented by

$$x(k+1) = A_o x(k) + D_o x(k-d(k)), \quad (73)$$

where for $k \in \mathbb{Z}_+ \triangleq \{0, 1, \dots\}$, $x(k) \in \mathbb{R}^n$ is the state and $A_o \in \mathbb{R}^{n \times n}$ and $D_o \in \mathbb{R}^{n \times n}$ are constant matrices. The delay factor $d(k)$ is unknown-but-bounded in the form

$$0 < d_m \leq d(k) \leq d_M, \quad d_s = d_M - d_m + 1, \quad (74)$$

where the scalars d_m and d_M represent the lower and upper bounds, respectively, and d_s denotes the number of samples within the delay interval.

Remark 31. By setting $d(k) \equiv 0$ in (73), it is readily seen that $|\lambda(A_o + D_o)| < 1$ is a necessary condition for stability of system (73). From all studies on discrete-time-delay systems, it is assumed that this is always the case.

Remark 32. The class of systems (73) represents a nominally linear model which emerges in many areas dealing with the applications functional difference equations or delay-difference equations. These applications include cold rolling mills, decision-making processes, and manufacturing systems.

Related results for a class of discrete-time systems with time-varying delays can be found in [47] where delay-dependent stability and stabilization conditions were derived. It should be stressed that although we consider only the case of single time-delay, extension to multiple time-delay systems can be easily attained using an augmentation procedure.

Intuitively if we associate with system (73) a positive-definite Lyapunov-Krasovskii functional $V(k, x(k)) > 0$ and we find that its first difference $\Delta V(k, x(k)) = V(k+1, x(k+1)) - V(k, x(k))$ is negative-definite along the solutions of (73), then the origin of system (73) is globally asymptotically stable. Formally, we present the following theorem for discrete-time systems of the type (73).

Theorem 33. *The equilibrium 0 of the discrete-time system*

$$x(k+1) = h(x(k)) \quad (75)$$

is globally asymptotically stable if there is a function $V : \{0, 1, 2, \dots\} \times \mathbb{R}^n \rightarrow \mathbb{R}$ such that

- (i) $V(k, x(k))$ is a positive-definite function, decrescent, and radially unbounded,
- (ii) $\Delta V(k, x(k)) = V(k+1, x(k+1)) - V(k, x(k))$ is negative-definite along the solutions of system (73).

For arbitrary value of $d(k)$, denote

$$z(k) = [x^t(k) \mid x^t(k-d(k))]^t. \quad (76)$$

We have

$$z(k+1) = \begin{bmatrix} A_o & 0 & \dots & 0 & D_o \\ I & 0 & \dots & 0 & 0 \\ \vdots & \ddots & \dots & \vdots & \vdots \\ 0 & 0 & \dots & I & 0 \end{bmatrix} z(k). \quad (77)$$

It is obvious that system (73) is globally asymptotically stable if and only if system (75) is globally asymptotically stable. For system (75), we define

$$\widehat{V}(k, z(k)) = z^t(k) \text{diag}[\mathcal{P} \quad \mathcal{Q} \quad \dots \quad \mathcal{Q}] z(k), \quad (78)$$

where $\mathcal{P} > 0$ and $\mathcal{Q} > 0$. It is easy to see that $\widehat{V}(k, z(k)) > 0$, decrescent and radially unbounded, and hence system (75) is globally asymptotically stable.

By selecting the Lyapunov-Krasovskii functional

$$V(k) = x^t(k) \mathcal{P} x(k) + \sum_{m=k-d(k)}^{k-1} x^t(m) \mathcal{Q} x(m), \quad (79)$$

$$0 < \mathcal{P}, \quad 0 < \mathcal{Q},$$

and invoking the Lyapunov-Krasovskii theorem, the following stability condition can be derived.

Theorem 34. *The discrete-delay system (73) is asymptotically stable if there exist matrices $\mathcal{P} > 0$ and $\mathcal{Q} > 0$ such that*

$$\begin{bmatrix} -(\mathcal{P} - \mathcal{Q}) & 0 & A_o^t \mathcal{P} \\ \bullet & -\mathcal{Q} & D_o^t \mathcal{P} \\ \bullet & \bullet & -\mathcal{P} \end{bmatrix} < 0. \quad (80)$$

We stress that LMI (80) is virtually delay-independent since it is satisfied no matter the size of delay $d(k)$ is.

Next, sufficient delay-dependent LMI-based stability conditions are given. The approach used here does not introduce any dynamics and leads to a product separation between the matrices of the system and those from the Lyapunov-Krasovskii functional. The following theorem provides some LMI conditions depending on the values d_m and d_M .

Theorem 35. *Given the delay sample number d_s , system (73) subject to (74) is delay-dependent asymptotically stable if one of the following equivalent conditions is satisfied:*

(A) *There exist matrices $0 < \mathcal{P} \in \mathfrak{R}^{n \times n}$ and $0 < \mathcal{Q} \in \mathfrak{R}^{n \times n}$ such that*

$$\Xi_a = \begin{bmatrix} A_o^t \mathcal{P} A_o + d_s \mathcal{Q} - \mathcal{P} & A_o^t \mathcal{P} D_o^t \\ \bullet & D_o^t \mathcal{P} D_o - \mathcal{Q} \end{bmatrix} < 0. \quad (81)$$

(B) *There exist matrices $0 < \mathcal{P} \in \mathfrak{R}^{n \times n}$, $0 < \mathcal{Q} \in \mathfrak{R}^{n \times n}$, $\mathcal{X} \in \mathfrak{R}^{n \times n}$, $\mathcal{Y} \in \mathfrak{R}^{n \times n}$, and $\mathcal{Z} \in \mathfrak{R}^{n \times n}$ such that*

$$\Xi_c = \begin{bmatrix} \mathcal{P} + \mathcal{X} + \mathcal{X}^t & \mathcal{Y} - \mathcal{X} A_o & \mathcal{Z} - \mathcal{X} D_o \\ \bullet & \Gamma_v & -A_o^t \mathcal{Z}^t - \mathcal{Y} D_o \\ \bullet & \bullet & \Gamma_w \end{bmatrix} < 0, \quad (82)$$

where

$$\begin{aligned} \Gamma_v &= -A_o^t \mathcal{Z}^t - \mathcal{Y} A_o + d_s \mathcal{Q} - \mathcal{P}, \\ \Gamma_w &= -\mathcal{Q} - \mathcal{Z} D_o - D_o^t \mathcal{Z}^t. \end{aligned} \quad (83)$$

In this case, the Lyapunov-Krasovskii functional (LKF)

$$\begin{aligned} \widetilde{V}(k) &= x^t(k) \mathcal{P} x(k) + \sum_{m=k-d(k)}^{k-1} x^t(m) \mathcal{Q} x(m) \\ &+ \sum_{s=2-d_M}^{1-d_m} \sum_{m=k+s-1}^{k-1} x^t(m) \mathcal{Q} x(m) > 0 \end{aligned} \quad (84)$$

is such that

$$\Delta \widetilde{V}(k) < 0, \quad \forall [x^t(k) \quad x^t(k-d(k))]^t \neq 0. \quad (85)$$

The result of Theorem 35 was developed in [47–49].

Next, we consider the following discrete-time piecewise linear systems with infinite distributed delays [50]:

$$x(k+1) = A_\ell x(k) + D_\ell \sum_{d=1}^{\infty} \mu_d x(k-d) + B_\ell u(k), \quad (86)$$

where $x(k) \in \mathfrak{R}^n$ is the state and $\{S_\ell\}_{\ell \in L}$ denotes a partition of the state-space into a number of closed polyhedral subspaces, L is the index set of subspaces, and $u(k) \in \mathfrak{R}^m$ is the control input. Matrices A_ℓ D_ℓ B_ℓ are constant matrices with appropriate dimensions corresponding to the ℓ th local model of the systems. When the state of the system transits from one region to another at the time k , the dynamics is governed by the local model of the former one. $\mu_d \geq 0$ is the convergence constants that satisfy the following condition:

$$\bar{\mu} \triangleq \sum_{d=1}^{\infty} \mu_d \leq \sum_{d=1}^{\infty} d \mu_d < +\infty. \quad (87)$$

Distributed time-delays have been widely recognized and intensively studied for continuous-time systems [51]. However, the corresponding results for discrete-time systems have been very few due mainly to the difficulty in formulating the distributed delays in a discrete-time domain. The distributed delay term $\sum_{d=1}^{\infty} \mu_d x(k-d)$ can be regarded as the discretization of the infinite integral form $\int_{-\infty}^t k(t-s)x(s)ds$ for the continuous-time system. The following result is recalled [51].

Lemma 36. *Let $0 \leq M \in \mathfrak{R}^{n \times n}$, $x_j \in \mathfrak{R}^n$, and $a_j > 0$, $j = 1, 2, \dots$, are constants. If the series concerned is convergent, then one has*

$$\left(\sum_{j=1}^{\infty} a_j x_j \right)^t M \left(\sum_{j=1}^{\infty} a_j x_j \right) \leq \left(\sum_{j=1}^{\infty} a_j \right) \sum_{j=1}^{\infty} a_j x_j^t M x_j. \quad (88)$$

Introduce the following Lyapunov-Krasovskii functional candidate:

$$V(k) = x^t(k) \mathcal{P}_\ell x(k) + \sum_{d=1}^{\infty} \mu_d \sum_{m=k-d}^{k-1} x^t(m) \mathcal{Q} x(m). \quad (89)$$

By setting $\bar{\mathcal{Q}} = \bar{\mu}_d \mathcal{Q}$ and invoking Theorem 34, the following result is obtained.

Theorem 37. Consider the piecewise linear system (86) with $u \equiv 0$. If there exist matrices $X_\ell > 0$ and $\bar{\mathcal{Q}} > 0$ such that the following linear matrix inequalities hold for $(\ell, j) \in \Omega \triangleq \{\ell, j \mid x(k) \in S_\ell, x(k+1) \in S_j, j \neq \ell\}$:

$$\begin{bmatrix} -\mathcal{P} + \bar{\mathcal{Q}} & 0 & A_o^t \mathcal{P} \\ \cdot & -\frac{\bar{\mathcal{Q}}}{\mu_d} & D_o^t \mathcal{P} \\ \cdot & \cdot & -\mathcal{P} \end{bmatrix} < 0. \quad (90)$$

We emphasize that Theorem 37 was established in [50].

7. Model Transformations

It must be recalled that the prototype system (30), the independent of delay (IOD) stability demands matrix A_0 to be Hurwitz which, coherently, can be found in condition (33). On the other hand, the criteria ensuring delay-dependent stability for $h \in [0, h_M)$ require the matrix $A_0 + A_d$ to be Hurwitz as evident in condition (36). On this basis, several results concerning delay-dependent stability were derived, from the formula

$$\int_{t-d}^t \dot{x}(s) ds = x(t) - x(t-d). \quad (91)$$

Consider the change of variables

$$\begin{aligned} A_j x(t-d) &= [A_j - L_j] x(t-d_j) \\ &+ L_j \left[x(t) - \int_{t-d_j}^t \dot{x}(s) ds \right]. \end{aligned} \quad (92)$$

This will transform the multiple-delay system with possibly $d_1 = 0$

$$\dot{x}(t) = \sum_{j=1}^m A_j x(t-d_j) \quad (93)$$

into the system having augmented delay $h = \max(h_j + h_k)$

$$\begin{aligned} \dot{x}(t) &= \left[\sum_{j=1}^m L_j \right] x(t) + \sum_{j=1}^m A_j x(t-d_j) \\ &+ \sum_{j=1, k=1}^m \int_{t-d_j}^t L_j A_k x(s-d_j) ds. \end{aligned} \quad (94)$$

Model (94) guarantees that the unstable nondelayed part A_d in system (30) is absorbed in the stable part $[\sum_{j=1}^m L_j]$. Indeed such decomposition can be conveniently handled using LMI

tools. It is shown in [5, 52] that the foregoing system can be written in the three following forms:

$$\begin{aligned} \dot{x}(t) &= Ax(t) - \sum_{j,k=1}^m A_{jk} \int_{t-d_{jk}}^{t-d_k} x(s) ds, \\ \dot{x}(t) &= Ax(t) - \sum_{j=1}^m A_j \int_{t-d_j}^t \dot{x}(s) ds, \\ \frac{d}{dt} \left[x(t) + \sum_{j=1}^m A_j \int_{t-d_j}^t x(s) ds \right] &= Ax(t), \end{aligned} \quad (95)$$

$$A = \sum_{j=1}^m A_j, \quad A_{jk} = A_j A_k, \quad d_{jk} = d_j + d_k.$$

It turns out that each of the above formulations can be studied by using specific Lyapunov-Krasovskii functionals (34) leading to the three different Riccati equations [5]:

$$\begin{aligned} \Pi + m d \mathcal{R} + \mathcal{P} \sum_{j,k=1}^m d_j A_{jk} \mathcal{R}^{-1} B_{jk}^t \mathcal{P} &= -\mathcal{Q}, \\ \Pi + \sum_{j=1}^m (d_j \mathcal{P} A_j \mathcal{R}^{-1} B_j^t \mathcal{P} + m d A_j^t \mathcal{R} A_j) &= -\mathcal{Q}, \\ \Pi + \sum_{j=1}^m d_j \mathcal{R}_j + \sum_{j,k=1}^m d_j A^t \mathcal{P} A_j \mathcal{R}_j^{-1} A_j^t \mathcal{P} A &= -\mathcal{Q}, \\ \Pi &= \mathcal{P} A + A^t \mathcal{P}. \end{aligned} \quad (96)$$

Remark 38. In the literature, there were other different methods to develop delay-dependent stability criteria. These methods include the discretized LKF approach [4], the descriptor system approach [53], and the delay-partitioning projection approach [54]. Declaring the stability result as conservative or not requires well-defined quantitative measures. More importantly, it must be pointed out that the issue of computational complexity and the associated number of manipulated matrices deserve a serious investigation.

8. Delay-Dependent Stabilization

Extending the time-delay system (30) for stabilization studies, we start with the form

$$\dot{x}(t) = A_0 x(t) + A_d x(t-d) + B_0 u(t), \quad t \geq t_0, \quad (97)$$

where $u(t)$ is the control input and B_0 is the input matrix with the pair A_0, B_0 being controllable. We seek to design a state feedback controller

$$u(t) = \mathbb{K}_0 x(t), \quad (98)$$

such that the closed-loop system

$$\dot{x}(t) = A_c x(t) + A_d x(t-d), \quad A_c = A_0 + B_0 \mathbb{K}_0, \quad (99)$$

is asymptotically stable [55]. This is attained by convex analysis [31] leading to the following theorem.

Theorem 39. The closed-loop time-delay system (97) is asymptotically stable for any $d \geq 0$ if there exist matrices $\mathcal{X} > 0$, \mathcal{Y} , $\mathcal{W} > 0$ verifying

$$\begin{bmatrix} A_o \mathcal{X} + \mathcal{X} A_o^t + B_o \mathcal{Y} + \mathcal{Y}^t B_o^t + \mathcal{W} & A_d \mathcal{X} \\ \cdot & -\mathcal{W} \end{bmatrix} < 0. \quad (100)$$

8.1. A Class of Nonlinear Systems. One of the standard classes of nonlinear time-delay systems is given by

$$\begin{aligned} \dot{x}(\sigma) &= A_o x(\sigma) + A_d x(\sigma - \sigma_d) + B_o u(\sigma) \\ &+ h(t, x, x(t-d)) \end{aligned} \quad (101)$$

in the dimensionless coordinates σ , where $x(\sigma)$ is the state vector, $u(t)$ is the control input, and A_o , B_o , and A_d are known real constant matrices. The nonlinear vector function $h(\cdot, \cdot)$ is a piecewise-continuous function in its arguments. In the discussions to follow, we assume that this function is uncertain satisfying the quadratic inequality

$$\begin{aligned} &h^t(t, x, x(t-d)) h(t, x, x(t-d)) \\ &\leq \alpha^2 x^t H_o^t H_o x + \theta^2 x^t(t-d) H_d^t H_d x(t-d), \end{aligned} \quad (102)$$

where $\alpha > 0$ and $\theta > 0$ are the bounding parameters. The matrices $H_o \in \mathbb{R}^{r \times n}$ and $H_d \in \mathbb{R}^{p \times n}$ are constants and characterize the upper bound on system nonlinearities.

For stability purposes, we let $\alpha^{-2} = \gamma$ and $\theta^{-2} = \psi$. The following convex optimization result holds.

$$\begin{aligned} &\min \quad \gamma, \psi \\ &\text{subject to} \quad \mathcal{X} > 0, \end{aligned}$$

\mathcal{Y}

$$\begin{bmatrix} A_o \mathcal{X} + \mathcal{X} A_o^t + B_o \mathcal{Y} + \mathcal{Y}^t B_o^t & \mathcal{X} \mathcal{W} & \mathcal{X} H_o^t & I & A_d & 0 \\ \cdot & -\mathcal{W} & 0 & 0 & 0 & 0 \\ \cdot & \cdot & -\gamma I & 0 & 0 & 0 \\ \cdot & \cdot & \cdot & -I & 0 & 0 \\ \cdot & \cdot & \cdot & \cdot & -W & H_d^t \\ \cdot & \cdot & \cdot & \cdot & \cdot & -\psi \end{bmatrix} < 0. \quad (105)$$

(S2) Next, to include bounds the gain matrix K_o , we set the bounding relations

$$\begin{aligned} M^t M &< \mu I, \quad \mu > 0, \\ X^{-1} &< \varphi I, \quad \varphi > 0. \end{aligned} \quad (106)$$

Theorem 40. Nonlinear system (101) with $u \equiv 0$ is robustly stable if the following LMI feasibility problem is solvable:

$$\begin{aligned} &\min \quad \gamma, \psi \\ &\text{subject to} \quad \mathcal{X} > 0 \\ &\begin{bmatrix} A_o \mathcal{X} + \mathcal{X} A_o^t & \mathcal{X} \mathcal{W} & \mathcal{X} H_o^t & I & A_d & 0 \\ \cdot & -\mathcal{W} & 0 & 0 & 0 & 0 \\ \cdot & \cdot & -\gamma I & 0 & 0 & 0 \\ \cdot & \cdot & \cdot & -I & 0 & 0 \\ \cdot & \cdot & \cdot & \cdot & -W & H_d^t \\ \cdot & \cdot & \cdot & \cdot & \cdot & -\psi \end{bmatrix} \\ &< 0. \end{aligned} \quad (103)$$

Given that the pair (A_o, B_o) is stabilizable. We achieve state feedback stabilization in two stages as follows.

(S1) Let the linear state feedback be $u(t) = K_o x(t)$, and then the closed-loop system becomes

$$\begin{aligned} \dot{x}(t) &= A_k x(t) + A_d x(t-d) + h(t, x, x(t-d)), \\ A_k &= (A_o + B_o K_o). \end{aligned} \quad (104)$$

This establishes the following theorem.

Theorem 41. Nonlinear system (101) is robustly stabilized by control law $u(t) = K_o x(t)$, if the following LMI problem has a feasible solution.

Moreover, to guarantee desired values $\{\bar{\alpha}, \bar{\theta}\}$ of the bounding factors $\{\alpha, \theta\}$, we enforce $\alpha^{-2} = \gamma$ and $\theta^{-2} = \psi$. The following theorem summarizes the main result.

Theorem 42. Nonlinear system (101) is robustly stabilized by control law $u(t) = K_o x(t)$, with constrained feedback gains if

following convex optimization problem over LMIs has a feasible solution:

$$\begin{aligned}
 & \min \quad \gamma + \psi + \mu + \varphi \\
 & \text{subject to} \quad \mathcal{X} > 0, \\
 & \quad \mathcal{Y} \\
 & \quad \begin{bmatrix} A_o \mathcal{X} + \mathcal{X} A_o^t + B_o \mathcal{Y} + \mathcal{Y}^t B_o^t & \mathcal{X} \mathcal{W} & \mathcal{X} H_o^t & I & A_d & 0 \\ \cdot & -\mathcal{W} & 0 & 0 & 0 & 0 \\ \cdot & \cdot & -\gamma I & 0 & 0 & 0 \\ \cdot & \cdot & \cdot & -I & 0 & 0 \\ \cdot & \cdot & \cdot & \cdot & -W & H_d^t \\ \cdot & \cdot & \cdot & \cdot & \cdot & -\psi \end{bmatrix} < 0 \\
 & \quad \gamma - \frac{1}{\alpha^2} < 0, \\
 & \quad \psi - \frac{1}{\sigma^2} < 0, \\
 & \quad \begin{bmatrix} -\mu I & \mathcal{Y}^t \\ \cdot & -I \end{bmatrix} < 0, \\
 & \quad \begin{bmatrix} -\varphi I & I \\ \cdot & -X \end{bmatrix} < 0.
 \end{aligned} \tag{107}$$

Remark 43. One can address the performance deterioration issue by considering that the actual linear state feedback controller has the form $u(t) = [K_o + \Delta K_o]x(t)$, $K_o \in \mathbb{R}^{m \times n}$ is a constant gain matrix, and ΔK_o is a gain perturbation matrix.

9. Kalman Filtering

The seminal Kalman filtering algorithm [56] is the optimal estimator over all possible linear ones and gives unbiased estimates of the unknown state vectors under the conditions that the system and measurement noise processes are mutually independent Gaussian distributions. Robust state-estimation arose out of the desire to estimate unmeasurable state variables when the plant model has uncertain parameters. In the sequel, we consider the state-estimation problem for a class of linear continuous-time-lag systems with norm-bounded parameter uncertainties. Specifically, we address the state-estimator design problem such that the estimation error covariance has a guaranteed bound for all admissible uncertainties.

9.1. A Class of Continuous-Time-Lag Systems. We consider a class of uncertain time-delay systems represented by

$$\begin{aligned}
 \dot{x}(t) &= [A(t) + \Delta A(t)] x(t) + A_d(t) x(t - \tau) \\
 &\quad + w(t) \\
 &= A_\Delta(t) x(t) + A_d(t) x(t - \tau) + w(t),
 \end{aligned} \tag{108}$$

$$\begin{aligned}
 y(t) &= [C(t) + \Delta C(t)] x(t) + v(t) \\
 &= C_\Delta(t) x(t) + v(t),
 \end{aligned} \tag{109}$$

where $x(t) \in \mathbb{R}^n$ is the state, $y(t) \in \mathbb{R}^m$ is the measured output, and $w(t) \in \mathbb{R}^n$ and $v(t) \in \mathbb{R}^m$ are, respectively, the process and measurement noises. In (1)-(2), $A(t) \in \mathbb{R}^{n \times n}$, $A_d(t) \in \mathbb{R}^{n \times n}$, and $C(t) \in \mathbb{R}^{m \times n}$ are piecewise-continuous matrix functions. Here, τ is a constant scalar representing the amount of time-lag in the state. The matrices $\Delta A(t)$ and $\Delta C(t)$ represent time-varying parametric uncertainties which are of the form:

$$\begin{bmatrix} \Delta A(t) \\ \Delta C(t) \end{bmatrix} = \begin{bmatrix} H(t) \\ H_c(t) \end{bmatrix} \Delta(t) E(t), \tag{110}$$

where $H(t) \in \mathbb{R}^{n \times \alpha}$, $H_c(t) \in \mathbb{R}^{m \times \alpha}$, and $E(t) \in \mathbb{R}^{\beta \times n}$ are known piecewise-continuous matrix functions and $\Delta(t) \in \mathbb{R}^{\alpha \times \beta}$ is an unknown matrix with Lebesgue measurable elements satisfying

$$\Delta^t(t) \Delta(t) \leq I \quad \forall t. \tag{111}$$

The initial condition is specified as $\langle x(0), x(s) \rangle = \langle x_o, \phi(s) \rangle$, where $\phi(\cdot) \in \mathcal{L}_2[-\tau, 0]$ which is assumed to be a zero-mean Gaussian random vector. The following standard assumptions on noise statistics are recalled.

Assumption 44. $\forall t, s \geq 0$

(a)

$$\begin{aligned} \mathbb{E}[w(t)] &= 0; \\ \mathbb{E}[w(t)w^t(s)] &= W(t)\delta(t-s); \\ W(t) &> 0. \end{aligned} \quad (112)$$

(b)

$$\begin{aligned} \mathbb{E}[v(t)] &= 0; \\ \mathbb{E}[v(t)v^t(s)] &= V(t)\delta(t-s); \\ V(t) &> 0. \end{aligned} \quad (113)$$

(c)

$$\begin{aligned} \mathbb{E}[x(0)w^t(t)] &= 0; \\ \mathbb{E}[x(0)v^t(t)] &= 0. \end{aligned} \quad (114)$$

(d)

$$\begin{aligned} \mathbb{E}[w(t)v^t(s)] &= 0; \\ \mathbb{E}[x(0)x^t(0)] &= R_o, \end{aligned} \quad (115)$$

where $\mathbb{E}[\cdot]$ stands for the mathematical expectation and $\delta(\cdot)$ is the Dirac function.

9.2. Robust Kalman Filtering. Our objective is to design a stable state estimator of the form:

$$\dot{\hat{x}}(t) = G(t)\hat{x}(t) + K(t)y(t), \quad \hat{x}(0) = 0, \quad (116)$$

where $G(t) \in \mathbb{R}^{n \times n}$ and $K(t) \in \mathbb{R}^{n \times m}$ are piecewise-continuous matrices to be determined such that there exists a matrix $\Psi \geq 0$ satisfying

$$\mathbb{E}[(x - \hat{x})(x - \hat{x})^t] \leq \Psi, \quad \forall \Delta : \Delta^t(t)\Delta(t) \leq I. \quad (117)$$

Note that (112) implies

$$\mathbb{E}[(x - \hat{x})^t(x - \hat{x})] \leq \text{tr}(\Psi), \quad \forall \Delta : \Delta^t(t)\Delta(t) \leq I. \quad (118)$$

In this case, the estimator (116) is said to provide a guaranteed cost (GC) matrix Ψ .

Examination of the proposed estimator proceeds by analyzing the estimation error

$$e(t) = x(t) - \hat{x}(t). \quad (119)$$

Substituting (109) and (116) into (119), we express the dynamics of the error in the form

$$\begin{aligned} \dot{e}(t) &= G(t)e(t) + [A(t) - G(t) - K(t)C(t)]x(t) \\ &\quad + [\Delta A(t) - K(t)\Delta C(t)]x(t) \\ &\quad + A_d(t)x(t - \tau) + [w(t) - K(t)v(t)]. \end{aligned} \quad (120)$$

By introducing the extended state vector

$$\xi(t) = \begin{bmatrix} x(t) \\ e(t) \end{bmatrix} \in \mathbb{R}^{2n}, \quad (121)$$

it follows from (108)-(109) and (120) that

$$\begin{aligned} \dot{\xi}(t) &= [\widehat{A}(t) + \widehat{H}(t)F(t)\widehat{E}(t)]\xi(t) + \widehat{D}(t)\xi(t - \tau) \\ &\quad + \widehat{B}(t)\eta(t) \\ &= \widehat{A}_\Delta(t)\xi(t) + \widehat{D}(t)\xi(t - \tau) + \widehat{B}(t)\eta(t), \end{aligned} \quad (122)$$

where $\eta(t)$ is a stationary zero-mean noise signal with identity covariance matrix and

$$\begin{aligned} \widehat{A}(t) &= \begin{bmatrix} A(t) & 0 \\ A(t) - G(t) - K(t)C(t) & G(t) \end{bmatrix}, \\ \widehat{H}(t) &= \begin{bmatrix} H(t) \\ H(t) - K(t)H_c(t) \end{bmatrix}, \\ \widehat{E}(t) &= [E(t) \ 0], \\ \widehat{B}\widehat{B}^t(t) &= \begin{bmatrix} W(t) & W(t) \\ W(t) & W(t) + K(t)V(t)K^t(t) \end{bmatrix}, \\ \widehat{D}(t) &= \begin{bmatrix} A_d(t) & 0 \\ A_d(t) & 0 \end{bmatrix}, \end{aligned} \quad (123)$$

$$\eta = \begin{bmatrix} w(t) \\ v(t) \end{bmatrix}.$$

Definition 45. Estimator (111) is said to be a quadratic estimator (QE) associated with a matrix $\Omega(t) > 0$ for system (108) if there exists a scalar $\lambda(t) > 0$ and a matrix

$$0 < \Omega(t) = \begin{bmatrix} \Omega_1(t) & \Omega_3(t) \\ \Omega_3^t(t) & \Omega_2(t) \end{bmatrix} \quad (124)$$

satisfying the algebraic inequality

$$\begin{aligned} -\dot{\Omega}(t) + \widehat{A}_\Delta(t)\Omega(t) + \Omega(t)\widehat{A}_\Delta^t(t) + \lambda(t)\Omega(t - \tau) \\ + \lambda^{-1}(t)\widehat{D}(t)\Omega(t - \tau)\widehat{D}^t(t) + \widehat{B}(t)\widehat{B}^t(t) \end{aligned} \quad (125)$$

$$\leq 0.$$

The next result shows that if (112) is QE for system (108)-(109) with cost matrix $\Omega(t)$, then $\Omega(t)$ defines an upper bound for the filtering error covariance; that is,

$$\mathbb{E}[e(t)e^t(t)] \leq \Omega_2(t) \quad \forall t \quad (126)$$

for all admissible uncertainties satisfying (110)-(111).

Theorem 46. Consider the time-delay (108)-(109) satisfying (110)-(111) and with known initial state. Suppose there exists a solution $\Omega(t) \geq 0$ to inequality (125) for some $\lambda(t) > 0$ and for all admissible uncertainties. Then the estimator (116) provides an upper bound for the filtering error covariance; that is,

$$\mathbb{E}[e(t)e^t(t)] \leq \Omega_2(t). \quad (127)$$

We employ hereafter a Riccati equation approach to solve the robust Kalman filtering for time-delay systems. To this end, we define piecewise matrices $P(t) = P^t(t) \in \mathbb{R}^{n \times n}$; $L(t) = L^t(t) \in \mathbb{R}^{n \times n}$ as the solutions of the Riccati differential equations (RDE):

$$\begin{aligned} \dot{P}(t) &= A(t)P(t) + P(t)A^t(t) + \lambda(t)P(t-\tau) \\ &\quad + \widehat{W}(t) + \lambda^{-1}(t)A_d(t)P(t-\tau)A_d^t(t) + \mu(t) \\ &\quad \cdot P(t)E^t(t)E(t)P(t); \\ P(t-\tau) &= 0 \quad \forall t \in [0, \tau], \\ \dot{L}(t) &= A(t)L(t) + L(t)A^t(t) + \lambda(t)L(t-\tau) \\ &\quad + \widehat{W}(t) + \lambda^{-1}(t)A_d(t)P(t-\tau)A_d^t(t) + \mu(t) \\ &\quad \cdot L(t)E^t(t)E(t)L(t) \\ &\quad - [L(t)C^t(t) + \mu^{-1}(t)H(t)H_c^t(t)]\widehat{V}^{-1}(t) \\ &\quad \cdot [C(t)L(t) + \mu^{-1}(t)H_c(t)H^t(t)]; \\ L(t-\tau) &= 0 \quad \forall t \in [0, \tau], \end{aligned} \quad (128)$$

where $\lambda(t) > 0$ and $\mu(t) > 0 \forall t$ are scaling parameters and the matrices $\widehat{A}(t)$, $\widehat{V}(t)$, and $\widehat{W}(t)$ are given by

$$\widehat{W}(t) = W(t) + \mu^{-1}(t)H(t)H^t(t), \quad (129)$$

$$\widehat{V}(t) = V(t) + \mu^{-1}(t)H_c(t)H_c^t(t), \quad (130)$$

$$\begin{aligned} \widehat{A}(t) &= A(t) + \delta A(t) \\ &= A(t) + \mu^{-1}(t)L^t(t)E^t(t)E(t). \end{aligned} \quad (131)$$

Let the (λ, μ) -parameterized estimator be expressed as

$$\begin{aligned} \dot{\hat{x}}(t) &= \{A(t) + \mu^{-1}(t)L^t(t)E^t(t)E(t)\}\hat{x}(t) \\ &\quad + K(t)\{y(t) - C(t)\hat{x}(t)\}, \end{aligned} \quad (132)$$

where the gain matrix $K_e(t) \in \mathbb{R}^{n \times m}$ is to be determined. The following theorem summarizes the main result.

Theorem 47. Consider system (108)-(109) satisfying the uncertainty structure (110)-(111) with zero initial condition. Suppose the process and measurement noises satisfy Assumption 44. For some $\mu(t) > 0$, $\lambda(t) > 0$, let $P(t) = P^t(t)$ and $L(t) = L^t(t)$ be the solutions of RDE (131)-(132), respectively. Then the (λ, μ) -parametrized estimator (132) is QE estimator with GC such that

$$\mathbb{E} \left[\{x(t) - \hat{x}(t)\}^t \{x(t) - \hat{x}(t)\} \right] \leq \text{tr} [L(t)]. \quad (133)$$

Moreover, the gain matrix $K(t)$ is given by

$$K_e(t) = \{L(t)C^t(t) + \mu^{-1}(t)H(t)H_c^t(t)\}\widehat{V}^{-1}(t). \quad (134)$$

Further details can be found in [57].

Remark 48. Had we considered a class of uncertain time-delay systems represented by

$$\begin{aligned} x_{k+1} &= [A_k + \Delta A_k]x_k + D_k x_{k-\tau} + w_k \\ &= A_{k,\Delta}x_k + D_k x_{k-\tau} + w_k, \\ y_k &= [C_k + \Delta C_k]x_k + v_k = C_{k,\Delta}x_k + v_k, \\ z_k &= C_{1,k}x_k, \end{aligned} \quad (135)$$

where $x_k \in \mathbb{R}^n$ is the state, $y_k \in \mathbb{R}^m$ is the measured output, $z_k \in \mathbb{R}^p$ is a linear combination of the state variables to be estimated, and $w_k \in \mathbb{R}^r$ and $v_k \in \mathbb{R}^m$ are, respectively, the process and measurement noise sequences, and following parallel development to the continuous-case, we would be able to generate a robust discrete-time Kalman filter.

10. Neural Networks

We consider a continuous-time-delayed uncertain neural network (UNN) which is described by the following nonlinear retarded functional differential equations:

$$\begin{aligned} \dot{y}(t) &= -(A_o + \Delta A_o)y(t) \\ &\quad + (W_o + \Delta W_o)g(y(t), t) \\ &\quad + (W_1 + \Delta W_1)g(y(t-\tau), t) + b, \end{aligned} \quad (136)$$

where $y(t) = [y_1(t), \dots, y_n(t)]^t \in \mathbb{R}^n$ is the neuron state vector with n being the number of neurons in NN, $g(y(t)) = [g_1(y_1(t)), \dots, g_n(y_n(t))]^t \in \mathbb{R}^n$ denotes the neuron activation function, $g(y(t-\tau(t))) = [g_1(y_1(t-\tau(t))), \dots, g_n(y_n(t-\tau(t)))]^t \in \mathbb{R}^n$, $A_o = \text{diag}\{a_{oj}\} \in \mathbb{R}^{n \times n}$ is a positive diagonal matrix, $W_o = (W_{jk}^o) \in \mathbb{R}^{n \times n}$ and $W_1 = (W_{jk}^1) \in \mathbb{R}^{n \times n}$ are the interconnection matrices representing the weight coefficients of the neurons, $b = [b_1, \dots, b_n]^t \in \mathbb{R}^n$ is a constant input vector, and $\Delta A(t)$, $\Delta W_o(t)$, and $\Delta W_1(t)$ are uncertain system matrices of the form

$$\begin{aligned} \Delta A_o &= EG(t)F, \\ \Delta W_o &= E_o G_o(t)F_o, \\ \Delta W_1 &= E_1 G_1(t)F_1, \end{aligned} \quad (137)$$

$$G^t(t)G(t) \leq I,$$

$$G_o^t(t)G_o(t) \leq I,$$

$$G_1^t(t)G_1(t) \leq I.$$

In the sequel, it is assumed that the delay $\tau(t)$ is a differentiable time-varying function satisfying

$$\begin{aligned} 0 &< \tau(t) \leq \varrho, \\ \dot{\tau}(t) &\leq \mu, \end{aligned} \quad (138)$$

where the bounds ϱ and μ are known constant scalars. Observe that there is no restriction on the derivative of the

time-varying delay function μ , thereby allowing fast time-delays to occur. This is in contrast with other methods which places $\mu < 1$, thereby limiting the method to slow variations in time-delay.

Assumption 49. The neuron activation functions, $g_{oj}(y_j(t))$, $j = 1, \dots, n$, and $g_{oj}((y_j(t - \tau(t))))$, $j = 1, \dots, n$, are assumed to be nondecreasing, bounded, globally Lipschitz and satisfy

$$0 \leq \frac{g_j(\zeta_j) - g_k(\zeta_k)}{\zeta_j - \zeta_k} \leq k_j, \quad (139)$$

$$\zeta_j, \zeta_k \in \mathbb{R}, \quad \zeta_j \neq \zeta_k, \quad j = 1, \dots, n,$$

where k_j , $j = 1, \dots, n$, are positive constants.

We note that the existence of an equilibrium point of system (136) is guaranteed by the fixed point theorem. Now let $y^* = [y_1^*, \dots, y_n^*]^t$ be an equilibrium of (136), and let

$$x(t) = y(t) - y^*. \quad (140)$$

It is easy to see that (136) is transformed to

$$\begin{aligned} \dot{x}(t) = & -[A_o + \Delta A_o(t)]x(t) \\ & + [W_o + \Delta W_o(t)]f(x(t)) \\ & + [W_1 + \Delta W_1(t)]f(x(t - \tau(t))) \quad (141) \\ = & -A_{o\Delta}x(t) + W_{o\Delta}f(x(t)) \\ & + W_{1\Delta}f(x(t - \tau(t))), \end{aligned}$$

where $f(x(t)) = [f_1(x(t)), \dots, f_n(x(t))]^t$ and $f_j(x_j(t)) = g_j(x_j(t) + y_j^*) - g_j(y_j^*)$ with $f_j(0) = 0$, $j = 1, \dots, n$. It is observed that $f(x(t))$ satisfies $f(0, t) = 0$, $\forall t$, and the following condition for all $(x, t) \in \mathbb{R}^n \times \mathbb{R}$:

$$\begin{aligned} f(x(t), t) & \leq kx, \\ f(x(t - \tau), t) & \leq kx(t - \tau), \end{aligned} \quad (142)$$

where $k > 0$ is a constant. In the absence of uncertainties, we get from (141) the nominal NN model

$$\dot{x}(t) = -A_o x(t) + W_o f(x(t)) + W_1 f(x(t - \tau(t))). \quad (143)$$

In the sequel, the global delay-dependent asymptotic stability the equilibrium of system (136) is investigated, which corresponds to the uniqueness of the equilibrium point.

The following theorem establishes the main result for global delay-dependent asymptotic stability of the NN system.

Theorem 50. Given $\varrho > 0$ and $\mu > 0$. System (143) is globally delay-dependent asymptotically stable if there exist weighting matrices $\mathcal{P} > 0$, $\mathcal{Q} > 0$, $\mathcal{R} > 0$, and $\mathcal{Z} > 0$ and free-weighting

parameter matrices $N_a, N_c, M_a, M_c, \mathcal{S} > 0, \mathcal{M} > 0$ satisfying the following LMI:

$$\Xi = \begin{bmatrix} \Xi_o & \widehat{\mathcal{P}}_o & \widehat{\mathcal{P}}_c & \varrho \mathcal{N} \\ \bullet & -2k^{-1}\mathcal{S} & 0 & 0 \\ \bullet & \bullet & -2k^{-1}\mathcal{M} & 0 \\ \bullet & \bullet & \bullet & -\varrho \mathcal{Z} \end{bmatrix} < 0, \quad (144)$$

where

$$\Xi_o = \begin{bmatrix} \Xi_{o1} & \Xi_{o2} & N_a & \mathcal{P} - M_a^t - A_o^t M_c \\ \bullet & \Xi_{o3} & N_c & 0 \\ \bullet & \bullet & -\mathcal{R} & 0 \\ \bullet & \bullet & \bullet & -M_c - M_c^t + \varrho \mathcal{Z} \end{bmatrix},$$

$$\Xi_{o1} = -M_a^t A_o - A_o^t M_a^+ \mathcal{Q} + \mathcal{R} + N_a + N_a^t,$$

$$\Xi_{o2} = -2N_a + N_c^t,$$

$$\Xi_{o3} = -(1 - \mu)\mathcal{Q} - 2N_c - 2N_c^t,$$

$$\mathcal{N} = \begin{bmatrix} N_a \\ N_c \\ 0 \\ 0 \end{bmatrix}, \quad (145)$$

$$\widehat{\mathcal{P}}_o = \begin{bmatrix} M_a^t W_o + \mathcal{S} \\ 0 \\ 0 \\ M_c^t W_o \end{bmatrix},$$

$$\widehat{\mathcal{P}}_c = \begin{bmatrix} M_a^t W_1 \\ \mathcal{M} \\ 0 \\ M_c^t W_1 \end{bmatrix}.$$

On considering the UNN system in (141) with the uncertainty in (137), it follows from Theorem 50 that the UNN system is globally delay-dependent asymptotically stable if there exist weighting matrices $\mathcal{P} > 0$, $\mathcal{Q} > 0$, $\mathcal{R} > 0$, and $\mathcal{Z} > 0$ and free-weighting parameter matrices $N_a, N_c, M_a, M_c, \mathcal{S} > 0, \mathcal{M} > 0$ satisfying the following LMI:

$$\Xi_{\Delta} = \begin{bmatrix} \Xi_{o\Delta} & \mathcal{P}_o & \mathcal{P}_c & \varrho \mathcal{N} \\ \bullet & -2k^{-1}\mathcal{S} & 0 & 0 \\ \bullet & \bullet & -2k^{-1}\mathcal{M} & 0 \\ \bullet & \bullet & \bullet & -\varrho \mathcal{Z} \end{bmatrix} < 0, \quad (146)$$

where

$$\Xi_{o\Delta} = \begin{bmatrix} \Xi_{o1\Delta} & \Xi_{o2} & N_a & \mathcal{P} - M_a^t - A_{o\Delta}^t M_c \\ \cdot & \Xi_{o3} & N_c & 0 \\ \cdot & \cdot & -\mathcal{R} & 0 \\ \cdot & \cdot & \cdot & -M_c - M_c^t + \mathcal{Q}\mathcal{Z} \end{bmatrix}, \quad (147)$$

$$\Xi_{o1\Delta} = -M_a^t A_{o\Delta} - A_{o\Delta}^t M_a + \mathcal{Q} + \mathcal{R} + N_a + N_a^t,$$

where $\Xi_{o2}, \Xi_{o3}, \mathcal{N}, \mathcal{P}_o, \mathcal{P}_c$ are given in (145). Applying Fact 1 for some scalars $\varepsilon_1 > 0, \varepsilon_2 > 0$, and $\varepsilon_3 > 0$ and invoking Schur complements, it is easy to show that the following theorem holds.

Theorem 51. *System (141) with norm-bounded uncertainty (137) is globally delay-dependent asymptotically stable if there exist weighting matrices $\mathcal{P} > 0, \mathcal{Q} > 0, \mathcal{R} > 0$, and $\mathcal{Z} > 0$, free-weighting parameter matrices $N_a, N_c, M_a, M_c, \mathcal{S} > 0, \mathcal{M} > 0$, and scalars $\sigma > 0, \kappa > 0, \varepsilon_i > 0, i = 1, 2, 3$, satisfying the following LMI:*

$$\hat{\Xi} = \begin{bmatrix} \Xi_s & \Xi_x \\ \cdot & \Xi_y \end{bmatrix} < 0, \quad (148)$$

where

$$\Xi_s = \begin{bmatrix} \Xi_{os} & \widehat{\mathcal{P}}_o & \widehat{\mathcal{P}}_c & \mathcal{Q}N_a \\ \cdot & \Xi_{f1} & 0 & \mathcal{Q}N_c \\ \cdot & \cdot & \Xi_{f2} & 0 \\ \cdot & \cdot & \cdot & -\mathcal{Q}\mathcal{W} \end{bmatrix},$$

$$\Xi_{os} = \begin{bmatrix} \Xi_{o1s} & \Xi_{o2} & N_a & \mathcal{P} - M_a^t - A^t M_c \\ \cdot & \Xi_{o3} & N_c & 0 \\ \cdot & \cdot & -\mathcal{R} & 0 \\ \cdot & \cdot & \cdot & -M_c - M_c^t + \mathcal{Q}\mathcal{Z} \end{bmatrix},$$

$$\Xi_{o1s} = -M_a^t A_o - A_o^t M_a + \mathcal{Q} + \mathcal{R} + N_a + N_a^t + \varepsilon_1 F^t F,$$

$$\Xi_{f1} = -2k^{-1} \mathcal{S} + \varepsilon_2 F_o^t F_o,$$

$$\Xi_{f2} = -2k^{-1} \mathcal{M} + \varepsilon_3 F_1^t F_1,$$

$$\Xi_x = \begin{bmatrix} -M_a^t E & M_a^t E_o & M_a^t E_1 \\ 0 & 0 & 0 \\ 0 & 0 & 0 \\ -M_c^t E & M_c^t E_o & M_c^t E_1 \\ 0 & 0 & 0 \\ 0 & 0 & 0 \\ 0 & 0 & 0 \end{bmatrix},$$

$$\Xi_y = \begin{bmatrix} -\varepsilon_1 I & 0 & 0 \\ \cdot & -\varepsilon_2 I & 0 \\ \cdot & \cdot & -\varepsilon_3 I \end{bmatrix}. \quad (149)$$

The reader is referred to [58] for further results on using expanded LKFs.

11. Networked Control Systems

Typically in process industries, a *network* used at the lowest level of a process/factory communication hierarchy is called a *fieldbus*. Fieldbuses are intended to replace the traditional wiring between sensors, actuators, and controllers. In distributed control system applications, a feedback control loop is often closed through the network, which is called a network-based control system (NBCS); see details in [44, 59–69]. In the NBCS, various delays with variable lengths occurred due to sharing a common network medium, which are called *network-induced delays*. These delays are dependent on configurations of the network and the given system. Those make the NBCS unstable.

In feedback control systems, it is significant that sampled data must be transmitted within a sampling period and stability of control systems should be guaranteed. While a shorter sampling period is preferable in most control systems, for some cases, it can be lengthened up to a certain bound within which stability of the system is guaranteed in spite of the performance degradation. This certain bound is called a *maximum allowable delay bound* (MADB). The MADB depends only on parameters and configurations of the given plant and the controller.

In addition, a faster sampling is said to be desirable in sampled-data systems because the performance of the discrete-time system controller can approximate that of the continuous-time system. But in NBCS (see Figure 1), the high sampling rate can increase network load, which in turn results in longer delay of the signals. Thus finding a sampling rate that can both tolerate the network-induced delay and achieve desired system performance is of fundamental importance in the NBCS design.

11.1. State Feedback Stabilization. Consider the plant model described as

$$\begin{aligned} \dot{x}(t) &= Ax(t) + Bu(t), \\ t &\in [kh + \tau_k, (k+1)h + \tau_{k+1}), \\ y(t) &= Cx(t), \\ u(t^+) &= -K_i x(t - \tau_k), \\ t &\in \{kh + \tau_k, k = 0, 1, 2, \dots\}. \end{aligned} \quad (150)$$

Sampling the above system with period h and defining $z(kh) = [x^T(h), u^T((k-1)h)]^T$ yielded the following closed-loop system:

$$z((k+1)h) = \widetilde{\Phi}(K_i) z(kh) \quad \forall i = 1, 2, \dots, p. \quad (151)$$

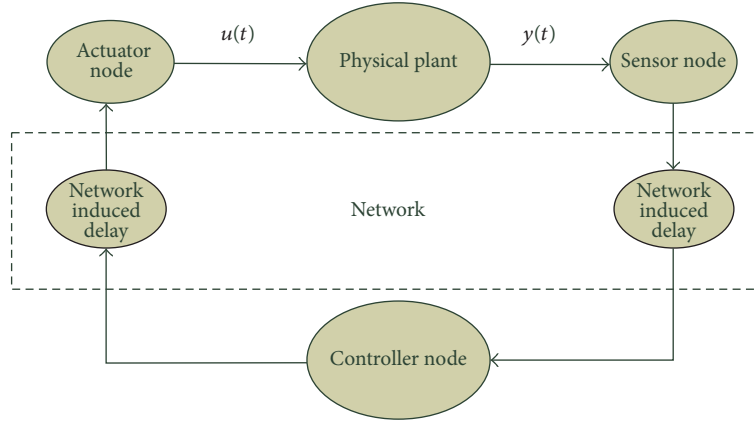


FIGURE 1: A feedback control loop with network-induced delays.

A recent survey of the stabilization methods is reported in [44].

11.2. Observer-Based Feedback Stabilization. An observer-based stabilizing controller can be designed for networked systems involving both random measurement and actuation delays. The LTI plant under consideration was assumed to be of the form

$$\begin{aligned} x_p(k+1) &= Ax_p + Bu_p, \\ y_p &= Cx_p, \end{aligned} \quad (152)$$

where $x_p(k) \in \mathfrak{R}^n$ is the state vector and $u_p(k) \in \mathfrak{R}^m$ and $y_p(k) \in \mathfrak{R}^p$ are the control input and output vectors of the plant, respectively. The measurement subjected to random communication delay is given by

$$y_c(k) = (1 - \delta(k)) y_p(k) + \delta(k) y_p(k - \tau_k^m), \quad (153)$$

where τ_k^m is the measurement delay, whose occurrence is governed by the Bernoulli distribution, and $\delta(k)$ is Bernoulli distributed sequence with

$$\begin{aligned} \text{Prob}\{\delta(k) = 1\} &= \mathbb{E}\{\delta(k)\} = \bar{\delta}, \\ \text{Prob}\{\delta(k) = 0\} &= 1 - \mathbb{E}\{\delta(k)\} = 1 - \bar{\delta}. \end{aligned} \quad (154)$$

The following observer-based controller is designed when the full state vector is not available.

Observer

$$\begin{aligned} \hat{x}(k+1) &= A\hat{x} + Bu_c(k) + L(y_c(k) - \hat{y}_c(k)), \\ \hat{y}_c(k) &= (1 - \bar{\delta})C\hat{x}(k) + \bar{\delta}C\hat{x}(k - \tau_k^m). \end{aligned} \quad (155)$$

Controller

$$\begin{aligned} u_c(k) &= K\hat{x}(k) \\ u_p &= (1 - \alpha)u_c(k) + \alpha u_c(k - \tau_k^a), \end{aligned} \quad (156)$$

where $\hat{x}(k) \in \mathfrak{R}^n$ is the estimate of system (152), $\hat{y}_c(k) \in \mathfrak{R}^p$ is the observer output, and $L \in \mathfrak{R}^{n \times p}$ and $K \in \mathfrak{R}^{m \times n}$ are the observer gain and the controller gain, respectively. The stochastic variable α , mutually independent of δ , is also a Bernoulli distributed white sequence with

$$\begin{aligned} \text{Prob}\{\alpha(k) = 1\} &= \mathbb{E}\{\alpha(k)\} = \bar{\alpha}, \\ \text{Prob}\{\alpha(k) = 0\} &= 1 - \mathbb{E}\{\alpha(k)\} = 1 - \bar{\alpha}, \end{aligned} \quad (157)$$

where τ_k^a is the actuation delay. It is assumed that τ_k^a and τ_k^m are time-varying and have the following bounded condition:

$$\begin{aligned} \underline{d}_m &\leq \tau_k^m \leq \bar{d}_m, \\ \underline{d}_a &\leq \tau_k^a \leq \bar{d}_a. \end{aligned} \quad (158)$$

The estimation error is defined by

$$e(k) = x_p(k) - \hat{x}(k). \quad (159)$$

This yields

$$\begin{aligned} x_p(k+1) &= [A + (1 - \bar{\alpha})BK]x_p(k) \\ &\quad - (1 - \bar{\alpha})BKe(k) + \bar{\alpha}BKx_p(k - \tau_k^a) \\ &\quad - \bar{\alpha}BKe(k - \tau_k^a) \\ &\quad - (\alpha - \bar{\alpha})BKx_p(k) \\ &\quad + (\alpha - \bar{\alpha})BKe(k) \\ &\quad + (\alpha - \bar{\alpha})BKx_p(k - \tau_k^a) \\ &\quad - (\alpha - \bar{\alpha})BKe(k - \tau_k^a), \\ e(k+1) &= [A - (1 - \bar{\delta})LC]e(k) \\ &\quad - \bar{\delta}Lce(k - \tau_k^m) \\ &\quad + (\delta - \bar{\delta})LCx_p(k) \\ &\quad - (\delta - \bar{\delta})LCx_p(k - \tau_k^m). \end{aligned} \quad (160)$$

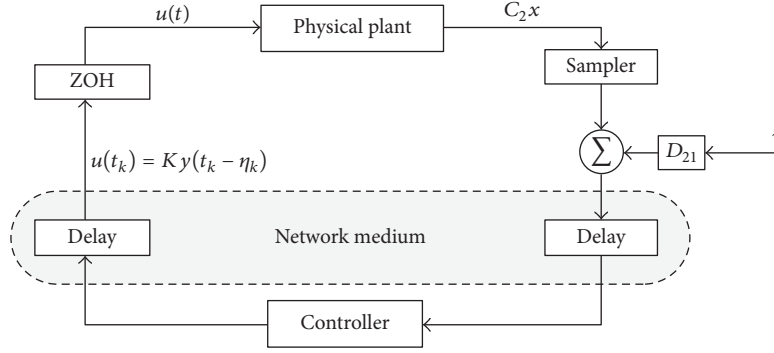


FIGURE 2: Networked output-feedback control system.

System (160) is equivalent to the following compact form:

$$\begin{aligned} \varepsilon(k+1) = & (\bar{A} + \tilde{A})\varepsilon(k) + (\bar{B} + \tilde{B})\varepsilon(k - \tau_k^m) \\ & + (\bar{C} - \tilde{C})\varepsilon(k - \tau_k^a), \end{aligned} \quad (161)$$

where

$$\begin{aligned} \varepsilon(k) &= \begin{bmatrix} x_p^T(k) & e^T(k) \end{bmatrix}^T, \\ \bar{A} &= \begin{bmatrix} A + (1 - \bar{\alpha})BK & -(1 - \bar{\alpha})BK \\ 0 & A - (1 - \bar{\delta})LC \end{bmatrix}, \\ \tilde{A} &= \begin{bmatrix} -(\alpha - \bar{\alpha})BK & (\alpha - \bar{\alpha})BK \\ (\delta - \bar{\delta})LC & 0 \end{bmatrix}, \\ \bar{B} &= \begin{bmatrix} 0 & 0 \\ 0 & -\bar{\delta}LC \end{bmatrix}, \\ \tilde{B} &= \begin{bmatrix} 0 & 0 \\ -(\delta - \bar{\delta})LC & 0 \end{bmatrix}, \\ \bar{C} &= \begin{bmatrix} \bar{\alpha}BK & -\bar{\alpha}BK \\ 0 & 0 \end{bmatrix}, \\ \tilde{C} &= \begin{bmatrix} (\alpha - \bar{\alpha})BK & -(\alpha - \bar{\alpha})BK \\ 0 & 0 \end{bmatrix}. \end{aligned} \quad (162)$$

Remark 52. It is noted that a majority of the existing works on the stability of NCS (in the framework of time-delay approach) are reduced to some Lyapunov-based analysis of systems with uncertain and bounded time-varying delays; see [44]. In the following sections, we will present alternative approaches that will lead to improved results.

11.3. Lyapunov-Based Sampled-Data Stabilization. Three main approaches have been used to the sampled-data control and later to the Networked Control Systems (NCS), where the plant is controlled via communication network:

- (A) The first one is based on discrete-time models [70, 71]. This approach is not applicable to the performance

analysis (like the exponential decay rate) of the resulting continuous-time closed-loop system.

- (B) The second one is a time-delay approach, where the system is modeled as a continuous-time system with a time-varying sawtooth delay in the control input [8, 72–74]. The time-delay approach via time-independent Lyapunov-Krasovskii functionals or Lyapunov-Razumikhin functions leads to linear matrix inequalities (LMIs) for analysis and design of linear uncertain NCS.
- (C) The third approach is based on the representation of the sampled-data system in the form of impulsive model [72, 73]. Recently, the impulsive model approach was extended to the case of uncertain sampling intervals [75] by employing a discontinuous Lyapunov function method, which improved the existing Lyapunov-based results. Recently, the latter result was recovered via an input-output approach by application of the vector extension of Wirtinger's inequality [76].

Consider the continuous-time system depicted in Figure 2:

$$\begin{aligned} \dot{x}(t) &= Ax(t) + Bu(t) + Ew(t), \\ z(t) &= C_1x(t) + D_1u(t), \end{aligned} \quad (163)$$

where $x(t) \in \mathbb{R}^n$ is the state, $z(t) \in \mathbb{R}^r$ is the signal to be controlled or estimated, $w(t) \in \mathbb{R}^q$ is the disturbance, $u(t) \in \mathbb{R}^m$ is the control input, and $A(t) \in \mathbb{R}^{n \times n}$, $B(t) \in \mathbb{R}^{n \times m}$, $C_1 \in \mathbb{R}^{p \times n}$, $D_1 \in \mathbb{R}^{p \times m}$, and $E \in \mathbb{R}^{n \times q}$ are system matrices.

In Figure 2, the sampler is time-driven, whereas the controller and the Zero-Order Hold (ZOH) are event-driven (in the sense that the controller and the ZOH update their outputs as soon as they receive a new sample). For simplicity in exposition, we assume that the measurement output $y(s_k) \in \mathbb{R}^p$ is available at discrete sampling instants

$$0 = s_0 < s_1 < \dots < s_k < \dots, \quad \lim_{k \rightarrow \infty} s_k = \infty, \quad (164)$$

and it may be corrupted by a measurement noise signal $v(s_k)$:

$$y(t) = Cx(t) + Du(t). \quad (165)$$

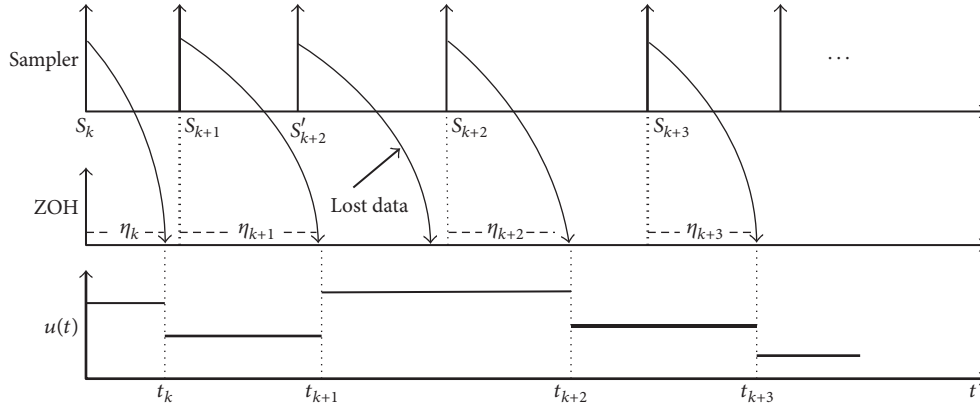


FIGURE 3: NCS timing diagram.

By considering nonuniform sampling, data packet dropouts can be accommodated. In this respect, $y(s_k)$, $k = 0, 1, 2, \dots$, correspond to the measurements that are not lost. The timing diagram of the considered NCS with both delay and packet dropout is shown in Figure 3, where $s_k = t_k - \lambda_k$ accounts for the sampling time of the data that has not been lost. In this setup, t_k denotes the updating instant time of the ZOH, and suppose that the updating signal at the instant t_k has experienced a signal transmission delay λ_k . Adopting the approach of [75], we allow the delays λ_k to grow larger than $s_{k+1} - s_k$, provided that the sequence of input update times t_k remains strictly increasing. This implies that if an old sample gets to the destination after the most recent one, it should be dropped.

The static output-feedback controller has a form

$$u(t_k) = K_o y(t_k - \lambda_k), \quad t_k \leq t \leq t_{k+1}, \quad (166)$$

where K_o is the controller gain and t_{k+1} is the next updating instant time of the ZOH after t_k . It is known that

$$t_{k+1} - t_k + \lambda_k \leq \tau_M, \quad 0 \leq \lambda_k \leq \lambda_M, \quad k = 0, 1, 2, \dots, \quad (167)$$

where λ_M is a known upper bound on the network-induced delays λ_k and τ_M denotes the maximum time span between the time $s_k = t_k - \lambda_k$ at which the state is sampled, and the time t_{k+1} at which next update arrives at the ZOH. Observe that the sampling intervals and the numbers of successive packet dropouts are uniformly bounded.

Within the foregoing representation, exponential stability, state feedback, and static output-feedback results are developed in [77]. More elaborate results can be found in [74].

12. Interconnected Systems

We consider a class of linear systems S structurally composed of n_s coupled subsystems S_j depicted in Figure 4 and modeled by the state-space model:

$$\begin{aligned} \dot{x}_j(t) &= A_{j\Delta} x_j(t) + A_{dj\Delta} x_j(t - \tau_j) + B_{j\Delta} u_j(t) \\ &\quad + c_j(k) + \Gamma_{j\Delta} w_j(t), \end{aligned}$$

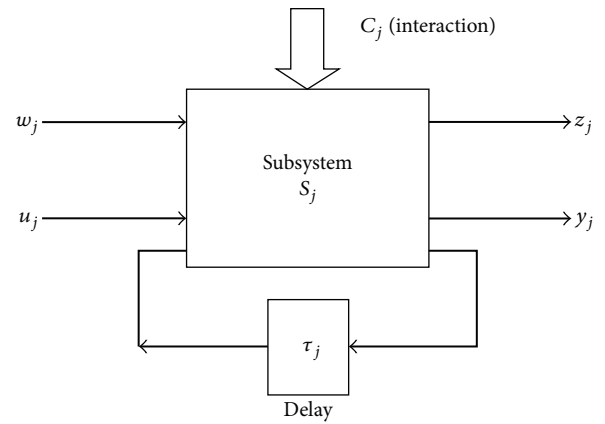


FIGURE 4: Subsystem model.

$$\begin{aligned} z_j(t) &= G_{j\Delta} x_j(t) + G_{dj\Delta} x_j(t - \tau_j) + D_{j\Delta} u_j(t) \\ &\quad + \Phi_{j\Delta} w_j(t), \end{aligned}$$

$$y_j(t) = C_{j\Delta} x_j(t) + C_{dj\Delta} x_j(t - \tau_j),$$

$$c_j(t) = \sum_{k=1}^{n_s} F_{jk\Delta} x_k(t) + \sum_{k=1}^{n_s} E_{jk\Delta} x_k(t - \eta_{jk}(t)) \quad (168)$$

whose matrices are containing uncertainties which belong to a real convex bounded polytopic model of the type

$$\begin{aligned} \begin{bmatrix} A_{j\Delta} & A_{dj\Delta} & B_{j\Delta} & \Gamma_{j\Delta} \\ G_{j\Delta} & G_{dj\Delta} & D_{j\Delta} & \Phi_{j\Delta} \\ C_{j\Delta} & C_{dj\Delta} & E_{jk\Delta} & F_{jk\Delta} \end{bmatrix} &\in \Pi_\lambda \\ &\triangleq \left\{ \begin{bmatrix} A_{j\lambda} & A_{dj\lambda} & B_{j\lambda} & \Gamma_{j\lambda} \\ G_{j\lambda} & G_{dj\lambda} & D_{j\lambda} & \Phi_{j\lambda} \\ C_{j\lambda} & C_{dj\lambda} & E_{jk\lambda} & F_{jk\lambda} \end{bmatrix} \right. \\ &\quad \left. = \sum_{s=1}^N \lambda_s \begin{bmatrix} A_{js} & A_{djs} & B_{js} & \Gamma_{js} \\ G_{js} & G_{djs} & D_{js} & \Phi_{js} \\ C_{js} & C_{djs} & E_{jks} & F_{jks} \end{bmatrix}, \lambda_s \in \Lambda \right\}, \end{aligned} \quad (169)$$

where Λ is the unit simplex:

$$\Lambda \triangleq \left\{ (\lambda_1, \dots, \lambda_N) : \sum_{j=1}^N \lambda_j = 1, \lambda_j \geq 0 \right\}. \quad (170)$$

Define the vertex set $\mathcal{N} = \{1, \dots, N\}$. We use $\{A, \dots, \Phi\}$ to imply generic system matrices and $\{A_j, \dots, \Phi_j, j \in \mathcal{N}\}$ to represent the respective values at the vertices.

In the absence of uncertainties, system (168) reduces to the nominal state-space model

$$\begin{aligned} \dot{x}_j(t) &= A_j x_j(t) + A_{dj} x_j(t - \tau_j(t)) + B_j u_j(t) \\ &\quad + c_j(t) + \Gamma_j w_j(t), \\ z_j(t) &= G_j x_j(t) + G_{dj} x_j(t - \tau_j(t)) + D_j u_j(t) \\ &\quad + \Phi_j w_j(t), \end{aligned} \quad (171)$$

$$\begin{aligned} y_j(t) &= C_j x_j(t) + C_{dj} x_j(t - \tau_j(t)), \\ c_j(t) &= \sum_{k=1}^{n_s} F_{jk} x_k(t) + \sum_{k=1}^{n_s} E_{jk} x_k(t - \eta_{jk}(t)), \end{aligned}$$

where, for $j \in \{1, \dots, n_s\}$, $x_j(t) \in \mathbb{R}^{n_j}$ is the state vector, $u_j(t) \in \mathbb{R}^{m_j}$ is the control input, $y_j(t) \in \mathbb{R}^{p_j}$ is the measured output, $w_j(t) \in \mathbb{R}^{q_j}$ is the disturbance input which belongs to $\mathcal{L}_2[0, \infty)$, $z_j(t) \in \mathbb{R}^{q_j}$ is the performance output, $c_j(t) \in \mathbb{R}^{n_j}$ is the coupling vector, and $\tau_j, \eta_{jk}, j, k \in \{1, \dots, n_s\}$, are unknown time-delay factors satisfying

$$\begin{aligned} 0 \leq \tau_j(t) \leq \varrho_j, \quad \dot{\tau}_j(t) \leq \mu_j, \\ 0 \leq \eta_{jk}(t) \leq \varrho_{jk}, \quad \dot{\eta}_{jk}(t) \leq \mu_{jk}, \end{aligned} \quad (172)$$

where the bounds $\varrho_j, \varrho_{jk}, \mu_j, \mu_{jk}$ are known constants in order to guarantee smooth growth of the state trajectories. The matrices $A_j \in \mathbb{R}^{n_j \times n_j}$, $B_j \in \mathbb{R}^{n_j \times m_j}$, $D_j \in \mathbb{R}^{q_j \times m_j}$, $A_{dj} \in \mathbb{R}^{n_j \times n_j}$, $\Phi_j \in \mathbb{R}^{q_j \times q_j}$, $\Gamma_j \in \mathbb{R}^{n_j \times q_j}$, $C_j \in \mathbb{R}^{p_j \times n_j}$, $C_{dj} \in \mathbb{R}^{p_j \times n_j}$, $G_j \in \mathbb{R}^{q_j \times n_j}$, $G_{dj} \in \mathbb{R}^{q_j \times n_j}$, $F_{jk} \in \mathbb{R}^{n_j \times n_k}$, and $E_{jk} \in \mathbb{R}^{n_j \times n_k}$ are real and constants. The initial condition $\langle x_j(0), x_j(r) \rangle = \langle x_{oj}, \phi_j \rangle$, $j \in \{1, \dots, n_s\}$, where $\phi_j(\cdot) \in \mathcal{L}_2[-\tau_j^*, 0]$, $j \in \{1, \dots, n_s\}$. The inclusion of the terms $A_{dj} x_j(t - \tau_j(t))$ and $E_{jk} x_k(t - \eta_{jk}(t))$ is meant to emphasize the delay within each subsystem (local delay) and among the subsystems (coupling delay), respectively.

We develop new criteria for LMI-based characterization of delay-dependent asymptotic stability and \mathcal{L}_2 gain analysis which requires only subsystem information thereby assuring decentralization. The criteria include some parameter matrices aims at expanding the range of applicability of the developed conditions. The following theorem establishes the main result subsystem S_j .

Theorem 53. Give $\varrho_j > 0$, $\mu_j > 0$, $\varrho_{jk} > 0$, and $\mu_{jk} > 0$, $j, k = 1, \dots, n_s$. The family of nominal subsystems $\{S_j\}$ with $u_j(\cdot) \equiv 0$ where S_j is described by (171) is delay-dependent asymptotically stable with \mathcal{L}_2 -performance bound γ_j , $j = 1, \dots, n_s$, if

there exist positive-definite matrices $\mathcal{P}_j, \mathcal{Q}_j, \mathcal{W}_j, \mathcal{X}_{kj}$, $k, j = 1, \dots, n_s$, and parameter matrices Θ_j and Υ_j satisfying the following LMIs for $j = 1, \dots, n_s$

$$\begin{bmatrix} \Xi_{oj} & \Xi_{aj} & -\varrho_j \Theta_j & \Xi_{cj} & \mathcal{P}_j \Gamma_j & G_j^t & \varrho_j A_{dj}^t \mathcal{W}_j \\ \bullet & -\Xi_{mj} & -\varrho_j \Upsilon_j & 0 & 0 & G_{dj}^t & \varrho_j A_{dj}^t \mathcal{W}_j \\ \bullet & \bullet & -\varrho_j \mathcal{W}_j & 0 & 0 & 0 & 0 \\ \bullet & \bullet & \bullet & -\Xi_{nj} & 0 & 0 & \varrho_j \sum_{k=1}^{n_s} E_{kj} \mathcal{W}_j \\ \bullet & \bullet & \bullet & \bullet & -\gamma_j^2 I_j & \Phi_j^t & \varrho_j \Gamma_j^t \mathcal{W}_j \\ \bullet & \bullet & \bullet & \bullet & \bullet & -I_j & 0 \\ \bullet & \bullet & \bullet & \bullet & \bullet & \bullet & -\varrho_j \mathcal{W}_j \end{bmatrix} < 0, \quad (173)$$

where

$$\begin{aligned} \Xi_{oj} &= \mathcal{P}_j \left[A_j + \sum_{k=1}^{n_s} F_{kj} \right] + \left[A_j + \sum_{k=1}^{n_s} F_{kj} \right]^t \mathcal{P}_j^t + \Theta_j \\ &\quad + \Theta_j^t + \mathcal{Q}_j + \sum_{k=1}^{n_s} \mathcal{X}_{kj}, \\ \Xi_{mj} &= \Upsilon_j + \Upsilon_j^t + (1 - \mu_j) \mathcal{Q}_j, \\ \Xi_{aj} &= \mathcal{P}_j A_{dj} - \Theta_j + \Upsilon_j^t, \\ \Xi_{nj} &= \sum_{k=1}^{n_s} (1 - \mu_{kj}) \mathcal{X}_{kj}, \\ \Xi_{cj} &= \mathcal{P}_j \sum_{k=1}^{n_s} E_{kj}. \end{aligned} \quad (174)$$

More detailed results can be found in [78].

13. Conclusions and Future Work

This paper has overviewed the research area of *stability and stabilization of systems with time-delays* with emphasis on the following topics:

- (i) Systems with time-delays constitute a good compromise between the too simple models with finite dimension and the great complexity of PDEs. The behavior features and the structural characteristics of delay systems are particular enough to justify specific techniques.
- (ii) The main Lyapunov-based tools have to be used developing robust stability in combination with model transformations. Several extensions are anticipated when examining different forms of Lyapunov-Krasovskii functionals.
- (iii) In the robust control area, existing results can be generally subdivided into two classes:

- (C1) The first class consists in systems with input or output delays (mainly, \mathcal{H}_∞ performance or predictor-like techniques).
- (C2) The second class in state delays (discrete or distributed). The intersection of the two classes is still to be addressed.
- (iv) Many contemporary dynamical systems with aftereffect are still requiring further investigation: this is the case, for instance, of delay systems with strong nonlinearities, as well as time-varying or state-dependent delays.
- (v) There are classes of nonlinear dynamical systems with delays including jump systems, fuzzy systems, and switched systems inviting additional research efforts.
- (vi) Recently, a surge of interests has been recently arisen regarding Wirtinger-based integral inequality and augmented Lyapunov-Krasovskii functionals [79–83]. The ensuing results triggered recent development in the time-delay system stability. Further discussions and assessments of these results and related issues suggest attractive research directions at least from the computational standpoint.
- (vii) The class of uncertain nonlinear networked systems with both multiple stochastic time-varying communication delays and multiple packet dropouts was addressed in [84] for filtering design and in [85] for reliable control. A promising research direction is to extend the role of delay patterns to alternative forms.

Conflicts of Interest

The author declares that there are no conflicts of interest regarding the publication of this paper.

Acknowledgments

This research work is supported by the Deanship of Scientific Research (DSR) at KFUPM through research Project no. IN 141048.

References

- [1] V. L. Kharitonov, "Robust stability analysis of time delay systems: a survey," in *Proceedings of the 4th IFAC Conference on System Structure and Control*, pp. 1–12, Nantes, France, 1998.
- [2] V. L. Kharitonov and D. Melchor-Aguilar, "On delay-dependent stability conditions," *Systems & Control Letters*, vol. 40, no. 1, pp. 71–76, 2000.
- [3] J. K. Hale and S. M. Verduyn Lunel, *Introduction to Functional-Differential Equations*, vol. 99 of *Applied Mathematical Sciences*, Springer, New York, NY, USA, 1993.
- [4] K. Gu, V. L. Kharitonov, and J. Chen, *Stability of Time-Delay Systems*, Control Engineering, Birkhäuser, Boston, Mass, USA, 2003.
- [5] J.-P. Richard, "Time-delay systems: an overview of some recent advances and open problems," *Automatica*, vol. 39, no. 10, pp. 1667–1694, 2003.
- [6] M. S. Mahmoud, *Robust Control and Filtering for Time-Delay Systems*, Marcel Dekker, New York, NY, USA, 2000.
- [7] A. Halanay, *Differential Equations: Stability, Oscillations, Time Lags*, Academic Press, New York, NY, USA, 1966.
- [8] E. Fridman, *Introduction to Time-delay Systems: Analysis and Control*, Springer, Berlin, Germany, 2014.
- [9] M. S. Mahmoud, *Switched Time-Delay Systems*, Springer, Boston, Mass, USA, 2010.
- [10] E. F. Infante, "A Liapunov functional for a matrix difference-differential equation," *Journal of Differential Equations*, vol. 29, no. 3, pp. 439–451, 1978.
- [11] W. Z. Huang, "Generalization of Liapunov's theorem in a linear delay system," *Journal of Mathematical Analysis and Applications*, vol. 142, no. 1, pp. 83–94, 1989.
- [12] J. Louisell, "A stability analysis for a class of differential-delay equations having time-varying delay," in *Delay Differential Equations and Dynamical Systems*, S. Busenberg and M. Martelli, Eds., vol. 1475 of *Lecture Notes in Mathematics*, pp. 225–242, Springer, Berlin, Germany, 1991.
- [13] M. S. Mahmoud and N. F. Al-Muthairi, "Design of robust controllers for time-delay systems," *IEEE Transactions on Automatic Control*, vol. 39, no. 5, pp. 995–999, 1994.
- [14] M. S. Mahmoud and N. F. Al-Muthairi, "Quadratic stabilization of continuous time systems with state-delay and norm-bounded time-varying uncertainties," *IEEE Transactions on Automatic Control*, vol. 39, no. 10, pp. 2135–2139, 1994.
- [15] K. Gu, "A generalized discretization scheme of Lyapunov functional in the stability problem of linear uncertain time-delay systems," *International Journal of Robust and Nonlinear Control*, vol. 9, no. 1, pp. 1–14, 1999.
- [16] K. Gu, "Discretization schemes for Lyapunov-Krasovskii functionals in time-delay systems," *Kybernetika*, vol. 37, no. 4, pp. 479–504, 2001.
- [17] X.-J. Jing, D.-L. Tan, and Y.-C. Wang, "An LMI approach to stability of systems with severe time-delay," *IEEE Transactions on Automatic Control*, vol. 49, no. 7, pp. 1192–1195, 2004.
- [18] S. Xu and T. Chen, "Robust H_∞ control for uncertain discrete-time systems with time-varying delays via exponential output feedback controllers," *Systems & Control Letters*, vol. 51, no. 3–4, pp. 171–183, 2004.
- [19] S. K. Nguang, P. Shi, and S. Ding, "Delay-dependent fault estimation for uncertain time-delay nonlinear systems: an LMI approach," *International Journal of Robust and Nonlinear Control*, vol. 16, no. 18, pp. 913–933, 2006.
- [20] G.-P. Liu, Y. Q. Xia, J. Chen, D. Rees, and W. S. Hu, "Networked predictive control of systems with random network delays in both forward and feedback channels," *IEEE Transactions on Industrial Electronics*, vol. 54, no. 3, pp. 1282–1297, 2007.
- [21] W.-A. Zhang and L. Yu, "A robust control approach to stabilization of networked control systems with time-varying delays," *Automatica*, vol. 45, no. 10, pp. 2440–2445, 2009.
- [22] X.-M. Sun, G.-P. Liu, W. Wang, and D. Rees, "Stability analysis for networked control systems based on average dwell time method," *International Journal of Robust and Nonlinear Control*, vol. 20, no. 15, pp. 1774–1784, 2010.
- [23] X.-G. Yu, "An LMI approach to robust H_∞ filtering for uncertain systems with time-varying distributed delays," *Journal of the Franklin Institute*, vol. 345, no. 8, pp. 877–890, 2008.
- [24] C. Peng and Y.-C. Tian, "Delay-dependent robust H_∞ control for uncertain systems with time-varying delay," *Information Sciences*, vol. 179, no. 18, pp. 3187–3197, 2009.

- [25] Y. Xia, M. Fu, H. Yang, and G.-P. Liu, "Robust sliding-mode control for uncertain time-delay systems based on delta operator," *IEEE Transactions on Industrial Electronics*, vol. 56, no. 9, pp. 3646–3655, 2009.
- [26] M. F. Miranda and V. J. S. Leite, "Robust stabilization of polytopic discrete-time systems with time-varying state delay: a convex approach," *Journal of the Franklin Institute*, vol. 348, no. 4, pp. 568–588, 2011.
- [27] F. Yang, Z. Wang, Y. S. Hung, and M. Gani, " H_∞ control for networked systems with random communication delays," *IEEE Transactions on Automatic Control*, vol. 51, no. 3, pp. 511–518, 2006.
- [28] W.-A. Zhang and L. Yu, "Modelling and control of networked control systems with both network-induced delay and packet-dropout," *Automatica*, vol. 44, no. 12, pp. 3206–3210, 2008.
- [29] H. Song, W.-A. Zhang, and L. Yu, " H_∞ filtering of network-based systems with communication constraints," *IET Signal Processing*, vol. 4, no. 1, pp. 69–77, 2010.
- [30] D. Wu, J. Wu, S. Chen, and J. Chu, "Stability of networked control systems with polytopic uncertainty and buffer constraint," *IEEE Transactions on Automatic Control*, vol. 55, no. 5, pp. 1202–1208, 2010.
- [31] S. Boyd, L. El Ghaoui, E. Feron, and V. Balakrishnan, *Linear Matrix Inequalities in System and Control Theory*, vol. 15 of *SIAM Studies in Applied Mathematics*, SIAM, Philadelphia, Pa, USA, 1994.
- [32] E. Fridman and U. Shaked, "An improved stabilization method for linear time-delay systems," *IEEE Transactions on Automatic Control*, vol. 47, no. 11, pp. 1931–1937, 2002.
- [33] E. Fridman and U. Shaked, "Delay-dependent stability and H_∞ control: constant and time-varying delays," *International Journal of Control*, vol. 76, no. 1, pp. 48–60, 2003.
- [34] M. Wu, Y. He, J.-H. She, and G.-P. Liu, "Delay-dependent criteria for robust stability of time-varying delay systems," *Automatica*, vol. 40, no. 8, pp. 1435–1439, 2004.
- [35] Y. He, Q.-G. Wang, C. Lin, and M. Wu, "Augmented Lyapunov functional and delay-dependent stability criteria for neutral systems," *International Journal of Robust and Nonlinear Control*, vol. 15, no. 18, pp. 923–933, 2005.
- [36] Y. He, Q.-G. Wang, L. Xie, and C. Lin, "Further improvement of free-weighting matrices technique for systems with time-varying delay," *IEEE Transactions on Automatic Control*, vol. 52, no. 2, pp. 293–299, 2007.
- [37] J. Sun, G. P. Liu, and J. Chen, "Delay-dependent stability and stabilization of neutral time-delay systems," *International Journal of Robust and Nonlinear Control*, vol. 19, no. 12, pp. 1364–1375, 2009.
- [38] J. Sun and G. P. Liu, "On improved delay-dependent stability criteria for neutral time-delay systems," *European Journal of Control*, vol. 15, no. 6, pp. 613–623, 2009.
- [39] P. Park, "A delay-dependent stability criterion for systems with uncertain time-invariant delays," *IEEE Transactions on Automatic Control*, vol. 44, no. 4, pp. 876–877, 1999.
- [40] Y. S. Moon, P. Park, W. H. Kwon, and Y. S. Lee, "Delay-dependent robust stabilization of uncertain state-delayed systems," *International Journal of Control*, vol. 74, no. 14, pp. 1447–1455, 2001.
- [41] V. Suplin, E. Fridman, and U. Shaked, " H_∞ control of linear uncertain time-delay systems—a projection approach," *IEEE Transactions on Automatic Control*, vol. 51, pp. 680–685, 2006.
- [42] K. Gu, "An integral inequality in the stability problem of time-delay systems," in *Proceedings of the 39th IEEE Conference on Decision and Control*, pp. 2805–2810, Sydney, Australia, 2000.
- [43] M. S. Mahmoud and A. Y. Al-Rayyah, "Efficient parameterisation to stability and feedback synthesis of linear time-delay systems," *IET Control Theory & Applications*, vol. 3, no. 8, pp. 1107–1118, 2009.
- [44] M. S. Mahmoud, *Control and Estimation Methods over Communication Networks*, Springer, London, UK, 2014.
- [45] F. Gouaisbaut and D. Peaucelle, "Delay-dependent robust stability of time delay systems," in *Proceedings of the 5th IFAC Symposium on Robust Control Design (ROCOND '06)*, pp. 453–458, Toulouse, France, July 2006.
- [46] W.-H. Chen, Z.-H. Guan, and X. Lu, "Delay-dependent guaranteed cost control for uncertain discrete-time systems with delay," *IEEE Proceedings: Control Theory and Applications*, vol. 150, no. 4, pp. 412–416, 2003.
- [47] E.-K. Boukas, "Discrete-time systems with time-varying time delay: stability and stabilizability," *Mathematical Problems in Engineering*, vol. 2006, Article ID 42489, 10 pages, 2006.
- [48] V. J. S. Leite, S. Tarbouriech, and P. L. D. Peres, "A convex approach for robust state-feedback control of discrete-time systems with state delay," in *Proceedings of the American Control Conference (AAC '04)*, pp. 2870–2875, Boston, Mass, USA, June 2004.
- [49] M. S. Mahmoud, "New results on robust control design of discrete-time uncertain systems," *IEEE Proceedings—Control Theory and Applications*, vol. 152, pp. 453–459, 2005.
- [50] Z. Wang, G. Wei, and G. Feng, "Reliable, H_∞ control for discrete-time piecewise linear systems with infinite distributed delays," *Automatica*, vol. 45, no. 12, pp. 2991–2994, 2009.
- [51] Y. Liu, Z. Wang, J. Liang, and X. Liu, "Synchronization and state estimation for discrete-time complex networks with distributed delays," *IEEE Transactions on Systems, Man, and Cybernetics Part B: Cybernetics*, vol. 38, no. 5, pp. 1314–1325, 2008.
- [52] V. B. Kolmanovskii and J.-P. Richard, "Stability of some linear systems with delays," *IEEE Transactions on Automatic Control*, vol. 44, no. 5, pp. 984–989, 1999.
- [53] E. Fridman, "New Lyapunov-Krasovskii functionals for stability of linear retarded and neutral type systems," *Systems and Control Letters*, vol. 43, no. 4, pp. 309–319, 2001.
- [54] S. Xu and J. Lam, "A survey of linear matrix inequality techniques in stability analysis of delay systems," *International Journal of Systems Science*, vol. 39, no. 12, pp. 1095–1113, 2008.
- [55] M. S. Mahmoud and M. Zribi, " H_∞ -controllers for time-delay systems using linear matrix inequalities," *Journal of Optimization Theory and Applications*, vol. 100, no. 1, pp. 89–122, 1999.
- [56] B. D. O. Anderson and J. B. Moore, *Optimal Filtering*, Prentice Hall, New York, NY, USA, 1979.
- [57] M. S. Mahmoud, N. F. Al-Muthairi, and S. Bingulac, "Robust Kalman filtering for continuous time-lag systems," *Systems & Control Letters*, vol. 38, no. 4–5, pp. 309–319, 1999.
- [58] M. S. Mahmoud, S. Z. Selim, and P. Shi, "Global exponential stability criteria for neural networks with probabilistic delays," *IET Control Theory and Applications*, vol. 4, no. 11, pp. 2405–2415, 2010.
- [59] G. C. Walsh, H. Ye, and L. G. Bushnell, "Stability analysis of networked control systems," *IEEE Transactions on Control Systems Technology*, vol. 10, no. 3, pp. 438–446, 2002.
- [60] S. Yin, L. Yu, and W.-A. Zhang, "A switched system approach to networked H_∞ filtering with packet losses," *Circuits, Systems, and Signal Processing*, vol. 30, no. 6, pp. 1341–1354, 2011.

- [61] R. A. Gupta and M.-Y. Chow, "Networked control system: overview and research trends," *IEEE Transactions on Industrial Electronics*, vol. 57, no. 7, pp. 2527–2535, 2010.
- [62] Y. Tipsuwan and M. Y. Chow, "Control methodologies in networked control systems," *Control Engineering Practice*, vol. 11, no. 10, pp. 1099–1111, 2003.
- [63] W. Zhang, M. S. Branicky, and S. M. Phillips, "Stability of networked control systems," *IEEE Control Systems*, vol. 21, no. 1, pp. 84–99, 2001.
- [64] S. Zampieri, "Trends in networked control systems," in *Proceedings of the 17th World Congress*, pp. 2886–2894, Seoul, Republic of Korea, July 2008.
- [65] L. A. Montestruque and P. J. Antsaklis, "On the model-based control of networked systems," *Automatica*, vol. 39, no. 10, pp. 1837–1843, 2003.
- [66] P. Seiler and R. Sengupta, "An H_∞ approach to networked control," *IEEE Transactions on Automatic Control*, vol. 50, no. 3, pp. 356–364, 2005.
- [67] M. S. Mahmoud, H. N. Nounou, and Y. Xia, "Robust dissipative control for internet-based switching systems," *Journal of the Franklin Institute. Engineering and Applied Mathematics*, vol. 347, no. 1, pp. 154–172, 2010.
- [68] P. Seiler and R. Sengupta, "Analysis of communication losses in vehicle control problems," in *Proceedings of the American Control Conference*, vol. 2, pp. 1491–1496, June 2001.
- [69] F.-L. Lian, J. Moyne, and D. Tilbury, "Network design consideration for distributed control systems," *IEEE Transactions on Control Systems Technology*, vol. 10, no. 2, pp. 297–307, 2002.
- [70] W. Zhang, M. S. Branicky, and S. M. Phillips, "Stability of networked control systems," *IEEE Control Systems Magazine*, vol. 21, no. 1, pp. 84–99, 2001.
- [71] W.-A. Zhang and L. Yu, "Modelling and control of networked control systems with both network-induced delay and packet-dropout," *Automatica*, vol. 44, no. 12, pp. 3206–3210, 2008.
- [72] Y. Mikheev, V. Sobolev, and E. Fridman, "Asymptotic analysis of digital control systems," *Automation and Remote Control*, vol. 49, pp. 1175–1180, 1988.
- [73] E. Fridman, A. Seuret, and J.-P. Richard, "Robust sampled-data stabilization of linear systems: an input delay approach," *Automatica*, vol. 40, no. 8, pp. 1441–1446, 2004.
- [74] K. Liu and E. Fridman, "Wirtinger's inequality and Lyapunov-based sampled-data stabilization," *Automatica*, vol. 48, no. 1, pp. 102–108, 2012.
- [75] P. Naghshtabrizi, J. P. Hespanha, and A. R. Teel, "Exponential stability of impulsive systems with application to uncertain sampled-data systems," *Systems and Control Letters*, vol. 57, no. 5, pp. 378–385, 2008.
- [76] K. Liu, V. Suplin, and E. Fridman, "Stability of linear systems with general sawtooth delay," *IMA Journal of Mathematical Control and Information*, vol. 27, no. 4, pp. 419–436, 2010.
- [77] K. Liu and E. Fridman, "Networked-based stabilization via discontinuous Lyapunov functionals," *International Journal of Robust and Nonlinear Control*, vol. 22, no. 4, pp. 420–436, 2012.
- [78] M. S. Mahmoud, "Decentralized stabilization of interconnected systems with time-varying delays," *IEEE Transactions on Automatic Control*, vol. 54, no. 11, pp. 2663–2668, 2009.
- [79] A. Seuret and F. Gouaisbaut, "Wirtinger-based integral inequality: application to time-delay systems," *Automatica*, vol. 49, no. 9, pp. 2860–2866, 2013.
- [80] O. M. Kwon, M. J. Park, J. H. Park, S. M. Lee, and E. J. Cha, "Improved results on stability of linear systems with time-varying delays via Wirtinger-based integral inequality," *Journal of the Franklin Institute. Engineering and Applied Mathematics*, vol. 351, no. 12, pp. 5386–5398, 2014.
- [81] M. J. Park, O. M. Kwon, J. H. Park, S. M. Lee, and E. J. Cha, "Stability of time-delay systems via Wirtinger-based double integral inequality," *Automatica*, vol. 55, pp. 204–208, 2015.
- [82] O. M. Kwon, M. J. Park, J. H. Park, and S. M. Lee, "Improvement on the feasible region of H_∞ performance and stability for systems with interval time-varying delays via augmented Lyapunov-Krasovskii functional," *Journal of the Franklin Institute. Engineering and Applied Mathematics*, vol. 353, no. 18, pp. 4979–5000, 2016.
- [83] O. M. Kwon, M. J. Park, J. H. Park, and S. M. Lee, "Stability and stabilization of T-S fuzzy systems with time-varying delays via augmented Lyapunov-Krasovskii functionals," *Information Sciences*, vol. 372, pp. 1–15, 2016.
- [84] H. Dong, Z. Wang, and H. Gao, "Robust H_∞ filtering for a class of nonlinear networked systems with multiple stochastic communication delays and packet dropouts," *IEEE Transactions on Signal Processing*, vol. 58, no. 4, pp. 1957–1966, 2010.
- [85] Y. Liu, Z. Wang, and W. Wang, "Robust reliable control for discrete-time-delay systems with stochastic nonlinearities and multiplicative noises," *Optimal Control Applications and Methods*, vol. 32, no. 3, pp. 285–297, 2011.

Research Article

Consensus Conditions for High-Order Multiagent Systems with Nonuniform Delays

Mengji Shi, Kaiyu Qin, Ping Li, and Jun Liu

School of Aeronautics and Astronautics, University of Electronic Science and Technology of China, Chengdu 611731, China

Correspondence should be addressed to Kaiyu Qin; kyqin@uestc.edu.cn

Received 20 May 2016; Revised 8 October 2016; Accepted 16 October 2016; Published 9 April 2017

Academic Editor: Guido Ala

Copyright © 2017 Mengji Shi et al. This is an open access article distributed under the Creative Commons Attribution License, which permits unrestricted use, distribution, and reproduction in any medium, provided the original work is properly cited.

Consensus of first-order and second-order multiagent systems has been widely studied. However, the convergence of high-order (especially the third-order to the sixth-order) state variables is also ubiquitous in various fields. The paper handles consensus problems of high-order multiagent systems in the presence of multiple time delays. Obtained by a novel frequency domain approach which properly resolves the challenges associated with nonuniform time delays, the consensus conditions for the first-order and second-order systems are proven to be nonconservative, and those for the third-order to the sixth-order systems are provided in the form of simple inequalities. The method revealed in this article is applicable to arbitrary-order systems, and the results are less conservative than those based on Lyapunov approaches, because it roots in sufficient and necessary criteria of stabilities. Simulations are carried out to validate the theoretical results.

1. Introduction

Consensus problems of multiagent systems have found many applications in the fields that hold great promise, including (but not limited to) biosciences, robotics, and computer sciences. Consensus is the agreement regarding a certain quality of interest on specific states of all the agents, which is widely demanded in the engineering applications. The research on consensus problems has lasted for decades. Various techniques are developed to solve consensus problems of numerous multiagent systems [1–23].

This paper addresses the consensus control problems of high-order multiagents systems with nonuniform time delays. One motivation for studying high-order systems is to achieve accurate control of complex motion: for example, when performing consensus motion that requires abrupt change of heading, a team of vehicles should maintain consistency of acceleration (as well as position and velocity) among them by controlling the third-order state (acceleration), while lower-order (first-order and second-order) consensus protocols are usually designed for more regular motion (e.g.,

rectilinear [16] and rotational [23] motion). Besides high-order dynamics [3–9], nonlinearities [1, 2, 24], time delays [8–21, 24, 25] and fuzziness [26, 27] also bring complexities to the control systems, which often lead to difficulties in stability analysis.

A novel frequency-domain-based method is developed to challenge the system complexities and derive the consensus conditions. Comparing to the universal stability analysis tool Lyapunov approaches, frequency domain methods are more possibly conducting to less conservative results as it roots in sufficient and necessary stability criteria. On the other hand, Lyapunov approaches applied in many literatures yield consensus conditions in the form of Linear Matrix Inequalities (LMIs) [7–9], while with frequency domain methods authors of [12–16, 22] as well as this note obtain consensus conditions in the form of inequalities which are more perspicuous and simple to calculate. However, frequency domain methods are limited to linear and time-invariant systems, and consequently most of the aforementioned articles [1–11, 24, 25] especially those coping with nonlinear and high-order systems have adopted Lyapunov

approaches instead. Moreover, both high-order dynamics and nonuniform time delays give rise to dramatic increment of the systems' dimensionality, which makes it a knotty problem. In existing literatures, methods based on the properties of nonnegative matrices [17, 18] and Nyquist stability theories [19–21] are introduced as alternative stability analysis tools.

The main idea of the proposed approach is to transform the high-order systems' dynamics into high-degree polynomials with respect to hypothetically existing imaginary eigenvalues of the systems. By studying the monotonicity of the polynomials and their derivatives, consensus conditions can be figured out in the form of inequalities. The present work first brings out sufficient consensus conditions for the first-order to sixth-order nonuniformly delayed systems which are most likely to apply to practical engineering applications [28]: if all the delays are bounded by a given value and all the parameters agree to corresponding inequalities, the systems can achieve consensus and in addition, for the sake of nonconservativeness, the paper provides stronger conditions for the first-order and second-order systems by thorough derivation: the states converge when all the delays are bounded by a given value but diverge when all the delays exceed that value.

Literature [29] has proposed a high-order nonlinear consensus tracking algorithm with unmeasurable system states which applies to wide-range multiagent systems and proven the achievement of consensus by constructing Lyapunov functions, while time delays are not considered. In [9], Zhang et al. have solved average consensus problem of high-order multiagent system with time-varying delays and provided stability conditions in the form of LMIs via a Lyapunov-Krasovskii approach. The authors of [19] have derived necessary and sufficient consensus conditions for large-scale high-order linear multiagent systems with heterogeneous communication delays by using the generalized Nyquist criterion; however, the derived consensus conditions are set-valued graphical conditions, and inequality conditions are only derived for the first-order system. The previous work in [30] has studied consensus motion of delayed second-order multiagent systems by a nonconservative frequency-domain-based method, while this article will present stationary consensus conditions for more complex high-order multiagent systems.

The remainder of this note is organized as follows: Section 2 states the consensus problem with the help of graph theory; Section 3 presents the main results by demonstrating the stability analysis; Section 4 depicts the selected simulation experiments; Section 5 draws conclusions with future research directions.

2. Problem Statement

This section starts with some definitions and results in graph theory.

Consider an n -agent system. The communication network topology among them is represented by an undirected graph $\mathcal{G}(\mathcal{V}, \mathcal{E}, \mathcal{A})$, which consists of a set of nodes $\mathcal{V} = \{s_i\}$, $i \in \mathcal{I} = \{1, 2, \dots, n\}$, a set of edges $\mathcal{E} \subseteq \mathcal{V} \times \mathcal{V}$, and a weighted

adjacency matrix $\mathcal{A} = [a_{ij}]$, where $a_{ii} = 0$ and $a_{ij} = a_{ji} \geq 0$ (for \mathcal{G} is undirected). $a_{ij} > 0$ if and only if there exists an edge $e_{ij} \in \mathcal{E}$ between the i th and j th nodes, which implies that they can get information from each other. The set of neighbors of node s_i is denoted by $N_i \triangleq \{s_j \in \mathcal{V} : e_{ji} \in \mathcal{E}\}$. The Laplacian corresponding to the graph \mathcal{G} is defined as $L_\sigma \triangleq [\ell_{ij}]$, where $\ell_{ii} = \sum_{j=1}^n a_{ij}$ and $\ell_{ij} = -a_{ij}$, $i \neq j$. A path is a sequence of indexed edges $e_{k_1 k_2}, e_{k_2 k_3}, \dots$, where $e_{k_i k_{i+1}} \in \mathcal{E}$. If there is a path between every pair of nodes in graph \mathcal{G} , the graph is said to be connected. The following lemma is given by [31].

Lemma 1. *If the undirected graph \mathcal{G} is connected, then its Laplacian L_σ has one singleton zero eigenvalue (with eigenvector $\mathbf{1}$), and the rest $n - 1$ eigenvalues of L_σ are all positive.*

Consider an l th-order multiagent system consisting of n agents. The dynamics of the i th agent ($i \in \mathcal{I}$) is

$$\begin{aligned} \dot{\psi}_i^{(0)}(t) &= \psi_i^{(1)}(t), \\ &\vdots \\ \dot{\psi}_i^{(l-2)}(t) &= \psi_i^{(l-1)}(t), \\ \dot{\psi}_i^{(l-1)}(t) &= u_i(t), \end{aligned} \quad (1)$$

where $\psi_i^{(k)} \in \mathbb{R}$ is the k th state variable of the i th agent, $k = 0, 1, \dots, l - 1$, and $u_i(t) \in \mathbb{R}$ is the control input. Let $\psi_i \triangleq [\psi_i^{(0)}, \psi_i^{(1)}, \dots, \psi_i^{(l-1)}]^T$ be the state vector of the i th agent; we assume that the initial conditions are $\psi_i^{(0)}(s) = \psi_i^{(0)}(0)$ and $\psi_i^{(k)}(s) = \psi_i^{(k)}(0) = 0$, $k = 1, 2, \dots, l - 1$, for $s \in (-\infty, 0]$. The control input $u_i(t)$ is said to solve the consensus problem asymptotically, if and only if $\lim_{t \rightarrow +\infty} [\psi_i(t) - \psi_j(t)] = 0$ for all $i, j \in \mathcal{I}$.

In [8], a discrete-time control input was introduced as

$$\begin{aligned} u_i(k) &= -\sum_{j=1}^{l-1} p_j \psi_i^{(j)}(k) \\ &\quad - \sum_{s_j \in N_i(k)} a_{ij}(k) [\psi_i^{(0)}(k) - \psi_j^{(0)}(k - \tau_{ij})]. \end{aligned} \quad (2)$$

In this paper, we introduce an continuous-time consensus algorithm for system (1) with multiple time delays, and the input delays are supposed to occur. The protocol is

$$\begin{aligned} u_i(t) &= -\sum_{j=1}^{l-1} p_j \psi_i^{(j)}(t) \\ &\quad - \sum_{s_j \in N_i} a_{ij} [\psi_i^{(0)}(t - \tau_{ij}) - \psi_j^{(0)}(t - \tau_{ij})], \end{aligned} \quad (3)$$

for any $i \in \mathcal{I}$, where $p_j > 0$ for $j = 1, 2, \dots, l - 1$; $a_{ij} > 0$ denotes the edge weight, and $\tau_{ij} = \tau_{ji}$ is the time delay for the i th agent to get the state information of the j th agent. We assume that the system has M different time delays, denoted by $\tau_m \in (\tau_{ij}, i, j \in \mathcal{I} (m = 1, 2, \dots, M))$.

Let $\psi(t) \triangleq [\psi_1(t), \psi_2(t), \dots, \psi_n(t)]$, and

$$A \triangleq \begin{bmatrix} 0 & 1 & 0 & 0 & 0 \\ 0 & 0 & 1 & 0 & 0 \\ \vdots & \ddots & \ddots & \ddots & 0 \\ 0 & \vdots & 0 & 0 & 1 \\ 0 & -p_1 & \dots & -p_{l-2} & -p_{l-1} \end{bmatrix} \in \mathbb{R}^{l \times l}, \quad (4)$$

$$B \triangleq \begin{bmatrix} 0 & 0 & \dots & 0 \\ \vdots & \vdots & \vdots & \vdots \\ 0 & 0 & \dots & 0 \\ 1 & 0 & \dots & 0 \end{bmatrix} \in \mathbb{R}^{l \times l}.$$

Under the control input given by (3), the network dynamics of the multiagent system becomes

$$\dot{\psi}(t) = (I_n \otimes A) \psi(t) - \sum_{m=1}^M (L_{\sigma m} \otimes B) \psi(t - \tau_m) \quad (5)$$

with the initial condition $\psi(s) = \psi(0)$, $s \in (-\infty, 0]$, where $L_{\sigma m}$ denotes the Laplacian of a subgraph associated with the delay τ_m . Clearly, $L_{\sigma} = \sum_{m=1}^M L_{\sigma m}$. If all the time delays are equal to zero, system (5) could be rewritten as

$$\dot{\psi}(t) = (I_n \otimes A - L_{\sigma} \otimes B) \psi(t). \quad (6)$$

This paper assumes that the graph \mathcal{G} is always connected and undirected.

3. Main Results

The following lemma presents a sufficient condition for the stability of high-degree polynomials given by [32], which is helpful in the present work.

Lemma 2. Consider a polynomial $f(x) = a_0 + a_1x + \dots + a_nx^n$, where $a_k > 0$, $k = 0, 1, \dots, n$, $n \geq 3$, with coefficients of determination defined as

$$\mu_i \triangleq \frac{a_{i-1}a_{i+2}}{a_i a_{i+1}}, \quad (7)$$

if all the coefficients of determination satisfy that $\mu_i < \beta/2 \approx 0.4655$, where $i = 1, 2, \dots, n-2$, $n \geq 3$, and β is the only real root of equation

$$\frac{\beta^3}{4} + \beta^2 + \beta - 2 = 0; \quad (8)$$

then all the roots of $f(x) = 0$ have negative real parts.

Let

$$\Phi \triangleq I_n \otimes A - L_{\sigma} \otimes B \quad (9)$$

and suppose that the eigenvalues of L_{σ} are $0 = \lambda_1 < \lambda_2 \leq \lambda_3 \leq \dots \leq \lambda_n$ according to Lemma 1.

Assumption 3. Assume for $l \geq 3$ that all $p_j > 0$ ($j = 1, 2, \dots, l-1$) satisfy the following:

$$\begin{aligned} p_{l-1}p_{l-2} &> 3p_l p_{l-3} \\ p_{l-2}p_{l-3} &> 3p_{l-1}p_{l-4} \\ &\vdots \\ p_3p_2 &> 3p_4p_1 \\ p_2p_1 &> 2.15p_3\lambda_n, \end{aligned} \quad (10)$$

where $p_l = 1$ and λ_n is the largest eigenvalue of L_{σ} .

Under Assumption 3, the following lemma can be proven.

Lemma 4. Matrix Φ has a singleton zero eigenvalue and all other eigenvalues have negative real parts if Assumption 3 is satisfied.

Proof. According to Lemma 1, there exists an orthogonal matrix W , such that

$$W^T L_{\sigma} W = \text{diag}\{0, \lambda_2, \dots, \lambda_n\}, \quad (11)$$

and then it follows that

$$\begin{aligned} (W \otimes I_l)^T \Phi (W \otimes I_l) \\ = \text{diag}\{A, A - \lambda_2 B, \dots, A - \lambda_n B\}. \end{aligned} \quad (12)$$

Through simple calculations, the eigenpolynomial of $(A - \lambda_j B)$ could be obtained; then we get

$$\det(sI_l - A + \lambda_j B) = s^l + \sum_{i=1}^{l-1} p_i s^i + \lambda_j = 0. \quad (13)$$

To simplify the following statements, let $p_l = 1$, and (13) could be written as

$$\sum_{i=1}^l p_i s^i + \lambda_j = 0. \quad (14)$$

For the first-order system, since $l = 1$, it is evident that $-\lambda_j$ are the eigenvalues of the system; thus the lemma is proven. For the second-order system, (14) becomes $s^2 + p_1 s + \lambda_j = 0$ and its roots are

$$\frac{-p_1 \pm \sqrt{p_1^2 - 4\lambda_j}}{2}. \quad (15)$$

If $p_1^2 < 4\lambda_j$, the real part of (15) is $-p_1/2 < 0$, and when $p_1^2 \geq 4\lambda_j$, (15) apparently is a pair of nonpositive real numbers, and the bigger one equals zero if and only if $\lambda_j = 0$; then the lemma is proven.

When $l \geq 3$, note that $p_i > 0$ for $i = 1, 2, \dots, l$, and λ_n is the largest eigenvalue of L_{σ} . It is apparent that $3 > 2.15 > 2.1482 \approx 1/0.4655$; according to Lemma 2, (10) is a group of more conservative condition, which ensures that all the roots of (14) have negative real parts except that there exists one singleton zero root for $\lambda_j = 0$. Thus, matrix Φ has a singleton zero eigenvalue and all its other $n * l - 1$ eigenvalues have negative real parts. \square

Remark 5. Lemma 4 has shown that each of the nondelayed multiagent systems given by (6) has all its eigenvalues on the open LHP except one equals zero. That implies that system (6) is stable, and all the states of each agent will reach a common value. The existence of the only zero root indicates that only the first-order state variable of each agent reaches a value that is decided by the initial state and all the other high-order state variables return to zero at last; that is, if all $\tau_m = 0$, multiagent system (5) will reach consensus.

By analyzing the effect of nonuniform time delays on the stability of the systems, we will give a proof to the ensuing theorem.

Theorem 6. Consider l th-order ($l = 1, 2, \dots, 6$) system given by (5) that satisfies Assumption 3, and the following inequalities (16), (17), and (18) are satisfied for $l = 4, 5, 6$, respectively:

$$p_2 > \frac{\lambda_n}{\sqrt{p_3 p_1}} + 2 \frac{p_1}{p_3}. \quad (16)$$

$$p_1 > \frac{1}{4} \left(\frac{p_2}{p_4} \right)^2 \quad (17)$$

$$p_1 > \max \left\{ \frac{p_5}{4} \left(\frac{p_2}{p_4} \right)^2, \lambda_n \sqrt{\frac{3}{p_4}} \right\}. \quad (18)$$

Define functions $\theta_l(\omega)$ and $T_l(\omega)$ ($l = 1, 2, \dots, 6$) as follows:

$$\theta_l(\omega) \triangleq \arg [F_l(\omega)] = \arg \left[-\sum_{i=1}^l (-j\omega)^i p_i \right] \quad (19)$$

$$\in (0, 2\pi],$$

$$T_l(\omega) \triangleq \frac{1}{\omega} \theta_l(\omega), \quad (20)$$

where $F_l(\omega)$ is defined in (27). If all τ_m satisfy $\tau_m < \bar{\tau}$ for l th-order multiagent system, where

$$\bar{\tau}$$

$$= \begin{cases} T_l(\lambda_n) & l = 1 \\ T_l(\sqrt{\lambda_n/p_2}) & l = 2, 3 \\ T_l(\sqrt{2\lambda_n/p_2}) & l = 4 \\ \min \{T_l(\sqrt{2\lambda_n/p_2}), T_l(\sqrt{p_{l-2}/(l-3)})\} & l = 5, 6, \end{cases} \quad (21)$$

then control input (3) can solve the consensus problem of system (5).

Proof. Consider the network of high-order multiagents with nonuniform time delays. Let $\Psi(s) = G_\tau^{-1} \Psi(0)$, where $\Psi(s)$ is the Laplace transform of $\psi(t)$, and

$$G_\tau(s) = sI_{n \times l} - (I_n \otimes A) + \sum_{m=1}^M (L_{\sigma m} \otimes B) e^{-\tau_m s}. \quad (22)$$

According to the foregoing discussions, to study the stability of the delayed system, we only need to investigate the values

of τ_m that guarantee the existence of nonzero roots of $G_\tau(s)$ on imaginary axis, which represents the crossing of the characteristic roots from the stable region to the unstable one. The roots of characteristic polynomials such as $G_\tau(s)$ are hereinafter referred to as “the eigenvalues of the system.”

Suppose $s = j\omega \neq 0$ is an imaginary root of $G_\tau(s)$, and $u = u_1 \otimes [1, 0, \dots, 0]^T + u_2 \otimes [0, 1, \dots, 0]^T + \dots + u_l \otimes [0, 0, \dots, 1]^T$ is a corresponding eigenvector, where $\|u\| = 1$, $u_i \in \mathbb{C}^n$, $i = 1, 2, \dots, n$. Then we have

$$\left[j\omega I_{n \times l} - (I_n \otimes A) + \sum_{m=1}^M (L_{\sigma m} \otimes B) e^{-j\omega \tau_m} \right] u = 0. \quad (23)$$

Note that all the complex roots of each $G_\tau(s)$ appeared in conjugated pairs; we only need to study the situation that $\omega_q > 0$. Since all of the first $l-1$ elements of the vector obtained by calculating the left part of (23) are equal to zero, we get

$$j\omega u_i = u_{i+1}, \quad (24)$$

for all $i = 1, 2, \dots, l-1$. Multiplied by u^* (the conjugate transpose of u) on the left side of the left part of (23), and with (24) substituted, we obtain

$$\sum_{m=1}^M \alpha_m e^{-j\omega \tau_m} + \sum_{i=1}^l (j\omega)^i p_i = 0, \quad (25)$$

where $p_i = 1$, and

$$\alpha_m = \frac{u^* (L_{\sigma m} \otimes I_l) u}{u^* u}. \quad (26)$$

Rewrite (25) as

$$\sum_{m=1}^M \alpha_m e^{j\omega \tau_m} = -\sum_{i=1}^l (-j\omega)^i p_i \triangleq F_l(\omega). \quad (27)$$

Take modulus of both sides of (27); then, we have

$$M_l(\omega) \triangleq |F_l(\omega)| = \left| \sum_{m=1}^M \alpha_m e^{j\omega \tau_m} \right| \leq \left| \sum_{m=1}^M \alpha_m \right| \quad (28)$$

$$= \frac{u^* (L_\sigma \otimes I_l) u}{u^* u} \leq \lambda_n.$$

Another necessary condition of (27) is

$$\arg \left(\sum_{m=1}^M \alpha_m e^{j\omega \tau_m} \right) = \arg [F_l(\omega)] = \theta_l(\omega). \quad (29)$$

As $\omega \tau_m > 0$, $\theta_l(\omega)$ should be discussed in the positive interval $(0, 2\pi]$. From (29), it is obvious that

$$\theta_l(\omega) = \arg \left(\sum_{m=1}^M \alpha_m e^{j\omega \tau_m} \right) \leq \max \{\omega \tau_m\}. \quad (30)$$

Define

$$R_l(\omega) \triangleq \frac{\text{Im} [F_l(\omega)]}{\text{Re} [F_l(\omega)]} = \tan [\theta_l(\omega)], \quad (31)$$

where $\text{Im}(c)$ and $\text{Re}(c)$ denote the imaginary part and real part of the complex number c , respectively. $R_l(\omega)$ is an access to $\theta_l(\omega)$.

Consider the first-order system; then, we have $F_1(\omega) = 0 + j\omega$ and $R_1(\omega) = \omega/0$. It is apparent that $\theta_1(\omega) = \pi/2$, and $M_1(\omega) = \omega$; according to (28), we should only consider $\omega \leq \lambda_n$; if we set all $\tau_m < \bar{\tau} = T_1(\lambda_n) = \pi/(2\lambda_n)$, then

$$\omega\tau_m < \lambda_n\bar{\tau} = \pi/2 = \theta_1(\omega), \quad (32)$$

$$\begin{aligned} R'_2 &= \frac{-p_1 p_2}{(p_2 \omega)^2} < 0, \\ R'_3 &= \frac{-p_2 p_3 \omega^2 - p_1 p_2}{(p_2 \omega)^2} < 0, \\ R'_4 &= \frac{-p_3 p_4 \omega^4 - (p_2 p_3 - 3p_1 p_4) \omega^2 - p_1 p_2}{(p_2 \omega - p_4 \omega^3)^2} < 0, \\ R'_5 &= \frac{-p_4 p_5 \omega^6 - (p_3 p_4 - 3p_2 p_5) \omega^4 - (p_2 p_3 - 3p_1 p_4) \omega^2 - p_1 p_2}{(p_2 \omega - p_4 \omega^3)^2} < 0, \\ R'_6 &= \frac{-p_5 p_6 \omega^8 - (p_4 p_5 - 3p_3 p_6) \omega^6 - (p_3 p_4 - 3p_2 p_5 + 5p_1 p_6) \omega^4 - (p_2 p_3 - 3p_1 p_4) \omega^2 - p_1 p_2}{(p_2 \omega - p_4 \omega^3)^2} < 0. \end{aligned} \quad (33)$$

$R'_l < 0$ means that $R_l = \tan[\theta_l(\omega)]$ are monotonically decreasing with the growth of ω . Then it can be deduced that the arguments $\theta_l(\omega)$ also decrease monotonically and continuously because the values of $F_l(\omega)$ vary smoothly. Evidently, we have

$$\lim_{\omega \rightarrow 0^+} R_l = \frac{p_1 \omega + o(\omega)}{p_2 \omega^2 + o(\omega)} = +\infty, \quad (34)$$

for $l \geq 2$, which implies that the arguments $\theta_l(\omega)$ start at $\pi/2$ when $\omega \rightarrow 0^+$.

By investigating the locus of $F_6(\omega)$ on a complex plane, we have found that the value of the argument $\theta_6(\omega)$ first falls from $\pi/2$, tending to 0; as the trajectory of $F_6(\omega)$ passes from the first quadrant to the fourth, $\theta_6(\omega)$ does not really turn negative but jumps to 2π instead and then it falls again, without second “jump” to perform. Similar phenomena occur in the other high-order systems when $l < 6$; in each system, the argument $\theta_l(\omega)$ performs a jump at most once and no jumps for some of these systems, such as the second-order system, because the real and imaginary parts of $F_2(\omega)$ are always positive when $\omega > 0$. The trajectories of $F_2(\omega)$ and $F_6(\omega)$ on the complex plane are shown in Figure 1 to give evidence of the variation on their arguments. For those whose arguments perform jumps, we consider the value of each $\theta_l(\omega)$ in two continuous intervals: $(0, \pi/2)$ and $(0, 2\pi]$.

For $l = 2, 3$, if $\omega > \sqrt{\lambda_n/p_2}$ then $\text{Re}[F_l(\omega)] = p_2 \omega^2 > \lambda_n$ and $M_l(\omega) > \lambda_n$, which we do not want. Thus, $\theta_l(\sqrt{\lambda_n/p_2})$ is the minimum to consider. Then $p_1 \omega - p_3 \omega^3 > 0$ holds when

which contradicts (30). Then when all $\tau_m < \bar{\tau}$, the first-order system is impossible to have an imaginary eigenvalue which presents the first contact of the eigenvalues from the stable region to the unstable one. Hence the system is still stable then, and it can reach consensus, and the theorem is proven for $l = 1$.

Unlike $\theta_1(\omega)$, $\theta_l(\omega)$ ($l \geq 2$) are not a fixed value. But we have found that the derivatives of $R_l(\omega)$ ($2 \leq l \leq 6$) listed below are negative values when Assumption 3 is applied:

$l = 3$, which implies $\theta_3(\omega) \in (0, \pi/2)$. Setting all $\tau_m < \bar{\tau} = T_1(\sqrt{\lambda_n/p_2})$, we have

$$\omega\tau_m < \sqrt{\frac{\lambda_n}{p_2}} T_1 \left(\sqrt{\frac{\lambda_n}{p_2}} \right) = \theta_l \left(\sqrt{\frac{\lambda_n}{p_2}} \right) < \theta_l(\omega), \quad (35)$$

which contradicts (30); then by the same idea of the proof for the first-order system, the theorem for $l = 2, 3$ is proven.

Investigate the following parabola when $\omega \in [\sqrt{2\lambda_n/p_2}, \sqrt{p_2/p_4 - 2\lambda_n/p_2}]$:

$$\xi(\omega) = -p_4 \omega^4 + p_2 \omega^2 - \lambda_n. \quad (36)$$

Apparently, its maximal value comes at the point when $\omega = \sqrt{p_2/2p_4}$. According to the symmetry of parabolas, $\xi(\sqrt{2\lambda_n/p_2}) = \xi(\sqrt{p_2/p_4 - 2\lambda_n/p_2})$ are the minima of $\xi(\omega)$. According to Assumption 3 that $p_2/p_4 > 3p_1/p_3 > 6\lambda_n/p_2$, which implies $p_2^2 > 4\lambda_n p_4$, we have

$$\begin{aligned} \xi \left(\sqrt{2\frac{\lambda_n}{p_2}} \right) &= 2\lambda_n - 4p_4 \frac{\lambda_n^2}{p_2^2} - \lambda_n = \frac{\lambda_n}{p_2^2} (p_2^2 - 4\lambda_n p_4) \\ &> 0. \end{aligned} \quad (37)$$

Thus, $\xi(\omega) \geq \xi(\sqrt{2\lambda_n/p_2}) > 0$. Then we have $M_l(\omega) \geq \text{Re}[F_l(\omega)] \geq p_2 \omega^2 - p_4 \omega^4 > \lambda_n$ for $l \geq 4$, when $\omega \in [\sqrt{2\lambda_n/p_2}, \sqrt{p_2/p_4 - 2\lambda_n/p_2}]$.

Let $F_l(\omega_0)$ be the first contact of its trajectory from the first quadrant to the fourth, as is shown in Figure 1. We analyze ω

in two intervals: $(0, \omega_0)$ and $[\omega_0, +\infty)$. Obviously, ω_0 is the smallest positive real root of $\text{Im}[F_l(\omega_0)] = 0$.

Consider the interval $\omega < \omega_0$. If $\omega_0 \in (\sqrt{2\lambda_n/p_2}, \sqrt{p_2/p_4 - 2\lambda_n/p_2})$, then $\theta_l(\sqrt{2\lambda_n/p_2})$ would be smaller than the minimal possible value of $\theta_l(\omega)$ to satisfy (27), because $M(\omega) > \lambda_n$ if $\sqrt{2\lambda_n/p_2} < \omega < \omega_0$.

Taking the fourth-order system into account, we have

$$\omega_0 = \sqrt{\frac{p_1}{p_3}} \in \left(\sqrt{\frac{2\lambda_n}{p_2}}, \sqrt{\frac{p_2}{p_4} - \frac{2\lambda_n}{p_2}} \right). \quad (38)$$

According to (16), one can obtain

$$\begin{aligned} & \left| \text{Im} \left[F_4 \left(\sqrt{\frac{p_2}{p_4} - \frac{2\lambda_n}{p_2}} \right) \right] \right| \\ &= p_3 \sqrt{\frac{p_2}{p_4} - \frac{2\lambda_n}{p_2}} \left(\frac{p_2}{p_4} - 2\frac{\lambda_n}{p_2} - \frac{p_1}{p_3} \right) \\ &> p_3 \sqrt{\frac{p_1}{p_3}} \left(\frac{p_2}{p_4} - 2\frac{p_1}{p_3} \right) = \sqrt{p_3 p_1} \left(\frac{p_2}{p_4} - 2\frac{p_1}{p_3} \right) \\ &> \lambda_n, \end{aligned} \quad (39)$$

where $p_4 = 1$. Because $|\text{Im}[F_4(\omega)]| = p_3\omega^3 - p_1\omega$ is monotonically increasing when $\omega \geq \omega_0$, we have $|\text{Im}[F_4(\omega)]| >$

$|\text{Im}[F_4(\sqrt{p_2/p_4 - 2\lambda_n/p_2})]| > \lambda_n$ for $\omega > \sqrt{p_2/p_4 - 2\lambda_n/p_2}$. Then we know that $M_4(\omega) > \lambda_n$ holds if $\omega > \sqrt{2\lambda_n/p_2}$. The only situation that needs to be considered is $\omega \leq \sqrt{2\lambda_n/p_2}$, where $\theta_l(\sqrt{2\lambda_n/p_2})$ is the smallest value of $\theta_l(\omega)$; if we set all $\tau_m < \bar{\tau} = T_4(\sqrt{2\lambda_n/p_2})$, it can be obtained that

$$\omega \tau_m < \sqrt{\frac{2\lambda_n}{p_2}} T_l \left(\sqrt{\frac{2\lambda_n}{p_2}} \right) = \theta_l \left(\sqrt{\frac{2\lambda_n}{p_2}} \right) < \theta_l(\omega), \quad (40)$$

which brings about the impossibility of (30) and provides the fourth-order system with consensus achievement.

For $l = 5, 6$, $\text{Im}[F_l(\omega)] = p_1\omega - p_3\omega^3 + p_5\omega^5$, then

$$\omega_0 = \sqrt{\frac{p_3 - \sqrt{p_3^2 - 4p_1p_5}}{2p_5}}. \quad (41)$$

Comparing ω_0^2 and $p_2/p_4 - 2\lambda_n/p_2$, we have

$$\begin{aligned} & \left(\frac{p_2}{p_4} - 2\frac{\lambda_n}{p_2} \right) - \left(\frac{p_3 - \sqrt{p_3^2 - 4p_1p_5}}{2p_5} \right) \\ &= \sqrt{\left(\frac{p_3}{2p_5} \right)^2 - \frac{p_1}{p_5}} - \left(\frac{p_3}{2p_5} - \frac{p_2}{p_4} + 2\frac{\lambda_n}{p_2} \right). \end{aligned} \quad (42)$$

According to (17) and (18), $4 - p_5p_2^2/p_1p_4^2 > 0$, so that

$$\begin{aligned} & \left[\left(\frac{p_3}{2p_5} \right)^2 - \frac{p_1}{p_5} \right] - \left(\frac{p_3}{2p_5} - \frac{p_2}{p_4} + 2\frac{\lambda_n}{p_2} \right)^2 \\ &= \frac{p_1}{p_5} \left[\left(2\frac{p_2p_3}{p_1p_4} - 6 \right) + 4\frac{p_5\lambda_n}{p_1p_2} \left(\frac{p_2}{p_4} - \frac{\lambda_n}{p_2} \right) + \left(4 - \frac{p_5p_2^2}{p_1p_4^2} \right) + \left(1 - 2\frac{p_3\lambda_n}{p_1p_2} \right) \right] > 0 \end{aligned} \quad (43)$$

under Assumption 3. Thus (42) is also positive, which means $\omega_0 < \sqrt{p_2/p_4 - 2\lambda_n/p_2}$. When $\omega < \omega_0$, if we set all $\tau_m < T_l(\sqrt{2\lambda_n/p_2})$, for $l = 5, 6$, (30) is impossible.

Consider the interval $\omega \geq \omega_0$. Evidently, when $\omega \geq \sqrt{p_3/2} > \sqrt{p_2/p_4}$, $|\text{Re}[F_5(\omega)]| = p_4\omega^4 - p_2\omega^2$ is monotonically increasing. According to Assumption 3, we have $p_2p_3 > 18\lambda_n$. Then

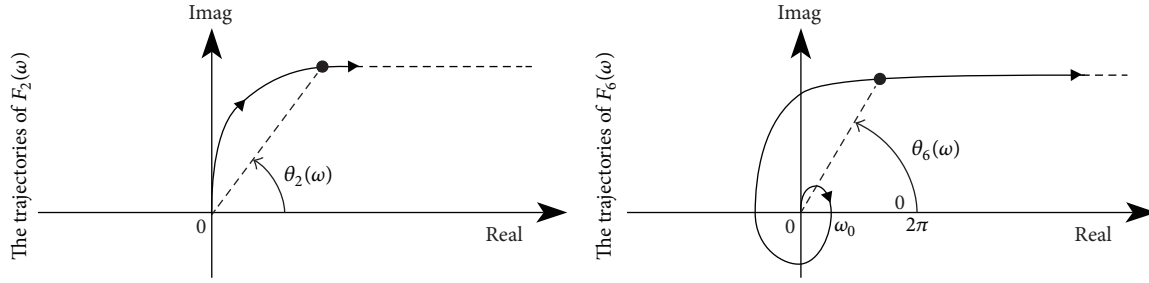
$$\begin{aligned} & \left| \text{Re} \left[F_5 \left(\sqrt{\frac{p_3}{2}} \right) \right] \right| = \frac{p_4p_3^2}{4} - \frac{p_2p_3}{2} > \frac{3p_2p_3}{4} - \frac{p_2p_3}{2} \\ &= \frac{p_2p_3}{4} > \lambda_n. \end{aligned} \quad (44)$$

Therefore, all $\tau_m < T_l(\sqrt{p_3/2})$ would make (30) impossible when $\omega \geq \omega_0$. As is described in Theorem 6, if all $\tau_m < \min\{T_l(\sqrt{2\lambda_n/p_2}), T_l(\sqrt{p_3/2})\}$, the consensus problem of the fifth-order system is solved.

Likewise, for $l = 6$, according to (18) we have

$$\begin{aligned} & \text{Re} \left[F_6 \left(\sqrt{\frac{p_4}{3}} \right) \right] - \lambda_n \\ &= \sqrt{\frac{p_4}{3}} \left[p_1 - p_3\frac{p_4}{3} + p_5\left(\frac{p_4}{3}\right)^2 \right] - \lambda_n \\ &= \left(\sqrt{\frac{p_4}{3}} \right)^3 \left[\frac{1}{3}(p_5p_4 - 3p_3) \right] + \left(p_1\sqrt{\frac{p_4}{3}} - \lambda_n \right) \\ &> 0; \end{aligned} \quad (45)$$

when $\omega > \sqrt{p_4/3} > \sqrt{p_3/p_5}$, $\text{Re}[F_6(\omega)]$ is a monotonically increasing function. Since $\text{Re}[F_6(\sqrt{p_4/3})] > \lambda_n$ is positive already, $M_6(\omega)$ would be further greater than λ_n as the growth of ω has passed through $\sqrt{p_4/3}$ where the situation should be ignored. Consequently, if all $\tau_m < \min\{T_l(\sqrt{2\lambda_n/p_2}), T_l(\sqrt{p_4/3})\}$, the sixth-order system is stable, and the theorem is proven out. \square

FIGURE 1: The trajectories of $F_2(\omega)$ and $F_6(\omega)$ on the complex plane.

Remark 7. Despite the fact that it is difficult to present a general solution in the form of inequality to consensus problems of all high-order multiagent systems because the monotonicity of each high-degree polynomial that the solution relies on requires specialized derivation to figure out, the process of deriving the consensus conditions for the first-to-sixth-order systems has demonstrated a general approach, with which one can work out consensus conditions for an arbitrary-order system. Moreover, by further calculation, we provide stronger consensus conditions for the first-order and second-order multiagent systems in the following theorem.

Theorem 8. Consider the first-order and second-order multiagent system (5) with the control input (3) ($l = 1, 2$); then, the systems reach consensus if all the delays $\tau_m < \bar{\tau}_l$, where

$$\begin{aligned} \bar{\tau}_1 &= \frac{\pi}{2\lambda_n}, \\ \bar{\tau}_2 &= \sqrt{\frac{2}{\sqrt{p_1^4 + 4\lambda_n^2} - p_1^2}} \cdot \arctan\left(\sqrt{\frac{2p_1^2}{\sqrt{p_1^4 + 4\lambda_n^2} - p_1^2}}\right). \end{aligned} \quad (46)$$

Moreover, if all the delays $\tau_m \geq \bar{\tau}_l$, the systems will be unstable, and the agents will fail to reach consensus.

Proof. For the first-order multiagent system, we have already proven in Theorem 6 that $\tau_m < \bar{\tau}_1$ is a sufficient condition for the system to reach consensus. If all $\tau_m = \bar{\tau}_1$, $j\lambda_n$ is the imaginary eigenvalue and its corresponding eigenvector u is the one ensuring $|\sum_{m=1}^M \alpha_m| = \lambda_n \triangleq \bar{\omega}_1$. With these values substituted into (27) ($l = 1$), the equation

$$\sum_{m=1}^M \alpha_m e^{j\bar{\omega}_1 \bar{\tau}_1} = F_1(\bar{\omega}_1) \quad (47)$$

holds true; that is, $\bar{\tau}_1$ is the “delay margin” equal to which the delays of the first-order system present the first contact of the eigenvalues from the stable region to the unstable one. When all the delays exceed the delay margin, the systems will be unstable, because there then exist eigenvalues in the unstable region (the RHP). The instabilities become stronger and the delays get greater distances exceeding the delay margin.

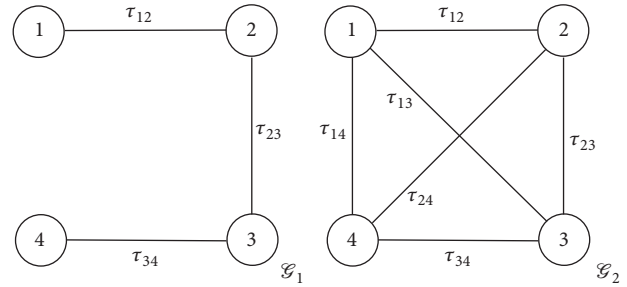


FIGURE 2: Two communication topologies of the 4-agent system.

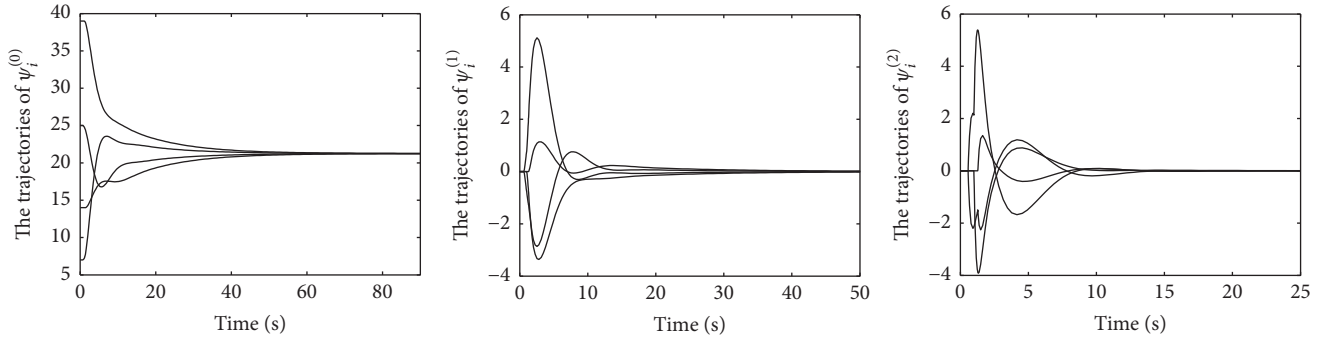
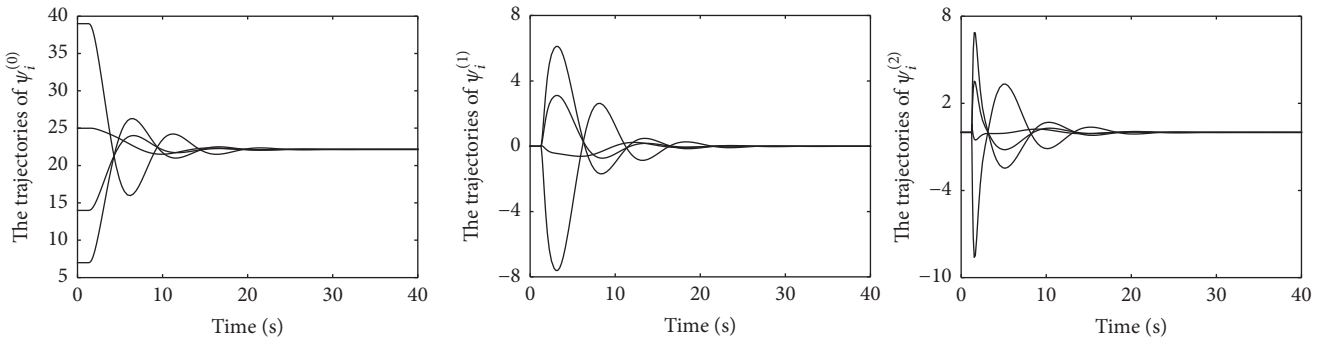
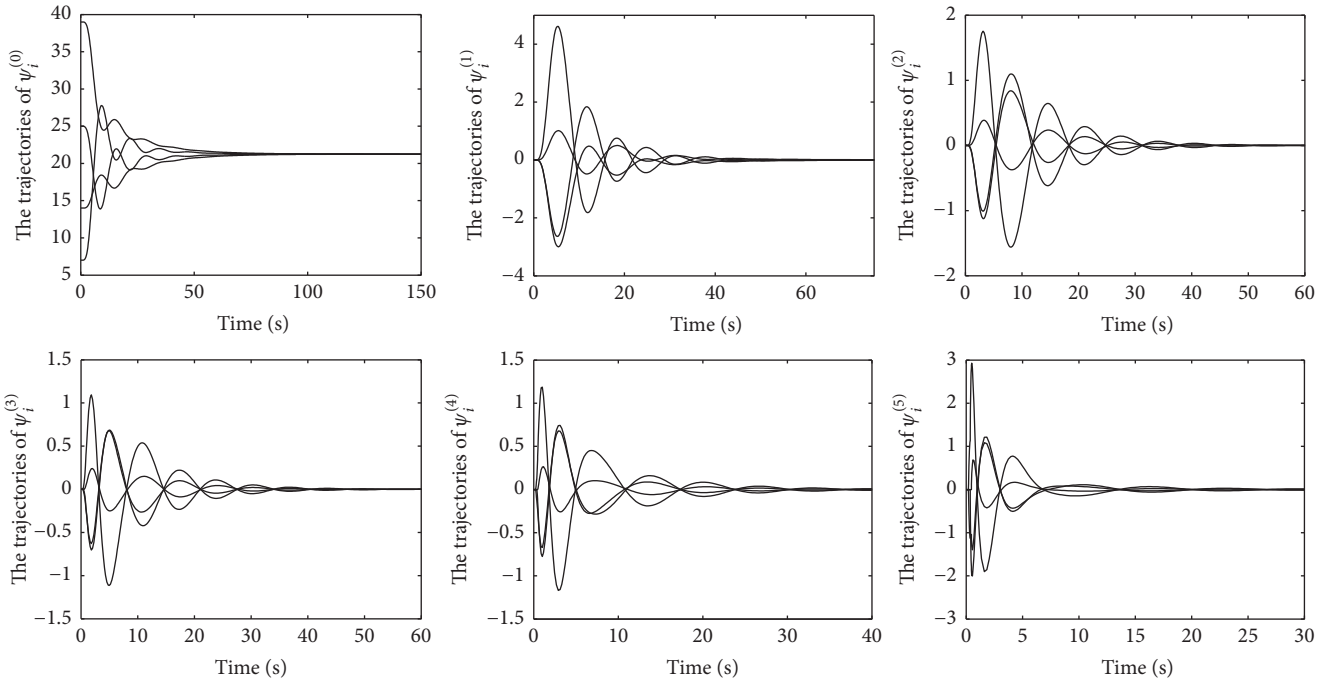
For $l = 2$, $M_2(\omega) = \sqrt{\omega^4 + p_1^2 \omega^2}$. Let $\omega^* = \sqrt{(\sqrt{p_1^4 + 4\lambda_n^2} - p_1^2)/2}$ be the only positive root of $M_2(\omega) = \lambda_n$; thus $M_2(\omega) \leq \lambda_n$ as long as $\omega \leq \omega^*$. Owing to the decline of $\theta(\omega)$, we can set all $\tau_m < \theta(\omega^*)/\omega^* = \bar{\tau}_2$ to avoid the possibility of (27) ($l = 2$). Therefore the sufficiency of the condition has been proven. By the same principle as that for the first-order system, $\bar{\tau}_2$ is also the delay margin bringing about the failure of the system to reach consensus. \square

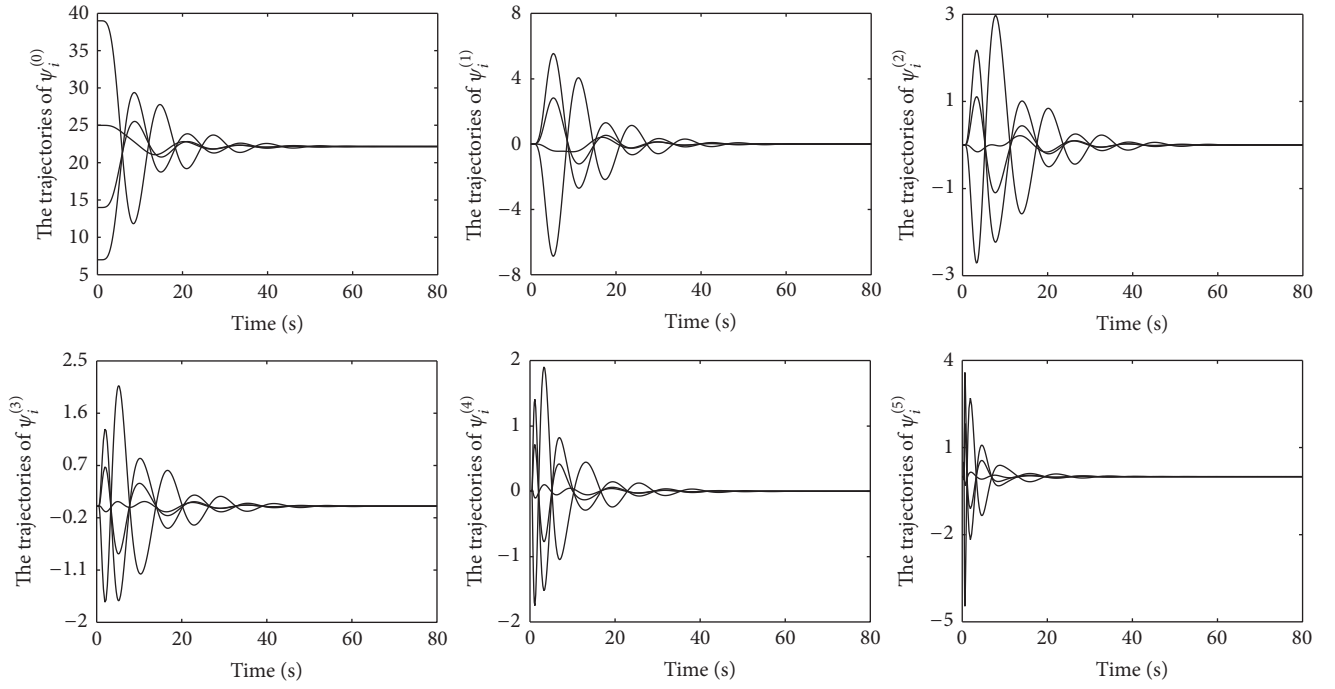
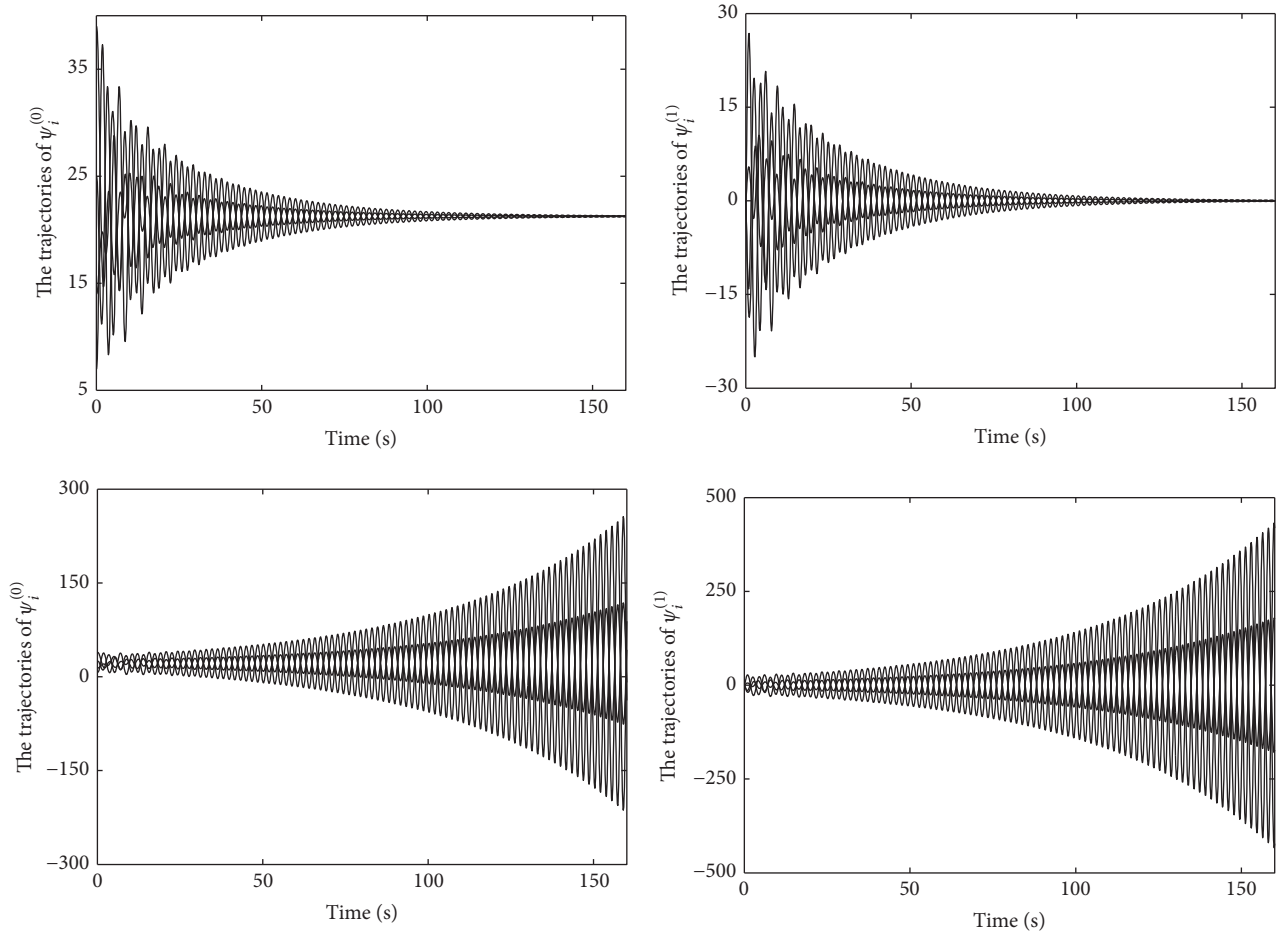
4. Numerical Simulations

In this section, some simulations are provided to illustrate the theoretical results obtained by the previous analysis.

Consider a multiagent system consisting of 4 agents. Figure 2 shows two different communication topologies described with undirected graphs \mathcal{G}_1 and \mathcal{G}_2 , respectively. With three different time delays on each connection, \mathcal{G}_1 presents the simplest connected topology, while \mathcal{G}_2 having six different time delays displays full connectivity. All the delays are marked with τ_{ij} , where i and j are the indices of the connected agents. Suppose the weight of each edge on both graphs is 1; then, for \mathcal{G}_1 , $\lambda_n \approx 3.4142$, and, for \mathcal{G}_2 , $\lambda_n = 4$. Selected experiments will be carried out to validate the obtained results on 4-agent systems with both topologies illustrated by \mathcal{G}_1 and \mathcal{G}_2 .

For a third-order multiagent system with simply connected graph \mathcal{G}_1 , set $p_1 = 9$ and $p_2 = 6$; thus $\bar{\tau} = 1.43$ according to Theorem 6. Let $\tau_{12} = 1.42$, $\tau_{23} = 1.40$, and $\tau_{34} = 1.38$. Seen from the simulation results shown in Figure 3, it is apparent that agents have reached consensus. And for the system with topology \mathcal{G}_2 showing full connectivity, let $p_1 = 9$

FIGURE 3: The trajectories of agents in the third-order system (the topology is \mathcal{T}_1).FIGURE 4: The trajectories of agents in the third-order system (the topology is \mathcal{T}_2).FIGURE 5: The trajectories of agents in the sixth-order system (the topology is \mathcal{T}_1).

FIGURE 6: The trajectories of agents in the sixth-order system (the topology is \mathcal{G}_2).FIGURE 7: The trajectories of agents in the second-order system (the topology is \mathcal{G}_1).

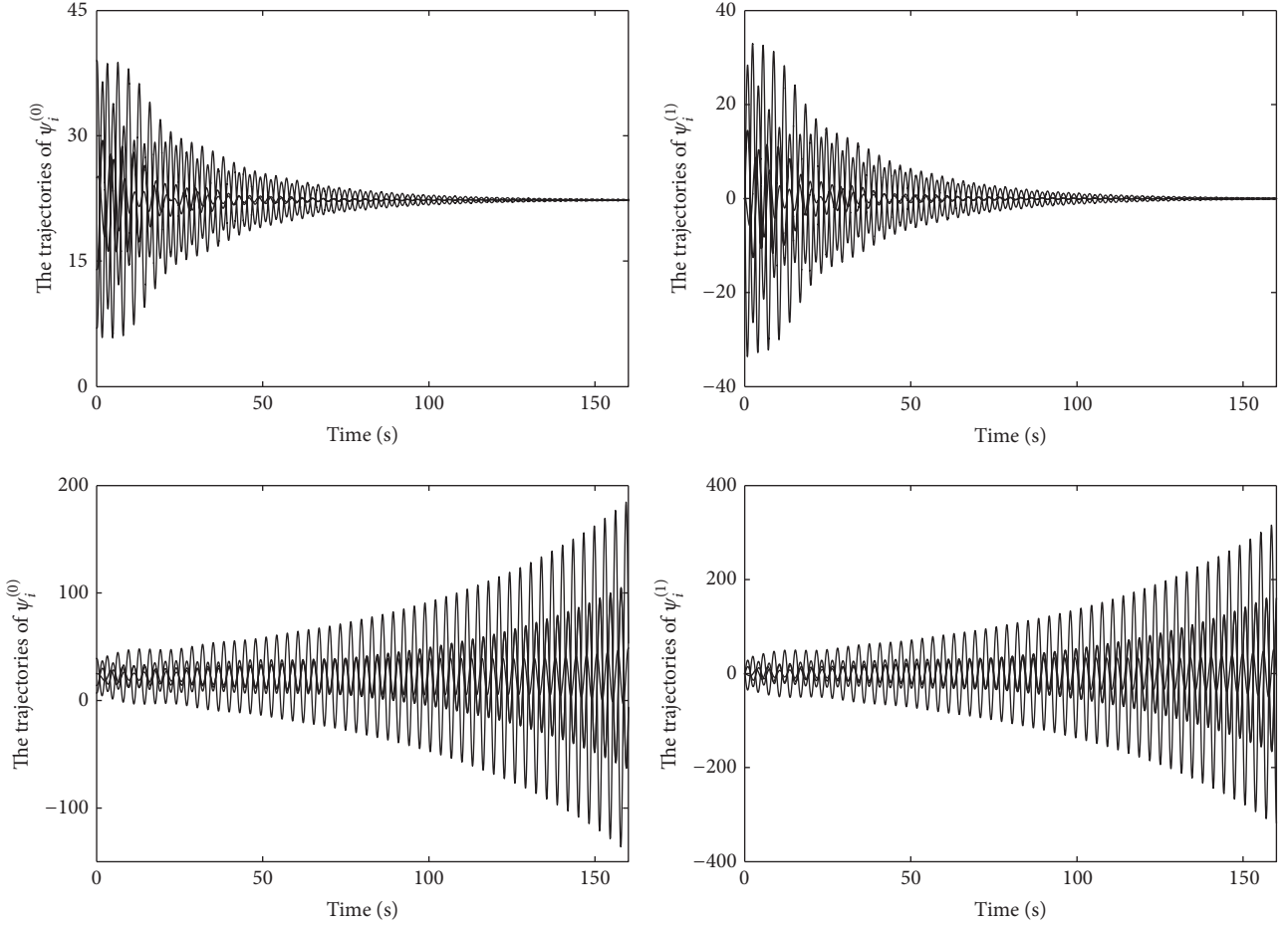


FIGURE 8: The trajectories of agents in the second-order system (the topology is \mathcal{G}_2).

and $p_2 = 6$, and then one gets $\bar{\tau} = 1.2729$. With time delays $\tau_{12} = 1.27$, $\tau_{23} = 1.26$, $\tau_{34} = 1.25$, $\tau_{14} = 1.24$, $\tau_{13} = 1.23$, and $\tau_{24} = 1.22$, simulation results are depicted in Figure 4, where the consensus achievement recurs.

For a sixth-order system connected as \mathcal{G}_1 , the parameters $p_1 = 12$, $p_2 = 27$, $p_3 = 40$, $p_4 = 28$, and $p_5 = 12$ yield $\bar{\tau} = 0.51$. Figure 5 has shown that the consensus achievement is guaranteed, where $\tau_{12} = 0.50$, $\tau_{23} = 0.48$, and $\tau_{34} = 0.46$. With connections in \mathcal{G}_2 , the system reaches consensus as shown in Figure 6, where $p_1 = 12$, $p_2 = 27$, $p_3 = 35$, $p_4 = 28$, and $p_5 = 12$ and time delays $\tau_{12} = 0.47$, $\tau_{23} = 0.46$, $\tau_{34} = 0.45$, $\tau_{14} = 0.44$, $\tau_{13} = 0.43$, and $\tau_{24} = 0.42$ which are bounded by $\bar{\tau} = 0.4713$ calculated according to Theorem 6.

To examine Theorem 8, we set $p_1 = 0.4$ for the second-order system. According to Theorem 8, for \mathcal{G}_1 , the delay margin $\bar{\tau} = 0.1181$. Two groups of delays are set: $\tau_{12} = 0.11$, $\tau_{23} = 0.10$, $\tau_{34} = 0.09$, which are bounded by the delay margin, and $\tau_{12} = 0.12$, $\tau_{23} = 0.13$, $\tau_{34} = 0.14$, which exceed the delay margin. The results are shown in Figure 7: the first two figures are the trajectories of agents when time delays are bounded, which indicates that consensus is reached; the last two figures are the trajectories of agents when all time delays exceed the delay margin, where the system is

unstable. These phenomena have attested the theorem. And for \mathcal{G}_2 , similar experiment is carried out: the delay margin is obtained as $\bar{\tau} = 0.1007$, and then, respectively, gives the bounded delays $\tau_{12} = 0.10$, $\tau_{23} = 0.09$, $\tau_{34} = 0.08$, $\tau_{14} = 0.07$, $\tau_{13} = 0.06$, and $\tau_{24} = 0.05$ and the exceeded delays $\tau_{12} = 0.101$, $\tau_{23} = 0.104$, $\tau_{34} = 0.107$, $\tau_{14} = 0.11$, $\tau_{13} = 0.113$, and $\tau_{24} = 0.116$. As shown in Figure 8, the simulation results validate the theorem again.

5. Conclusions

This paper has studied consensus problem of high-order multiagent systems with nearest-neighbor control rules in the presence of nonuniform time delays. For each delayed l th-order ($l = 1, 2, \dots, 6$) system, a sufficient condition has been provided in the form of inequalities and, for the first-order and second-order system, consensus conditions have been presented in the form of delay margins, which are less conservative and simpler in calculation than the existing results by Lyapunov methods in the form of LMIs. Numerical simulations on systems with two sets of different topologies have been carried out to testify the theorems. The simulation results show that the selected experiments have

reached expected effect: the systems achieve consensus under given conditions.

Future research will seek solutions to consensus problems of nonuniformly delayed high-order systems with directed topologies by applying this method. The main challenge is the calculation of $F_l(\omega)$'s arguments (see (27)), because the eigenvalues of systems with directed topologies are complex values even in the absence of time delays and it is hard to tell the relationship among the arguments of several complex values and their summation.

Competing Interests

The authors declare that they have no competing interests.

Acknowledgments

This work has been supported by the Specialized Research Fund for the Doctoral Program of Higher Education (20130185110023).

References

- [1] Z. Li, G. Wen, Z. Duan, and W. Ren, "Designing fully distributed consensus protocols for linear multi-agent systems with directed graphs," *IEEE Transactions on Automatic Control*, vol. 60, no. 4, pp. 1152–1157, 2015.
- [2] Z. Li, W. Ren, X. Liu, and M. Fu, "Consensus of multi-agent systems with general linear and lipschitz nonlinear dynamics using distributed adaptive protocols," *IEEE Transactions on Automatic Control*, vol. 58, no. 7, pp. 1786–1791, 2013.
- [3] G. Zhang, J. Xu, J. Zeng, J. Xi, and W. Tang, "Consensus of high-order discrete-time linear networked multi-agent systems with switching topology and time delays," *Transactions of the Institute of Measurement and Control*, 2016.
- [4] C. Sun, G. Hu, and L. Xie, "Robust consensus tracking for a class of high-order multi-agent systems," *International Journal of Robust and Nonlinear Control*, vol. 26, no. 3, pp. 578–598, 2016.
- [5] X. Dong, Z. Shi, G. Lu, and Y. Zhong, "Time-varying output formation control for high-order linear time-invariant swarm systems," *Information Sciences*, vol. 298, pp. 36–52, 2015.
- [6] C.-C. Hua, X. You, and X.-P. Guan, "Leader-following consensus for a class of high-order nonlinear multi-agent systems," *Automatica*, vol. 73, pp. 138–144, 2016.
- [7] W. Ren, K. Moore, and Y.-Q. Chen, "High-order consensus algorithms in cooperative vehicle systems," in *Proceedings of the IEEE International Conference on Networking, Sensing and Control (ICNSC '06)*, pp. 457–462, Ft. Lauderdale, Fla, USA, April 2006.
- [8] P. Lin, Z. Li, Y. Jia, and M. Sun, "High-order multi-agent consensus with dynamically changing topologies and time-delays," *IET Control Theory and Applications*, vol. 5, no. 8, pp. 976–981, 2011.
- [9] Q.-J. Zhang, Y.-F. Niu, L. Wang, L.-C. Shen, and H.-Y. Zhu, "Average consensus seeking of high-order continuous-time multi-agent systems with multiple time-varying communication delays," *International Journal of Control, Automation and Systems*, vol. 9, no. 6, pp. 1209–1218, 2011.
- [10] G. Wen, Z. Duan, W. Yu, and G. Chen, "Consensus of second-order multi-agent systems with delayed nonlinear dynamics and intermittent communications," *International Journal of Control*, vol. 86, no. 2, pp. 322–331, 2013.
- [11] P. Lin and Y. Jia, "Multi-agent consensus with diverse time-delays and jointly-connected topologies," *Automatica*, vol. 47, no. 4, pp. 848–856, 2011.
- [12] W. Yu, G. Chen, M. Cao, and W. Ren, "Delay-induced consensus and quasi-consensus in multi-agent dynamical systems," *IEEE Transactions on Circuits and Systems I: Regular Papers*, vol. 60, no. 10, pp. 2679–2687, 2013.
- [13] Y.-P. Tian and C.-L. Liu, "Robust consensus of multi-agent systems with diverse input delays and asymmetric interconnection perturbations," *Automatica*, vol. 45, no. 5, pp. 1347–1353, 2009.
- [14] P.-A. Bliman and G. Ferrari-Trecate, "Average consensus problems in networks of agents with delayed communications," *Automatica*, vol. 44, no. 8, pp. 1985–1995, 2008.
- [15] Y.-P. Tian and C.-L. Liu, "Consensus of multi-agent systems with diverse input and communication delays," *IEEE Transactions on Automatic Control*, vol. 53, no. 9, pp. 2122–2128, 2008.
- [16] P. Lin, Y.-M. Jia, J.-P. Du, and S.-Y. Yuan, "Distributed consensus control for second-order agents with fixed topology and time-delay," in *Proceedings of the 26th IEEE Chinese Control Conference (CCC '07)*, pp. 577–581, Zhangjiajie, China, July 2007.
- [17] P. Lin and Y. Jia, "Consensus of second-order discrete-time multi-agent systems with nonuniform time-delays and dynamically changing topologies," *Automatica*, vol. 45, no. 9, pp. 2154–2158, 2009.
- [18] V. D. Blondel, J. M. Hendrickx, A. Olshevsky, and J. N. Tsitsiklis, "Convergence in multiagent coordination, consensus, and flocking," in *Proceedings of the 44th IEEE Conference on Decision and Control and European Control Conference (CDC-ECC '05)*, pp. 2996–3000, IEEE, 2005.
- [19] U. Munz, A. Papachristodoulou, and F. Allgower, "Generalized Nyquist consensus condition for high-order linear multi-agent systems with communication delays," in *Proceedings of the 48th IEEE Conference on Decision and Control, Held Jointly with the 28th Chinese Control Conference (CDC/CCC '09)*, pp. 4765–4771, IEEE, Shanghai, China, December 2009.
- [20] U. Munz, A. Papachristodoulou, and F. Allgower, "Delay robustness in non-identical multi-agent systems," *IEEE Transactions on Automatic Control*, vol. 57, no. 6, pp. 1597–1603, 2012.
- [21] A. Popov and H. Werner, "Robust stability of a multi-agent system under arbitrary and time-varying communication topologies and communication delays," *IEEE Transactions on Automatic Control*, vol. 57, no. 9, pp. 2343–2347, 2012.
- [22] H. Fang, Z. Wu, and J. Wei, "Improvement for consensus performance of multi-agent systems based on weighted average prediction," *IEEE Transactions on Automatic Control*, vol. 57, no. 1, pp. 249–254, 2012.
- [23] P. Lin, K.-Y. Qin, Z.-K. Li, and W. Ren, "Collective rotating motions of second-order multi-agent systems in three-dimensional space," *Systems & Control Letters*, vol. 60, no. 6, pp. 365–372, 2011.
- [24] B. Mirkin, P.-O. Gutman, and Y. Shtessel, "Asymptotic sliding mode control approach to adaptive distributed tracking problem for multi-agent nonlinear delayed systems," *International Journal of Control*, vol. 85, no. 11, pp. 1671–1682, 2012.
- [25] P. Deshpande, P. P. Menon, C. Edwards, and I. Postlethwaite, "Formation control of multi-agent systems with double integrator dynamics using delayed static output feedback," in

- Proceedings of the 50th IEEE Conference on Decision and Control and European Control Conference (CDC-ECC '11)*, pp. 3446–3451, Orlando, Fla, USA, December 2011.
- [26] H. Zhang, J. Zhang, G. H. Yang, and Y. Luo, “Leader-based optimal coordination control for the consensus problem of multiagent differential games via fuzzy adaptive dynamic programming,” *IEEE Transactions on Fuzzy Systems*, vol. 23, no. 1, pp. 152–163, 2015.
 - [27] T. H. Lee, J. H. Park, D. H. Ji, and H. Y. Jung, “Leader-following consensus problem of heterogeneous multi-agent systems with nonlinear dynamics using fuzzy disturbance observer,” *Complexity*, vol. 19, no. 4, pp. 20–31, 2014.
 - [28] R. Ponalagusamy and S. Senthilkumar, “Investigation on numerical solution for a robot arm problem,” *Journal of Automation Mobile Robotics and Intelligent Systems*, vol. 3, pp. 34–40, 2009.
 - [29] C. P. Chen, G.-X. Wen, Y.-J. Liu, and Z. Liu, “Observer-based adaptive backstepping consensus tracking control for high-order nonlinear semi-strict-feedback multiagent systems,” *IEEE Transactions on Cybernetics*, vol. 46, no. 7, pp. 1591–1601, 2016.
 - [30] M. Shi and K. Qin, “Distributed control for multiagent consensus motions with nonuniform time delays,” *Mathematical Problems in Engineering*, vol. 2016, Article ID 3567682, 10 pages, 2016.
 - [31] C. D. Godsil, G. Royle, and C. Godsil, *Algebraic Graph Theory*, vol. 8, Springer, New York, NY, USA, 2001.
 - [32] Y.-Y. Nie and X.-K. Xie, “New criteria for polynomial stability,” *IMA Journal of Mathematical Control and Information*, vol. 4, no. 1, pp. 1–12, 1987.

Research Article

Consensus Control for a Multiagent System with Time Delays

Yiran Cao,¹ Toshiki Oguchi,¹ Paul Verhoeckx,² and Henk Nijmeijer²

¹Department of Mechanical Engineering, Graduate School of Science and Engineering, Tokyo Metropolitan University, 1-1 Minami-Osawa, Hachioji-shi, Tokyo 192-0397, Japan

²Department of Mechanical Engineering, Eindhoven University of Technology, P.O. Box 513, 5600MB Eindhoven, Netherlands

Correspondence should be addressed to Yiran Cao; cao-yiran@ed.tmu.ac.jp

Received 2 September 2016; Revised 14 December 2016; Accepted 26 December 2016; Published 28 February 2017

Academic Editor: Olfa Boubaker

Copyright © 2017 Yiran Cao et al. This is an open access article distributed under the Creative Commons Attribution License, which permits unrestricted use, distribution, and reproduction in any medium, provided the original work is properly cited.

In this paper, we consider the consensus control problem for a multiagent system (MAS) consisting of integrator dynamics with input and output time delays. First, we investigate a consensus condition for the MAS with a linear controller and without any delay compensation. We then propose a consensus controller with a state predictor to compensate the effect of time delay. The consensus condition for this controller is derived and investigated. Finally, we present an example of solving the consensus control problem for two-wheel mobile robots with feedback loops that pass through a computer network with time delays. To demonstrate the validity of the predictor-based controller, we conduct experiments with two-wheel mobile robots and present the results.

1. Introduction

Achieving cooperative control of robotic systems is of increasing interest and has attracted a great attention in recent years. There are many potential applications for multirobot systems, including unmanned aerial vehicles, satellite clusters, automated highways, and search and rescue operations. Control tasks for robotic systems include consensus [1, 2], flocking [3–5], formation control [6, 7], and tracking [8–10]. Of these, consensus constitutes a fundamental problem for the coordination control of distributed systems. Since cooperative multirobot systems rely on communication between robots in order to collaborate, time delays due to communication through networks and computations are a problem that cannot be neglected. Time delays in general can degrade system performance or even destroy stability. When each robot is considered to be an individual agent, multirobot systems can be considered multiagent systems (MASs). Here, we consider the consensus problem of MASs with time delay.

For nonlinear systems with input delay, Oguchi and Nijmeijer [11] proposed a delay compensation method with a state predictor based on anticipating synchronization. Several studies [1, 12–16] have focused on the consensus problem in a MAS with time delay. The papers [12, 13] showed the

upper bound of allowable input time delay under which consensus could be achieved. We attempt to consider both input and output time delay due to both communication and computation. In this study, we first introduce a linear time-delay control protocol with a corresponding consensus condition, similar to that in [12]. The consensus condition is used to give the consensus region of the allowable time delay corresponding to coupling strength. To compensate the time-delay effect, we focus on using a prediction control scheme for MASs with input and output time delays to allow the system to achieve consensus. A previously proposed state predictor-based controller for nonlinear systems with time delay is based on anticipating synchronization [11]. Kojima et al. used it for a tracking-control problem with time delay [17], as did Alvarez-Aguirre et al. [18]. In our previous work [2], we used a controller based on this predictor [11] to solve the consensus problem of MASs in undirected graph networks with time delay and derived the corresponding consensus condition. In this paper, by extending the results, we show that the system achieves the average consensus, and the MASs with directed communication graph can also achieve consensus under the consensus condition. To show the validity of the obtained results, we make the experiments in a multirobot system with the proposed controllers to solve the consensus problem of the coordinates of mobile robots.

This article is organized as follows. In Section 2, we introduce consensus problems for networks of dynamic agents with input and output time delays and show the necessary and sufficient conditions with linear coupling without the predictor to achieve consensus. We then propose a predictor-based consensus controller, for which we derive the necessary and sufficient conditions. Simulation results are presented in Section 3. Section 4 shows experimental results of nonholonomic mobile robots with input and output time delays to show the effectiveness of the proposed control scheme. Finally, Section 5 contains our conclusions.

2. Problem Formulation

Consider a network that consists of N identical integrator agents with invariant input and output time delays given as the following dynamics:

$$\begin{aligned}\dot{\mathbf{x}}_i(t) &= \mathbf{u}_i(t - \tau_i^{\text{in}}) \\ \mathbf{y}_i(t) &= \mathbf{x}_i(t - \tau_i^{\text{out}}) \\ &\text{for } i = 1, 2, \dots, N.\end{aligned}\quad (1)$$

Here $\mathbf{x}_i = [x_{1i}, x_{2i}, \dots, x_{ni}]^T \in \mathbb{R}^n$, $\mathbf{y}_i = [y_{1i}, y_{2i}, \dots, y_{ni}]^T \in \mathbb{R}^n$, and $\mathbf{u}_i = [u_{1i}, u_{2i}, \dots, u_{ni}]^T \in \mathbb{R}^n$ denote the state, output, and input vectors of the i th agent, respectively. τ_i^{in} and $\tau_i^{\text{out}} \in \mathbb{R}^+$ separately denote the input and output delays corresponding to agent i .

For this system, the consensus problem is formulated as follows.

Definition 1 (consensus problem). For multiagent system (1) with input and output time delays, the consensus problem is to find a control protocol to make the states of all agents reach agreement such that $\mathbf{x}_i(t) = \mathbf{x}_j(t)$ for all $i, j \in \{1, \dots, N\}$ as $t \rightarrow \infty$.

Following the consensus control protocol proposed by [12], we assume that these agents are interconnected by the following controller:

$$\mathbf{u}_i(t) = - \sum_{j \in \mathcal{N}_i} k_{ij} (\mathbf{y}_i(t) - \mathbf{y}_j(t)) \quad (2)$$

for $i = 1, \dots, N$, where $k_{ij} \in \mathbb{R}_+$ denotes the coupling strength between agents i and j . \mathcal{N}_i denotes the set of agents adjacent to agent i , which means these agents are connected to agent i in the network topology. We now introduce some definitions about a graph \mathcal{G} . $L(\mathcal{G})$ is the Laplacian matrix of a graph \mathcal{G} corresponding to the network topology constructed by the interconnection of the agents. If the information communication between agent i and j is bidirectional, the graph \mathcal{G} is undirected, and the corresponding Laplacian $L(\mathcal{G})$ has the following entries:

$$\ell_{ij} = \begin{cases} -1 & \text{if } j \in \mathcal{N}_i \\ 0 & \text{if } j \notin \mathcal{N}_i, j \neq i \\ |\mathcal{N}_i| & \text{if } j = i. \end{cases} \quad (3)$$

It is well known that the bidirectional graph Laplacian $L(\mathcal{G})$ is diagonalized and has a zero eigenvalue, and $N-1$ positive real eigenvalues such as $0 = \lambda_0 < \lambda_1 \leq \dots \leq \lambda_{N-1}$ corresponding to the N agents system.

Assuming that $\tau_i^{\text{in}} = \tau_i^{\text{out}} = \tau$, each round-trip time delay is given by 2τ for $i = 1, \dots, N$. All coupling strengths are identical and denoted as k . Controller (2) is simplified as

$$\mathbf{u}(t) = -k(L(\mathcal{G}) \otimes \mathbf{I}_n) \mathbf{y}(t), \quad (4)$$

where \otimes denotes the Kronecker product of two matrices and $\mathbf{y} = [\mathbf{y}_1^T, \mathbf{y}_2^T, \dots, \mathbf{y}_N^T]^T \in \mathbb{R}^{nN}$ and $\mathbf{u} = [\mathbf{u}_1^T, \mathbf{u}_2^T, \dots, \mathbf{u}_N^T]^T \in \mathbb{R}^{nN}$ denote the output vector and the input vector, respectively.

The dynamics of the total system can then be derived as

$$\dot{\mathbf{x}}(t) = -k(L(\mathcal{G}) \otimes \mathbf{I}_n) \mathbf{x}(t - 2\tau), \quad (5)$$

where $\mathbf{x} = [\mathbf{x}_1^T, \dots, \mathbf{x}_N^T]^T \in \mathbb{R}^{nN}$ denotes the state vector. The initial condition of the states is given as $\mathbf{x}(\theta) = \varphi(\theta)$ ($-2\tau \leq \theta \leq 0$), where $\varphi(\theta) \in C([-2\tau, 0], \mathbb{R}^{nN})$.

Therefore, from the stability of system (5), the following consensus condition is proven following the results of Olfati-Saber and Murray [12].

Theorem 2. Assume that each system (1) is interconnected by (2) with a coupling strength k and constant input and output time delay τ . The constructed network topology is fixed, undirected, and connected. If the pair (k, τ) satisfies

$$0 < k\tau < \frac{\pi}{4\lambda_{N-1}}, \quad (6)$$

the delayed system achieves consensus. Here λ_{N-1} is the maximum eigenvalue of $L(\mathcal{G})$ for an N -agents system.

Rewriting $k\lambda_{N-1}$ as \bar{k} , pairs of (\bar{k}, τ) satisfying $0 < \tau < \pi/4\bar{k}$ can stabilise the delayed system. Thus, τ has a maximum value boundary corresponding to each value of \bar{k} . In general, if the number of agents increases, λ_{N-1} corresponding to the network structure also tends to increase. Based on $k = \bar{k}/\lambda_{N-1}$, for a fixed time delay τ , k decreases as λ_{N-1} increases, and this slows the convergence rate. Therefore, this condition means that the convergence rate gets slower as the number of agents and the allowable delay increases. To overcome this problem, in the next section, we propose a state predictor-based controller that can counteract the effect of λ_{N-1} .

Moreover, if the graph is undirected and connected, [12] shows that MAS without time delays achieve the consensus, and the consensus solution is given as the average of the states of all agents; that is, $\text{Ave}(\mathbf{x}(t)) = (1/N) \sum_{i=1}^N \mathbf{x}_i(t)$. In [19], the necessary and sufficient condition for an average consensus problem for MAS with nonuniform and asymmetric time delay is given. From these results, we know that the MAS

in Theorem 2 achieves the average consensus and that the consensus value is given as

$$\begin{aligned}\alpha &:= \frac{\mathbf{1}_N^T \otimes \mathbf{I}_n}{N} \left\{ \varphi(0) + \int_{-2\tau}^0 (L(\mathcal{G}) \otimes \mathbf{I}_n) \varphi(s) ds \right\} \\ &= \frac{\mathbf{1}_N^T \otimes \mathbf{I}_n}{N} \varphi(0),\end{aligned}\quad (7)$$

where $\mathbf{1}_N = [1, \dots, 1]^T \in \mathbb{R}^N$.

3. Main Results

Based on the MAS (1) with controller (2), we propose a controller with a state predictor based on anticipating synchronization for the consensus control of agents. We present the consensus controller and discuss its stability problem in this section.

3.1. State Predictor-Based Controller. Anticipating synchronization is a kind of master-slave synchronization. The predictor is constituted by the given system dynamics and coupling of the difference of the system output and delayed predictor states. The dynamics of this predictor can be stated as follows:

$$\dot{\hat{\mathbf{y}}}(t) = \mathbf{u}(t) - k_p (\hat{\mathbf{y}}(t - 2\tau) - \mathbf{y}(t)), \quad (8)$$

where $k_p \in \mathbb{R}^+$ is the prediction gain. Meanwhile, $\hat{\mathbf{y}} = [\hat{\mathbf{y}}_1^T, \dots, \hat{\mathbf{y}}_N^T]^T \in \mathbb{R}^{nN}$, where $\hat{\mathbf{y}}_i(t) = [\hat{y}_{1i}(t), \dots, \hat{y}_{ni}(t)]^T \in \mathbb{R}^n$, $i \in \{1, \dots, N\}$ denotes the predicted outputs. The initial condition of the predicted states is given as $\hat{\mathbf{y}}(\theta) = \phi(\theta)$ ($-2\tau \leq \theta \leq 0$), where $\phi(\theta) \in C([-2\tau, 0], \mathbb{R}^{nN})$. Then, using the output of the predictor instead of the output of the actual system, the main controller is given as

$$\mathbf{u}(t) = -k (L(\mathcal{G}) \otimes \mathbf{I}_n) \hat{\mathbf{y}}(t). \quad (9)$$

Controller (9) with state predictor (8) compensates the effect of time delays at input and output. If the predictor has prior knowledge of the initial states of the system, the prediction error always remains 0, and the predictor can predict the exact future value of the states of the system. Thereafter, the total system is shown as

$$\begin{aligned}\dot{\mathbf{x}}(t) &= \mathbf{u}(t - \tau), \\ \mathbf{y}(t) &= \mathbf{x}(t - \tau), \\ \mathbf{u}(t) &= -k (L(\mathcal{G}) \otimes \mathbf{I}_n) \hat{\mathbf{y}}(t), \\ \dot{\hat{\mathbf{y}}}(t) &= \mathbf{u}(t) - k_p (\hat{\mathbf{y}}(t - 2\tau) - \mathbf{y}(t)).\end{aligned}\quad (10)$$

3.2. Consensus Condition. As we use a predictor to predict the states, it is important to prove that the prediction error converges to 0. The prediction error is defined as

$$\hat{\mathbf{e}}(t) = \hat{\mathbf{y}}(t - \tau) - \mathbf{x}(t). \quad (11)$$

When the prediction error $\hat{\mathbf{y}}(t - \tau) - \mathbf{x}(t)$ converges to zero, this means that $\hat{\mathbf{y}}(t)$ estimates the exact future value of $\mathbf{x}(t)$,

which is $\mathbf{x}(t + \tau)$. The time-delay 2τ is totally compensated at this time.

With the use of (8) and (9), the dynamics of prediction error can be obtained as

$$\dot{\hat{\mathbf{e}}}(t) = -k_p \hat{\mathbf{e}}(t - 2\tau). \quad (12)$$

To derive the necessary and sufficient conditions such that the whole system converges to consensus, we consider the coordinate transformation as follows:

$$\begin{aligned}\mathbf{e}_s(t) &= \begin{bmatrix} \sum_{i=1}^N \mathbf{x}_i(t) \\ \mathbf{e}(t) \end{bmatrix} = \begin{bmatrix} \mathbf{x}_1(t) + \dots + \mathbf{x}_N(t) \\ \mathbf{x}_1(t) - \mathbf{x}_2(t) \\ \vdots \\ \mathbf{x}_1(t) - \mathbf{x}_N(t) \end{bmatrix} \\ &= (\mathbf{M}_0 \otimes \mathbf{I}_n) \mathbf{x}(t),\end{aligned}\quad (13)$$

where

$$\mathbf{M}_0 = \begin{bmatrix} 1 & 1 & \dots & 1 \\ 1 & -1 & & \mathbf{0} \\ \vdots & & \ddots & \\ 1 & \mathbf{0} & & -1 \end{bmatrix} \in \mathbb{R}^{N \times N} \quad (14)$$

and $\mathbf{e}(t) = [\mathbf{x}_1(t) - \mathbf{x}_2(t), \dots, \mathbf{x}_1(t) - \mathbf{x}_N(t)]^T$ denotes the synchronization error. Substituting (8), (9), and (11) for the derivative of (13), we obtain the following dynamics:

$$\begin{aligned}\dot{\mathbf{e}}_s(t) &= -k (\mathbf{M}_0 L(\mathcal{G}) \mathbf{M}_0^{-1} \otimes \mathbf{I}_n) \mathbf{e}_s(t) \\ &\quad - k (\mathbf{M}_0 L(\mathcal{G}) \otimes \mathbf{I}_n) \hat{\mathbf{e}}(t).\end{aligned}\quad (15)$$

The prediction error dynamics (12) and the dynamics (15) can be rewritten in a matrix form as

$$\begin{aligned}\begin{bmatrix} \dot{\mathbf{e}}_s(t) \\ \dot{\hat{\mathbf{e}}}(t) \end{bmatrix} &= \begin{bmatrix} 0 & 0 \\ 0 & -k_p \end{bmatrix} \begin{bmatrix} \mathbf{e}_s(t - 2\tau) \\ \hat{\mathbf{e}}(t - 2\tau) \end{bmatrix} \\ &\quad + \begin{bmatrix} -k (\mathbf{M}_0 L(\mathcal{G}) \mathbf{M}_0^{-1} \otimes \mathbf{I}_n) & -k (\mathbf{M}_0 L(\mathcal{G}) \otimes \mathbf{I}_n) \\ 0 & 0 \end{bmatrix} \begin{bmatrix} \mathbf{e}_s(t) \\ \hat{\mathbf{e}}(t) \end{bmatrix}.\end{aligned}\quad (16)$$

From this equation, the consensus condition is given in the following theorem.

Theorem 3. Assume that each agent (1) is controlled by predictor (8) and controller (9) with gain k , constant input and output time delay τ and prediction gain k_p . The constructed network topology is fixed, undirected, and connected. Then, if the pair (k_p, τ) and k satisfy

$$\begin{aligned}k &> 0, \\ 0 &< k_p \tau < \frac{\pi}{4},\end{aligned}\quad (17)$$

the MAS achieves consensus.

Proof. The proof is given for the stability of the total synchronization error dynamics (16). After the Laplace transformation, the characteristic equation of (16) can be derived as

$$\det \begin{bmatrix} s\mathbf{I}_{nN} + k(\mathbf{M}_0 L(\mathcal{G}) \mathbf{M}_0^{-1} \otimes \mathbf{I}_n) & k(\mathbf{M}_0 L(\mathcal{G}) \otimes \mathbf{I}_n) \\ 0 & s\mathbf{I}_{nN} + k_p(\mathbf{e}^{-2\tau s} \mathbf{I}_{nN}) \end{bmatrix} \quad (18)$$

$$= \det(s\mathbf{I}_{nN} + k(\mathbf{M}_0 L(\mathcal{G}) \mathbf{M}_0^{-1} \otimes \mathbf{I}_n)) \cdot \det(s\mathbf{I}_{nN} + k_p(\mathbf{e}^{-2\tau s} \mathbf{I}_{nN})) = 0.$$

To make the equation hold, one of the above determinates should be equal to 0. As can be seen, the first determinant of (18) represents the synchronization error, and the latter represents the prediction error. To make both errors converge to 0, all solutions satisfying the following equations must have negative real parts:

$$\det(s\mathbf{I}_{nN} + k(\mathbf{M}_0 L(\mathcal{G}) \mathbf{M}_0^{-1} \otimes \mathbf{I}_n)) = 0, \quad (19)$$

$$\det(s\mathbf{I}_{nN} + k_p(\mathbf{e}^{-2\tau s} \mathbf{I}_{nN})) = 0.$$

Since $L(\mathcal{G})$ for a fixed, undirected, and connected graph is a symmetric real matrix and for the eigenvalues it holds that $0 < \lambda_1 \leq \dots \leq \lambda_{N-1}$, the term of the first equation in (19) satisfies the following results:

$$\mathbf{P} \mathbf{M}_0 L(\mathcal{G}) \mathbf{M}_0^{-1} \mathbf{P}^{-1} = \begin{bmatrix} 0 & 0 & \dots & 0 \\ 0 & \lambda_1 & \dots & 0 \\ \vdots & \vdots & \ddots & \vdots \\ 0 & 0 & \dots & \lambda_{N-1} \end{bmatrix}, \quad (20)$$

where $\mathbf{P} \in \mathbb{R}^{N \times N}$ is the matrix that transforms $\mathbf{M}_0 L(\mathcal{G}) \mathbf{M}_0^{-1}$ into the diagonalized form. Thus, the first equation can be written as $s + k\lambda_i = 0$, $i = 1, \dots, N-1$. To make s have negative real part, we get the condition $k > 0$ from the first equation.

For the second equation, we consider the smallest value of τ , such that $s = j\omega$, which has a zero real part on the imaginary axis. Then we have

$$\omega - k_p \sin(\omega\tau) = 0, \quad (21)$$

$$k_p \cos(\omega\tau) = 0.$$

Assuming $\omega > 0$, we can get $\omega\tau = (\pi/2) + 2k\pi$, $k = 0, 1, \dots, N$ and $\omega = k_p$. Since the delay-free system is described by $s + k_p = 0$ (which is exponentially stable for $k_p > 0$), and the continuity of eigenvalues for LTI systems holds, the roots of the dynamics of the second equation of (19) lie on the open left half-plane. Therefore, from the second equation, we get $0 < k_p\tau < \pi/2$. \square

The first condition corresponds to the consensus condition for the system without delay, and the second comes from the stability of the prediction error. This discussion means

that the synchronization-based predictor is an extension of the full-state observer, and a counterpart of the separation principle holds for the stability of the system with the synchronization-based predictor.

Compared with the consensus condition (6) of Theorem 2, the ranges of both k and τ are extended. The coupling strength k is independent of time delay in Theorem 3 and $k_p < \pi/4\tau$ holds for any constant τ . Moreover, if the prediction error is not zero, both k and k_p affect the convergence rate. If the predictor has prior knowledge of the initial condition, k is the only influence factor for the convergence rate. We can choose a larger value of k in order to make the system converge to consensus faster.

Remark 4. It is known that a directed graph contains a directed spanning tree, if and only if the corresponding graph Laplacian $L(\mathcal{G})$ always has one zero eigenvalue and $N-1$ eigenvalues that have positive real parts [20]. In this network topology, the MAS satisfying inequalities (17) can also reach a consensus.

Concerning the average value of agent states, we have the following results.

Theorem 5. Consider that the system with agent (1) satisfies Theorem 3, so that the MAS achieves consensus. This MAS achieves average consensus for any initial states $\varphi(0) \in \mathbb{R}^{nN}$ and the consensus solution is given as

$$\alpha_p := \frac{\mathbf{1}_N^T \otimes \mathbf{I}_n}{N} \varphi(0). \quad (22)$$

Proof. The total system can be summarised as

$$\dot{\mathbf{x}}(t) = -k(L(\mathcal{G}) \otimes \mathbf{I}_n) \hat{\mathbf{y}}(t - \tau),$$

$$\dot{\hat{\mathbf{y}}}(t) = -k(L(\mathcal{G}) \otimes \mathbf{I}_n) \hat{\mathbf{y}}(t) \quad (23)$$

$$- k_p(\hat{\mathbf{y}}(t - 2\tau) - \mathbf{x}(t - \tau)).$$

Following the method shown in [19], we consider the following functional vector $F_1 : C([-\tau, 0], \mathbb{R}^{nN}) \rightarrow \mathbb{R}^n$:

$$F_1(\mathbf{x}_t) = \frac{1}{N} (\mathbf{1}_N^T \otimes \mathbf{I}_n) \cdot \left(\mathbf{x}(t) + \int_{t-\tau}^t -k(L(\mathcal{G}) \otimes \mathbf{I}_n) \hat{\mathbf{y}}(s) ds \right) \quad (24)$$

$$= \frac{1}{N} (\mathbf{1}_N^T \otimes \mathbf{I}_n) \mathbf{x}(t),$$

where $\mathbf{x}_t \in C([-\tau, 0], \mathbb{R}^{nN})$ represents the solution $\mathbf{x}(t) \in \mathbb{R}^{nN}$ on the time interval $[t-\tau, t]$ such that $\mathbf{x}_t(s) = \mathbf{x}(t+s)$, $s \in [-\tau, 0]$. Since this graph Laplacian $L(\mathcal{G})$ is a symmetric zero column-sum matrix, $\mathbf{1}_N^T L(\mathcal{G}) = \mathbf{0}$ holds. Thus, the integral

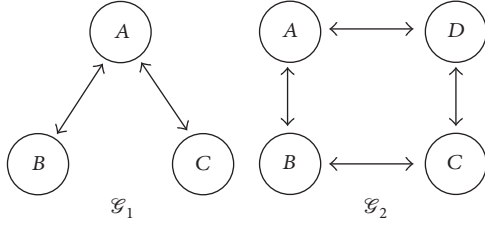


FIGURE 1: Network structures for three and four agents.

term is vanished in (24). The time-derivative of (24) along the solution of (23) is given as

$$\begin{aligned} \frac{d}{dt} F_1(\mathbf{x}_t) &= \frac{1}{N} (\mathbf{1}_N^T \otimes \mathbf{I}_n) \\ &\cdot \left(\mathbf{x}(t) + \int_{t-\tau}^t -k(L(\mathcal{G}) \otimes \mathbf{I}_n) \hat{\mathbf{y}}(s) ds \right) \\ &= \frac{1}{N} (\mathbf{1}_N^T \otimes \mathbf{I}_n) (-k(L(\mathcal{G}) \otimes \mathbf{I}_n) \hat{\mathbf{y}}(t - \tau)) = 0. \end{aligned} \quad (25)$$

Therefore, the functional vector $F_1(\mathbf{x}_t)$ is time-invariant, and the value always equals the average of the initial state $\mathbf{x}(0)$ given as

$$\begin{aligned} F_1(\mathbf{x}_t) &= \frac{\mathbf{1}_N^T \otimes \mathbf{I}_n}{N} \mathbf{I}_{nN} (\mathbf{1}_N \otimes \boldsymbol{\alpha}_p) = \boldsymbol{\alpha}_p \\ &= \frac{\mathbf{1}_N^T \otimes \mathbf{I}_n}{N} \boldsymbol{\varphi}(0). \end{aligned} \quad (26)$$

□

3.3. Simulation Results. By using controller (9) and predictor (8), we can obtain the simulation results for the system (10) of three and four agents, respectively, connected by networks in Figure 1.

The graph Laplacian $L(\mathcal{G}_1)$ for three agents is

$$L(\mathcal{G}_1) = \begin{bmatrix} 2 & -1 & -1 \\ -1 & 1 & 0 \\ -1 & 0 & 1 \end{bmatrix} \quad (27)$$

and the corresponding eigenvalues are $\lambda_i = [0, 1, 3]$, $i = 0, 1, 2$.

In this simulation the coupling strength is $k = 2$, the prediction gain $k_p = 0.8$, and the time-delay is set as $\tau = 0.25$ s. The initial states are set as $\mathbf{x}_A = [1.35, 2.54]^T$, $\mathbf{x}_B = [0.98, 2.99]^T$, and $\mathbf{x}_C = [1.60, 3.07]^T$ for each agent, and the initial states of the predictor are given as $\hat{\mathbf{y}}(t) = \mathbf{0}$ for $-2\tau \leq t \leq 0$. The simulation results are shown in Figure 2. It is clearly shown that both the prediction error and the synchronization error converge to 0 for each state. The consensus values of the system are the average of the states at $t = 0$; that is, $\boldsymbol{\alpha}_p = [3.93, 2.9]^T$.

For a four-agent system, the graph Laplacian $L(\mathcal{G}_2)$ of the communication network in Figure 1 is

$$L(\mathcal{G}_2) = \begin{bmatrix} 2 & -1 & 0 & -1 \\ -1 & 2 & -1 & 0 \\ 0 & -1 & 2 & -1 \\ -1 & 0 & -1 & 2 \end{bmatrix} \quad (28)$$

and the corresponding eigenvalues are $\lambda_i = [0, 2, 2, 4]$, $i = 0, 1, 2, 3$. The time delay is set as $\tau = 1$ s, coupling strength $k = 2$, and prediction gain $k_p = 0.4$ satisfying the consensus condition shown in Theorem 3. We set $\hat{\mathbf{y}}(t) = \mathbf{0}$ for $-2\tau \leq t \leq 0$ as the initial states of the predictor; the initial states of dynamics (1) are $\mathbf{x}_A = [1.12, 2.56]^T$, $\mathbf{x}_B = [1.62, 2.57]^T$, $\mathbf{x}_C = [1.59, 3.06]^T$, and $\mathbf{x}_D = [1.15, 3.06]^T$ for the four agents, respectively.

With more agents and a longer time delay, the MAS satisfies Theorem 3 and converges to consensus, and the prediction error converges to 0, as shown in Figure 3. Since the simulation results show that the two MASs all converge to consensus under the conditions given in Theorem 3, the validity of the predictor-based controller is verified.

4. Experimental Results

In this section, by applying controller (9) with state predictor (8), we show experimental results for multirobot systems.

Consider the two-wheel mobile robot shown in Figure 4. Let us suppose that the robot moves on a flat plane under a fixed global frame without drift. Let $\xi_i(t)$ and $\zeta_i(t)$ denote the global coordinates of the centre of the i th mobile robot; $\theta_i(t)$ denotes the current angle between the direction of velocity $v_i(t)$ of the centre and the x -axis, and $\omega_i(t) = d\theta_i(t)/dt$ is the angular velocity. The kinematic model of the i th mobile robot is expressed as

$$\begin{bmatrix} \dot{\xi}_i(t) \\ \dot{\zeta}_i(t) \\ \dot{\theta}_i(t) \end{bmatrix} = \begin{bmatrix} \cos \theta_i(t) & 0 \\ \sin \theta_i(t) & 0 \\ 0 & 1 \end{bmatrix} \begin{bmatrix} v_i(t) \\ \omega_i(t) \end{bmatrix} \quad (29)$$

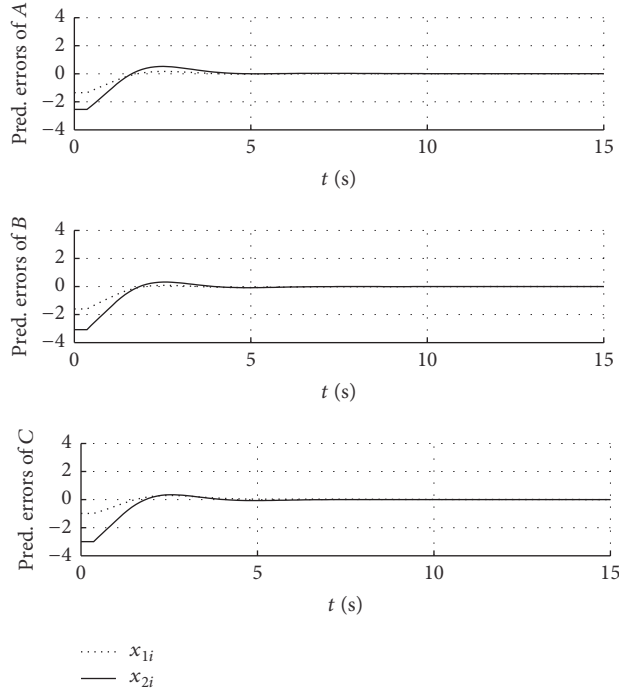
for $i = 1, \dots, N$. Then, the coordinate $(\xi_o^i(t), \zeta_o^i(t))$ of point O^i on the head of the robot used as the outputs is represented by the coordinate transformation

$$\begin{bmatrix} \xi_o^i(t) \\ \zeta_o^i(t) \end{bmatrix} = \begin{bmatrix} \xi_i(t) + R \cos \theta_i(t) \\ \zeta_i(t) + R \sin \theta_i(t) \end{bmatrix}, \quad (30)$$

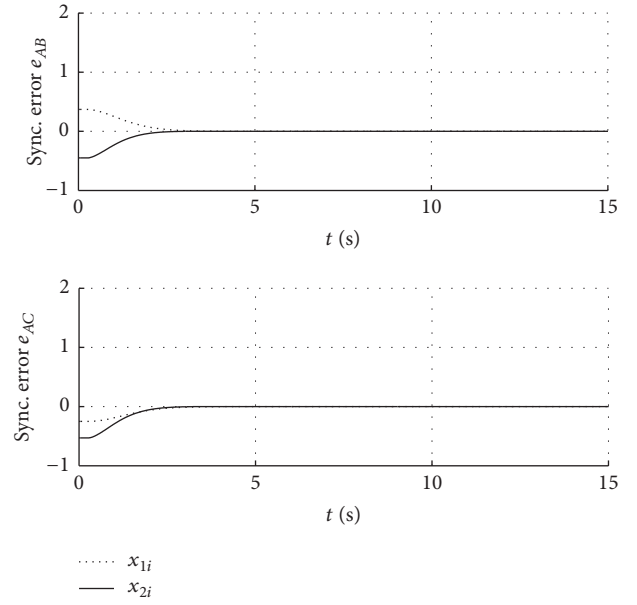
where $R \in \mathbb{R}^+$ is the radius of the mobile robot.

Applying (30) into (29), we obtain

$$\begin{bmatrix} \dot{\xi}_o^i(t) \\ \dot{\zeta}_o^i(t) \end{bmatrix} = \begin{bmatrix} \cos \theta_i(t) & -R \sin \theta_i(t) \\ \sin \theta_i(t) & R \cos \theta_i(t) \end{bmatrix} \begin{bmatrix} v_i(t) \\ \omega_i(t) \end{bmatrix}. \quad (31)$$

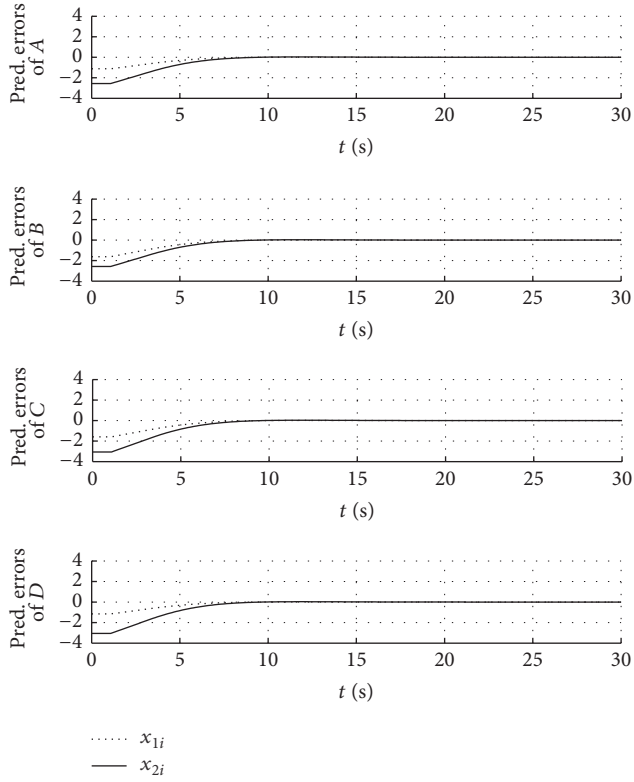


(a) Prediction error

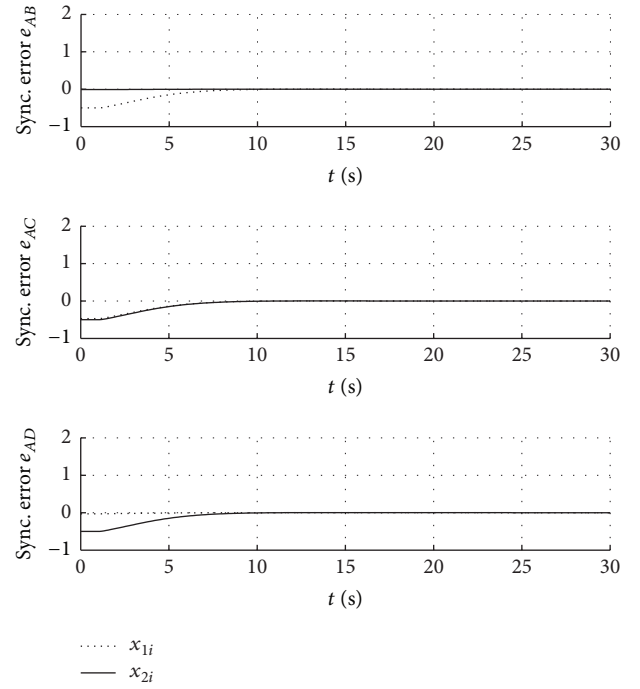


(b) Synchronization error

FIGURE 2: Simulation results for three agents with controller (9) and state predictor (8).



(a) Prediction error



(b) Synchronization error

FIGURE 3: Simulation results for four agents with controller (9) and state predictor (8).

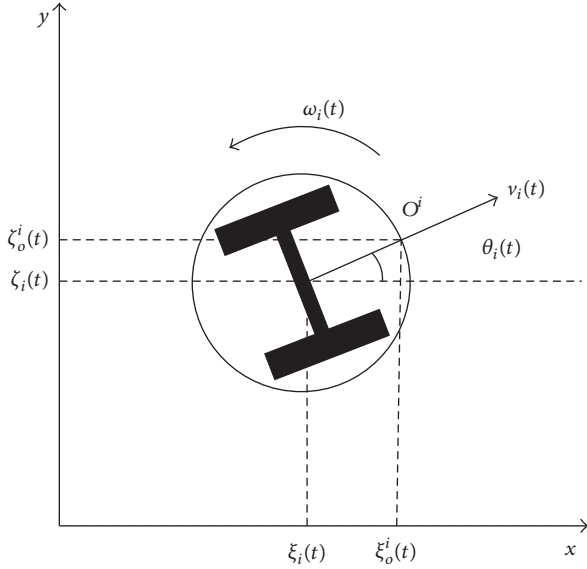


FIGURE 4: Kinematic model of a mobile robot.

For clarity, we simplify $[\xi_o^i(t), \zeta_o^i(t)]^T$ as $\mathbf{x}_i(t) = [\xi_i(t), \zeta_i(t)]^T$ for the i th mobile robot. Then (31) can be rewritten as

$$\begin{aligned} \dot{\mathbf{x}}_i(t) &= \begin{bmatrix} \dot{\xi}_i(t) \\ \dot{\zeta}_i(t) \end{bmatrix} = \begin{bmatrix} \cos \theta_i(t) & -R \sin \theta_i(t) \\ \sin \theta_i(t) & R \cos \theta_i(t) \end{bmatrix} \begin{bmatrix} v_i(t) \\ \omega_i(t) \end{bmatrix} \\ &= \mathbf{B}(\theta_i(t)) \mathbf{p}_i(t), \end{aligned} \quad (32)$$

where $\mathbf{p}_i(t) = [v_i(t), \omega_i(t)]^T$. Since $\det(\mathbf{B}(\theta_i(t))) = R$, the matrix $\mathbf{B}(\theta_i(t))$ is invertible for any $\theta_i(t)$.

The schematic for the system in the experiment is depicted in Figure 5. Time delay occurs in the communication between each robot and a centralized controller. Such a configuration corresponds with a system that has a separate central controller and several local controllers as simple on-board controllers. By using this system, each robot needs only weak computation capability for the local controller, which makes the robots smaller and cheaper. We implement the delayed system by using e-pucks [21], which are two-wheel mobile robots.

We assume that there is a unified constant input and output time delay τ between each robot and a centralized controller. Applying the input-output feedback linearization technique, we design the local controller carried by each robot as follows:

$$\mathbf{p}_i(t) = \mathbf{B}^{-1}(\theta_i(t)) \mathbf{u}_i(t - \tau), \quad (33)$$

where $\mathbf{u}_i(t - \tau) \in \mathbb{R}^2$ denotes the output from the centralized controller with time delay $\tau \in \mathbb{R}^+$. In this way, $\theta_i(t)$ is the local information without time delay for each robot i . The differential of an angular $\dot{\theta}_i(t) = \omega_i(t)$ depends on the control input $\omega_i(t)$; $\theta_i(t)$ is a variant local state, and $\dot{\theta}_i(t)$ converges to zero when the control input $\omega_i(t)$ converges to zero. By

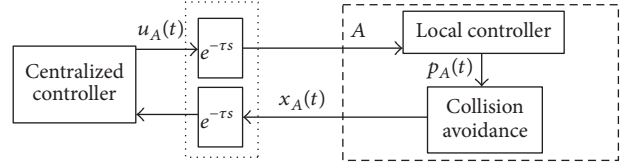


FIGURE 5: Schematic of the robot A system. The local controller and collision avoidance are on-board the robot. Time delay happens on communications between robot A and the centralized controller.

applying (33) to (32), the system is linearized as an integrator system with input and output time delay given as

$$\begin{aligned} \dot{\mathbf{x}}_i(t) &= \mathbf{u}_i(t - \tau), \\ \mathbf{y}_i(t) &= \mathbf{x}_i(t - \tau) \end{aligned} \quad (34)$$

for $i = 1, \dots, N$. Then the predictor-based control scheme can be used for this multirobot system to converge the output of the robot to consensus.

4.1. Collision Avoidance. On the way to convergence consensus, a robot may collide with other robots. Here, we assume for robot i that the other robots are obstacles. The robot j in danger of colliding with robot i is denoted as belonging to the set

$$M_i = \{\mathbf{x}_j(t) \mid x_{ij}^2(t) < d_{\min}^2, j \neq i (j = 1, \dots, N)\}, \quad (35)$$

where $x_{ij}^2(t) = (\xi_i(t) - \xi_j(t))^2 + (\zeta_i(t) - \zeta_j(t))^2$ denotes the square of the distance between robots i and j and d_{\min} is the minimum safe distance between two robots. Here, the following RPF proposed in [22] is adopted as

$$V_{ij}(t) = \begin{cases} \eta \left(\frac{1}{x_{ij}^2(t)} - \frac{1}{d^2} \right)^2 & \text{if } x_{ij}(t) < d_{\min} \\ 0 & \text{if } x_{ij}(t) \geq d_{\min}, \end{cases} \quad (36)$$

where $\eta \in \mathbb{R}^+$ is the gain of the RPF. The collision avoidance algorithm can be implemented by the following local controller:

$$\begin{aligned} \mathbf{u}_i(t) &= - \sum_{j \in M_i} \frac{\partial V_{ij}(t)}{\partial \mathbf{x}_i(t)} \\ &= 4 \sum_{j \in M_i} \eta \left(\frac{1}{x_{ij}^2(t)} - \frac{1}{d^2} \right) \left(\frac{1}{x_{ij}^2(t)} \right)^2 (\mathbf{x}_i(t) - \mathbf{x}_j(t)). \end{aligned} \quad (37)$$

Here, the distance $x_{ij}(t)$ is measured by sensing under the measuring range of robot i and the angle $\theta_i(t)$ is available as local information. With such local information, the RPF approach can be utilized without time delay, as in $\mathbf{x}_i(t) - \mathbf{x}_j(t) = [x_{ij}(t) \cos(\theta_i(t)), x_{ij}(t) \sin(\theta_i(t))]^T$. With

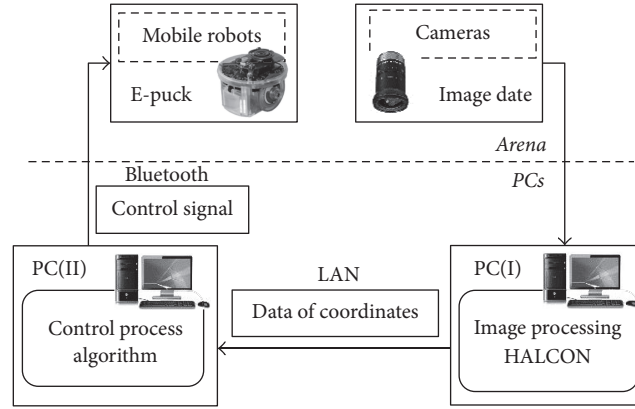


FIGURE 6: Structure of experimental system.

collision avoidance, the controller for the experiment is given as

$$\mathbf{p}_i(t) = \mathbf{B}^{-1}(\theta_i(t)) \mathbf{u}_i(t - \tau), \quad (38)$$

$$\hat{\mathbf{y}}_i(t) = \mathbf{u}_i(t) - k_p(\hat{\mathbf{y}}_i(t - 2\tau) - \mathbf{y}_i(t)), \quad (39)$$

$$\mathbf{u}_i(t) = \begin{cases} -k \sum_{j \in N_i} (\hat{\mathbf{y}}_i(t) - \hat{\mathbf{y}}_j(t)) & \text{if } x_{ij}(t) > d_{\max} \\ 0 & \text{if } d_{\min} \leq x_{ij}(t) \leq d_{\max} \\ 4 \sum_{j \in M_i} \eta \left(\frac{1}{x_{ij}^2(t)} - \frac{1}{d^2} \right) \left(\frac{1}{x_{ij}^2(t)} \right)^2 (\mathbf{x}_i(t) - \mathbf{x}_j(t)) & \text{if } x_{ij}(t) < d_{\min} \end{cases} \quad (40)$$

for $i = 1, \dots, N$.

The consensus problem is to converge the coordinates of point O^i on mobile robots to one point. However, considering the possibility of collision, we first use Δr as the transformed distance instead of the radius R of the robot. Thus, the transformed coordinates are on the line between point O^i and the centre of the robot. Then, if $x_{ij}(t) \in [d_{\min}, d_{\max}]$ for all $i, j = 1, \dots, N$, the robots are considered to have achieved consensus, and the control program stops. Since the actual volume of the robot should be considered, $d_{\min} = 2R - 2\Delta r + \delta$ and $d_{\max} = 2R + 2\Delta r + \delta$, where δ is the tolerance.

4.2. Experiment Configuration. As shown in Figure 6, the experimental setup is composed of robots named e-puck, which move on a smooth plane with two overhead CCD cameras to obtain the images of the robots moving. PC(i) is used to analyse the position and angle information of the robots by image processing designed using the software HALCON, and another PC(ii) is applied to calculate the control input $u_i(t)$ and send the control signal to each robot through a Bluetooth module.

In the experiment, the radius of each robot is $R = 37.5$ mm, the transformed distance is set as $\Delta r = 5$ mm, and the tolerance is set as $\delta = 10$ mm. Therefore, d_{\max} and d_{\min} in (37) are defined as $d_{\max} = 95$ mm and $d_{\min} = 75$ mm. The

gain of RPF is given as $\eta = 0.002$. To show the effect of the predictor, time delays are set artificially.

Figure 7 shows the experimental results in the graph topology of the three robots in Figure 1 using controller (40). The initial states, $(\xi_i(0), \zeta_i(0), \theta_i(0))$, are $A(1.35, 2.54, 1.33)$, $B(0.98, 2.99, -0.29)$, and $C(1.60, 3.07, -2.13)$, respectively. The design parameters are set as the coupling strength $k = 2$ and prediction gain $k_p = 0.8$. Time delay is set as $\tau = 0.25$ s artificially. The initial states of the predictor are set as $\hat{\mathbf{y}}(t) = \mathbf{0}$ for $-2\tau \leq t \leq 0$.

In Figure 7(a), the \times marks indicate the starting positions and the solid circles show the final positions of the robots in which the radius of the small circles is Δr and the transformed coordinates are on these circles. Both the final positions of the robots and the synchronization errors given in Figure 7(b) show that the robots converged to consensus intuitively.

Figure 8 shows the experimental results for controller (40) for four e-pucks in the graph topology in Figure 1. The initial coordinates are $A(1.12, 2.56, 0.98)$, $B(1.62, 2.57, 2.46)$, $C(1.59, 3.06, -2.29)$, and $D(1.15, 3.06, -0.84)$ for the four robots, respectively, and we set $\hat{\mathbf{y}}(t) = \mathbf{0}$ for $-2\tau \leq t \leq 0$ as the initial state of the predictor. Time delay is set as $\tau = 1$ s artificially, coupling strength is $k = 2$, and prediction gain $k_p = 0.4$.

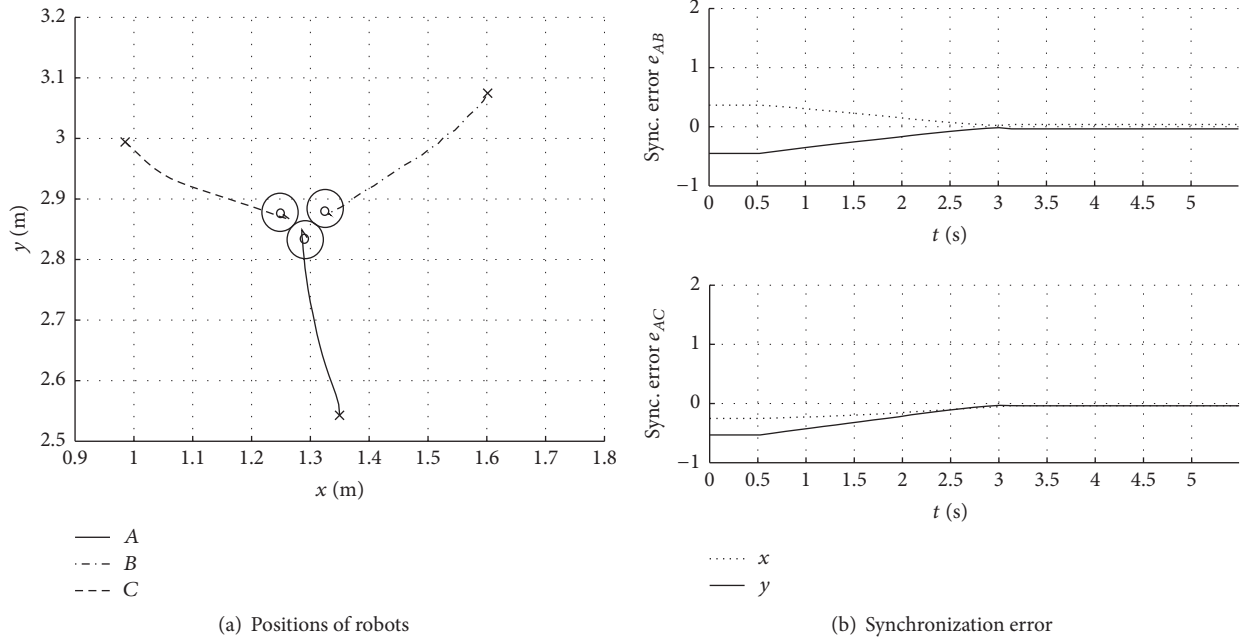


FIGURE 7: Experimental results for three robots with controller (40).

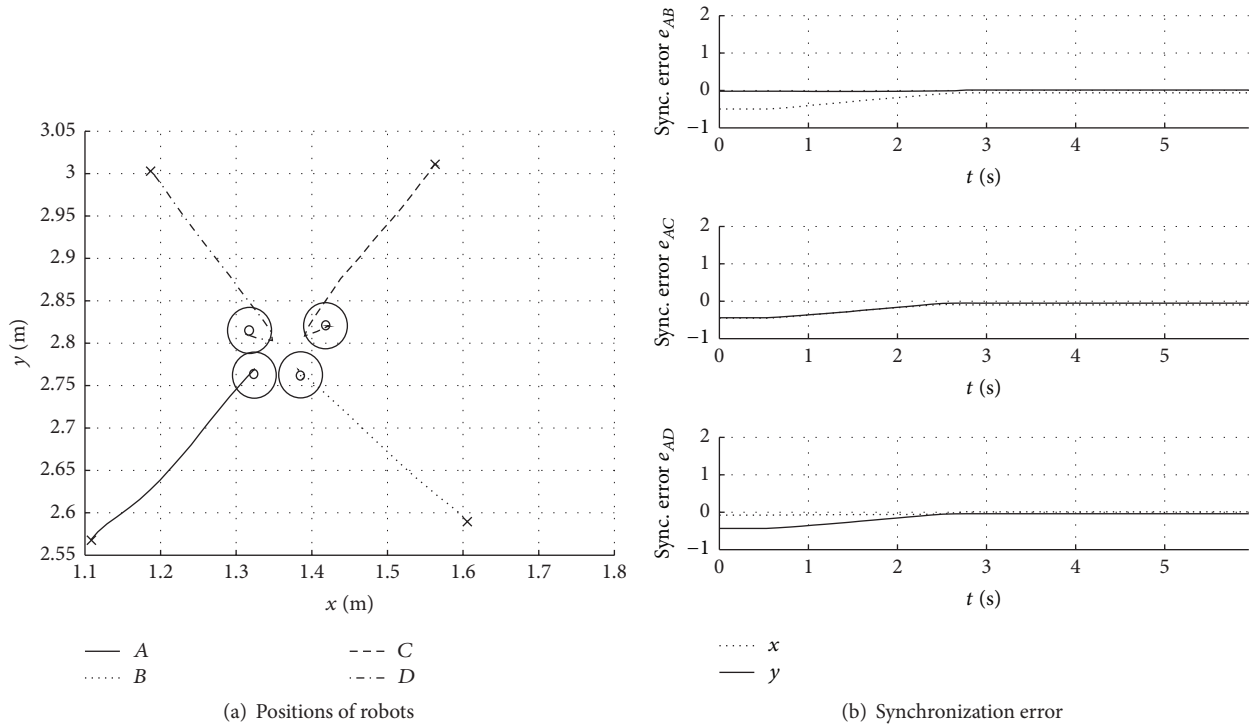


FIGURE 8: Experimental results for four robots with controller (40).

From the experimental results in Figure 8, we confirmed that consensus is achieved. Figure 8(a) shows the trajectories of the four robots that converge to one point. Figure 8(b) shows that the robots converge to consensus.

Figure 7 shows an experimental result for the same network topology, coupling strength, prediction gain, and initial

conditions as the simulation shown in Figure 2 by using the robots. In Figures 2(b) and 7(b), the synchronization errors both have the tendency of convergence to zero and the agents finally achieve consensus. In the experiment, we considered the volume of the robot and the collision problem. The achieved synchronization error is between $[d_{\min}, d_{\max}]$

due to the controller (37) in Figure 7(b). In Figures 3 and 8, the similar results are obtained for four agents.

Remark 6. In real applications, time-delay in network communication may be time-varying and/or unknown. According to the experimental results in [18], Internet-induced time delays between different countries are almost constant. If the variation of time-varying delay is relatively slower comparing with the velocity of convergence of prediction error, the delay can be considered as constant. In this case, the proposed method is available for the MAS using communication networks. Even if the practical time-delay is time-varying, it is possible to add artificial delay to true up the length of delay to a constant value and adopt the proposed scheme by overestimating the maximum size of delay.

5. Conclusions

In this paper, we considered the consensus problem of MAS with input and output time delays. A controller with a state predictor based on anticipating synchronization was proposed for this system. The consensus conditions for the controller were given, and we discussed the average consensus. We concluded that the proposed controller and predictor could cope with longer time delays, since the number of robots increased. We provided numerical simulations to show the validity of the control scheme. Validity was further confirmed in experiments with nonholonomic mobile robots based on the theoretical stability criteria and collision avoidance mechanism. It was shown that the validity of the proposed predictor-based controller could be used in real applications to control multiple mobile robots converging to consensus. In this study, to apply the predictor-based control approach, time-delay is considered as a constant value. Since time-delay is variable in real applications, we would like to discuss this problem in the future study.

Competing Interests

The authors declare that they have no competing interests.

Acknowledgments

This research is an extended version of a conference paper [2] which was presented at the 2015 IEEE Multi-Conference on Systems and Control. This work was partially supported by the Japan Society for the Promotion of Science (JSPS) Grant-in-Aid for Scientific Research (no. 26420424).

References

- [1] W. Qiao and R. Sipahi, "Consensus control under communication delay in a three-robot system: design and experiments," *IEEE Transactions on Control Systems Technology*, vol. 24, no. 2, pp. 687–694, 2016.
- [2] Y. Cao, T. Oguchi, P. B. Verhoeckx, and H. Nijmeijer, "Predictor-based consensus control of a multi-agent system with time-delays," in *Proceedings of the IEEE Conference on Control and Applications (CCA '15)*, pp. 113–118, Sydney, Australia, September 2015.
- [3] S. Ferrari, G. Foderaro, P. Zhu, and T. A. Wettergren, "Distributed optimal control of multiscale dynamical systems: a tutorial," *IEEE Control Systems*, vol. 36, no. 2, pp. 102–116, 2016.
- [4] G. Antonelli, F. Arrichiello, and S. Chiaverini, "Flocking for multi-robot systems via the Null-space-based behavioral control," *Swarm Intelligence*, vol. 4, no. 1, pp. 37–56, 2010.
- [5] N. Moshtagh, A. Jadbabaie, and K. Daniilidis, "Vision-based control laws for distributed flocking of nonholonomic agents," in *Proceedings of the IEEE International Conference on Robotics and Automation (ICRA '06)*, pp. 2769–2774, IEEE, Orlando, Fla, USA, May 2006.
- [6] W. Ren, "Multi-vehicle consensus with a time-varying reference state," *Systems and Control Letters*, vol. 56, no. 7-8, pp. 474–483, 2007.
- [7] K. D. Listmann, M. V. Masalawala, and J. Adamy, "Consensus for formation control of nonholonomic mobile robots," in *Proceedings of the IEEE International Conference on Robotics and Automation (ICRA '09)*, pp. 3886–3891, Kobe, Japan, May 2009.
- [8] G.-B. Dai and Y.-C. Liu, "Leaderless and leader-following consensus for networked mobile manipulators with communication delays," in *Proceedings of the IEEE Conference on Control and Applications (CCA '15)*, pp. 1656–1661, IEEE, Sydney, Australia, September 2015.
- [9] Y. Cai, Q. Zhan, and X. Xi, "Path tracking control of a spherical mobile robot," *Mechanism and Machine Theory*, vol. 51, pp. 58–73, 2012.
- [10] Y. Lan, G. Yan, and Z. Lin, "Synthesis of distributed control of coordinated path following based on hybrid approach," *Institute of Electrical and Electronics Engineers. Transactions on Automatic Control*, vol. 56, no. 5, pp. 1170–1175, 2011.
- [11] T. Oguchi and H. Nijmeijer, "Control of nonlinear systems with time-delay using state predictor based on synchronization," in *Proceedings of the Euromech Nonlinear Dynamics Conference (ENOC '05)*, pp. 1150–1156, Eindhoven, The Netherlands, August 2005.
- [12] R. Olfati-Saber and R. M. Murray, "Consensus problems in networks of agents with switching topology and time-delays," *Institute of Electrical and Electronics Engineers. Transactions on Automatic Control*, vol. 49, no. 9, pp. 1520–1533, 2004.
- [13] R. Olfati-Saber, J. A. Fax, and R. M. Murray, "Consensus and cooperation in networked multi-agent systems," *Proceedings of the IEEE*, vol. 95, no. 1, pp. 215–233, 2007.
- [14] A. Papachristodoulou, A. Jadbabaie, and U. Munz, "Effects of delay in multi-agent consensus and oscillator synchronization," *IEEE Transactions on Automatic Control*, vol. 55, no. 6, pp. 1471–1477, 2010.
- [15] X. Liu, W. Lu, and T. Chen, "Consensus of multi-agent systems with unbounded time-varying delays," *Institute of Electrical and Electronics Engineers. Transactions on Automatic Control*, vol. 55, no. 10, pp. 2396–2401, 2010.
- [16] K. H. Movric and F. L. Lewis, "Cooperative optimal control for multi-agent systems on directed graph topologies," *IEEE Transactions on Automatic Control*, vol. 59, no. 3, pp. 769–774, 2014.
- [17] K. Kojima, T. Oguchi, A. Alvarez-Aguirre, and H. Nijmeijer, "Predictor-based tracking control of a mobile robot with time-delays," in *Proceedings of the 8th IFAC Symposium on Nonlinear Control Systems (NOLCOS '10)*, pp. 167–172, Bologna, Italy, September 2010.
- [18] A. Alvarez-Aguirre, N. Van De Wouw, T. Oguchi, and H. Nijmeijer, "Predictor-based remote tracking control of a mobile

- robot,” *IEEE Transactions on Control Systems Technology*, vol. 22, no. 6, pp. 2087–2102, 2014.
- [19] K. Sakurama and K. Nakano, “Average-consensus problem for networked multi-agent systems with heterogeneous time-delays,” *IFAC Proceedings Volumes*, vol. 44, no. 1, pp. 2368–2375, 2011.
- [20] R. Wei and W. B. Randal, *Distributed Consensus in Multi-Vehicle Cooperative Control*, Springer, London, UK, 2008.
- [21] F. Mondada, M. Bonani, X. Raemy et al., “The e-puck, a robot designed for education in engineering,” in *Proceedings of the 9th Conference on Autonomous Robot Systems and Competitions*, pp. 59–65, Castelo Branco, Portugal, May 2009.
- [22] E. Rimon and D. E. Koditschek, “Exact robot navigation using artificial potential functions,” *IEEE Transactions on Robotics and Automation*, vol. 8, no. 5, pp. 501–518, 1992.

Research Article

MIMO PI Controllers for LTI Systems with Multiple Time Delays Based on ILMIs and Sensitivity Functions

Wajdi Belhaj and Olfa Boubaker

National Institute of Applied Sciences and Technology (INSAT), Centre Urbain Nord, BP 676, 1080 Tunis Cedex, Tunisia

Correspondence should be addressed to Olfa Boubaker; olfa.boubaker@insat.rnu.tn

Received 12 August 2016; Revised 9 November 2016; Accepted 5 December 2016; Published 20 February 2017

Academic Editor: Tamas Kalmar-Nagy

Copyright © 2017 Wajdi Belhaj and Olfa Boubaker. This is an open access article distributed under the Creative Commons Attribution License, which permits unrestricted use, distribution, and reproduction in any medium, provided the original work is properly cited.

In this paper, a MIMO PI design procedure is proposed for linear time invariant (LTI) systems with multiple time delays. The controller tuning is established in two stages and guarantees performances for set-point changes, disturbance variations, and parametric uncertainties. In the first stage, an iterative linear matrix inequality (ILMI) approach is extended to design PI controllers for systems with multiple time delays without performance guarantee, a priori. The second stage is devoted to improve the closed-loop performances by minimizing sensitivity functions. Simulations results carried out on the unstable distillation column, the stable industrial scale polymerization (ISP) reactor, and the non-minimum phase 4-tank benchmark prove the efficiency of the proposed approach. A comparative analysis with the conventional internal model control (IMC) approach, a multiloop IMC-PI approach, and a previous ILMI PID approach proves the superiority of the proposed approach compared to the related ones.

1. Introduction

PID controllers have been at the heart of control engineering practice for several decades [1, 2]. They are widely used in industrial applications as no other controllers match simple control structure, fewer tuning parameters, and robustness against uncertainties. However, until now, a high percentage of PID control systems seem to be badly tuned and many difficulties occur essentially when the multi-input multi-output systems are considered [3–5]. One major reason may be explained by coupling interactions between the different loops and mainly the negligence of uncertain and immeasurable dead times. Tuning multiloop PID controllers for LTI systems with multiple time delays [6–9] is then considered until now as a challenging problem in control theory. In this framework, the internal model control (IMC) method is considered as the most conventional and effective approach for PID controller design while taking into account time delays [10–12]. The design of MIMO IMC-PID controllers is based on a series of SISO controllers using IMC interaction measures between the different loops. This method becomes

very hard when the number of inputs/outputs increases. Even more, its implementation may fail when the interaction measures between the different loops are so high. The last difficulty represents the main disadvantage of this method and an alternative solution was proposed by Vu and Lee [13] to solve such a problem. Unfortunately, this result remains applicable only when the first-order MIMO systems are considered.

On the other hand, iterative linear matrix inequalities (ILMIs) are known to be powerful tools to solve multivariable control problems. Particularly, ILMI approaches were already used to design PID controllers for LTI systems without delays [14–18]. The basic idea was based on transforming the PID controller into an equivalent static output feedback (SOF) stabilization one by augmenting, using some new state variables, the dimension of the controlled system. Unfortunately, such controllers are known by their bad performances compared to those designed via IMC approaches (when applicable).

As Loop Shaping (LS) techniques [19, 20] are well known for their abilities to improve the closed-loop system performances by minimizing the signal transmission from

load disturbances and measurement noise to input and output process or in terms of requirements on the sensitivity functions and/or complementary sensitivity functions [21–23], this paper suggests using this concept for improving the MIMO PI controller performances computed via ILMIs. The proposed approach overcomes the problems introduced by the well known IMC method when the fully cross-coupled multivariable systems are considered. Its implementation requires two steps: in the first step, the ILMI method proposed by Zheng et al. [14], appropriate for systems without delays, is extended for the design of PI controller for multiple time delay systems. As such approach generally gives bad performances, a second stage is then launched in order to improve the performances of the closed-loop system by shaping the already designed PI controller by minimizing the sensitivity function of the system.

To illustrate the effectiveness and the performances of the proposed approach, three examples of multiple time delay systems including unstable, stable, and non-minimum systems are considered. A comparative analysis with related approaches is also given to prove the superiority of the proposed approach.

The paper is organized as follows: The problem formulation is stated in Section 2. Model reduction of the MIMO system with multiple time delays is detailed in Section 3. Section 4 is devoted to the main results. Section 5 shows the validity of the proposed approach where a comparative study with related approaches using typical examples for set-point tracking, disturbance rejection, and parametric uncertainties scenarios is considered.

2. Problem Statement

Consider a nominal multivariable LTI system with multiple time delays described by

$$\begin{aligned}\dot{x}(t) &= A_0 x(t) + A_1 x(t - \tau_1) + B_0 u(t - \tau_2) \\ &\quad + B_1 u(t - \tau_3), \\ y(t) &= Cx(t),\end{aligned}\quad (1)$$

where $x(t) \in \mathcal{R}^n$, $u(t) \in \mathcal{R}^m$, and $y(t) \in \mathcal{R}^p$ are the state vector, the control vector, and the output vector, respectively. $A_0 \in \mathcal{R}^{n \times n}$, $A_1 \in \mathcal{R}^{n \times n}$, $B_0 \in \mathcal{R}^{n \times m}$, $B_1 \in \mathcal{R}^{n \times m}$, and $C \in \mathcal{R}^{p \times n}$ are known constant matrices. τ_1 , τ_2 , and τ_3 are time delays.

The objective is to design a finite dimensional PI controller described by

$$u(t) = F_1 e(t) + F_2 \int_0^t e(t) dt, \quad (2)$$

where $e(t) = r(t) - y(t)$, $r(t) \in \mathcal{R}^p$, is the set-point vector and $F_1, F_2 \in \mathcal{R}^{m \times p}$ are proportional and time integral gain matrices, respectively, that stabilize the system (1) to the set-point vector.

Let $G(s) \in \mathcal{R}^{p \times m}$ be the general transfer matrix of the delayed system (1), computed as described in [24], and $K(s) =$

$[K_{ij}(s)] \in \mathcal{R}^{m \times p}$ the transfer matrix of the PI controller given by

$$K_{ij}(s) = F_{1ij} + \frac{F_{2ij}}{s}, \quad (3)$$

where $K_{ij}(s)$ is the ij th element of the transfer matrix $K(s)$, F_{1ij} is the proportional gain of the ij th element of $K(s)$, and F_{2ij} is the integral gain of the ij th element of $K(s)$.

For such PI controller there are $2 \times m \times p$ parameters to be tuned for a plant with m inputs and p outputs.

The last control problem is very complex since system (1) is a MIMO infinite dimensional system. To be relaxed, the control problem will be organized in two subproblems.

2.1. Subproblem 1: Design a Finite Dimensional PI Controller for Just SOF Stabilization. In this stage, the infinite dimensional system (1) will be reduced to the finite dimensional system (4)–(5) whereas the PI controller (2) will be transformed into the SOF controller (6) described, respectively, by

$$\dot{\tilde{z}} = \tilde{A}\tilde{z} + \tilde{B}u, \quad (4)$$

$$\tilde{y} = \tilde{C}\tilde{z}, \quad (5)$$

$$u = \tilde{F}\tilde{y}, \quad (6)$$

where $\tilde{z}(t) \in \mathcal{R}^{n'}$, $u(t) \in \mathcal{R}^m$, and $\tilde{y}(t) \in \mathcal{R}^{p'}$ are the state vector, the control vector, and the output vector of the approximated system, respectively. $\tilde{A} \in \mathcal{R}^{n' \times n'}$, $\tilde{B} \in \mathcal{R}^{n' \times m}$, and $\tilde{C} \in \mathcal{R}^{p' \times n'}$ are matrices related to the approximated system to be computed using the approximation method and the SOF transformation and $\tilde{F} \in \mathcal{R}^{m \times p'}$ and is the SOF feedback gain matrix, to be designed under the following assumptions.

Assumption 1. The set-point vector $r(t)$ in (2) is assumed to be null ($r(t) = 0$).

Assumption 2. τ_1 , τ_2 , and τ_3 are assumed to be uncertain but constant delays.

Assumption 3. The PI controller (2) is well-posed.

Assumption 4. The finite dimensional closed-loop dynamics $\dot{\tilde{z}} = (\tilde{A} + \tilde{B}\tilde{F}\tilde{C})\tilde{z}$ with a realization $(\tilde{A}, \tilde{B}, \tilde{C})$ is stabilizable via SOF controller.

To this end, the PI design procedure is proposed in Section 4.1.

2.2. Subproblem 2: Set-Point Stabilization and Output Disturbance Attenuation by Minimizing Sensitivity Functions. The objective of the subproblem 2 is to design a shaped controller described by

$$K_{sh}(s) = V_1(s) K(s) V_2(s) \quad (7)$$

that improves the closed-loop response considering a shaped system described by

$$G_{sh}(s) = V_1(s) G(s) V_2(s), \quad (8)$$

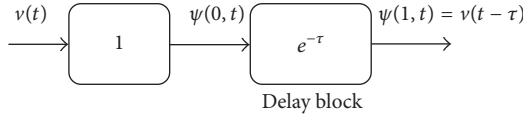


FIGURE 1: Modeling a delayed variable via a distributed parameter system.

where $V_1(s) \in \mathbb{R}^{p \times p}$ and $V_2(s) \in \mathbb{R}^{m \times m}$ are a pre- and postcompensators to be chosen in order to satisfy, in closed-loop, performance specifications such as set-point stabilization and load disturbance rejection.

The most crucial part of the design procedure is to find the appropriate weighting matrices $V_1(s)$ and $V_2(s)$. Note that the shape of the weights is determined by the closed-loop design specifications. Once the desired loop shape is achieved, the final controller $K_{\text{fin}}(s)$ to be applied to the nominal transfer matrix $G(s)$ is then constructed. To this end, a Loop Shaping design procedure is proposed in Section 4.2.

3. Model Reduction of the MIMO System with Multiple Time Delays

Each delayed variable can be modeled as a distributed parameter system described by a partial differential equation as follows [25]:

$$\frac{\partial \psi(z, t)}{\partial t} = -\frac{1}{\tau} \frac{\partial \psi(z, t)}{\partial z} \quad (9)$$

with the boundary condition

$$v(t) = \psi(0, t) \quad (10)$$

and the output equations:

$$v(t - \tau) = \psi(1, t), \quad (11)$$

where t and z are time and pseudospace variables, respectively. As shown by Figure 1, $v(t)$, $\psi(z, t)$, and $v(t - \tau)$ are the input, the state variable, and the output of the delay block, respectively. τ is a constant time delay.

For numerical simulation or control design purposes, an infinite dimensional system is generally reduced to a finite dimensional system by using an approximation method. Within the framework of weighted residuals methods, the orthogonal collocation method is applied in this paper to approximate the partial differential equations described by relation (9) augmented by boundary conditions (10)-(11) for its simplicity since it avoids integration [26].

The principle of the orthogonal collocation method is to search a finite dimensional approximation for the distributed parameter variable $\psi(z, t)$ in the following form [27]:

$$\psi^*(z, t) = \sum_{i=0}^N c_i(t) L_i^N(z), \quad (12)$$

where ψ^* denotes the approximation of $\psi(z, t)$; N is the order reduction; $c_i(t)$ are unknown time-varying coefficients chosen such that the approximated solution is the exact one at the collocation points such that

$$c_i(t) = \psi^*(z_i, t) = \psi(z, t)|_{z=z_i}, \quad \forall i \in \{0, \dots, N\} \quad (13)$$

and $L_i^N(z)$ are the N th order Lagrange interpolation polynomials; that is:

$$L_i^N(z) := \prod_{\substack{j=0 \\ j \neq i}}^N \frac{z - z_j}{z_j - z_i}, \quad (14)$$

where $z_0, z_1, \dots, z_N \in [0, 1]$ are the collocation points of the method. In this paper, the internal collocation points are considered as the zeros of the $(N + 2)$ th order Jacobi polynomial defined for $i = 1, \dots, N + 2$ by Lefèvre et al. [27] as follows:

$$p_N^{(p,q)} = (z - g_N^{(p,q)}) p_{N-1}^{(p,q)} - h_N^{(p,q)} p_{N-2}^{(p,q)} \quad (15)$$

with $p_0^{(p,q)} = 1$ and where coefficients $h_N^{(p,q)}$ and $g_N^{(p,q)}$ are defined as follows:

$$h_N^{(p,q)} := \begin{cases} \frac{(N-1)(N+p-1)(N+q-1)(N+p+q-1)}{(2N+p+q-1)(2N+p+q-2)^2(2N+p+q-3)}, & \text{if } N > 2, \\ \frac{(p+1)(q+1)}{(p+q+2)^2(p+q+3)}, & \text{if } N = 2, \\ 0, & \text{otherwise,} \end{cases} \quad (16)$$

$$g_N^{(p,q)} := \begin{cases} \frac{1}{2} \left(1 - \frac{p^2 - q^2}{(2N+p+q-1)^2 - 1} \right), & \text{if } N > 1, \\ \frac{q+1}{p+q+2}, & \text{if } N = 1, \end{cases}$$

where p and q are two constant parameters affecting the position of the collocation points.

By applying delay variable approximation on each delayed variable of the vectors $x(t - \tau_1)$, $u(t - \tau_2)$, and $u(t - \tau_3)$, the

following $3(N + 1)$ finite dimensional equations can be then obtained from the partial differential equation (9), [28]:

$$\begin{aligned}\dot{\psi}_1(t) &= -\frac{1}{\tau_1}\bar{A}_1\psi_1(t) + \frac{1}{\tau_1}\bar{B}_1x(t), \\ \dot{\psi}_2(t) &= -\frac{1}{\tau_2}\bar{A}_2\psi_2(t) + \frac{1}{\tau_2}\bar{B}_2u(t), \\ \dot{\psi}_3(t) &= -\frac{1}{\tau_3}\bar{A}_3\psi_3(t) + \frac{1}{\tau_3}\bar{B}_3u(t),\end{aligned}\quad (17)$$

augmented by the following outputs:

$$\begin{aligned}x(t - \tau_1) &= \psi_1(1, t) = \bar{C}_1\psi_1(t), \\ u(t - \tau_2) &= \psi_2(1, t) = \bar{C}_2\psi_2(t), \\ u(t - \tau_3) &= \psi_3(1, t) = \bar{C}_3\psi_3(t),\end{aligned}\quad (18)$$

where for $k = 1, 2, 3$, $\bar{A}_i, \bar{B}_i, \bar{C}_i$ are computed as given in [28].

Let consider Cauchy's formula for the interpolation error defined by Lefèvre et al. [27] as follows:

$$e_N(z, t) = \psi(z, t) - \psi^*(z, t) \quad (19)$$

and assume that the unknown solution $\psi(z, t)$ is sufficiently continuously differentiable; we have then

$$e_N(z, t) = w(z) \frac{\psi(z)^{(N+1)}(\eta(z), t)}{(N+1)!}, \quad (20)$$

where $w(z) := \prod_{j=0}^N (z - z_j)$ and $\eta(z) \in [-1, +1]$.

Hence, we try to choose the interior collocation points z_1, \dots, z_{N-1} that minimize the interpolation error (19). Without any a priori knowledge on the behavior of the exact solution, this problem reduces to finding z_1, \dots, z_{N-1} such that $\psi(z)$ is minimal.

By considering the case study of the Chebyshev polynomials belonging to the family of Jacobi polynomials, and, corresponding to the values of the parameters $p = q = -1/2$, the corresponding minimal norm is given by Lefèvre et al. [27] as follows:

$$\|e_N\|_\infty \leq \frac{\|\psi(z)^{N+1}(\eta(z), t)\|_\infty}{(N+1)!2^{N-2}}. \quad (21)$$

Through the result (21), we demonstrate that the interpolation error for a variable delay approximation is always bounded for the parameters $p = q = -1/2$.

4. Main Results

4.1. PI Controller Design via ILMIs. In the following, the SOF transformation of the PI controller of the delayed system (1) will be detailed. Using (18), the system (1) can be written as follows:

$$\begin{aligned}\dot{x}(t) &= A_0x(t) + A_1\bar{C}_1\psi_1(t) + B_0\bar{C}_2\psi_2(t) \\ &\quad + B_1\bar{C}_3\psi_3(t), \\ y(t) &= Cx(t).\end{aligned}\quad (22)$$

Let now

$$\tilde{z}^T = [\tilde{z}_1^T \quad \tilde{z}_2^T]^T, \quad (23)$$

where:

$$\begin{aligned}\tilde{z}_1 &= [x(t) \quad \psi_1(t) \quad \psi_2(t) \quad \psi_3(t)] \in \mathfrak{R}^{4n}, \\ \tilde{z}_2(t) &= \int_0^t y(t) dt\end{aligned}\quad (24)$$

and let:

$$\tilde{y} = [\tilde{y}_1 \quad \tilde{y}_2]^T = \tilde{C}\tilde{z}, \quad (25)$$

where:

$$\begin{aligned}\tilde{y}_1 &= y = Cx = [C \quad 0 \quad 0 \quad 0 \quad 0] \tilde{z}, \\ \tilde{y}_2 &= \int_0^t y(t) dt = [0 \quad 0 \quad 0 \quad 0 \quad I] \tilde{z}.\end{aligned}\quad (26)$$

The state space of a new augmented system controlled via an SOF controller is then deduced as follows:

$$\begin{aligned}\dot{\tilde{z}} &= \tilde{A}\tilde{z} + \tilde{B}u, \\ \tilde{y} &= \tilde{C}\tilde{z}, \\ u &= \tilde{F}\tilde{y},\end{aligned}\quad (27)$$

where:

$$\begin{aligned}\tilde{A} &= \begin{pmatrix} A_0 & A_1\bar{C}_1 & B_0\bar{C}_2 & B_1\bar{C}_3 & 0 \\ \frac{1}{\tau_1}\bar{B}_1 & -\frac{1}{\tau_1}\bar{A}_1 & 0 & 0 & 0 \\ 0 & 0 & -\frac{1}{\tau_2}\bar{A}_2 & 0 & 0 \\ 0 & 0 & 0 & -\frac{1}{\tau_3}\bar{A}_3 & 0 \\ C & 0 & 0 & 0 & 0 \end{pmatrix} \\ &\in \mathfrak{R}^{n' \times n'}, \\ \tilde{B} &= \begin{pmatrix} 0 \\ 0 \\ \frac{1}{\tau_2}\bar{B}_2 \\ \frac{1}{\tau_3}\bar{B}_3 \\ 0 \end{pmatrix} \in \mathfrak{R}^{n' \times m},\end{aligned}\quad (28)$$

$$\tilde{C} = [\bar{C}_1^T \quad \bar{C}_2^T]^T \in \mathfrak{R}^{p' \times n'},$$

$$\bar{C}_1 = [C \quad 0 \quad 0 \quad 0 \quad 0] \in \mathfrak{R}^{p \times n'},$$

$$\bar{C}_2 = [0 \quad 0 \quad 0 \quad 0 \quad I_{p \times p}] \in \mathfrak{R}^{p \times n'}.$$

Taking into account (27), the control law (2) under Assumption 1 can be written as follows:

$$u = -(F_1\tilde{y}_1 + F_2\tilde{y}_2). \quad (29)$$

On the other hand, we have from (27) the following:

$$u = -(\tilde{F}_1 \tilde{y}_1 + \tilde{F}_2 \tilde{y}_2) = \tilde{F} \tilde{y}. \quad (30)$$

We can deduce that once the matrix $\tilde{F} = [\tilde{F}_1 \quad \tilde{F}_2] \in \mathfrak{R}^{m \times p'}$ is designed the closed-loop system (4)–(6) is asymptotically stable. Considering analogy between (29) and (30), the original PI gains can be recovered as follows:

$$[F_1 \quad F_2] = [\tilde{F}_1 \quad \tilde{F}_2]. \quad (31)$$

Theorem 5. *The multivariable LTI system with multiple time delays (1) is stabilizable via SOF if and only if there exist a constant matrix $\tilde{F} = [\tilde{F}_1 \quad \tilde{F}_2] \in \mathfrak{R}^{m \times p'}$ and a symmetric positive definite matrix $X = X^T > 0$, $X \in \mathfrak{R}^{n' \times n'}$ satisfying the following matrix inequality:*

$$\begin{aligned} & \tilde{A}^T X + X \tilde{A} - X \tilde{B} \tilde{B}^T X + \left(\tilde{B}^T X + \tilde{F} \tilde{C} \right)^T \left(\tilde{B}^T X + \tilde{F} \tilde{C} \right) \\ & < 0 \end{aligned} \quad (32)$$

such that

$$\begin{aligned} F_1 &= \tilde{F}_1, \\ F_2 &= \tilde{F}_2. \end{aligned} \quad (33)$$

Proof.

Sufficiency. Note that

$$\begin{aligned} & (\tilde{A} + \tilde{B} \tilde{F} \tilde{C})^T X + X (\tilde{A} + \tilde{B} \tilde{F} \tilde{C}) \\ & \leq (\tilde{A} + \tilde{B} \tilde{F} \tilde{C})^T X + X (\tilde{A} + \tilde{B} \tilde{F} \tilde{C}) + \tilde{C}^T \tilde{F}^T \tilde{F} \tilde{C} \\ & = \tilde{A}^T X + X \tilde{A} - X \tilde{B} \tilde{B}^T X \\ & \quad + \left(\tilde{B}^T X + \tilde{F} \tilde{C} \right)^T \left(\tilde{B}^T X + \tilde{F} \tilde{C} \right) < 0. \end{aligned} \quad (34)$$

From Lyapunov's theory, the closed-loop system $\Sigma_c : \dot{z} = (\tilde{A} + \tilde{B} \tilde{F} \tilde{C})z$ is then asymptotically stable.

Necessity. Suppose that Σ_c is asymptotically stable for some \tilde{F} . Then there exists $X = X^T > 0$ such that

$$(\tilde{A} + \tilde{B} \tilde{F} \tilde{C})^T X + X (\tilde{A} + \tilde{B} \tilde{F} \tilde{C}) < 0. \quad (35)$$

It is easy to find that there exists a scalar $\rho > 0$ such that

$$(\tilde{A} + \tilde{B} \tilde{F} \tilde{C})^T X + X (\tilde{A} + \tilde{B} \tilde{F} \tilde{C}) + \frac{1}{\rho^2} \tilde{C}^T \tilde{F}^T \tilde{F} \tilde{C} < 0; \quad (36)$$

that is,

$$\begin{aligned} & \tilde{A}^T X + X \tilde{A} - \rho^2 X \tilde{B} \tilde{B}^T X \\ & \quad + \left(\rho \tilde{B}^T X + \frac{1}{\rho} \tilde{F} \tilde{C} \right)^T \left(\rho \tilde{B}^T X + \frac{1}{\rho} \tilde{F} \tilde{C} \right) < 0, \\ & \tilde{A}^T X + X \tilde{A} - \rho^2 X \tilde{B} \tilde{B}^T X \\ & \quad + \left(\rho \tilde{B}^T X + \frac{1}{\rho} \tilde{F} \tilde{C} \right)^T \left(\rho \tilde{B}^T X + \frac{1}{\rho} \tilde{F} \tilde{C} \right) < 0. \end{aligned} \quad (37)$$

Obviously, (37) is equivalent to

$$\begin{aligned} & \rho^2 \tilde{A}^T X + \rho^2 X \tilde{A} - \rho^4 X \tilde{B} \tilde{B}^T X \\ & \quad + \left(\rho^2 \tilde{B}^T X + \tilde{F} \tilde{C} \right)^T \left(\rho^2 \tilde{B}^T X + \tilde{F} \tilde{C} \right) < 0. \end{aligned} \quad (38)$$

By substituting $\rho^2 X$ with X in (38), we obtain inequality (32). Condition (33) is already proved in (31).

Due to the term $-X \tilde{B} \tilde{B}^T X$, (32) cannot be simplified to an LMI. Similarly to SOF control problem described in [14–16], an ILMI algorithm can be addressed to solve the Bilinear Matrix Inequality (BMI) in (32). To accommodate the $-X \tilde{B} \tilde{B}^T X$ term, an additional design variable Y is introduced. Because $(Y - X)^T \tilde{B} \tilde{B}^T (Y - X) \geq 0$ for any $Y > 0$ and X for the same dimension, we obtain

$$Y^T \tilde{B} \tilde{B}^T X + X^T \tilde{B} \tilde{B}^T Y - Y^T \tilde{B} \tilde{B}^T Y \leq X^T \tilde{B} \tilde{B}^T X. \quad (39)$$

By combining (32) and (39), a sufficient condition for the existence of SOF gain matrix \tilde{F} is obtained such that

$$\begin{aligned} & \tilde{A}^T X + X \tilde{A} - Y \tilde{B} \tilde{B}^T X - X \tilde{B} \tilde{B}^T Y + Y \tilde{B} \tilde{B}^T Y \\ & \quad + \left(\tilde{B}^T X + \tilde{F} \tilde{C} \right)^T \left(\tilde{B}^T X + \tilde{F} \tilde{C} \right) < 0. \end{aligned} \quad (40)$$

Considering the $\alpha/2$ stabilizability via SOF concept [29], if the matrix inequality (40) has a solution ($X > 0$, \tilde{F}), then there exist a real number $\alpha \geq 0$ and a fixed matrix $Y > 0$ such that

$$\begin{aligned} & \tilde{A}^T X + X \tilde{A} - Y \tilde{B} \tilde{B}^T X - X^T \tilde{B} \tilde{B}^T Y + Y^T \tilde{B} \tilde{B}^T Y \\ & \quad + \left(\tilde{B}^T X + \tilde{F} \tilde{C} \right)^T \left(\tilde{B}^T X + \tilde{F} \tilde{C} \right) - \alpha X < 0. \end{aligned} \quad (41)$$

Based on the idea that all eigenvalues of $\tilde{A} + \tilde{B} \tilde{F} \tilde{C}$ are shifted progressively towards the left-half-plane through the reduction of α , we may close in on the feasibility of (32) [29]. Using Schur complement, inequality (41) is equivalent to the following matrix inequality:

$$\begin{bmatrix} \tilde{A}^T X + X \tilde{A} - Y \tilde{B} \tilde{B}^T X - X^T \tilde{B} \tilde{B}^T Y + Y^T \tilde{B} \tilde{B}^T Y - \alpha X & \left(\tilde{B}^T X + \tilde{F} \tilde{C} \right)^T \\ \left(\tilde{B}^T X + \tilde{F} \tilde{C} \right) & -I \end{bmatrix} < 0. \quad (42)$$

The previous inequality (42) points to an iterative approach to solve \tilde{F} and $X > 0$; namely, if Y is fixed in (42), then it reduces to an LMI problem in the unknowns α , \tilde{F} and X . \square

The following is a constructive ILMI algorithm for PI control of LTI MIMO with multiple delays systems, and the explanations are given in Remark 7.

Algorithm 6.

Step 1. Define the orthogonal collocation method parameters N , p , and q .

Step 2. Transform the infinite dimensional system (1) to a finite dimensional system (17)-(18) by computing matrices $\bar{A}_1, \bar{A}_2, \bar{A}_3, \bar{B}_1, \bar{B}_2, \bar{B}_3, \bar{C}_1, \bar{C}_2$, and \bar{C}_3 .

Step 3. Design the SOF transformation to give the system's state space realization $(\tilde{A}, \tilde{B}, \tilde{C})$. If it does proceed to Step 4.

Step 4. Set $i = 1$ and choose $Y_1 = I_{n'} + \varepsilon_1$ where $\varepsilon_1 \geq 0$.

Step 5. Solve the following optimization problem for X_i, \tilde{F} , and α_i :

OP1: Minimize α_i subject to the following LMI constraints:

$$\begin{bmatrix} \Sigma_{1i} & (\tilde{B}^T X_i + \tilde{F}\tilde{C})^T \\ \tilde{B}^T X_i + \tilde{F}\tilde{C} & -I \end{bmatrix} < 0, \quad X_i > 0, \quad (43)$$

where $\Sigma_{1i} = \tilde{A}^T X_i + X_i \tilde{A} - Y_i \tilde{B} \tilde{B}^T X_i - X_i \tilde{B} \tilde{B}^T Y_i + Y_i \tilde{B} \tilde{B}^T Y_i - \alpha_i X_i$. Denote by α_i^* the minimized value of α_i .

Step 6. If $\alpha_i^* \leq 0$, the feedback matrix gains are $F_1 = \tilde{F}_1$ and $F_2 = \tilde{F}_2$. Stop. Otherwise, go to Step 7.

Step 7. Solve the following optimization problem for X_i and \tilde{F} .

OP2: Minimize $\text{tr}(X_i)$ subject to LMI constraints (43) with $\alpha_i = \alpha_i^*$, where tr stands for the trace of a square matrix. Denote by X_i^* the optimal X_i . The feedback matrix gains are $F_1 = \tilde{F}_1$ and $F_2 = \tilde{F}_2$.

Step 8. If $\|Y_i \tilde{B} - X_i^* \tilde{B}\| < \delta$, where δ is a prescribed tolerance, go to Step 9; otherwise, set $i := i + 1$, $Y_i = X_i^*$ and go to Step 5.

Step 9. It cannot be decided by this algorithm whether SOF problem is solvable. Stop.

Remark 7. Due to the bad performances generated by initial data selection in ILMI algorithms [14, 15], $Y_1 = I_{n'} + \varepsilon_1$ is proposed in this paper where $\varepsilon_1 > 0$, yielding to a feasible solution.

4.2. Improving Closed-Loop Performances. In this section, a modified approach of Loop Shaping technique [19] will be introduced to design the multiloop PI controller as

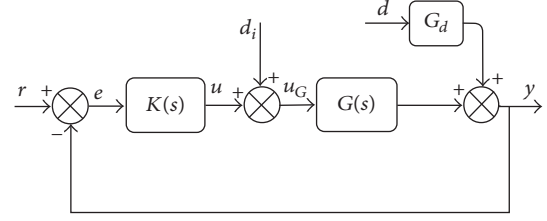


FIGURE 2: Block diagram of the controlled system.

described in subproblem 2. Figure 2 shows the block diagram of the controlled system where r, y, u, u_G, e, d and d_i denote the set-point vector, the output vector, the control signal vector, the process control signal vector, the error vector, the output disturbance vector, and the input disturbance vector, respectively.

Let us define the input loop transfer matrix, L_i , and the output transfer matrix, L_o , respectively, as follows [20]:

$$\begin{aligned} L_i &= KG, \\ L_o &= GK. \end{aligned} \quad (44)$$

The input sensitivity matrix is defined as the transfer matrix from d_i to u_G such as

$$\begin{aligned} S_i &= (I + L_i)^{-1}, \\ u_G &= S_i d_i \end{aligned} \quad (45)$$

and the output sensitivity matrix is defined as the transfer matrix from d to y such that

$$\begin{aligned} S_o &= (I + L_o)^{-1}, \\ y &= S_o G_d d. \end{aligned} \quad (46)$$

The input and output complementary sensitivity matrices are defined as follows:

$$\begin{aligned} T_i &= I - S_i = L_i (I + L_i)^{-1}, \\ T_o &= I - S_o = L_o (I + L_o)^{-1}. \end{aligned} \quad (47)$$

It is easy to see that the closed-loop system, if it is internally stable, satisfies the following equations:

$$y = T_o r + S_o G_d d_i + S_o G_d d, \quad (48)$$

$$u = K S_o r - K S_o G_d d - T_i d_i, \quad (49)$$

$$e = S_o (r - G_d d) - S_o G_d d_i, \quad (50)$$

$$u_G = K S_o r - K S_o G_d d + S_i d_i. \quad (51)$$

Equation (48) shows that the effects of the disturbance d on the plant output y can be made "small" by making the output sensitivity function S_o small, as G_d is fixed. Similarly, (50) shows the effect of the set-point r to the error e by making S_o as small as possible. The notion of smallness for a transfer matrix in a certain range of frequencies can

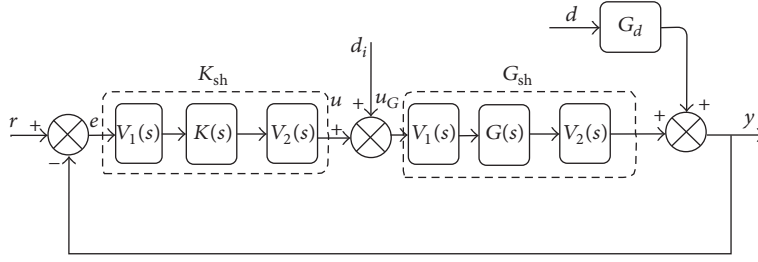


FIGURE 3: Block diagram of a controlled shaped system.

be made explicit using frequency dependent singular values particularly minimizing $\bar{\sigma}(S_o)$ where $\bar{\sigma}$ is the maximum singular value. Similarly to the conventional Loop Shaping design [19, 20], shaping the open-loop nominal system corresponds to shaping the loop gain GK using the pre- and postcompensators $V_1(s)$ and $V_2(s)$. The new shaped control system is shown in Figure 3. It is obvious that a well designed control system should meet, at least, the following requirements: (1) stability, (2) set-point tracking, and (3) output disturbance attenuation. Let us then define the input loop transfer matrix, L_{ish} , and the output transfer matrix, L_{osh} , as

$$\begin{aligned} L_{ish} &= K_{sh} G_{sh}, \\ L_{osh} &= G_{sh} K_{sh}. \end{aligned} \quad (52)$$

The input sensitivity matrix is defined as the transfer matrix from d_i to u_G as follows:

$$\begin{aligned} S_{ish} &= (I + L_{ish})^{-1}, \\ u_G &= S_{ish} d_i \end{aligned} \quad (53)$$

and the output sensitivity matrix is defined as the transfer matrix from d to y as follows:

$$\begin{aligned} S_{osh} &= (I + L_{osh})^{-1}, \\ y &= S_{osh} G_d d. \end{aligned} \quad (54)$$

The input and output complementary sensitivity matrices are defined as

$$\begin{aligned} T_{ish} &= I - S_{ish} = L_{ish} (I + L_{ish})^{-1}, \\ T_{osh} &= I - S_{osh} = L_{osh} (I + L_{osh})^{-1}. \end{aligned} \quad (55)$$

It is easy to see that the closed-loop system, if it is internally stable, satisfies the following equations:

$$y = T_{osh} r + S_{osh} G_{sh} d_i + S_{osh} G_d d, \quad (56)$$

$$u = K_{sh} S_{osh} r - K_{sh} S_{osh} G_d d - T_{ish} d_i, \quad (57)$$

$$e = S_{osh} (r - G_d d) - S_{osh} G_{sh} d_i, \quad (58)$$

$$u_G = K_{sh} S_{osh} r - K_{sh} S_{osh} G_d d + S_{ish} d_i. \quad (59)$$

As G_d is fixed, from (56) and (58), good set-point tracking and output disturbance attenuation would require the maximum singular value of the output sensitivity matrix of the shaped system $\bar{\sigma}(S_{osh})$ be made small such as

$$\begin{aligned} \bar{\sigma}(S_{osh}) &= \bar{\sigma}((I + G_{sh} K_{sh})^{-1}) = \frac{1}{\underline{\sigma}(I + G_{sh} K_{sh})} \\ &\leq \frac{1}{\underline{\sigma}(G_{sh} K_{sh})}. \end{aligned} \quad (60)$$

It should be indicated that improving the closed-loop shaped system performances over those of the nominal system would require $\bar{\sigma}(S_{osh})$ be made smaller than $\bar{\sigma}(S_o)$, particularly in the low frequency range where d is usually significant. As $G(s)$ and $K(s)$ are fixed by subproblem 1, $V_1(s)$ and $V_2(s)$ play a key role in the Loop Shaping design procedure. Thus, synthesis of the shaped controller K_{sh} is reduced to choose an appropriate $V_1(s)$ and $V_2(s)$ in order to guarantee closed-loop performances, under the following:

$$\min \bar{\sigma}(S_{osh}) \quad (61)$$

such that

$$\bar{\sigma}(S_{osh}) < \bar{\sigma}(S_o). \quad (62)$$

Figure 4 synthesizes the Loop Shaping design procedure proposed in this paper where the proposed Loop Shaping design procedure is stated below:

Algorithm 8.

Step 1. Consider the PI controller designed via Algorithm 6. Assume that the closed-loop system performances are not well performed and define the control objectives for the desired closed-loop system responses (good disturbance rejection, steady state error minimization).

Step 2. Choose a precompensator $V_1(s)$ and a postcompensator $V_2(s)$ such that the singular values of the nominal plant $G(s)$ are shaped to give a desired open-loop shape (high low frequency gain and low high frequency gain).

Step 3. For the shaped plant $G_{sh}(s)$, if the control objectives and constraint (62) are satisfied then go to Step 4. Else adjust $V_1(s)$ and $V_2(s)$ and go to Step 2.

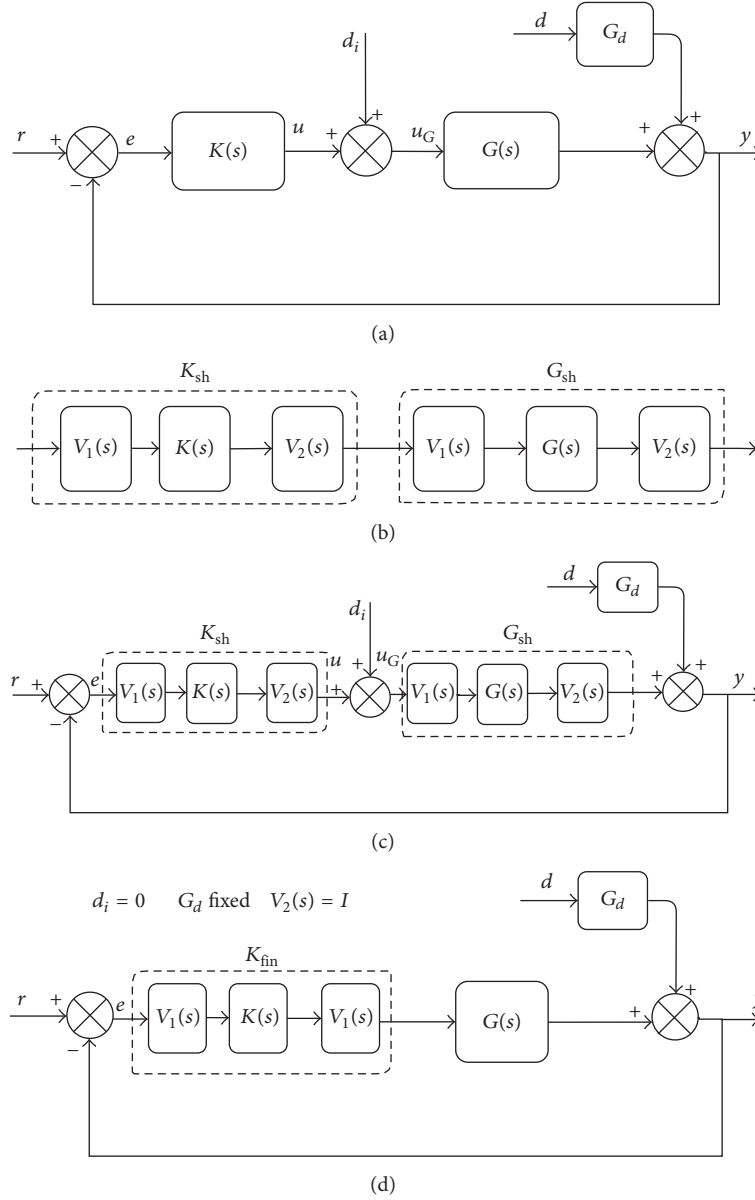


FIGURE 4: Loop Shaping design procedure.

Step 4. Synthesize a final feedback controller $K_{fin}(s)$ for the nominal plant $G(s)$ by

$$K_{fin}(s) = K_{sh}(s) V_1(s), \quad (63)$$

where $K_{sh}(s)$ is given in (7). For tuning purpose, we always choose $V_2(s) = I$; then

$$K_{fin}(s) = V_1(s) K(s) V_1(s). \quad (64)$$

Step 5. Verify that the desired closed-loop system responses are met. If yes stop. Else adjust $V_1(s)$ and $V_2(s)$ and go to Step 2.

Remark 9. If $G(s)$ is a nonsquare matrix such as $p > m$ or $p < m$, then it is obvious that the proposed algorithm does not

hold. Some minor modifications are required to tackle this problem. In fact, compatible dimensions for the shaped plant $G_{sh}(s)$ and the shaped controller $K_{sh}(s)$ require taking $V_1(s)$, $V_2(s)$, $G(s)$, and $K(s)$ with the same dimension $(\max(p, m)) \times (\max(p, m))$. Thereby, the dimensions of $G_{sh}(s)$ and $K_{sh}(s)$ are chosen to be equal to $(\max(p, m)) \times (\max(p, m))$ and the proposed Loop Shaping design procedure still holds.

Remark 10. Note that the final PI controller designed in Algorithm 8 is related to the PI controller designed in Algorithm 6. Indeed, $K_{fin}(s)$, given by relation (64), is designed, on one hand, using the full MIMO PI controller $K(s)$ given by relation (3) computed via Algorithm 6, and, on the other hand, using weighting functions $V_1(s)$ properly designed following Algorithm 8.

Remark 11. It must be noted that there are severe limitations when the conventional Loop Shaping design procedure is used for MIMO systems as discussed in [20]. Among these limitations, it may still be much harder to find a stabilizing K_{sh} if G_{sh} for non-minimum phase or unstable systems. However, this paper succeeds in overcoming these limitations thanks to the first stage of the design procedure that guarantees internally stable closed-loop.

5. Application

In this section, simulation results will be performed using three typical examples: the distillation column (unstable system), the ISP reactor (stable system), and the 4-tank process (non-minimum phase system). Furthermore, we will illustrate the superiority of the proposed approach over related ones for set-point tracking, disturbance rejection, and parametric uncertainties scenarios. The comparative study will be established between the following approaches:

- (i) The proposed PI controller designed via the Algorithms 6 and 8.
- (ii) The PI controller designed via Algorithm 6.
- (iii) The PID controller designed in [14].
- (iv) IMC-PI controller approach [13]
- (v) The conventional IMC-PID approach [10]

Sedumi and Yalmip Toolbox [30] are used to solve ILMI. To evaluate the closed-loop performances, the Integral Absolute Error (IAE) and the Total Variation (TV) criteria are considered. They are defined, respectively, by Vu and Lee [13] as follows:

$$\begin{aligned} \text{IAE} &= \int_0^T |e(t)| dt, \\ \text{TV} &= \sum_{k=1}^T |u(k+1) - u(k)|, \end{aligned} \quad (65)$$

where T is finite time chosen for the integral approach steady state value and $e(t)$ is defined as the total error between the set-points and the outputs.

For the different simulations, unit step changes in the set-points and disturbances are made to the 1st and 2nd loops. Furthermore, the robustness of the controller is evaluated by considering a perturbation uncertainty of $\pm 10\%$ in the important parameters, particularity, gains, and delays of the process.

Just for the second example, we will prove that the most conventional multiloop IMC-PID control approach proposed by Economou and Morari [10] fails and that the multiloop IMC-PI proposed by Vu and Lee [13] has less TV performances. This last approach will not be tested on the third example since it is only appropriate for first-order systems.

For systems with given transfer matrix, the passage from the matrix transfer to a minimal state space model is established using Gilbert method detailed in [31].

For the orthogonal collocation method, optimal parameters are chosen such as $N = 3$ and $p = q = -1/2$. The different performances singular values are plotted by means of $1/\bar{\sigma}(S)$ and $1/\bar{\sigma}(S_{sh})$ by noting that $\max 1/\bar{\sigma}(S_{sh})$ is equal to $\min \bar{\sigma}(S_{sh})$.

To prove the validity of the transformation between the state space representation and the corresponding transfer matrix and the approximation of the delayed system, let us introduce the following errors: let e_1 be the error between the unit step response to the state space representation (1) and the corresponding transfer matrix of the LTI MIMO with multiple time delays $G(s)$. e_2 is defined as the total error between the delayed system (1) outputs and the approximated ones by model (4)-(5) using the orthogonal collocation method.

Remark 12. Due the bad performances obtained via the PID controller designed via the approach given in [14], an additive filter is joined to the derivative action to attenuate noises. Thus, the transfer matrix of the PID controller with filter considered is described by

$$K_{PID,f}(s) = F_{1,PID} + \frac{F_{2,PID}}{s} + F_{3,PID} \times \frac{s}{\tau_d s + 1}, \quad (66)$$

$\tau_d > 0.$

It should be noted that the PID controller with filter (66) is applied to stable and non-minimum phase systems. Due to bad simulation results performed for the unstable system, the PID controller with filter is not considered.

5.1. Example 1: The Distillation Column System. Consider the typical example of the distillation column described in [6, 32, 33] belonging to the class of MIMO unstable plants with input delays; its transfer matrix model is described by Mete et al. [32] as follows:

$$G(s) = \begin{bmatrix} \frac{3.0400e^{-\tau_2 s}}{s} & \frac{-278.2000e^{-\tau_3 s}}{s(s+6)(s+30)} \\ \frac{0.0520e^{-\tau_2 s}}{s} & \frac{206.6000e^{-\tau_3 s}}{(s+6)(s+30)} \end{bmatrix}. \quad (67)$$

Applying a column decomposition method [31] for (67), the state space representation (1) can be deduced as follows:

$$\begin{aligned} A_0 &= \begin{pmatrix} 0 & 0 & 0 & 0 \\ 0 & 0 & 0 & 0 \\ 0 & 0 & -6 & 0 \\ 0 & 0 & 0 & -30 \end{pmatrix}, \\ B_0 &= \begin{pmatrix} 1 & 0 \\ 0 & 0 \\ 0 & 0 \\ 0 & 0 \end{pmatrix}, \end{aligned}$$

$$B_1 = \begin{pmatrix} 0 & 0 \\ 0 & 1 \\ 0 & 1 \\ 0 & 1 \end{pmatrix},$$

$$C = \begin{pmatrix} 3.0400 & -1.5400 & 1.9300 & 0.3800 \\ 0.0520 & 1.1400 & -1.4300 & 0.2800 \end{pmatrix} \quad (68)$$

for $\tau_2 = 0.5$ h and $\tau_3 = 0.6$ h.

Using the orthogonal collocation method, the following matrices are obtained for model (4)-(5):

$$\bar{A}_2 = \bar{A}_3 = \begin{pmatrix} 10.3923 & 1.1547 & -1.1547 & 0.8038 \\ -4.6188 & -0.0000 & 4.6188 & -3 \\ 1.1547 & -1.1547 & -10.3923 & 11.1962 \\ -1.4291 & 1.3333 & -19.9043 & 19 \end{pmatrix},$$

$$\bar{B}_2 = \bar{B}_3 = \begin{pmatrix} -11.1962 & -11.1962 \\ 3 & 3 \\ -0.8038 & -0.8038 \\ 1 & 1 \end{pmatrix},$$

$$\bar{C}_2 = \bar{C}_3 = \begin{pmatrix} 0 & 0 & 0 & 1 \\ 0 & 0 & 0 & 1 \end{pmatrix}. \quad (69)$$

By solving Algorithm 6 with $X_1 = I_{14} + 0.0010$ and $\delta = 0.1000$ yielding to $\alpha = 1.5000$, the following PI gains are obtained:

$$F_1 = \begin{pmatrix} 0.1945 & 0.2953 \\ 0.1946 & 0.2955 \end{pmatrix},$$

$$F_2 = \begin{pmatrix} 0.0432 & 0.0006 \\ 0.0429 & 0.0006 \end{pmatrix}. \quad (70)$$

Thus, the PI controller transfer matrix is given by

$$K(s) = \begin{bmatrix} \frac{0.1945s + 0.0432}{s} & \frac{0.2953s + 0.0006}{s} \\ \frac{0.1946s + 0.0429}{s} & \frac{0.2955s + 0.0006}{s} \end{bmatrix}. \quad (71)$$

Figure 5 illustrates the validity of the passage between the transfer matrix model (67) and the state space representation (1) and also the validity of the approximated model (4)-(5) obtained via the orthogonal collocation method.

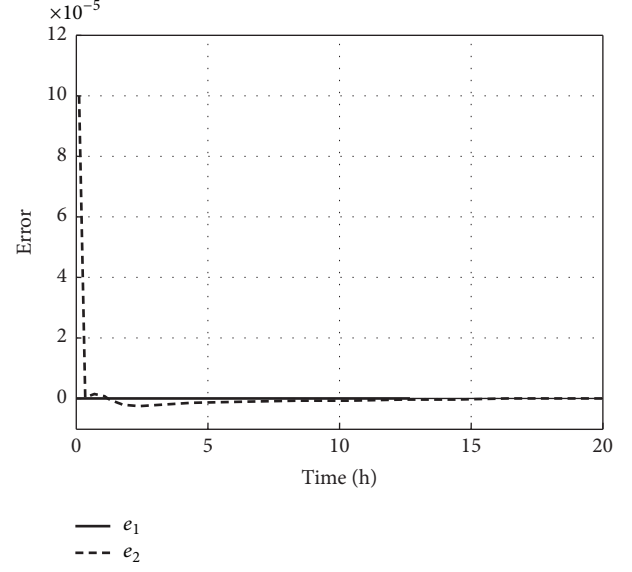


FIGURE 5: Models validation of the distillation column.

TABLE 1: Comparative analysis of controller's performances: the distillation column case study.

| Tuning method | Set-point | | Disturbance | |
|---------------|-----------|-------|-------------|-------|
| | IAE | TV | IAE | TV |
| Proposed | 175.16 | 19.82 | 453.14 | 19.77 |
| PI controller | 494.05 | 1.810 | 1366.10 | 6.69 |

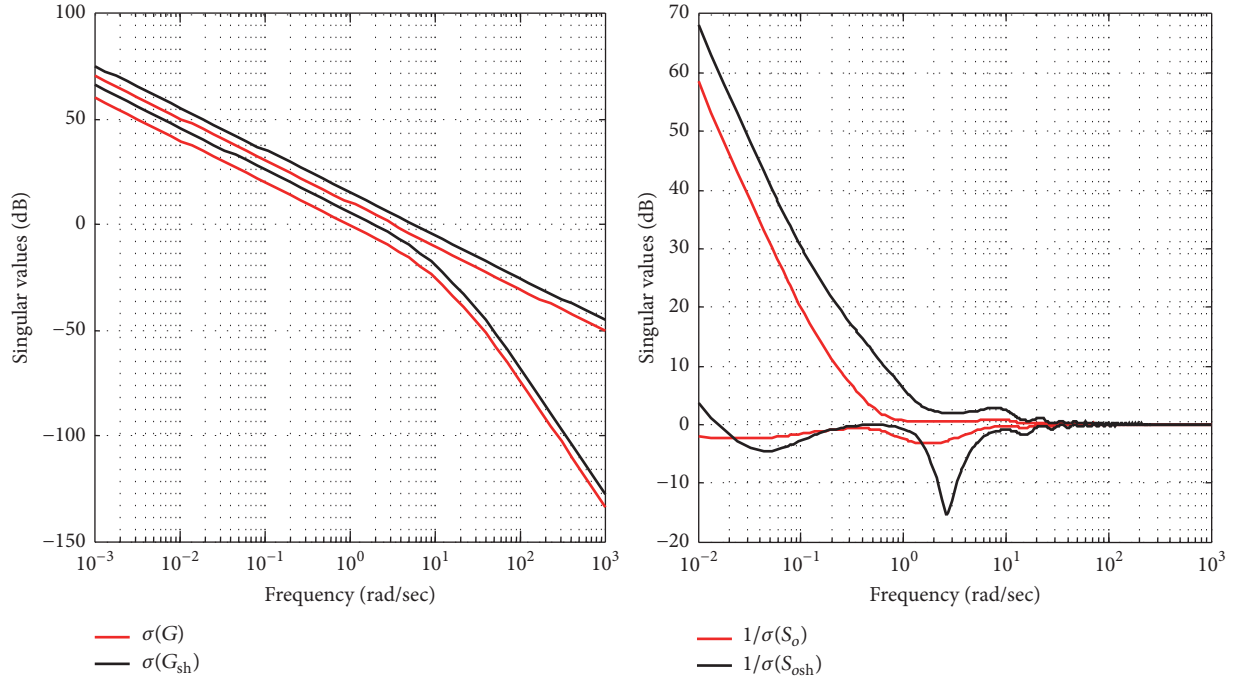
Figure 6 proves that the PI design procedure satisfies the desired specifications for a precompensator $V_1(s)$ and postcompensator $V_2(s)$ chosen as follows:

$$V_1(s) = \begin{bmatrix} 1.8000 \frac{s+1}{s+1.0400} & 0 \\ 0 & 2 \frac{s+1}{s+1.0200} \end{bmatrix}, \quad (72)$$

$$V_2(s) = \begin{bmatrix} 1 & 0 \\ 0 & 1 \end{bmatrix}.$$

To boost the low frequency gain and give almost zero steady state error, $V_1(s)$ is chosen accordingly as an approximated PI precompensator.

The resulting performance indices for the proposed multivariable controller and the one computed by ILMI method for the nominal and perturbed system cases are summarized in Tables 1 and 2. The proposed controller affords better performances especially for the second output and better disturbance rejection over PI controller as shown by Figures 8 and 9. As listed in Tables 1 and 2, the controller settings of the proposed method provide superior performances by the smallest total IAE for both case studies: set-point changes, disturbances changes, and parametric uncertainties. Acceptable TV indices are also shown by the proposed method for this process.

FIGURE 6: Singular values of G , G_{sh} , $1/S_o$, and $1/S_{osh}$ for the distillation column.TABLE 2: Robustness analysis under $\pm 10\%$ in the gain and delay: the distillation column with input delays.

| Tuning method | The distillation column with input delays (+10%) | | | | The distillation column with input delays (-10%) | | | |
|---------------|--|-------|-------------|-------|--|-------|-------------|-------|
| | Set-point | | Disturbance | | Set-point | | Disturbance | |
| | IAE | TV | IAE | TV | IAE | TV | IAE | TV |
| Proposed | 166.17 | 60.42 | 453.14 | 19.77 | 189.34 | 11.97 | 371.23 | 15.83 |
| PI controller | 457.45 | 1.82 | 1366.10 | 6.69 | 537.84 | 1.80 | 1118 | 5.18 |

5.2. Example 2: The Industrial Scale Polymerization (ISP) Reactor. Consider the ISP reactor system described by its transfer matrix given by Chien et al. [34] as follows:

$$G(s) = \begin{bmatrix} \frac{22.8900e^{-\tau_2 s}}{4.5720s + 1} & \frac{-11.6400e^{-\tau_3 s}}{1.8070s + 1} \\ \frac{4.6890e^{-\tau_2 s}}{2.1740s + 1} & \frac{5.8000e^{-\tau_3 s}}{1.8010s + 1} \end{bmatrix}. \quad (73)$$

Its minimal realization via Gilbert method gives the state space model (1) where

$$A_0 = \begin{pmatrix} -0.2187 & 0 & 0 & 0 \\ 0 & -0.5534 & 0 & 0 \\ 0 & 0 & -0.4600 & 0 \\ 0 & 0 & 0 & -0.5552 \end{pmatrix},$$

$$B_0 = \begin{pmatrix} 5.0065 & 0 \\ 0 & 0 \\ 2.1569 & 0 \\ 0 & 0 \end{pmatrix},$$

$$B_1 = \begin{pmatrix} 0 & 0 \\ 0 & -6.4416 \\ 0 & 0 \\ 0 & 3.2204 \end{pmatrix},$$

$$C = \begin{pmatrix} 1 & 1 & 0 & 0 \\ 0 & 0 & 1 & 1 \end{pmatrix}$$

(74)

for $\tau_2 = 0.2$ h and $\tau_3 = 0.4$ h.

Let us first test for the previous system the conventional IMC-PID approach proposed by Economou & Morari [10]. In this approach, the IMC interaction measure surfaces are practical tools to assess the potential value of the multiloop design. By their definitions, they must vary between 0 and 1 such that for the i th input/output pair of a particular system configuration, the Row IMC interaction measure R_i is the quantity defined by

$$R_i(i\omega) \triangleq \frac{1}{1 + f_{R_i}^*(i\omega)} = \frac{\sum_{j, j \neq i} g_{ij}(i\omega)}{\sum_j |g_{ij}(i\omega)|}, \quad 0 \leq \omega < \infty \quad (75)$$

TABLE 3: Interaction measures of the ISP reactor via the IMC-PID approach [10].

| Pairing | IMC interaction measure | |
|-----------------------|---|---|
| | R_i | C_i |
| $(u_1, y_1) = (1, 1)$ | $R_i(i\omega) = \frac{ g_{12} }{ g_{11} + g_{12} }$ | $C_i(i\omega) = \frac{ g_{21} }{ g_{11} + g_{21} }$ |
| $(u_2, y_2) = (2, 2)$ | $R_i(i\omega) = \frac{ g_{21} }{ g_{21} + g_{22} }$ | $C_i(i\omega) = \frac{ g_{12} }{ g_{12} + g_{22} }$ |
| $(u_2, y_1) = (1, 2)$ | $R_i(i\omega) = \frac{ g_{11} }{ g_{11} + g_{12} }$ | $C_i(i\omega) = \frac{ g_{22} }{ g_{12} + g_{22} }$ |
| $(u_1, y_2) = (2, 1)$ | $R_i(i\omega) = \frac{ g_{22} }{ g_{21} + g_{22} }$ | $C_i(i\omega) = \frac{ g_{11} }{ g_{11} + g_{21} }$ |

whereas, for the same input/output pair and configuration, the complementary quantity C_i is defined by

$$C_i(i\omega) \triangleq \frac{1}{1 + f_{C_i}^*(i\omega)} = \frac{\sum_{j \neq i} g_{ji}(i\omega)}{\sum_j |g_{ji}(i\omega)|}, \quad 0 \leq \omega < \infty. \quad (76)$$

The following scenarios are expected:

- (i) $0.5 < R_i, C_i < 1.0$ corresponds to significant interactions between the multiple loops and an overall poor performances of the multiloop structure are expected.
- (ii) $0 < R_i, C_i \leq 0.5$ corresponds to good pairing and SISO controllers can be designed for each loop and granting good performances.

For the ISP reactor, the transfer function matrix (73) can be written as follows:

$$G(s) = \begin{bmatrix} \frac{y}{u} \end{bmatrix} = \begin{bmatrix} \frac{22.8900e^{-0.2s}}{4.5720s + 1} & \frac{-11.6400e^{-0.4s}}{1.8070s + 1} \\ \frac{4.6890e^{-0.2s}}{2.1740s + 1} & \frac{5.8000e^{-0.4s}}{1.8010s + 1} \end{bmatrix} \quad (77)$$

$$= \begin{bmatrix} g_{11}e^{-\theta_{11}} & g_{12}e^{-\theta_{12}} \\ g_{21}e^{-\theta_{21}} & g_{22}e^{-\theta_{22}} \end{bmatrix}.$$

From (75) and (76), we compute the IMC interactions measure for each pairing as summarized in Table 3. Figure 10 shows the IMC interaction measure for u_1 controlling y_1 and u_2 controlling y_2 for the original pairing whereas reverse pairing is shown as the IMC interaction measure for u_1 controlling y_2 and u_2 controlling y_1 . As it can be observed by the IMC measure interaction, the original pairing as the reverse pairing cannot guarantee good performances that is why such an approach fails.

Let us now apply the extended IMC-PI controller approach proposed by Vu and Lee [13] for the class of TITO multidelay processes with first-order plus delay time

TABLE 4: Multiloop PI controller design of the ISP reactor via the IMC-PI approach [13].

| Loop | K_{Ci} | K_{Ii} |
|------|----------|----------|
| 1 | 0.4211 | 0.1068 |
| 2 | 0.1320 | 0.1121 |

(FOPDT) systems. From the ISP reactor and referring to [13], the following data are deduced:

$$\begin{aligned}
 K_{11} &= 22.8900, \\
 K_{12} &= -11.6400, \\
 K_{21} &= 4.6890, \\
 K_{22} &= 5.8000, \\
 T_{11} &= 4.5720, \\
 T_{12} &= 1.8070, \\
 T_{21} &= 2.1740, \\
 T_{22} &= 1.8010, \\
 \theta_{11} &= 0.2000, \\
 \theta_{12} &= 0.4000, \\
 \theta_{21} &= 0.2000, \\
 \theta_{22} &= 0.4000, \\
 \lambda_1 &= 0.0900, \\
 \lambda_2 &= 0.6900, \\
 K_{ei} &= -0.4111, \\
 T_{ei} &= -2.1800.
 \end{aligned} \quad (78)$$

The steady state relative gain array of the ISP reactor is $\Lambda_{ii}(0) = 0.7087 < 1$, which proves that the closed-loop gain is greater than the open-loop gain. The ISP reactor system does not then exhibit open-loop diagonal dominance. The diagonal PI-multi-loop controller parameters K_{Ci} and K_{Ii} for each loop $i, i = 1, 2$ are then designed and given by Table 4.

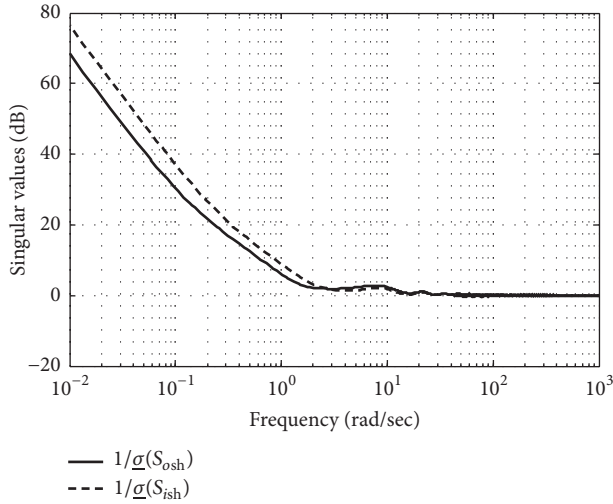


FIGURE 7: Input and output sensitivity matrices of the shaped model for the distillation column.

TABLE 5: Comparative analysis of the controller's performances: the ISP reactor case study.

| Tuning method | Set-point | | Disturbance | |
|---------------|-----------|-------|-------------|------|
| | IAE | TV | IAE | TV |
| Proposed | 20.24 | 10.74 | 123.08 | 2.66 |
| PI | 174.42 | 1.97 | 224.96 | 1.33 |
| PID [14] | 440.57 | 4.93 | 417.66 | 1.48 |
| IMC-PI [13] | 3.97 | 1.98 | 49.05 | 9.13 |

We have also verified that the two outputs converge to the set-points in response to a unit step.

For $\tau_2 = 0.2$ h and $\tau_3 = 0.4$ h, the reduced model (4)-(5) is obtained via the collocation method. Figure 11 proves the validity of models (1) and (4)-(5). By solving Algorithm 6 using the parameters $Y_1 = I_{18} + 0.0020$ and $\delta = 0.1000$ and yielding $\alpha = 0.7549$, the following PI matrix gains are given:

$$\begin{aligned} F_1 &= \begin{pmatrix} 0.2059 & 0.3061 \\ 0.2062 & 0.3060 \end{pmatrix}, \\ F_2 &= \begin{pmatrix} 0.0302 & 0.0332 \\ 0.0292 & 0.0335 \end{pmatrix}. \end{aligned} \quad (79)$$

The transfer matrix of the related computed PI controller is given by

$$K(s) = \begin{bmatrix} \frac{0.2059s + 0.0302}{s} & \frac{0.3061s + 0.0332}{s} \\ \frac{0.2062s + 0.0292}{s} & \frac{0.3060s + 0.0335}{s} \end{bmatrix}. \quad (80)$$

By solving algorithm in [14], the PID feedback matrix gains are given by

$$\begin{aligned} F_{1,\text{PID}} &= \begin{pmatrix} 0.0187 & 0.2988 \\ 0.0192 & 0.2989 \end{pmatrix}, \\ F_{2,\text{PID}} &= \begin{pmatrix} -0.0132 & 0.0812 \\ -0.0135 & 0.0812 \end{pmatrix}, \\ F_{3,\text{PID}} &= \begin{pmatrix} 0.0151 & 0.0661 \\ 0.0151 & 0.0660 \end{pmatrix}. \end{aligned} \quad (81)$$

Figure 12 proves that PI design procedure satisfies the desired specifications for a precompensator $V_1(s)$ and postcompensator $V_2(s)$ chosen as follows:

$$\begin{aligned} V_1(s) &= \begin{bmatrix} 3.5000 \times \frac{0.5000s + 1}{s + 1} & 0 \\ 0 & 3 \times \frac{0.1500s + 1}{s + 1} \end{bmatrix}, \\ V_2(s) &= \begin{bmatrix} 1 & 0 \\ 0 & 1 \end{bmatrix}. \end{aligned} \quad (82)$$

For a sequential unit step change in the set-points at $t = 0$ and $t = 600$ h, one can see that the proposed controller has the faster rising time and settling response over other ILMI approaches as shown by Figure 14. The disturbance model G_d is taken as $G_d = [-4.2430e^{-0.4s}/(3.4450s + 1) \quad -0.6010e^{-0.4s}/(1.9820s + 1)]^T$ as in [34]. Unit step changes in the disturbance were also made to the 1st and 2nd loops, respectively, as shown by Figure 15. The resulting performance indices for the nominal and perturbed system cases for various tuning methods are given in Tables 5 and 6. The proposed MIMO PI controller provides superior performances over PI controller and PID controller designed via ILMI approaches by means of the smallest total IAE. Acceptable TV values are also listed by the proposed method.

5.3. Example 3: The 4-Tank Process. Consider the quadruple-tank process for which one of the two transmission-zeros of the linearized system dynamics can be moved between the positive and negative real axis [35]. The corresponding model with multiple delays is described in [36] by taking into account transport delays between valves and tanks. Applying the numerical values corresponding to the non-minimum phase model found in [35], system (1) is given by

$$A_0 = \begin{pmatrix} -0.1993 & 0 & 0 & 0 \\ 0 & -0.1422 & 0 & 0 \\ 0 & 0 & -0.1230 & 0 \\ 0 & 0 & 0 & -0.0873 \end{pmatrix},$$

TABLE 6: Robustness analysis under $\pm 10\%$ parametric uncertainties: The ISP reactor case study.

| Tuning method | ISP (+10%) | | | | ISP (-10%) | | | |
|---------------|------------|------|-------------|------|------------|------|-------------|-------|
| | Set-point | | Disturbance | | Set-point | | Disturbance | |
| | IAE | TV | IAE | TV | IAE | TV | IAE | TV |
| Proposed | 19.75 | 8.72 | 120.67 | 2.90 | 21.28 | 9.27 | 127.46 | 2.54 |
| PI | 158.68 | 1.95 | 224.06 | 1.33 | 193.50 | 1.94 | 225.85 | 1.33 |
| PID [14] | 404.24 | 4.82 | 415.56 | 1.28 | 482.68 | 4.94 | 418.84 | 1.52 |
| IMC-PI [13] | 4.36 | 2.05 | 48.33 | 8.26 | 3.58 | 1.92 | 49.95 | 10.32 |

$$\begin{aligned}
 A_1 &= \begin{pmatrix} 0 & 0 & 0.1230 & 0 \\ 0 & 0 & 0 & 0.0873 \\ 0 & 0 & 0 & 0 \\ 0 & 0 & 0 & 0 \end{pmatrix}, \\
 B_0 &= \begin{pmatrix} 0.0482 & 0 \\ 0 & 0.0350 \\ 0 & 0 \\ 0 & 0 \end{pmatrix}, \\
 B_1 &= \begin{pmatrix} 0 & 0 \\ 0 & 0 \\ 0 & 0.0775 \\ 0.0559 & 0 \end{pmatrix}.
 \end{aligned} \tag{83}$$

The measurement level signals y_1 and y_2 are $k_c h_1$ and $k_c h_2$ where $k_c = 0.5$ V/cm. The output matrix is then given by

$$C = \begin{pmatrix} 0.5000 & 0 & 0 & 0 \\ 0 & 0.5000 & 0 & 0 \end{pmatrix}. \tag{84}$$

Its transfer matrix is described by

$$\begin{aligned}
 G(s) &= \begin{bmatrix} \frac{0.0241e^{-s\tau_2}}{s + 0.1993} & \frac{0.0047e^{-s(\tau_1 + \tau_3)}}{(s + 0.1995)(s + 0.1230)} \\ \frac{0.0024e^{-s(\tau_1 + \tau_3)}}{(s + 0.1422)(s + 0.0873)} & \frac{0.0175e^{-s\tau_2}}{s + 0.1422} \end{bmatrix}.
 \end{aligned} \tag{85}$$

For simulation results, the constant delays are chosen as follows: $\tau_1 = 5$ s, $\tau_2 = 2$ s, and $\tau_3 = 4$ s.

To investigate the validity of the 4-tank process, the different model errors are depicted in Figure 16. By solving Algorithm 6 using the parameters $Y_1 = I_{18} + 0.2050$, $\delta =$

0.1000, and yielding $\alpha = 0.2500$, the following PI gains are given:

$$\begin{aligned}
 F_1 &= \begin{pmatrix} 0.1569 & 0.1532 \\ 0.0236 & 0.0154 \end{pmatrix}, \\
 F_2 &= \begin{pmatrix} 0.1569 & 0.1532 \\ 0.0236 & 0.0154 \end{pmatrix}.
 \end{aligned} \tag{86}$$

Thus, the PI controller transfer matrix is given by

$$K(s) = \begin{bmatrix} \frac{0.1569s + 0.1569}{s} & \frac{0.1532s + 0.1532}{s} \\ \frac{0.0236s + 0.0236}{s} & \frac{0.0154s + 0.0154}{s} \end{bmatrix}. \tag{87}$$

The feedback matrix gains designed by solving algorithm in [14] are given by

$$\begin{aligned}
 F_{1,\text{PID}} &= \begin{pmatrix} 0.1562 & 0.1515 \\ 0.0231 & 0.0150 \end{pmatrix}, \\
 F_{2,\text{PID}} &= \begin{pmatrix} 0.1562 & 0.1515 \\ 0.0231 & 0.0150 \end{pmatrix}, \\
 F_{3,\text{PID}} &= \begin{pmatrix} -3.7924 & 5.5584 \\ -3.7924 & 5.5584 \end{pmatrix}.
 \end{aligned} \tag{88}$$

Figure 17 shows that PI design procedure satisfies the desired specifications for a precompensator $V_1(s)$ and postcompensator $V_2(s)$ chosen as follows:

$$\begin{aligned}
 V_1(s) &= \begin{bmatrix} 3 \times \frac{2s + 1}{s + 1} & 0 \\ 0 & 3 \times \frac{3s + 1}{s + 1} \end{bmatrix}, \\
 V_2(s) &= \begin{bmatrix} 1 & 0 \\ 0 & 1 \end{bmatrix}.
 \end{aligned} \tag{89}$$

The resulting performance indices for the proposed multivariable controller and those of other ILMI methods for the nominal and perturbed system cases are summarized in Tables 7 and 8. For a sequential unit step changes in the set-point and disturbance, Figures 19 and 20 compare the closed-loop time responses and controller output responses afforded

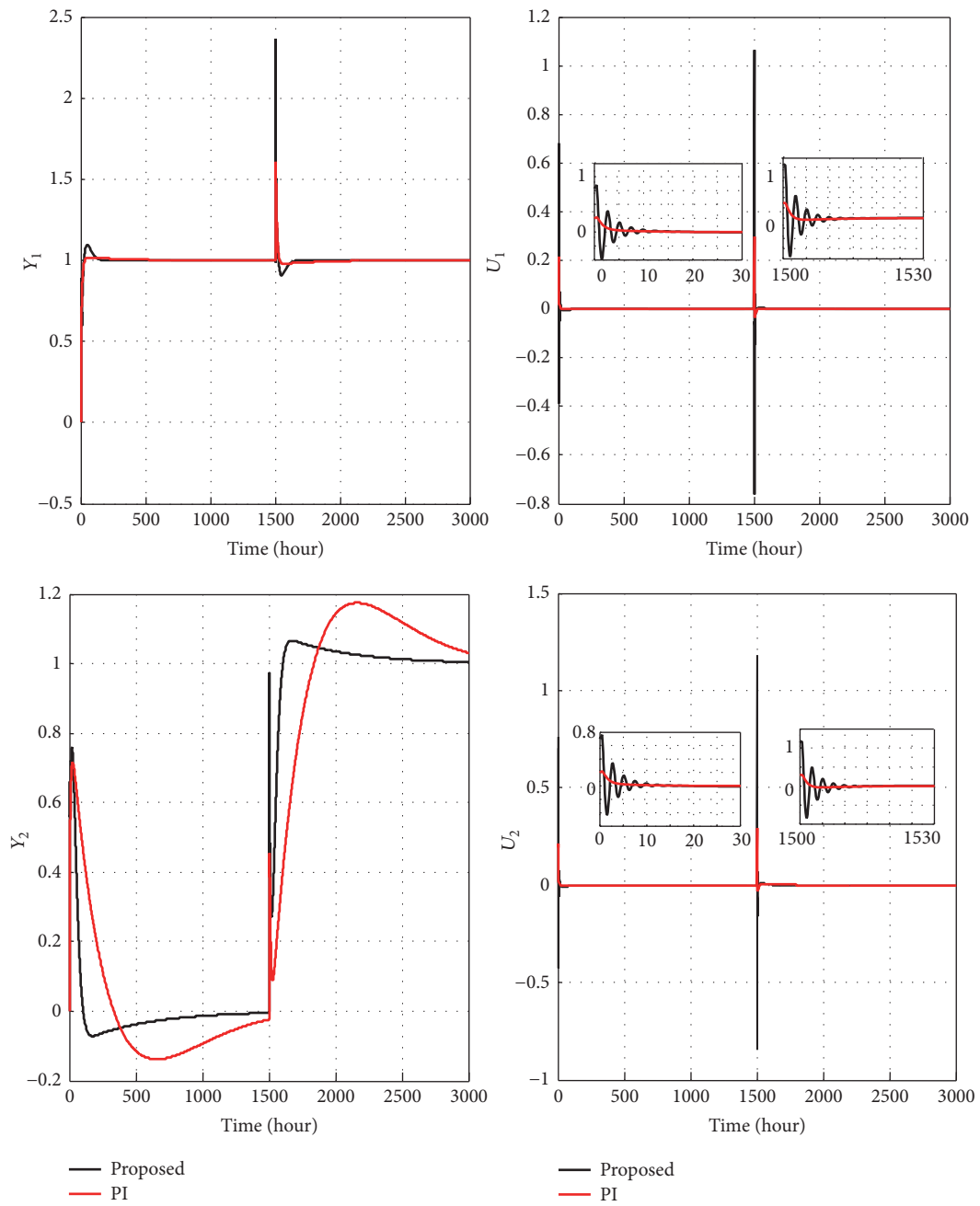


FIGURE 8: Closed-loop responses and controller output responses to set-point changes for the distillation column.

TABLE 7: Comparative analysis of controller's performances. The non-minimum phase 4-tank process.

| Tuning method | Set-point | | Disturbance | |
|---------------|-----------|--------|-------------|-------|
| | IAE | TV | IAE | TV |
| Proposed | 479.04 | 119.47 | 98.24 | 15.20 |
| PI | 4005.50 | 39.10 | 105.91 | 11.48 |
| PID [14]. | 4100.80 | 338.06 | 105.22 | 6.75 |

TABLE 8: Robustness analysis under $\pm 10\%$ in the gain and delay: the non-minimum phase 4-tank process case study.

| Tuning method | 4-tank process (+10%) | | | | 4-tank process (−10%) | | | |
|---------------|-----------------------|--------|-------------|-------|-----------------------|--------|-------------|-------|
| | Set-point | | Disturbance | | Set-point | | Disturbance | |
| | IAE | TV | IAE | TV | IAE | TV | IAE | TV |
| Proposed | 418.26 | 120.51 | 99.43 | 15.84 | 510.06 | 98.66 | 94.85 | 13.21 |
| PI | 3678.10 | 37.14 | 106.96 | 11.99 | 4383.80 | 41.88 | 102.31 | 11.58 |
| PID [14]. | 3768.90 | 333.93 | 106.24 | 7.04 | 4482.50 | 339.06 | 101.65 | 5.76 |

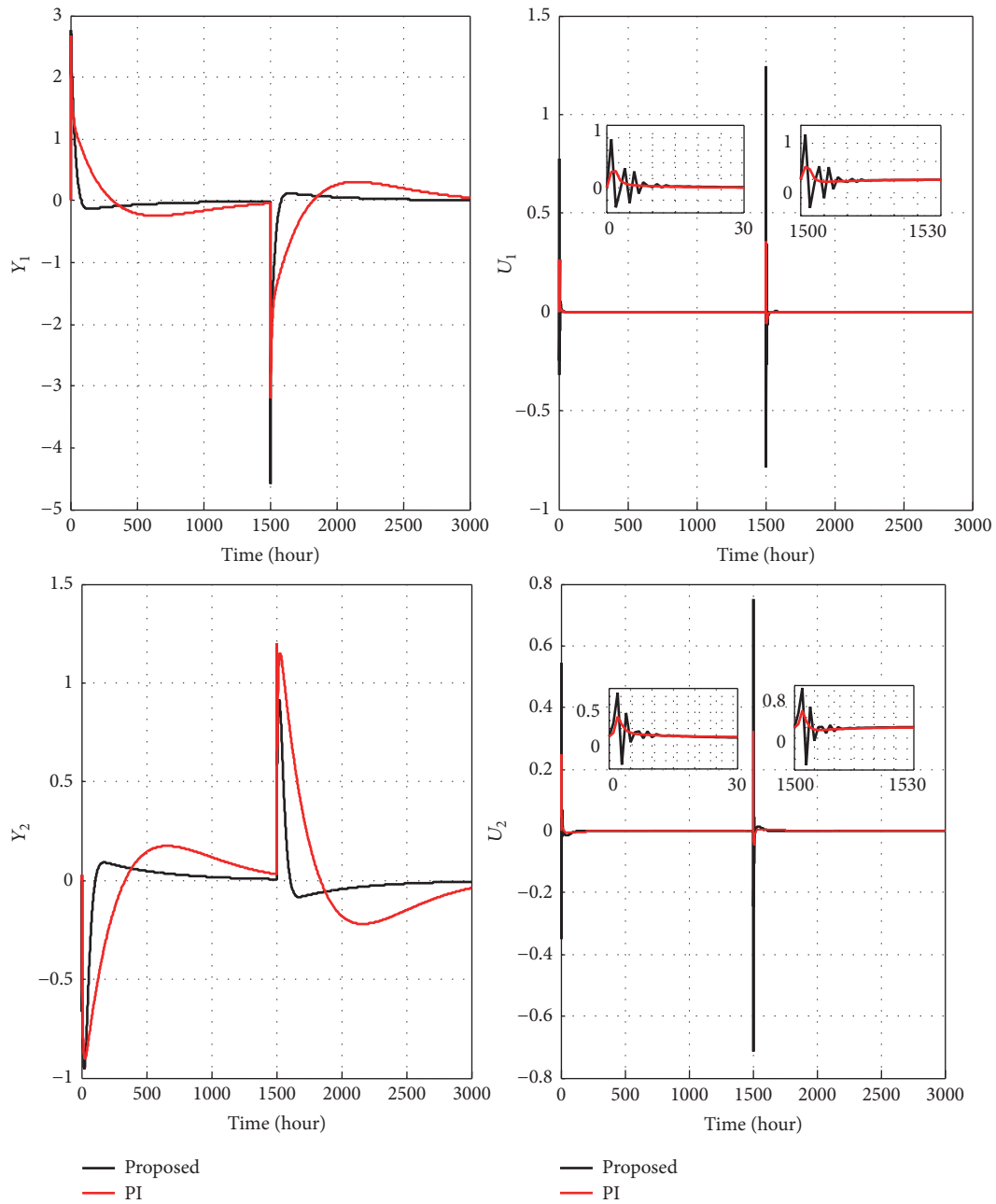


FIGURE 9: Closed-loop responses and controller output responses to unit step changes in the disturbance for the distillation column.

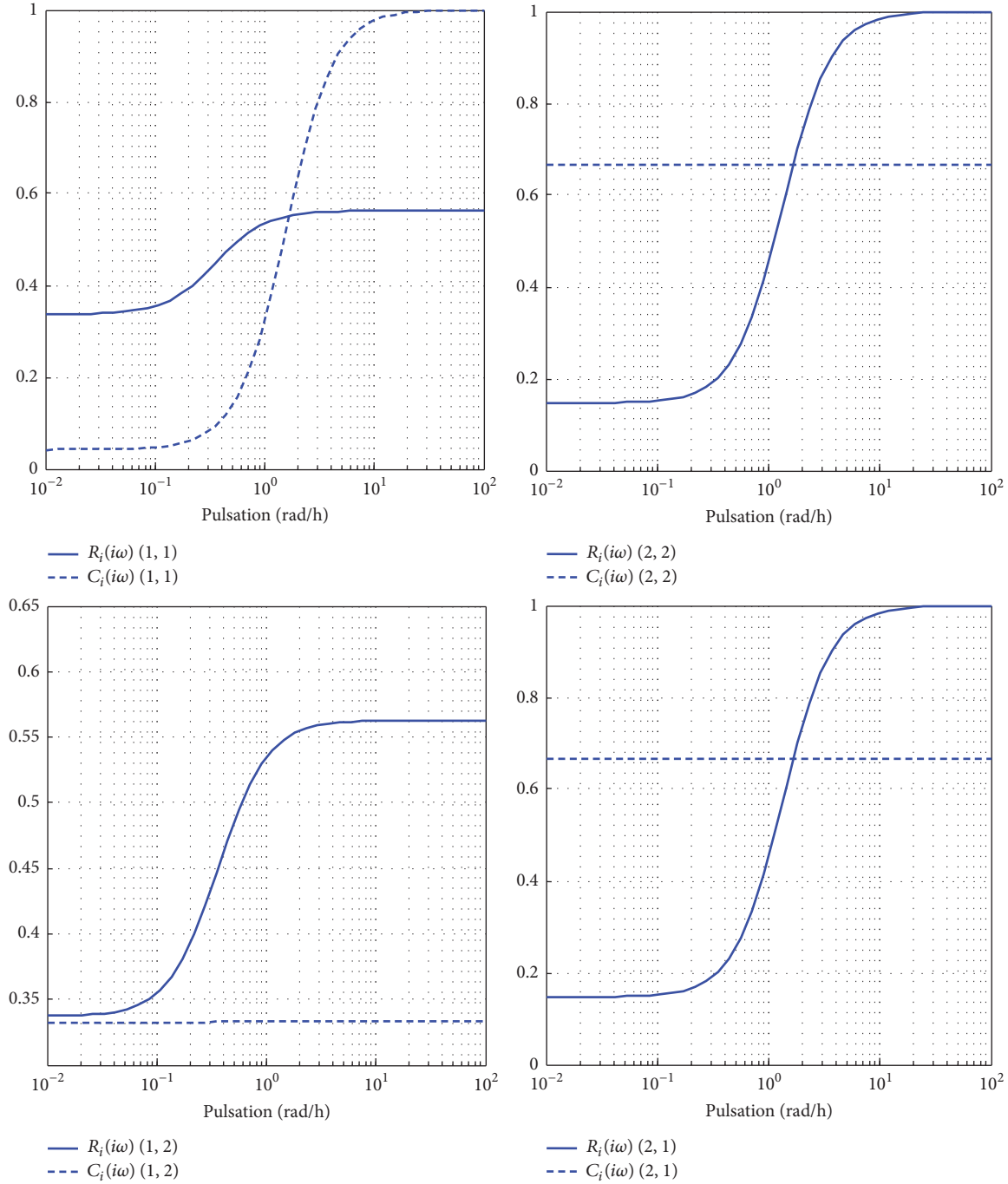


FIGURE 10: IMC interaction measures for the ISP reactor: fail of the conventional IMC-PID approach.

by the proposed controller with those given by PI and PID with filter controllers. The disturbance model G_d is taken as a perturbation uncertainty of +10% in the process gain and time delay into the actual process, simultaneously. As listed in Tables 7 and 8, the proposed MIMO PI controller settings provide superior performance over PI and PID controllers by means of the smallest total IAE. High TV values are

explained by non-minimum phase system characteristics for this process.

Furthermore, noise rejection in high frequencies is also known as an important requirement in a control system design. In order to evaluate the effect of such noise on the closed-loop performances of the most complex examples considered in this paper, simulation results have been

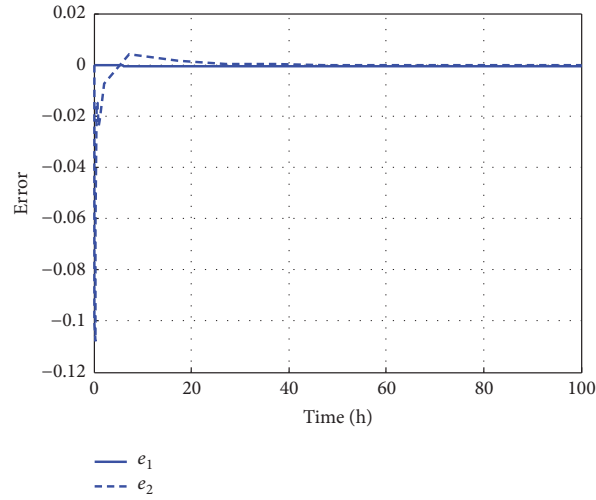


FIGURE 11: Models validation of the ISP reactor.

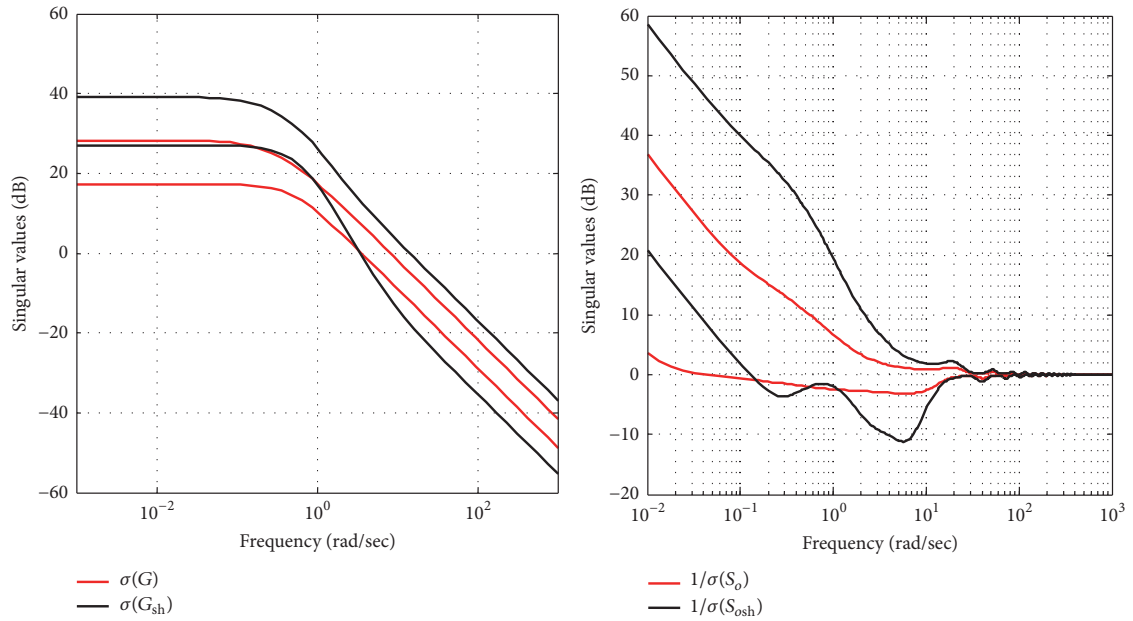
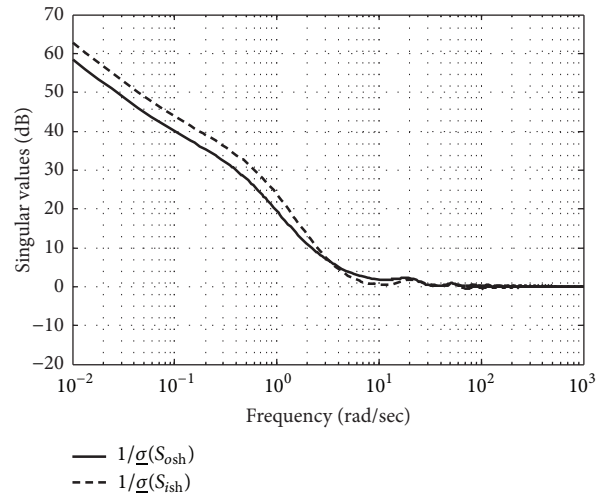
FIGURE 12: Singular values of G , G_{sh} , $1/S_o$, and $1/S_{osh}$ for the ISP reactor.

FIGURE 13: Input and output sensitivity matrices of the shaped model for the ISP reactor.

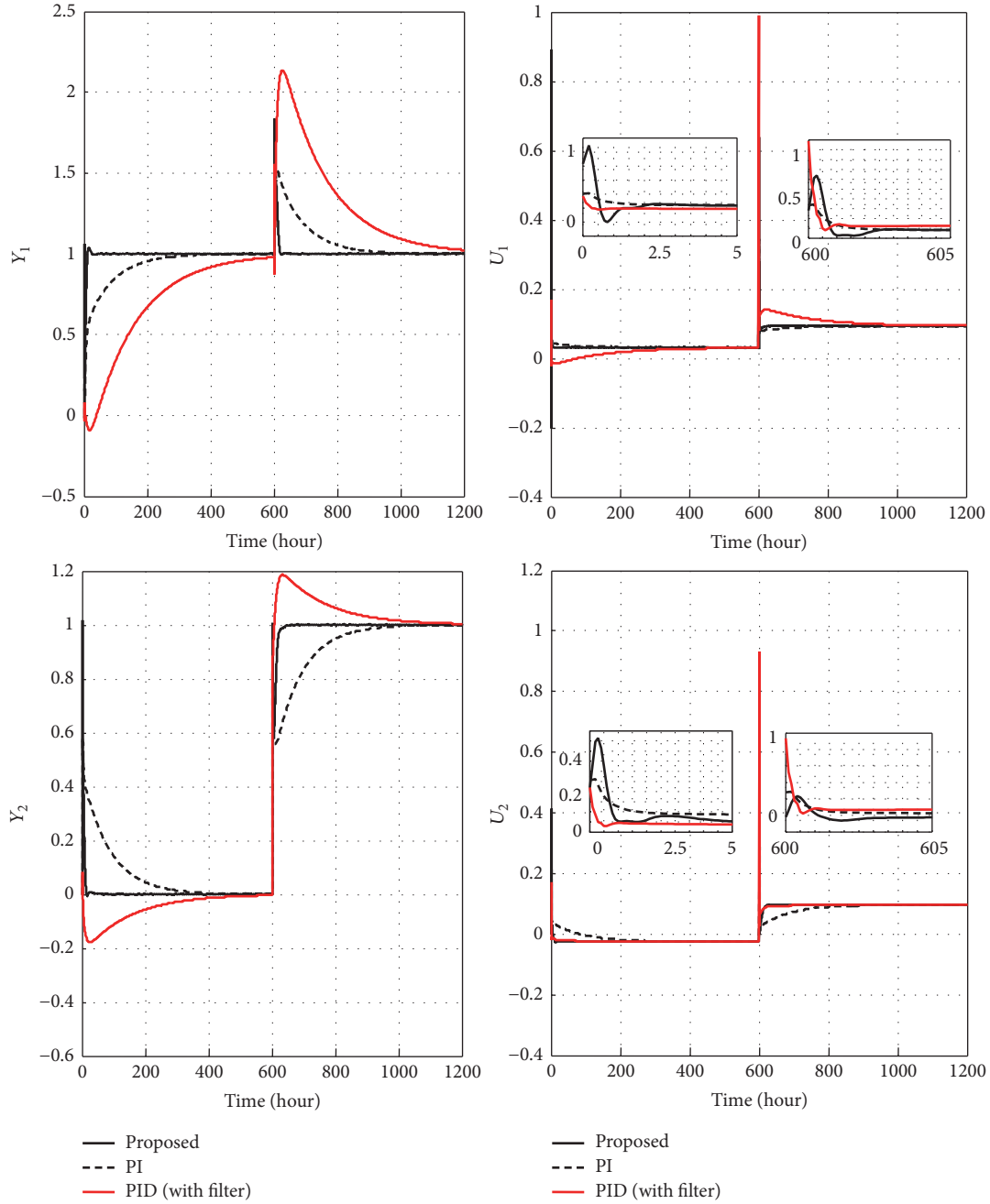


FIGURE 14: Closed-loop responses and controller output responses to set-point changes for the ISP reactor.

conducted taking into account of White Gaussian Noise Measurements (WGNM) with a variation of 0.01 V and zero mean. It is apparent from Figure 21 that the output responses are not sensitive to WGNM whereas acceptable fluctuations are however observed for the control inputs. Improving such performances will be considered in future works.

Remark 13. Equations (56) and (59) show the effects of the disturbances d and d_i on the output vector y and the control

signal vector u_G , respectively. This can be obviously made small by making the output sensitivity function S_{osh} and the input sensitivity function S_{ish} small. In other words, a good disturbance attenuation can be improved by making the sensitivity functions $1/S_{osh}$ and $1/S_{ish}$ decrease faster in low frequencies. From Figures 7, 13, and 18, it is clear that this principle is well managed for the three examples. Indeed, a high frequency roll-off is shown over 0.01 rad/s and 1 rad/s with 31 dB/decade, 20 dB/decade and 17.5 dB/decade for $1/S_{osh}$

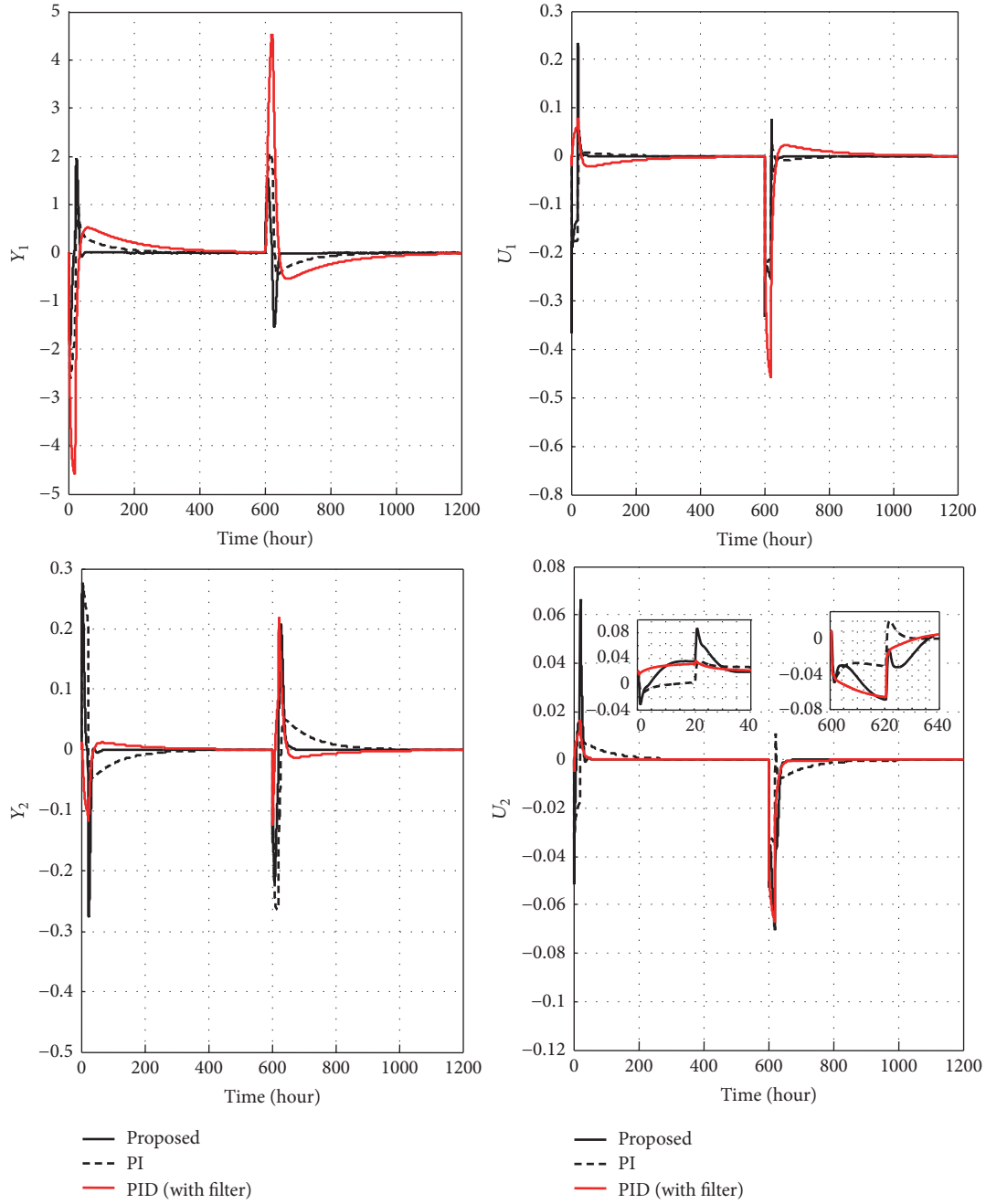


FIGURE 15: Closed-loop responses and controller output responses to unit step changes in the disturbance for the ISP reactor.

and with 33.5 dB/decade, 20 dB/decade, and 18 dB/decade for $1/S_{ish}$ for the considered unstable, stable, and non-minimum phase systems, respectively.

5.4. Comparative Analysis. Previous results can be summarized as follows:

- (i) Even more the controller design procedure has not considered decoupling principle of multivariable systems; the proposed approach provides generally superior performances by the smallest total IAE for the

set-point changes, disturbance changes and parametric uncertainties, over related approaches, for the unstable distillation column, the ISP reactor, and the 4-tank process as summarized by Tables 1-2 and 5-8. Low TV values are also shown for the ISP reactor.

- (ii) The proposed method succeeds to synthesize a MIMO PI controller for the ISP reactor when the IMC-PID approach proposed by Economou and Morari [10] fails due to high interactions measure for the original and reverse pairings. Furthermore, the

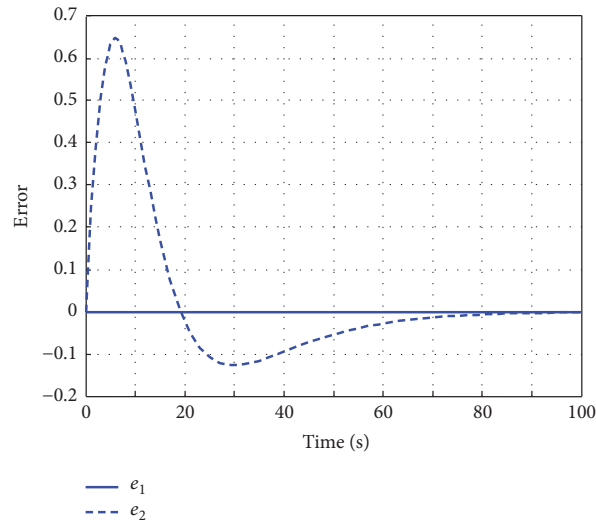


FIGURE 16: Models validation of the 4-tank process.

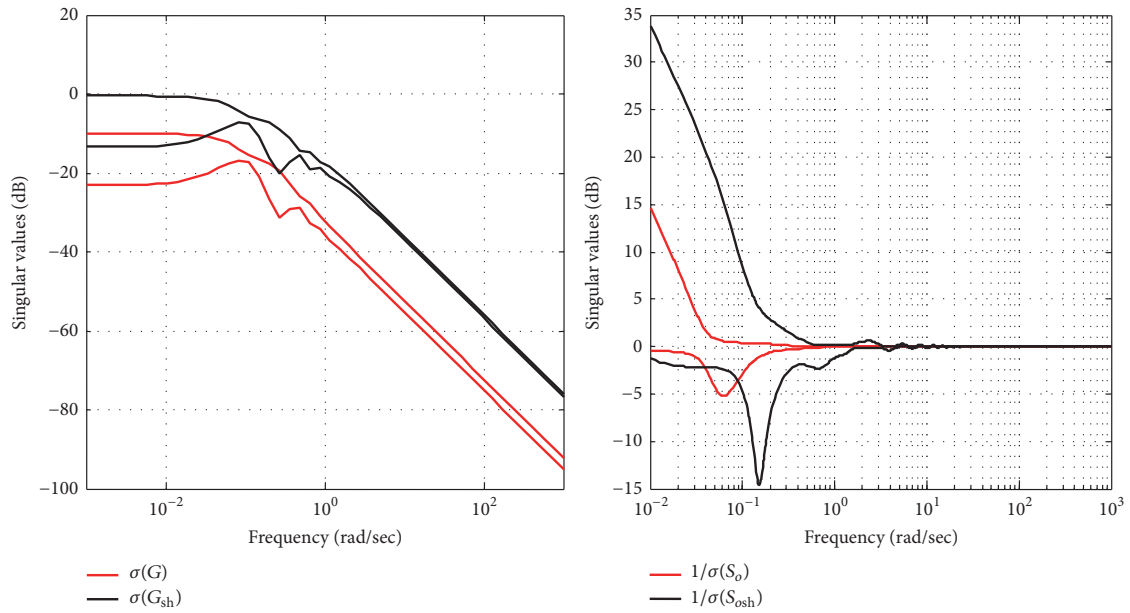
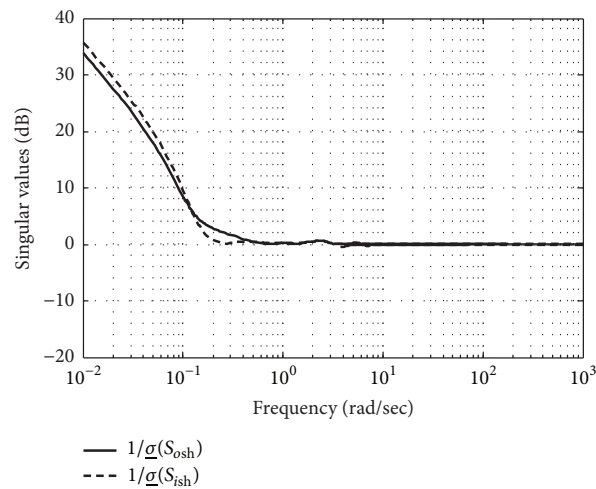
FIGURE 17: Singular values of G , G_{sh} , $1/S_o$, and $1/S_{osh}$ for the 4-tank process.

FIGURE 18: Input and output sensitivity matrices of the shaped model for the 4-tank process.

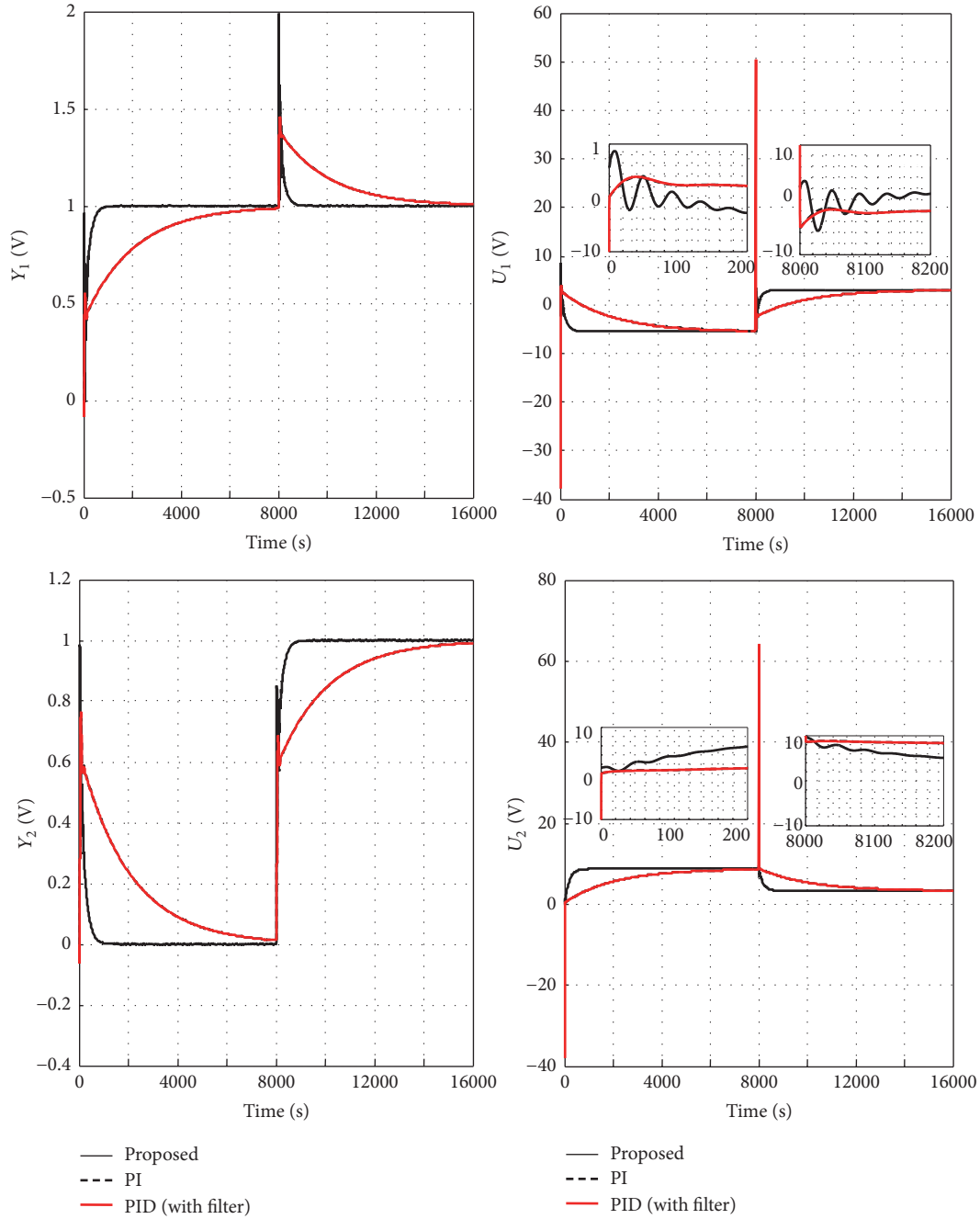


FIGURE 19: Closed-loop responses and controller output responses to set-point changes for the 4-tank process.

proposed controller settings give a much smoother response for the disturbance rejection case with ($TV = 2.66$, $TV = 2.90$ and $TV = 2.54$) over the IMC-PI approach [13] with ($TV = 9.13$, $TV = 8.26$, $TV = 10.32$) for both the nominal and the perturbed models.

- (iii) The proposed method is applicable to the 4-tank process where the IMC-PI approach [13] is not applicable due to the presence of second-order functions in the

transfer matrix. The IMC-PI approach proposed by Vu and Lee [13] is only applicable for FOPTD systems.

- (iv) The proposed method is applicable to the unstable distillation column with input delays where the IMC-PI approach proposed by Vu and Lee [13] is only applicable for FOPTD systems and where the IMC-PID approach proposed by Economou and Morari [10] is limited to models with first or second orders.

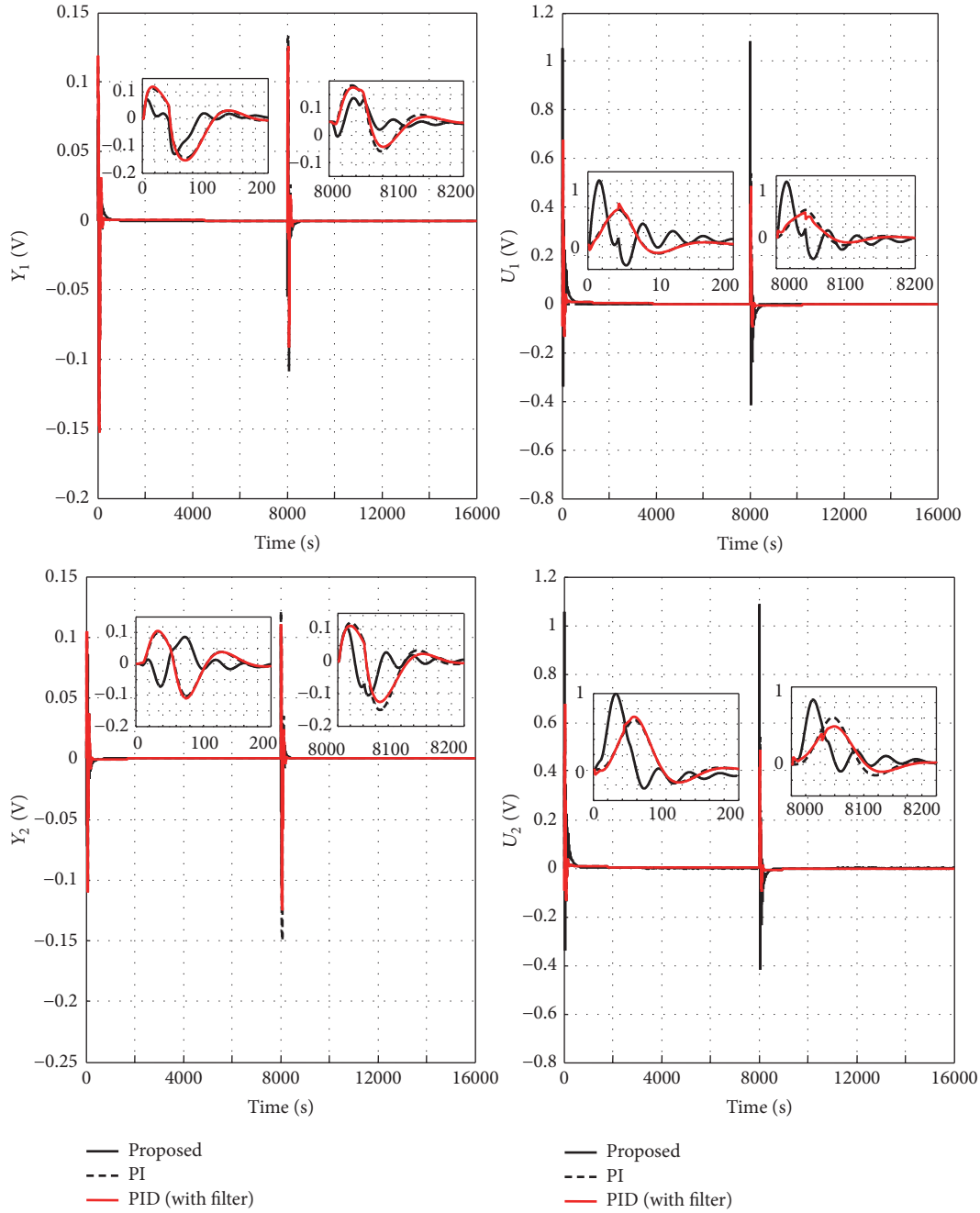


FIGURE 20: Closed-loop responses and controller output responses to unit step changes in the disturbance for the 4-tank process.

It should be pointed out that the unstable distillation column holds third-order elements.

- (v) For the 4-tank process, some large IAE and TV values listed are due to non-minimum phase system characteristics; it is obvious that non-minimum zero dynamics cause performance deterioration of the closed-loop system responses (initial undershoot, overshoot and zero crossings) and then increase IAE and TV performances indices.

6. Conclusion

This paper presents a MIMO PI controller design procedure for LTI MIMO systems with multiple time delays by means of ILMI and sensitivity functions. The proposed Loop Shaping design procedure with minimizing sensibility functions yields to optimized closed-loop system responses. The distillation column, the ISP reactor, and the 4-tank process as benchmarks of unstable, stable, and non-minimum phase systems are provided to illustrate the validity, effectiveness,

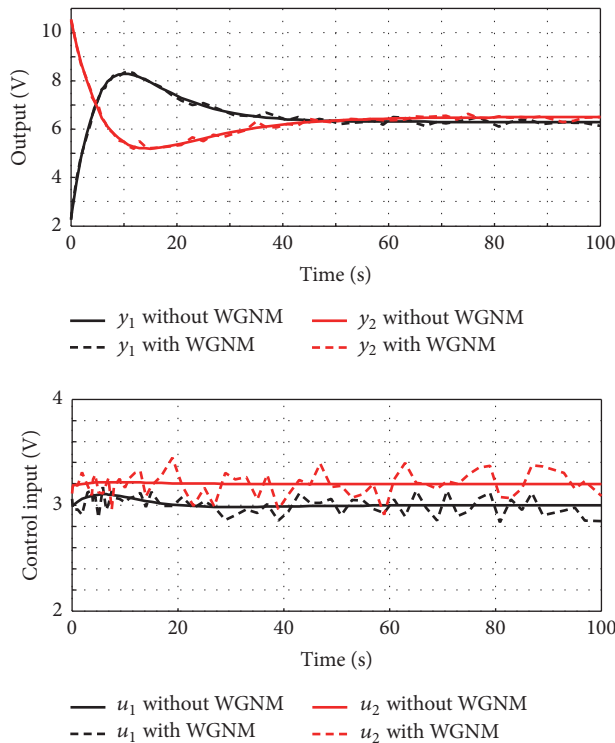


FIGURE 21: Closed-loop responses and controller output responses without WGNM and under WGNM.

and robustness of the proposed method. Considering different case studies (set-point tracking, disturbance rejection, and parametric uncertainties), a comparative analysis between the proposed method and related ones showed that the proposed method afforded the superior performances both in the nominal and in the perturbed case studies.

Competing Interests

The authors declare that there is no conflict of interests regarding the publication of this paper.

References

- [1] K. J. Astrom and T. Hagglund, "Advanced PID control," in *ISA-The Instrumentation, Systems, and Automation Society*, 2005.
- [2] R. Vilanova and A. Visioli, *PID Control in the Third Millennium: Lessons Learned and New Approaches*, Springer, New York, NY, USA, 2012.
- [3] F. D. Bianchi, R. J. Mantz, and C. F. Christiansen, "Multivariable PID control with set-point weighting via BMI optimisation," *Automatica*, vol. 44, no. 2, pp. 472–478, 2008.
- [4] X. Luan, Q. Chen, and F. Liu, "Equivalent transfer function based multi-loop PI control for high dimensional multivariable systems," *International Journal of Control, Automation and Systems*, vol. 13, no. 2, pp. 346–352, 2015.
- [5] S. Boyd, M. Hast, and K. J. Åström, "MIMO PID tuning via iterated LMI restriction," *International Journal of Robust and Nonlinear Control*, vol. 26, no. 8, pp. 1718–1731, 2016.
- [6] A. N. Gündeş, H. Özbay, and A. B. Özgüler, "PID controller synthesis for a class of unstable MIMO plants with I/O delays," *Automatica*, vol. 43, no. 1, pp. 135–142, 2007.
- [7] T. N. L. Vu and M. Lee, "Analytical design of robust multi-loop PI controller for multi-time delay processes," in *Advances in Machine Learning and Data Analysis*, vol. 48 of *Lecture Notes in Electrical Engineering*, pp. 95–108, Springer, Berlin, Germany, 2010.
- [8] A. N. Gündeş and H. Özbay, "Reliable decentralised control of delayed MIMO plants," *International Journal of Control*, vol. 83, no. 3, pp. 516–526, 2010.
- [9] Q. Jin, F. Hao, and Q. Wang, "IMC-PID controller based on diagonal equivalent model for multivariable systems with multiple time delays," *Journal of Chemical Engineering of Japan*, vol. 46, no. 3, pp. 209–218, 2013.
- [10] C. G. Economou and M. Morari, "Internal Model Control: multi-loop design," *Industrial and Engineering Chemistry Process Design and Development*, vol. 25, no. 2, pp. 411–419, 1986.
- [11] S. Cha, D. Chun, and J. Lee, "Two-step IMC-PID method for multiloop control system design," *Industrial and Engineering Chemistry Research*, vol. 41, no. 12, pp. 3037–3041, 2002.
- [12] M. Lee, K. Lee, C. Kim, and J. Lee, "Analytical design of multiloop PID controllers for desired closed-loop responses," *AIChE Journal*, vol. 50, no. 7, pp. 1631–1635, 2004.
- [13] T. N. L. Vu and M. Lee, "Multi-loop PI controller design based on the direct synthesis for interacting multi-time delay processes," *ISA Transactions*, vol. 49, no. 1, pp. 79–86, 2010.
- [14] F. Zheng, Q.-G. Wang, and T. H. Lee, "On the design of multivariable PID controllers via LMI approach," *Automatica*, vol. 38, no. 3, pp. 517–526, 2002.
- [15] C. Lin, Q.-G. Wang, and T. H. Lee, "An improvement on multivariable PID controller design via iterative LMI approach," *Automatica*, vol. 40, no. 3, pp. 519–525, 2004.
- [16] Y. He and Q. G. Wang, "An improved ILMI method for static output feedback control with application to multivariable PID control," *IEEE Transactions on Automatic Control*, vol. 51, no. 10, pp. 1678–1683, 2006.
- [17] W. Belhaj and O. Boubaker, "On MIMO PID control of the quadruple-tank process via ILMI approaches: minimum and non-minimum case studies," in *Proceedings of the 10th IFAC Symposium on Dynamics and Control of Process Systems (DYCOPS '13)*, pp. 481–486, Mumbai, India, December 2013.
- [18] W. Belhaj and O. Boubaker, "Multivariable PID controller via LMIs: performances assessment," *International Journal of Smart Sensing and Intelligent Systems*, vol. 8, no. 4, pp. 1896–1916, 2015.
- [19] D. McFarlane and K. Glover, *Robust Controller Design Using Normalized Coprime Factor Plant Descriptions*, vol. 138 of *Lecture Notes in Control and Information Sciences*, Springer, Berlin, Germany, 1990.
- [20] K. Zhou, J. C. Doyle, and K. Glover, *Robust and Optimal Control*, Prentice Hall, Upper Saddle River, NJ, USA, 1996.
- [21] H. Panagopoulos and K. J. Astrom, "PID control design and loop shaping," in *Proceedings of the IEEE International Conference on Control Applications*, pp. 103–108, Honolulu, Hawaii, USA, 1999.
- [22] W. Tan, T. Chen, and H. J. Marquez, "Robust controller design and PID tuning for multivariable processes," *Asian Journal of Control*, vol. 4, no. 4, pp. 439–451, 2002.

- [23] B. Vanavil, K. K. Chaitanya, and A. S. Rao, "Improved PID controller design for unstable time delay processes based on direct synthesis method and maximum sensitivity," *International Journal of Systems Science*, vol. 46, no. 8, pp. 1349–1366, 2015.
- [24] J.-P. Richard, "Time-delay systems: an overview of some recent advances and open problems," *Automatica*, vol. 39, no. 10, pp. 1667–1694, 2003.
- [25] P. J. Davis, *Interpolation and Approximation*, Blaisdell, Boston, Mass, USA, 1975.
- [26] O. Boubaker, J. P. Babary, and M. Ksouri, "MIMO sliding mode control of a distributed parameter denitrifying biofilter," *Applied Mathematical Modelling*, vol. 25, no. 8, pp. 671–682, 2001.
- [27] L. Lefèvre, D. Dochain, S. Feyo De Azevedo, and A. Magnus, "Optimal selection of orthogonal polynomials applied to the integration of chemical reactor equations by collocation methods," *Computers and Chemical Engineering*, vol. 24, no. 12, pp. 2571–2588, 2000.
- [28] M. T. Nihtila, T. Damak, and J. P. Babary, "Recursive input delay estimation in linear systems," in *Proceedings of the IFAC Symposium on Identification and System Parameter Estimation*, July 1994.
- [29] Y.-Y. Cao, L. James, and Y.-X. Sun, "Static output feedback stabilization: an ILMI approach," *Automatica*, vol. 34, no. 12, pp. 1641–1645, 1998.
- [30] J. Löfberg, "YALMIP: a toolbox for modeling and optimization in MATLAB," in *Proceedings of the IEEE International Symposium on Computer Aided Control Systems Design*, pp. 284–289, Taipei, Taiwan, September 2004.
- [31] T. Kailath, *Linear Systems*, Prentice-Hall, New Jersey, NJ, USA, 1980.
- [32] A. N. Mete, A. N. Gundes, and H. Özbay, "Decoupled PID controller synthesis for MIMO plants with I/O delays," in *Proceedings of the 45th IEEE Conference on Decision and Control (CDC '06)*, pp. 852–857, San Diego, Calif, USA, December 2006.
- [33] B. Friedland, *Control System Design: An Introduction to State Space Methods*, Dover Publications, New York, NY, USA, 1986.
- [34] I.-L. Chien, H.-P. Huang, and J.-C. Yang, "A simple multiloop tuning method for PID controllers with no proportional kick," *Industrial and Engineering Chemistry Research*, vol. 38, no. 4, pp. 1456–1468, 1999.
- [35] K. H. Johansson, "The quadruple-tank process: a multivariable laboratory process with an adjustable zero," *IEEE Transactions on Control Systems Technology*, vol. 8, no. 3, pp. 456–465, 2000.
- [36] F. El Haoussi, E. H. Tissir, F. Tadeo, and A. Hmamed, "Delay-dependent stabilisation of systems with time-delayed state and control: application to a quadruple-tank process," *International Journal of Systems Science*, vol. 42, no. 1, pp. 41–49, 2011.

Research Article

Direct Yaw-Moment Control of All-Wheel-Independent-Drive Electric Vehicles with Network-Induced Delays through Parameter-Dependent Fuzzy SMC Approach

Wanke Cao,^{1,2} Zhiyin Liu,² Yuhua Chang,² and Antoni Szumanowski²

¹The National Engineering Laboratory for Electric Vehicles and the Collaborative Innovation Center of Electric Vehicles in Beijing, School of Mechanical Engineering, Beijing Institute of Technology (BIT), Beijing 100081, China

²The Department of Multisource Propulsion System, Faculty of Automotive and Construction Machinery Engineering, Warsaw University of Technology (WUT), Narbutta 84, Warsaw 02-524, Poland

Correspondence should be addressed to Wanke Cao; caowanke@bit.edu.cn

Received 25 August 2016; Revised 20 November 2016; Accepted 20 December 2016; Published 22 January 2017

Academic Editor: Quanmin Zhu

Copyright © 2017 Wanke Cao et al. This is an open access article distributed under the Creative Commons Attribution License, which permits unrestricted use, distribution, and reproduction in any medium, provided the original work is properly cited.

This paper investigates the robust direct yaw-moment control (DYC) through parameter-dependent fuzzy sliding mode control (SMC) approach for all-wheel-independent-drive electric vehicles (AWID-EVs) subject to network-induced delays. AWID-EVs have obvious advantages in terms of DYC over the traditional centralized-drive vehicles. However it is one of the most principal issues for AWID-EVs to ensure the robustness of DYC. Furthermore, the network-induced delays would also reduce control performance of DYC and even deteriorate the EV system. To ensure robustness of DYC and deal with network-induced delays, a parameter-dependent fuzzy sliding mode control (FSMC) method based on the real-time information of vehicle states and delays is proposed in this paper. The results of cosimulations with Simulink® and CarSim® demonstrate the effectiveness of the proposed controller. Moreover, the results of comparison with a conventional FSMC controller illustrate the strength of explicitly dealing with network-induced delays.

1. Introduction

In recent years, all-wheel-independent-drive electric vehicles (AWID-EVs) have attracted increasing research efforts from both the academia and industry [1–3]. Equipped by advanced electric motors with more accurate and quicker torque generations than internal combustion engine (ICE) and hydraulic braking systems, AWID-EVs have obvious advantages in terms of direct yaw-moment control (DYC) through flexible differential driving/braking functions over traditional centralized drive vehicles [1, 3–6]. Plenty of existing studies have focused on the more flexible DYC and its integration control with active steering for AWID-EVs [2, 7–13]. However, considering the presence of model uncertainties, system parameter variations and external disturbances such as road rough or wind gust, it is one of the most principal issues for AWID-EVs to ensure the robustness of DYC.

To improve and ensure the robustness of DYC, in the existing lateral dynamics control strategies of AWID-EVs, sliding mode control (SMC) has been widely adopted, which is robust and suitable for nonlinear systems such as vehicles. Goodarzi and Esmailzadeh used a sliding mode controller in low-level control to improve the robustness of vehicle dynamics control system for AWID-EVs [1]. Li et al. employed a sliding mode controller in the main loop to offer enough robustness for an integrated vehicle chassis control system based on DYC, active steering, and active stabilizer [14]. Wang and Longoria designed three sliding mode controllers to ensure control system robustness in a new coordinated-reconfigurable vehicle dynamics control strategy for AWID-EVs [15] and [16, 17] presented a terminal sliding mode control method to improve the robustness of yaw rate tracking control and torque distribution control. But, in all of these aforementioned control strategies based on

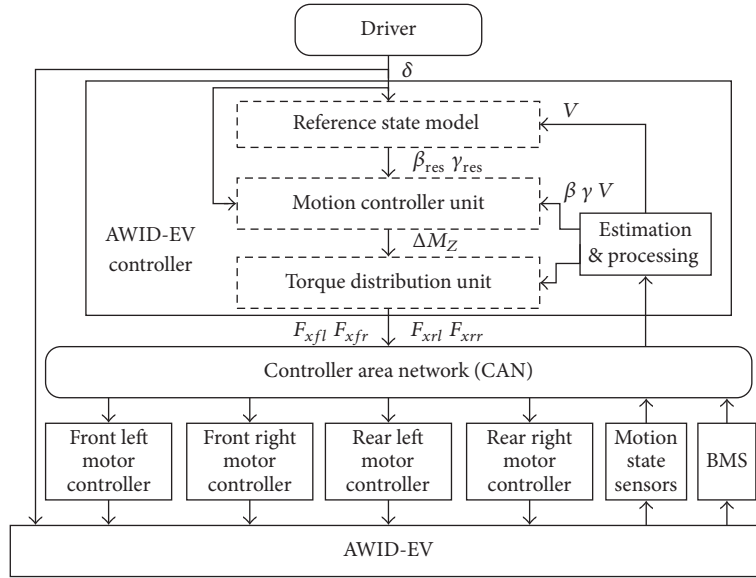


FIGURE 1: Overall structure for DYC of networked AWID-EVs.

SMC, the interference from electronic control systems such as networked-induced delays is not considered.

However, in a modern AWID-EV, the control signals from controllers and the measurements from sensors are usually exchanged through an in-vehicle communication network, for example, controller area network (CAN) or FlexRay [2]. In other words, a modern AWID-EV is a networked control system (NCS) rather than a conventional centralized control system [2, 7, 9, 10]. Thus, the network-induced delays cannot be ignored. According to these research results in [2, 7, 9, 10], the network-induced delays caused by CAN could reduce the control performance of DYC and even deteriorate the EV system. Some researchers proposed H_∞ -based linear quadratic regulator (LQR) control method against CAN network delays as in [2, 7, 10]. However, research on SMC-based DYC of AWID-EVs is rare.

Furthermore, as a variable structure control technology, SMC is more vulnerable to network-induced delays than continuous control technologies such as LQR or PID [18, 19]. There are numerous approaches to improve SMC. Among these approaches, the state-dependent boundary layer tuning method [20] has been widely used to improve the robustness of SMC. However the conventional state-dependent boundary layer tuning method is not sufficiently effective to deal with network-induced delay.

The main work is as follows: firstly, the network-induced delays are explicitly considered in the DYC through SMC control method. Considering that the network-induced delays lead to a challenging problem for the DYC based on SMC, the chattering problem of SMC caused by the delays is analyzed in detail and the delays are determined with a command-first scheme, which is a more accurate method than the existing approaches. Furthermore, a parameter-dependent fuzzy sliding mode control (FSMC) method based on the real-time information of vehicle states and system

delays is proposed to ensure the robustness of DYC for AWID-EVs against network-induced delays.

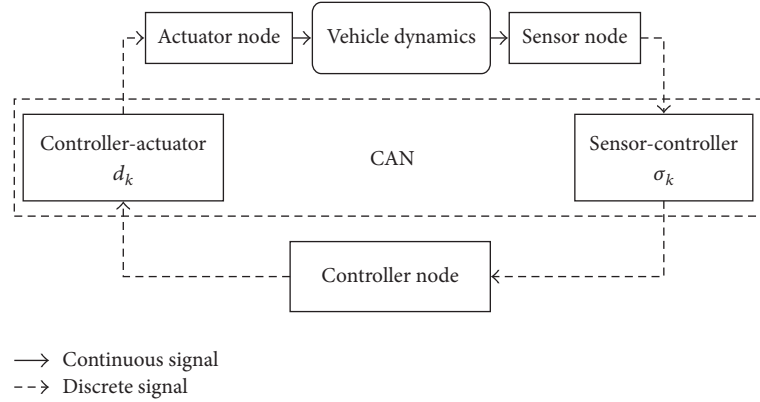
The remaining sections of this paper are organized as follows: In Section 2, problem formulation is described containing overall structure for DYC of networked AWID-EVs, control-oriented vehicle lateral dynamics model, and reference state model. The negative impact that resulted from NCS on the lateral dynamics model of AWID-EVs is also analyzed in detail in this section. In Section 3, an integrated state-dependent and delay-dependent fuzzy SMC is proposed to improve the robustness of DYC for networked AWID-EVs. In Section 4, the results of cosimulations with Matlab®/Simulink and CarSim are demonstrated. Conclusions are summarized in Section 5.

2. Problem Formulation

2.1. Overall Structure for DYC of Networked AWID-EVs.

According to vehicle dynamics, the main working principle of the DYC of AWID-EVs is to keep the vehicle lateral motion state variables such as the yaw rate and the slip angle tracking the reference states by using the external yaw moment [21], which is directly generated by active longitude tire forces distribution of all wheels. As shown in Figure 1, a typical overall structure for DYC of networked 4-wheel-independent drive vehicles mainly consists of AWID-EV controller, controller area network (CAN), 4 motor controllers, motion state sensors, and BMS. The overall control system is integrated by CAN.

The DYC function is implemented by AWID-EV controller, which is usually designed as a hierarchical controller including reference state model, motion controller unit, torque distribution unit, and estimation and processing unit as in Figure 1. The reference state model is used to solve the



In this study, the motion controller unit, which influences the system robustness against network-induced delays, will be studied, whereas the reference state model, torque distribution unit, and estimation and processing unit are simplified.

2.2. Control-Oriented Vehicle Lateral Dynamics Model. As shown in Figure 3, a two-degree-of-freedom (2-DOF) vehicle model, which has been widely studied as the control-oriented vehicle lateral dynamics model in various researches on DYC of vehicles [2, 21], is used in the paper, where CG is the center of gravity; m is the vehicle mass; I_z is the vehicle yaw inertia; M_z is the yaw moment; F_{xf} and F_{xr} are the longitude tire forces of front and rear wheels, respectively; F_{yf} and F_{yr} are the lateral tire forces of front and rear wheels, respectively; α_f and α_r are the slip angle of front and rear wheels, respectively.

With the 2-DOF vehicle model, the state-space formulation of control-oriented vehicle lateral dynamics model for DYC of AWID-EVs is expressed as follows [10]:

$$\dot{x} = Ax + Bu + E\delta, \quad (1)$$

where

$$\begin{aligned} x &= [\beta \quad \gamma]^T, \\ u &= \Delta M_z, \\ A &= \begin{bmatrix} -2 \frac{c_f + c_r}{mV} & -2 \frac{c_f l_f - c_r l_r}{mV^2} - 1 \\ -2 \frac{c_f l_f - c_r l_r}{I_z} & -2 \frac{c_f l_f^2 + c_r l_r^2}{I_z V} \end{bmatrix}, \\ B &= \begin{bmatrix} 0 \\ \frac{1}{I_z} \end{bmatrix}, \end{aligned}$$

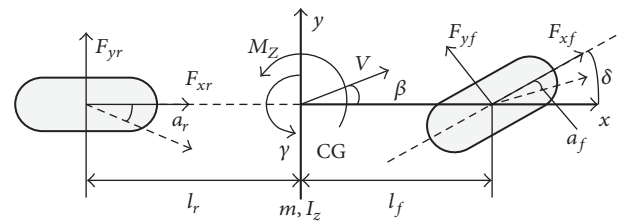


FIGURE 3: 2-DOF model of control-oriented vehicle lateral dynamics.

$$E = \begin{bmatrix} \frac{2c_f}{mV} \\ \frac{2c_f l_f}{I_z} \end{bmatrix}. \quad (2)$$

c_f and c_r are the cornering stiffness of the front and rear tires, respectively.

2.3. Reference State Model. In vehicle lateral motion control, the desired sideslip angle is generally selected to be zero to ensure vehicle stability, while the desired yaw rate is usually defined to ensure good handling performance [10]. A widespread expression of the desired yaw rate is described in [2, 10]. Therefore, the reference state model can be written as follows:

$$r = R\delta, \quad (3)$$

where

$$\begin{aligned} r &= \begin{bmatrix} \beta_{\text{res}} \\ \gamma_{\text{res}} \end{bmatrix}, \\ R &= \begin{bmatrix} 0 & \frac{V}{l_f + l_r + mV^2 (c_r l_r - c_f l_f) / 2c_f c_r (l_f + l_r)} \end{bmatrix}^T. \end{aligned} \quad (4)$$

2.4. The Impact Resulted from NCS on Vehicle Lateral Dynamics Model. Firstly, without loss of generality as in [22], it is possible to make following assumption. In the NCS of DYC for AWID-EVs shown in Figure 2, the sensor node

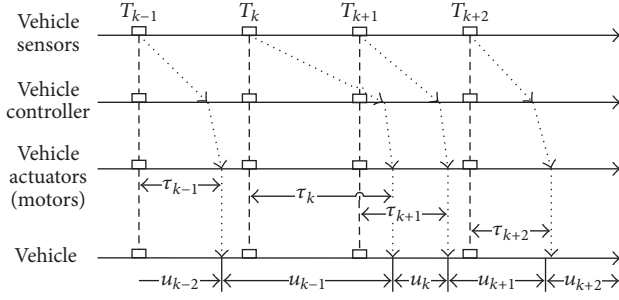


FIGURE 4: The network-induced delays.

periodically samples the vehicle states with fixed period T_s , the controller node and the actuator node operate in event-driven mode which means a task will be immediately implemented once a message arrives via CAN, and the task implementation time in each node is ignored. With such assumption and without considering network-induced delays, the NCS of DYC for AWID-EVs runs like an ideal centralized control system with fixed sampling period T_s . The control-oriented discrete-time model of the vehicle lateral dynamics along with reference state model can be written as [2]

$$\begin{aligned} x_{k+1} &= A_d x_k + B_d u_k + E_d \delta_k, \\ r_k &= R_d \delta_k, \end{aligned} \quad (5)$$

where

$$\begin{aligned} A_d &= e^{A T_s}, \\ R_d &= R, \\ B_d &= \int_0^{T_s} e^{A(T_s-\theta)} d\theta \cdot B, \\ E_d &= \int_0^{T_s} e^{A(T_s-\theta)} d\theta \cdot E \end{aligned} \quad (6)$$

with x_k , δ_k , u_k , and r_k indicating the state vector, steering angle vector, control input vector, and the reference state vector at time kT_s , respectively.

Secondly, considering the network-induced delays and the same assumption mentioned above, the control input u will be delayed by CAN as shown in Figure 4.

Thus, the control input u of the vehicle model at time t can be expressed as follows [22]:

$$u(t) = u_k, \quad \forall t \in [kT_s + \tau_k, (k+1)T_s + \tau_{k+1}]. \quad (7)$$

If the delay τ_k is expressed as

$$\tau_k = (\Upsilon + \nu) T_s, \quad (8)$$

where $\Upsilon \in \mathbb{Z}_+$ and $\nu \in R_{[0,1)}$.

Then, the control-oriented discrete-time model of the vehicle lateral dynamics with network-induced delays can be expressed as follows [2]:

$$\begin{aligned} x_{k+1} &= A_d x_k + E_d \delta_k + B_d u_k + \Delta_{0,k} (u_{k-1} - u_k) \\ &\quad + \Delta_{1,k} (u_{k-2} - u_{k-1}) + \dots \\ &\quad + \Delta_{\Upsilon,k} (u_{k-\Upsilon-1} - u_{k-\Upsilon}) \\ &= A_d x_k + E_d \delta_k + B_d u_k + \sum_{i=0}^{\Upsilon} \Delta_{i,k} (u_{k-i-1} - u_{k-i}), \end{aligned} \quad (9)$$

where the coefficient of each disturbance element induced by network-induced delays is expressed as follows [2]:

$$\Delta_{i,k} = \begin{cases} 0, & \tau_{k-i} - i \cdot T_s \leq 0 \\ \int_0^{\tau_{k-i} - i \cdot T_s} e^{A(T_s - \theta)} d\theta \cdot B, & 0 \leq \tau_{k-i} - i \cdot T_s \leq T_s \\ \int_0^{T_s} e^{A(T_s - \theta)} d\theta \cdot B, & T_s \leq \tau_{k-i} - i \cdot T_s. \end{cases} \quad (10)$$

For analyzing, expression (9) is rewritten as follows:

$$x_{k+1} = A_d x_k + B_d u_k + E_d \delta_k + f(k), \quad (11)$$

where the disturbance item

$$f(k) = \sum_{i=0}^{\Upsilon} \Delta_{i,k} (u_{k-i-1} - u_{k-i}). \quad (12)$$

$f(k)$ is the function of the network-induced delay τ and the input u .

Thus, the control-oriented model of vehicle lateral dynamics for networked AWID-EVs is described as a discrete-time model with the disturbance elements caused by network-induced delays.

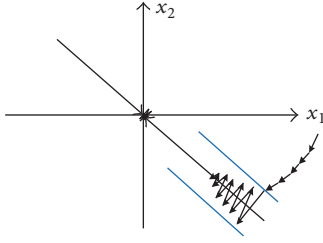


FIGURE 5: Trajectories of quasi-sliding mode.

3. Controller Design

3.1. Sliding Mode Controller Design for DYC of 4WID-EV. Firstly, without considering network-induced delays, a general SMC for the discrete-time model (5) is designed. According to the typical design methodology of an general SMC [18], the sliding mode surface can be defined as

$$s(x) = c^T (x - r) = c^T e. \quad (13)$$

e denotes the tracing error of motion states and $c^T = [c_1 c_2]$ is the weight coefficient of elements of e .

A reach law has been widely used [15, 18], which is written as

$$s_{k+1} - s_k = -qT_s s_k - \varepsilon T_s \text{sgn}(s_k), \quad (14)$$

$$\varepsilon > 0, q \geq 0, 1 - qT_s > 0,$$

where s_k denotes $s(x_k)$ at the time T_k .

With the reach law (14), the control law can be solved as follows:

$$u_k = - (c^T B_d)^{-1} \left\{ c^T A_d x_k + c^T E_d \delta_k - c^T r_{k+1} - c^T (x_k - r_k) + qT_s c^T (x_k - r_k) + \varepsilon T_s \text{sgn} [c^T (x_k - r_k)] \right\}. \quad (15)$$

However, according to the research in [18], for a discrete-time system, the state trajectory hardly occurs on the sliding mode surface (13) but zigzags around the sliding mode surface cause a quasi-sliding mode with a quasi-sliding mode band (QSMB) as in Figure 5. The QSMB is expressed as follows [18]:

$$\left\{ x \mid |s(x)| < \frac{\varepsilon T_s}{1 - qT_s} \right\}. \quad (16)$$

In order to avoid the chattering phenomenon in the QSMB, a boundary layer technique [1, 14] is usually adopted by defining a saturation function $\text{sat}(s_k)$ instead of $\text{sgn}(s_k)$ in (14) and (15)

$$\text{sat}(s_k) = \begin{cases} 1, & \text{if } s_k > w_{bl} \\ ks_k, & \text{if } |s_k| \leq w_{bl}, k = \frac{1}{w_{bl}} \\ -1, & \text{if } s_k < -w_{bl} \end{cases} \quad (17)$$

where w_{bl} is the boundary layer width.

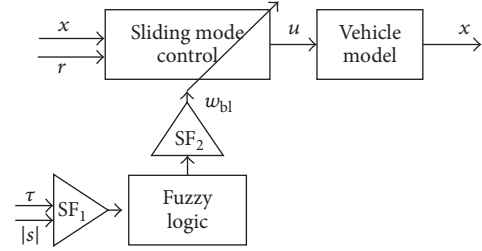


FIGURE 6: Fuzzy sliding mode controller for DYC of AWID-EV.

Thus, the reach law (14) and control law (15) can be rewritten as

$$s_{k+1} - s_k = -qT_s s_k - \varepsilon T_s \text{sat}(s_k), \quad (18)$$

$$u_k = - (c^T B_d)^{-1} \left\{ c^T A_d x_k + c^T E_d \delta_k - c^T r_{k+1} - c^T (x_k - r_k) + qT_s c^T (x_k - r_k) + \varepsilon T_s \text{sat} [c^T (x_k - r_k)] \right\}. \quad (19)$$

According to the expression (16), it is necessary to tune the boundary layer width w_{bl} based on the dynamics of $s(x)$ in the controller design stage. When the control law (19) is used for the discrete-time system (5), the $s(x)$ dynamics can be expressed as [18]:

$$s_{k+1} = s_k - qT_s s_k - \varepsilon T_s \text{sat}(s_k). \quad (20)$$

The $s(x)$ dynamics can be solved by (5) and (12).

However, when the control law (19) is used for the DYC of networked AWID-EVs, according to formulas (11), (13), (14), and (19), the $s(x)$ dynamics will be changed as follows:

$$s_{k+1} = s_k - qT_s s_k - \varepsilon T_s \text{sat}(s_k) - c^T f(k). \quad (21)$$

Comparing (21) with (20), the disturbance item $c^T f(k)$, which is caused by network-induced delays, will impose a new uncertainty item on the $s(x)$ dynamics and will result in adverse impact on the robustness of DYC.

3.2. Integrated State-Dependent and Delay-Dependent Sliding Mode Controller Design. A state-dependent boundary layer tuning method [20], which can tune the boundary layer width actively according to the dynamic state such as $s(x)$ instead of a fixed boundary layer, has been widely used to improve the robustness of SMC in the real-time system applications [20].

However, according to (21), the network-induced delays cause the uncertainty of the $s(x)$ dynamics. Consequently, it is reasonable to create an integrated state-dependent and delay-dependent method to tune the boundary layer width for SMC dynamically (see Figure 6).

TABLE 1: Fuzzy linguistic variable value terms.

| Name | Description (relative value) |
|------|------------------------------|
| NB | Negative big |
| NS | Negative small |
| ZE | Zero |
| PS | Positive small |
| PB | Positive big |
| PB1+ | Positive big + level 1 |
| PB2+ | Positive big + level 2 |
| PB3+ | Positive big + level 3 |
| PB4+ | Positive big + level 4 |

However, according to expressions (10), (12), and (21), the mathematic function between the $s(x)$ and the network-induced delay τ is complicated nonlinear. It is too difficult to be solved online in general in-vehicle ECUs. Thus, a fuzzy logic unit is designed to deal with the complicated nonlinear mathematic problem as in Figure 6.

3.3. Fuzzy Logic Unit Design for the Integrated State-Dependent and Delay-Dependent Method. As shown in Figure 6, the fuzzy logic unit is used to solve the boundary layer width w_{bl} according to the state norm $|s|$ and the network-induced delay τ . Thus the fuzzy logic unit has two input values and one unique output value, which are, respectively, defined as follows.

Input 1

$$|S| \in \{NB, NS, ZE, PS, PB\} \quad (22)$$

Input 2

$$\tau \in \{NB, NS, ZE, PS, PB\} \quad (23)$$

Output

$$W_{bl} \in \{NB, NS, ZE, PS, PB, PB1+, PB2+, PB3+, PB4+\} \quad (24)$$

And the fuzzy linguistic variable values are defined in Table 1. As shown in Figure 7, the triangular membership functions are used for the fuzzification of the two input variables and the one output variable. The scaling factors SF_1 and SF_2 (see Figure 6), which are tuned at the design stage by trial and extensive simulations performed in this study, are used to map the actual values of the input and output variables to their fuzzified values [23]. The rule base for the proposed fuzzy logic unit is described in Table 2.

The variable domains such as the inputs $|s| \in [0, 0.5]$ and $\tau \in [0, 20]$ and the output $w_{bl} \in [0.6, 1.4]$ are selected based on the simulation results with a high-fidelity full-vehicle model in CarSim and Matlab in this study.

TABLE 2: Rule base of the fuzzy logic unit.

| $ S $ | τ | W_{bl} |
|-------|--------|----------|
| NB | NB | NB |
| NS | NB | NS |
| ZE | NB | ZE |
| PS | NB | PS |
| PB | NB | PB |
| NB | PS | PS |
| NS | PS | PB |
| ZE | PS | PB1+ |
| PS | PS | PB2+ |
| PB | PS | PB3+ |
| NB | NS | NS |
| NS | NS | ZE |
| ZE | NS | PS |
| PS | NS | PB |
| PB | NS | PB1+ |
| NB | PB | PB |
| NS | PB | PB1+ |
| ZE | PB | PB2+ |
| PS | PB | PB3+ |
| PB | PB | PBPB4+ |
| NB | ZE | ZE |
| NS | ZE | PS |
| ZE | ZE | PB |
| PS | ZE | PB1+ |
| PB | ZE | PB1+ |

The fuzzy unit employs the Mamdani Fuzzy Inference System (FIS), which is described by the following schema:

$$\text{IF } |S| \text{ is } A, \tau \text{ is } B, \text{ THEN } W_{bl} \text{ is } C. \quad (25)$$

$$\text{IF } |S| \text{ is } A', \tau \text{ is } B', \text{ THEN } W_{bl} \text{ is } C',$$

where A, A', B, B', C , and C' are fuzzy values defined as the input and output variables, respectively. The *centre of area* method is used in the defuzzification to solve W_{bl} .

The rule base in detail between the inputs and the outputs is shown in Figure 8. Thus, once the state norm $|s|$ and the network-induced delay τ are known, the boundary layer width can be calculated by the fuzzy unit, and these rules could be easily implemented into the microprocessor of vehicle controller with a look-up mode. According to definition (13), the state norm $|s|$ is known, and the unknown network-induced delay τ will be discussed in the following section.

3.4. Determination of the Network-Induced Time Delay. To implement the proposed method, the network-induced delay τ should be determined. According to the assumption above (see Figures 2 and 4), the network-induced delay τ_k , which consists of the delays in both the forward and feedback links in the k th cycle, can be expressed as follows:

$$\tau_k = d_k + \sigma_k. \quad (26)$$

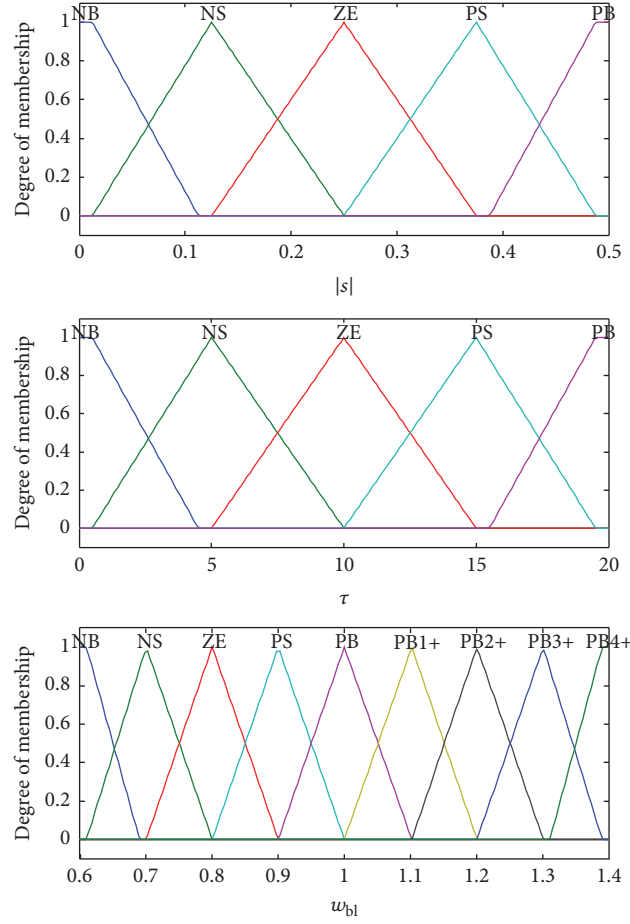


FIGURE 7: Membership functions for three variables.

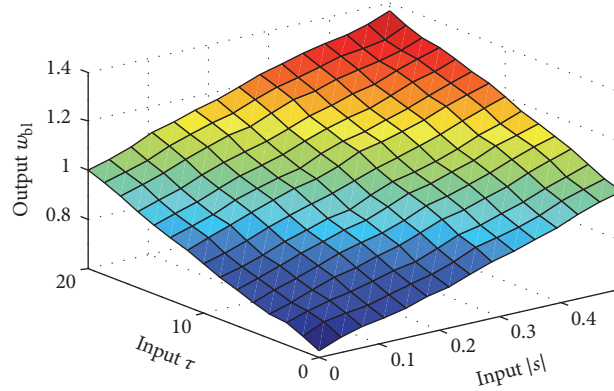


FIGURE 8: The rule relations between the inputs and the outputs for the proposed controller.

Generally, the feedback link delay σ_k in a NCS is known, which can be measured by using a “time sampling technology” with the time tag within each received message sent by sensor node. However, the current delay d_k in the forward link cannot be measured. In this paper, a “delay estimating technology,” which is based on *Network Calculus Theory* [24],

is introduced to estimate the forward link delay d_k with an explicit expression as follows [24]:

$$\tau_{\text{large},j} = \frac{(j+2)l}{R - \sum_{i=0}^{j-1} (l/c_i)}, \quad (27)$$

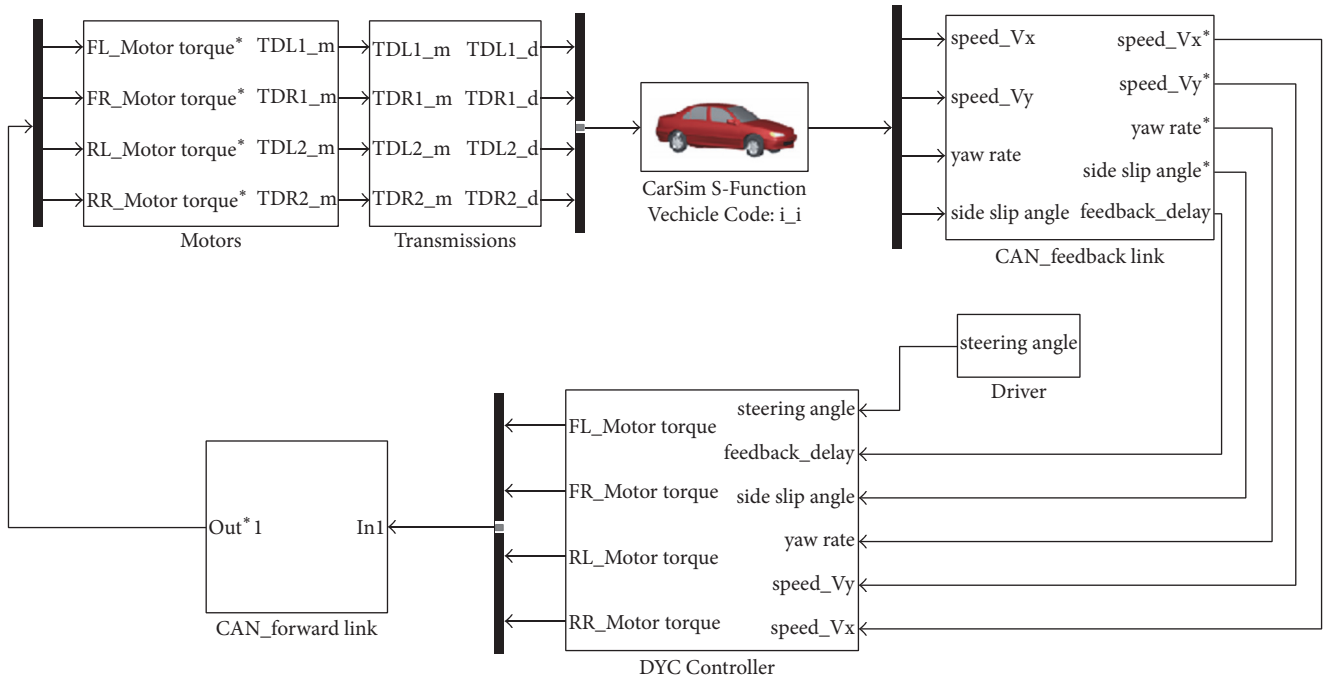


FIGURE 9: The cosimulation model with Simulink and CarSim.

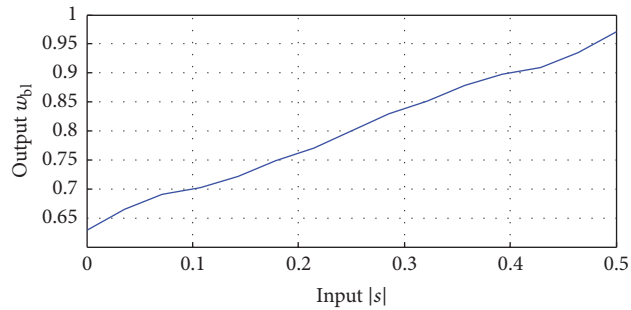


FIGURE 10: The rule relations between the input and the output for conventional FSMC.

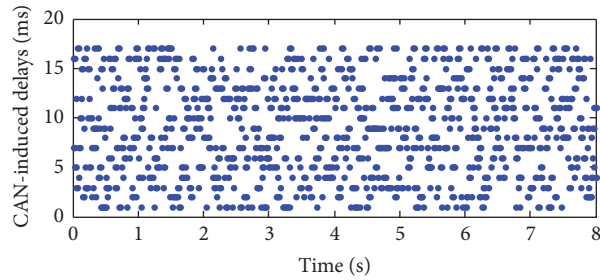


FIGURE 11: The network-induced delays in control loop over CAN.

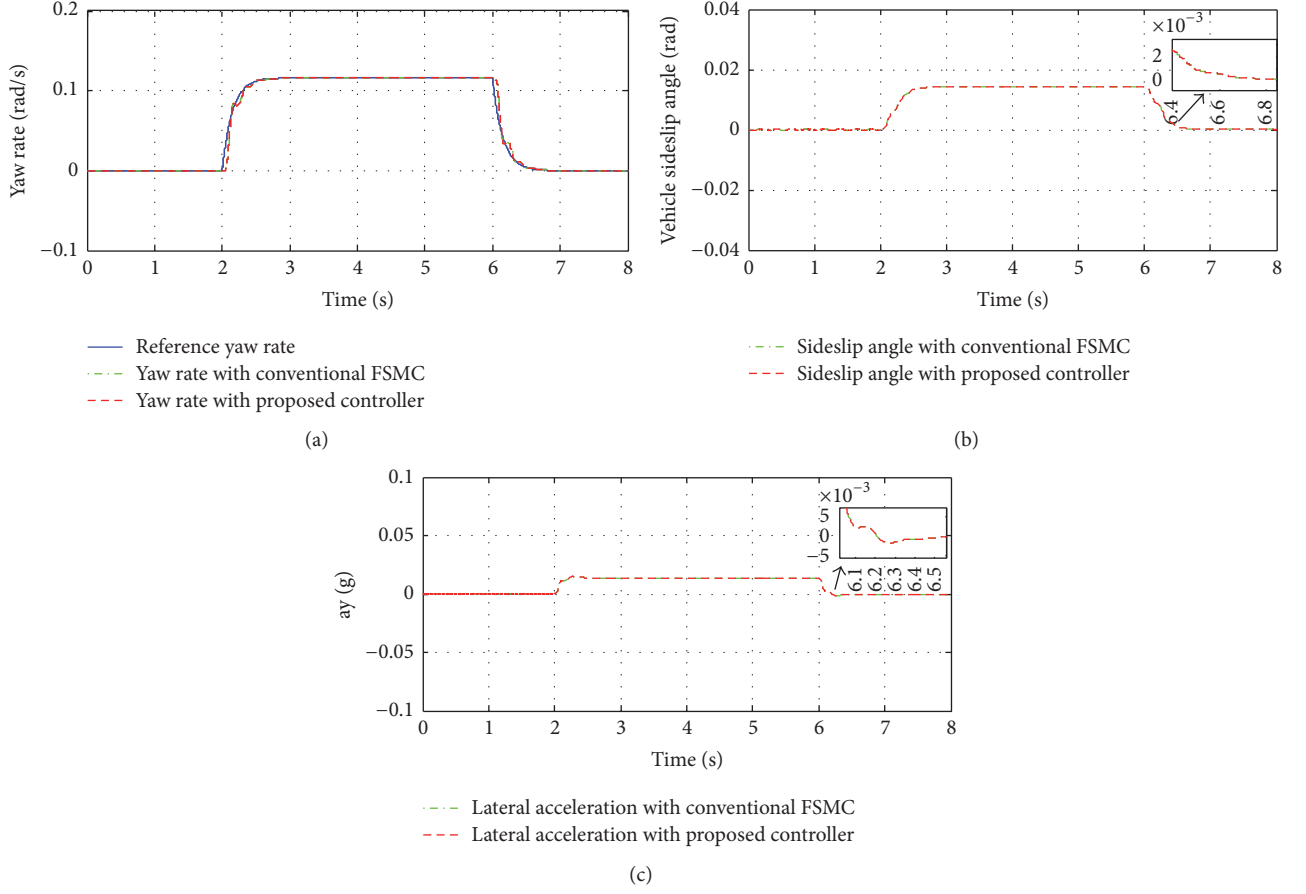


FIGURE 12: Control performance in J -turn maneuver under the ideal network condition. (a) Vehicle yaw rate. (b) Vehicle sideslip angle. (c) Vehicle lateral acceleration.

where $\tau_{\text{large},j}$ is the upper bound of delay of a message with the j th priority sent by CAN; l indicates the maximum data frame length; R is the baud rate of the CAN; c_i is the cycle length of the message with the i th priority.

According to the research result in [24], the network-induced delay of the message with the highest priority sent by CAN network can be accurately estimated through the expression (27). Therefore, this paper uses a “command-first scheme,” in which the command message in the forward link is sent with the highest priority to ensure the accuracy of d_k as follows:

$$d_k = \tau_{\text{large},j} = \frac{(j+2)l}{R - \sum_{i=0}^{j-1} (l/c_i)}, \quad \text{setting } j = 0. \quad (28)$$

Thus, the network-induced delay τ_k can be precisely determined by the following formula:

$$\tau_k = \sigma_k + \frac{(j+2)l}{R - \sum_{i=0}^{j-1} (l/c_i)}, \quad \text{setting } j = 0. \quad (29)$$

TABLE 3: Main vehicle parameters.

| Parameter | Description | Quantity |
|-----------|------------------------------------|------------------------|
| M | Vehicle mass | 1350 kg |
| I_z | Yaw moment of inertia | 1975 kg·m ² |
| l_f | Front semiwheelbase | 1.085 m |
| l_r | Rear semiwheelbase | 1.386 m |
| c_f | Cornering stiffness of front tires | 58000 N/rad |
| c_r | Cornering stiffness of rear tires | 60000 N/rad |

4. Simulation Results

To study the effectiveness of the proposed controller, the cosimulations are carried out in Matlab/Simulink with a full-vehicle model constructed by CarSim (see Figure 9). The vehicle parameters used in the simulations are based on a prototyped 4WID-EV, and main parameters are listed in Table 3.

The proposed controller is used in motion controller unit (see Figure 1) and a simple torque distribution strategy, which distributes the direct yaw-moment equally to the driving or braking torques of 4 wheels, is used in torque distribution

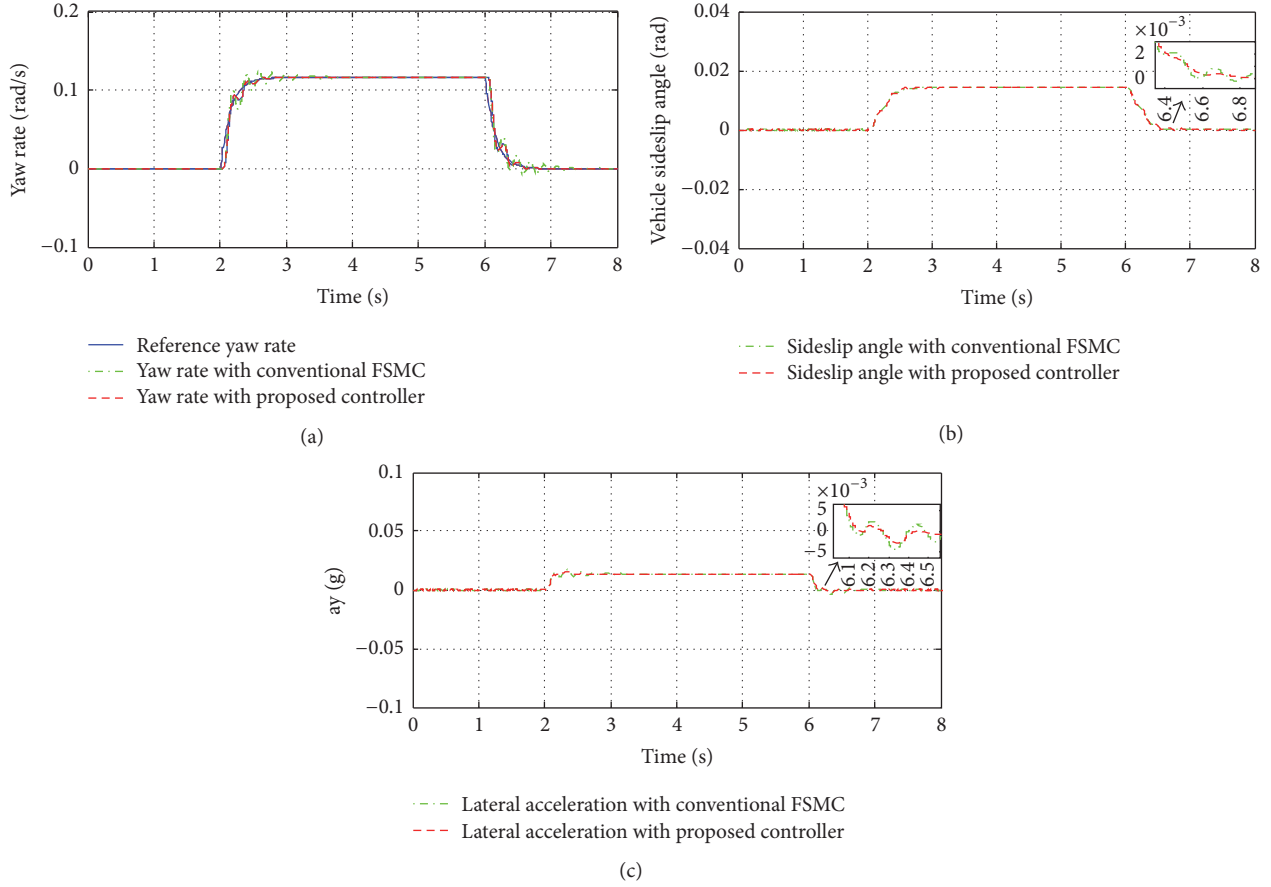


FIGURE 13: Control performance in *J*-turn maneuver with the network-induced delays caused by CAN. (a) Vehicle yaw rate. (b) Vehicle sideslip angle. (c) Vehicle lateral acceleration.

unit (see Figure 1). For comparison, a conventional state-dependent fuzzy SMC controller (the conventional FSMC) without considering network-induced delays is also designed. And the designed rule base of the conventional FSMC is shown in Figure 10.

The reaching law parameters of SMC are chosen as $\varepsilon = 27.5$ and $q = 0$. According to the results in [22], the upper bound of network-induced delays in a practical vehicle control system is about as high as $1.7T_s$. The sampling period of the closed-loop system is adopted as $T_s = 10$ ms. Thus, CAN-induced delays in simulations are assumed to change randomly in time range $[0, 1.7T_s]$ (see Figure 11).

Two different steering maneuvers, which are commonly used in vehicle tests, are considered: a ramp steering maneuver and a double lane-changing maneuver. The ramp steering maneuver is often adopted in the *J*-turn test and the double lane-changing maneuver is usually used in extreme cases, for example, high-speed overtaking or obstacle avoidance.

In each driving maneuver, simulations are carried out in two stages. The first stage is under the ideal network condition to evaluate the effectiveness of controllers without considering network-induced delays. The second stage is

to verify the robustness of the proposed controller with network-induced delays.

4.1. *J*-Turn Steering Maneuver. In this case, the vehicle runs at a low speed of 40 km/h on a slippery road with a low road friction ($\mu = 0.4$). During the *J*-turn maneuver, the steering wheel angle first increases from 0 deg to 18 deg in 0.5 s, which is used to simulate a sharp turn. Then it decreases to 0 deg again in 4 s.

Figure 12 shows the results of cosimulations in the *J*-turn steering maneuver under the ideal network condition. It is obvious in Figures 12(a), 12(b), and 12(c) that the vehicle yaw rate can precisely track the desired reference by the driver, the vehicle sideslip angle can be restrained in a narrow scope around 0.014 rad, and the lateral acceleration can be restrained in a narrow scope around 0.013 g. For the two controllers, the control performance is satisfactory. The results demonstrate the effectiveness of the conventional FSMC and the proposed controller.

Figure 13 shows the results of cosimulations in the *J*-turn steering maneuver with the network-induced delays caused by CAN. It is obvious in Figures 13(a), 13(b), and 13(c) that, with the conventional FSMC, the vehicle motion cannot track

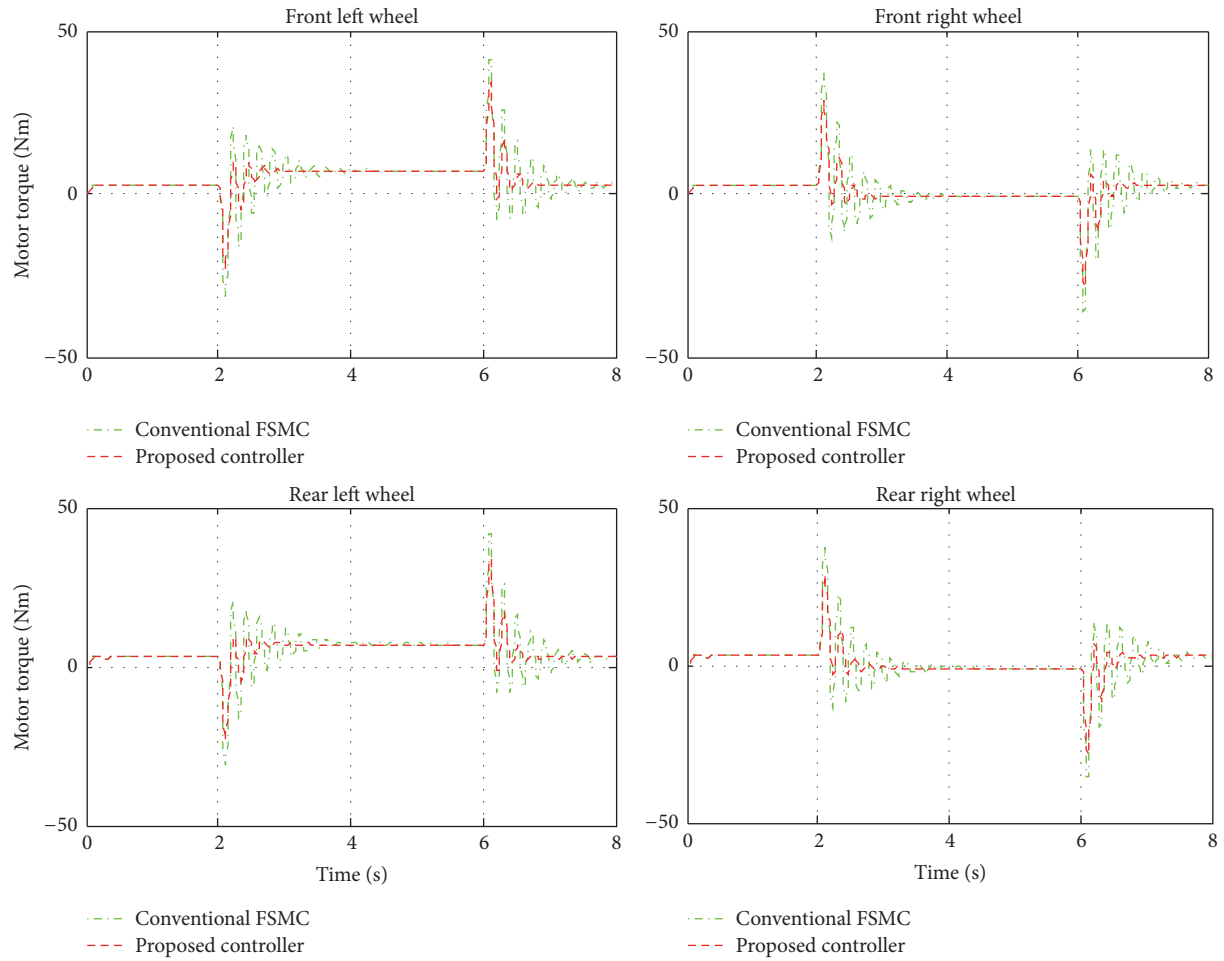


FIGURE 14: Motor torques of 4 wheels with two different controllers for DYC of 4WID-EV in double J -turn maneuver with the network-induced delays caused by CAN.

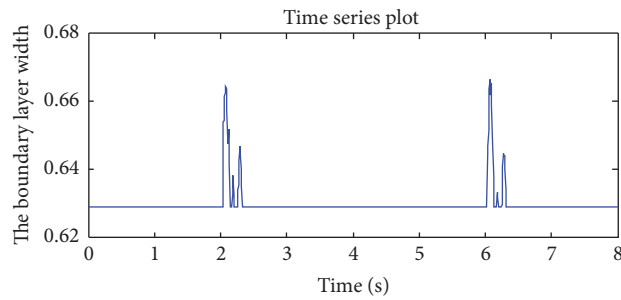


FIGURE 15: Tuning the boundary layer width process by the conventional FSMC in double J -turn steering maneuver with the network-induced delays caused by CAN.

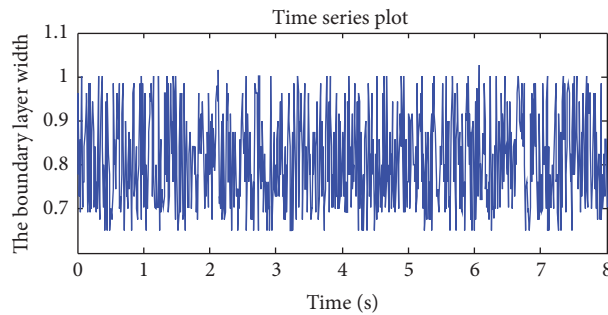


FIGURE 16: Tuning the boundary layer width process by the proposed controller in double J -turn steering maneuver with the network-induced delays caused by CAN.

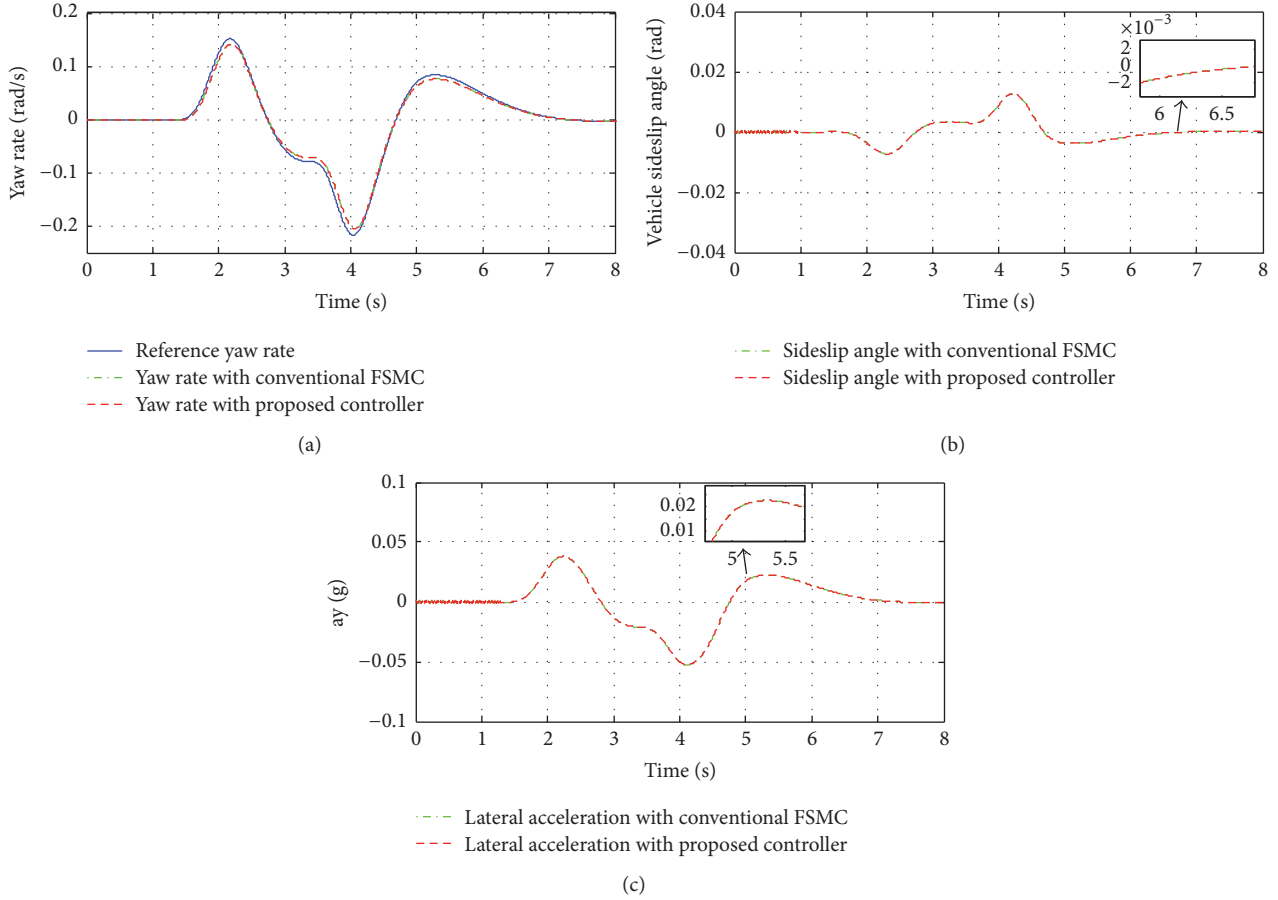


FIGURE 17: Control performance in double lane-changing maneuver under the ideal network condition. (a) Vehicle yaw rate. (b) Vehicle sideslip angle. (c) Vehicle lateral acceleration.

the desired yaw rate in the transient phase but can keep tracking the desired yaw rate in the steady phase, and the yaw rate overshoot is about 10.3% in the transient phase, while, for the proposed controller, the adverse impact of delays can be eliminated and the control performance is still satisfactory. The yaw rate overshoot is about 3.4%. Therefore the results of comparison explicitly illustrate the strength of the proposed controller dealing with network-induced delays.

Figure 14 shows the torque response of 4 motors in the *J*-turn steering maneuver with the network-induced delays caused by CAN. It is obvious that, with the conventional FSMC, the chattering phenomenon of each motor is severe in the transient phase, which would reduce control performance of DYC and even deteriorate the EV system, while, for the proposed controller, the performance of the torque response of each motor is satisfactory.

Figures 15 and 16 show the dynamic boundary layers of two controllers in the *J*-turn steering maneuver with the network-induced delays caused by CAN.

The results show that the conventional FSMC can tune the boundary layer width according to the vehicle states but not the network-induced delays. The proposed controller can tune the boundary layer width according to both the vehicle states and the network-induced delays.

4.2. Double Lane-Changing Steering Maneuver. In this case, the vehicle runs at a high speed of 100 km/h on a road with a high road friction ($\mu = 0.85$).

The following cosimulation process is quite similar to that for the *J*-turn steering maneuver. Under different network conditions, the results are shown in Figures 17, 18, 19, 20, and 21. Under the ideal network condition, the actual vehicle yaw rate can track the desired reference very well, and the vehicle sideslip angle and the vehicle lateral acceleration can also be kept regulated for both controllers. When with the network-induced delays, the proposed control can still keep the vehicle yaw rate tracking the desired reference very well, whereas the conventional FSMC results in significant oscillations due to the effect of the network-induced delays. Furthermore, a similar observation can be found in the vehicle sideslip angle and the vehicle lateral acceleration. The torque response of each motor is also shown as in Figure 19. The results show that network-induced delays have a significant impact on the stability of the closed-loop control system and can obviously reduce the robustness of the conventional FSMC.

The tuning boundary layer width processes of two controllers in double lane-changing maneuver are shown in Figures 20 and 21. The results also show that the conventional FSMC only can tune the boundary layer width according to

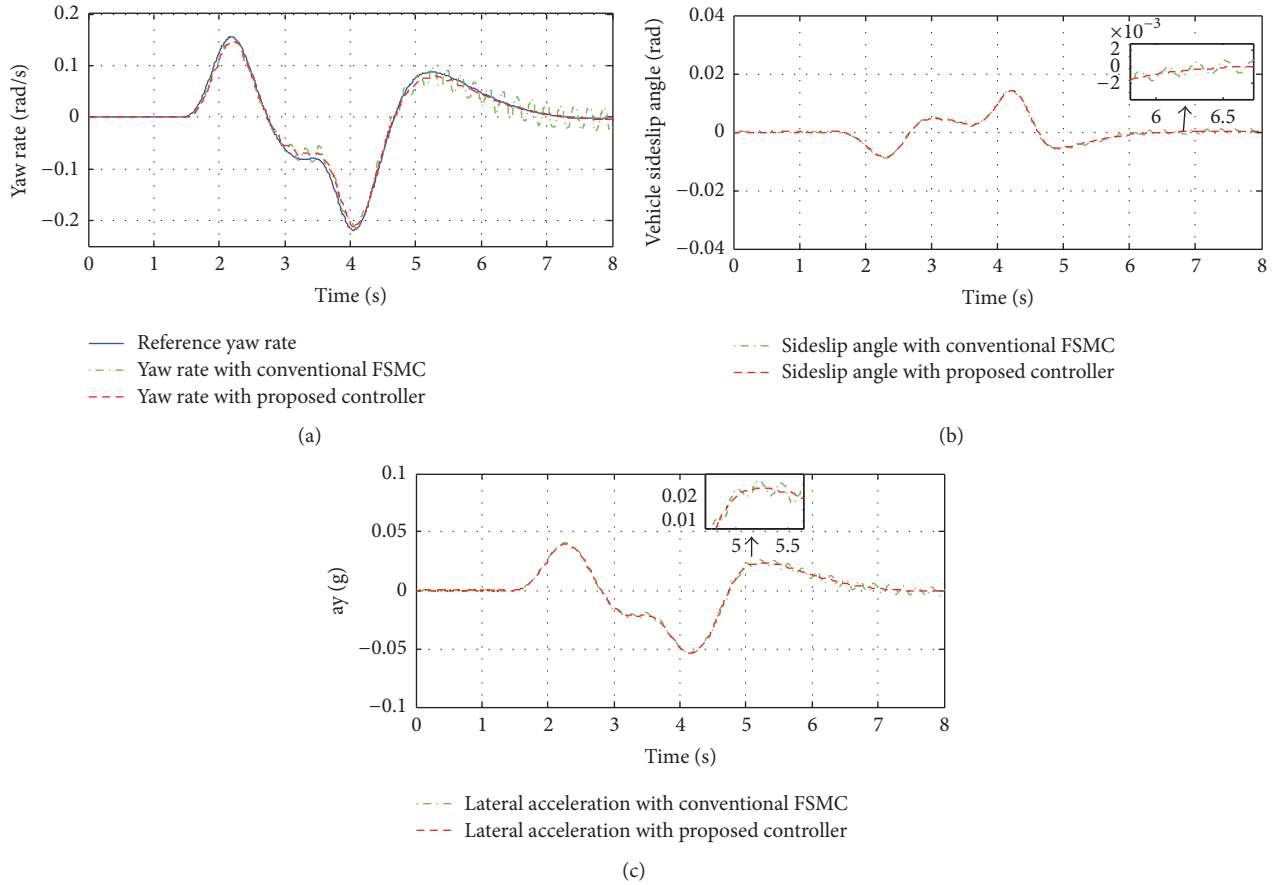


FIGURE 18: Control performance in double lane-changing maneuver with the network-induced delays caused by CAN. (a) Vehicle yaw rate. (b) Vehicle sideslip angle. (c) Vehicle lateral acceleration.

the vehicle states but not the network-induced delays, while the proposed controller can tune the boundary layer width actively according to both the vehicle states and the system delays, which makes the control system more robust.

5. Conclusions

This paper proposed an integrated state-dependent and delay-dependent fuzzy sliding mode control method to improve the robustness of DYC of AWID-EVs subject to network-induced delays. The SMC, which can effectively deal with model uncertainties, system parameter variations, and external disturbances, has been widely used to improve the robustness of DYC of AWID-EVs instead of common continuous control technologies such as LQR and PID. However, on the other hand, the SMC, which is a variable structure control, is more vulnerable to the system delays from electronic control systems. Meanwhile, in modern AWID-EVs, the networked control system based on in-vehicle networks such as CAN would inevitably impose network-induced delays on the vehicle control system. In order to improve the robustness of DYC of AWID-EVs, this paper first analyzed the adverse impact resulted from NCS on DYC based on SMC in detail.

Then an integrated state-dependent and delay-dependent fuzzy SMC method is proposed to improve the robustness of DYC for AWID-EVs.

The results of comparison in both typical steering maneuver cases show that the proposed controller can effectively improve the robustness of DYC for AWID-EVs subject to network-induced delays. Moreover, the proposed controller also inherits the robustness of SMC in terms of dealing with model uncertainties, system parameter variations, and external disturbances.

Competing Interests

The authors declare that they have no competing interests.

Acknowledgments

This work was supported in part by the National Natural Science Foundation of China (Grants 51205022, 51575044), the National Key Technology Support Program of China (Grant 2014BAG02B02), the China-Poland Collaborative Project of Electric City Bus (Grant 2015DFG81930), and the Basic Research Foundation of BIT (Grant 20140342015).

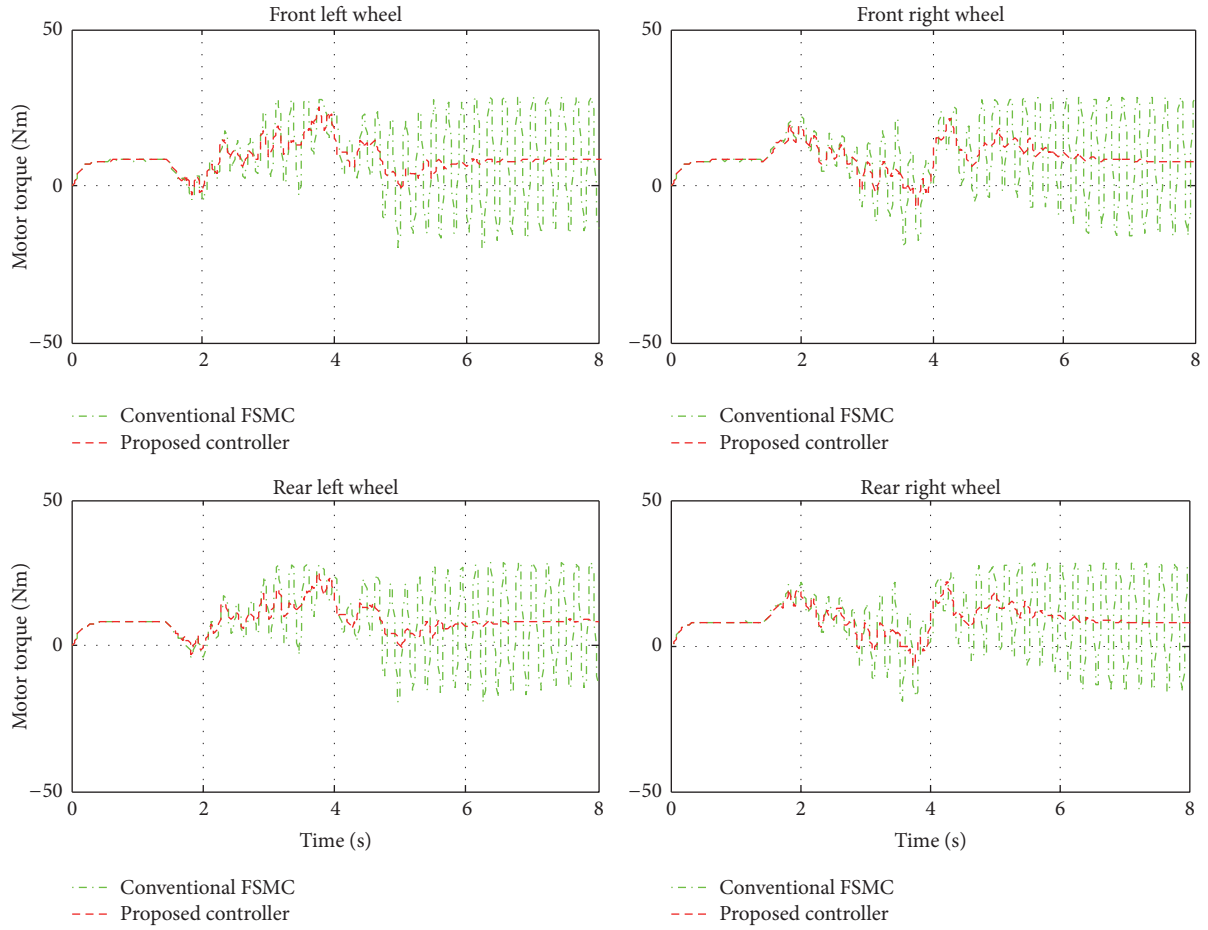


FIGURE 19: Motor torques of 4 wheels with two different controllers for DYC of 4WID-EV in double lane-changing maneuver with the network-induced delays caused by CAN.

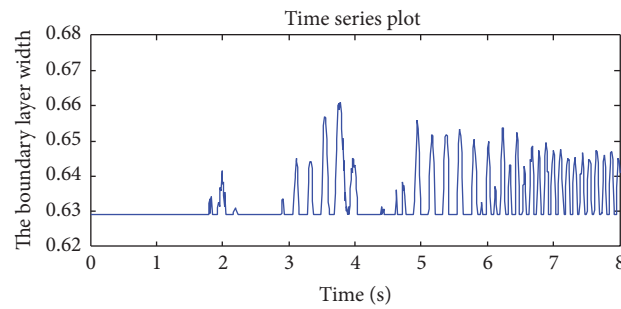


FIGURE 20: Tuning the boundary layer width process by the conventional FSMC in double lane-changing steering maneuver with the network-induced delays caused by CAN.

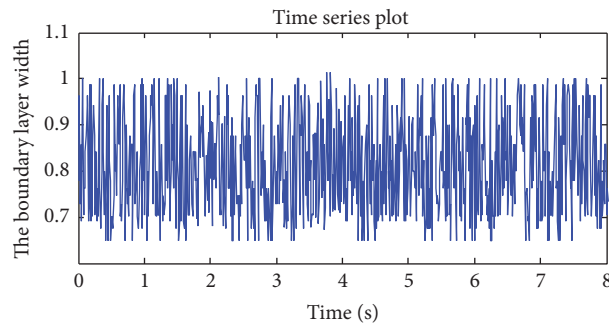


FIGURE 21: Tuning the boundary layer width process by the proposed controller in double lane-changing steering maneuver with the network-induced delays caused by CAN.

References

- [1] A. Goodarzi and E. Esmailzadeh, "Design of a VDC system for all-wheel independent drive vehicles," *IEEE/ASME Transactions on Mechatronics*, vol. 12, no. 6, pp. 632–639, 2007.
- [2] Z. Shuai, H. Zhang, J. Wang, J. Li, and M. Ouyang, "Combined AFS and DYC control of four-wheel-independent-drive electric vehicles over CAN Network with time-varying delays," *IEEE Transactions on Vehicular Technology*, vol. 63, no. 2, pp. 591–602, 2014.
- [3] Y. H. Shen, Y. Gao, and T. Xu, "Multi-axle vehicle dynamics stability control algorithm with all independent drive wheel," *International Journal of Automotive Technology*, vol. 17, no. 5, pp. 795–805, 2016.
- [4] L. De Novellis, A. Sorniotti, P. Gruber et al., "Direct yaw moment control actuated through electric drivetrains and friction brakes: theoretical design and experimental assessment," *Mechatronics*, vol. 26, pp. 1–15, 2015.
- [5] R. Wang, C. Hu, F. Yan, and M. Chadli, "Composite nonlinear feedback control for path following of four-wheel independently actuated autonomous ground vehicles," *IEEE Transactions on Intelligent Transportation Systems*, vol. 17, no. 7, pp. 2063–2074, 2016.
- [6] L. Xiong, G. W. Teng, Z. P. Yu, W. X. Zhang, and Y. Feng, "Novel stability control strategy for distributed drive electric vehicle based on driver operation intention," *International Journal of Automotive Technology*, vol. 17, no. 4, pp. 651–663, 2016.
- [7] G. Qin and J. Zou, " H_∞ control of four-wheel-independent-drive electric vehicles with random time-varying delays," *Mathematical Problems in Engineering*, vol. 2015, Article ID 245493, 10 pages, 2015.
- [8] R. Wang and J. Wang, "Fault-tolerant control with active fault diagnosis for four-wheel independently driven electric ground vehicles," *IEEE Transactions on Vehicular Technology*, vol. 60, no. 9, pp. 4276–4287, 2011.
- [9] Z. Shuai, H. Zhang, J. Wang, J. Li, and M. Ouyang, "Lateral motion control for four-wheel-independent-drive electric vehicles using optimal torque allocation and dynamic message priority scheduling," *Control Engineering Practice*, vol. 24, no. 1, pp. 55–66, 2014.
- [10] X. Zhu, H. Zhang, J. Wang, and Z. Fang, "Robust lateral motion control of electric ground vehicles with random network-induced delays," *IEEE Transactions on Vehicular Technology*, vol. 64, no. 11, pp. 4985–4995, 2015.
- [11] H. Alipour, M. Sabahi, and M. B. B. Sharifian, "Lateral stabilization of a four wheel independent drive electric vehicle on slippery roads," *Mechatronics*, vol. 30, pp. 275–285, 2015.
- [12] Y. Hori, Y. Toyoda, and Y. Tsuruoka, "Traction control of electric vehicle: basic experimental results using the test EV 'UOT electric march,'" *IEEE Transactions on Industry Applications*, vol. 34, no. 5, pp. 1131–1138, 1998.
- [13] S.-I. Sakai, H. Sado, and Y. Hori, "Motion control in an electric vehicle with four independently driven in-wheel motors," *IEEE/ASME Transactions on Mechatronics*, vol. 4, no. 1, pp. 9–16, 1999.
- [14] D. Li, S. Du, and F. Yu, "Integrated vehicle chassis control based on direct yaw moment, active steering and active stabiliser," *Vehicle System Dynamics*, vol. 46, no. 1, pp. 341–351, 2008.
- [15] J. Wang and R. G. Longoria, "Coordinated and reconfigurable vehicle dynamics control," *IEEE Transactions on Control Systems Technology*, vol. 17, no. 3, pp. 723–732, 2009.
- [16] D. B. Ren, J. Y. Zhang, J. M. Zhang, and S. M. Cui, "Trajectory planning and yaw rate tracking control for lane changing of intelligent vehicle on curved road," *Science China Technological Sciences*, vol. 54, no. 3, pp. 630–642, 2011.
- [17] P. Song, C.-F. Zong, and M. Tomizuka, "A terminal sliding mode based torque distribution control for an individual-wheel-drive vehicle," *Journal of Zhejiang University: Science A*, vol. 15, no. 9, pp. 681–693, 2014.
- [18] W. Gao, Y. Wang, and A. Homaifa, "Discrete-time variable structure control systems," *IEEE Transactions on Industrial Electronics*, vol. 42, no. 2, pp. 117–122, 1995.
- [19] S. Z. Sarpturk, Y. I Stefanopulos, and O. Kaynak, "On the stability of discrete-time sliding mode control systems," *IEEE Transactions on Automatic Control*, vol. 32, pp. 930–932, 1987.
- [20] M.-S. Chen, Y.-R. Hwang, and M. Tomizuka, "A state dependent boundary layer design for sliding mode control," *Institute of Electrical and Electronics Engineers. Transactions on Automatic Control*, vol. 47, no. 10, pp. 1677–1681, 2002.
- [21] B. L. Boada, M. J. L. Boada, and V. Díaz, "Fuzzy-logic applied to yaw moment control for vehicle stability," *Vehicle System Dynamics*, vol. 43, no. 10, pp. 753–770, 2005.
- [22] C. F. Caruntu, M. Lazar, R. H. Gielen, P. P. J. van den Bosch, and S. Di Cairano, "Lyapunov based predictive control of vehicle drivetrains over CAN," *Control Engineering Practice*, vol. 21, no. 12, pp. 1884–1898, 2013.
- [23] N. Yagiz, Y. Hacioglu, and Y. Taskin, "Fuzzy sliding-mode control of active suspensions," *IEEE Transactions on Industrial Electronics*, vol. 55, no. 11, pp. 3883–3890, 2008.
- [24] T. Herpel, K.-S. Hielscher, U. Klehmet, and R. German, "Stochastic and deterministic performance evaluation of automotive CAN communication," *Computer Networks*, vol. 53, no. 8, pp. 1171–1185, 2009.

Research Article

Multiple Periodic Solutions for a Class of Second-Order Neutral Impulsive Functional Differential Equations

Jingli Xie,¹ Zhiguo Luo,² and Yuhua Zeng³

¹College of Mathematics and Statistics, Jishou University, Jishou, Hunan 416000, China

²Department of Mathematics, Hunan Normal University, Changsha, Hunan 410081, China

³Department of Mathematics, Hunan First Normal University, Changsha, Hunan 410205, China

Correspondence should be addressed to Jingli Xie; xiejingli721124@163.com

Received 29 August 2016; Revised 1 December 2016; Accepted 20 December 2016; Published 12 January 2017

Academic Editor: Olfa Boubaker

Copyright © 2017 Jingli Xie et al. This is an open access article distributed under the Creative Commons Attribution License, which permits unrestricted use, distribution, and reproduction in any medium, provided the original work is properly cited.

In this paper, we study a class of second-order neutral impulsive functional differential equations. Under certain conditions, we establish the existence of multiple periodic solutions by means of critical point theory and variational methods. We propose an example to illustrate the applicability of our result.

1. Introduction and Main Results

In this paper we consider a class of second-order neutral impulsive functional differential equations

$$\begin{aligned} u''(t - \tau) - u(t - \tau) \\ + \lambda f(t, u(t), u(t - \tau), u(t - 2\tau)) = 0, \\ t \neq t_j, \quad t \in J = [0, 2k\tau], \quad (1) \end{aligned}$$

$$\Delta u'(t_j) = I_j(u(t_j)), \quad j = 1, 2, \dots, l,$$

$$u(0) - u(2k\tau) = u'(0) - u'(2k\tau) = 0,$$

where $f \in C(\mathbb{R}^4, \mathbb{R})$, $I_j \in C(\mathbb{R}, \mathbb{R})$, and $0 = t_0 < t_1 < t_2 < \dots < t_l < t_{l+1} = 2k\tau$. The operator Δ is defined as $\Delta u'(t_j) = u'(t_j^+) - u'(t_j^-)$, where $u'(t_j^+)(u'(t_j^-))$ denotes the right-hand (left-hand) limit of u' at t_j . $\lambda \in \mathbb{R}$, τ is a constant with $\tau > 0$ and k is a given positive integer.

The necessity to study delay differential equations is due to the fact that these equations are useful mathematical tools in modeling many real processes and phenomena studied in biology, medicine, chemistry, physics, engineering, economics, and so forth [1, 2].

On the other hand, impulsive differential equation not only is richer than the corresponding theory of differential equations but also represents a more natural framework for mathematical modeling of real world phenomena. People generally consider impulses in positions u and u' for the second-order differential equation $u'' = f(t, u, u')$. However it is well known that in the motion of spacecraft instantaneous impulses depend on the position which result in jump discontinuities in velocity, with no change in position.

Thus, it is more realistic to consider the case of combined effects: impulses and time delays. This motivates us to consider neutral impulsive functional differential system (1).

The existence of periodic solutions of delay differential equations has been focused on by many researchers [3–6]. Several available approaches to tackle them include Lyapunov method, Fourier analysis method, fixed point theory, and coincidence degree theory [7–10]. Recently, some researchers have studied the existence of solutions for delay differential equations via variational methods [11–13]. In recent years, some researchers, by using critical point theory, have studied the existence of solutions for boundary value problems, periodic solutions, and homoclinic orbits of impulsive differential systems [14–19].

In this paper, we aim to establish existence of multiple periodic solutions for the second-order neutral impulsive

functional differential equation (1) by using critical point theory and variational methods.

For (1) with $I_j = 0$, Shu and Xu [20] obtained the following periodic solutions result.

Theorem A. Assume that the following conditions are satisfied.

(H1) $\partial f(t, u_1, u_2, u_3)/\partial t \neq 0$.

(H2) There exists a function $F(t, u_1, u_2) \in C^1(\mathbb{R}^3, \mathbb{R})$ such that

$$\frac{\partial F(t, u_1, u_2)}{\partial u_2} + \frac{\partial F(t, u_2, u_3)}{\partial u_2} = f(t, u_1, u_2, u_3). \quad (2)$$

(H3) $F(t, u_1, u_2)$ is τ -periodic in t .

(H4) F satisfies $F(t, -u_1, -u_2) = F(t, u_1, u_2)$ and $f(t, -u_1, -u_2, -u_3) = -f(t, u_1, u_2, u_3)$.

(H5) $F(t, u_1, u_2) = 0$ if and only if $(u_1, u_2) = 0, \forall t \in [0, \tau]$.

(H6) $\lim_{|u| \rightarrow 0} (F(t, u_1, u_2)/|u|^2) = 1$, where $|u| = (|u_1|^2 + |u_2|^2)^{1/2}, t \in [0, \tau]$.

(H7) There exists a constant $\alpha > 0$ such that when $|u_1|^2 + |u_2|^2 > \alpha^2, F(t, u_1, u_2) < 0, t \in [0, \tau]$.

Moreover, if there exists an integer $m > 0$ such that λ satisfying

$$\lambda > \frac{m^2 (\pi^2 + k^2 \tau^2)}{4k\tau^2}, \quad (3)$$

then the system

$$\begin{aligned} u''(t - \tau) - u(t - \tau) \\ + \lambda f(t, u(t), u(t - \tau), u(t - 2\tau)) &= 0, \\ u(0) - u(2k\tau) = u'(0) - u'(2k\tau) &= 0 \end{aligned} \quad (4)$$

possesses at least $2m$ nonzero solutions with the period $2k\tau$.

Our main result is stated as follows.

Theorem 1. Assume that (H1)–(H7) and the following condition are satisfied.

(H8) I_j is odd about u , and there exists a constant $0 \leq D < 1$ such that $|I_j(u)| \leq D|u|$, where $j = 1, 2, \dots, l$.

Moreover, if there exists an integer $m > 0$ such that

$$\lambda > \frac{m^2 (\pi^2 + (1 + D)k^2 \tau^2)}{4k^2 \tau^2}, \quad (5)$$

then system (1) admits at least $2m$ nonzero solutions with the period $2k\tau$.

Clearly, when $I_j = 0$, Theorem 1 generalizes Theorem A.

Note that the first equation of system (1) is equivalent to the following equation:

$$\begin{aligned} u''(t - \tau) - u(t - \tau) + \lambda (F'_1(t, u(t - \tau), u(t - 2\tau)) \\ + F'_2(t, u(t), u(t - \tau))) &= 0, \end{aligned} \quad (6)$$

where $F'_1(t, u(t - \tau), u(t - 2\tau)) = \partial F(t, u(t - \tau), u(t - 2\tau))/\partial u(t - \tau)$ and $F'_2(t, u(t), u(t - \tau)) = \partial F(t, u(t), u(t - \tau))/\partial u(t - \tau)$.

The rest of this paper is organized as follows. In Section 2, we present some preliminaries, which will be used to prove our main result. In Section 3 we prove our main result and provide an example to illustrate the applicability of our results.

2. Some Preliminaries

Let

$$\begin{aligned} H_{2k\tau}^1 &= \{u : \mathbb{R} \rightarrow \mathbb{R} \mid u, u' \in L^2([0, 2k\tau]), u(0) \\ &= u(2k\tau), u'(0) = u'(2k\tau)\}. \end{aligned} \quad (7)$$

Then $H_{2k\tau}^1$ is a separable and reflexive Banach space and the inner product

$$(u, v) = \int_0^{2k\tau} (u'(t) v'(t) + u(t) v(t)) dt \quad (8)$$

induces the norm

$$\|u\|_{H_{2k\tau}^1} = \left(\int_0^{2k\tau} |u'(t)|^2 + |u(t)|^2 dt \right)^{1/2}. \quad (9)$$

Definition 2. A function $u \in H_{2k\tau}^1$ is a solution of system (1) if the function u satisfies system (1).

Define a functional φ as

$$\begin{aligned} \varphi(u) &= \frac{1}{2} \int_0^{2k\tau} (|u(t)|^2 + |u'(t)|^2) dt \\ &\quad - \lambda \int_0^{2k\tau} F(t, u(t), u(t - \tau)) dt \\ &\quad + \sum_{j=1}^l \int_0^{u(t_j)} I_j(s) ds, \quad u \in H_{2k\tau}^1. \end{aligned} \quad (10)$$

Then φ is Fréchet differentiable at any $u \in H_{2k\tau}^1$. For any $v \in H_{2k\tau}^1$, by a simple calculation, we have

$$\begin{aligned} \varphi'(u)(v) &= \int_0^{2k\tau} (u'(t) v'(t) + u(t) v(t)) dt \\ &\quad - \lambda \int_0^{2k\tau} (F'_1(t, u(t), u(t - \tau)) v(t) \\ &\quad + F'_2(t, u(t), u(t - \tau)) v(t - \tau)) dt \\ &\quad + \sum_{j=1}^l I_j(u(t_j)) v(t_j). \end{aligned} \quad (11)$$

From (H3), we get

$$\begin{aligned} \varphi'(u)(v) &= \int_0^{2k\tau} (-u''(t) + u(t)) v(t) dt \\ &\quad - \lambda \int_0^{2k\tau} (F'_1(t, u(t), u(t - \tau)) v(t) \\ &\quad + F'_2(t, u(t + \tau), u(t)) v(t)) dt. \end{aligned} \quad (12)$$

Therefore, the corresponding Euler equation of functional φ is

$$\begin{aligned} u''(t) - u(t) \\ + \lambda (F'_1(t, u(t), u(t - \tau)) + F'_2(t, u(t + \tau), u(t))) \\ = 0. \end{aligned} \quad (13)$$

$$\gamma(A) = \begin{cases} \min \{n \in \mathbb{Z}^+ : \text{there exists an odd continuous map } \varphi : A \rightarrow \mathbb{R}^n \setminus \{0\}\}; \\ 0, & \text{if } A = \emptyset; \\ +\infty, & \text{if there is no odd continuous map } \varphi : A \rightarrow \mathbb{R}^n \setminus \{0\} \text{ for any } n \in \mathbb{Z}^+. \end{cases} \quad (15)$$

Then we say γ is the genus of Σ .

Denote $i_1(\varphi) = \lim_{a \rightarrow -0} \gamma(\varphi_a)$ and $i_2(\varphi) = \lim_{a \rightarrow -\infty} \gamma(\varphi_a)$, where $\varphi_a = \{u \in E \mid \varphi(u) \leq a\}$.

Lemma 4 (see [22]). *Let E be a real Banach space and $\varphi \in C^1(E, \mathbb{R})$ with φ even functional and satisfying the Palais-Smale (PS) condition. Suppose $\varphi(0) = 0$ and*

- (i) *if there exist an m -dimensional subspace X of E and a constant $r > 0$ such that*

$$\sup_{u \in X \cap B_r} \varphi(u) < 0, \quad (16)$$

where B_r is an open ball of radius r in E centered at 0, then we have $i_1(\varphi) \geq m$;

- (ii) *if there exists j -dimensional subspace V of E such that*

$$\inf_{u \in V^\perp} \varphi(u) > -\infty, \quad (17)$$

then we have $i_2(\varphi) \leq j$.

Moreover, if $m \geq j$, then φ possesses at least $2(m - j)$ distinct critical points.

3. Proof of Theorem 1 and an Example

We apply Lemma 4 to finish the proof. Under assumption (H4), it is easy to see that if function u is a solution of system (1), then function $-u$ is also a solution of system (1). Therefore, the solutions of system (1) are a set which is symmetric with respect to the origin in $H_{2k\tau}^1$. It follows directly from (10), (H5), and (H8) that φ is even in u and $\varphi(0) = 0$. The rest of the proof is divided into three steps.

Step 1. We show that the functional φ satisfies assumption (ii) of Lemma 4.

It follows from (H7) that there exists a constant $M > 0$ such that

$$\max_{t \in \mathbb{R}} F(t, u(t), u(t - \tau)) \leq \max_{(t, u_1, u_2) \in \Omega} F(t, u_1, u_2) \leq M, \quad (18)$$

Note that (6) is equivalent to system (13) and critical points of the functional φ are classical $2k\tau$ -periodic solutions of system (1).

Definition 3 (see [21]). Let E be a real reflexive Banach space, and

$$\Sigma = \{A \mid A \subset E \setminus \{0\} \text{ is closed, symmetric set}\}. \quad (14)$$

Define $\gamma : \Sigma \rightarrow \mathbb{Z}^+ \cup \{+\infty\}$ as follows:

where $\Omega = [0, \tau] \times [-\alpha, \alpha] \times [-\alpha, \alpha]$. Combining (10) and (18), we get

$$\begin{aligned} \varphi(u) &= \frac{1}{2} \int_0^{2k\tau} (|u(t)|^2 + |u'(t)|^2) dt \\ &\quad - \lambda \int_0^{2k\tau} F(t, u(t), u(t - \tau)) dt \\ &\quad + \sum_{j=1}^l \int_0^{u(t_j)} I_j(s) ds \\ &\geq \frac{1}{2} \int_0^{2k\tau} |u'(t)|^2 dt + \frac{1-D}{2} \int_0^{2k\tau} |u(t)|^2 dt \\ &\quad - 2\lambda M k \tau \geq \frac{1-D}{2} \|u\|_{H_{2k\tau}^1}^2 - 2\lambda M k \tau > -\infty, \end{aligned} \quad (19)$$

which implies that φ is bounded from below. By condition (ii) of Lemma 4, we have $i_2(\varphi) = 0$.

Step 2. We show that the functional φ satisfies the PS condition.

For any given sequence $\{u_n\} \in H_{2k\tau}^1$ such that $\{\varphi(u_n)\}$ is bounded and $\lim_{n \rightarrow \infty} \varphi'(u_n) = 0$, there exists a constant C_1 such that

$$\begin{aligned} |\varphi(u_n)| &\leq C_1, \\ \|\varphi'(u_n)\|_{(H_{2k\tau}^1)^*} &\leq C_1, \\ \forall n \in \mathbb{N}, \end{aligned} \quad (20)$$

where $(H_{2k\tau}^1)^*$ is the dual space of $H_{2k\tau}^1$.

Combining (19) and (20), we have

$$\frac{1}{2} \|u\|_{H_{2k\tau}^1}^2 \leq C_1 + 2\lambda M k \tau. \quad (21)$$

It follows that $\|u_n\|_{H_{2k\tau}^1}$ is bounded.

Since $H_{2k\tau}^1$ is a reflexive Banach space, so we may extract a weakly convergent subsequence, for simplicity, we also note again by $\{u_n\}$, $u_n \rightharpoonup u$ in $H_{2k\tau}^1$. So we have

$$\begin{aligned} & \int_0^{2k\tau} (F_1'(t, u_n(t), u_n(t-\tau)) - F_1'(t, u(t), u(t-\tau))) \\ & \quad \cdot (u_n(t) - u(t)) dt \longrightarrow 0, \\ & \int_0^{2k\tau} (F_2'(t, u_n(t), u_n(t-\tau)) - F_2'(t, u(t), u(t-\tau))) \\ & \quad \cdot (u_n(t-\tau) - u(t-\tau)) dt \longrightarrow 0, \\ & \sum_{j=1}^l (I_j(u_n(t_j)) - I_j(u(t_j))) (u_n(t_j) - u(t_j)) \\ & \longrightarrow 0, \\ & u_n(t) - u(t) \longrightarrow 0 \text{ as } n \longrightarrow \infty, t \in [0, 2k\tau]. \end{aligned} \quad (22)$$

Therefore, by (22), we have $\|u_n - u\|_{H_{2k\tau}^1} \rightarrow 0$. Hence the functional φ satisfies the PS condition.

Step 3. We show that the functional φ satisfies assumption (i) of Lemma 4.

Let $\beta_j(t) = (k\tau/j\pi)\sin(j\pi/\kappa\tau)t$, $j = 1, 2, \dots, m$. By calculations, we obtain

$$\begin{aligned} & \int_0^{2k\tau} |\beta_j(t)|^2 dt = \left(\frac{k\tau}{j\pi}\right)^2 k\tau, \\ & \int_0^{2k\tau} |\beta_j'(t)|^2 dt = k\tau. \end{aligned} \quad (23)$$

Define the m -dimensional linear subspace as follows:

$$E_m = \text{span}\{\beta_1(t), \beta_2(t), \dots, \beta_m(t)\}. \quad (24)$$

It is clear to see that E_m is a symmetric set. Take $r > 0$, when $u(t) \in E_m \cap S_r$, where S_r denotes boundary of B_r , $u(t)$ has expansion $u(t) = \sum_{j=1}^m b_j \beta_j(t)$, $b_j \in \mathbb{R}$, and

$$\begin{aligned} r^2 &= \|u(t)\|_{H_{2k\tau}^1}^2 = \int_0^{2k\tau} (|u'(t)|^2 + |u(t)|^2) dt \\ &\leq k\tau \sum_{j=1}^m b_j^2 \left(1 + \frac{k^2 \tau^2}{j^2 \pi^2}\right). \end{aligned} \quad (25)$$

By (H6), for given ε with $0 < \varepsilon < (\lambda m^2 / 4k^2 \tau^2)(4k^2 \tau^2 / m^2 - (\pi^2 + (1+D)k^2 \tau^2) / \lambda)$, there exists $0 < \delta < 1$ such that when $(|u(t)|^2 + |u(t-\tau)|^2)^{1/2} < \delta$, we have

$$\begin{aligned} & \lambda F(t, u(t), u(t-\tau)) \\ & > (\lambda - \varepsilon) (|u(t)|^2 + |u(t-\tau)|^2). \end{aligned} \quad (26)$$

Combining (10), (25), and (26), when $u(t) \in E_m \cap S_r$, we have

$$\begin{aligned} \varphi(u) &= \frac{1}{2} \int_0^{2k\tau} (|u(t)|^2 + |u'(t)|^2) dt \\ &\quad - \lambda \int_0^{2k\tau} F(t, u(t), u(t-\tau)) dt \\ &\quad + \sum_{j=1}^l \int_0^{u(t_j)} I_j(s) ds \leq \frac{1}{2} \|u\|_{H_{2k\tau}^1}^2 - (\lambda - \varepsilon) \\ &\quad \cdot \int_0^{2k\tau} (|u(t)|^2 + |u(t-\tau)|^2) dt + \frac{D}{2} \\ &\quad \cdot \int_0^{2k\tau} |u(t)|^2 dt \leq \frac{k\tau}{2} \sum_{j=1}^m b_j^2 \left(1 + \frac{(1+D)k^2 \tau^2}{j^2 \pi^2}\right) \\ &\quad - \frac{2(\lambda - \varepsilon)k^2 \tau^2}{m^2 \pi^2} k\tau \sum_{j=1}^m b_j^2 \leq \frac{k\tau}{2\pi^2} \\ &\quad \cdot \sum_{j=1}^m b_j^2 \left(\pi^2 + (1+D)k^2 \tau^2 - \frac{4(\lambda - \varepsilon)k^2 \tau^2}{m^2}\right) \\ &= \frac{\lambda k\tau}{2\pi^2} \\ &\quad \cdot \sum_{j=1}^m b_j^2 \left(\frac{\pi^2 + (1+D)k^2 \tau^2}{\lambda} - \frac{4k^2 \tau^2}{m^2} + \varepsilon \frac{4k^2 \tau^2}{\lambda m^2}\right) \\ &< 0. \end{aligned} \quad (27)$$

Therefore $i_1(\varphi) \geq m$. Consequently, system (1) admits at least $2m$ nonzero $2k\tau$ -periodic solutions.

We conclude this section with the following example.

Example 5. Consider (1) with

$$\begin{aligned} & f(t, u(t), u(t-\tau), u(t-2\tau)) \\ &= 4u(t-\tau) - 4\left(2 + \cos \frac{2\pi t}{\tau}\right)u(t-2\tau) \\ &\quad \cdot (u^2(t) + 2u^2(t-\tau) + u^2(t-2\tau)), \end{aligned} \quad (28)$$

$$F(t, u_1, u_2) = u_1^2 + u_2^2 - \left(2 + \cos \frac{2\pi t}{\tau}\right)(u_1^2 + u_2^2),$$

$$I_j(u) = 0.5u.$$

It is easy to see that $\partial f(t, u_1, u_2, u_3) / \partial t \neq 0$ and when $(u_1, u_2) = 0$, $F(t, u_1, u_2) = 0$; then (H1) and (H5) hold. Set $u_1 = u(t)$, $u_2 = u(t-\tau)$, $u_3 = u(t-2\tau)$, and then $\partial F(t, u(t), u(t-\tau)) / \partial u(t-\tau) + \partial F(t, u(t-\tau), u(t-2\tau)) / \partial u(t-\tau) = f(t, u(t), u(t-\tau), u(t-2\tau))$. By a simple computation, we have $F(t+\tau, u_1, u_2) = F(t, u_1, u_2)$, $F(t, -u_1, -u_2) = F(t, u_1, u_2)$, and $f(t, -u_1, -u_2, -u_3) = -f(t, u_1, u_2, u_3)$. So conditions (H2)–(H4) hold. Clearly, the conditions (H6)–(H8) hold. Therefore system (1) admits at least $2m$ nonzero solutions with the period $2k\tau$.

Competing Interests

The authors declare that there is no conflict of interests regarding the publication of this paper.

Acknowledgments

This work was partially supported by Hunan Provincial Natural Science Foundation of China (no. 2016JJ6122), National Natural Science Foundation of China (nos. 11661037 and 11471109), and Jishou University Doctor Science Foundation (no. jsdxxcfbskyxm201504).

References

- [1] J. K. Hale, *Theory of Functional Differential Equations*, Springer, New York, NY, USA, 1977.
- [2] Y. Kuang, *Delay differential equations with applications in population dynamics*, Mathematics in Science and Engineering, Academic Press, Inc., Boston, MA, USA, 1993.
- [3] W. Wang, P. Fergola, and C. Tenneriello, "Global attractivity of periodic solutions of population models," *Journal of Mathematical Analysis and Applications*, vol. 211, no. 2, pp. 498–511, 1997.
- [4] R. Olach, "Positive periodic solutions of delay differential equations," *Applied Mathematics Letters*, vol. 26, no. 12, pp. 1141–1145, 2013.
- [5] J. Yu and H. Xiao, "Multiple periodic solutions with minimal period 4 of the delay differential equation $\dot{x}(t) = -f(t, x(t-1))$," *Journal of Differential Equations*, vol. 254, no. 5, pp. 2158–2172, 2013.
- [6] E. Serra, "Periodic solutions for some nonlinear differential equations of neutral type," *Nonlinear Analysis: Theory, Methods & Applications*, vol. 17, no. 2, pp. 139–151, 1991.
- [7] B. Yang, R. Ma, and C. Gao, "Positive periodic solutions of delayed differential equations," *Applied Mathematics and Computation*, vol. 218, no. 8, pp. 4538–4545, 2011.
- [8] X. M. Li and X. P. Yuan, "Quasi-periodic solutions for perturbed autonomous delay differential equations," *Journal of Differential Equations*, vol. 252, no. 6, pp. 3752–3796, 2012.
- [9] K. Wu and X. Wu, "Multiplicity results of periodic solutions for a class of first order delay differential equations," *Journal of Mathematical Analysis and Applications*, vol. 390, no. 2, pp. 427–438, 2012.
- [10] J. Wu and Z. Wang, "Two periodic solutions of second-order neutral functional differential equations," *Journal of Mathematical Analysis and Applications*, vol. 329, no. 1, pp. 677–689, 2007.
- [11] H. Xiao and Z. Guo, "Multiplicity and minimality of periodic solutions to delay differential system," *Electronic Journal of Differential Equations*, vol. 39, no. 115, pp. 1–12, 2014.
- [12] X.-B. Shu, Y.-T. Xu, and L. H. Huang, "Infinite periodic solutions to a class of second-order Sturm-Liouville neutral differential equations," *Nonlinear Analysis: Theory, Methods & Applications*, vol. 68, no. 4, pp. 905–911, 2008.
- [13] Z.-M. Guo and Y.-T. Xu, "Existence of periodic solutions to a class of second-order neutral differential difference equations," *Acta Analysis Functionalis Applicata*, vol. 5, no. 1, pp. 13–19, 2003.
- [14] J. J. Nieto and D. O'Regan, "Variational approach to impulsive differential equations," *Nonlinear Analysis: Real World Applications*, vol. 10, no. 2, pp. 680–690, 2009.
- [15] Z. Zhang and R. Yuan, "An application of variational methods to Dirichlet boundary value problem with impulses," *Nonlinear Analysis. Real World Applications*, vol. 11, no. 1, pp. 155–162, 2010.
- [16] L. Bai and B. X. Dai, "An application of variational method to a class of Dirichlet boundary value problems with impulsive effects," *Journal of the Franklin Institute*, vol. 348, no. 9, pp. 2607–2624, 2011.
- [17] Y. Tian, J. Wang, and W. Ge, "Variational methods to mixed boundary value problem for impulsive differential equations with a parameter," *Taiwanese Journal of Mathematics*, vol. 13, no. 4, pp. 1353–1370, 2009.
- [18] J. Xie and Z. Luo, "Subharmonic solutions with prescribed minimal period of an impulsive forced pendulum equation," *Applied Mathematics Letters*, vol. 52, pp. 169–175, 2016.
- [19] J. Xie and Z. Luo, "Homoclinic orbits for Hamiltonian systems induced by impulses," *Mathematical Methods in the Applied Sciences*, vol. 39, no. 9, pp. 2239–2250, 2016.
- [20] X. B. Shu and Y. T. Xu, "Multiple periodic solutions to a class of second-order functional differential equations of mixed type," *Acta Mathematicae Applicatae Sinica*, vol. 29, no. 5, pp. 821–831, 2006.
- [21] J. Mawhin and M. Willem, *Critical Point Theory and Hamiltonian Systems*, Springer, Berlin, Germany, 1989.
- [22] C. Q. Ching, *Critical Point Theory and Its Applications*, Shanghai Scientific and Technical Publishers, Shanghai, China, 1986.

Research Article

Stabilization for Damping Multimachine Power System with Time-Varying Delays and Sector Saturating Actuator

Linlin Ma,^{1,2} Yanping Liang,¹ and Jian Chen²

¹Electrical and Electronic Engineering College, Harbin University of Science and Technology, Harbin 150080, China

²College of Automation Engineering, Qingdao University of Technology, Qingdao 266520, China

Correspondence should be addressed to Yanping Liang; liangyanping2010@126.com

Received 4 August 2016; Accepted 16 October 2016

Academic Editor: Abdellah Benzaouia

Copyright © 2016 Linlin Ma et al. This is an open access article distributed under the Creative Commons Attribution License, which permits unrestricted use, distribution, and reproduction in any medium, provided the original work is properly cited.

This paper studies the stabilization problem for damping multimachine power system with time-varying delays and sector saturating actuator. The multivariable proportional plus derivative (PD) type stabilizer is designed by transforming the problem of PD controller design to that of state feedback stabilizer design for a system in descriptor form. A new sufficient condition of closed-loop multimachine power system asymptomatic stability is derived based on the Lyapunov theory. Computer simulation of a two-machine power system has verified the effectiveness and efficiency of the proposed approach.

1. Introduction

To cope with the increasing demand for quality electric power, excitation control, power system stabilizer (PSS), and other power system controllers are playing important roles in power system stability and maintaining dynamic performance. Conventional PSS is mainly designed based on a linear model and considered one operating point. Recently, to interconnect large energy pools connecting neighboring electric grids together and transmit bulk energy during peak times of load demand can satisfy the growing demand for energy [1]. But it introduces some modes of electromechanical oscillations and frequency deviations within the range of 0.2–2 Hz in the power system which will make power system more complicated [2, 3]. A conventional PSS cannot guarantee to have the best performance. Hence, a variety of control strategies have been used to obtain PSS, such as lead-lag controller [4], variable structure controller [5–7], robust controller [8], PID controller [9–11], and fuzzy logic controller [10]. Most of the controllers are nonlinear. Some researchers have designed the PSS by using searching algorithms such as genetic algorithms [10, 12], particle swarm optimization [13, 14], and chaotic optimization algorithm [15, 16]. But these algorithms are hard to program and are not sure to find the optimum solutions.

It is well known that the amplitude of the controller is always bounded in the real world [17]. So it is very necessary that the actuator saturation is taken into consideration. Time-delay is very common in power systems which can be a source of instability of performance degradation [18]. Multimachine power system with time-varying delay and sector saturating actuator [19] is a complex interconnected large-scale system that is composed of many electric devices and mechanical components with a better description of real world. The state feedback control problem for such a system is addressed by [19] based on the LMI methods. However, the conditions in [19] are conservative because of the amplifying technique to deal with the nonlinear terms in the conditions. Moreover, we usually cannot find the state feedback controller to satisfy demand when system becomes more complex.

The purpose of this paper is to design a PD controller for damping multimachine power systems with time-varying delay and sector saturating actuator. Under a descriptor transformation, the problem of PD type controller design is transformed into the state feedback controller design for a descriptor system. Then, a new sufficient condition is derived for the admissible of the descriptor system based on the Lyapunov theory. Compared with the existing LMI methods in [19], our method introduces more relax matrix variables. Therefore, it is less conservative. Compared with some of the

nondeterministic methods, our method has the advantages of low complexity.

This paper is organized as follows. Section 2 is the problem formulation and preliminaries. Section 3 gives the main results. Section 4 provides an example to show the merits and effectiveness of the results and Section 5 concludes this paper.

Notation. R^n denotes n -dimensional Euclidean space; the superscripts -1 and T denote the matrix inverse and transpose, respectively; $X > 0$ ($X \geq 0$) means that X is positive definite (positive semidefinite); the star $*$ denotes the symmetric term in a matrix.

2. Problem Formulation and Preliminaries

Consider N -machine power system with time-varying delays and input constraints which is described by the interconnection of N subsystems as follows:

$$\dot{x}_i(t) = A_i x_i(t) + B_i u_{si}(t) + \sum_{j=1}^N p_{ij} G_{ij} g_{ij}(x_i(t), x_j(t - \tau_{ij}(t))), \quad (1)$$

$$u_{si}(t) = \text{sat}(u_i(t)),$$

$$x_i(t) = \phi_i(t), \quad t \in [-\tau, 0],$$

where $x_i(t) = [\Delta\delta_i(t) \ \Delta W_i(t) \ \Delta E'_{qi}(t) \ \Delta E_{fdi}(t) \ \Delta V_{DCi}(t)]^T$, $u_i(t) = [\Delta m_i]$, $u_i(t)$ is the control input vector to the actuator, and $u_{si}(t)$ is the control input vector to the plant.

$g_{ij}(x_i(t), x_j(t - \tau_{ij}(t)))$ is the nonlinear function vector characterizing the interconnection between i th generator and j th generator with

$$\begin{aligned} g_{ij}(x_i(t), x_j(t - \tau_{ij}(t))) \\ = -\cos \beta_i(\delta) (\Delta\delta_i(t) - \Delta\delta_j(t - \tau_{ij}(t))) \\ = -\cos \beta_i(\delta) W(x_i(t) - x_j(t - \tau_{ij}(t))), \end{aligned} \quad (2)$$

where $\tau_{ij}(t)$ is the time-varying delay and satisfied $0 \leq \tau_{ij}(t) \leq \tau \leq \infty$, $\dot{\tau}_{ij}(t) \leq \dot{\tau}^* < 1$, and $\beta_i(\delta) = (\delta_i(t) - \delta_j(t - \tau_{ij}(t)) + \delta_{j0} - \delta_{i0})/2$, $W = [1 \ 0 \ 0 \ 0 \ 0]$.

The nominal system matrices are represented as follows:

$$A_i = \begin{bmatrix} 0 & \omega_0 & 0 & 0 & 0 \\ -\frac{K_{1i}}{M_i} & -\frac{P_i}{M_i} & -\frac{K_{2i}}{M_i} & 0 & -\frac{K_{pdci}}{M_i} \\ -\frac{K_{4i}}{T'_{d0i}} & 0 & -\frac{K_{3i}}{T'_{d0i}} & \frac{1}{T'_{d0i}} & -\frac{K_{pdci}}{T'_{d0i}} \\ -\frac{K_{Ai}K_{5i}}{T_{Ai}} & 0 & -\frac{K_{Ai}K_{6i}}{T_{Ai}} & -\frac{1}{T_{Ai}} & -\frac{K_{Ai}K_{VDCi}}{T_{Ai}} \\ K_{7i} & 0 & K_{8i} & 0 & K_{9i} \end{bmatrix},$$

$$B_i = [0 \ -K_{pmi} \ -K_{qmi} \ -K_{vmi} \ -K_{DCmi}]^T,$$

$$G_{ij} = \begin{bmatrix} -(\omega_0 E'_{qi} E'_{qj} B_{ij}) \\ 0 \quad \frac{M_i}{M_i} \quad 0 \quad 0 \quad 0 \end{bmatrix}^T. \quad (3)$$

In this modeling, the single-machine infinite bus is modeled by Heffron-Phillips model which is shown in Figure 1.

The nonlinear saturation function $u_{si}(t)$ is considered to be inside sector $(a_i, 1)$ and is shown in Figure 1, where $0 \leq a_i \leq 1$.

From Figure 2, it is obvious that $u_{si}(t) - 0.5(1 + a_i)u_i(t) = \Delta t_i u_i(t) \Rightarrow u_{si}(t) = \psi_i u_i(t)$, where $\psi_i = 0.5(1 + a_i) + \Delta t_i$, Δt_i is a real number which varying between $-0.5(1 - \bar{a}_i)$ and $0.5(1 + \bar{a}_i)$, $a_i < \bar{a}_i < 1$.

The control law for a PD controller is

$$u_i(t) = K_{pi} x_i(t) + K_{Di} \dot{x}_i(t). \quad (4)$$

Substituting (4) into (1), we have

$$\begin{aligned} (I - \psi_i B_i K_{Di}) \dot{x}_i(t) \\ = (A_i + \psi_i B_i K_{pi}) x_i(t) \\ + \sum_{j=1}^N p_{ij} G_{ij} g_{ij}(x_i(t), x_j(t - \tau_{ij}(t))), \end{aligned} \quad (5)$$

$$x_i(t) = \phi_i(t), \quad t \in [-\tau, 0].$$

Taking the inverse of the left-hand side of (5), we obtain

$$\begin{aligned} \dot{x}_i(t) = (I - \psi_i B_i K_{Di})^{-1} \left((A_i + \psi_i B_i K_{pi}) x_i(t) \right. \\ \left. + \sum_{j=1}^N p_{ij} G_{ij} g_{ij}(x_i(t), x_j(t - \tau_{ij}(t))) \right), \end{aligned} \quad (6)$$

$$x_i(t) = \phi_i(t), \quad t \in [-\tau, 0].$$

Properly selecting the controller gains K_{pi} and K_{Di} , so that the closed-loop systems are stable, then we have the PD controller design. It is obvious from (6) that the PD controller is nonlinear. Some researchers have designed such a controller with the aid of searching algorithms [10]. A huge amount of computation burden is foreseeable. In the following, we introduce a new state variable $\bar{x}_i(t) = [x_i^T(t) \ \dot{x}_i^T(t)]^T$, then system (1) with controller (4) is transformed into the following PD control system:

$$\begin{aligned} E \dot{\bar{x}}_i(t) = \bar{A}_i \bar{x}_i(t) + \bar{B}_i \bar{u}_{si}(t) \\ + \sum_{j=1}^N p_{ij} \bar{G}_{ij} \bar{g}_{ij}(\bar{x}_i(t), \bar{x}_j(t - \tau_{ij}(t))), \end{aligned} \quad (7)$$

$$\bar{u}_{si}(t) = \text{sat}(\bar{u}_i(t)),$$

$$\bar{u}_i(t) = \bar{K}_i \bar{x}_i(t),$$

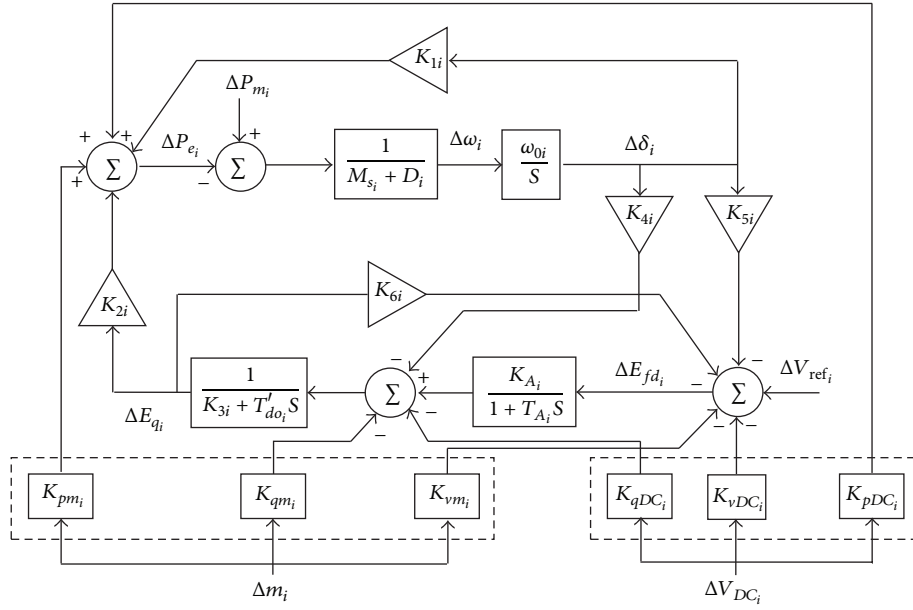


FIGURE 1: Heffron-Phillips model for single-machine power system connected to infinite bus along with SSSC series in the transmission line.

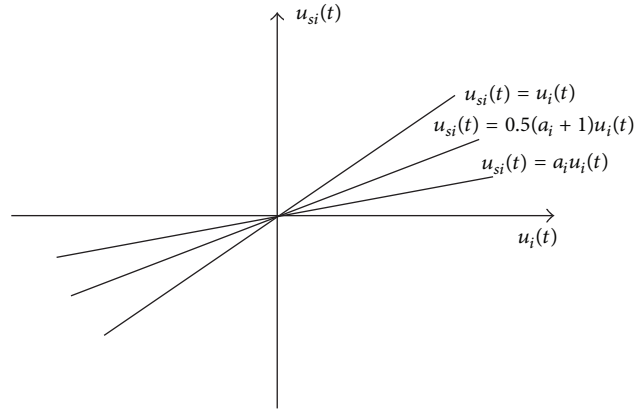


FIGURE 2: Sector saturation function.

where

$$\bar{A}_i = \begin{bmatrix} 0 & I \\ A_i & -I \end{bmatrix},$$

$$\bar{B}_i = \begin{bmatrix} 0 \\ B_i \end{bmatrix},$$

$$\bar{G}_{ij} = \begin{bmatrix} 0 \\ G_{ij} \end{bmatrix},$$

$$E = \begin{bmatrix} I_n & 0 \\ 0 & 0 \end{bmatrix},$$

$$\begin{aligned} \bar{g}_{ij}(\bar{x}_i(t), \bar{x}_j(t - \tau_{ij}(t))) &= g_{ij}(x_i(t), x_j(t - \tau_{ij}(t))) \\ &= -\cos \beta_i(\delta) \bar{W}(\bar{x}_i(t) - \bar{x}_j(t - \tau_{ij}(t))), \end{aligned} \quad (8)$$

$$\bar{K}_i = [K_{pi} \ K_{Di}], \text{ and } \bar{W} = [W \ 0].$$

System (7) is a descriptor system as $\text{rank}(E) = n < \dim(E)$, $\bar{u}_i(t) = K_{pi}x_i(t) + K_{Di}\dot{x}_i(t) = \bar{K}_i\bar{x}_i(t)$; then, we have

$$\begin{aligned} E\dot{\bar{x}}_i(t) &= (\bar{A}_i + \psi_i\bar{B}_i\bar{K}_i)\bar{x}_i(t) \\ &\quad + \sum_{j=1}^N p_{ij}\bar{G}_{ij}\bar{g}_{ij}(\bar{x}_i(t), \bar{x}_j(t - \tau_{ij}(t))) \end{aligned}$$

$$\begin{aligned}
&= (\bar{A}_i + \psi_i \bar{B}_i \bar{K}_i) \bar{x}_i(t) \\
&\quad - \cos \beta_i(\delta) \sum_{j=1}^N p_{ij} \bar{G}_{ij} \bar{W} (\bar{x}_i(t) - \bar{x}_j(t - \tau_{ij}(t))) \\
&= \left(\bar{A}_{ci} - \sum_{j=1}^N A_{dij} \right) \bar{x}_i(t) + \sum_{j=1}^N A_{dij} \bar{x}_j(t - \tau_{ij}(t)),
\end{aligned} \tag{9}$$

where $A_{dij} = \cos \beta_i(\delta) p_{ij} \bar{G}_{ij} \bar{W}$ and $\bar{A}_{ci} = \bar{A}_i + \psi_i \bar{B}_i \bar{K}_i$.

The following definition and lemmas will be useful in this paper.

Definition 1 (see [20]). (i) Descriptor system

$$E \dot{x}(t) = Ax(t) + \sum_{j=1}^N A_{dj} x(t - d_j) \tag{10}$$

is said to be regular and impulse-free, if pair (E, A) is regular and impulse-free.

(ii) System (10) is said to be stable if for any scalar $\varepsilon > 0$, there exists a scalar $\delta(\varepsilon) > 0$ such that, for any compatible initial conditions $\phi(k)$ satisfying $\sup_{-d \leq t \leq 0} \|\phi(t)\| \leq \delta(\varepsilon)$, solution $x(t)$ of system (10) satisfies $\|x(t)\| \leq \varepsilon$ for any $t \geq 0$; moreover, $\lim_{t \rightarrow \infty} x(t) = 0$.

(iii) System (10) is said to be admissible if it is regular, impulse-free, and stable.

Lemma 2 (see [18]). For any constant matrix $M > 0$, scalar $\gamma > 0$, and vector function $W : [0, \gamma] \rightarrow R^n$, such that integrations concerned are well defined, the following inequality holds:

$$\begin{aligned}
&\left(\int_0^\gamma W(s) ds \right)^T M \left(\int_0^\gamma W(s) ds \right) \\
&\leq \gamma \left(\int_0^\gamma W^T(s) M W(s) ds \right).
\end{aligned} \tag{11}$$

Lemma 3. Given any matrices D and E with appropriate dimensions, the inequality

$$DE + E^T D^T \leq DTD^T + E^T T^{-1} E \tag{12}$$

holds for any matrix $T > 0$.

3. Main Results

In this section, we will give the following condition for system (9).

Theorem 4. The delay descriptor system (9) is admissible with $\bar{K}_i = Y_i X_i^{-T}$ if there exist matrices $X_i = \begin{bmatrix} X_{1i} & X_{2i} \\ 0 & X_{3i} \end{bmatrix}$, $Q_{ij} > 0$, $T > 0$, $Y_i, U_{ij} > 0$, $(i, j = 1, 2, \dots, N)$, such that the following inequalities hold:

$$EX_i^T = X_i E^T \geq 0, \tag{13}$$

$$\begin{bmatrix}
\text{sym} \{ \bar{A}_i X_i^T + \psi_i \bar{B}_i Y_i \} & * & \cdots & * & * \\
+ \tau \sum_{j=1}^N p_{ji} E^T Q_{ji} E - \frac{1 - \dot{\tau}^*}{\tau} \sum_{j=1}^N p_{ji} E^T Q_{ji} E & & & & \\
+ \sum_{j=1}^N p_{ji} U_{ji} + \sum_{j=1}^N p_{ij} \bar{G}_{ij} \bar{W} T \bar{W}^T \bar{G}_{ij}^T & & & & \\
\frac{1 - \dot{\tau}^*}{\tau} E^T Q_{1i} E & -\alpha(1 - \dot{\tau}^*) U_{1i} & & & \\
& -\frac{1 - \dot{\tau}^*}{\tau} E^T Q_{1i} E & & & \\
\vdots & & \ddots & & \\
\frac{1 - \dot{\tau}^*}{\tau} E^T Q_{Ni} E & & & -\alpha(1 - \dot{\tau}^*) U_{Ni} & \\
& & & -\frac{1 - \dot{\tau}^*}{\tau} E^T Q_{Ni} E & \\
X_i^T & & & & -\frac{T}{N-1}
\end{bmatrix} < 0, \tag{14}$$

$$\begin{bmatrix}
-(1 - \alpha)(1 - \dot{\tau}^*) U_{ij} & X_i \\
X_i^T & -T
\end{bmatrix} < 0, \tag{15}$$

where α is a fixed scalar which satisfies $0 < \alpha < 1$.

Proof. Firstly, we prove that system (9) with PD gain matrices \bar{K}_i is regular and impulse-free. System (9) can be rewritten as

$$\begin{aligned} \bar{E}\dot{X}(t) = & \left(\bar{A} + \psi\bar{B}\bar{K} - \sum_{i=1}^N \sum_{j=1}^N \bar{A}_{dij} \right) X(t) \\ & + \sum_{i=1}^N \sum_{j=1}^N \bar{A}_{dij} X(t - \tau_{ij}(t)), \end{aligned} \quad (16)$$

where $X(t) = [\bar{x}_1^T(t), \bar{x}_2^T(t), \dots, \bar{x}_N^T(t)]^T$, matrices $\bar{E} = \text{diag}\{E, E, \dots, E\}$, $\bar{A} = \text{diag}\{\bar{A}_1, \bar{A}_2, \dots, \bar{A}_N\}$, $\psi = \text{diag}\{\psi_1, \psi_2, \dots, \psi_N\}$, $\bar{B} = \text{diag}\{\bar{B}_1, \bar{B}_2, \dots, \bar{B}_N\}$, $\bar{K} = \text{diag}\{\bar{K}_1, \bar{K}_2, \dots, \bar{K}_N\}$, and

$$\bar{A}_{dij} = \begin{bmatrix} 0 & \dots & 0 & \dots & 0 \\ 0 & \dots & \cos \beta_i(\delta) p_{ij} \bar{G}_{ij} \bar{W} & \dots & 0 \\ 0 & \dots & 0 & \dots & 0 \end{bmatrix} \quad i \quad j. \quad (17)$$

From (14), it is easy to see that

$$\begin{aligned} \text{sym} \{ \bar{A}_i X_i^T + \psi_i B_i Y_i \} - \frac{1 - \dot{\tau}^*}{\tau} \sum_{j=1}^N p_{ji} E^T Q_{ji} E \\ = \text{sym} \left\{ \left(\bar{A}_i + \psi_i \bar{B}_i \bar{K}_i \right) X_i^T \right\} - \frac{1 - \dot{\tau}^*}{\tau} \sum_{j=1}^N p_{ji} E^T Q_{ji} E \\ < 0. \end{aligned} \quad (18)$$

That is

$$\begin{aligned} \text{sym} \{ (\bar{A} + \psi\bar{B}\bar{K}) X^T \} \\ - \frac{1 - \dot{\tau}^*}{\tau} E^T \text{diag} \left\{ \sum_{j=1}^N p_{ji} Q_{ji} \right\} \bar{E} < 0, \end{aligned} \quad (19)$$

where $X = \text{diag}\{X_1, \dots, X_N\}$. Since \bar{E} is descriptor, there exist nonsingular matrices G and H such that

$$G\bar{E}H = \begin{bmatrix} I_{nN} & 0 \\ 0 & 0 \end{bmatrix}. \quad (20)$$

Suppose

$$\begin{aligned} G(\bar{A} + \psi\bar{B}\bar{K})H &= \begin{bmatrix} A_{11} & A_{12} \\ A_{21} & A_{22} \end{bmatrix}, \\ GXH &= \begin{bmatrix} X_{11} & X_{12} \\ 0 & X_{22} \end{bmatrix}. \end{aligned} \quad (21)$$

Equation (19) yields $\text{sym}\{A_{22}X_{22}^T\} < 0$, which implies that the pair $(\bar{E}, \bar{A} + \psi\bar{B}\bar{K})$ is regular and impulse-free. By Definition 1, system (16) is regular and impulse-free. It also shows that system (9) is regular and impulse-free.

Next, we will show that system (9) is stable. Consider a Lyapunov-Krasovskii functional as

$$\begin{aligned} V(t) = & \sum_{i=1}^N \left\{ x_i^T(t) P_{11i} x_i(t) + \sum_{j=1}^N p_{ij} \right. \\ & \cdot \left[\int_{t-\tau_{ij}(t)}^t \bar{x}_j^T(\xi) U_{ij} \bar{x}_j(\xi) d\xi \right. \\ & \left. \left. + \int_{-\tau_{ij}(t)}^0 \int_{t+\alpha}^t \dot{\bar{x}}_j^T(\xi) E^T Q_{ij} E \dot{\bar{x}}_j(\xi) d\xi d\alpha \right] \right\}. \end{aligned} \quad (22)$$

Taking the time derivative of $V(t)$ along the solution of system (9) yields

$$\begin{aligned} \dot{V}(t) = & \sum_{i=1}^N \left\{ \dot{x}_i^T(t) P_{11i} x_i(t) + x_i^T(t) P_{11i} \dot{x}_i(t) + \sum_{j=1}^N p_{ij} \right. \\ & \cdot \left[\bar{x}_j^T(t) U_{ij} \bar{x}_j(t) \right. \\ & - (1 - \dot{\tau}_{ij}(t)) \bar{x}_j^T(t) (t - \tau_{ij}(t)) U_{ij} \bar{x}_j(t - \tau_{ij}(t)) \\ & + \tau_{ij}(t) \bar{x}_j^T(t) E^T Q_{ij} E \bar{x}_j(t) \\ & \left. \left. - (1 - \dot{\tau}_{ij}(t)) \int_{t-\tau_{ij}(t)}^t \dot{\bar{x}}_j(\alpha) E^T Q_{ij} E \bar{x}_j(\alpha) d\alpha \right] \right\}. \end{aligned} \quad (23)$$

By Lemma 2, we obtain

$$\begin{aligned} & - (1 - \dot{\tau}_{ij}(t)) \int_{t-\tau_{ij}(t)}^t \dot{\bar{x}}_j(\alpha) E^T Q_{ij} E \bar{x}_j(\alpha) d\alpha \\ & \leq - \frac{1 - \dot{\tau}_{ij}(t)}{\tau_{ij}(t)} (\bar{x}_j(t) - x_j(t - \tau_{ij}(t)))^T \\ & \cdot E^T Q_{ij} E (\bar{x}_j(t) - \bar{x}_j(t - \tau_{ij}(t))). \end{aligned} \quad (24)$$

Then,

$$\begin{aligned}
 \dot{V}(t) \leq & \sum_{i=1}^N \left\{ \dot{\bar{x}}_i^T(t) E^T P_i \bar{x}_i(t) + \bar{x}_i^T(t) P_i^T E \bar{x}_i(t) \right. \\
 & + \sum_{j=1}^N p_{ij} \left[\bar{x}_j^T(t) U_{ij} \bar{x}_j(t) - (1 - \dot{\tau}^*) \bar{x}_j^T(t - \tau_{ij}(t)) \right. \\
 & \cdot U_{ij} \bar{x}_j(t - \tau_{ij}(t)) + \tau_{ij}^T(t) E^T Q_{ij} E \bar{x}_j(t) \\
 & \left. \left. - \frac{1 - \dot{\tau}^*}{\tau} (\bar{x}_j(t) - \bar{x}_j(t - \tau_{ij}(t)))^T \right. \right. \\
 & \left. \cdot E^T Q_{ij} E (\bar{x}_j(t) - \bar{x}_j(t - \tau_{ij}(t))) \right] \Big\} = \sum_{i=1}^N \left\{ \bar{x}_i^T(t) \right. \\
 & \cdot \left[(\bar{A}_i + \psi_i \bar{B}_i \bar{K}_i)^T P_i + P_i^T (\bar{A}_i + \psi_i \bar{B}_i \bar{K}_i) \right] \bar{x}_i(t) \\
 & + \text{sym} \left\{ \bar{x}_i^T(t) P_i^T (-\cos \beta_i(\delta)) \sum_{j=1}^N p_{ij} \right. \\
 & \cdot \bar{G}_{ij} \bar{W} (\bar{x}_i(t) - \bar{x}_j(t - \tau_{ij}(t))) \Big\} + \sum_{j=1}^N p_{ij} \bar{x}_j^T(t) \\
 & \cdot U_{ij} \bar{x}_j(t) - \sum_{j=1}^N (1 - \dot{\tau}^*) p_{ij} \bar{x}_j^T(t - \tau_{ij}(t)) U_{ij} \bar{x}_j(t - \tau_{ij}(t)) \\
 & - \tau_{ij}(t) + \sum_{j=1}^N p_{ij} \tau_{ij}^T(t) E^T Q_{ij} E \bar{x}_j(t) - \sum_{j=1}^N p_{ij} \\
 & \cdot \frac{1 - \dot{\tau}^*}{\tau} (\bar{x}_j(t) - \bar{x}_j(t - \tau_{ij}(t)))^T E^T Q_{ij} E (\bar{x}_j(t) \\
 & \left. - \bar{x}_j(t - \tau_{ij}(t))) \right\}, \tag{25}
 \end{aligned}$$

where

$$P_i = \begin{bmatrix} P_{11i} & P_{12i} \\ 0 & P_{22i} \end{bmatrix}. \tag{26}$$

It is obvious that $\dot{V}(t) < 0$ can be obtained by the following equation:

$$\begin{aligned}
 \dot{V} = & \text{diag} \{ \dot{V}_1(t), \dots, \dot{V}_N(t) \} = X^T(t) \left[(\bar{A} + \psi \bar{B} \bar{K})^T P \right. \\
 & + P^T (\bar{A} + \psi \bar{B} \bar{K}) \Big] X(t) + \text{sym} \left\{ -X^T(t) P^T \sum_{i=1}^N \sum_{j=1}^N \bar{A}_{dij} X(t) \right. \\
 & \left. + X^T(t) P^T \sum_{i=1}^N \sum_{j=1}^N \bar{A}_{dij} X(t - \tau_{ij}(t)) \right\} \\
 & + X^T(t) \text{diag} \left\{ \sum_{j=1}^N p_{j1} U_{j1}, \dots, \sum_{j=1}^N p_{jN} U_{jN} \right\} X(t) \\
 & - \sum_{i=1}^N \sum_{j=1}^N (1 - \dot{\tau}^*) X^T(t - \tau_{ij}(t)) \mathbf{U}_{ij} X(t - \tau_{ij}(t)) \\
 & + \tau X^T(t) \text{diag} \left\{ \sum_{j=1}^N p_{j1} E^T Q_{j1} E, \dots, \sum_{j=1}^N p_{jN} E^T Q_{jN} E \right\} X(t) \\
 & - \sum_{i=1}^N \sum_{j=1}^N p_{ij} \frac{1 - \dot{\tau}^*}{\tau} (X(t) - X(t - \tau_{ij}(t)))^T \mathbf{Q}_{ij} (X(t) \\
 & - X(t - \tau_{ij}(t))), \tag{27}
 \end{aligned}$$

where

$$\begin{aligned}
 P &= \text{diag} \{ P_1, P_2, \dots, P_N \}, \\
 \mathbf{U}_{ij} &= \begin{bmatrix} 0 & \dots & 0 & \dots & 0 \\ 0 & \dots & p_{ji} U_{ji} & \dots & 0 \\ 0 & \dots & 0 & \dots & 0 \end{bmatrix}_i, \tag{28} \\
 \mathbf{Q}_{ij} &= \begin{bmatrix} 0 & \dots & 0 & \dots & 0 \\ 0 & \dots & E^T Q_{ji} E & \dots & 0 \\ 0 & \dots & 0 & \dots & 0 \end{bmatrix}_i.
 \end{aligned}$$

It is obtained from Lemma 3 that

$$\begin{aligned}
 & \text{sym} \left\{ -X^T(t) P^T \sum_{i=1}^N \sum_{j=1}^N \bar{A}_{dij} X(t) \right\} + X^T(t) P^T \sum_{i=1}^N \sum_{j=1}^N \bar{A}_{dij} X(t - \tau_{ij}(t)) \\
 & \leq X^T(t) \text{diag} \left\{ P_1^T \sum_{j=1}^N p_{1j} \bar{G}_{1j} \bar{W} T \bar{W}^T G_{1j}^T P_1, \dots, P_N^T \sum_{j=1}^N p_{Nj} \bar{G}_{Nj} \bar{W} T \bar{W}^T G_{Nj}^T P_N \right\} X(t)
 \end{aligned}$$

$$+ X^T(t) \text{diag} \left\{ \sum_{j=1}^N p_{1j} T^{-1}, \dots, \sum_{j=1}^N p_{Nj} T^{-1} \right\} X(t) + \sum_{i=1}^N \sum_{j=1}^N p_{ij} X^T(t - \tau_{ij}(t)) \mathfrak{T} X(t - \tau_{ij}(t)), \quad (29)$$

where $\mathfrak{T} = \text{diag}\{0, \dots, 0, T^{-1}, 0, \dots, 0\}$.

Substituting (29) into (27), we obtain

$$\begin{aligned} \dot{\bar{V}} &\leq X^T(t) \Phi X(t) + \sum_{i=1}^N \sum_{j=1}^N p_{ij} X^T(t - \tau_{ij}(t)) \\ &\quad \cdot \left(\mathfrak{T} - (1 - \dot{\tau}^*) \mathbf{U}_{ij} - \frac{1 - \dot{\tau}^*}{\tau} \mathfrak{Q}_{ij} \right) X(t - \tau_{ij}(t)) \end{aligned} \quad (30)$$

where $\bar{\xi}(t) = [X^T(t) \quad X^T(t - \tau_{ij})]_{i,j=1,\dots,N,i \neq j}^T$,

$$\begin{aligned} \Phi &= (\bar{A} + \psi \bar{B} \bar{K})^T P + P^T (\bar{A} + \psi \bar{B} \bar{K}) + \text{diag} \left\{ P_1^T \sum_{j=1}^N p_{1j} \bar{G}_{1j} \bar{W}^T \bar{W}^T G_{1j}^T P_1, \dots, P_N^T \sum_{j=1}^N p_{Nj} \bar{G}_{Nj} \bar{W}^T \bar{W}^T G_{Nj}^T P_N \right\} \\ &\quad + \text{diag} \left\{ \sum_{j=1}^N p_{1j} T^{-1}, \dots, \sum_{j=1}^N p_{Nj} T^{-1} \right\} + \text{diag} \left\{ \sum_{j=1}^N p_{j1} U_{j1}, \dots, \sum_{j=1}^N p_{jN} U_{jN} \right\} \end{aligned} \quad (31)$$

$$- \frac{1 - \dot{\tau}^*}{\tau} \text{diag} \left\{ \sum_{j=1}^N p_{j1} E^T Q_{j1} E, \dots, \sum_{j=1}^N p_{jN} E^T Q_{jN} E \right\} + \tau \text{diag} \left\{ \sum_{j=1}^N p_{j1} E^T Q_{j1} E, \dots, \sum_{j=1}^N p_{jN} E^T Q_{jN} E \right\},$$

$$\bar{\Xi} = \begin{bmatrix} \Phi & * & \dots & * \\ \sum_{i=1}^N \frac{1 - \dot{\tau}^*}{\tau} \mathfrak{Q}_{1i} & \sum_{i=1}^N \left(\mathfrak{T} - (1 - \dot{\tau}^*) \mathbf{U}_{1i} - \frac{1 - \dot{\tau}^*}{\tau} \mathfrak{Q}_{1i} \right) & & \\ \vdots & & \ddots & \\ \sum_{i=1}^N \frac{1 - \dot{\tau}^*}{\tau} \mathfrak{Q}_{Ni} & & \sum_{i=1}^N \left(\mathfrak{T} - (1 - \dot{\tau}^*) \mathbf{U}_{Ni} - \frac{1 - \dot{\tau}^*}{\tau} \mathfrak{Q}_{Ni} \right) & \end{bmatrix} < 0. \quad (32)$$

From (30), we obtain that

$$\dot{V}(t) \leq \sum_{i=1}^N \xi_i^T(t) \Xi_i \xi_i(t), \quad (33)$$

$$[T^{-1} - (1 - \alpha)(1 - \dot{\tau}^*) U_{ji}] < 0, \quad i \neq j, \quad (34)$$

where $\xi_i(t) = [\bar{x}_i^T(t), \bar{x}_i^T(t - \tau_{1i}(t)), \dots, \bar{x}_i^T(t - \tau_{(i-1)i}(t)), \bar{x}_i^T(t - \tau_{(i+1)i}(t)), \dots, \bar{x}_i^T(t - \tau_{Ni}(t))]^T$ and

$$\Xi = \begin{bmatrix} \text{sym} \left\{ (\bar{A}_i + \psi_i \bar{B}_i \bar{K}_i)^T P_i \right\} & * & \cdots & * \\ +P_i^T \sum_{j=1}^N p_{ij} \bar{G}_{ij} \bar{W} T \bar{W}^T \bar{G}_{ij}^T P_i & & & \\ + \sum_{j=1}^N p_{ij} T^{-1} + \sum_{j=1}^N p_{ji} U_{ji} & & & \\ + \tau \sum_{j=1}^N p_{ji} E^T Q_{ji} E & & & \\ - \frac{1 - \dot{\tau}^*}{\tau} \sum_{j=1}^N p_{ji} E^T Q_{ji} E & & & \\ \frac{1 - \dot{\tau}^*}{\tau} \sum_{j=1}^N E^T Q_{1i} E & -\alpha(1 - \dot{\tau}^*) U_{1i} & & \\ & - \frac{1 - \dot{\tau}^*}{\tau} \sum_{j=1}^N E^T Q_{1i} E & & \\ \vdots & & \ddots & \\ \frac{1 - \dot{\tau}^*}{\tau} \sum_{j=1}^N E^T Q_{Ni} E & & -\alpha(1 - \dot{\tau}^*) U_{Ni} & \\ & & - \frac{1 - \dot{\tau}^*}{\tau} \sum_{j=1}^N E^T Q_{Ni} E & \end{bmatrix} < 0. \quad (35)$$

Pre- and postmultiply (45) by $\text{diag}\{X_i, X_i, \dots, X_i\}$ and its transpose, respectively, where $X_i = P_i^{-T}$, and define $Y_i = \bar{K}_i X_i^T$, $Q_{ji} = X_i Q_{ji} X_i^T$, and $U_{ji} = X_i U_{ji} X_i^T$; we arrive at

$$\begin{bmatrix} \text{sym} \left\{ \bar{A}_i X_i^T + \psi_i \bar{B}_i Y_i \right\} + \sum_{j=1}^N p_{ji} U_{ji} & * & \cdots & * \\ + \sum_{j=1}^N \tau p_{ji} E^T Q_{ji} E - \sum_{j=1}^N \frac{1 - \dot{\tau}^*}{\tau} p_{ji} E^T Q_{ji} E & & & \\ + \sum_{j=1}^N p_{ij} \bar{G}_{ij} \bar{W} T \bar{W}^T \bar{G}_{ij}^T + X_i \sum_{j=1}^N p_{ji} T^{-1} X_i^T & & & \\ \frac{1 - \dot{\tau}^*}{\tau} E^T Q_{1i} E & -\alpha(1 - \dot{\tau}^*) U_{1i} & & \\ & - \frac{1 - \dot{\tau}^*}{\tau} E^T Q_{1i} E & & \\ \vdots & & \ddots & \\ \frac{1 - \dot{\tau}^*}{\tau} E^T Q_{Ni} E & & -\alpha(1 - \dot{\tau}^*) U_{Ni} & \\ & & - \frac{1 - \dot{\tau}^*}{\tau} E^T Q_{Ni} E & \end{bmatrix} < 0. \quad (36)$$

By Schur complement, (44) is equivalent to (14).

Pre-and postmultiplying (34) by X_i and its transpose, respectively, and by Schur complement, (34) is equivalent to (15).

Since A_{22} is nonsingular, there exist two nonsingular matrices \bar{G} and \bar{H} such that

$$\begin{aligned}\bar{G}\bar{E}\bar{H} &= \begin{bmatrix} I_{nN} & 0 \\ 0 & 0 \end{bmatrix}, \\ \bar{G}(A + \psi BK)\bar{H} &= \begin{bmatrix} A_1 & 0 \\ 0 & I_{nN} \end{bmatrix}, \\ \bar{H}^T \bar{E}^T P \bar{E} \bar{H} &= \begin{bmatrix} \bar{P}_1 & 0 \\ 0 & 0 \end{bmatrix}, \\ \bar{G} \bar{A} d_{ij} \bar{H} &= \begin{bmatrix} A_{dij11} & A_{dij12} \\ A_{dij21} & A_{dij22} \end{bmatrix}, \\ \bar{H}^T P \bar{H} &= \begin{bmatrix} \bar{P}_{11} & \bar{P}_{12} \\ 0 & \bar{P}_{22} \end{bmatrix}, \\ \bar{H}^T \mathfrak{U}_{ji} \bar{H} &= \begin{bmatrix} U_{ji11} & U_{ji12} \\ U_{ji21} & U_{ji22} \end{bmatrix}.\end{aligned}\quad (37)$$

Denote $V(t) = \bar{H}^{-1} X(t) = \begin{bmatrix} v_1(t) \\ v_2(t) \end{bmatrix}$, where $Q_1(t) \in \mathbb{R}^{nN}$ and $v_2(t) \in \mathbb{R}^{nN}$. We obtain

$$\begin{aligned}-\|X(t)\|^2 &\leq -\|\bar{H}^{-1}\|^{-2} \|V(t)\|^2 \\ &\leq -\|\bar{H}^{-1}\|^{-2} \|v_1(t)\|^2.\end{aligned}\quad (38)$$

By (30), we obtain that there exists scalar $\varepsilon > 0$ such that

$$\dot{V}(t) < -\varepsilon \|X(t)\|^2, \quad (39)$$

which implies

$$\begin{aligned}\lambda \min(\bar{P}_1) \|v_1(t)\|^2 - V(0) &\leq \int_0^t \dot{V}(s) ds \\ &\leq -\varepsilon \|\bar{H}^{-1}\|^{-2} \int_0^t \|v_1(s)\|^2 ds.\end{aligned}\quad (40)$$

Then, $\sum_{i=1}^N \|v_1(t)\|^2 \leq V(0)/\lambda \min(\bar{P}_1)$, and $\int_0^t \|v_1(s)\|^2 ds \leq (1/\varepsilon)V(0)\|\bar{H}^{-1}\|^{-2}$.

Thus,

$$\lim_{t \rightarrow \infty} v_1(t) = 0. \quad (41)$$

Next, we will prove that $\lim_{t \rightarrow \infty} v_2(t) = 0$, which is equivalent to the stability of system (5).

Pre-and postmultiplying (32) by $\text{diag}(\bar{H}^T, \bar{H}^T, \dots, \bar{H}^T)$ and its transpose, respectively, we obtain

$$\begin{bmatrix} \bar{P}_{22} + \bar{P}_{22}^T + \sum_{i=1}^N \sum_{j=1}^N U_{ji22} & * & \dots & * \\ \sum_{i=1}^N \bar{P}_{22}^T A_{di122} & -\sum_{i=1}^N (1 - \tau^*) U_{1i22} & & \\ \vdots & & \ddots & \\ \sum_{i=1}^N \bar{P}_{22}^T A_{diN22} & & & -\sum_{i=1}^N (1 - \tau^*) U_{Ni22} \end{bmatrix} < 0. \quad (42)$$

Pre- and postmultiplying (42) by $[-\sum_{i=1}^N \sum_{j=1}^N A_{dij22}^T \ I \dots I]$ and its transpose, respectively, we obtain $\sum_{i=1}^N \sum_{j=1}^N A_{dij22}^T \cdot \sum_{i=1}^N \sum_{j=1}^N U_{ji22} \sum_{i=1}^N \sum_{j=1}^N A_{dij22} - \sum_{i=1}^N \sum_{j=1}^N (1 - \tau^*) U_{ji22} < 0$, which implies that

$$\rho\left(\sum_{i=1}^N \sum_{j=1}^N A_{dij22}\right) < 1. \quad (43)$$

Using the expression in (37), the singular delay system (16) can be decomposed as

$$\begin{aligned}\dot{v}_1(t) &= A_1 v_1(t) + \sum_{i=1}^N \sum_{j=1}^N A_{dij11} v_1(t - \tau_{ij}(t)) \\ &\quad + \sum_{i=1}^N \sum_{j=1}^N A_{dij12} v_2(t - \tau_{ij}(t)),\end{aligned}\quad (44)$$

$$\begin{aligned}0 &= v_2(t) + \sum_{i=1}^N \sum_{j=1}^N A_{dij21} v_1(t - \tau_{ij}(t)) \\ &\quad + \sum_{i=1}^N \sum_{j=1}^N A_{dij22} v_2(t - \tau_{ij}(t)).\end{aligned}\quad (45)$$

Noting that, for any $t > 0$, there exists positive integer k .

Such that $k\tau - \tau \leq t \leq k\tau$, and considering (44), we have

$$\begin{aligned}v_2(t) &= \left(-\sum_{i=1}^N \sum_{j=1}^N A_{dij22}\right)^k v_2(t - k\tau) \\ &\quad - \sum_{l=1}^k \left(\sum_{i=1}^N \sum_{j=1}^N A_{dij22}\right)^{l-1} \sum_{i=1}^N \sum_{j=1}^N A_{dij21} v_1(t - k\tau).\end{aligned}\quad (46)$$

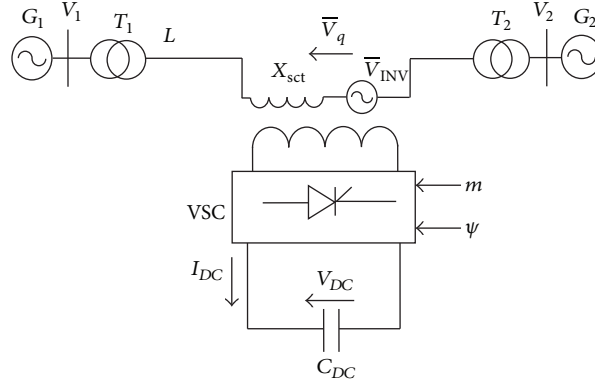


FIGURE 3: Connecting diagram of two-machine system.

This, together with (43) and (41), we obtain $\lim_{t \rightarrow \infty} v_2(t) = 0$, and this completes the proof. \square

Remark 5. Theorem 4 provides a PD control method for system (1). An LMI based criterion is obtained by transforming a regular system into the state feedback stabilizer design for a descriptor system. It is worth noting that if \bar{A}_i , \bar{B}_i , \bar{G}_{ij} ,

\bar{W} , and E are replaced with A_i , B_i , G_{ij} , W , and I_n , the state feedback controller can be solved by the following corollary. It is obvious that Theorem 4 has wider range of application.

Corollary 6. The delay system (5) with $K_{Di} = 0$ is stable with $K_{pi} = Y_i X_i^{-T}$ if there exist matrices $X_i > 0$, $Q_{ij} > 0$, $T > 0$, $Y_i, U_{ij} > 0$, ($i, j = 1, 2, \dots, N$), such that the following inequalities hold:

$$\begin{bmatrix} \text{sym} \{A_i X_i^T + \psi_i B_i Y_i\} & * & \cdots & * & * \\ +\tau \sum_{j=1}^N p_{ji} Q_{ji} - \frac{1-\hat{\tau}^*}{\tau} \sum_{j=1}^N p_{ji} Q_{ji} & & & & \\ +\sum_{j=1}^N p_{ji} U_{ji} + \sum_{j=1}^N p_{ij} G_{ij} W T W^T G_{ij}^T & & & & \\ \frac{1-\hat{\tau}^*}{\tau} Q_{1i} & -\alpha(1-\hat{\tau}^*) U_{1i} & & & \\ & -\frac{1-\hat{\tau}^*}{\tau} Q_{1i} & & & \\ \vdots & & \ddots & & \\ \frac{1-\hat{\tau}^*}{\tau} Q_{Ni} & & & -\alpha(1-\hat{\tau}^*) U_{Ni} & \\ & & & -\frac{1-\hat{\tau}^*}{\tau} Q_{Ni} & \\ X_i^T & & & & -\frac{T}{N-1} \end{bmatrix} < 0, \quad (47)$$

$$\begin{bmatrix} -(1-\alpha)(1-\hat{\tau}^*) U_{ij} & X_i \\ X_i^T & -T \end{bmatrix} < 0, \quad (48)$$

where α is a fixed scalar which satisfies $0 < \alpha < 1$.

Remark 7. Both Theorem 4 and Corollary 6 are LMIs. The solutions of X_i , Y_i are obtained, and the corresponding controller gain matrices are derived as $\bar{K}_i = Y_i X_i^{-T}$. Our method is a deterministic method which can be solved easier than some of the nondeterministic methods, such as the genetic algorithm [10] and particle swarm optimization [13].

Remark 8. Compared with Theorem 2 in [19], Corollary 6 is less conservative in two aspects. Firstly, By using constraint (48), U_{ij} , and T_i in Corollary 6 can be variables matrices, while relatives u_{ij} , v_i in Theorem 2 in [19] are fixed scalars. Secondly, the integral term $-(\hat{\tau}_{ij}(t)) \int_{t-\tau_{ij}(t)}^t \dot{\bar{x}}_j(\alpha) E^T Q_{ij} E \dot{\bar{x}}_j(\alpha) d\alpha$ in the proof is enlarged by using Lemma 2 instead of being removed in the proof in [19].

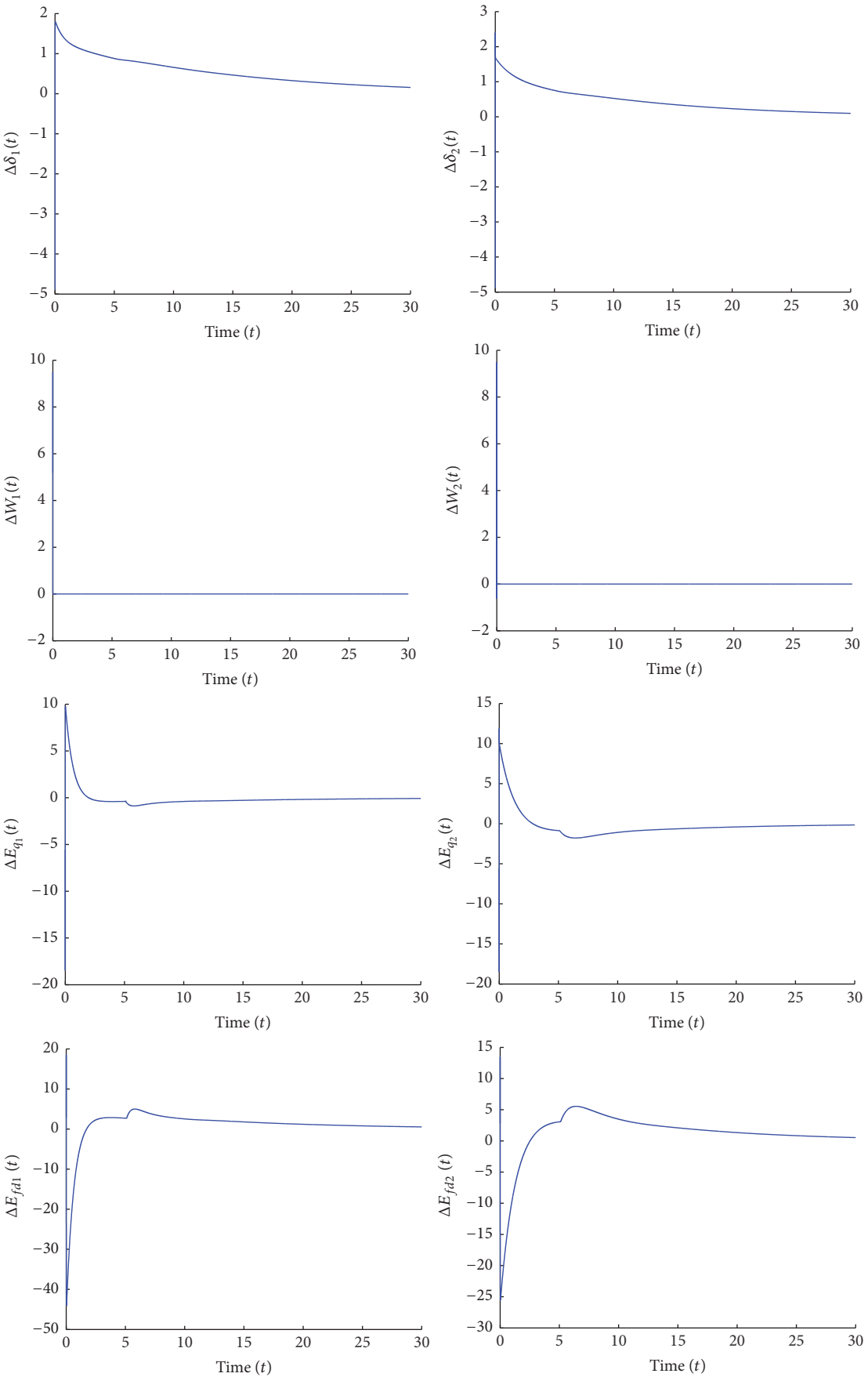


FIGURE 4: Continued.

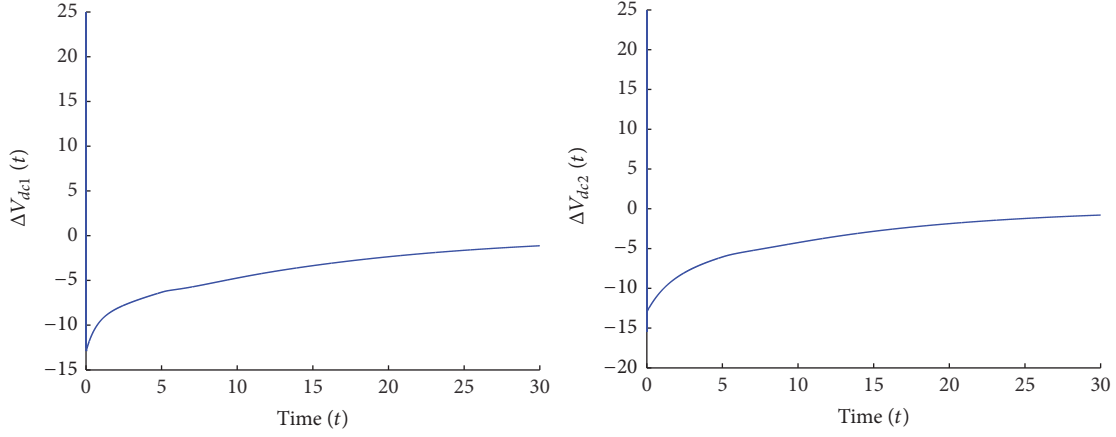


FIGURE 4: The close-loop state trajectories.

4. Simulation

In this section, a two-machine infinite bus example system is chosen to show the effectiveness of the proposed method, which is shown in Figure 3. The system parameters used in the simulation are as follows:

$$p_{11} = p_{22} = 0,$$

$$p_{12} = p_{21} = 1,$$

$$D_1 = 5,$$

$$D_2 = 3,$$

$$A_1$$

$$= \begin{bmatrix} 0 & 379.2000 & 0 & 0 & 0 \\ -0.3169 & -0.8333 & -0.1123 & 0 & -0.0041 \\ -0.0099 & 0 & -0.2266 & 0.1983 & -0.0048 \\ 12.7000 & 0 & -951.7000 & -200.0000 & -24.4000 \\ -0.1759 & 0 & 0.0302 & 0 & 0.0257 \end{bmatrix}, \quad (49)$$

$$A_2$$

$$= \begin{bmatrix} 0 & 379.2000 & 0 & 0 & 0 \\ -0.4054 & -0.5000 & -0.0463 & 0 & -0.0041 \\ -0.0495 & 0 & -0.0283 & 0.1983 & -0.0048 \\ -12.7000 & 0 & -551.7000 & -200.0000 & -24.4000 \\ -0.2759 & 0 & 0 & 0 & 0.0257 \end{bmatrix},$$

$$B_1 = B_2 = [0 \ 1.0000 \ -3.0000 \ 0.8000 \ 4.0000]^T,$$

$$G_{12} = G_{13} = [0 \ 0 \ -2.7 \ 0 \ 0]^T,$$

$$G_{21} = G_{23} = [0 \ 0 \ -2.3 \ 0 \ 0]^T.$$

If we set $a_1 = a_2 = 0.3$ and $\hat{a}_1 = \hat{a}_2 = 0.5$, so $\psi_1 = \psi_2$ varies between 0.4 and 0.9. The upper bound of delay $\tau = 5$ and $\hat{\tau}^* = 0.5$. The method in [19] fails to find a state feedback

controller for this system. According to Theorem 4, the PD controller can be solved as

$$K_{D1} = [0.2057 \ 0.0837 \ -0.3127 \ -0.1429 \ 0.3615],$$

$$K_{p1}$$

$$= [-645.2015 \ -107.9008 \ -156.5715 \ -33.0835 \ -94.0722], \quad (50)$$

$$K_{D2} = [0.1030 \ 0.0874 \ -0.3113 \ -0.2068 \ 0.3635],$$

$$K_{p2} = [-559.7891 \ 5.6352 \ -95.1653 \ -35.7473 \ -74.1156].$$

The close-loop state trajectories of generator 1-2 are shown in Figure 4.

5. Conclusion

In this paper, a decentralized PD control scheme has been proposed to deal with the time-delay multimachine power system with sector saturating actuator. A sufficient condition of closed-loop system asymptotic stability is presented in terms of LMIs, which can be solved easily by LMI toolbox. Then, a sufficient condition of state feedback control is also obtained which is less conservative than that in [19]. A two-machine infinite bus system is considered as an example, and the simulation result shows the effectiveness of proposed method.

Nomenclature

p_{ij} : Constant of either 1 or 0 and $p_{ij} = 0$ means that j th generator has no connection with i th generator

B_{ij} : i th row and j th column element of nodal susceptance matrix at the internal nodes after eliminated all physical buses, in pu

H_i : Inertia constant for i th generator, in seconds

| | |
|---------------------------|---|
| D_i : | Damping coefficient for i th generator, in pu |
| ω_i : | Relative speed for i th machine, in radian/s |
| δ_i : | Rotor angle for i th machine, in radian |
| ω_0 : | The synchronous machine speed |
| E'_{qi} and E'_{qj} : | Internal transient voltage for i th and j th machine, in pu, which are assumed to be constant |
| δ_{i0} : | The initial values of δ_i |
| ΔP_{ei} : | The generator power for i th machine |
| ΔE_{fdi} : | The generator stimulus voltage for i th machine. |

Competing Interests

The authors declare that there are no competing interests regarding the publication of this paper.

References

- [1] A. Khodabakhshian and R. Hemmati, "Robust decentralized multi-machine power system stabilizer design using quantitative feedback theory," *International Journal of Electrical Power and Energy Systems*, vol. 41, no. 1, pp. 112–119, 2012.
- [2] P. Kundur, *Power System Stability and Control*, Prentice-Hall, New York, NY, USA, 1994.
- [3] P. M. Anderson and A. A. Fouad, *Power System Control and Stability*, IEEE Press, 1997.
- [4] A. M. El-Zonkoly, A. A. Khalil, and N. M. Ahmied, "Optimal tuning of lead-lag and fuzzy logic power system stabilizers using particle swarm optimization," *Expert Systems with Applications*, vol. 36, no. 2, pp. 2097–2106, 2009.
- [5] V. G. D. C. Samarasinghe and N. C. Pahalawaththa, "Design of universal variable-structure controller for dynamic stabilisation of power systems," *IEE Proceedings: Generation, Transmission and Distribution*, vol. 141, no. 4, pp. 363–368, 1994.
- [6] G. Kenné, A. M. Fombu, and J. D. D. Nguimfack-Ndongmo, "Coordinated excitation and steam valve control for multimachine power system using high order sliding mode technique," *Electric Power Systems Research*, vol. 131, pp. 87–95, 2016.
- [7] J. Fernández-Vargas and G. Ledwich, "Variable structure control for power systems stabilization," *International Journal of Electrical Power and Energy Systems*, vol. 32, no. 2, pp. 101–107, 2010.
- [8] Q. Zhao and J. Jiang, "Robust controller design for generator excitation systems," *IEEE Transactions on Energy Conversion*, vol. 10, no. 2, pp. 201–209, 1995.
- [9] C. S. Ali Nandar, "Robust PI control of smart controllable load for frequency stabilization of microgrid power system," *Renewable Energy*, vol. 56, pp. 16–23, 2013.
- [10] Y.-J. Lin, "Proportional plus derivative output feedback based fuzzy logic power system stabiliser," *International Journal of Electrical Power & Energy Systems*, vol. 44, no. 1, pp. 301–307, 2013.
- [11] M. S. Baumud and A. R. Shamekh, "A comparative study between the performance of the fixed gain PID and the adaptive self-tuning power system stabilisers," in *Proceedings of the International Conference on Power System Technology (PowerCon '02)*, vol. 2, pp. 1233–1238, Kunming, China, October 2002.
- [12] M. G. Jolfaei, A. M. Sharaf, S. M. Shariatmadar, and M. B. Poudeh, "A hybrid PSS-SSSC GA-stabilization scheme for damping power system small signal oscillations," *International Journal of Electrical Power and Energy Systems*, vol. 75, pp. 337–344, 2016.
- [13] H. E. Mostafa, M. A. El-Sharkawy, A. A. Emary, and K. Yassin, "Design and allocation of power system stabilizers using the particle swarm optimization technique for an interconnected power system," *International Journal of Electrical Power and Energy Systems*, vol. 34, no. 1, pp. 57–65, 2012.
- [14] N. A. Singh, K. A. Muraleedharan, and K. Gomathy, "Particle swarm intelligence tuned fuzzy controller for damping modal oscillations of power system," in *Proceedings of the IEEE Region 10 Conference (TENCON '08)*, pp. 1–6, Hyderabad, India, November 2008.
- [15] A. Chatterjee, S. P. Ghoshal, and V. Mukherjee, "Chaotic ant swarm optimization for fuzzy-based tuning of power system stabilizer," *International Journal of Electrical Power and Energy Systems*, vol. 33, no. 3, pp. 657–672, 2011.
- [16] H. Shayeghi, H. A. Shayanfar, S. Jalilzadeh, and A. Safari, "Multi-machine power system stabilizers design using chaotic optimization algorithm," *Energy Conversion and Management*, vol. 51, no. 7, pp. 1572–1580, 2010.
- [17] Z. Xi, G. Feng, D. Cheng, and Q. Lu, "Nonlinear decentralized saturated controller design for power systems," *IEEE Transactions on Control Systems Technology*, vol. 11, no. 4, pp. 539–547, 2003.
- [18] K. Gu, V. L. Kharitonov, and J. Chen, *Stability of Time-Delay Systems*, Birkhäuser, Boston, Mass, USA, 2003.
- [19] M.-P. Sun, X.-H. Nian, and H. Pan, "Delay-dependent robust stabilization for steam valve opening of uncertain time-delay multi-machine power system with sector saturating actuator," *International Journal of Electrical Power & Energy Systems*, vol. 44, no. 1, pp. 153–159, 2013.
- [20] S. Xu and J. Lam, *Robust Control and Filtering of Singular Systems*, Springer, Berlin, Germany, 2006.

Research Article

High Precision Clock Bias Prediction Model in Clock Synchronization System

Zan Liu,¹ Xihong Chen,¹ Jin Liu,² and Chenglong Li¹

¹Air and Missile Defense College, Air Force Engineering University, Xi'an 710051, China

²Unit 95425 of the Chinese People's Liberation Army, Qujing 655000, China

Correspondence should be addressed to Zan Liu; kgdliuzan@163.com

Received 19 July 2016; Revised 18 October 2016; Accepted 23 October 2016

Academic Editor: Magdi S. Mahmoud

Copyright © 2016 Zan Liu et al. This is an open access article distributed under the Creative Commons Attribution License, which permits unrestricted use, distribution, and reproduction in any medium, provided the original work is properly cited.

Time synchronization is a fundamental requirement for many services provided by a distributed system. Clock calibration through the time signal is the usual way to realize the synchronization among the clocks used in the distributed system. The interference to time signal transmission or equipment failures may bring about failure to synchronize the time. To solve this problem, a clock bias prediction module is paralleled in the clock calibration system. And for improving the precision of clock bias prediction, the first-order grey model with one variable (GM(1, 1)) model is proposed. In the traditional GM(1, 1) model, the combination of parameters determined by least squares criterion is not optimal; therefore, the particle swarm optimization (PSO) is used to optimize GM(1, 1) model. At the same time, in order to avoid PSO getting stuck at local optimization and improve its efficiency, the mechanisms that double subgroups and nonlinear decreasing inertia weight are proposed. In order to test the precision of the improved model, we design clock calibration experiments, where time signal is transferred via radio and wired channel, respectively. The improved model is built on the basis of clock bias acquired in the experiments. The results show that the improved model is superior to other models both in precision and in stability. The precision of improved model increased by 66.4%~76.7%.

1. Introduction

Time synchronization technology has been widely used in the distributed system [1–4], such as global navigation satellite system (GNSS) and multistatic radar and electric network. Clock calibration is that devices of distributed system use reference time to synchronize the local clock. Hence, process of clock calibration determines the accuracy of time synchronization [5–7]. Nowadays, the way to calibrate local clock is that finite impulse response (FIR) filter uses the bias between local and remote clock measured by time interval counter (TIC) or discriminator to get a control signal [8–10], which is used to regulate clock until the clocks are synchronized. In the distributed system with far distance, time signal is always conveyed by electric cable, satellite, or microwave. Recently, troposphere scatter has also been proposed to transfer the time signal [6]. In a process of time signal's transmission, channel interruption or equipment failure will lead to the failure to get clock bias, and the absence of clock bias can make synchronization system abnormal.

In order to guarantee the distributed system work normally and add anti-interference ability of the synchronization system, clock bias prediction module is paralleled in the clock calibration system. In this parallel module, clock bias could be acquired through the prediction module, when the system cannot get clock bias. And system uses the predicted clock bias to generate a control signal, which is used to adjust the local clock. Above all, the performance of clock bias prediction has a direct impact on synchronization precision when accidents occur. At present, the clock bias prediction is an important work in GNSS; researchers have put forward several prediction models [8, 9], such as first-order grey model with one variable (GM(1, 1)) model, artificial neural network (ANN) model, and least squares support vector machine (LSSVM) model. The sampling interval of satellite clock bias is generally 15 min, which lead to a relatively low real-time requirement. Nevertheless, in the clock calibration system, the short sampling time puts forward a great requirement for real-time performance. GM(1, 1) model needs less data sample and has better real-time than

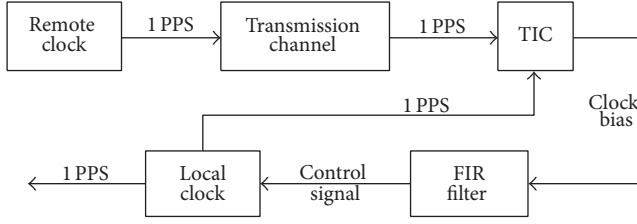


FIGURE 1: Workflow of clock calibration.

artificial intelligence algorithms, which need more data to train themselves. However, parameters of GM(1, 1) model are usually determined by the least square criterion (LSC), which cannot guarantee the parameters are optimal.

Aiming at this problem, we introduce the particle swarm optimization (PSO) algorithm to optimize GM(1, 1) model. Also, in order to avoid the PSO getting stuck at local optimization and improve its efficiency, the mechanisms that double subgroups and nonlinear decreasing inertia weight are proposed.

The rest of this paper is organized as follows. The mechanism that clock bias module is paralleled in clock calibration system is described in the next section. In Section 3, GM(1, 1) model optimized by improved particle swarm optimization (IPSO) is introduced. In Section 4, we design two clock calibration experiments that time signal is transferred via wired and radio channel, respectively. And the improved model is built through clock bias acquired by these calibration experiments. Finally, some conclusions are drawn in Section 5.

2. Clock Bias Prediction in Clock Calibration

Figure 1 shows the workflow of the clock calibration model in time synchronization system.

As shown in Figure 1, TIC is used to calculate the bias between these two one pulse per second (1 PPS), which come from the local and remote clock, respectively. FIR filter is used to generate a control signal on the basis of clock bias. Local clock continues to be adjusted according to the control signal until clocks are synchronous. Briefly, when the transmission channel or equipment is in a fault state, the local system cannot get the essential clock bias. Namely, absence of clock bias will bring a failure to time synchronization system. At present, no effective solutions exist or are proposed to overcome this failure. So to overcome this shortcoming, clock bias module is paralleled in clock calibration system; this mechanism is described in Figure 2.

In Figure 2, prediction module paralleled with the original system can predict clock bias, which may not be got when exceptions occur. Also, bias prediction module is paralleled with the original system, so under normal circumstances, this new module has no influence on the original system. Generally speaking, this parallel mechanism can ameliorate anti-interference ability and guarantee the synchronization system work normally. And the accuracy of clock bias prediction has great influence on the performance of time synchronization, when an exception happens. Therefore, an excellent clock bias prediction model is urgently needed.

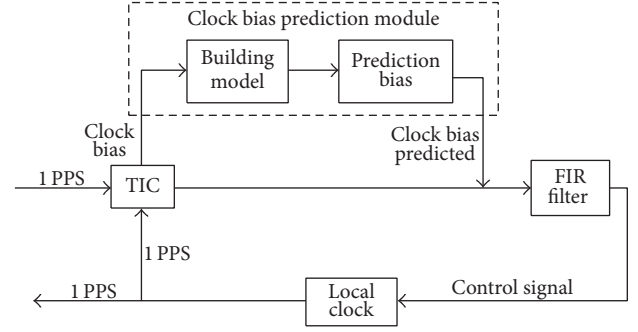


FIGURE 2: Clock error prediction in calibration.

3. GM(1, 1) Model Improved by IPSO

3.1. GM(1, 1) Model. The GM(1, 1) model has advantage not only in calculation speed but also in prediction accuracy. Also, building GM(1, 1) model needs less data [11–14]. GM(1, 1) model can be finally expressed as

$$\hat{x}^0(k) = e^{-a(k-1)} \cdot \left[x^0(1) - \frac{u}{a} \right] \cdot (1 - e^a), \quad (1)$$

where $x^0(k)$ and $\hat{x}^0(k)$ stand for the primitive and predicted k th element in sequence, respectively. a and u are the parameters of this model. According to LSC, the estimated value of parameters can be expressed as

$$[\hat{a}, \hat{u}]^T = (G^T G)^{-1} G^T Y_n, \quad (2)$$

where $G = [-Z(K+1), 1]_{(n-1) \times 2}$, $Z(K+1) = [x^1(k+1) + x^1(k)]/2$, and $Y_n = [x^1(2), \dots, x^1(k), \dots, x^1(n)]^T$. $x^1(k)$ stand for the first accumulation of the primitive sequence. Equation (1) indicates that parameters directly affect the performance of GM(1, 1) model. However, LSC cannot guarantee parameters are optimal.

For demonstrating that parameters obtained by LSC are not optimal, clock bias of satellite PG01 provided by the international GNSS service (IGS) in June 10 of 2012 is selected; the sampling interval is 15 min. GM(1, 1) models with different parameters are established by using these data during the first 18 hours. Data during last 6 hours are used to evaluate the performance of different models. Values of mean errors (ME) and mean square error (MSE) are used to evaluate accuracy of the model. MSE can be expressed as

$$\text{MSE} = \frac{1}{n} \sum_{i=1}^n (x_i - \hat{x}_i)^2, \quad (3)$$

where x_i and \hat{x}_i stand for the real and predicted clock bias, respectively. As shown in (3), the minimum value of MSE refers to the optimal combination of parameters. There are two strategies to get different combinations of parameters. *Strategy 1:* combination of parameters is determined by LSC, shown as (2). *Strategy 2:* different combinations of parameters are chosen close to the parameters determined by LSC.

The values of ME and MSE are got through using different combinations of parameters. In these different models, the

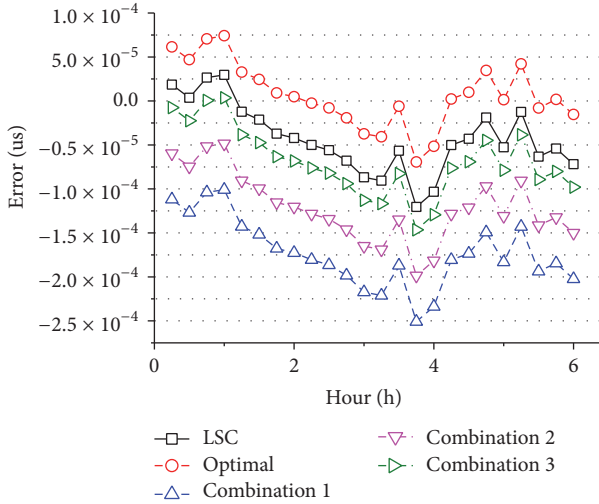


FIGURE 3: Prediction errors of different models.

optimal combination of a and u is $(-5.965 \times 10^{-6}, 260.74)$. And values of MSE and ME are $1.36 \times 10^{-3} \text{ ns}^2$ and 0.0066 ns , respectively. The combination of a and u determined by LSC is $(-5.963 \times 10^{-6}, 260.63)$. And the values of MSE and ME are $3.32 \times 10^{-3} \text{ ns}^2$ and -0.043 ns , respectively. Prediction errors are shown as in Figure 3.

In Figure 3, the labels “combination 1,” “combination 2,” and “combination 3” stand for the different combinations close to parameters determined by LSC, respectively. And the label “optimal” stands for the optimal combination. As described in Figure 3, the parameters determined by LSC are not optimal. Therefore, using IPSO algorithm to optimize the GM(1, 1) model is necessary.

3.2. IPSO Algorithm. PSO algorithm is widely used as a global optimization algorithm, which has the characteristics of simple programming, high efficiency, and fast computing speed [15–17]. The solution space is considered as a multidimension search space. Particle flying in the search space as an individual bird stands for a candidate solution. And the swarm is a collection of these particles. Candidate solution is judged by a fitness function, which usually depends on the problem to be optimized. During the process of optimization, each particle maintains a $Pbest$ value as individual experience, which represents the best solution until now. Meanwhile, swarm maintains a $Gbest$ value as social knowledge, which represents the best point achieved by the whole collection until now.

During iterative procedure, these particles fly through the problem space following the current optimum particle and corporate with each other to find the global optimum. The algorithm updates velocity and position of each particle as follows:

$$\begin{aligned} v_{id}^k &= \omega v_{id}^{k-1} + c_1 r_1 (p_{id} - x_{id}^{k-1}) + c_2 r_2 (g_{id} - x_{id}^{k-1}), \\ x_{id}^k &= x_{id}^{k-1} + v_{id}^{k-1}, \end{aligned} \quad (4)$$

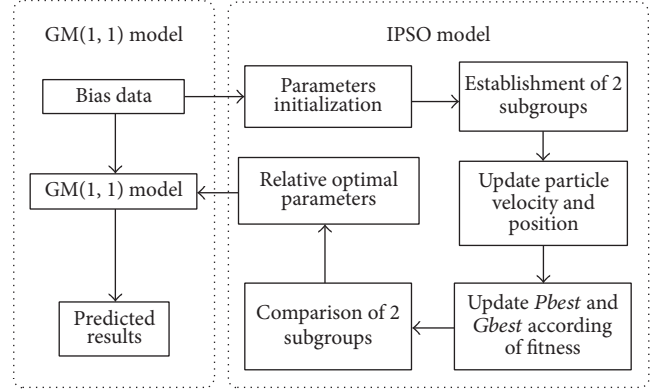


FIGURE 4: Flow of the improved model.

where r_1 and r_2 are random values between 0 and 1. v_{id}^k and x_{id}^k are velocity and position of particle i in dimension d at time k , respectively. c_1 and c_2 stand for acceleration constants known as the cognitive and social learning parameters, which pull each particle towards $Pbest$ and $Gbest$ positions, respectively. ω stands for the inertia weight reflecting the search ability of algorithm. Hence, in order to improve the accuracy and convergence rate of PSO, ω changing with the optimized iteration is proposed as follows:

$$\omega_k = (\omega_{\max} - \omega_{\min}) \cdot e^{-\beta \cdot (k/k_{\max})^2} + \omega_{\min}, \quad (5)$$

where ω_{\max} and ω_{\min} stand for the maximum and minimum of inertia weights, respectively. The value of β is between 15 and 20. As described in (5), at the early optimization stage, a larger inertia weight factor is applied to promote global exploration; then, in order to facilitate local exploitation with algorithm running, it decreases in exponential form. At the same time, for avoiding PSO getting stuck at local optimization and improving its efficiency, the mechanism that double subgroups simultaneously search is proposed. On the basis of original algorithm, the backward searching subgroup is described as follows:

$$x_{id}(t+1) = x_{id}(t) - v_{id}(t+1). \quad (6)$$

After each cycle is complete, these two subgroups will compare with each other. This mechanism can make the algorithm avoid local optimization on the basis of not increasing the optimal algebra obviously.

3.3. GM(1, 1) Model Improved by IPSO. In the time synchronization system, channel interruption or equipment failure will lead to a failure to get clock bias. Under these negative circumstances, clock bias acquired through a prediction model can guarantee the distributed system work normally. We use GM(1, 1) model to predict these clock bias. In order to find the optimal parameters of GM(1, 1) model, IPSO algorithm is proposed. The process of improved model is shown as in Figure 4.

As shown in Figure 4, GM(1, 1) model improved by IPSO mainly follows the basic steps of standard PSO. The detailed steps are as follows.

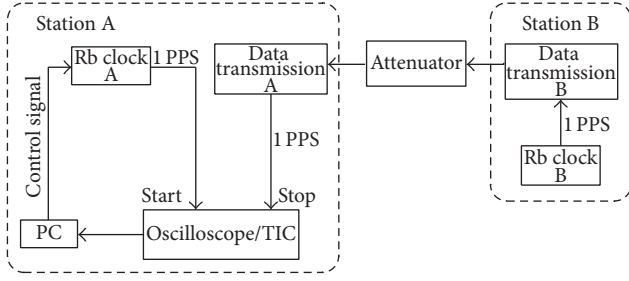


FIGURE 5: Clock calibration through wired channel.

Step 1. The parameters of IPSO are firstly initialized, including ω_{\min} (ω_{\max}), c_1 (c_2), β , threshold of fitness, and the maximum number of circulating times.

Step 2. IPSO algorithm establishes two subgroups, which search in opposite direction according to (6).

Step 3. Velocity and position of particles are updated, and the P_{best} and G_{best} of particles are also updated according to the value of fitness.

Step 4. In order to find the optimal combination of parameters, fitness of two subgroups is compared.

Step 5. IPSO algorithm continues to find the relative optimal combination of parameters, until it reaches the maximum number of circulating times or the value of fitness meets the threshold.

Step 6. After IPSO algorithm finishes, GM(1,1) model with the relative optimal combination of parameters determined by IPSO is used to predict the clock bias.

4. Example Analysis

4.1. Clock Bias Acquisition Schemes. In order to evaluate the performance of GM(1,1) model improved by IPSO, clock bias acquisition experiment is conducted with PSR10-type rubidium clock, Agilent53230A-type TIC, Tektronix DPO3054-type Oscilloscope, and so forth. The wired data transmission experiment is firstly performed as the layout shown in Figure 5.

As shown in Figure 5, 1PPS produced by Rb clock B is transferred through an electric cable and an attenuator to the data transmission A. Attenuation of long distance cable is simulated by attenuator. 1PPS output from the data transmission A is regarded as a reference; bias between these two clocks is tested by TIC. PC takes note of the clock bias, which is used to produce a control signal according to the principle of FIR filter. The sampling interval is 10 seconds. 150 data pieces are chosen, and the trend terms after invariance in those data is removed are shown in Figure 6.

Devices are also used to design the clock calibration experiment that time signal is transmitted through radio channel. Layout is shown in Figure 7.

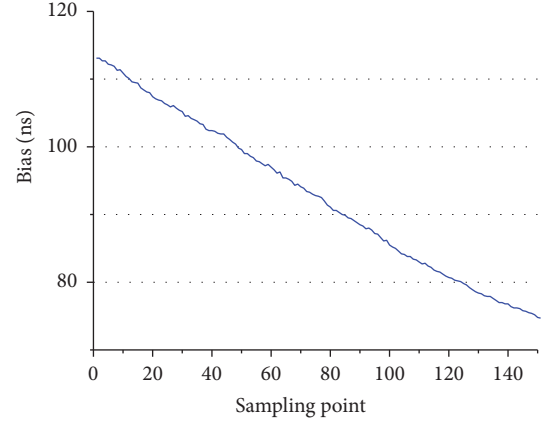


FIGURE 6: Clock bias acquired by wired channel.

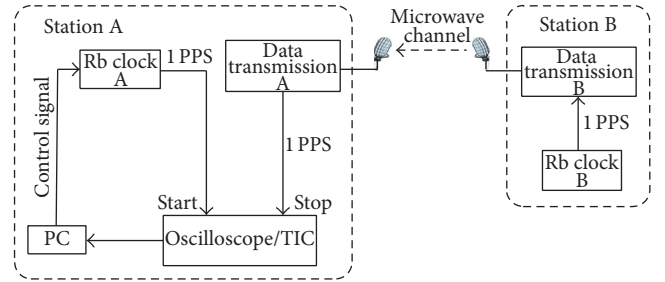


FIGURE 7: Clock calibration through radio channel.

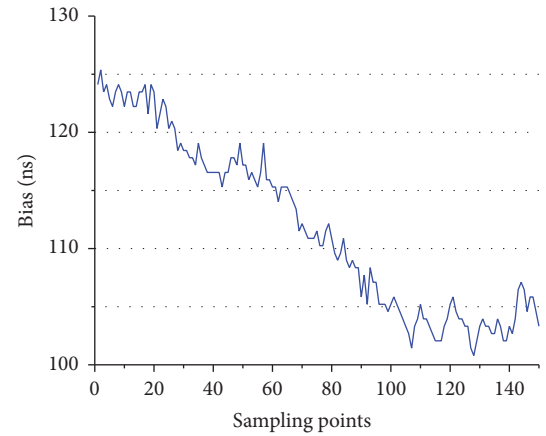


FIGURE 8: Clock bias acquired by radio channel.

The sampling interval of this experiment is also 10 seconds. Figure 8 shows the trend terms of these data.

As shown in Figures 6 and 8, the downward trend of bias indicates that these two clocks tend to be synchronized with calibration running. Noises in microwave channel and multipath effect bring jitter to the clock bias, which indicates that noises have negative effect on clock calibration.

4.2. Prediction Results. In order to get the accuracy of GM(1,1) model improved by IPSO, polynomial model,

TABLE 1: Statistics of the different models (ns).

| Clock bias | Polynomial model | | | GM(1, 1) model | | | IPSO-GM(1, 1) model | | |
|------------|------------------|--------|-------|----------------|--------|-------|---------------------|--------|-------|
| | E_{\max} | ME | SD | E_{\max} | ME | SD | E_{\max} | ME | SD |
| Data 1 | 1.543 | -0.414 | 0.641 | 0.822 | 0.383 | 0.325 | 0.544 | 0.127 | 0.301 |
| Data 2 | 3.247 | -1.776 | 0.850 | 2.758 | -1.248 | 0.799 | 1.614 | -0.323 | 0.623 |

GM(1, 1) model, and GM(1, 1) improved by IPSO are, respectively, established by using 120 sets of data acquired in these two experiments; the last 30 sets of data are used to test these different models.

Individual atomic clocks have different frequency offset characteristic, the relationship between order of polynomial and atomic clock is defined as

$$x(t) = a + bt + \beta \cdot \frac{ct^2}{2}, \quad \beta = \begin{cases} 1, & \text{Rb,} \\ 0, & \text{Cs.} \end{cases} \quad (7)$$

Considering that Rb atomic clock is used in these experiments, polynomial with one order is used. Figure 9 shows the prediction errors of different models.

In Figure 9, the clock bias acquired by wired channel and microwave channel is expressed as data 1 and data 2, respectively. Judgments are made in several aspects, such as maximum absolute error (E_{\max}), ME, and standard error (SD). Table 1 describes the values of these judgments.

Figure 9 and Table 1 illustrate that the MEs of two results predicted through GM(1, 1) model improved by IPSO are less than 0.5 ns. Accuracy of ME increases by 66.4%~76.7% compared to the traditional GM(1, 1) model. Also, in terms of accuracy and stability, the improved model is superior to other models. Therefore, when a channel interruption or equipment failure happens, the bias predicted by GM(1, 1) model improved by IPSO can be used to produce the control signal, which is used to synchronize the clock.

Also, the limitation of parameters selection range at the beginning can not only overcome the blindness in IPSO but also reduce the calculation time in a certain degree. The simulation process on PC platform indicates that running time of improved prediction model is less than 5 s, which concludes that the improved prediction model can completely match the real-time requirement.

At the same time, the accuracy of all prediction models built using data 1 is better than using data 2. The noises in clock bias have negative effect not only on performance of clock calibration, but also on the accuracy of clock bias prediction.

5. Conclusion

The failure to transfer time signal and equipment's breakdown will bring the failure to time synchronization system. Aiming at this problem, we parallel the clock bias system with clock calibration system. Also, GM(1, 1) model improved by IPSO is proposed to predict the clock bias. Clock calibration experiments that time signal is transferred through wire and microwave channel are conducted. The parts of clock bias recorded in the process of the experiment are used to evaluate

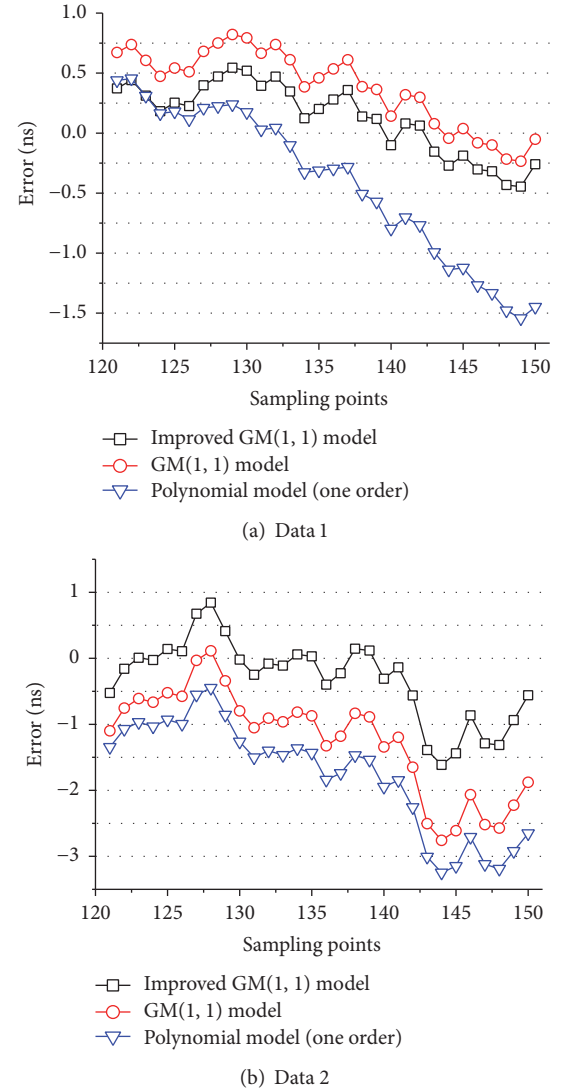


FIGURE 9: Errors of different prediction models.

this improved model. The consequence indicates that the ME of improved model is less than 0.5 ns. Also, in view of accuracy and stability, the improved model is superior to other models. Therefore, when a failure happens, the clock bias predicted through GM(1, 1) model improved by IPSO can be used to produce the control signal, which is vital to synchronize the clock.

Competing Interests

The authors declare that there is no conflict of interests regarding the publication of this paper.

Acknowledgments

This work was supported by the National Natural Science Foundation of China under Grant no. 61571459. The authors also would like to thank IGS for granting access to satellite clock bias data.

References

- [1] E. Mallada, X. Meng, M. Hack, L. Zhang, and A. Tang, "Skewless network clock synchronization without discontinuity: convergence and performance," *IEEE/ACM Transactions on Networking*, vol. 23, no. 5, pp. 1619–1633, 2015.
- [2] M. R. Kosanovic and M. K. Stojcev, "RPATS-Reliable power aware time synchronization protocol," *Microelectronics Reliability*, vol. 54, no. 1, pp. 303–315, 2014.
- [3] Z. Wang, L. Zhao, S. Wang, J. Zhang, B. Wang, and L. Wang, "COMPASS time synchronization and dissemination—toward centimetre positioning accuracy," *Science China Physics, Mechanics & Astronomy*, vol. 57, no. 9, pp. 1788–1804, 2014.
- [4] A. V. Makarenko, "Analysis of the time structure of synchronization in multidimensional chaotic systems," *Journal of Experimental and Theoretical Physics*, vol. 120, no. 5, pp. 912–921, 2015.
- [5] W. Xiang, B. Xu, W. Mou, and F. Wang, "A clock error calibration algorithm based on phase lock loop in GNSS time synchronization receiver," *Journal of National University of Defense Technology*, vol. 35, no. 2, pp. 115–119, 2013.
- [6] Q. Liu, J. Sun, X. Chen, J. Liu, and Q. Zhang, "Analysis of two way troposphere time transfer and its delay errors," *Acta Geodaetica et Cartographica Sinica*, vol. 43, no. 4, pp. 341–347, 2014.
- [7] M. Jabbarifar, M. Dagenais, and A. Shameli-Sendi, "Online incremental clock synchronization," *Journal of Network and Systems Management*, vol. 23, no. 4, pp. 1034–1066, 2015.
- [8] S.-G. Lin, "Assisted adaptive extended Kalman filter for low-cost single-frequency GPS/SBAS kinematic positioning," *GPS Solutions*, vol. 19, no. 2, pp. 215–223, 2015.
- [9] H. Xiong and D. Li, "Nuclear reactor doubling time calculation using FIR filter," *Energy Procedia*, vol. 39, pp. 3–11, 2013.
- [10] L. Arceo-Miquel, Y. S. Shmaliy, and O. Ibarra-Manzano, "Optimal synchronization of local clocks by GPS 1PPS signals using predictive FIR filters," *IEEE Transactions on Instrumentation and Measurement*, vol. 58, no. 6, pp. 1833–1840, 2009.
- [11] X. Cui and W. Jiao, "Grey system model for the satellite clock error predicting," *Geomatics and Information Science of Wuhan University*, vol. 30, no. 5, pp. 447–450, 2005.
- [12] G. W. Huang, Q. Zhang, and G. C. Xu, "Real-time clock offset prediction with an improved model," *GPS Solutions*, vol. 18, no. 1, pp. 95–104, 2014.
- [13] L. Wu, S. Liu, D. Chen, L. Yao, and W. Cui, "Using gray model with fractional order accumulation to predict gas emission," *Natural Hazards*, vol. 71, no. 3, pp. 2231–2236, 2014.
- [14] H. P. Tserng, T. L. Ngo, P. C. Chen, and L. Quyen Tran, "A grey system theory-based default prediction model for construction firms," *Computer-Aided Civil and Infrastructure Engineering*, vol. 30, no. 2, pp. 120–134, 2015.
- [15] A. B. Hashemi and M. R. Meybodi, "Cellular PSO: a PSO for dynamic environments," in *Advances in Computation and Intelligence: 4th International Symposium, ISICA 2009 Huangshi, China, October 23–25, 2009 Proceedings*, vol. 5821 of *Lecture Notes in Computer Science*, pp. 422–433, Springer, Berlin, Germany, 2009.
- [16] B. Tran, B. Xue, and M. Zhang, "Improved PSO for feature selection on high-dimensional datasets," in *Simulated Evolution and Learning*, vol. 8886, pp. 912–921, Springer, 2014.
- [17] C. Sudheer, R. Maheswaran, B. K. Panigrahi, and S. Mathur, "A hybrid SVM-PSO model for forecasting monthly streamflow," *Neural Computing and Applications*, vol. 24, no. 6, pp. 1381–1389, 2014.

Research Article

Robust Quadratic Stabilizability and H_∞ Control of Uncertain Linear Discrete-Time Stochastic Systems with State Delay

Xiushan Jiang,¹ Xuemin Tian,¹ and Weihai Zhang²

¹College of Information and Control Engineering, China University of Petroleum (East China), Qingdao 266510, Shandong Province, China

²College of Electrical Engineering and Automation, Shandong University of Science and Technology, Qingdao 266590, Shandong Province, China

Correspondence should be addressed to Weihai Zhang; w.hzhang@163.com

Received 20 May 2016; Revised 9 August 2016; Accepted 5 October 2016

Academic Editor: Abdellah Benzaouia

Copyright © 2016 Xiushan Jiang et al. This is an open access article distributed under the Creative Commons Attribution License, which permits unrestricted use, distribution, and reproduction in any medium, provided the original work is properly cited.

This paper mainly discusses the robust quadratic stability and stabilization of linear discrete-time stochastic systems with state delay and uncertain parameters. By means of the linear matrix inequality (LMI) method, a sufficient condition is, respectively, obtained for the stability and stabilizability of the considered system. Moreover, we design the robust H_∞ state feedback controllers such that the system with admissible uncertainties is not only quadratically internally stable but also robust H_∞ controllable. A sufficient condition for the existence of the desired robust H_∞ controller is obtained. Finally, an example with simulations is given to verify the effectiveness of our theoretical results.

1. Introduction

It is well known that stability and stabilization are very important concepts in linear system theory. Due to a great number of applications of stochastic systems in the realistic world, the studies of stability and stabilization for stochastic systems attract lots of researchers' attention in recent years; we refer the reader to the classic book [1] and the follow-up books [2, 3], together with references [4–11] and the references therein, which include robust stochastic stability [4], exponential stabilization [6], mean-square stability, and \mathcal{D} -stability and \mathcal{D}_R -stability [8]. The stabilization of various systems, including impulsive Markovian jump delay systems [4], stochastic singular systems [10, 12, 13], uncertain stochastic T-S fuzzy systems [14], and time-delay systems [6, 11, 15–17], has been studied extensively. H_∞ control is one of the most important robust control approaches when the system is subject to the influence of external disturbance, which has been shown to be effective in attenuating the disturbance. The objective of standard H_∞ control requires designing a controller to attenuate l^2 -gain from the external disturbance to controlled output below a given level $\gamma > 0$; see [18]. The study of H_∞ control of general linear discrete-time stochastic

systems with multiplicative noise seems to be first initiated by [19]. Then, stochastic H_∞ control and its applications have been investigated extensively; see [14, 16, 20–24].

Because time-delay exists widely in practice and affects the system stability, there have been many works concerning the study in stability or H_∞ control of stochastic systems [4, 6, 9, 11, 14–16, 22, 25]. Due to limitations of measurement technique and tools, it is not easy to construct exact mathematical models. Compared with the nominal stochastic systems without uncertain terms investigated in [2, 5, 24], our considered system allows the coefficient matrix to vary in a certain range.

Discrete-time stochastic difference systems have attracted a great deal of attention with the development of computer technology in recent years. In our viewpoint, there are at least two motivations to study discrete-time stochastic systems. Firstly, discrete-time stochastic systems are ideal mathematical models in practical modeling such as genetic regulatory networks [23]. Secondly, discrete-time stochastic systems provide a better approach to understand extensively continuous-time stochastic Itô systems [2, 3, 26]. Therefore, it is of significance to study the stabilization and H_∞ control of discrete-time stochastic time-delay uncertain systems.

This paper will study quadratic stability, stabilization, and robust state feedback H_∞ control for uncertain discrete-time stochastic systems with state delay. The parameter uncertainties are time varying and norm bounded. It can be found that, up to now, many criteria for testing quadratic stabilization and H_∞ control have been given in terms of LMIs and algebraic Riccati equations by applying Lyapunov function approach. One of our main contributions is to study quadratic stability and stabilization via LMIs instead of algebraic Riccati equations which is hardly solved. What we have obtained extended the work of [15] about the quadratic stability and stabilization of deterministic uncertain systems. Another contribution is to solve the state feedback H_∞ control and present a state feedback H_∞ controller design.

The paper is organized as follows. In Section 2 we give some adequate preliminaries and useful definitions. In Section 3, sufficient conditions for quadratic stability and stabilization are given in terms of LMIs which is convenient to compute by the MATLAB LMI toolbox. Section 4 designs a state feedback H_∞ controller. Two numerical examples with simulations are given in Section 5 to verify the efficiency of the proposed results. Finally, we end this paper in Section 6 with a brief conclusion.

For convenience, the notations in this paper are quite standard such as the following: we let \mathcal{R}^n and $\mathcal{R}^{m \times n}$ represent the set of all real n -dimensional vectors and $m \times n$ real matrices. For symmetric matrices X and Y , $X \geq Y$ (resp., $X > Y$) stands for the idea that the matrix $X - Y$ is positive semidefinite (resp., positive definite). I denotes the identity matrix of appropriate dimensions and X^T denotes the matrix transpose of X . $\|x\| = \sqrt{\sum_{k=0}^{\infty} |x_k|^2}$ represents the Euclidean norm or spectral norm of the vector x . $\mathcal{N}_{k_0} := \{k_0, k_0 + 1, k_0 + 2, \dots\}$, especially, $\mathcal{N}_1 := \{1, 2, \dots\}$, $\mathcal{N}_0 := \{0, 1, 2, \dots\}$, and $[\tau_1, \tau_2]$, represents the set of integers between τ_1 and τ_2 (inclusive). In symmetric block matrices, the symbol “*” is used as an ellipsis for terms induced by symmetry. $\mathcal{E}(\cdot)$ is the expectation operator.

2. Preliminaries

Consider a class of uncertain linear discrete-time stochastic systems with state delay described by

$$\begin{aligned} x(k+1) &= (A_0 + \Delta A_0(k))x(k) + (A_{0d} + \Delta A_{0d}(k)) \\ &\quad \cdot x(k-d) + (B_0 + \Delta B_0(k))u(k) \\ &\quad + \sum_{i=1}^s \{[C_0 + \Delta C_0(k)]x(k) \\ &\quad + [C_{0d} + \Delta C_{0d}(k)]x(k-d) \\ &\quad + [D_0 + \Delta D_0(k)]u(k)\} w_i(k), \\ x(j) &= \phi(j) \in \mathcal{R}^n, \\ j &\in \{-d, -d+1, \dots, 0\}, \quad k \in \mathcal{N}_0, \end{aligned} \quad (1)$$

where $x(k) \in \mathcal{R}^n$ is the system state and $u(k) \in \mathcal{R}^m$ is the control input, and $\{w(k)\}_{k \geq 0}$ are independent white noise process satisfying the following assumptions:

- (H₁) $\mathcal{E}[w_k] = 0$, $\mathcal{E}[w_k w_j] = \delta_{kj}$, where δ_{kj} is a Kronecker function defined by $\delta_{kj} = 0$ for $k \neq j$ while $\delta_{kj} = 1$ for $k = j$.
- (H₂) $\{w(k)\}_{k \geq 0}$ are defined on the filtered probability space $(\Omega, \mathcal{F}, \mathcal{F}_k, \mathcal{P})$ with $\mathcal{F}_k = \sigma\{w(0), \dots, w(k)\}$. In addition, $\{\mathcal{F}_k\}_{k \in \mathcal{N}_0}$ is an increasing sequence of σ -algebras with $\mathcal{F}_t \subset \mathcal{F}$.

$A_0, A_{0d}, B_0, C_0, C_{0d}, D_0$ are known real constant matrices with compatible dimensions. $\Delta A_0(k), \Delta A_{0d}(k), \Delta B_0(k), \Delta C_0(k), \Delta D_0(k), \Delta C_{0d}(k)$ are norm bounded and time-varying uncertain parameter which are assumed to have the following form:

$$\begin{aligned} &[\Delta A_0(k) \quad \Delta A_{0d}(k) \quad \Delta B_0(k) \quad \Delta C_0(k) \quad \Delta C_{0d}(k) \quad \Delta D_0(k)] \\ &= EF(k) [G_{A_0} \quad G_{A_{0d}} \quad G_{B_0} \quad G_{C_0} \quad G_{C_{0d}} \quad G_{D_0}], \end{aligned} \quad (2)$$

where $E, G_{A_0}, G_{A_{0d}}, G_{B_0}, G_{C_0}, G_{C_{0d}}, G_{D_0}$ are constant matrices and $F(k) \in \mathcal{R}^{m \times n}$ is the uncertain matrix satisfying

$$F(k)^T F(k) \leq I, \quad k \in \mathcal{N}_0. \quad (3)$$

For the purpose of simplicity, throughout this paper, we write system (1) in the following form:

$$\begin{aligned} x(k+1) &= A_{0\Delta}x(k) + A_{0d\Delta}x(k-d) + B_{0\Delta}u(k) \\ &\quad + \sum_{i=1}^s [C_{0\Delta}x(k) + C_{0d\Delta}x(k-d) + D_{0\Delta}u(k)] w_i(k), \\ x(j) &= \phi(j) \in \mathcal{R}^n, \quad j \in [-d, 0], \quad k \in \mathcal{N}_0, \end{aligned} \quad (4)$$

where $A_{0\Delta}, A_{0d\Delta}, B_{0\Delta}, C_{0\Delta}, C_{0d\Delta}$ are bounded uncertain system matrices with

$$\begin{aligned} A_{0\Delta} &= A_0 + \Delta A_0(k) = A_0 + EF(k) G_{A_0}, \\ A_{0d\Delta} &= A_{0d} + \Delta A_{0d}(k) = A_{0d} + EF(k) G_{A_{0d}}, \\ B_{0\Delta} &= B_0 + \Delta B_0(k) = B_0 + EF(k) G_{B_0}, \\ C_{0\Delta} &= C_0 + \Delta C_0(k) = C_0 + EF(k) G_{C_0}, \\ C_{0d\Delta} &= C_{0d} + \Delta C_{0d}(k) = C_{0d} + EF(k) G_{C_{0d}}, \\ D_{0\Delta} &= D_0 + \Delta D_0(k) = D_0 + EF(k) G_{D_0}. \end{aligned} \quad (5)$$

Below, we define robust quadratic stability and robust quadratic stabilizability for the uncertain time-delay discrete-time system (1), which generalize Definition 1 of [15] to stochastic systems.

Definition 1. Uncertain discrete time-delay system (1) is said to be robustly quadratically stable, if there exist matrices $P > 0$, $Q > 0$ and a scalar $\omega > 0$ such that, for all admissible

uncertain terms and given initial condition $x(j) = \phi(j) \in \mathcal{R}^n$ for $j = 0, -1, \dots, -d$, the unforced system of (1) (with $u(k) \equiv 0$) satisfies

$$\mathcal{E}(\Delta V_k) = \mathcal{E}V_{k+1} - \mathcal{E}V_k \leq -\omega \mathcal{E} \|\hat{x}(k)\|^2 \quad (6)$$

for $\hat{x}(k) \in \mathcal{R}^{2n}$ with $\hat{x}(k) = (x(k)^T, x(k-d)^T)^T$ and

$$V_k = x(k)^T P x(k) + \sum_{j=1}^d x(k-j)^T Q x(k-j). \quad (7)$$

Definition 2. Uncertain discrete time-delay system (1) is said to be robustly quadratically stabilizable if there exists a matrix $K \in \mathcal{R}^{m \times n}$ such that closed-loop system (1) with $u(k) = Kx(k)$, that is,

$$\begin{aligned} x(k+1) &= (A_{0\Delta} + B_{0\Delta}K)x(k) + A_{0d\Delta}(k)x(k-d) \\ &\quad + \sum_{i=1}^s [(C_{0\Delta} + D_{0\Delta}K)x(k) + C_{0d\Delta}x(k-d)] w_i(k), \end{aligned} \quad (8)$$

is robustly quadratically stable for given $x(j) = \phi(j) \in \mathcal{R}^n$ for $j = 0, -1, \dots, -d$.

3. Robust Quadratic Stabilization

In this section, a sufficient condition about robust quadratic stability and robust quadratic stabilization will be presented via LMIs, respectively. First, we cite the following lemma which is essential in proving our main results.

Lemma 3 (see [27]). Suppose that $W = W^T$, $F(k)$ satisfies (2), and then for any real matrices W , M , and N of suitable dimensions we have

$$W + MF(k)N + N^T F(k)^T M^T < 0 \quad (9)$$

if and only if (iff), for some $\alpha > 0$,

$$W + \alpha MM^T + \alpha^{-1} N^T N < 0. \quad (10)$$

Theorem 4. Consider uncertain discrete-time stochastic delay system (1) with $u(k) = 0$. This system is robustly quadratically

stable if there exist positive definite matrices $X > 0$, $Y > 0$ such that the following LMI holds.

$$\begin{bmatrix} \Delta_{11} & \Delta_{12} & A_0^T X & s^{1/2} C_0^T X & 0 & 0 \\ * & \Delta_{22} & A_{0d}^T X & s^{1/2} C_{0d}^T X & 0 & 0 \\ * & * & -X & 0 & XE & 0 \\ * & * & * & -X & 0 & XE \\ * & * & * & * & -I & 0 \\ * & * & * & * & * & -I \end{bmatrix} < 0, \quad (11)$$

where

$$\begin{aligned} \Delta_{11} &= Y - X + G_{A_0}^T G_{A_0} + s G_{C_0}^T G_{C_0}, \\ \Delta_{12} &= G_{A_{0d}}^T G_{A_{0d}} + s G_{C_{0d}}^T G_{C_{0d}}, \\ \Delta_{22} &= -Y + G_{A_{0d}}^T G_{A_{0d}} + s G_{C_{0d}}^T G_{C_{0d}}. \end{aligned} \quad (12)$$

Proof. From Definition 1, taking a Lyapunov function V_k as in the form of (7), if uncertain discrete time-delay stochastic system (1) is quadratically stable, then, for all admissible uncertainties of (1), there exist matrices $P > 0$, $Q > 0$ and a scalar $\alpha > 0$ such that $\mathcal{E}(\Delta V_k)$ associated with unforced system (8) satisfies (6). In view of the assumption (H_1) , it is easy to compute

$$\begin{aligned} \mathcal{E}V_{k+1} - \mathcal{E}V_k &= \mathcal{E} \left\{ x(k)^T [A_{0\Delta}(k)^T P A_{0\Delta}(k) \right. \\ &\quad + s C_{0\Delta}(k)^T P C_{0\Delta}(k) + Q - P] x(k) + x(k)^T \\ &\quad \cdot [A_{0\Delta}(k)^T P A_{0d\Delta}(k) + s C_{0\Delta}(k)^T P C_{0d\Delta}(k)] x(k) \\ &\quad - d) + x(k-d)^T [A_{0d\Delta}(k)^T P A_{0\Delta}(k) \\ &\quad + s C_{0d\Delta}(k)^T P C_{0\Delta}(k)] x(k) + x(k-d)^T \\ &\quad \cdot [A_{0d\Delta}(k)^T P A_{0d\Delta}(k) + s C_{0d\Delta}(k)^T P C_{0d\Delta}(k) \\ &\quad - Q] x(k-d) \Big\} = \begin{bmatrix} x(k) \\ x(k-d) \end{bmatrix}^T \Pi \begin{bmatrix} x(k) \\ x(k-d) \end{bmatrix}, \end{aligned} \quad (13)$$

where $A_{0\Delta}$, $A_{0d\Delta}$, $C_{0\Delta}$, and $C_{0d\Delta}$ are given in (5) and Π is shown as

$$\Pi = \begin{bmatrix} A_{0\Delta}(k)^T P A_{0\Delta}(k) + s C_{0\Delta}(k)^T P C_{0\Delta}(k) + Q - P & A_{0\Delta}(k)^T P A_{0d\Delta}(k) + s C_{0\Delta}(k)^T P C_{0d\Delta}(k) \\ A_{0d\Delta}(k)^T P A_{0\Delta}(k) + s C_{0d\Delta}(k)^T P C_{0\Delta}(k) & A_{0d\Delta}(k)^T P A_{0d\Delta}(k) + s C_{0d\Delta}(k)^T P C_{0d\Delta}(k) - Q \end{bmatrix}. \quad (14)$$

By Definition 1, system (1) with $u(k) = 0$ is robustly quadratically stable, only if

$$\Pi < 0 \quad (15)$$

which is equivalent to

$$\Pi = \Pi_1 + \Pi_2$$

$$\begin{aligned} &= \begin{bmatrix} s C_{0\Delta}(k)^T P C_{0\Delta}(k) + Q - P & s C_{0\Delta}(k)^T P C_{0d\Delta}(k) \\ s C_{0d\Delta}(k)^T P C_{0\Delta}(k) & s C_{0d\Delta}(k)^T P C_{0d\Delta}(k) - Q \end{bmatrix} \\ &\quad + \begin{bmatrix} A_{0\Delta}(k)^T P A_{0\Delta}(k) & A_{0\Delta}(k)^T P A_{0d\Delta}(k) \\ A_{0d\Delta}(k)^T P A_{0\Delta}(k) & A_{0d\Delta}(k)^T P A_{0d\Delta}(k) \end{bmatrix} < 0. \end{aligned} \quad (16)$$

Note that Π_2 can be rewritten as

$$\Pi_2 = \begin{bmatrix} A_{0\Delta}(k)^T P \\ A_{0d\Delta}(k)^T P \end{bmatrix} P^{-1} [PA_{0\Delta}(k) \ PA_{0d\Delta}(k)]. \quad (17)$$

By Schur's complement, it is easy to derive that $\Pi < 0$ is equivalent to

$$\widehat{\Pi} = \begin{bmatrix} \pi_{11} & sC_{0\Delta}(k)^T PC_{0d\Delta}(k) & A_{0\Delta}(k)^T P \\ * & \pi_{22} & A_{0d\Delta}(k)^T P \\ * & * & -P \end{bmatrix}, \quad (18)$$

where

$$\begin{aligned} \pi_{11} &= sC_{0\Delta}(k)^T PC_{0\Delta}(k) + Q - P, \\ \pi_{22} &= sC_{0d\Delta}(k)^T PC_{0d\Delta}(k) - Q. \end{aligned} \quad (19)$$

Then, using the same way as in (16)–(19) yields

$$\widehat{\Pi} = \begin{bmatrix} Q - P & 0 & A_{0\Delta}(k)^T P & s^{1/2}C_{0\Delta}(k)^T P \\ * & -Q & A_{0d\Delta}(k)^T P & s^{1/2}C_{0d\Delta}(k)^T P \\ * & * & -P & 0 \\ * & * & * & -P \end{bmatrix} < 0. \quad (20)$$

The above inequality can be rewritten as

$$\begin{aligned} \widehat{\Pi} &= \Pi_3 + \begin{bmatrix} 0 & 0 \\ 0 & 0 \\ PE & 0 \\ 0 & PE \end{bmatrix} \text{diag}(F(k), F(k)) \\ &\cdot \begin{bmatrix} G_{A0} & G_{A0d} & 0 & 0 \\ s^{1/2}G_{C0} & s^{1/2}G_{C0d} & 0 & 0 \end{bmatrix} + \begin{bmatrix} G_{A0}^T & s^{1/2}G_{C0}^T \\ G_{A0d}^T & s^{1/2}G_{C0d}^T \\ 0 & 0 \\ 0 & 0 \end{bmatrix} \\ &\cdot \text{diag}(F(k)^T, F(k)^T) \begin{bmatrix} 0 & 0 & E^T P & 0 \\ 0 & 0 & 0 & E^T P \end{bmatrix} < 0, \end{aligned} \quad (21)$$

where

$$\Pi_3 = \begin{bmatrix} Q - P & 0 & A_0^T P & s^{1/2}C_0^T P \\ * & -Q & A_{0d}^T P & s^{1/2}C_{0d}^T P \\ * & * & -P & 0 \\ * & * & * & -P \end{bmatrix}. \quad (22)$$

Because Π_3 is a symmetric matrix, applying Lemma 3, (21) holds iff the following inequality holds:

$$\begin{aligned} \Pi_3 + \alpha \begin{bmatrix} 0 & 0 \\ 0 & 0 \\ PE & 0 \\ 0 & PE \end{bmatrix} &\begin{bmatrix} 0 & 0 & E^T P & 0 \\ 0 & 0 & 0 & E^T P \end{bmatrix} \\ + \alpha^{-1} \begin{bmatrix} G_{A0}^T & s^{1/2}G_{C0}^T \\ G_{A0d}^T & s^{1/2}G_{C0d}^T \\ 0 & 0 \\ 0 & 0 \end{bmatrix} &\begin{bmatrix} G_{A0} & G_{A0d} & 0 & 0 \\ s^{1/2}G_{C0} & s^{1/2}G_{C0d} & 0 & 0 \end{bmatrix} \\ = \begin{bmatrix} \Lambda_{11} & \Lambda_{12} & A_0^T P & s^{1/2}C_0^T P \\ * & \Lambda_{22} & A_{0d}^T P & s^{1/2}C_{0d}^T P \\ * & * & \Lambda_{33} & 0 \\ * & * & * & \Lambda_{44} \end{bmatrix} &< 0, \end{aligned} \quad (23)$$

where

$$\begin{aligned} \Lambda_{11} &= Q - P + \alpha^{-1}G_{A0}^T G_{A0} + s\alpha^{-1}G_{C0}^T G_{C0}, \\ \Lambda_{12} &= \alpha^{-1}G_{A0}^T G_{A0d} + s\alpha^{-1}G_{C0}^T G_{C0d}, \\ \Lambda_{22} &= -Q + \alpha^{-1}G_{A0d}^T G_{A0d} + s\alpha^{-1}G_{C0d}^T G_{C0d}, \\ \Lambda_{33} &= \Lambda_{44} = -P + \alpha PEE^T P. \end{aligned} \quad (24)$$

Take

$$\begin{aligned} P &= \alpha^{-1}X, \\ Q &= \alpha^{-1}Y \end{aligned} \quad (25)$$

and then by substituting (25) into (23), for $\alpha > 0$, we get

$$\begin{bmatrix} \Delta_{11} & \Delta_{12} & A_0^T X & s^{1/2}C_0^T X \\ * & \Delta_{22} & A_{0d}^T X & s^{1/2}C_{0d}^T X \\ * & * & -X + XEE^T X & 0 \\ * & * & * & -X + XEE^T X \end{bmatrix} < 0, \quad (26)$$

where $\Delta_{11}, \Delta_{12}, \Delta_{22}$ are shown in (12).

Using the same method as in (16)–(20), (11)–(12) follow immediately from the above inequality. \square

Theorem 5. System (1) is robustly quadratically stabilizable if there exist positive matrices $X > 0, Y > 0, K \in \mathcal{R}^{m \times n}$ and a scalar $\varepsilon > 0$ with $\varepsilon I - X^{-1} < 0$ such that the following LMI holds.

$$\begin{bmatrix} \Theta_{11} & \Theta_{12} & (A_0 + B_0 K)^T & s^{1/2} (C_0 + D_0 K)^T & 0 & 0 & (G_{A0} + G_{B0} K)^T & s^{1/2} (G_{C0} + G_{D0} K)^T \\ * & \Theta_{22} & A_{0d}^T & s^{1/2} C_{0d}^T & 0 & 0 & 0 & 0 \\ * & * & -\varepsilon I & 0 & E & 0 & 0 & 0 \\ * & * & * & -\varepsilon I & 0 & E & 0 & 0 \\ * & * & * & * & -I & 0 & 0 & 0 \\ * & * & * & * & * & -I & 0 & 0 \\ * & * & * & * & * & * & -I & 0 \\ * & * & * & * & * & * & * & -I \end{bmatrix} < 0, \quad (27)$$

where

$$\Theta_{11} = Y - X,$$

$$\Theta_{12} = (G_{A0} + G_{B0} K)^T G_{A0d} + (G_{C0} + G_{D0} K)^T G_{C0d}, \quad (28)$$

$$\Theta_{22} = -Y + G_{A0d}^T G_{A0d} + G_{C0d}^T G_{C0d}.$$

Moreover, a quadratically stabilizing state feedback controller is given by

$$u(k) = Kx(k). \quad (29)$$

Proof. By Definition 2, using the same way as in the proof of Theorem 4, the following inequality which has a similar form to (11)-(12) can be obtained by taking $u(k) = Kx(k)$

$$\begin{bmatrix} \widehat{\Theta}_{11} & \widehat{\Theta}_{12} & (A_0 + B_0 K)^T X & s^{1/2} (C_0 + D_0 K)^T X & 0 & 0 \\ * & \widehat{\Theta}_{22} & A_{0d}^T X & s^{1/2} C_{0d}^T X & 0 & 0 \\ * & * & -X & 0 & XE & 0 \\ * & * & * & -X & 0 & XE \\ * & * & * & * & -I & 0 \\ * & * & * & * & * & -I \end{bmatrix} < 0, \quad (30)$$

where

$$\begin{aligned} \widehat{\Theta}_{11} &= Y - X + (G_{A0} + G_{B0} K)^T (G_{A0} + G_{B0} K) \\ &+ (G_{C0} + G_{D0} K)^T (G_{C0} + G_{D0} K). \end{aligned} \quad (31)$$

In order to eliminate the nonlinear quadratic terms

$$\begin{aligned} (A_0 + B_0 K)^T X, \\ (C_0 + D_0 K)^T X, \end{aligned} \quad (32)$$

pre- and postmultiplying

$$\text{diag}(I, I, X^{-1}, I, I, I) \quad (33)$$

on both sides of (30) and considering $X^{-1} > \varepsilon I$, (27)-(28) can be obtained easily. This theorem is proved. \square

Remark 6. Compared with the results about quadratic stability and quadratic stabilizability of deterministic systems given in [14], our two theorems not only extend the results of [14] to stochastic systems, but also provide the corresponding LMI criteria which can be easily tested by MATLAB LMI toolbox.

Remark 7. From these two theorems, we also can get the result about quadratic stability with the given decay rate. Take the function

$$x_\lambda(k) = x(k) e^{k\lambda}, \quad (34)$$

and then, substituting (34) into (8), we obtain the following new system:

$$\begin{aligned} x_\lambda(k+1) &= (\widetilde{A}_{0\Delta} + \widetilde{B}_{0\Delta} K) x_\lambda(k) + \widetilde{A}_{0d\Delta} x_\lambda(k-d) \\ &+ \sum_{i=1}^s [(\widetilde{C}_{0\Delta} + \widetilde{D}_{0\Delta} K) x_\lambda(k) + \widetilde{C}_{0d\Delta} x_\lambda(k-d)] \\ &\cdot w_i(k), \end{aligned} \quad (35)$$

where

$$\begin{aligned} \widetilde{A}_{0\Delta} &= e^\lambda A_{0\Delta}, \\ \widetilde{B}_{0\Delta} &= e^\lambda B_{0\Delta}, \\ \widetilde{C}_{0\Delta} &= e^\lambda C_{0\Delta}, \\ \widetilde{D}_{0\Delta} &= e^\lambda D_{0\Delta}, \\ \widetilde{A}_{0d\Delta} &= e^{(d+1)\lambda} A_{0d\Delta}, \\ \widetilde{C}_{0d\Delta} &= e^{(d+1)\lambda} C_{0d\Delta}. \end{aligned} \quad (36)$$

So system (1) is quadratically stabilizable with decay rate λ if system (35) is quadratically stabilizable.

where

$$\begin{aligned} \hbar_{12} &= \alpha^{-1} \left[s^{1/4} (G_{C0} + G_{D0}K)^T G_{C0d} \right. \\ &\quad \left. + (G_{A0} + G_{B0}K)^T G_{A0d} \right], \\ \hbar_{22} &= -Q + \alpha^{-1} \left(s^{1/4} G_{C0d}^T G_{C0d} + G_{A0d}^T G_{A0d} \right), \\ \hbar_{17} &= \alpha^{-1} s^{1/2} (G_{C0} + G_{D0}K)^T, \\ \hbar_{18} &= \alpha^{-1} (G_{A0} + G_{B0}K)^T, \end{aligned} \quad (43)$$

then system (37) is robustly H_∞ controllable with a control law $u(k) = Kx(k)$.

Proof. By Theorem 5, when disturbance $\xi(k) = 0$, it is easy to test that system (37) is internally stabilizable with $u^*(k) = Kx(k)$. Now we only need to show $\|\mathcal{E}_{z\xi}\| < \gamma$. By Definition 1, choose the Lyapunov function $V_k = x(k)^T Px(k) + \sum_{j=1}^d x(k-j)^T Qx(k-j)$ with $P > 0$ and $Q > 0$ to be determined, and then

$$\begin{aligned} \mathcal{E}\Delta V_k &= \mathcal{E}V_{k+1} - \mathcal{E}V_k = \mathcal{E} \left[x^T(k+1) Px(k+1) \right. \\ &\quad \left. + \sum_{j=1}^d x^T(k+1-j) Qx(k+1-j) - x^T(k) Px(k) \right. \\ &\quad \left. - \sum_{j=1}^d x^T(k-j) Qx(k-j) \right] \\ &= \mathcal{E} \left[x^T(k+1) Px(k+1) + x^T(k) (Q - P) x(k) \right. \\ &\quad \left. - x^T(k-d) Qx(k-d) \right]. \end{aligned} \quad (44)$$

So in the case of $x(j) = 0, j = 0, -1, \dots, -d$, we have

$$\begin{aligned} \|z(k)\|_{l_w^2(\mathcal{N}_0, \mathcal{R}^{n_z})} - \gamma^2 \|\xi(k)\|_{l_w^2(\mathcal{N}_0, \mathcal{R}^q)} &= \mathcal{E} \sum_{k=0}^{\infty} \left\{ x^T(k) \right. \\ &\quad \cdot (C^T C + K^T D^T D K) x(k) + \Delta V - \gamma^2 \xi^T(k) \xi(k) \} \\ &\quad + V(x(0)) - \liminf_{t \rightarrow \infty} \mathcal{E}V(x(k)) \leq \mathcal{E} \sum_{k=0}^{\infty} \left\{ x^T(k) \right. \\ &\quad \cdot (A_{0\Delta} + B_{0\Delta}K)^T P (A_{0\Delta} + B_{0\Delta}K) x(k) + x^T(k) \\ &\quad \cdot (A_{0\Delta} + B_{0\Delta}K)^T P A_{0d\Delta} x(k-d) + x^T(k) \\ &\quad \cdot (A_{0\Delta} + B_{0\Delta}K)^T P B \xi(k) + x^T(k-d) \\ &\quad \cdot A_{0d\Delta}^T P (A_{0\Delta} + B_{0\Delta}K) x(k) + x^T(k-d) \\ &\quad \cdot A_{0d\Delta}^T P A_{0d\Delta} x(k-d) + x^T(k-d) A_{0d\Delta}^T P B \xi(k) \\ &\quad + \xi^T(k) B^T P (A_{0\Delta} + B_{0\Delta}K) x(k) + \xi^T(k) \\ &\quad \cdot B^T P A_{0d\Delta} x(k-d) + \xi^T(k) B^T P B \xi(k) + x^T(k) \\ &\quad \cdot (C_{0\Delta}K)^T P (C_{0\Delta} + D_{0\Delta}K) x(k) \\ &\quad + x^T(k) (C_{0\Delta} + D_{0\Delta}K)^T P C_{0d\Delta} x(k-d) \\ &\quad + x^T(k-d) C_{0d\Delta}^T P (C_{0\Delta} + D_{0\Delta}K) x(k) \\ &\quad + x^T(k-d) C_{0d\Delta} P C_{0d\Delta} x(k-d) - x^T(k) Px(k) \\ &\quad + x^T(k) (Q - P) x(k) - x^T(k-d) Qx(k-d) \\ &\quad + x^T(k) (C^T C + K^T D^T D K) x(k) - \gamma^2 \xi^T(k) \\ &\quad \cdot \xi(k) \} = \mathcal{E} \sum_{k=0}^{\infty} \begin{bmatrix} x(k) \\ x(k-d) \\ \xi(k) \end{bmatrix}^T \Xi \begin{bmatrix} x(k) \\ x(k-d) \\ \xi(k) \end{bmatrix}, \end{aligned} \quad (45)$$

where

$$\Xi = \begin{bmatrix} \Xi_{11} & (A_{0\Delta} + B_{0\Delta}K)^T P A_{0d\Delta} & (A_{0\Delta} + B_{0\Delta}K)^T P B & s^{1/2} (C_{0\Delta} + D_{0\Delta}K)^T P \\ * & A_{0d\Delta}^T P A_{0d\Delta} - Q & A_{0d\Delta}^T P B & s^{1/2} C_{0d\Delta}^T P \\ * & * & B^T P B - \gamma^2 I & 0 \\ * & * & * & -P \end{bmatrix}, \quad (46)$$

$$\Xi_{11} = (A_{0\Delta} + B_{0\Delta}K)^T P (A_{0\Delta} + B_{0\Delta}K) - 2P + Q + C^T C + K^T D^T D K.$$

Obviously, it is easy to get that $\|\mathcal{G}_{z\hat{x}}\| < \gamma$ if $\Xi < 0$. Then, we need to eliminate the uncertainties. Using the same method as in the proof of Theorem 4, we know that, for some $\alpha > 0$, a sufficient condition for $\Xi < 0$ can be got from the following matrix inequality.

$$\begin{bmatrix} \Gamma_{11} & \Gamma_{12} & 0 & s^{1/2}(C_0 + D_0K)^T P & (A_0 + B_0K)^T P \\ * & \Gamma_{22} & 0 & s^{1/2}C_{0d}^T P & A_{0d}^T P \\ * & * & -\gamma^2 I & 0 & B^T P \\ * & * & * & -P + \alpha PEE^T P & 0 \\ * & * & * & * & -P + \alpha PEE^T P \end{bmatrix} < 0, \quad (47)$$

where

$$\begin{aligned} \Gamma_{11} &= -2P + Q + C^T C + K^T D^T D K + \alpha^{-1} s^{1/4} (G_{C0} \\ &\quad + G_{D0}K)^T (G_{C0} + G_{D0}K) + \alpha^{-1} (G_{A0} + G_{B0}K)^T \\ &\quad \cdot (G_{A0} + G_{B0}K), \\ \Gamma_{12} &= \alpha^{-1} [s^{1/4} (G_{C0} + G_{D0}K)^T G_{C0d} \\ &\quad + (G_{A0} + G_{B0}K)^T G_{A0d}], \\ \Gamma_{22} &= -Q + \alpha^{-1} (s^{1/4} G_{C0d}^T G_{C0d} + G_{A0d}^T G_{A0d}). \end{aligned} \quad (48)$$

Then, by pre- and postmultiplying

$$\text{diag}[I \ I \ I \ P^{-1} \ P^{-1}] \quad (49)$$

on both sides of (47), we have

$$\begin{bmatrix} \Gamma_{11} & \Gamma_{12} & 0 & s^{1/2}(C_0 + D_0K)^T & (A_0 + B_0K)^T \\ * & \Gamma_{22} & 0 & s^{1/2}C_{0d}^T & A_{0d}^T \\ * & * & -\gamma^2 I & 0 & B^T \\ * & * & * & -P^{-1} + \alpha EE^T & 0 \\ * & * & * & * & -P^{-1} + \alpha EE^T \end{bmatrix} < 0. \quad (50)$$

For some constant $\beta > 0$ with $P^{-1} > \beta I$, Theorem 10 is concluded; that is, an H_∞ control of system (37) is obtained by solving LMIs (42)-(43). This completes the proof. \square

5. Simulation Example

In this section, we consider two simple examples with simulations to illustrate the effectiveness of the proposed approach.

Example 11. Consider discrete-time stochastic system (1) with the following parameters:

$$\begin{aligned} A_0 &= \begin{bmatrix} 1 & 0 \\ 0 & 0.8 \end{bmatrix}, \\ A_{0d} &= \begin{bmatrix} 0.02 & 0 \\ 0 & 0.1 \end{bmatrix}, \\ B_0 &= \begin{bmatrix} 3 \\ 1 \end{bmatrix}, \\ C_0 &= \begin{bmatrix} 0.2 & 0 \\ 0 & 0.4 \end{bmatrix}, \\ C_{0d} &= \begin{bmatrix} 0.1 & 0 \\ 0 & 0.2 \end{bmatrix}, \\ D_0 &= \begin{bmatrix} 0.2 \\ 0.7 \end{bmatrix}, \\ E &= \begin{bmatrix} 0.2 & 0 \\ 0 & 0.4 \end{bmatrix}, \\ G_{A_0} &= \begin{bmatrix} 0.01 & 0 \\ 0 & 0.03 \end{bmatrix}, \\ G_{A_{0d}} &= \begin{bmatrix} 0.04 & 0 \\ 0 & 0.05 \end{bmatrix}, \\ G_{B_0} &= \begin{bmatrix} 0.2 \\ 0.1 \end{bmatrix}, \\ G_{C_0} &= \begin{bmatrix} 0.3 & 0 \\ 0 & 0.1 \end{bmatrix}, \\ G_{D_0} &= \begin{bmatrix} 0.1 \\ 0.7 \end{bmatrix}, \\ G_{C_{0d}} &= \begin{bmatrix} 0.1 & 0 \\ 0 & 0.01 \end{bmatrix}, \\ F(k) &= \begin{bmatrix} \cos(w(k)) & 0 \\ 0 & \sin(w(k)) \end{bmatrix}, \\ s &= 1. \end{aligned} \quad (51)$$

Using LMI toolbox to solve (11)-(12) in Theorem 4, we find out that $t_{\min} = 0.0086 > 0$ which means that there is no feasible solution and indicates that system (1) with $u \equiv 0$ is unstable. Figure 1 verifies the result. By solving LMI (27), a group of feasible solutions with $t_{\min} = -0.9649 < 0$ are shown as $\varepsilon = 16.7436$ and

$$\begin{aligned} X &= \begin{bmatrix} 22.1026 & 0.6519 \\ 0.6519 & 20.0007 \end{bmatrix}, \\ Y &= \begin{bmatrix} 11.3608 & -0.6710 \\ -0.6710 & 13.2231 \end{bmatrix}. \end{aligned} \quad (52)$$

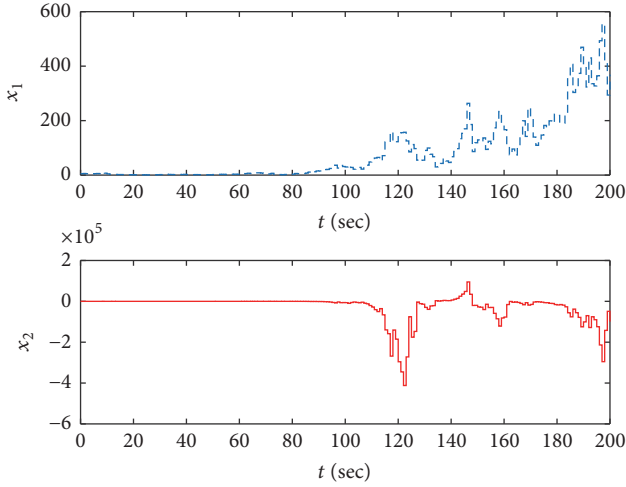


FIGURE 1: State trajectories of the autonomous system.

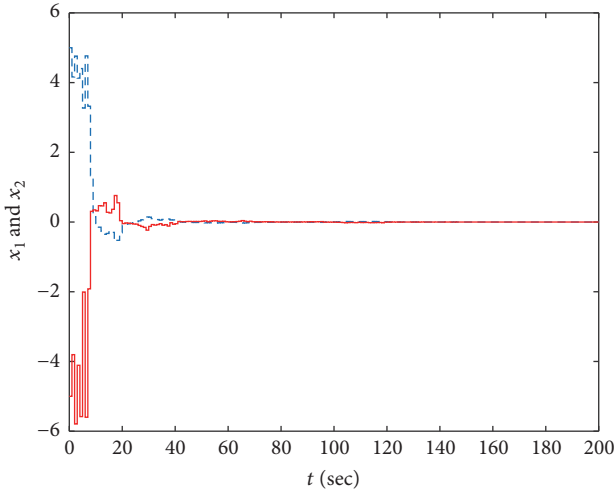


FIGURE 2: State trajectories of the closed-loop system.

By Theorem 5, the system is mean-square stabilizable which is verified by Figure 2. A robust stabilizing controller is given by

$$u(k) = Kx(k) = [-0.092 \quad -0.1344] x(k). \quad (53)$$

Example 12. Consider system (42) with the following parameters:

$$A_0 = \begin{bmatrix} 1.2 & 0 \\ 0 & 1.1 \end{bmatrix},$$

$$A_{0d} = \begin{bmatrix} 0.2 & 0 \\ 0 & 0.1 \end{bmatrix},$$

$$B_0 = \begin{bmatrix} 1.3 \\ 1 \end{bmatrix},$$

$$C_0 = \begin{bmatrix} 0.2 & 0 \\ 0 & 0.4 \end{bmatrix},$$

$$B = \begin{bmatrix} 1 \\ 0.65 \end{bmatrix},$$

$$C = \begin{bmatrix} 0.4 & 0.2 \\ 0.1 & 0.8 \end{bmatrix},$$

$$D = \begin{bmatrix} 0.8 \\ 1 \end{bmatrix},$$

$$C_{0d} = \begin{bmatrix} 0.1 & 0 \\ 0 & 0.2 \end{bmatrix},$$

$$D_0 = \begin{bmatrix} 0.2 \\ 0.7 \end{bmatrix},$$

$$E = \begin{bmatrix} 0.2 & 0 \\ 0 & 0.4 \end{bmatrix},$$

$$G_{A_0} = \begin{bmatrix} 0.1 & 0 \\ 0 & 0.3 \end{bmatrix},$$

$$G_{A_{0d}} = \begin{bmatrix} 0.4 & 0 \\ 0 & 0.5 \end{bmatrix},$$

$$G_{B_0} = \begin{bmatrix} 0.2 \\ 0.1 \end{bmatrix},$$

$$G_{C_0} = \begin{bmatrix} 0.3 & 0 \\ 0 & 0.1 \end{bmatrix},$$

$$G_{D_0} = \begin{bmatrix} 0.1 \\ 0.7 \end{bmatrix},$$

$$G_{C_{0d}} = \begin{bmatrix} 0.1 & 0 \\ 0 & 0.1 \end{bmatrix},$$

$$F(k) = \begin{bmatrix} \cos(w(k)) & 0 \\ 0 & \sin(w(k)) \end{bmatrix},$$

$$s = 1.$$

(54)

For perturbed system (42), we take the external disturbance as $\xi(k) = e^{-k}$ and the certain level as $\gamma = 0.8$. In addition, according to Lemma 3, an appropriate α is given as $\alpha = 4.9$. Then, by the result of Theorem 10, using LMI toolbox to solve (43) and (47), we find that $t_{\min} = -0.1046$, which means we have got a group of feasible solutions with

$$P = \begin{bmatrix} 1.7258 & 0.0320 \\ 0.0320 & 1.8314 \end{bmatrix},$$

$$Q = \begin{bmatrix} 1.6581 & -0.0480 \\ -0.0480 & 1.5180 \end{bmatrix},$$

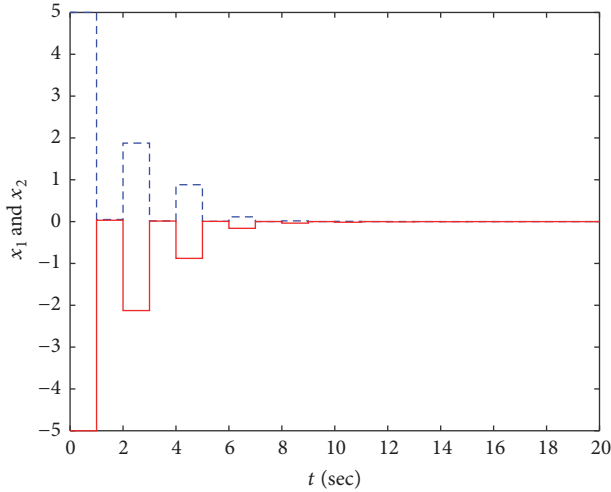


FIGURE 3: State trajectories of the closed-loop system.

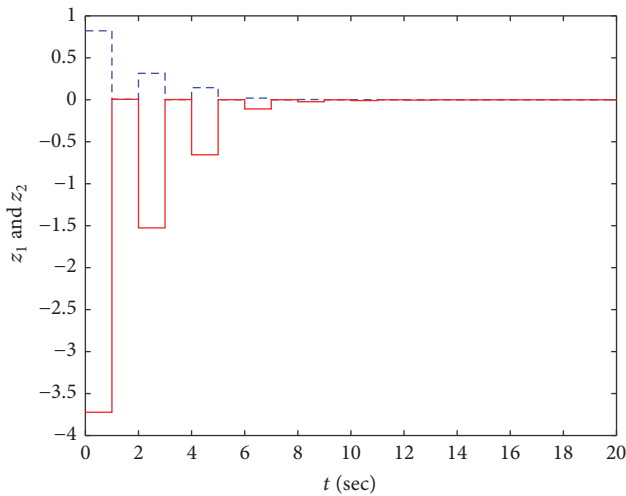


FIGURE 4: Controlled output trajectories of the closed-loop system.

$$K = [-0.3281 \quad -0.2836],$$

$$\beta = 3.0531. \quad (55)$$

The simulation results of state trajectories and controlled output trajectories of system (42) are given in Figures 3 and 4 with the H_∞ controller

$$u(k) = Kx(k) = [-0.3281 \quad -0.2836] x(k). \quad (56)$$

This further verifies the effectiveness of Theorem 10.

6. Conclusion

In this paper, we have studied the robust quadratic stability, quadratic stabilization, and robust H_∞ state feedback control of discrete-time stochastic systems with state delay and uncertain parameters. Based on LMI technique, a sufficient condition about quadratic stability and quadratic

stabilization of our considered system is, respectively, given. Moreover, an H_∞ state feedback controller is obtained by solving two LMIs. Finally, we supply two simulation examples to show the validity of the proposed results. It is expected to solve the H_∞ output feedback control and H_∞ filtering in our forthcoming work.

Competing Interests

The authors declare that there is no conflict of interests regarding the publication of this paper.

Acknowledgments

This work was supported by the National Natural Science Foundation of China (no. 61573227 and no. 61273160), Natural Science Foundation of Shandong Province of China (no. 2013ZRE28089), the Research Fund for the Taishan Scholar Project of Shandong Province of China, the Postgraduate Innovation Funds of China University of Petroleum (East China) (no. YCX2015051), and the SDUST Research Fund (no. 2015TDJH105).

References

- [1] T. Söderström, *Discrete-Time Stochastic Systems*, Springer, New York, NY, USA, 2002.
- [2] V. Dragan, T. Morozan, and A.-M. Stoica, *Mathematical Methods in Robust Control of Discrete-Time Linear Stochastic Systems*, Springer, New York, NY, USA, 2010.
- [3] A. Seierstad, *Stochastic Control in Discrete and Continuous Time*, Springer, New York, NY, USA, 2009.
- [4] Y. Zhang and C. Wang, "Robust stochastic stability of uncertain discrete-time impulsive Markovian jump delay systems with multiplicative noises," *International Journal of Systems Science*, vol. 46, no. 12, pp. 2210–2220, 2015.
- [5] W. Zhang and B.-S. Chen, "On stabilizability and exact observability of stochastic systems with their applications," *Automatica*, vol. 40, no. 1, pp. 87–94, 2004.
- [6] Z. Wang, Y. Liu, and X. Liu, "Exponential stabilization of a class of stochastic system with Markovian jump parameters and mode-dependent mixed time-delays," *IEEE Transactions on Automatic Control*, vol. 55, no. 7, pp. 1656–1662, 2010.
- [7] X. Li, X. Y. Zhou, and M. Ait Rami, "Indefinite stochastic linear quadratic control with Markovian jumps in infinite time horizon," *Journal of Global Optimization Theory and Applications*, vol. 27, no. 2-3, pp. 149–175, 2003.
- [8] T. Hou, W. Zhang, and B.-S. Chen, "Study on general stability and stabilizability of linear discrete-time stochastic systems," *Asian Journal of Control*, vol. 13, no. 6, pp. 977–987, 2011.
- [9] J. Lian and Z. Feng, "Passivity analysis and synthesis for a class of discrete-time switched stochastic systems with time-varying delay," *Asian Journal of Control*, vol. 15, no. 2, pp. 501–511, 2013.
- [10] W. Zhang, Y. Zhao, and L. Sheng, "Some remarks on stability of stochastic singular systems with state-dependent noise," *Automatica*, vol. 51, pp. 273–277, 2015.
- [11] F. Li, L. Wu, and P. Shi, "Stochastic stability of semi-Markovian jump systems with mode-dependent delays," *International Journal of Robust and Nonlinear Control*, vol. 24, no. 18, pp. 3317–3330, 2014.

- [12] L. Huang and X. Mao, "Stability of singular stochastic systems with Markovian switching," *IEEE Transactions on Automatic Control*, vol. 56, no. 2, pp. 424–429, 2011.
- [13] M. Sun, W. Zhang, and G. Li, "Stochastic admissibility of continuous-time singular Markov jump systems with general uncertain transition rates," *Journal of Shandong University of Science and Technology*, vol. 35, no. 4, pp. 86–92, 2016.
- [14] T. Senthilkumar and P. Balasubramaniam, "Delay-dependent robust stabilization and H_∞ control for uncertain stochastic T-S fuzzy systems with multiple time delays," *Iranian Journal of Fuzzy Systems*, vol. 9, no. 2, pp. 89–111, 2012.
- [15] S. Xu, J. Lam, and C. Yang, "Quadratic stability and stabilization of uncertain linear discrete-time systems with state delay," *Systems and Control Letters*, vol. 43, no. 2, pp. 77–84, 2001.
- [16] G. Chen and Y. Shen, "Robust H_∞ filter design for neutral stochastic uncertain systems with time-varying delay," *Journal of Mathematical Analysis and Applications*, vol. 353, no. 1, pp. 196–204, 2009.
- [17] J.-N. Li, Y. Zhang, and Y.-J. Pan, "Mean-square exponential stability and stabilisation of stochastic singular systems with multiple time-varying delays," *Circuits, Systems, and Signal Processing*, vol. 34, no. 4, pp. 1187–1210, 2015.
- [18] O. L. V. Costa, M. D. Fragoso, and R. P. Marques, *Discrete-Time Markov Jump Linear Systems*, Probability and Its Applications, Springer, New York, NY, USA, 2005.
- [19] A. E. Bouhtouri, D. Hinrichsen, and A. J. Pritchard, " H^∞ -type control for discrete-time stochastic systems," *International Journal of Robust Nonlinear Control*, vol. 9, no. 13, pp. 923–948, 1999.
- [20] Z. Lin, Y. Lin, and W. Zhang, "A unified design for state and output feedback H_∞ control of nonlinear stochastic Markovian jump systems with state and disturbance-dependent noise," *Automatica*, vol. 45, no. 12, pp. 2955–2962, 2009.
- [21] Y. Zhang, P. Shi, S. K. Nguang, and Y. Song, "Robust finite-time H_∞ control for uncertain discrete-time singular systems with Markovian jumps," *IET Control Theory & Applications*, vol. 8, no. 12, pp. 1105–1111, 2014.
- [22] H. Li and Y. Shi, "State-feedback H_∞ control for stochastic time-delay nonlinear systems with state and disturbance-dependent noise," *International Journal of Control*, vol. 85, no. 10, pp. 1515–1531, 2012.
- [23] K. Mathiyalagan and R. Sakthivel, "Robust stabilization and H_∞ control for discrete-time stochastic genetic regulatory networks with time delays," *Canadian Journal of Physics*, vol. 90, no. 10, pp. 939–953, 2012.
- [24] W. Zhang, Y. Huang, and L. Xie, "Infinite horizon stochastic H_2/H_∞ control for discrete-time systems with state and disturbance dependent noise," *Automatica*, vol. 44, no. 9, pp. 2306–2316, 2008.
- [25] X. Jiang, X. Tian, T. Zhang, and W. Zhang, "Robust quadratic stability and stabilizability of uncertain linear discrete-time stochastic systems with state delay," in *Proceedings of the 28th Chinese Control and Decision Conference (CCDC '16)*, pp. 1728–1732, Yinchuang, China, 2016.
- [26] W. Wang, Y. Zhang, and X. Liang, "Exact observability of Markov jump stochastic systems with multiplicative noise," *Journal of Shandong University of Science and Technology*, vol. 35, no. 3, pp. 99–105, 2016.
- [27] W. Zhang, Q. Li, and Y. Hua, "Quadratic stabilization and output feedback H_∞ control of stochastic uncertain systems," in *Proceedings of the 5th World Congress on Intelligent Control and Automation (WCICA '04)*, pp. 728–732, Hangzhou, China, June 2004.

Research Article

Robust Stability Criteria for T-S Fuzzy Systems with Time-Varying Delays via Nonquadratic Lyapunov-Krasovskii Functional Approach

Sung Hyun Kim

School of Electrical Engineering, University of Ulsan, Daehak-ro 93, Nam-Gu, Ulsan 680-749, Republic of Korea

Correspondence should be addressed to Sung Hyun Kim; ie222.kim@gmail.com

Received 17 May 2016; Revised 13 September 2016; Accepted 5 October 2016

Academic Editor: Olfa Bouabaker

Copyright © 2016 Sung Hyun Kim. This is an open access article distributed under the Creative Commons Attribution License, which permits unrestricted use, distribution, and reproduction in any medium, provided the original work is properly cited.

This paper tackles the issue of stability analysis for uncertain T-S fuzzy systems with interval time-varying delays, especially based on the nonquadratic Lyapunov-Krasovskii functional (NLKF). To this end, this paper first provides a less conservative relaxation technique and then derives a relaxed robust stability criterion that enhances the interactions among delayed fuzzy subsystems. The effectiveness of our method is verified by two examples.

1. Introduction

Over the past few decades, Takagi-Sugeno (T-S) fuzzy model has attracted great attention since it can systematically represent nonlinear systems via a kind of interpolation method that connects smoothly some local linear systems based on fuzzy weighting functions [1]. In particular, the T-S fuzzy model has the advantage that it allows the well-established linear system theory to be applied to the analysis and synthesis of nonlinear systems. For this reason, the T-S fuzzy model has been a popular choice not only in consumer products but also in industrial processes (refer to [2] and references therein).

As well-known, time-delay phenomena are ubiquitous in practical engineering systems such as aircraft systems, biological systems, and chemical engineering system [3–5]. Recently, thus, the research on nonlinear systems with state delays has been an important issue in the stability analysis of T-S fuzzy systems. In the literature, there are two major research trends to deal with such systems: one focuses on decreasing computational burdens required to solve a set of conditions from the Lyapunov-Krasovskii functional (LKF) approach, and the other focuses on improving the solvability of delay-dependent stability conditions despite significant computational efforts. Strictly speaking, the first trend is

mainly based on Jensen's inequality approach [6–11] and the second one is based on the free-weighting matrix approach [12–16].

Recently, it is recognized that the common quadratic Lyapunov function approach leads to overconservative performance for a large number of fuzzy rules [17, 18]. For this reason, it is essential to tackle the issue of stability analysis in the light of the nonquadratic Lyapunov-Krasovskii functional (NLKF) [19–23]. However, to our best knowledge, up to now, little progress has been made toward using NLKFs for the stability analysis. Motivated by the above concern, this paper proposes a relaxed stability criterion for uncertain T-S fuzzy systems with interval time-varying delays, especially obtained by the NLKF approach. To this end, this paper offers a proper relaxation method that can enhance the interactions among delayed fuzzy subsystems. Further, it is worth noticing that Jensen's inequality, given in [24], is applicable only to the case where the internal matrix is constant, that is, to the case where the common quadratic Lyapunov-Krasovskii functional (CQLKF) is employed. Thus, this paper focuses more on exploring the second trend in the direction of reducing the conservatism that stems from the CQLKF approach, without resorting to any delay-decomposition method. In this sense, this paper provides two examples numerically to show the effectiveness of our method.

The rest of the paper is organized as follows. Section 2 gives a mathematical description of the system considered here and presents a useful lemma. Section 3 presents the main result of this paper. Furthermore, through numerical examples, Section 4 shows the verification of our results. Finally, Section 5 makes the concluding remarks.

Notation. Throughout this paper, standard notions will be adopted. The notations $X \geq Y$ and $X > Y$ mean that $X - Y$ is positive semidefinite and positive definite, respectively. In symmetric block matrices, $(*)$ is used as an ellipsis for terms that are induced by symmetry. For a square matrix \mathcal{X} , $\text{He}(\mathcal{X})$ denotes $\mathcal{X} + \mathcal{X}^T$, where \mathcal{X}^T is the transpose of \mathcal{X} . The notation $\text{Conv}(\cdot)$ denotes the convex hull; $\text{col}(v_1, v_2, \dots, v_n) = [v_1^T \ v_2^T \ \dots \ v_n^T]^T$ for any vector v_i ; $\text{diag}(\mathcal{A}, \mathcal{B})$ denotes a diagonal matrix with diagonal entries \mathcal{A} and \mathcal{B} ; and $\mathbb{N}_r^+ = \{1, 2, \dots, r\}$. For any matrix \mathcal{S}_i or \mathcal{S}_{ij} ,

$$\begin{aligned} [\mathcal{S}_i]_r &= [\mathcal{S}_1 \ \mathcal{S}_2 \ \dots \ \mathcal{S}_r], \\ [\mathcal{S}_{ij}]_{r \times r} &= [[\mathcal{S}_{1i}]_r^T \ [\mathcal{S}_{2i}]_r^T \ \dots \ [\mathcal{S}_{ri}]_r^T]^T. \end{aligned} \quad (1)$$

All matrices, if their dimensions are not explicitly stated, are assumed to be compatible for algebraic operation.

2. System Description and Preliminaries

Consider the following uncertain T-S fuzzy system, which represents a class of nonlinear systems: for $i \in \mathbb{N}_r^+$,

Plant Rule i. IF $\eta_1(t)$ is \mathcal{F}_{i1} and \dots $\eta_s(t)$ is \mathcal{F}_{is} , THEN

$$\begin{aligned} \dot{x}(t) &= A_i x(t) + A_{d,i} x(t - d(t)) + E_i p(t), \\ q(t) &= G_i x(t) + G_{d,i} x(t - d(t)), \\ x(t) &= \psi(t), \end{aligned} \quad (2)$$

$$t \in [-d_2, 0],$$

where $x(t) \in \mathbb{R}^{n_x}$ and $x(t - d(t)) \in \mathbb{R}^{n_x}$ denote the state and the delayed state, respectively; the initial condition $\psi(t)$ is a continuously differentiable vector-valued function; \mathcal{F}_{ij} denotes a fuzzy set; $\eta_i(t)$ denotes the i th premise variable; and r denotes the number of IF-THEN rules. In (2), $p(t) \in \mathbb{R}^{n_p}$ and $q(t) \in \mathbb{R}^{n_q}$ are used to describe the structured feedback uncertainty such that $p(t) = \Delta(t)q(t)$ and $\Delta^T(t)\Delta(t) \leq I \in \mathbb{R}^{n_q \times n_q}$. Further, the state delay $d(t)$ is assumed to be unknown and time-varying with known bounds as follows: $d_1 \leq d(t) \leq d_2$, where d_1 and d_2 are constant. Then, the overall T-S fuzzy model is inferred as follows:

$$\begin{aligned} \dot{x}(t) &= A(\Theta_t) x(t) + A_d(\Theta_t) x(t - d(t)) \\ &\quad + E(\Theta_t) p(t), \\ q(t) &= G(\Theta_t) x(t) + G_d(\Theta_t) x(t - d(t)), \end{aligned} \quad (3)$$

where $A(\Theta_t) = \sum_{i=1}^r \theta_i A_i$, $A_d(\Theta_t) = \sum_{i=1}^r \theta_i A_{d,i}$, $E(\Theta_t) = \sum_{i=1}^r \theta_i E_i$, $G(\Theta_t) = \sum_{i=1}^r \theta_i G_i$, and $G_d(\Theta_t) = \sum_{i=1}^r \theta_i G_{d,i}$ in

which $\theta_i (= \theta_i(\eta(t)))$ denotes the normalized fuzzy weighting function for the i th rule; $\eta(t) = \text{col}(\eta_1(x(t)), \dots, \eta_s(x(t)))$ denotes the premise variable vector; and $\Theta_t = \text{col}(\theta_1, \dots, \theta_r)$ belongs to

$$\begin{aligned} \mathbb{S}_\Theta &= \left\{ \text{col}(\theta_1, \dots, \theta_r) \mid \sum_{i=1}^r \theta_i = 1, \alpha_i \leq \theta_i \leq \beta_i, \forall i \right. \\ &\quad \left. \in \mathbb{N}_r^+ \right\}. \end{aligned} \quad (4)$$

Assumption 1. The fuzzy weighting functions θ_i are differentiable and $\dot{\Theta}_t = \text{col}(\dot{\theta}_1, \dots, \dot{\theta}_r)$ belongs to

$$\begin{aligned} \mathbb{S}_{\dot{\Theta}} &= \left\{ \text{col}(\dot{\theta}_1, \dots, \dot{\theta}_r) \mid \sum_{i=1}^r \dot{\theta}_i = 0, \varrho_{1,i} \leq \dot{\theta}_i \leq \varrho_{2,i}, \forall i \right. \\ &\quad \left. \in \mathbb{N}_r^+ \right\}. \end{aligned} \quad (5)$$

To simplify the notations, we use $\theta_i^{d_1} = \theta_i(\eta(t - d_1))$ and $\theta_i^{d_2} = \theta_i(\eta(t - d_2))$. And, for later convenience, we define $\bar{x}(t) = \text{col}(x(t), x(t - d_1), x(t - d(t)), x(t - d_2))$, $\eta(t) = \text{col}(\bar{x}(t), p(t)) \in \mathbb{R}^{n_\eta}$, and $n_\eta = 4n_x + n_p$. And we use some block entry matrices \mathbf{e}_i ($i = 1, 2, \dots, 5$) such that $x(t) = \mathbf{e}_1 \eta(t)$, $x(t - d_1) = \mathbf{e}_2 \eta(t)$, $x(t - d(t)) = \mathbf{e}_3 \eta(t)$, $x(t - d_2) = \mathbf{e}_4 \eta(t)$, and $p(t) = \mathbf{e}_5 \eta(t)$, which implies $\bar{x}(t) = \mathbf{e}_{14} \eta(t)$ by defining $\mathbf{e}_{14}^T = [\mathbf{e}_1^T \ \dots \ \mathbf{e}_4^T]$. Then, (3) becomes

$$\begin{aligned} \dot{x}(t) &= \Phi_t \eta(t), \\ q(t) &= \Psi_t \eta(t), \end{aligned} \quad (6)$$

where $\Phi_t = A(\Theta_t)\mathbf{e}_1 + A_d(\Theta_t)\mathbf{e}_3 + E(\Theta_t)\mathbf{e}_5$ and $\Psi_t = G(\Theta_t)\mathbf{e}_1 + G_d(\Theta_t)\mathbf{e}_3$.

Lemma 2. Let $\Theta_t \in \mathbb{S}_\Theta$ be satisfied. Then, the following condition holds:

$$\begin{aligned} 0 &> \mathcal{M} \\ &= \mathcal{M}_0 + \sum_{i=1}^r \theta_i \text{He}(\mathcal{M}_i) + \sum_{i=1}^r \theta_i^2 \mathcal{M}_{ii} \\ &\quad + \sum_{i=1}^r \left(\sum_{j=i+1}^r \theta_i \theta_j \mathcal{M}_{ij} + \sum_{j=1}^{i-1} \theta_i \theta_j \mathcal{M}_{ji}^T \right) \end{aligned} \quad (7)$$

if there are all decision variables such that

$$\begin{aligned} 0 &> \mathcal{L} = \left[\begin{array}{c|c} \mathcal{L}_0 & [\mathcal{L}_i]_r \\ (*) & [\mathcal{L}_{ij}]_{rr} \end{array} \right], \\ 0 &< X_i + X_i^T, \end{aligned} \quad (8)$$

$$\forall i \in \mathbb{N}_r^+,$$

where $\mathcal{L}_0 = \mathcal{M}_0 + \text{He}(S_0 - \sum_{i=1}^r \alpha_i \beta_i X_i)$, $\mathcal{L}_i = \mathcal{M}_i + S_i - S_0 + (\alpha_i + \beta_i)X_i$, $\mathcal{L}_{ii} = \mathcal{M}_{ii} + \text{He}(-S_i - X_i)$, and $\mathcal{L}_{ij} = \mathcal{M}_{ij} - S_i - S_j$.

Lemma 3. Let $\dot{\Theta}_t \in \mathbb{S}_{\dot{\Theta}}$ be satisfied. Then, the following condition holds:

$$0 > \Omega + \sum_{i=1}^r \dot{\Theta}_i \mathcal{P}_i \quad (9)$$

if there are all decision variables such that

$$0 > \Omega + \sum_{i=1}^r \varrho_{\ell_i, i} (\mathcal{P}_i + \mathcal{Q}), \quad (10)$$

$$\forall \ell \in \mathbb{L} = \{(\ell_1, \dots, \ell_r) \mid \ell_i \in \mathbb{N}_2^+, i \in \mathbb{N}_r^+\}.$$

Proof. In view of $\dot{\Theta}_t \in \mathbb{S}_{\dot{\Theta}}$, we can get

$$\begin{aligned} \dot{\Theta}_i &= \sum_{\ell_i=1}^2 \lambda_{\ell_i}(t) \varrho_{\ell_i, i}, \\ 0 &= \sum_{i=1}^r \dot{\Theta}_i \mathcal{N}, \end{aligned} \quad (11)$$

where coefficients λ_{ℓ_i} are all positive and sum to one and \mathcal{N} is a constant slack variable. Then, (9) leads to

$$0 > \Omega + \sum_{i=1}^r \left(\sum_{\ell_i=1}^2 \lambda_{\ell_i}(t) \varrho_{\ell_i, i} \right) (\mathcal{P}_i + \mathcal{N}), \quad (12)$$

which holds if (10) holds because $\sum_{\ell_i=1}^2 \lambda_{\ell_i}(t) \varrho_{\ell_i, i} (\mathcal{P}_i + \mathcal{N}) \in \text{Conv}(\varrho_{\ell_i, i} (\mathcal{P}_i + \mathcal{N}))$, where ℓ_i denotes the i th element of $\ell \in \mathbb{L}$. \square

3. Θ_t -Dependent Stability Criterion

Based on a nonquadratic Lyapunov-Krasovskii functional (NLKF), this section provides a less conservative stability criterion. To this end, we first choose an NLKF of the following form:

$$\begin{aligned} V(t) &= V_1(t) + V_2(t) + V_3(t), \\ V_1(t) &= x^T(t) P(\Theta_t) x(t), \\ V_2(t) &= \int_{t-d_1}^t x^T(\alpha) Q_1(\Theta_\alpha) x(\alpha) d\alpha \\ &\quad + \int_{t-d_2}^t x^T(\alpha) Q_2(\Theta_\alpha) x(\alpha) d\alpha, \\ V_3(t) &= \int_{-d_1}^0 \int_{t+\alpha}^t \dot{x}^T(\beta) R_1(\Theta_\beta) \dot{x}(\beta) d\beta d\alpha \\ &\quad + \int_{-d_2}^{-d_1} \int_{t+\alpha}^t \dot{x}^T(\beta) R_2(\Theta_\beta) \dot{x}(\beta) d\beta d\alpha, \end{aligned} \quad (13)$$

where $P(\Theta_t)$, $Q_1(\Theta_\alpha)$, $Q_2(\Theta_\alpha)$, $R_1(\Theta_\beta)$, and $R_2(\Theta_\beta)$ are positive definite for all admissible grades. Then, the time

derivative of each $V_i(t)$ along the trajectories of (6) is given by

$$\begin{aligned} \dot{V}_1(t) &= \eta^T(t) \left(\text{He} \left(\mathbf{e}_1^T P(\Theta_t) \Phi_t \right) + \mathbf{e}_1^T \dot{P}(\Theta_t) \mathbf{e}_1 \right) \eta(t), \\ \dot{V}_2(t) &= \eta^T(t) \left(\mathbf{e}_1^T (Q_1(\Theta_t) + Q_2(\Theta_t)) \mathbf{e}_1 \right. \\ &\quad \left. - \mathbf{e}_2^T Q_1(\Theta_{t-d_1}) \mathbf{e}_2 - \mathbf{e}_4^T Q_2(\Theta_{t-d_2}) \mathbf{e}_4 \right) \eta(t), \\ \dot{V}_3(t) &= \eta^T(t) \left(d_1 \Phi_t^T R_1(\Theta_t) \Phi_t + \delta \Phi_t^T R_2(\Theta_t) \Phi_t \right) \\ &\quad \cdot \eta(t) - \int_{t-d_1}^t \dot{x}^T(\alpha) R_1(\Theta_\alpha) \dot{x}(\alpha) d\alpha \\ &\quad - \int_{t-d_2}^{t-d_1} \dot{x}^T(\alpha) R_2(\Theta_\alpha) \dot{x}(\alpha) d\alpha, \end{aligned} \quad (14)$$

which leads to

$$\dot{V}(t) = \eta^T(t) \Pi_1 \eta(t) + \mathcal{O}_1 + \mathcal{O}_2, \quad (15)$$

where

$$\begin{aligned} \Pi_1 &= \text{He} \left(\mathbf{e}_1^T P(\Theta_t) \Phi_t \right) \\ &\quad + \mathbf{e}_1^T \left(\dot{P}(\Theta_t) + Q_1(\Theta_t) + Q_2(\Theta_t) \right) \mathbf{e}_1 \\ &\quad - \mathbf{e}_2^T Q_1(\Theta_{t-d_1}) \mathbf{e}_2 - \mathbf{e}_4^T Q_2(\Theta_{t-d_2}) \mathbf{e}_4 \\ &\quad + d_1 \Phi_t^T R_1(\Theta_t) \Phi_t + \delta \Phi_t^T R_2(\Theta_t) \Phi_t, \\ \mathcal{O}_1 &= - \int_{t-d_1}^t \dot{x}^T(\alpha) R_1(\Theta_\alpha) \dot{x}(\alpha) d\alpha, \quad \delta = d_2 - d_1, \\ \mathcal{O}_2 &= - \int_{t-d_2}^{t-d_1} \dot{x}^T(\alpha_1) R_2(\Theta_{\alpha_1}) \dot{x}(\alpha_1) d\alpha_1 \\ &\quad - \int_{t-d(t)}^{t-d_1} \dot{x}^T(\alpha_2) R_2(\Theta_{\alpha_2}) \dot{x}(\alpha_2) d\alpha_2. \end{aligned} \quad (16)$$

Remark 4. Indeed, it is hard to directly use Jensen's inequality approach to obtain the upper bounds of \mathcal{O}_1 and \mathcal{O}_2 because $R_1(\Theta_\alpha)$ and $R_2(\Theta_\alpha)$ are set to be dependent on Θ_α , which motivates the present study.

Lemma 5. Suppose that there exist matrices $U_0(\Theta_t)$, $U_1(\Theta_t)$, and $U_2(\Theta_t) \in \mathbb{R}^{4n_x \times n_x}$ and symmetric matrices $0 < P(\Theta_t)$, $\dot{P}(\Theta_t)$, $0 < Q_1(\Theta_{t-d_1})$, $0 < Q_2(\Theta_{t-d_2})$, $0 < Q_1(\Theta_t)$, $0 < Q_2(\Theta_t)$, $0 < R_1(\Theta_\alpha)$, $0 < R_2(\Theta_{\alpha_p})$, $0 < R_1(\Theta_t)$, $0 < R_2(\Theta_t) \in \mathbb{R}^{n_x \times n_x}$, $M_0(\Theta_t)$, $M_1(\Theta_t)$, and $M_2(\Theta_t) \in \mathbb{R}^{4n_x \times 4n_x}$ such that

$$0 > \Pi_1 + \Pi_2 + \Gamma_p, \quad \forall p \in \mathbb{N}_2^+, \quad (17)$$

$$\begin{aligned} 0 &\leq \begin{bmatrix} M_0(\Theta_t) & U_0(\Theta_t) \\ (*) & R_1(\Theta_\alpha) \end{bmatrix}, \\ 0 &\leq \begin{bmatrix} M_p(\Theta_t) & U_p(\Theta_t) \\ (*) & R_2(\Theta_{\alpha_p}) \end{bmatrix}, \end{aligned} \quad (18)$$

$$\forall p \in \mathbb{N}_2^+,$$

where

$$\begin{aligned}
\Pi_1 &= \text{He} \left(\mathbf{e}_1^T P(\Theta_t) \Phi_t \right) + \mathbf{e}_1^T \left(\dot{P}(\Theta_t) + Q_1(\Theta_t) \right. \\
&\quad \left. + Q_2(\Theta_t) \right) \mathbf{e}_1 - \mathbf{e}_2^T Q_1(\Theta_{t-d_1}) \mathbf{e}_2 - \mathbf{e}_4^T Q_2(\Theta_{t-d_2}) \mathbf{e}_4 \\
&\quad + d_1 \Phi_t^T R_1(\Theta_t) \Phi_t + \delta \Phi_t^T R_2(\Theta_t) \Phi_t, \\
\Pi_2 &= \Psi_t^T \Psi_t - \mathbf{e}_5^T \mathbf{e}_5, \\
\Gamma_p &= \text{He} \left(\mathbf{e}_{14}^T U_0(\Theta_t) (\mathbf{e}_1 - \mathbf{e}_2) + \mathbf{e}_{14}^T U_1(\Theta_t) (\mathbf{e}_3 - \mathbf{e}_4) \right. \\
&\quad \left. + \mathbf{e}_{14}^T U_2(\Theta_t) (\mathbf{e}_2 - \mathbf{e}_3) \right) + d_1 \mathbf{e}_{14}^T M_0(\Theta_t) \mathbf{e}_{14} \\
&\quad + \delta \mathbf{e}_{14}^T M_p(\Theta_t) \mathbf{e}_{14}.
\end{aligned} \tag{19}$$

Then, (6) is robustly asymptotically stable for $d_1 \leq d(t) \leq d_2$.

Proof. First of all, by incorporating the following equalities into (15),

$$\begin{aligned}
0 &= \bar{x}^T(t) M_0(\Theta_t) \bar{x}(t) \left(d_1 - \int_{t-d_1}^t d\alpha \right), \\
0 &= \bar{x}^T(t) M_1(\Theta_t) \bar{x}(t) \left((d_2 - d(t)) - \int_{t-d_2}^{t-d(t)} d\alpha_1 \right), \\
0 &= \bar{x}^T(t) M_2(\Theta_t) \bar{x}(t) \left((d(t) - d_1) - \int_{t-d(t)}^{t-d_1} d\alpha_2 \right), \\
0 &= 2\bar{x}^T(t) U_0(\Theta_t) \left((\mathbf{e}_1 - \mathbf{e}_2) \eta(t) - \int_{t-d_1}^t \dot{x}(\alpha) d\alpha \right), \\
0 &= 2\bar{x}^T(t) U_1(\Theta_t) \\
&\quad \cdot \left((\mathbf{e}_3 - \mathbf{e}_4) \eta(t) - \int_{t-d_2}^{t-d(t)} \dot{x}(\alpha_1) d\alpha_1 \right), \\
0 &= 2\bar{x}^T(t) U_2(\Theta_t) \\
&\quad \cdot \left((\mathbf{e}_2 - \mathbf{e}_3) \eta(t) - \int_{t-d(t)}^{t-d_1} \dot{x}(\alpha_2) d\alpha_2 \right),
\end{aligned} \tag{20}$$

we can get

$$\dot{V}(t) = \eta^T(t) (\Pi_1 + \bar{\Gamma}_p) \eta(t) + \bar{\mathcal{O}}_1 + \bar{\mathcal{O}}_2, \tag{21}$$

where

$$\begin{aligned}
\bar{\Gamma}_p &= \text{He} \left(\mathbf{e}_{14}^T U_0(\Theta_t) (\mathbf{e}_1 - \mathbf{e}_2) + \mathbf{e}_{14}^T U_1(\Theta_t) (\mathbf{e}_3 - \mathbf{e}_4) \right. \\
&\quad \left. + \mathbf{e}_{14}^T U_2(\Theta_t) (\mathbf{e}_2 - \mathbf{e}_3) \right) + d_1 \mathbf{e}_{14}^T M_0(\Theta_t) \mathbf{e}_{14} \\
&\quad + \delta \mathbf{e}_{14}^T \left(\sum_{p=1}^2 \lambda_p(t) M_p(t) \right) \mathbf{e}_{14},
\end{aligned}$$

$$\begin{aligned}
\bar{\mathcal{O}}_1 &= - \int_{t-d_1}^t \left[\bar{x}(t) \right]^T \\
&\quad \cdot \begin{bmatrix} M_0(\Theta_t) & U_0(\Theta_t) \\ (*) & R_1(\Theta_{\alpha}) \end{bmatrix} \begin{bmatrix} \bar{x}(t) \\ \dot{x}(\alpha) \end{bmatrix} d\alpha,
\end{aligned}$$

$$\begin{aligned}
\bar{\mathcal{O}}_2 &= - \int_{t-d_2}^{t-d(t)} \left[\bar{x}(t) \right]^T \\
&\quad \cdot \begin{bmatrix} M_1(\Theta_t) & U_1(\Theta_t) \\ (*) & R_2(\Theta_{\alpha_1}) \end{bmatrix} \begin{bmatrix} \bar{x}(t) \\ \dot{x}(\alpha_1) \end{bmatrix} d\alpha_1 \\
&\quad - \int_{t-d(t)}^{t-d_1} \left[\bar{x}(t) \right]^T \\
&\quad \cdot \begin{bmatrix} M_2(\Theta_t) & U_2(\Theta_t) \\ (*) & R_2(\Theta_{\alpha_2}) \end{bmatrix} \begin{bmatrix} \bar{x}(t) \\ \dot{x}(\alpha_2) \end{bmatrix} d\alpha_2
\end{aligned} \tag{22}$$

in which $\lambda_1(t) = (d_2 - d(t))/(d_2 - d_1)$ and $\lambda_2(t) = (d(t) - d_1)/(d_2 - d_1)$. Next, the structured feedback uncertainty, given as $0 \leq q^T(t)q(t) - p^T(t)p(t)$, can be converted into $0 \leq \eta^T(t)(\Psi_t^T \Psi_t - \mathbf{e}_5^T \mathbf{e}_5)\eta(t)$, which yields $\dot{V}(t) \leq \eta^T(t)(\Pi_1 + \Pi_2 + \bar{\Gamma}_p)\eta(t) + \bar{\mathcal{O}}_1 + \bar{\mathcal{O}}_2$. That is, the robust stability for (6) is assured by $0 > \eta^T(t)(\Pi_1 + \Pi_2 + \bar{\Gamma}_p)\eta(t) + \bar{\mathcal{O}}_1 + \bar{\mathcal{O}}_2$. Therefore, if (18) holds, then $\bar{\mathcal{O}}_1 + \bar{\mathcal{O}}_2 \leq 0$, and hence the robust stability criterion is given by (17) because $\sum_{p=1}^2 \lambda_p(t) M_p(t) \in \text{Conv}(M_p(\Theta_t))$. \square

In the absence of uncertainties, the T-S fuzzy system becomes $\dot{x}(t) = \Phi_t \bar{x}(t)$, where $\Phi_t = A(\Theta_t)\mathbf{e}_1 + A_d(\Theta_t)\mathbf{e}_3$. The following corollary presents the stability criterion for nominal T-S fuzzy systems with time-varying delays.

Corollary 6. Suppose that there exist matrices $U_0(\Theta_t)$, $U_1(\Theta_t)$, and $U_2(\Theta_t) \in \mathbb{R}^{4n_x \times n_x}$ and symmetric matrices $0 < P(\Theta_t)$, $\dot{P}(\Theta_t)$, $0 < Q_1(\Theta_{t-d_1})$, $0 < Q_2(\Theta_{t-d_2})$, $0 < Q_1(\Theta_t)$, $0 < Q_2(\Theta_t)$, $0 < R_1(\Theta_{\alpha})$, $0 < R_2(\Theta_{\alpha_p})$, $0 < R_1(\Theta_t)$, $0 < R_2(\Theta_t) \in \mathbb{R}^{n_x \times n_x}$, $M_0(\Theta_t)$, $M_1(\Theta_t)$, and $M_2(\Theta_t) \in \mathbb{R}^{4n_x \times 4n_x}$ such that

$$\begin{aligned}
0 &> \Pi_1 + \Gamma_p, \quad \forall p \in \mathbb{N}_2^+, \\
0 &\leq \begin{bmatrix} M_0(\Theta_t) & U_0(\Theta_t) \\ (*) & R_1(\Theta_{\alpha}) \end{bmatrix}, \\
0 &\leq \begin{bmatrix} M_p(\Theta_t) & U_p(\Theta_t) \\ (*) & R_2(\Theta_{\alpha_p}) \end{bmatrix}, \\
&\quad \forall p \in \mathbb{N}_2^+,
\end{aligned} \tag{23}$$

where

$$\begin{aligned}
\Pi_1 &= \text{He} \left(\mathbf{e}_1^T P(\Theta_t) \Phi_t \right) + \mathbf{e}_1^T \left(\dot{P}(\Theta_t) + Q_1(\Theta_t) \right. \\
&\quad \left. + Q_2(\Theta_t) \right) \mathbf{e}_1 - \mathbf{e}_2^T Q_1(\Theta_{t-d_1}) \mathbf{e}_2 - \mathbf{e}_4^T Q_2(\Theta_{t-d_2}) \mathbf{e}_4 \\
&\quad + d_1 \Phi_t^T R_1(\Theta_t) \Phi_t + \delta \Phi_t^T R_2(\Theta_t) \Phi_t,
\end{aligned}$$

$$\begin{aligned}
\Gamma_p &= \text{He}(\mathbf{e}_{14}^T U_0(\Theta_t)(\mathbf{e}_1 - \mathbf{e}_2) + \mathbf{e}_{14}^T U_1(\Theta_t)(\mathbf{e}_3 - \mathbf{e}_4) \\
&\quad + \mathbf{e}_{14}^T U_2(\Theta_t)(\mathbf{e}_2 - \mathbf{e}_3)) + d_1 \mathbf{e}_{14}^T M_0(\Theta_t) \mathbf{e}_{14} \\
&\quad + \delta \mathbf{e}_{14}^T M_p(\Theta_t) \mathbf{e}_{14}.
\end{aligned} \tag{24}$$

Then, (6) without uncertainties is asymptotically stable for $d_1 \leq d(t) \leq d_2$.

Proof. The proof is omitted since it is analogous to the derivation of Lemma 5. \square

4. LMI-Based Stability Criterion

Based on Lemmas 2 and 3, to derive a finite number of solvable LMI conditions from (17), this paper simply sets all the decision variables to be of affine dependence on fuzzy-weighting functions:

$$\begin{aligned}
P(\Theta_t) &= \sum_{i=1}^r \theta_i P_i, \\
\dot{P}(\Theta_t) &= \sum_{i=1}^r \dot{\theta}_i P_i,
\end{aligned} \tag{25}$$

$$\begin{aligned}
Q_1(\Theta_t) &= \sum_{i=1}^r \theta_i Q_{1,i}, \\
Q_2(\Theta_t) &= \sum_{i=1}^r \theta_i Q_{2,i}, \\
Q_1(\Theta_{t-d_1}) &= \sum_{q=1}^r \theta_q^{d_1} Q_{1,q}, \\
Q_2(\Theta_{t-d_2}) &= \sum_{\phi=1}^r \theta_\phi^{d_2} Q_{2,\phi},
\end{aligned} \tag{26}$$

$$\begin{aligned}
R_1(\Theta_t) &= \sum_{i=1}^r \theta_i R_{1,i}, \\
R_2(\Theta_t) &= \sum_{i=1}^r \theta_i R_{2,i}, \\
R_1(\Theta_\alpha) &= \sum_{i=1}^r \theta_i^\alpha R_{1,i}, \\
R_2(\Theta_{\alpha_p}) &= \sum_{i=1}^r \theta_i^{\alpha_p} R_{2,i}, \\
U_0(\Theta_t) &= \sum_{i=1}^r \theta_i U_{0,i}, \\
U_1(\Theta_t) &= \sum_{i=1}^r \theta_i U_{1,i},
\end{aligned} \tag{27}$$

$$U_2(\Theta_t) = \sum_{i=1}^r \theta_i U_{2,i},$$

$$M_0(\Theta_t) = \sum_{i=1}^r \theta_i M_{0,i},$$

$$M_1(\Theta_t) = \sum_{i=1}^r \theta_i M_{1,i},$$

$$M_2(\Theta_t) = \sum_{i=1}^r \theta_i M_{2,i}.$$

(28)

Remark 7. As a way to improve the performance to be considered, we can increase the degree of polynomial dependence on fuzzy-weighting functions, as in [31–33] but this is outside of the intended scope of this paper.

Theorem 8. Let $\dot{\Theta}_t \in \mathbb{S}_{\dot{\Theta}}$ be satisfied. Suppose that there exist matrices $U_{0,i}, U_{1,i}, U_{2,i} \in \mathbb{R}^{4n_x \times n_x}$ and $S_0, S_i, X_i \in \mathbb{R}^{n_c \times n_c}$ ($n_c = 6n_x + n_p + n_q$), for $i \in \mathbb{N}_r^+$, symmetric matrices $N, 0 < P_i, 0 < Q_{1,i}, 0 < Q_{2,i}, 0 < R_{1,i}$, and $0 < R_{2,i} \in \mathbb{R}^{n_x \times n_x}$, for $i \in \mathbb{N}_r^+$, and $M_{0,i}, M_{1,i}, M_{2,i} \in \mathbb{R}^{4n_x \times 4n_x}$ such that, for all $q, \phi \in \mathbb{N}_r^+$, $p \in \mathbb{N}_2^+$, and $\ell \in \mathbb{L}$,

$$0 > \left[\begin{array}{c|c} \mathcal{L}_{\ell q \phi, 0} & [\mathcal{L}_{p,i}]_r \\ (*) & [\mathcal{L}_{ij}]_{r \times r} \end{array} \right], \tag{29}$$

$$\begin{aligned}
0 &< X_q + X_q^T, \\
0 &\leq \left[\begin{array}{cc} M_{0,\phi} & U_{0,\phi} \\ (*) & R_{1,q} \end{array} \right], \\
0 &\leq \left[\begin{array}{cc} M_{p,\phi} & U_{p,\phi} \\ (*) & R_{2,q} \end{array} \right],
\end{aligned} \tag{30}$$

where $\mathcal{L}_{\ell q \phi, 0} = \mathcal{M}_{\ell q \phi, 0} + \text{He}(S_0 - \sum_{i=1}^r \alpha_i \beta_i X_i)$, $\mathcal{L}_{p,i} = \mathcal{M}_{p,i} + S_i - S_0 + (\alpha_i + \beta_i) X_i$, $\mathcal{L}_{ii} = \mathcal{M}_{ii} + \text{He}(-S_i - X_i)$, and $\mathcal{L}_{ij} = \mathcal{M}_{ij} - S_i - S_j$ in which

$$\mathcal{M}_{\ell q \phi, 0} = \text{diag}(-I, 0, 0, (4, 4)_{\ell q \phi, 0}), \tag{31}$$

$$\mathcal{M}_{p,i} = \left[\begin{array}{cccc} 0 & 0 & 0 & (1, 4)_i \\ 0 & -\frac{1}{2} \delta R_{2,i} & 0 & 0 \\ 0 & 0 & -\frac{1}{2} d_1 R_{1,i} & 0 \\ 0 & 0 & 0 & (4, 4)_{p,i} \end{array} \right], \tag{32}$$

$$\mathcal{M}_{ii} = \left[\begin{array}{cccc} 0 & 0 & 0 & 0 \\ 0 & 0 & 0 & (2, 4)_{ii} \\ 0 & 0 & 0 & (3, 4)_{ii} \\ 0 & (*) & (*) & \text{He}((4, 4)_{ii}) \end{array} \right],$$

$$\mathcal{M}_{ij} = \begin{bmatrix} 0 & 0 & 0 & 0 \\ 0 & 0 & 0 & (2,4)_{ij} + (2,4)_{ji} \\ 0 & 0 & 0 & (3,4)_{ij} + (3,4)_{ji} \\ 0 & 0 & 0 & (4,4)_{ij} + (4,4)_{ji} \end{bmatrix}, \quad (33)$$

$$\begin{aligned} (4,4)_{\ell q\phi,0} &= \mathbf{e}_1^T \left(\sum_{i=1}^r \varrho_{\ell,i} (P_i + N) \right) \mathbf{e}_1 - \mathbf{e}_2^T Q_{1,q} \mathbf{e}_2 \\ &\quad - \mathbf{e}_4^T Q_{2,\phi} \mathbf{e}_4 - \mathbf{e}_5^T \mathbf{e}_5, \\ (1,4)_i &= G_i \mathbf{e}_1 + G_{d,i} \mathbf{e}_3, \\ (4,4)_{p,i} &= \mathbf{e}_1^T \left(\frac{1}{2} Q_{1,i} + \frac{1}{2} Q_{2,i} \right) \mathbf{e}_1 + \Gamma_{p,i}, \\ (2,4)_{ij} &= \delta (R_{2,j} A_i \mathbf{e}_1 + R_{2,j} A_{d,i} \mathbf{e}_3 + R_{2,j} E_i \mathbf{e}_5), \\ (3,4)_{ij} &= d_1 (R_{1,j} A_i \mathbf{e}_1 + R_{1,j} A_{d,i} \mathbf{e}_3 + R_{1,j} E_i \mathbf{e}_5), \\ (4,4)_{ij} &= \mathbf{e}_1^T P_j A_i \mathbf{e}_1 + \mathbf{e}_1^T P_j A_{d,i} \mathbf{e}_3 + \mathbf{e}_1^T P_j E_i \mathbf{e}_5, \\ \Gamma_{p,i} &= \mathbf{e}_{14}^T U_{0,i} (\mathbf{e}_1 - \mathbf{e}_2) + \mathbf{e}_{14}^T U_{1,i} (\mathbf{e}_3 - \mathbf{e}_4) \\ &\quad + \mathbf{e}_{14}^T U_{2,i} (\mathbf{e}_2 - \mathbf{e}_3) + \frac{1}{2} d_1 \mathbf{e}_{14}^T M_{0,i} \mathbf{e}_{14} \\ &\quad + \frac{1}{2} \delta \mathbf{e}_{14}^T M_{p,i} \mathbf{e}_{14}. \end{aligned} \quad (34)$$

Then, the system in (6) is robustly asymptotically stable for $d_1 \leq d(t) \leq d_2$.

Proof. Note that $\dot{\Theta}_t \in \mathbb{S}_{\Theta}$. Thus, in view of Lemma 3, applying the Schur complement to (17) is given by

$$0 > \begin{bmatrix} -I & 0 & 0 & \Psi_t \\ 0 & -\delta R_2(\Theta_t) & 0 & \delta R_2(\Theta_t) \Phi_t \\ 0 & 0 & -d_1 R_1(\Theta_t) & d_1 R_1(\Theta_t) \Phi_t \\ (*) & (*) & (*) & \Omega_\ell + \Gamma_p \end{bmatrix}, \quad (35)$$

$\forall p \in \mathbb{N}_2^+, \ell \in \mathbb{L},$

where $\Omega_\ell = \text{He}(\mathbf{e}_1^T P(\Theta_t) \Phi_t) - \mathbf{e}_2^T Q_1(\Theta_t) \mathbf{e}_2 - \mathbf{e}_4^T Q_2(\Theta_t) \mathbf{e}_4 - \mathbf{e}_5^T \mathbf{e}_5 + \mathbf{e}_1^T (\sum_{i=1}^r \varrho_{\ell,i} (P_i + N) + Q_1(\Theta_t) + Q_2(\Theta_t)) \mathbf{e}_1$. Further, from (26) and (27), (35) and (18) can be converted into

$$\begin{aligned} 0 &> \sum_{q=1}^r \sum_{\phi=1}^r \theta_q^{d_1} \theta_\phi^{d_2} \mathcal{M}_{p,\ell q\phi}(\Theta_t) \in \mathbb{R}^{n_c \times n_c}, \\ &\quad \forall p \in \mathbb{N}_2^+, \ell \in \mathbb{L}, \\ 0 &\leq \sum_{\phi=1}^r \sum_{q=1}^r \theta_\phi \theta_q^\alpha \begin{bmatrix} M_{0,\phi} & U_{0,\phi} \\ (*) & R_{1,q} \end{bmatrix}, \\ 0 &\leq \sum_{\phi=1}^r \sum_{q=1}^r \theta_\phi \theta_q^{\alpha_p} \begin{bmatrix} M_{p,\phi} & U_{p,\phi} \\ (*) & R_{2,q} \end{bmatrix}, \end{aligned} \quad (36)$$

where

$$\begin{aligned} &\mathcal{M}_{p,\ell q\phi}(\Theta_t) \\ &= \begin{bmatrix} -I & 0 & 0 & \Psi_t \\ 0 & -\delta R_2(\Theta_t) & 0 & \delta R_2(\Theta_t) \Phi_t \\ 0 & 0 & -d_1 R_1(\Theta_t) & d_1 R_1(\Theta_t) \Phi_t \\ (*) & (*) & (*) & \Omega_{\ell q\phi} + \Gamma_p \end{bmatrix}, \end{aligned} \quad (37)$$

$\Omega_{\ell q\phi}$

$$\begin{aligned} &= \text{He}(\mathbf{e}_1^T P(\Theta_t) \Phi_t) - \mathbf{e}_2^T Q_{1,q} \mathbf{e}_2 - \mathbf{e}_4^T Q_{2,\phi} \mathbf{e}_4 - \mathbf{e}_5^T \mathbf{e}_5 \\ &\quad + \mathbf{e}_1^T \left(\sum_{i=1}^r \varrho_{\ell,i} (P_i + N) + Q_1(\Theta_t) + Q_2(\Theta_t) \right) \mathbf{e}_1. \end{aligned}$$

As a result, from the convexity of fuzzy-weighting functions, (17) and (18) can be assured by (30),

$$0 > \mathcal{M}_{p,\ell q\phi}(\Theta_t), \quad \forall q, \phi \in \mathbb{N}_r^+, p \in \mathbb{N}_2^+, \ell \in \mathbb{L}. \quad (38)$$

Further, note that representing (38) in the form of (7) becomes

$$\begin{aligned} 0 &> \mathcal{M}_{\ell q\phi,0} + \sum_{i=1}^r \theta_i \text{He}(\mathcal{M}_{p,i}) + \sum_{i=1}^r \theta_i^2 \mathcal{M}_{ii} \\ &\quad + \sum_{i=1}^r \left(\sum_{j=i+1}^r \theta_i \theta_j \mathcal{M}_{ij} + \sum_{j=1}^{i-1} \theta_i \theta_j \mathcal{M}_{ji}^T \right), \end{aligned} \quad (39)$$

where $\mathcal{M}_{\ell q\phi,0}$, $\mathcal{M}_{p,i}$, \mathcal{M}_{ii} , and \mathcal{M}_{ij} are defined in (31)–(33). Therefore, from Lemma 2, we can obtain (29) in the sequel without loss of generality. \square

The following corollary presents the LMI-based stability criterion for nominal T-S fuzzy systems with time-varying delays.

Corollary 9. Let $\dot{\Theta}_t \in \mathbb{S}_{\Theta}$ be satisfied. Suppose that there exist matrices $U_{0,i}, U_{1,i}, U_{2,i} \in \mathbb{R}^{4n_x \times n_x}$ and $S_0, S_i, X_i \in \mathbb{R}^{n_c \times n_c}$ ($n_c = 6n_x$), for $i \in \mathbb{N}_r^+$, symmetric matrices $N, 0 < P_i, 0 < Q_{1,i}, 0 < Q_{2,i}, 0 < R_{1,i}$, and $0 < R_{2,i} \in \mathbb{R}^{n_x \times n_x}$, for $i \in \mathbb{N}_r^+$, and $M_{0,i}, M_{1,i}, M_{2,i} \in \mathbb{R}^{4n_x \times 4n_x}$ such that, for all $q, \phi \in \mathbb{N}_r^+, p \in \mathbb{N}_2^+$, and $\ell \in \mathbb{L}$,

$$\begin{aligned} 0 &> \begin{bmatrix} \mathcal{L}_{\ell q\phi,0} & \left[\mathcal{L}_{p,i} \right]_r \\ (*) & \left[\mathcal{L}_{ij} \right]_{r \times r} \end{bmatrix}, \\ 0 &< X_q + X_q^T, \\ 0 &\leq \begin{bmatrix} M_{0,\phi} & U_{0,\phi} \\ (*) & R_{1,q} \end{bmatrix}, \\ 0 &\leq \begin{bmatrix} M_{p,\phi} & U_{p,\phi} \\ (*) & R_{2,q} \end{bmatrix}, \end{aligned} \quad (40)$$

where $\mathcal{L}_{\ell p\phi,0} = \mathcal{M}_{\ell p\phi,0} + \text{He}(S_0 - \sum_{i=1}^r \alpha_i \beta_i X_i)$, $\mathcal{L}_{p,i} = \mathcal{M}_{p,i} + S_i - S_0 + (\alpha_i + \beta_i)X_i$, $\mathcal{L}_{ii} = \mathcal{M}_{ii} + \text{He}(-S_i - X_i)$, and $\mathcal{L}_{ij} = \mathcal{M}_{ij} - S_i - S_j$ in which

$$\begin{aligned}
 \mathcal{M}_{\ell p\phi,0} &= \text{diag}(0, 0, (3, 3)_{\ell p\phi,0}), \\
 \mathcal{M}_{p,i} &= \begin{bmatrix} -\frac{1}{2}\delta R_{2,i} & 0 & 0 \\ 0 & -\frac{1}{2}d_1 R_{1,i} & 0 \\ 0 & 0 & (3, 3)_{p,i} \end{bmatrix}, \\
 \mathcal{M}_{ii} &= \begin{bmatrix} 0 & 0 & (1, 3)_{ii} \\ 0 & 0 & (2, 3)_{ii} \\ (*) & (*) & \text{He}((3, 3)_{ii}) \end{bmatrix}, \\
 \mathcal{M}_{ij} &= \begin{bmatrix} 0 & 0 & (1, 3)_{ij} + (1, 3)_{ji} \\ 0 & 0 & (2, 3)_{ij} + (2, 3)_{ji} \\ 0 & 0 & (3, 3)_{ij} + (3, 3)_{ji} \end{bmatrix}, \\
 (3, 3)_{\ell q\phi,0} &= \mathbf{e}_1^T \left(\sum_{i=1}^r \mathcal{Q}_{\ell,i} (P_i + N) \right) \mathbf{e}_1 - \mathbf{e}_2^T Q_{1,q} \mathbf{e}_2 \\
 &\quad - \mathbf{e}_4^T Q_{2,\phi} \mathbf{e}_4, \\
 (3, 3)_{p,i} &= \mathbf{e}_1^T \left(\frac{1}{2} Q_{1,i} + \frac{1}{2} Q_{2,i} \right) \mathbf{e}_1 + \Gamma_{p,i}, \\
 (1, 3)_{ij} &= \delta (R_{2,j} A_i \mathbf{e}_1 + R_{2,j} A_{d,i} \mathbf{e}_3), \\
 (2, 3)_{ij} &= d_1 (R_{1,j} A_i \mathbf{e}_1 + R_{1,j} A_{d,i} \mathbf{e}_3), \\
 (3, 3)_{ij} &= \mathbf{e}_1^T P_j A_i \mathbf{e}_1 + \mathbf{e}_1^T P_j A_{d,i} \mathbf{e}_3, \\
 \Gamma_{p,i} &= \mathbf{e}_{14}^T U_{0,i} (\mathbf{e}_1 - \mathbf{e}_2) + \mathbf{e}_{14}^T U_{1,i} (\mathbf{e}_3 - \mathbf{e}_4) \\
 &\quad + \mathbf{e}_{14}^T U_{2,i} (\mathbf{e}_2 - \mathbf{e}_3) + \frac{1}{2} d_1 \mathbf{e}_{14}^T M_{0,i} \mathbf{e}_{14} \\
 &\quad + \frac{1}{2} \delta \mathbf{e}_{14}^T M_{p,i} \mathbf{e}_{14}.
 \end{aligned} \tag{41}$$

Then, (6) without uncertainties is asymptotically stable for $d_1 \leq d(t) \leq d_2$.

Proof. The proof is omitted since it is analogous to the derivation of Theorem 8. \square

Remark 10. The number of scalar variables involved in Theorem 8 and Corollary 9 is given as follows: $\# = n_c^2(2r+1) + 0.5n_x(n_x+1) + n_x(38.5n_x+8.5)r$. Table 1 shows the number for each case of (n_x, r) . Since the use of slack variables requires more computation cost compared with other methods, there may be the need to balance the tradeoffs between the computational cost and the performance enhancement.

5. Numerical Examples

To verify the effectiveness of our methods, this paper provides two examples that make some comparisons with other results: one is related to the stability analysis for nominal T-S fuzzy systems and the other is related to the robust stability analysis for T-S fuzzy systems with uncertainties.

Example 1. Consider the following T-S fuzzy system, adopted in [25]:

$$\begin{aligned}
 A_1 &= \begin{bmatrix} -2 & 0 \\ 0 & -0.9 \end{bmatrix}, \\
 A_2 &= \begin{bmatrix} -1 & 0.5 \\ 0 & -1 \end{bmatrix}, \\
 A_{d,1} &= \begin{bmatrix} -1 & 0 \\ -1 & -1 \end{bmatrix}, \\
 A_{d,2} &= \begin{bmatrix} -1 & 0 \\ 0.1 & -1 \end{bmatrix},
 \end{aligned} \tag{42}$$

where $\theta_1 = 1/(1 + \exp(-2x_1(t)))$ and $\theta_2 = 1 - \theta_1$. Table 2 shows the maximum allowable upper bound (MAUB) for each $d_1 \in \{0.0, 0.4, 0.8, 1.0, 1.2\}$, where m denotes the number of delay segments and $(m-1)$ denotes the degree of delay partitioning. From Table 2, we can see that our method (Corollary 9) provides larger MAUBs in comparison with those of [25, 26]. Hence it can be concluded that the stability criterion in Corollary 9, obtained based on the NLKF, is less conservative than other results. In particular, for $d_1 = 1.2$ and $d_2 = 1.531$, Corollary 9 offers the following solutions:

$$\begin{aligned}
 P_1 &= 10^{-2} \begin{bmatrix} 1.485 & -0.227 \\ -0.227 & 0.368 \end{bmatrix}, \\
 P_2 &= 10^{-2} \begin{bmatrix} 1.078 & -0.290 \\ -0.290 & 0.799 \end{bmatrix}, \\
 Q_{1,1} &= 10^{-3} \begin{bmatrix} 3.315 & 0.253 \\ 0.253 & 0.785 \end{bmatrix}, \\
 Q_{1,2} &= 10^{-3} \begin{bmatrix} 3.082 & 0.163 \\ 0.163 & 0.930 \end{bmatrix}, \\
 Q_{2,1} &= 10^{-3} \begin{bmatrix} 5.607 & 0.254 \\ 0.254 & 3.137 \end{bmatrix}, \\
 Q_{2,2} &= 10^{-3} \begin{bmatrix} 5.708 & -0.001 \\ -0.001 & 3.323 \end{bmatrix}, \\
 R_{1,1} &= 10^{-3} \begin{bmatrix} 4.661 & -0.847 \\ -0.847 & 1.669 \end{bmatrix}, \\
 R_{1,2} &= 10^{-3} \begin{bmatrix} 4.647 & -0.813 \\ -0.813 & 1.671 \end{bmatrix},
 \end{aligned}$$

TABLE 1: # involved in Corollary 9 and Theorem 8 ($n_p = 1, n_q = 1$).

| (n_x, r) | (2, 2) | (2, 3) | (2, 4) | (3, 2) | (3, 3) | (3, 4) | (4, 2) | (4, 3) | (4, 4) |
|-------------|--------|--------|--------|--------|--------|--------|--------|--------|--------|
| Corollary 9 | 1065 | 1524 | 1983 | 2370 | 3390 | 4410 | 4190 | 5992 | 7794 |
| Theorem 8 | 1325 | 1888 | 2451 | 2750 | 3922 | 5094 | 4690 | 6692 | 8694 |

TABLE 2: Maximum allowable upper bound (MAUB) for each d_1 , where m denotes the number of delay segments and $(m - 1)$ denotes the degree of delay partitioning.

| d_1 | 0.0 | 0.4 | 0.8 | 1.0 | 1.2 | $(m - 1)$ |
|-------------|-------|-------|-------|-------|-------|-----------|
| [25] | 0.982 | 1.038 | 1.158 | 1.252 | 1.359 | 0 |
| [26] | 1.221 | 1.277 | 1.311 | 1.358 | 1.419 | 1 |
| [26] | 1.278 | 1.303 | 1.316 | 1.361 | 1.425 | 2 |
| Corollary 9 | 1.302 | 1.380 | 1.413 | 1.462 | 1.531 | 0 |

TABLE 3: Maximum allowable upper bound (MAUB) for $d_1 = 0$.

| Methods | [27] | [28] | [29] | [30] | Theorem 8 |
|---------|------|-------|-------|-------|-----------|
| d_2 | — | 0.443 | 0.499 | 1.081 | 1.132 |

$$R_{2,1} = 10^{-3} \begin{bmatrix} 7.232 & -1.319 \\ -1.319 & 2.747 \end{bmatrix},$$

$$R_{2,2} = 10^{-3} \begin{bmatrix} 6.538 & -0.704 \\ -0.704 & 2.583 \end{bmatrix}.$$

(43)

$$G_{d1} = \begin{bmatrix} 0.1 & 0 \\ 0 & 0.3 \end{bmatrix},$$

$$G_{d2} = \begin{bmatrix} 0.1 & 0 \\ 0 & 0.3 \end{bmatrix},$$

(44)

where

$$\theta_1 = \left(1 - \frac{1}{1 + \exp(-6(x_2 - \pi/4))} \right) \times \left(\frac{1}{1 + \exp(-6(x_2 + \pi/4))} \right), \quad (45)$$

$$\theta_2 = 1 - \theta_1.$$

The maximum allowable upper bound (MAUB) for each method is tabulated in Table 3. And, from Table 3, we can see that the proposed method (Theorem 8) achieves larger MAUBs than those of other methods [27–30]. Hence, it can be concluded that the robust stability criterion in Theorem 8, established from the NLKF approach and Lemma 2, is less conservative than those of [27–30].

6. Concluding Remarks

This paper proposed an NLKF-based method of deriving a less conservative stability criterion for T-S fuzzy systems with time-varying delays. Of course, the proposed method may increase the burden of numerical computation. However, if the computational complexity is out of the practical problem, then our results can be significantly useful.

Competing Interests

The author declares that there is no conflict of interests regarding the publication of this paper.

Example 2. Consider the following T-S fuzzy system:

$$A_1 = \begin{bmatrix} -2 & 1 \\ 0.5 & -1 \end{bmatrix},$$

$$A_2 = \begin{bmatrix} -2 & 0 \\ 0 & -1 \end{bmatrix},$$

$$A_{d1} = \begin{bmatrix} -1 & 0 \\ -1 & -1 \end{bmatrix},$$

$$A_{d2} = \begin{bmatrix} -1.6 & 0 \\ 0 & -1 \end{bmatrix},$$

$$E_1 = \begin{bmatrix} 0.03 & 0 \\ 0 & -0.03 \end{bmatrix},$$

$$E_2 = \begin{bmatrix} 0.03 & 0 \\ 0 & -0.03 \end{bmatrix},$$

$$G_1 = \begin{bmatrix} 1.6 & 0 \\ 0 & 0.05 \end{bmatrix},$$

$$G_2 = \begin{bmatrix} 1.6 & 0 \\ 0 & -0.05 \end{bmatrix},$$

Acknowledgments

This work was supported by the National Research Foundation of Korea Grant funded by the Korean Government (NRF-2015R1A1A1A05001131).

References

- [1] T. Takagi and M. Sugeno, "Fuzzy identification of systems and its applications to modeling and control," *IEEE Transactions on Systems, Man and Cybernetics*, vol. 15, no. 1, pp. 116–132, 1985.
- [2] G. Feng, "A survey on analysis and design of model-based fuzzy control systems," *IEEE Transactions on Fuzzy Systems*, vol. 14, no. 5, pp. 676–697, 2006.
- [3] J. Cheng, H. Wang, S. Chen, Z. Liu, and J. Yang, "Robust delay-derivative-dependent state-feedback control for a class of continuous-time system with time-varying delays," *Neurocomputing*, vol. 173, pp. 827–834, 2016.
- [4] Y. Ren, Z. Feng, and G. Sun, "Improved stability conditions for uncertain neutral-type systems with time-varying delays," *International Journal of Systems Science*, vol. 47, no. 8, pp. 1982–1993, 2016.
- [5] S. H. Kim, "Relaxed inequality approach to robust H_∞ stability analysis of discrete-time systems with time-varying delay," *IET Control Theory & Applications*, vol. 6, no. 13, pp. 2149–2156, 2012.
- [6] C.-H. Lien and K.-W. Yu, "Robust control for Takagi-Sugeno fuzzy systems with time-varying state and input delays," *Chaos, Solitons and Fractals*, vol. 35, no. 5, pp. 1003–1008, 2008.
- [7] C. Peng, D. Yue, and Y.-C. Tian, "New approach on robust delay-dependent H_∞ control for uncertain T-S fuzzy systems with interval time-varying delay," *IEEE Transactions on Fuzzy Systems*, vol. 17, no. 4, pp. 890–900, 2009.
- [8] K.-W. Yu and C.-H. Lien, "Robust H_∞ control for uncertain T-S fuzzy systems with state and input delays," *Chaos, Solitons and Fractals*, vol. 37, no. 1, pp. 150–156, 2008.
- [9] L. Li and X. Liu, "New results on delay-dependent robust stability criteria of uncertain fuzzy systems with state and input delays," *Information Sciences*, vol. 179, no. 8, pp. 1134–1148, 2009.
- [10] W.-J. Chang, C.-C. Ku, and Z.-G. Fu, "Robust and passive constrained fuzzy control for discrete fuzzy systems with multiplicative noises and interval time delay," *Mathematical Problems in Engineering*, vol. 2013, Article ID 159279, 12 pages, 2013.
- [11] S. Ahmad, R. Majeed, K.-S. Hong, and M. Rehan, "Observer design for one-sided Lipschitz nonlinear systems subject to measurement delays," *Mathematical Problems in Engineering*, vol. 2015, Article ID 879492, 13 pages, 2015.
- [12] L. Li and X. Liu, "New approach on robust stability for uncertain T-S fuzzy systems with state and input delays," *Chaos, Solitons & Fractals*, vol. 40, no. 5, pp. 2329–2339, 2009.
- [13] P. G. Park, J. W. Ko, and C. Jeong, "Reciprocally convex approach to stability of systems with time-varying delays," *Automatica*, vol. 47, no. 1, pp. 235–238, 2011.
- [14] Y. S. Moon, P. Park, W. H. Kwon, and Y. S. Lee, "Delay-dependent robust stabilization of uncertain state-delayed systems," *International Journal of Control*, vol. 74, no. 14, pp. 1447–1455, 2001.
- [15] Y. S. Lee, W. H. Kwon, and P. G. Park, "Authors reply: comments on delay-dependent robust H_∞ control for uncertain systems with a state-delay," *Automatica*, vol. 43, no. 3, pp. 572–573, 2007.
- [16] Z. Yang and Y.-P. Yang, "New delay-dependent stability analysis and synthesis of T-S fuzzy systems with time-varying delay," *International Journal of Robust and Nonlinear Control*, vol. 20, no. 3, pp. 313–322, 2010.
- [17] D. H. Lee, J. B. Park, and Y. H. Joo, "A new fuzzy lyapunov function for relaxed stability condition of continuous-time takagi-sugeno fuzzy systems," *IEEE Transactions on Fuzzy Systems*, vol. 19, no. 4, pp. 785–791, 2011.
- [18] L. A. Mozelli, R. M. Palhares, F. O. Souza, and E. M. A. M. Mendes, "Reducing conservativeness in recent stability conditions of T-S fuzzy systems," *Automatica*, vol. 45, no. 6, pp. 1580–1583, 2009.
- [19] T. M. Guerra and L. Vermeiren, "LMI-based relaxed nonquadratic stabilization conditions for nonlinear systems in the Takagi-Sugeno's form," *Automatica*, vol. 40, no. 5, pp. 823–829, 2004.
- [20] S. Zhou, J. Lam, and W. X. Zheng, "Control design for fuzzy systems based on relaxed nonquadratic stability and H_∞ performance conditions," *IEEE Transactions on Fuzzy Systems*, vol. 15, no. 2, pp. 188–199, 2007.
- [21] S. H. Kim, "Relaxation technique for a T-S fuzzy control design based on a continuous-time fuzzy weighting-dependent lyapunov function," *IEEE Transactions on Fuzzy Systems*, vol. 21, no. 4, pp. 761–766, 2013.
- [22] S. H. Kim and P. Park, "Relaxed H_∞ stabilization conditions for discrete-time fuzzy systems with interval time-varying delays," *IEEE Transactions on Fuzzy Systems*, vol. 17, no. 6, pp. 1441–1449, 2009.
- [23] S. H. Kim, "Robust stability analysis of T-S fuzzy systems with interval time-varying delays via a relaxation technique," in *Proceedings of the 8th IEEE International Conference on Automation Science and Engineering*, pp. 829–832, Seoul, Korea, August 2012.
- [24] K. Gu, "An integral inequality in the stability problem of time-delay systems," in *Proceedings of the 39th IEEE Conference on Decision and Control*, pp. 2805–2810, Sydney, Australia, December 2000.
- [25] L. Li, X. Liu, and T. Chai, "New approaches on H_∞ control of T-S fuzzy systems with interval time-varying delay," *Fuzzy Sets and Systems*, vol. 160, no. 12, pp. 1669–1688, 2009.
- [26] J. An and G. Wen, "Improved stability criteria for time-varying delayed T-S fuzzy systems via delay partitioning approach," *Fuzzy Sets and Systems*, vol. 185, no. 1, pp. 83–94, 2011.
- [27] C. G. Li, H. J. Wang, and X. F. Liao, "Delay-dependent robust stability of uncertain fuzzy systems with time-varying delays," *IEE Proceedings—Control Theory and Applications*, vol. 151, no. 4, pp. 417–421, 2004.
- [28] C.-H. Lien, "Further results on delay-dependent robust stability of uncertain fuzzy systems with time-varying delay," *Chaos, Solitons & Fractals*, vol. 28, no. 2, pp. 422–427, 2006.
- [29] C. H. Lien, K. W. Yu, W. D. Chen, Z. L. Wan, and Y. J. Chung, "Stability criteria for uncertain Takagi-Sugeno fuzzy systems with interval time-varying delay," *IET Control Theory and Applications*, vol. 1, no. 3, pp. 764–769, 2007.
- [30] F. Liu, M. Wu, Y. He, and R. Yokoyama, "New delay-dependent stability criteria for T-S fuzzy systems with time-varying delay," *Fuzzy Sets and Systems*, vol. 161, no. 15, pp. 2033–2042, 2010.
- [31] A. Sala and C. Ariño, "Relaxed stability and performance conditions for Takagi-Sugeno fuzzy systems with knowledge on membership-function overlap," *IEEE Transactions on Systems, Man, and Cybernetics, Part B: Cybernetics*, vol. 37, no. 3, pp. 727–732, 2007.

- [32] S. H. Kim and P. Park, " H_∞ state-feedback-control design for discrete-time fuzzy systems using relaxation technique for parameterized LMI," *IEEE Transactions on Fuzzy Systems*, vol. 18, no. 5, pp. 985–993, 2010.
- [33] M. Bernal, A. Sala, A. Jaadari, and T.-M. Guerra, "Stability analysis of polynomial fuzzy models via polynomial fuzzy Lyapunov functions," *Fuzzy Sets and Systems*, vol. 185, no. 1, pp. 5–14, 2011.

Research Article

Fixed Points and Exponential Stability for Impulsive Time-Delays BAM Neural Networks via LMI Approach and Contraction Mapping Principle

Ruofeng Rao,¹ Zhilin Pu,^{1,2} Shouming Zhong,^{1,3} and Xingui Li^{1,3}

¹Department of Mathematics, Chengdu Normal University, Chengdu, Sichuan 611130, China

²Institute of Mathematics, Chengdu Normal University, Chengdu, Sichuan 611130, China

³Institute of Mathematical Education, Chengdu Normal University, Chengdu, Sichuan 611130, China

Correspondence should be addressed to Ruofeng Rao; ruofengrao@163.com

Received 12 August 2016; Revised 24 September 2016; Accepted 29 September 2016

Academic Editor: Quanmin Zhu

Copyright © 2016 Ruofeng Rao et al. This is an open access article distributed under the Creative Commons Attribution License, which permits unrestricted use, distribution, and reproduction in any medium, provided the original work is properly cited.

The fixed point technique has been employed in the stability analysis of time-delays bidirectional associative memory (BAM) neural networks with impulse. By formulating a contraction mapping in a product space, a new LMI-based exponential stability criterion was derived. Lately, fixed point methods have achieved various good results inspiring this work, but those criteria cannot be programmed by a computer. In this paper, LMI conditions of the obtained result can be applicable to computer Matlab LMI toolbox which meets the need of the large-scale calculation in real engineering. Moreover, a numerical example and a comparable table are presented to illustrate the effectiveness of the proposed methods.

1. Introduction

Bidirectional associative memory (BAM) neural networks model was originally introduced by Kosko [1, 2]:

$$\begin{aligned}\dot{x}_i &= -a_i x_i(t) + \sum_{j=1}^p w_{ji} g_j(y_j(t)) + I_i, \quad i = 1, 2, \dots, n, \\ \dot{y}_j &= -b_j y_j(t) + \sum_{i=1}^n v_{ij} g_i(x_i(t)) + J_j, \quad j = 1, 2, \dots, n.\end{aligned}\tag{1}$$

Thanks to its generalization of the single-layer autoassociative Hebbian correlation to two-layer pattern-matched heteroassociative circuits, widespread applications have been found in various areas, such as automatic control, signal and image processing, pattern recognition, artificial intelligence, parallel computation, and optimization problems. Often, a stable equilibrium of BAM neural networks is the important precondition of the successful applications. There are many factors influencing the stability of neural networks, in which pulse and time delay are usually the main reasons [3–8].

So, the stability analysis of impulse or delays system has become a hot topic. All the time, the Lyapunov functional method is employed to deduce stability criteria [9–20]. But every method may have its limitations. During the recent decades, other techniques have been developed to investigate the stability, in which the fixed point method is always one of those alternatives [21–27]. For example, in 2015, Zhou utilized Brouwer's fixed point theorem to prove the existence and uniqueness of equilibrium of the hybrid BAM neural networks with proportional delays and finally constructed appropriate delay differential inequalities to derive the stability of equilibrium [28]. In [29], Banach fixed point theorem was applied to show the existence of the unique equilibrium of BAM neural networks with time-varying delays in the leakage terms, and then the Lyapunov functional method was for demonstrating the global exponential stability. Different from [28, 29], we shall use Banach fixed point theorem deriving straightway the stability criterion of impulsive time-delay BAM neural networks, in which LMI conditions facilitate computer programming. Finally, a numerical example is presented to illustrate the effectiveness of the proposed methods.

For the sake of convenience, we introduce the following standard notations [18]:

- (i) $L = (l_{ij})_{n \times n} > 0 (< 0)$: a positive (negative) definite matrix; that is, $y^T L y > 0 (< 0)$ for any $0 \neq y \in R^n$.
- (ii) $L = (l_{ij})_{n \times n} \geq 0 (\leq 0)$: a semipositive (seminegative) definite matrix; that is, $y^T L y \geq 0 (\leq 0)$ for any $y \in R^n$.
- (iii) $L_1 \geq L_2 (L_1 \leq L_2)$: this means matrix $(L_1 - L_2)$ is a semipositive (seminegative) definite matrix.
- (iv) $L_1 > L_2 (L_1 < L_2)$: this means matrix $(L_1 - L_2)$ is a positive (negative) definite matrix.
- (v) $\lambda_{\max}(\Phi)$ and $\lambda_{\min}(\Phi)$ denote the largest and the smallest eigenvalue of matrix Φ , respectively.
- (vi) Denote $|L| = (|l_{ij}|)_{n \times n}$ for any matrix $L = (l_{ij})_{n \times n}$.
- (vii) $|u| = (|u_1|, |u_2|, \dots, |u_n|)^T$ for any vector $u = (u_1, u_2, \dots, u_n)^T \in R^n$.
- (viii) $u \leq (\geq) v$ implies that $u_i \leq (\geq) v_i, \forall i$, and $u < (>) v$ implies that $u_i < (>) v_i, \forall i$, for any vectors $u = (u_1, u_2, \dots, u_n)^T \in R^n$ and $v = (v_1, v_2, \dots, v_n)^T \in R^n$.
- (ix) I is identity matrix with compatible dimension.

Remark 1. Different from the methods of [28, 29], it will be the first time to utilize contraction mapping principle to infer directly the LMI-based stability criterion of BAM neural networks, convenient for computer programming. Recently, there have been a lot of good results and methods [21–29] enlightening our current work. In this paper, we shall propose the LMI-based criterion, novel against the existing results, published from 2013 to 2016 (see Remark 10 and Table 1).

2. Preliminaries

Consider the following delayed differential equations:

$$\begin{aligned} \frac{dx(t)}{dt} &= -Ax(t) + Cf(y(t - \tau(t))), \\ t &\in [0, +\infty), \quad t \neq t_k, \quad k = 1, 2, \dots, \\ \frac{dy(t)}{dt} &= -By(t) + Dg(x(t - h(t))), \\ t &\in [0, +\infty), \quad t \neq t_k, \quad k = 1, 2, \dots, \\ x(t_k^+) - x(t_k) &= \rho(x(t_k)), \\ y(t_k^+) - y(t_k) &= \rho(y(t_k)), \\ k &= 1, 2, \dots, \\ x(s) &= \xi(s), \\ y(s) &= \eta(s), \\ s &\in [-\tau, 0], \end{aligned} \quad (2)$$

where $x(t) = (x_1(t), x_2(t), \dots, x_n(t))^T$, $y(t) = (y_1(t), y_2(t), \dots, y_n(t))^T \in R^n$, and $\xi(s), \eta(s) \in \mathcal{C}([-\tau, 0], R^n)$. Here, $\mathcal{C}([-\tau, 0], R^n)$ represents the space of continuous functions from $[-\tau, 0]$ to R^n . Active functions $f(x(t - \tau(t))) = (f_1(x_1(t - \tau(t))), f_2(x_2(t - \tau(t))), \dots, f_n(x_n(t - \tau(t))))^T$, $g(x(t - h(t))) = (g_1(x_1(t - h(t))), g_2(x_2(t - h(t))), \dots, g_n(x_n(t - h(t))))^T \in R^n$, impulsive function $\rho(x(t)) = (\rho_1(x_1(t)), \rho_2(x_2(t)), \dots, \rho_n(x_n(t)))^T \in R^n$, and time delays $0 \leq \tau(t), h(t) \leq \tau$. The fixed impulsive moments t_k ($k = 1, 2, \dots$) satisfy $0 < t_1 < t_2 < \dots$ with $\lim_{k \rightarrow \infty} t_k = \infty$. $x(t_k^+)$ and $x(t_k^-)$ stand for the right-hand and left-hand limit of $x(t)$ at time t_k , respectively. We always assume $x(t_k^-) = x(t_k)$, for all $k = 1, 2, \dots$. Similar to [23], we assume in this paper that $f(0) = g(0) = \rho(0) = 0 \in R^n$. Constant matrices $A = \text{diag}(a_1, a_2, \dots, a_n)$, $B = \text{diag}(b_1, b_2, \dots, b_n)$ are positive definite diagonal matrices, and both $C = (c_{ij})_{n \times n}$ and $D = (d_{ij})_{n \times n}$ are matrices with $n \times n$ dimension.

Throughout this paper, we assume that $F = \text{diag}(F_1, F_2, \dots, F_n)$, $G = \text{diag}(G_1, G_2, \dots, G_n)$, and $H = \text{diag}(H_1, H_2, \dots, H_n)$ are diagonal matrices, satisfying

$$(A1) \quad |f(x) - f(y)| \leq F|x - y|, \quad x, y \in R^n.$$

$$(A2) \quad |g(x) - g(y)| \leq G|x - y|, \quad x, y \in R^n.$$

$$(A3) \quad |\rho(x) - \rho(y)| \leq H|x - y|, \quad x, y \in R^n.$$

Definition 2. Dynamic equations (2) are said to be globally exponentially stable if, for any initial condition $\xi(s), \eta(s) \in \mathcal{C}([-\tau, 0], R^n)$, there exist a pair of positive constants a and b such that

$$\left\| \begin{pmatrix} x(t; s, \xi, \eta) \\ y(t; s, \xi, \eta) \end{pmatrix} \right\| \leq be^{-at}, \quad \forall t > 0, \quad (3)$$

where the norm $\left\| \begin{pmatrix} x(t) \\ y(t) \end{pmatrix} \right\| = (\sum_{i=1}^n |x_i(t)|^2 + \sum_{i=1}^n |y_i(t)|^2)^{1/2}$, and $x = (x_1, \dots, x_n)$, $y = (y_1, \dots, y_n) \in R^n$.

Definition 3. For a diagonal constants matrix $B = \text{diag}(b_1, b_2, \dots, b_n)$, one denotes the matrix exponential function $e^{Bt} = \text{diag}(e^{b_1 t}, e^{b_2 t}, \dots, e^{b_n t})$ for all $t \in R$.

Lemma 4 (see [31] contraction mapping theorem). *Let P be a contraction operator on a complete metric space Θ ; then, there exists a unique point $\theta \in \Theta$ for which $P(\theta) = \theta$.*

Lemma 5. *Let B be a diagonal constants matrix and e^{Bt} be the matrix exponential function of B . Then, one has*

$$(1) \quad (d/dt)e^{Bt} = Be^{Bt}, \quad t \in R;$$

$$(2) \quad (d/dt)(e^{Bt}\alpha) = Be^{Bt}\alpha, \quad t \in R,$$

where $\alpha = (\alpha_1, \alpha_2, \dots, \alpha_n)^T \in R^n$ and each $\alpha_i \in R$ ($i = 1, 2, \dots, n$) is a constant.

3. Main Result

Theorem 6. Assume that there exists a positive constant δ such that $\inf_{k=1,2,\dots} (t_{k+1} - t_k) \geq \delta$. In addition, there exists a constant $0 < \lambda < 1$ such that

$$\begin{aligned} |C| F + \frac{1}{\delta} H + A H - \lambda A &< 0, \\ |D| G + \frac{1}{\delta} H + B H - \lambda B &< 0, \end{aligned} \quad (4)$$

and then the impulsive fuzzy dynamic equations (2) are globally exponentially stable, where $\delta = \inf_{k=1,2,\dots} (t_{k+1} - t_k) > 0$.

Proof. To apply the fixed point theory, we firstly define a complete metric space $\Omega = \Omega_1 \times \Omega_2$ as follows.

Let Ω_i ($i = 1, 2$) be the space consisting of functions $q_i(t) : [-\tau, \infty) \rightarrow R^n$, satisfying the following:

- (a) $q_i(t)$ is continuous on $t \in [0, +\infty) \setminus \{t_k\}_{k=1}^\infty$.
- (b) $q_1(t) = \xi(t)$, $q_2(t) = \eta(t)$, for $t \in [-\tau, 0]$.
- (c) $\lim_{t \rightarrow t_k^-} q_i(t) = q_i(t_k)$, and $\lim_{t \rightarrow t_k^+} q_i(t)$ exists, for all $k = 1, 2, \dots$
- (d) $e^{\gamma t} q_i(t) \rightarrow 0 \in R^n$ as $t \rightarrow \infty$, where $\gamma > 0$ is a positive constant, satisfying $\gamma < \min\{\lambda_{\min} A, \lambda_{\min} B\}$.

It is not difficult to verify that the product space Ω is a complete metric space if it is equipped with the following metric:

$$\text{dist}(\bar{q}, \tilde{q}) = \max_{i=1,2,\dots,2n-1,2n} \left(\sup_{t \geq -\tau} |\bar{q}^{(i)}(t) - \tilde{q}^{(i)}(t)| \right), \quad (5)$$

where

$$\begin{aligned} \bar{q} = \bar{q}(t) &= \begin{pmatrix} \bar{q}_1(t) \\ \bar{q}_2(t) \end{pmatrix} = (\bar{q}^{(1)}(t), \bar{q}^{(2)}(t), \dots, \bar{q}^{(2n)}(t))^T \\ &\in \Omega, \end{aligned} \quad (6)$$

$$\tilde{q} = \tilde{q}(t) = \begin{pmatrix} \tilde{q}_1(t) \\ \tilde{q}_2(t) \end{pmatrix} = (\tilde{q}^{(1)}(t), \dots, \tilde{q}^{(2n)}(t))^T \in \Omega,$$

and $\bar{q}_i \in \Omega_i$, $\tilde{q}_i \in \Omega_i$, $i = 1, 2$.

Next, we are to construct a contraction mapping $P : \Omega \rightarrow \Omega$, which may be divided into three steps.

Step 1 (formulating the mapping). Let $(x^T(t), y^T(t))^T = (x_1(t), x_2(t), \dots, x_n(t), y_1(t), \dots, y_n(t))^T$ be a solution of system (2).

Then, for $t \geq 0$, $t \neq t_k$, we have

$$\begin{aligned} \frac{dx(t)}{dt} (e^{At} x(t)) &= A e^{At} x(t) + e^{At} \frac{dx(t)}{dt} \\ &= e^{At} C f(y(t - \tau(t))). \end{aligned} \quad (7)$$

Further, we get by the integral property

$$x(t) = e^{-At} \left[\int_0^t e^{As} C f(y(s - \tau(s))) ds + \chi \right], \quad t \geq 0, \quad (8)$$

where $\chi \in R^n$ is the vector to be determined.

Next, we claim that $\chi = \xi(0) + \sum_{0 < t_k < t} e^{At_k} \rho(x_{t_k})$, and

$$\begin{aligned} x(t) &= e^{-At} \xi(0) + e^{-At} \left[\int_0^t e^{As} C f(y(s - \tau(s))) ds \right. \\ &\quad \left. + \sum_{0 < t_k < t} e^{At_k} \rho(x_{t_k}) \right], \quad t \geq 0. \end{aligned} \quad (9)$$

Indeed, on the one hand, we can conclude from (9) that

$$\begin{aligned} e^{At} x(t) &= \xi(0) + \int_0^t e^{As} C f(y(s - \tau(s))) ds \\ &\quad + \sum_{0 < t_k < t} e^{At_k} \rho(x_{t_k}). \end{aligned} \quad (10)$$

For $t \geq 0$, $t \neq t_k$, taking the time derivative of both sides leads to

$$\begin{aligned} e^{At} \frac{dx(t)}{dt} + A e^{At} x(t) &= \frac{d}{dt} (e^{At} x(t)) \\ &= e^{At} C f(y(t - \tau(t))), \end{aligned} \quad (11)$$

or

$$\frac{dx(t)}{dt} + A x(t) = C f(y(t - \tau(t))), \quad (12)$$

which is the first equation of system (2).

Moreover, as $t \rightarrow t_j^-$, we can gain by (9)

$$\begin{aligned} x(t_j^-) &= \lim_{\varepsilon \rightarrow 0^+} x(t_j - \varepsilon) = x(t_j), \quad j = 1, 2, \dots, \\ x(t_j^+) &= \lim_{\varepsilon \rightarrow 0^+} x(t_j + \varepsilon) = x(t_j) + \rho(x(t_j)), \\ &\quad j = 1, 2, \dots. \end{aligned} \quad (13)$$

On the other hand, multiplying both sides of the first equation of system (2) by e^{At} yields

$$\begin{aligned} e^{At} \frac{dx(t)}{dt} + A e^{At} x(t) &= e^{At} C f(y(t - \tau(t))), \\ t \geq 0, \quad t \neq t_k. \end{aligned} \quad (14)$$

Moreover, integrating from $t_{k-1} + \varepsilon$ to $t \in (t_{k-1}, t_k)$ gives

$$\begin{aligned} e^{At} x(t) &= e^{A(t_{k-1} + \varepsilon)} x(t_{k-1} + \varepsilon) \\ &\quad + \int_{t_{k-1} + \varepsilon}^t e^{As} [C f(y(s - \tau(s)))] ds, \end{aligned} \quad (15)$$

which yields, after letting $\varepsilon \rightarrow 0^+$,

$$\begin{aligned} e^{At} x(t) &= e^{A(t_{k-1})} x(t_{k-1}^+) \\ &\quad + \int_{t_{k-1}}^t e^{As} [C f(y(s - \tau(s)))] ds, \end{aligned} \quad (16)$$

$$t \in (t_{k-1}, t_k).$$

Throughout this paper, we assume that ε is a sufficient small positive number. Now, taking $t = t_k - \varepsilon$ in the above equation yields

$$e^{At_k - \varepsilon} x(t_k - \varepsilon) = e^{At_{k-1}} x(t_{k-1}^+) + \int_{t_{k-1}}^{t_k - \varepsilon} e^{As} [Cf(y(s - \tau(s)))] ds, \quad (17)$$

which yields by letting $\varepsilon \rightarrow 0^+$

$$e^{At_k} x(t_k) = e^{At_{k-1}} x(t_{k-1}^+) + \int_{t_{k-1}}^{t_k} e^{As} [Cf(y(s - \tau(s)))] ds. \quad (18)$$

So, we have actually got

$$\begin{aligned} e^{At} x(t) &= e^{At_{k-1}} x(t_{k-1}^+) \\ &\quad + \int_{t_{k-1}}^t e^{As} [Cf(y(s - \tau(s)))] ds \\ &= e^{At_{k-1}} x(t_{k-1}) \\ &\quad + \int_{t_{k-1}}^t e^{As} [Cf(y(s - \tau(s)))] ds \\ &\quad + e^{At_{k-1}} \rho(x(t_{k-1})), \end{aligned} \quad (19)$$

for all $t \in (t_{k-1}, t_k]$, $k = 1, 2, \dots$. Furthermore, (19) generates

$$\begin{aligned} e^{At_{k-1}} x(t_{k-1}) &= e^{At_{k-2}} x(t_{k-2}) \\ &\quad + \int_{t_{k-2}}^{t_{k-1}} e^{As} [Cf(y(s - \tau(s)))] ds \\ &\quad + e^{At_{k-2}} \rho(x(t_{k-2})), \\ &\quad \vdots \end{aligned} \quad (20)$$

$$\begin{aligned} e^{At_2} x(t_2) &= e^{At_1} x(t_1) \\ &\quad + \int_{t_1}^{t_2} e^{As} [Cf(y(s - \tau(s)))] ds + e^{At_1} \rho(x(t_1)), \\ e^{At_1} x(t_1) &= \xi(0) + \int_0^{t_1} e^{As} [Cf(y(s - \tau(s)))] ds. \end{aligned}$$

Making a synthesis of the above equations results in (9).

Similarly, we can obtain

$$\begin{aligned} y(t) &= e^{-Bt} \eta(0) + e^{-Bt} \left[\int_0^t e^{Bs} Dg(x(s - h(s))) ds \right. \\ &\quad \left. + \sum_{0 < t_k < t} e^{Bt_k} \rho(y_{t_k}) \right], \quad t \geq 0. \end{aligned} \quad (21)$$

So, we may define the mapping P on the space Ω as follows:

$$P \begin{pmatrix} x(t) \\ y(t) \end{pmatrix} = \begin{pmatrix} e^{-At} \xi(0) + e^{-At} \left[\int_0^t e^{As} Cf(y(s - \tau(s))) ds + \sum_{0 < t_k < t} e^{At_k} \rho(x_{t_k}) \right] \\ e^{-Bt} \eta(0) + e^{-Bt} \left[\int_0^t e^{Bs} Dg(x(s - h(s))) ds + \sum_{0 < t_k < t} e^{Bt_k} \rho(y_{t_k}) \right] \end{pmatrix}, \quad \text{for } t \in [0, +\infty), \quad (22)$$

$$P \begin{pmatrix} x(t) \\ y(t) \end{pmatrix} = \begin{pmatrix} \xi(t) \\ \eta(t) \end{pmatrix}, \quad \text{for } t \in [-\tau, 0]. \quad (23)$$

Step 2. We claim that $P \begin{pmatrix} x(t) \\ y(t) \end{pmatrix} \in \Omega$ for any $\begin{pmatrix} x(t) \\ y(t) \end{pmatrix} \in \Omega$.

In other words, we need to prove that $P \begin{pmatrix} x(t) \\ y(t) \end{pmatrix}$ must satisfy conditions (a)–(d) of Ω .

Indeed, $P(\cdot)$ satisfies condition (b) due to (23).

Besides, let ε be a real number; we have

$$P \begin{pmatrix} x(t + \varepsilon) \\ y(t + \varepsilon) \end{pmatrix} = \begin{pmatrix} e^{-A(t+\varepsilon)} \xi(0) + e^{-A(t+\varepsilon)} \left[\int_0^{t+\varepsilon} e^{As} Cf(y(s - \tau(s))) ds + \sum_{0 < t_k < t+\varepsilon} e^{At_k} \rho(x_{t_k}) \right] \\ e^{-B(t+\varepsilon)} \eta(0) + e^{-B(t+\varepsilon)} \left[\int_0^{t+\varepsilon} e^{Bs} Dg(x(s - h(s))) ds + \sum_{0 < t_k < t+\varepsilon} e^{Bt_k} \rho(y_{t_k}) \right] \end{pmatrix}. \quad (24)$$

In (24), letting $\varepsilon \rightarrow 0$ brings about

$$\lim_{\varepsilon \rightarrow 0} P \begin{pmatrix} x(t + \varepsilon) \\ y(t + \varepsilon) \end{pmatrix} = P \begin{pmatrix} x(t) \\ y(t) \end{pmatrix}, \quad \forall t \neq t_k, \quad t \geq 0, \quad (25)$$

which implies that $P \begin{pmatrix} x(t) \\ y(t) \end{pmatrix}$ is continuous on $t \geq 0, t \neq t_k$. Here, the convergences are under the metric defined on the space Ω . Below, all the convergences of vector functions are in this sense. Thus, condition (a) is satisfied.

Furthermore, letting $t = t_j, j = 1, 2, \dots$, in (24), we have

$$\begin{aligned} \lim_{\varepsilon \rightarrow 0^-} P \begin{pmatrix} x(t_j + \varepsilon) \\ y(t_j + \varepsilon) \end{pmatrix} &= P \begin{pmatrix} x(t_j) \\ y(t_j) \end{pmatrix}, \\ \lim_{\varepsilon \rightarrow 0^+} P \begin{pmatrix} x(t_j + \varepsilon) \\ y(t_j + \varepsilon) \end{pmatrix} &= P \begin{pmatrix} x(t_j) \\ y(t_j) \end{pmatrix} + \begin{pmatrix} \rho(x(t_j)) \\ \rho(y(t_j)) \end{pmatrix}, \end{aligned} \quad (26)$$

which implies that condition (c) is also satisfied.

Next, condition (d) is satisfied if only

$$e^{\gamma t} \begin{pmatrix} e^{-At} \xi(0) + e^{-At} \left[\int_0^t e^{As} C f(y(s - \tau(s))) ds + \sum_{0 < t_k < t} e^{At_k} \rho(x_{t_k}) \right] \\ e^{-Bt} \eta(0) + e^{-Bt} \left[\int_0^t e^{Bs} D g(x(s - h(s))) ds + \sum_{0 < t_k < t} e^{Bt_k} \rho(y_{t_k}) \right] \end{pmatrix} \rightarrow \begin{pmatrix} 0 \\ 0 \end{pmatrix} \in R^{2n}, \quad t \rightarrow +\infty. \quad (27)$$

Indeed, obviously, $e^{\gamma t} e^{-At} \xi(0) \rightarrow 0 \in R^n$ and $e^{\gamma t} e^{-Bt} \eta(0) \rightarrow 0 \in R^n$ as $t \rightarrow \infty$.

Below, we may firstly prove

$$e^{\gamma t} e^{-At} \int_0^t e^{As} C f(y(s - \tau(s))) ds \rightarrow 0 \in R^n, \quad (28)$$

$$t \rightarrow \infty.$$

In fact, it follows from $e^{\gamma t} x(t) \rightarrow 0$ that, for any given $\varepsilon > 0$, there exists a corresponding constant $t^* > \tau$ such that

$$|e^{\gamma t} x(t)| + |e^{\gamma t} y(t)| < \varepsilon \mu, \quad (29)$$

$$\forall t \geq t^*, \text{ where } \mu = (1, 1, \dots, 1)^T \in R^n.$$

Next, we get by (A1)

$$\begin{aligned} & \left| e^{\gamma t} e^{-At} \int_0^t e^{As} C f(y(s - \tau(s))) ds \right| \\ & \leq e^{-(A-\gamma I)t} \int_0^{t^*} e^{As} |C| F |y(s - \tau(s))| ds \\ & \quad + e^{-(A-\gamma I)t} \int_{t^*}^t e^{As} |C| F |y(s - \tau(s))| ds. \end{aligned} \quad (30)$$

On the one hand,

$$\begin{aligned} & e^{-(A-\gamma I)t} \int_0^{t^*} e^{As} |C| F |y(s - \tau(s))| ds \\ & \leq t^* e^{-(A-\gamma I)t} e^{At^*} |C| F \left[\max_i \left(\sup_{s \in [-\tau, t^*]} |y_i(s)| \right) \right] \mu \\ & \rightarrow 0 \in R^n, \quad t \rightarrow \infty. \end{aligned} \quad (31)$$

On the other hand, obviously, there exists a positive number a_0 such that $|C| F \mu \leq a_0 \mu$. So, we have

$$\begin{aligned} & e^{-(A-\gamma I)t} \int_{t^*}^t e^{As} |C| F |y(s - \tau(s))| ds \\ & \leq \varepsilon e^{\gamma t} e^{-(A-\gamma I)t} \int_{t^*}^t e^{(A-\gamma I)s} |C| F \mu ds \end{aligned}$$

$$\begin{aligned} & \leq \varepsilon a_0 e^{\gamma t} e^{-(A-\gamma I)t} \begin{pmatrix} \frac{e^{(a_1-\gamma)t}}{a_1-\gamma} & 0 & \dots & 0 & 0 \\ 0 & \frac{e^{(a_2-\gamma)t}}{a_2-\gamma} & 0 & \dots & 0 \\ & & \ddots & & \\ 0 & 0 & \dots & 0 & \frac{e^{(a_n-\gamma)t}}{a_n-\gamma} \end{pmatrix} \mu \\ & = \varepsilon a_0 e^{\gamma t} \left(\frac{1}{a_1-\gamma}, \frac{1}{a_2-\gamma}, \dots, \frac{1}{a_n-\gamma} \right)^T. \end{aligned} \quad (32)$$

Combining (30)–(32) yields (28). Similarly, we can prove

$$e^{\gamma t} e^{-Bt} \int_0^t e^{Bs} D g(x(s - h(s))) ds \rightarrow 0 \in R^n, \quad (33)$$

$$t \rightarrow \infty.$$

Next, we need to prove that if $t \rightarrow +\infty$,

$$\begin{aligned} & e^{\gamma t} \begin{pmatrix} e^{-At} \sum_{0 < t_k < t} e^{At_k} \rho(x_{t_k}) \\ e^{-Bt} \sum_{0 < t_k < t} e^{Bt_k} \rho(y_{t_k}) \end{pmatrix} \\ & = e^{\gamma t} \begin{pmatrix} e^{-At} \sum_{0 < t_k < t^*} e^{At_k} \rho(x_{t_k}) \\ e^{-Bt} \sum_{0 < t_k < t^*} e^{Bt_k} \rho(y_{t_k}) \end{pmatrix} \\ & \quad + e^{\gamma t} \begin{pmatrix} e^{-At} \sum_{t^* < t_k < t} e^{At_k} \rho(x_{t_k}) \\ e^{-Bt} \sum_{t^* < t_k < t} e^{Bt_k} \rho(y_{t_k}) \end{pmatrix} \rightarrow 0 \in R^{2n}. \end{aligned} \quad (34)$$

Indeed, it is obvious that

$$\begin{aligned} e^{\gamma t} \begin{pmatrix} e^{-At} \sum_{0 < t_k < t^*} e^{At_k} \rho(x_{t_k}) \\ e^{-Bt} \sum_{0 < t_k < t^*} e^{Bt_k} \rho(y_{t_k}) \end{pmatrix} \\ = \begin{pmatrix} e^{(\gamma I - A)t} \sum_{0 < t_k < t^*} e^{At_k} \rho(x_{t_k}) \\ e^{(\gamma I - B)t} \sum_{0 < t_k < t^*} e^{Bt_k} \rho(y_{t_k}) \end{pmatrix} \longrightarrow 0 \in R^{2n}, \\ t \longrightarrow +\infty. \end{aligned} \quad (35)$$

Below, we shall prove

$$\begin{aligned} e^{\gamma t} \begin{pmatrix} e^{-At} \sum_{t^* < t_k < t} e^{At_k} \rho(x_{t_k}) \\ e^{-Bt} \sum_{t^* < t_k < t} e^{Bt_k} \rho(y_{t_k}) \end{pmatrix} \longrightarrow 0 \in R^{2n}, \\ t \longrightarrow +\infty. \end{aligned} \quad (36)$$

Firstly, we may assume that $t_{m-1} < t^* \leq t_m$ and $t_j < t \leq t_{j+1}$ for any given $t > t^*$. Hence,

$$\begin{aligned} \left| e^{\gamma t} e^{-At} \sum_{t^* < t_k < t} e^{At_k} \rho(x_{t_k}) \right| \\ \leq e^{\gamma t} e^{-At} \sum_{t^* < t_k < t} e^{At_k - \gamma t_k} H e^{\gamma t_k} |x_{t_k}| \leq \frac{\varepsilon}{\delta} \\ \cdot \begin{pmatrix} e^{-(\gamma - a_1)t} \left(\delta e^{(a_1 - \gamma)t_{j+1}} + \int_{t^*}^t e^{(a_1 - \gamma)s} ds \right) H_1 \\ \vdots \\ e^{-(\gamma - a_n)t} \left(\delta e^{(a_n - \gamma)t_{j+1}} + \int_{t^*}^t e^{(a_n - \gamma)s} ds \right) H_n \end{pmatrix} \\ \leq \frac{\varepsilon}{\delta} \\ \cdot \begin{pmatrix} e^{-(\gamma - a_1)t} \left(\delta e^{(a_1 - \gamma)t_{j+1}} + \frac{1}{a_1 - \gamma} e^{(a_1 - \gamma)t} \right) H_1 \\ \vdots \\ e^{-(\gamma - a_n)t} \left(\delta e^{(a_n - \gamma)t_{j+1}} + \frac{1}{a_n - \gamma} e^{(a_1 - \gamma)t} \right) H_n \end{pmatrix}, \end{aligned} \quad (37)$$

which together with the arbitrariness of the positive number ε implies that

$$e^{-At} \sum_{t^* < t_k < t} e^{At_k} \rho(x_{t_k}) \longrightarrow 0 \in R^n, \quad t \longrightarrow +\infty. \quad (38)$$

Similarly, we can also get

$$e^{-Bt} \sum_{t^* < t_k < t} e^{Bt_k} \rho(y_{t_k}) \longrightarrow 0 \in R^n, \quad t \longrightarrow +\infty. \quad (39)$$

Hence, we have proved (36) and (34). And so we can conclude (27) from (28), (33), and (34). This means that condition (d) is satisfied, too.

Therefore, $P \begin{pmatrix} x(t) \\ y(t) \end{pmatrix} \in \Omega$ for any $\begin{pmatrix} x(t) \\ y(t) \end{pmatrix} \in \Omega$.

Step 3. Below, we only need to prove that P is a contraction mapping.

Indeed, for any $\begin{pmatrix} x(t) \\ y(t) \end{pmatrix}, \begin{pmatrix} \bar{x}(t) \\ \bar{y}(t) \end{pmatrix} \in \Omega$, we have

$$\begin{aligned} \left| P \begin{pmatrix} x(t) \\ y(t) \end{pmatrix} - P \begin{pmatrix} \bar{x}(t) \\ \bar{y}(t) \end{pmatrix} \right| \\ \leq \begin{pmatrix} e^{-At} \int_0^t e^{As} |C| |f(y(s - \tau(s))) - f(\bar{y}(s - \tau(s)))| ds \\ e^{-Bt} \int_0^t e^{Bs} |D| |g(x(s - h(s))) - g(\bar{x}(s - h(s)))| ds \end{pmatrix} \\ + \begin{pmatrix} e^{-At} \sum_{0 < t_k < t} e^{At_k} |\rho(x_{t_k}) - \rho(\bar{x}_{t_k})| \\ e^{-Bt} \sum_{0 < t_k < t} e^{Bt_k} |\rho(y_{t_k}) - \rho(\bar{y}_{t_k})| \end{pmatrix} \leq \begin{bmatrix} (A^{-1} |C| F \mu) \\ (B^{-1} |D| G \mu) \end{bmatrix} \\ + \frac{1}{\delta} \\ \cdot \begin{pmatrix} e^{-At} \left(\int_0^t e^{As} ds + \delta e^{At} \right) H \mu \\ e^{-Bt} \left(\int_0^t e^{Bs} ds + \delta e^{Bt} \right) H \mu \end{pmatrix} \text{dist} \left(\begin{pmatrix} x(t) \\ y(t) \end{pmatrix}, \begin{pmatrix} \bar{x}(t) \\ \bar{y}(t) \end{pmatrix} \right) \\ \leq \begin{pmatrix} (A^{-1} |C| F + \frac{1}{\delta} A^{-1} H + H) \mu \\ (B^{-1} |D| G + \frac{1}{\delta} B^{-1} H + H) \mu \end{pmatrix} \text{dist} \left(\begin{pmatrix} x(t) \\ y(t) \end{pmatrix}, \begin{pmatrix} \bar{x}(t) \\ \bar{y}(t) \end{pmatrix} \right) \\ < \lambda \begin{pmatrix} \mu \\ \mu \end{pmatrix} \text{dist} \left(\begin{pmatrix} x(t) \\ y(t) \end{pmatrix}, \begin{pmatrix} \bar{x}(t) \\ \bar{y}(t) \end{pmatrix} \right), \end{aligned} \quad (40)$$

and hence

$$\begin{aligned} \text{dist} \left(P \begin{pmatrix} x(t) \\ y(t) \end{pmatrix}, P \begin{pmatrix} \bar{x}(t) \\ \bar{y}(t) \end{pmatrix} \right) \\ \leq \lambda \text{dist} \left(\begin{pmatrix} x(t) \\ y(t) \end{pmatrix}, \begin{pmatrix} \bar{x}(t) \\ \bar{y}(t) \end{pmatrix} \right), \end{aligned} \quad (41)$$

where A^{-1} and B^{-1} are the inverse matrices of A and B , respectively.

Therefore, $P : \Omega \rightarrow \Omega$ is a contraction mapping such that there exists the fixed point $\begin{pmatrix} x(t) \\ y(t) \end{pmatrix}$ of P in Ω , which implies that $\begin{pmatrix} x(t) \\ y(t) \end{pmatrix}$ is a solution of the impulsive fuzzy dynamic equations (2), satisfying $e^{\gamma t} \left\| \begin{pmatrix} x(t) \\ y(t) \end{pmatrix} \right\| \rightarrow 0$ as $t \rightarrow +\infty$. And the proof is completed. \square

Remark 7. Impulsive BAM neural networks model brings some mathematical difficulties to contraction mapping technique. However, in this paper, we set up the contraction mapping on the complete product space to overcome obstacles.

4. Numerical Example

Example 8. We equip the impulsive system with the following parameters:

$$\begin{aligned} A &= \begin{pmatrix} 1.8 & 0 \\ 0 & 2.1 \end{pmatrix}, \\ B &= \begin{pmatrix} 2 & 0 \\ 0 & 1.9 \end{pmatrix}, \end{aligned}$$

TABLE 1: Comparing Theorem 6 with other existing results.

| | Types of equations | Fixed point methods | LMI-based? |
|------------------------|--------------------------------|-----------------------------------|------------|
| Theorem 6 | Impulsive BAM neural networks | Contraction mapping principle | Yes |
| [28, Th. 2–4] | BAM neural networks | Brouwer's fixed theorem | No |
| [29, Th. 2.1, Th. 3.1] | BAM neural networks | Contraction mapping principle | No |
| [22, Th. 1.2] | Neural networks | Contraction mapping principle | No |
| [23, Th. 3.1] | Cellular neural networks | Krasnoselskii fixed point theorem | No |
| [21, Th. 2.1] | Neutral differential equations | Contraction mapping principle | No |
| [30, Th. 1.1–1.2] | Neural networks | Schauder fixed point theorem | No |

$$\begin{aligned}
C &= \begin{pmatrix} -0.2 & 0.01 \\ 0 & 0.3 \end{pmatrix}, \\
D &= \begin{pmatrix} 0.3 & 0.02 \\ 0 & -0.1 \end{pmatrix}, \\
F &= \begin{pmatrix} 0.1 & 0 \\ 0 & 0.2 \end{pmatrix}, \\
G &= \begin{pmatrix} 0.2 & 0 \\ 0 & 0.1 \end{pmatrix}, \\
H &= \begin{pmatrix} 0.3 & 0 \\ 0 & 0.2 \end{pmatrix}.
\end{aligned} \tag{42}$$

Let $\delta = 1.5$. Then, we can use Matlab LMI toolbox to solve LMI conditions (4), obtaining the datum feasible as follows:

$$\lambda = 0.9913. \tag{43}$$

Obviously, $0 < \lambda < 1$. Thereby, we can conclude from Theorem 6 that the impulsive equations (2) are globally exponentially stable.

Remark 9. Example 8 illustrates the effectiveness of LMI-based criterion (Theorem 6). Table 1 presents a comparable result among the related literature, mainly published from 2013 to 2016.

Remark 10. From Table 1, we know that there are many existing literatures involving fixed point technique and stability analysis, and a lot of interesting conclusions are derived [21–23, 28–30]. Motivated by some methods of those literatures, we utilized Banach contraction mapping theorem to obtain the LMI-based stability criterion applicable to computer Matlab LMI toolbox. It is well known that computer software can solve large-scale computations in actual engineering, which demonstrates the superiority of the proposed method in this paper to a certain extent.

5. Conclusion

Recently, fixed point technique and methods are employed to the stability analysis to BAM neural networks, and some stability criteria are derived (see, e.g., [28, 29]). Some good

methods and results of related literature [21–23, 28–30] inspire our current work. Different from existing papers, we utilized Banach fixed point theorem deriving immediately the exponential stability criterion applicable to computer Matlab LMI toolbox. Computer programming is suitable for large-scale computation in practical engineering.

Competing Interests

The authors declare that they have no competing interests.

Authors' Contributions

Ruofeng Rao wrote the original manuscript, Zhilin Pu and Shouming Zhong checked it, and Xinggui Li and Ruofeng Rao were in charge of correspondence. All authors typed, read, and approved the final manuscript.

Acknowledgments

This work was supported by the Scientific Research Fund of Science Technology Department of Sichuan Province (2010JY0057, 2012JYZ010) and the Scientific Research Fund of Sichuan Provincial Education Department (12ZB349).

References

- [1] B. Kosko, "Adaptive bidirectional associative memories," *Applied Optics*, vol. 26, no. 23, pp. 4947–4960, 1987.
- [2] B. Kosko, "Bidirectional associative memories," *IEEE Transactions on Systems, Man, and Cybernetics*, vol. 18, no. 1, pp. 49–60, 1988.
- [3] R. Rao, X. Wang, and S. Zhong, "LMI-based stability criterion for impulsive delays Markovian jumping time-delays reaction-diffusion BAM neural networks via Gronwall-Bellman-type impulsive integral inequality," *Mathematical Problems in Engineering*, vol. 2015, Article ID 185854, 11 pages, 2015.
- [4] X. Li and S. Song, "Research on synchronization of chaotic delayed neural networks with stochastic perturbation using impulsive control method," *Communications in Nonlinear Science and Numerical Simulation*, vol. 19, no. 10, pp. 3892–3900, 2014.
- [5] X. Li and X. Fu, "Effect of leakage time-varying delay on stability of nonlinear differential systems," *Journal of the Franklin Institute*, vol. 350, no. 6, pp. 1335–1344, 2013.
- [6] H. Chen, S. Zhong, M. Li, X. Liu, and F. Adu-Gyamfi, "Stability criteria for T-S fuzzy systems with interval time-varying delays

- and nonlinear perturbations based on geometric progression delay partitioning method,” *ISA Transactions*, vol. 63, pp. 69–77, 2016.
- [7] X. Liu and S. Zhong, “T-S fuzzy model-based impulsive control of chaotic systems with exponential decay rate,” *Physics Letters, Section A: General, Atomic and Solid State Physics*, vol. 370, no. 3–4, pp. 260–264, 2007.
 - [8] Q. Zhu, X. Li, and X. Yang, “Exponential stability for stochastic reaction-diffusion BAM neural networks with time-varying and distributed delays,” *Applied Mathematics and Computation*, vol. 217, no. 13, pp. 6078–6091, 2011.
 - [9] M. De la Sen, “About robust stability of Caputo linear fractional dynamic systems with time delays through fixed point theory,” *Fixed Point Theory and Applications*, vol. 2011, article 867932, 2011.
 - [10] D. Li, X. Wang, and D. Xu, “Existence and global p-exponential stability of periodic solution for impulsive stochastic neural networks with delays,” *Nonlinear Analysis: Hybrid Systems*, vol. 6, no. 3, pp. 847–858, 2012.
 - [11] Q. Song, Z. Zhao, and Y. Li, “Global exponential stability of BAM neural networks with distributed delays and reaction-diffusion terms,” *Physics Letters A*, vol. 335, no. 2–3, pp. 213–225, 2005.
 - [12] J. Hu, S. Zhong, and L. Liang, “Exponential stability analysis of stochastic delayed cellular neural network,” *Chaos, Solitons & Fractals*, vol. 27, no. 4, pp. 1006–1010, 2006.
 - [13] M. De la Sen, “Total stability properties based on fixed point theory for a class of hybrid dynamic systems,” *Fixed Point Theory and Applications*, vol. 2009, Article ID 826438, pp. 1–19, 2009.
 - [14] M. De la Sen, “About robust stability of dynamic systems with time delays through fixed point theory,” *Fixed Point Theory and Applications*, vol. 2008, article 480187, 2008.
 - [15] Q. Song and Z. Wang, “An analysis on existence and global exponential stability of periodic solutions for BAM neural networks with time-varying delays,” *Nonlinear Analysis: Real World Applications*, vol. 8, no. 4, pp. 1224–1234, 2007.
 - [16] W. Peng, Q. Wu, and Z. Zhang, “LMI-based global exponential stability of equilibrium point for neutral delayed BAM neural networks with delays in leakage terms via new inequality technique,” *Neurocomputing*, vol. 199, pp. 103–113, 2016.
 - [17] X. Li and X. Fu, “Global asymptotic stability of stochastic Cohen-Grossberg-type BAM neural networks with mixed delays: an LMI approach,” *Journal of Computational and Applied Mathematics*, vol. 235, no. 12, pp. 3385–3394, 2011.
 - [18] R. Rao, S. Zhong, and X. Wang, “Stochastic stability criteria with LMI conditions for Markovian jumping impulsive BAM neural networks with mode-dependent time-varying delays and nonlinear reaction-diffusion,” *Communications in Nonlinear Science and Numerical Simulation*, vol. 19, no. 1, pp. 258–273, 2014.
 - [19] R. Sakthivel, R. Anbuviya, K. Mathiyalagan, A. Arunkumar, and P. Prakash, “New LMI-based passivity criteria for neutral-type BAM neural networks with randomly occurring uncertainties,” *Reports on Mathematical Physics*, vol. 72, no. 3, pp. 263–286, 2013.
 - [20] J. Tian, W. Xiong, and F. Xu, “Improved delay-partitioning method to stability analysis for neural networks with discrete and distributed time-varying delays,” *Applied Mathematics and Computation*, vol. 233, pp. 152–164, 2014.
 - [21] J. Luo, “Fixed points and stability of neutral stochastic delay differential equations,” *Journal of Mathematical Analysis and Applications*, vol. 334, no. 1, pp. 431–440, 2007.
 - [22] G. Chen, O. van Gaans, and S. Verduyn Lunel, “Fixed points and p th moment exponential stability of stochastic delayed recurrent neural networks with impulses,” *Applied Mathematics Letters*, vol. 27, pp. 36–42, 2014.
 - [23] C. Guo, D. O’Regan, F. Deng, and R. P. Agarwal, “Fixed points and exponential stability for a stochastic neutral cellular neural network,” *Applied Mathematics Letters*, vol. 26, no. 8, pp. 849–853, 2013.
 - [24] X. Lai and Y. Zhang, “Fixed point and asymptotic analysis of cellular neural networks,” *Journal of Applied Mathematics*, vol. 2012, Article ID 689845, 12 pages, 2012.
 - [25] R. Rao and Z. Pu, “LMI-based stability criterion of impulsive T-S fuzzy dynamic equations via fixed point theory,” *Abstract and Applied Analysis*, vol. 2013, Article ID 261353, 9 pages, 2013.
 - [26] G.-Q. Wang and S. S. Cheng, “Fixed point theorems arising from seeking steady states of neural networks,” *Applied Mathematical Modelling*, vol. 33, no. 1, pp. 499–506, 2009.
 - [27] P. Wawrzyński and B. Papis, “Fixed point method for autonomous on-line neural network training,” *Neurocomputing*, vol. 74, no. 17, pp. 2893–2905, 2011.
 - [28] L. Zhou, “Novel global exponential stability criteria for hybrid BAM neural networks with proportional delays,” *Neurocomputing*, vol. 161, pp. 99–106, 2015.
 - [29] B. Liu, “Global exponential stability for BAM neural networks with time-varying delays in the leakage terms,” *Nonlinear Analysis: Real World Applications*, vol. 14, no. 1, pp. 559–566, 2013.
 - [30] J. Deng and Z. Deng, “Existence and exponential stability of solutions of NNs with continuously distributed delays,” *Neurocomputing*, vol. 171, pp. 492–496, 2016.
 - [31] D. Smart, *Fixed Point Theorems*, Cambridge University Press, Cambridge, UK, 1980.

Research Article

A Control Method to Balance the Efficiency and Reliability of a Time-Delayed Pump-Valve System

Zhounian Lai,^{1,2} Peng Wu,^{1,2} Shuai Yang,^{1,2} and Dazhuan Wu^{1,2,3}

¹*Institute of Process Equipment, Zhejiang University, Hangzhou 310027, China*

²*College of Chemical and Biological Engineering, Zhejiang University, Hangzhou 310027, China*

³*State Key Laboratory of Fluid Power and Mechatronic Systems, Zhejiang University, Hangzhou 310027, China*

Correspondence should be addressed to Dazhuan Wu; wudazhuan@zju.edu.cn

Received 26 May 2016; Revised 8 August 2016; Accepted 30 August 2016

Academic Editor: Olfa Boubaker

Copyright © 2016 Zhounian Lai et al. This is an open access article distributed under the Creative Commons Attribution License, which permits unrestricted use, distribution, and reproduction in any medium, provided the original work is properly cited.

The efficiency and reliability of pumps are highly related to their operation conditions. The concept of the optimization pump operation conditions is to adjust the operation point of the pump to obtain higher reliability at the cost of lower system efficiency using a joint regulation of valve and frequency convertor. This paper realizes the control of the fluid conveying system based on the optimization results. The system is a nonlinear Multi-Input Multioutput (MIMO) system with time delays. In this paper, the time delays are separated from the system. The delay-free system is linearized using input-output linearization and controlled using a sliding mode method. A modified Smith predictor is used to compensate time delays of the system. The control strategy is validated to be effective on the test bench. The comparison of energy consumption and operation point deviation between conventional speed regulation and the new method is presented.

1. Introduction

As a key component of fluid conveying systems, pumps are widely used in industries, of which 45% are centrifugal pumps [1]. Pumps account for nearly 20% of electrical energy consumption and are in the range of 25%~50% of energy consumption in many industries [2]. Therefore energy saving in pumps is one main goal in industries, which requires pumps work in good operation points. Bad operation point leads to a low efficiency and reliability of a pump, causing serious consequences.

Many researchers focused on the energy saving of pump systems. The variable speed pump technology is widely used to reduce energy cost in industries. It varies the rotational speed of centrifugal pumps to accommodate pipeline requirements [3]. According to surveys and researches [4, 5], speed regulation can save 5%~50% energy relative to valve regulation. In recent years, the scheduling of pumps has progressed greatly. Wang et al. [6] proposed an enhanced genetic algorithm for pump scheduling in water supply system to reduce the energy cost and slow land subsidence.

Hashemi et al. [7] developed an ant-colony optimization of pumping schedule using variable speed pumps and saved about 10% energy cost compared to single speed pumps. However, few studies on the pump reliability have been conducted so far.

Efficiency and reliability of a centrifugal pump are related to operation point of the pump. Efficiency of a centrifugal pump reaches its peak value at its design point and decreases as its operation point deviates from its design point [8]. Barringer [9] found out that reliability curve is similar to its efficiency curve. Reliability of a pump is a statistics term, which is defined as the mean time between failure (MTBF) relative to the mission time. Reliability of a centrifugal pump reaches a peak value at the Best Efficiency Point (BEP), near its design point, but decreases sharply as operation point deviates from design point, shown in Figure 1. Thus the operation point plays a decisive role in pump reliability. Long operating time at part load or overload may increase the component failure rate. High temperature rise, suction recirculation, and discharge recirculation may occur in a pump operating at part load, while low sealing life, low

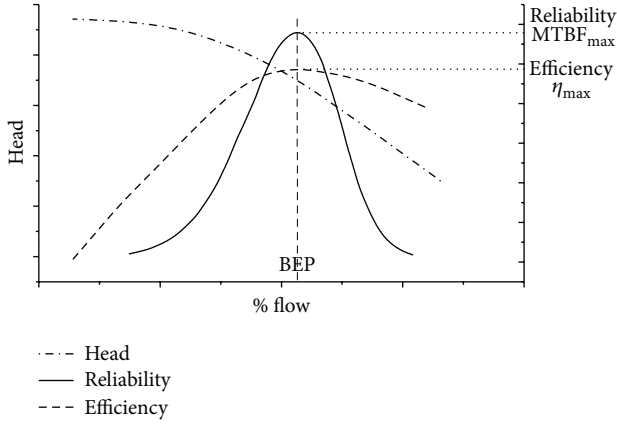


FIGURE 1: Reliability curve, efficiency curve, and head curve of a centrifugal pump.

bear life, and cavitation may occur in a pump operating at overload, leading to a poor pump efficiency and reliability.

In our previous work [10], we developed an optimization algorithm to improve centrifugal pump reliability and efficiency for pump systems at the cost of a decline in system efficiency, using throttling valves and a pump number selection strategy to restrict the pump operation point to a neighbourhood of BEP. Compared with conventional speed regulation, one of the key concepts of our previous work [10] is to use a frequency converter to enlarge the BEP to a larger flow rate point and use a valve to enlarge pipeline characteristics to a certain point; therefore the operation point of the pump is limited to the BEP at the cost of increasing energy consumption at the valve. The genetic algorithm in our previous work [10] will calculate the pressure loss across the valve. However, the flow rate and the pressure loss across the valve are coupled, making it difficult to control these two variables simultaneously. In our previous work [10], the author was concerned with the allocation of flow rate and the pressure loss at the valve but did not mention the way to reach the desired flow rate and pressure loss.

Figure 2 shows a comparison of valve regulation, speed regulation, and the new method in our previous work [10] for a typical pump-valve system, where the x -axis is the flow rate Q and the y -axis is the head Y . Supposing the flow rate of the system is to regulate from Q_0 to Q_1 , valve regulation changes pipeline characteristics from curve R_0 to R_1 , resulting in a change of operation point from A to B , while speed regulation changes pump characteristics from curve n_0 to n_1 , causing the operation point to change from A to C . It is clear that valve regulation causes a surplus head ($Y_B - Y_C$) and thus leads to a significant energy waste, appearing as the shadowed area in Figure 2. Therefore substituting throttling valve regulations with speed regulations has become a widespread energy saving method [11]. In the case of conventional speed regulation in Figure 2, the Best Efficiency Point of speed regulation might be located at somewhere (point E) left of the operation point C ; therefore the pump is operating at high flow rate point. Compared with conventional speed regulation, one of the key concepts of Wu's method [10] is to

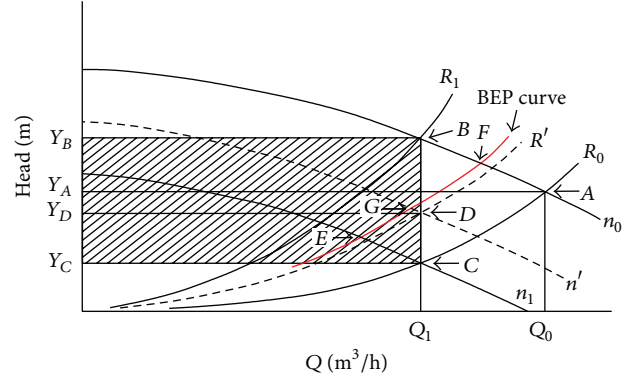


FIGURE 2: Comparison of valve regulation and speed regulation.

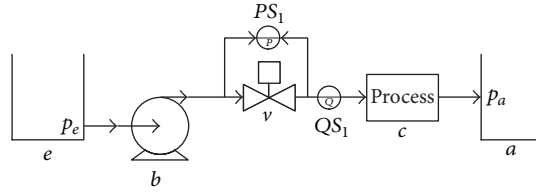
use a frequency converter to enlarge the BEP to a larger flow rate point D and use a valve to change pipeline characteristics to R ; therefore the operation point of the pump is limited to the BEP D at the cost of increasing energy consumption at the valve. The genetic algorithm in our previous work [10] will calculate the pressure loss across the valve. However, the flow rate and the pressure loss across the valve are coupled, making it difficult to control these two variables simultaneously.

This paper is an inherited work of our previous work [10] and aims at achieving the control of the two variables, flow rate and pressure loss across the valve of the pump-valve system, based on the optimization result of our previous work [10]. To emphasize the impact of valve on the pump operation point, this paper focuses on a one-pump system and gets rid of pump number selection strategy in our previous work [10]. This one-pump system is a special case of the multipump system in our previous work [10], because it can be regarded as small flow rate situation when only one pump is put into operation. The controlled variables of the pump-valve system are flow rate and the pressure loss across the valve, and the control variables are the pump speed and the valve lift. Since there are time delays in the valve actuator and the flow rate sensor, the pump-valve system is a nonlinear Multi-Input Multioutput (MIMO) system with time delays.

Many progresses have been made in the study of nonlinear MIMO systems during the past half century. The nonlinear MIMO systems with precise model are developed using input-output linearization to convert the nonlinear system into an equivalent linear systems in [12–14]. The nonlinear system with modelling imprecisions is presented using sliding model control in [13, 14] and adaptive control in [14]. As a simple approach to robust control, the sliding mode control for nonlinear systems with modelling imprecisions is implemented in a wide range of applications, such as electrohydraulic servo-mechanism [15, 16], electric drives [17], mechanical systems [18], and rigid manipulators [19]. During the past two decades, many approaches for uncertain nonlinear MIMO systems have been published. Shaocheng et al. [20] proposed a fuzzy adaptive indirect control for nonlinear MIMO systems with uncertainties using H_∞ tracking theory. The disturbances and fuzzy approximation errors are attenuated by a robust compensator to guarantee the



(a) Photograph of the test bench



(b) Schematic of the test bench

FIGURE 3: Test bench.

robustness. Lin and Chen [21] developed a fuzzy sliding mode control for the nonlinear MIMO systems with uncertainties. Ge and Tee [22] and Chen et al. [23] proposed fuzzy adaptive method for nonlinear MIMO system with time delays. However, the complexity and the model restrictions of fuzzy adaptive method may limit their industrial applications.

The time delays of control systems are commonly balanced by Smith predictor which is used in many applications, such as water distribution system [24] and jet engine fuel controls [25]. Many modified Smith predictors have been put into application such as filtered Smith predictor [26].

In this paper, the time delays of the pump-valve system are isolated from the system, dividing the system into a delay-free system and a time-delay module. The delay-free system is controlled by a sliding mode controller while the time delays are compensated by a modified Smith predictor. This method takes full advantage of the existing imprecise system model and greatly decreases the complexity of the control algorithm compared to fuzzy adaptive method. In Section 2, a test bench composed of one pump and one valve is presented and modelled in state space model. In Section 3, the delay-free system is controlled by a sliding mode controller and the time delays are compensated by a modified Smith predictor. Section 4 presents the simulation result of the controller. The optimization strategy in our previous work [10] and the control strategy in Section 3 are combined and applied on the one-pump system and compared with conventional speed regulation.

2. System Model

A typical fluid conveying system test bench is built. The bench consists of two parallel installed centrifugal pumps (Etanorm 32-160, rated flow $25 \text{ m}^3/\text{h}$ and rated speed 2950 rpm, equipped with a frequency converter) with manual valves installed at both ends of each pump, two pneumatic control valves (BOA-CVP H), and a water tank. As previously described, only one pump is applied in this paper; the other pump will not be used. The fluid in this study is chosen as water due to easy access and low costs. Water flows from the tank and flows back to the tank after a circulation through the centrifugal pump and the valves. Therefore the test bench

can be described as Figures 3(a) and 3(b), where b denotes the centrifugal pump, v denotes the pneumatic control valve, c denotes a typical pressure load (represented by the other pneumatic control valve), PS_1 denotes the pressure sensor that measures the pressure difference across the valve, QS_1 denotes the flow sensor, and e/a denotes the tank.

The mathematical model of the system can be developed by applying Bernoulli's principle [27] at entry e and exit a , as shown in

$$\rho g z_e + P_e + \frac{\rho}{2} v_e^2 = \rho g z_a + P_a + \frac{\rho}{2} v_a^2 + \rho \int_e^a \frac{\partial v(l, t)}{\partial t} dl + \rho g h_f, \quad (1)$$

where g denotes the gravitational acceleration, z denotes vertical height, v denotes flow velocity, ρ denotes fluid density, P denotes fluid pressure, t denotes time, h_f denotes the friction head, and l denotes the location along streamline coordinate. The diameter of pipes is constant and the water is considered to be incompressible since the compressibility of liquid is very low [27]; therefore the flow velocity is independent of the streamline coordinate. Therefore the inertia term in (1) can be simplified to (2) according to [27]

$$\rho \int_e^a \frac{\partial v(l, t)}{\partial t} dl = \frac{\rho L}{A} \dot{Q}, \quad (2)$$

where L denotes the length of the pipe between entry e and exit a ; A denotes the cross-sectional area of the pipe; Q denotes the flow rate in the pipe; and the overdot denotes its time derivative. The friction term $\rho g h_f$ can be considered as a sum of pressure loss ΔP (valve v) and ΔP_c (process load) as well as pressure source ΔP_p (pump b); (1) yields to

$$\begin{aligned} & \rho g (z_a - z_e) + P_a - P_e + \frac{\rho}{2} (v_a^2 - v_e^2) \\ &= -\frac{\rho L}{A} \dot{Q} + \Delta P_p - \Delta P - \Delta P_c. \end{aligned} \quad (3)$$

Since the entry e and the exit a are the same tank with small difference in vertical height, therefore it is reasonable

to assume $z_a = z_e$, $P_a = P_e$, and $v_a = v_e$. Ultimately, (1) can be written as fluid dynamic equation (4) as follows:

$$\dot{Q} = \frac{A}{\rho L} [\Delta P_p - \Delta P - \Delta P_c]. \quad (4)$$

The pump performance at rated speed n_r is a quadratic polynomial of flow rate and $\Delta P_{pn_r} = d'_1 Q_{n_r}^2 + d'_2 Q_{n_r} + d'_3$, which can be expanded to (6) at any given speed n by applying pump similarity law equation (5) [8]. The pressure loss ΔP (valve v) is relevant to installation conditions, fluid type, flow rate Q , and flow coefficient $K(H)$, where H denotes valve lift. In this paper, the fluid is water and the valve is standardly installed, which yields (7) [28], where $\Delta P_{\text{ref}} = 1 \times 10^5$ Pa. The pressure loss of ΔP_c (process load) is quadratic to flow rate [8], as shown in (8) as follows:

$$\frac{Q}{Q_{n_r}} = \frac{n}{n_r}, \quad (5)$$

$$\frac{\Delta P_p}{\Delta P_{pn_r}} = \left(\frac{n}{n_r} \right)^2,$$

$$\Delta P_p = d'_1 \left(\frac{n}{n_r} \right)^2 + d'_2 \left(\frac{n}{n_r} \right) Q + d'_3 Q^2 \quad (6)$$

$$\triangleq d_1 n^2 + d_2 n Q + d_3 Q^2,$$

$$\Delta P = \frac{Q^2}{K^2(H)} \Delta P_{\text{ref}}, \quad (7)$$

$$\Delta P_c = K_c Q^2, \quad (8)$$

where d'_1 , d'_2 , d'_3 , d_1 , d_2 , and d_3 are the pump parameters; n denotes speed of the pump; K_c denotes the resistance coefficient of the process load c . The dynamic response of the pneumatic valve and the frequency convertor can be described as first-order linear systems [29, 30], as shown in

$$\begin{aligned} \dot{H} &= \frac{1}{T_H} (H_{\text{set}} - H), \\ \dot{n} &= \frac{1}{T_n} (n_{\text{set}} - n), \end{aligned} \quad (9)$$

where T_H and T_n are the time constant of valve actuator and frequency converter and H_{set} and n_{set} denote the set values of H and n . According to the aims of the controller, the controlled variables are chosen to be flow rate requirement Q_{set} and pressure loss ΔP_{set} . The pressure loss across the valve ΔP_{set} equals the difference of pump head and system required head by the genetic algorithm in our previous work [10]. By applying (6), (7), and (8) to (4) and combining with (9), a state space model of the plant can be derived. The overall state space model can be described by (10). The system is a nonlinear MIMO system, whose time delays are omitted in (10) due to a comprehensible description:

$$\begin{aligned} \dot{x} &= f(x) + g(x)u, \\ y &= h(x), \end{aligned} \quad (10)$$

where

$$x = [x_1 \ x_2 \ x_3]^T = [Q \ H \ n]^T, \quad (11)$$

$$f(x) = \begin{bmatrix} \frac{A}{\rho L} \left[d_1 n^2 + d_2 n Q + \left(d_3 - \frac{\Delta P_{\text{ref}}}{K^2(H)} - K_c \right) Q^2 \right] \\ -\frac{1}{T_H} H \\ -\frac{1}{T_n} n \end{bmatrix} \triangleq \begin{bmatrix} w_1 \\ -\frac{1}{T_H} H \\ -\frac{1}{T_n} n \end{bmatrix}, \quad (12)$$

$$g(x) = (g_1 \ g_2) = \begin{pmatrix} 0 & 0 \\ \frac{1}{T_H} & 0 \\ 0 & \frac{1}{T_n} \end{pmatrix}, \quad (13)$$

$$u = [u_1 \ u_2]^T = [H_{\text{set}} \ n_{\text{set}}]^T, \quad (14)$$

$$y = [Q \ \Delta P]^T, \quad (15)$$

$$h(x) = \left[Q \ \frac{\Delta P_{\text{ref}}}{K^2(H)} Q^2 \right]^T, \quad (16)$$

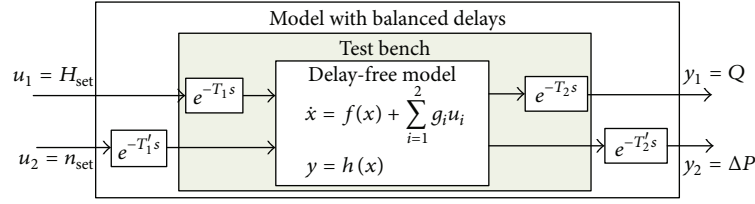


FIGURE 4: Test bench model, delay-free model, and model with balanced delays.

$$\begin{aligned}
 & (g_1 \quad g_2 \quad ad_f g_1 \quad ad_f g_2 \quad ad_f^2 g_1 \quad ad_f^2 g_2) \\
 & = \begin{pmatrix} 0 & 0 & -\frac{1}{T_H} \frac{\partial w_1}{\partial Q} & -\frac{1}{T_n} \frac{\partial w_1}{\partial n} & \left(-\frac{1}{T_H^2} + \frac{1}{T_H T_n}\right) \frac{\partial w_1}{\partial H} & \left(-\frac{1}{T_n^2} + \frac{1}{T_H T_n}\right) \frac{\partial w_1}{\partial n} \\ \frac{1}{T_H} & 0 & \frac{1}{T_H^2} & 0 & \frac{1}{T_H^3} & 0 \\ 0 & \frac{1}{T_n} & 0 & \frac{1}{T_n^2} & 0 & \frac{1}{T_n^3} \end{pmatrix}. \quad (17)
 \end{aligned}$$

As to the real test bench, time delays are observed in the valve actuator and the flow sensor. The time delays cannot be neglected due to the connection with system dynamics. The inputs and outputs of the system can be observed visually from the system model in Figure 4, where T_1 denotes time delay of the valve actuator and T_2 denotes time delay of the flow sensor. Since the actuators and the sensors of the systems have different delays, virtual delays $T_1' = T_1$ and $T_2' = T_2$ are added to the other input-output channels to balance the delays and obtain a synchronization performance of the system outputs.

3. Controller Design

Considering the pump-valve system is a time-delay system, we isolate the time delays of the system. The system without delays is controlled by a sliding mode controller and the time delays are compensated by a modified Smith predictor.

3.1. Control the Delay-Free Model. By applying Lie-derivative to the delay-free system equation (10), it is simple to linearize the input-output as

$$\begin{bmatrix} y_1^{(r_1)} \\ y_2^{(r_2)} \end{bmatrix} = \begin{bmatrix} y_1^{(2)} \\ y_2^{(1)} \end{bmatrix} = F + G \begin{bmatrix} u_1 \\ u_2 \end{bmatrix}, \quad (18)$$

where r_1 and r_2 are the relative degrees of the system, $r_1 = 2$ and $r_2 = 1$, respectively.

$$\begin{aligned}
 F & = \begin{bmatrix} L_f^2 h_1(x) \\ L_f h_2(x) \end{bmatrix} \\
 & = \begin{bmatrix} w_1 \frac{\partial w_1}{\partial Q} - \frac{1}{T_H} H \frac{\partial w_1}{\partial H} - \frac{1}{T_n} n \frac{\partial w_1}{\partial n} \\ w_1 \frac{2\Delta P_{ref} Q}{K^2(H)} + \frac{2\Delta P_{ref} Q^2}{T_H K^3(H)} \frac{dK(H)}{dH} \end{bmatrix} \triangleq \begin{bmatrix} f_1 \\ f_2 \end{bmatrix}, \quad (19)
 \end{aligned}$$

$$\begin{aligned}
 G & = \begin{pmatrix} L_{g_1} L_f h_1(x) & L_{g_2} L_f h_1(x) \\ L_{g_1} h_2(x) & L_{g_2} h_2(x) \end{pmatrix} \\
 & = \begin{pmatrix} -\frac{2A\Delta P_{ref} Q^2}{\rho L T_H K^3(H)} \frac{dK(H)}{dH} & \frac{A}{\rho L T_n} (2d_1 n + d_2 Q) \\ -\frac{2\Delta P_{ref} Q^2}{T_H K^3(H)} \frac{dK(H)}{dH} & 0 \end{pmatrix} \quad (20) \\
 & \triangleq \begin{pmatrix} g_{11} & g_{12} \\ g_{21} & g_{22} \end{pmatrix}.
 \end{aligned}$$

The singularity of G should be validated. The valve flow coefficient $K(H)$ is monotonically decreasing with valve lift H [28]; therefore its derivative is negative. The pump parameters d_1 and d_2 are positive; therefore G is nonsingular and invertible. By applying Lie bracket to (10), the controllability matrix can be obtained as (17). It has rank 3; therefore the system is controllable [31].

The r_i th derivative of output y_i is linearly related to the inputs u . By controlling the r_i th derivative of output y_i , the control of the output y_i is achieved. The model described by (10) in this paper yields to two decoupled single-input-single-output systems, one two-order (relative degree $r_1 = 2$) system for flow rate Q and one one-order (relative degree $r_2 = 1$) system for pressure loss across the control valve. It is easier to implement decoupling controller on the linear MIMO system. Since $r_1 = 2$ and $r_2 = 1$, the total relative degree equals the number of states; therefore the system will have no internal dynamics [14] and all the states of the system are observable.

In order to track target signal y_{di} , define a sliding surface $s_i = 0$ as (21), where $e_1 = y_{d1} - y_1$ and $e_2 = y_{d2} - y_2$ are the tracking errors of outputs.

$$S = \begin{bmatrix} s_1 \\ s_2 \end{bmatrix} = \begin{bmatrix} e_1^{(r_1-1)} + \alpha_{1(r_1-1)} e_1^{(r_1-2)} + \dots + \alpha_{11} e_1 \\ e_2^{(r_2-1)} + \alpha_{2(r_2-1)} e_2^{(r_2-2)} + \dots + \alpha_{21} e_2 \end{bmatrix}$$

$$= \begin{bmatrix} \dot{e}_1 + \alpha_{11}e_1 \\ e_2 \end{bmatrix}. \quad (21)$$

Combining (18), the derivative of s_i can be written as

$$\dot{S} = \begin{bmatrix} \dot{s}_1 \\ \dot{s}_2 \end{bmatrix} = \begin{bmatrix} m_1 \\ m_2 \end{bmatrix} - F - Gu, \quad (22)$$

where

$$\begin{aligned} \begin{pmatrix} m_1 \\ m_2 \end{pmatrix} &= \begin{pmatrix} y_{d1}^{(r_1)} + \alpha_{1(r_1-1)}e_1^{(r_1-1)} + \cdots + \alpha_{11}\dot{e}_1 \\ y_{d2}^{(r_2)} + \alpha_{1(r_2-1)}e_2^{(r_2-1)} + \cdots + \alpha_{21}\dot{e}_2 \end{pmatrix} \\ &= \begin{pmatrix} y_{d1}^{(2)} + \alpha_{11}\dot{e}_1 \\ \dot{y}_{d2} \end{pmatrix} \triangleq m, \end{aligned} \quad (23)$$

and the coefficients α_{ij} are chosen so that the polynomial in m_i is Hurwitz. In this case, we can simply choose $\alpha_{11} = 1$. Choose control law as

$$u = G^{-1} [-F + m + K \cdot \text{sgn}(S)], \quad (24)$$

where $\text{sgn}(s_i)$ is the sign function: $\text{sgn}(s_i) = +1$ if $s_i > 0$, $\text{sgn}(s_i) = 0$ if $s_i = 0$, $\text{sgn}(s_i) = -1$ if $s_i < 0$, and $K = [k_1, k_2]^T$ with $k_1 > 0$ and $k_2 > 0$. By substituting (24) into (22), we get

$$\begin{aligned} \dot{s}_1 &= -k_1 \cdot \text{sgn}(s_1), \\ \dot{s}_2 &= -k_2 \cdot \text{sgn}(s_2), \end{aligned} \quad (25)$$

which means $\lim_{t \rightarrow \infty} s_1 = 0$ and $\lim_{t \rightarrow \infty} s_2 = 0$; thus s_i goes to zero in finite time. Once the trajectory reaches the sliding surfaces, it follows that $\lim_{t \rightarrow \infty} e_1 = 0$ and $\lim_{t \rightarrow \infty} e_2 = 0$. Therefore the tracking performance is achieved.

Choose Lyapunov function as $V = V_1 + V_2 = s_1^2 + s_2^2$. The time derivative of V is

$$\begin{aligned} \dot{V} &= \dot{V}_1 + \dot{V}_2 = s_1\dot{s}_1 + s_2\dot{s}_2 \\ &= -k_1 \cdot \text{sgn}(s_1) - k_2 \cdot \text{sgn}(s_2) \leq 0. \end{aligned} \quad (26)$$

Therefore the stability of the system is guaranteed.

3.2. Compensating Time Delays. As illustrated in Figure 4, the time delays of valve actuator T_1 and flow sensor T_2 as well as the balanced delays T'_1 and T'_2 will affect system controllability; thus the delays should be compensated. The most common method to compensate time delays is Smith predictor [32]. The concept of Smith predictor is separating time delays from the system, controlling the delay-free part in an inner loop, and correcting modelling error and disturbance in an outer loop [33]. Since the inner control loop does not contain any time delays, the main controller can obtain a quick response to the system. The time delays of the bench or plant as a whole cannot be taken apart directly, so the model of the bench without time delays is needed for a quick response, which makes Smith predictor a model-based

control method. However, the conventional Smith predictor is sensitive to modelling error of the system.

To overcome the dependence of modelling accuracy, a modified Smith predictor [34] is applied for the pump-valve system in Figure 4, as shown in Figure 5. Compared with conventional Smith predictor, the modified Smith predictor introduces a first-order filter to attenuate the oscillations of the error between the real system and the predicted one. Therefore it can tolerate larger modelling errors, reduce the dependence on model accuracy, and improve the robustness of the system [35]. The first-order filter can be chosen as (27). T_f can be chosen as half of the pure time delay [35]; $T_f = 0.5 \times (T_1 + T_2)$ for both outputs for the model equation (10) since the time delays are balanced.

$$G_f(s) = \frac{1}{T_f s + 1}. \quad (27)$$

Therefore the overall control flow chart can be modified as Figure 6.

4. Experiment Validation and Analysis

To validate the control method developed in this paper, the experiment is done on the test bench as shown in Figure 3(b). The PLC is chosen as ABB PM554; the upper computer software is Simulink on an Intel 2.3 GHz PC. The upper computer and PLC communicate via OPC protocol at a sample frequency of 1 Hz. Other parameters are chosen as $T_1 = 0.3$ s, $T_2 = 0.9$ s, $T_H = 1$ s, and $T_n = 0.4$ s based on the actual characteristics of the bench components. The control law is chosen as (24). The time constants of filters in (27) are chosen as $T_f = 0.5 \times (T_1 + T_2) = 0.6$ s.

The experiment result is shown in Figure 7. The set point trajectories are chosen as the outputs of the optimization algorithm in our previous work [10], which are two step signals. It is shown that the actual trajectories converge to the set point trajectories. A step disturbance triggered by decreasing the lift of the pneumatic valve representing pressure load ΔP_c from 60% to 40%, which is very common in industrial applications, is added to the system at $t = 300$ s. The disturbance caused a fluctuation in both ΔP and Q and the fluctuation is soon suppressed in 25 seconds. Therefore the controller is satisfying in tracking performance and antidisturbance performance.

To verify the cooperation of the optimization method in our previous work [10] and the control method in this paper on this one-pump system, a comparison of operation point deviation and power consumption between conventional speed regulation in [3] and the new method in this paper on a low pipeline resistance system at different flow rate requirements is simulated. The results are shown in Figures 8(a) and 8(b), respectively. The operation point deviation θ is defined as (28) [10]. The genetic algorithm is applied on the single pump system and its optimization result is used as the input of the controller. The conventional speed regulation does not regulate valve and only regulates the pump speed using a simple PID controller; therefore the operation point is always far away from BEP if the pump is oversized for

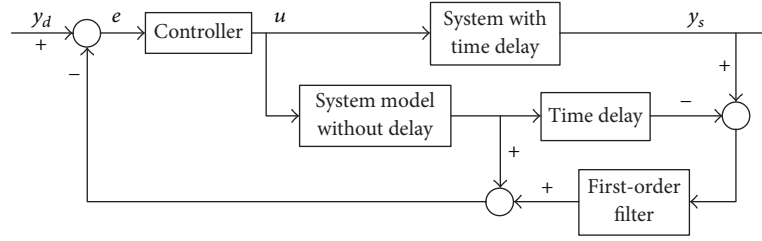


FIGURE 5: Schematic of modified Smith predictor.

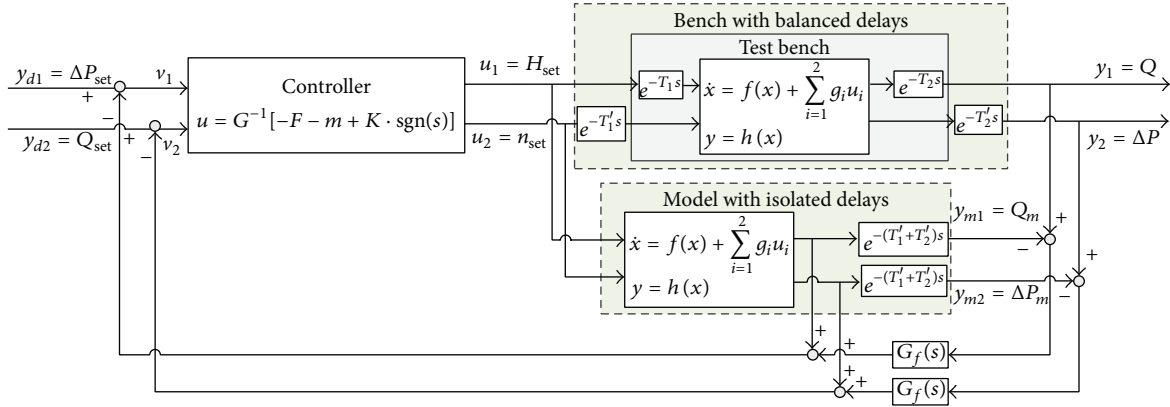


FIGURE 6: Overall control flow chart.

the system. Since the system in Figure 3(a) is a closed-loop test rig, the static head for the system curve is very small. In this case, the system curve is a parabolic curve similar to the BEP curve as pump speed varies. Figure 2 gives a qualitative explanation. For the initial operation point A, the BEP at operation speed n_0 is point F. When the operation point changes to point C using conventional speed regulation, the BEP becomes point E. However, the changes of BEP and operation point are almost equally proportional due to the similarity of the BEP curve and the system curve R_0 . Therefore the deviation almost remains constant as the flow varies for the conventional speed regulation.

$$\theta = \frac{Q - Q_{\text{BEP}}}{Q_{\text{BEP}}}. \quad (28)$$

The new method combines the optimization in our previous work [10] and the controller in this paper, optimizing the operation point and regulating both speed and valve. The new method obtains a wide flow range ($15 \text{ m}^3/\text{h} \sim 30 \text{ m}^3/\text{h}$) of small operation point deviation ($\leq 20\%$ from BEP). The deviations from the BEPs are clearly decreased at all flow rates for the new method; thus the reliability of the pump is improved. However, the power consumption is higher, due to extra energy consumed at part open control valve compared to conventional speed regulation method. In other words, the overall efficiency of the system is decreased for a better pump reliability. Better operation point cuts down the component failure rate and reduces maintenance cost, while lower system efficiency increases energy cost. If the benefits gained from better pump reliability win over the

costs of higher power consumption, it is suitable to apply this strategy to obtain higher reliability. The method is applicable for situation that requires high reliability but is insensitive to power consumption. If the flow rate far exceeds the BEP, the valve consumes a large amount of energy to shrink the operation point deviation. When the energy cost increased exceeds the maintenance cost reduced, it becomes uneconomic for this one-pump system. In this case, it is suggested to substitute the pump to a smaller pump or apply pump number optimization in our previous work [10].

5. Conclusion

In this paper, a typical fluid conveying system that consists of one pump and one valve is built to study the control of balancing efficiency and reliability. A control strategy aimed at achieving the control of the pump-valve system based on the optimization result in our previous work [10] is developed. The pump-valve system is a time-delayed nonlinear MIMO system. In this paper, the time delays are isolated from the system to form a delay-free system and a time-delay component. A sliding mode controller is developed to control the delay-free system and the time delays of the system are compensated by a modified Smith predictor. The experiment results show that the controller achieves good tracking performance and robustness. This method takes full advantage of the existing imprecise system model and greatly decreases the complexity of the control algorithm compared to fuzzy adaptive method.

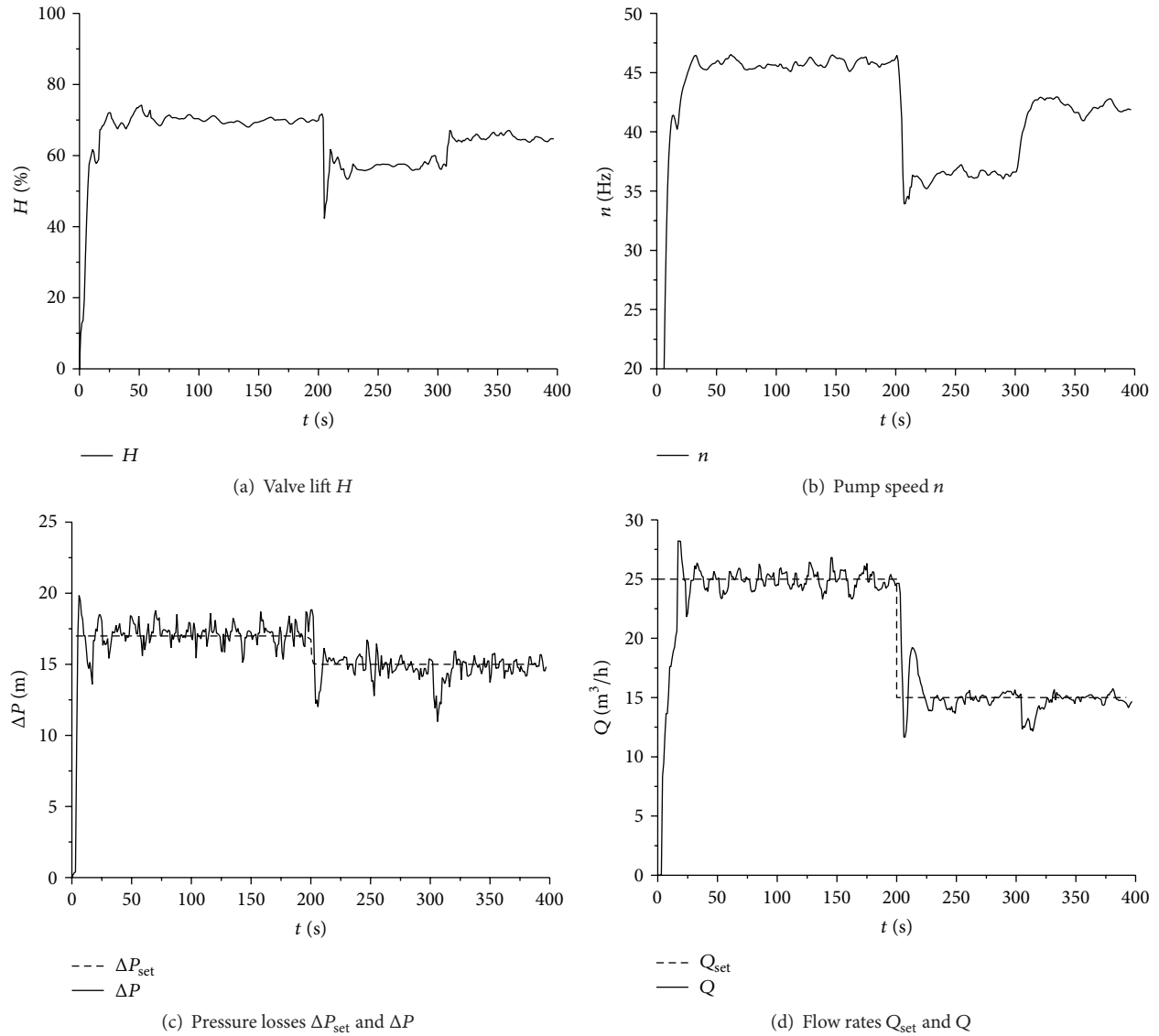


FIGURE 7: Experiment results.

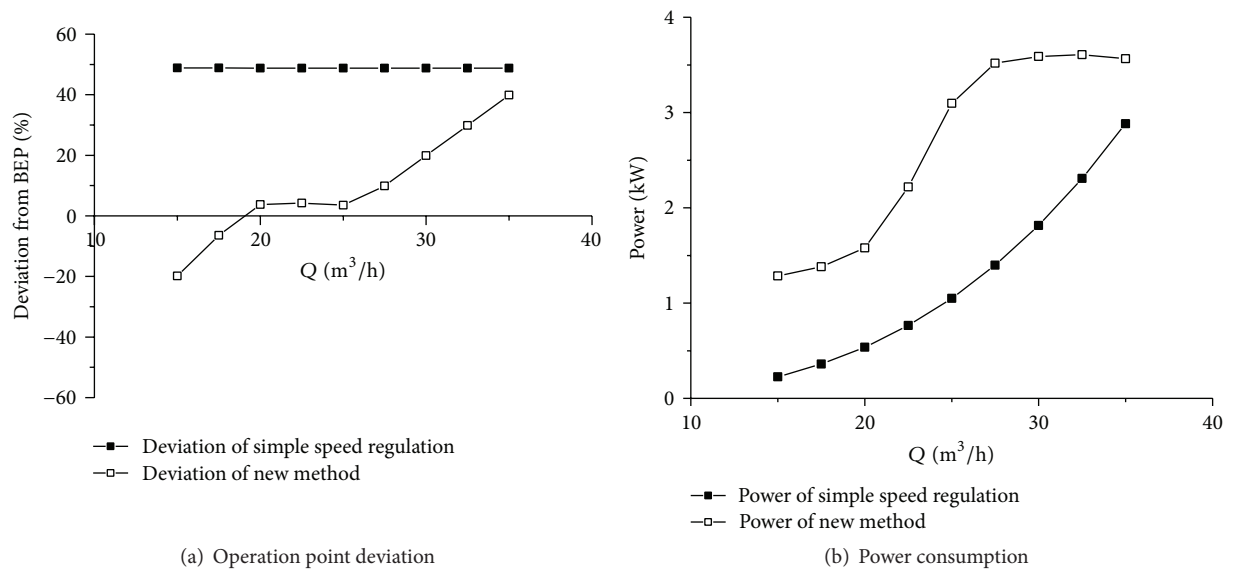


FIGURE 8: Comparison between conventional speed regulation and the new method.

A comparison of conventional speed regulation and the method combined with our previous work [10] is conducted. The comparison shows that the method can significantly reduce the operation point deviation at the cost of increasing power consumption. It is clearly shown in the comparison result that the new method sacrifices system efficiency for a better operation point. This paper offers an option to improve reliability of a class of fluid conveying systems, but it is worthwhile to weigh the better operation point against the higher energy consumption.

Competing Interests

The authors declare that they have no competing interests.

Acknowledgments

The authors would like to thank the support of National Natural Science Foundation of China (no. 51276213), Selected Postdoctoral Research Projects Foundation of Zhejiang Province (no. BSH1401015), and KSB AG.

References

- [1] Freedonia, *Industry Report—Machinery Pumps in China. Industry Report*, Freedonia Group, Cleveland, Ohio, USA, 2011.
- [2] L. Frenning, *Pump Life Cycle Costs: A Guide to LCC Analysis for Pumping Systems*, Hydraulic Institute & Europum & U.S. Department of Energy's Office of Industrial Technologies, 2001.
- [3] L. Jiang, Y. Chen, and G. Fan, "The design of constant pressure water supply system based on ABB inverter," *Procedia Engineering*, vol. 15, pp. 436–442, 2011.
- [4] S. Paul and U.S. Department of Energy, *United States Industrial Electric Motor Systems Market Opportunities Assessment. Government Report*, Office of Energy Efficiency and Renewable Energy, Washington, DC, USA, 2002.
- [5] M. Ciontu, D. Popescu, and M. Motocu, "Analysis of energy efficiency by replacing the throttle valve with variable speed drive condensate pump from E.C. Turceni," in *Proceedings of the 3rd International Symposium on Electrical and Electronics Engineering (ISEEE '10)*, pp. 293–297, IEEE, New York, NY, USA, September 2010.
- [6] J.-Y. Wang, T.-P. Chang, and J.-S. Chen, "An enhanced genetic algorithm for bi-objective pump scheduling in water supply," *Expert Systems with Applications*, vol. 36, no. 7, pp. 10249–10258, 2009.
- [7] S. S. Hashemi, M. Tabesh, and B. Ataekia, "Ant-colony optimization of pumping schedule to minimize the energy cost using variable-speed pumps in water distribution networks," *Urban Water Journal*, vol. 11, no. 5, pp. 335–347, 2014.
- [8] V. M. Cherkassky and B. Nikolaev, *Pumps Fans Compressors*, vol. 10, Mir, Moscow, Russia, 1980.
- [9] H. P. Barringer, "How to use reliability engineering principles for business issues," in *Proceedings of the YPF Reliability Symposium*, La Plata, Argentina, November 1998.
- [10] P. Wu, Z. Lai, D. Wu, and L. Wang, "Optimization research of parallel pump system for improving energy efficiency," *Journal of Water Resources Planning and Management*, vol. 141, no. 8, Article ID 04014094, 8 pages, 2015.
- [11] F. J. T. E. Ferreira, J. A. C. Fong, and A. T. de Almeida, "Ecoanalysis of variable-speed drives for flow regulation in pumping systems," *IEEE Transactions on Industrial Electronics*, vol. 58, no. 6, pp. 2117–2125, 2011.
- [12] A. Isidori, *Nonlinear Control Systems*, vol. 1 of *Communications and Control Engineering Series*, Springer, Berlin, Germany, 3rd edition, 1995.
- [13] S. Sastry, *Nonlinear Systems: Analysis, Stability, and Control*, vol. 10, Springer, New York, NY, USA, 2013.
- [14] J. J. E. Slotine and W. Li, *Applied Nonlinear Control*, vol. 199, Prentice Hall, New Jersey, NJ, USA, 1991.
- [15] C. Hwang, C. Lan, and W. Jieng, "The trajectory tracking of an electrohydraulic servo-mechanism via a sliding mode controller," *Proceedings of the Institution of Mechanical Engineers, Part I: Journal of Systems and Control Engineering*, vol. 207, no. 3, pp. 135–142, 1993.
- [16] S. Wang, S. Habibi, and R. Burton, "Sliding mode control for an electrohydraulic actuator system with discontinuous non-linear friction," *Proceedings of the Institution of Mechanical Engineers, Part I: Journal of Systems and Control Engineering*, vol. 222, no. 8, pp. 799–815, 2008.
- [17] V. I. Utkin, "Sliding mode control design principles and applications to electric drives," *IEEE Transactions on Industrial Electronics*, vol. 40, no. 1, pp. 23–36, 1993.
- [18] G. Bartolini, A. Pisano, E. Punta, and E. Usai, "A survey of applications of second-order sliding mode control to mechanical systems," *International Journal of Control*, vol. 76, no. 9–10, pp. 875–892, 2003.
- [19] Y. Feng, X. Yu, and Z. Man, "Non-singular terminal sliding mode control of rigid manipulators," *Automatica*, vol. 38, no. 12, pp. 2159–2167, 2002.
- [20] T. Shaocheng, T. Jiantao, and W. Tao, "Fuzzy adaptive control of multivariable nonlinear systems," *Fuzzy Sets and Systems*, vol. 111, no. 2, pp. 153–167, 2000.
- [21] W.-S. Lin and C.-S. Chen, "Robust adaptive sliding mode control using fuzzy modelling for a class of uncertain MIMO nonlinear systems," *IEE Proceedings: Control Theory and Applications*, vol. 149, no. 3, pp. 193–202, 2002.
- [22] S. S. Ge and K. P. Tee, "Approximation-based control of nonlinear MIMO time-delay systems," *Automatica*, vol. 43, no. 1, pp. 31–43, 2007.
- [23] B. Chen, X. P. Liu, K. F. Liu, and C. Lin, "Adaptive control for nonlinear MIMO time-delay systems based on fuzzy approximation," *Information Sciences*, vol. 222, pp. 576–592, 2013.
- [24] V. Feliu-Batlle, R. Rivas Pérez, F. J. Castillo García, and L. Sanchez Rodriguez, "Smith predictor based robust fractional order control: application to water distribution in a main irrigation canal pool," *Journal of Process Control*, vol. 19, no. 3, pp. 506–519, 2009.
- [25] M. Nasiri and M. Montazeri-Gh, "Time-delay compensation for actuator-based hardware-in-the-loop testing of a jet engine fuel control unit," *Proceedings of the Institution of Mechanical Engineers Part I: Journal of Systems and Control Engineering*, vol. 226, no. 10, pp. 1371–1380, 2012.
- [26] J. M. Romero-García, J. L. Guzmán, J. C. Moreno, F. G. Acien, and J. M. Fernández-Sevilla, "Filtered Smith Predictor to control pH during enzymatic hydrolysis of microalgae to produce L-aminoacids concentrates," *Chemical Engineering Science*, vol. 82, pp. 121–131, 2012.
- [27] G. Biswas, *Introduction to Fluid Mechanics and Fluid Machines*, McGraw-Hill Education, Columbus, Ohio, USA, 2nd edition, 2003.

- [28] IEC-60534-2-1, Flow Equations for Sizing Control Valve, 2007.
- [29] C. A. Smith and A. B. Corripio, *Principles and Practice of Automatic Process Control*, John Wiley & Sons, New York, NY, USA, 2nd edition, 1997.
- [30] A. Hughes and B. Drury, *Electric Motors and Drives: Fundamentals, Types and Applications*, Newnes, Burlington, Mass, USA, 4th edition, 2013.
- [31] V. G. Ivancevic and T. T. Ivancevic, *Geometrical Dynamics of Complex Systems: A Unified Modelling Approach to Physics, Control, Biomechanics, Neurodynamics and Psycho-Socioeconomical Dynamics*, vol. 31, Springer, Dordrecht, Netherlands, 2006.
- [32] M. Rao and H. Qiu, *Process Control Engineering: A Textbook for Chemical, Mechanical, and Electrical Engineering*, vol. 1, Gordon and Breach Science, New York, NY, USA, 1993.
- [33] O. J. Smith, "A controller to overcome dead time," *ISA Journal*, vol. 6, no. 2, pp. 28–33, 1959.
- [34] C. Hang and F. Wong, "Modified smith predictors for the control of processes with dead time," in *Proceedings of the ISA Annual Conference*, pp. 33–44, Chicago, Ill, USA, October 1979.
- [35] J. E. Normey-Rico, *Control of Dead-Time Processes*, Advanced Textbooks in Control and Signal Processing, Springer, London, UK, 2007.

Research Article

A Decoupling Control Strategy for Multilayer Register System in Printed Electronic Equipment

Shanhui Liu, Bingzheng Yin, Li'e Ma, Hongwei Xu, and Geshun Zhu

Faculty of Printing, Packaging Engineering and Digital Media Technology, Xi'an University of Technology, No. 5, Jinhua South Road, Xi'an 710048, China

Correspondence should be addressed to Shanhui Liu; shanhui.liu@xaut.edu.cn

Received 30 June 2016; Revised 13 August 2016; Accepted 16 August 2016

Academic Editor: Valentina E. Balas

Copyright © 2016 Shanhui Liu et al. This is an open access article distributed under the Creative Commons Attribution License, which permits unrestricted use, distribution, and reproduction in any medium, provided the original work is properly cited.

Register accuracy is an important index to evaluate the quality of electronic products printed by gravure printed electronic equipment. However, the complex relationships of multilayer register system make the problem of decoupling control difficult to be solved, which has limited the improvement of register accuracy for the gravure printed electronic equipment. Therefore, this paper presents an integrated decoupling control strategy based on feedforward control and active disturbance rejection control (ADRC) to solve the strong coupling, strong interference, and time-delay problems of multilayer register system. First of all, a coupling and nonlinear model is established according to the multilayer register working principle in gravure printing, and then a linear model of the register system is derived based on the perturbation method. Secondly, according to the linear model, a decoupling control strategy is designed based on feedforward control and ADRC for the multilayer register system. Finally, the results of computer simulation show that the proposed control methodology can realize a decoupling control and has good control performance for multilayer register system.

1. Introduction

Roll-to-roll (R2R) gravure printing machine is considered one of the highest throughput printed electronic equipment for manufacturing disposable and flexible electronic devices on flexible substrates at a low cost [1]. Register accuracy is an important index to evaluate the quality of printed electronic products. Unfortunately, because of the characteristics of multilayer register system including multi-input multioutput, strong coupling, strong disturbance, and time delay, it is difficult to solve the overshoot and concussion problems in the control process, which has limited the improvement of register accuracy for gravure electronic equipment. Hence, a decoupling control strategy is essential to improve the quality of printed electronic products.

Register errors directly reflect the register accuracy, including two kinds [2, 3]: machine directional register errors and cross directional register errors. In general, cross directional register errors can be ignored because the lateral jitter of a moving web is very small. Thus, the focus of this paper is on machine directional register errors which are

affected by many factors and are the emphasis and difficulty of multilayer register control system. In previous works, the synthesis control methods based on the PID control are the most common control strategy for the multilayer register system in the gravure printing machines. Yoshida et al. [4] established a mathematical model and proposed a cooperative register control method using feedforward and PD control for gravure printing presses. Based on the model established in [4], a speed variation compensation PD control was presented to eliminate the nondeterministic disturbance of the tension variation in speed-up process in [5]. Li et al. [6] established the mathematical model of two-layer register error and designed a control methodology based on feedforward and PID control to eliminate the interference caused by the speed and tension of upstream web. In [7], the mathematical model of register errors was established and a feedforward PID controller was proposed to cancel out the upstream speed disturbance and achieved good control effect. Chen et al. [8] developed an optimized feedforward decoupling PD register control method with membrane algorithm to generate optimized control signal

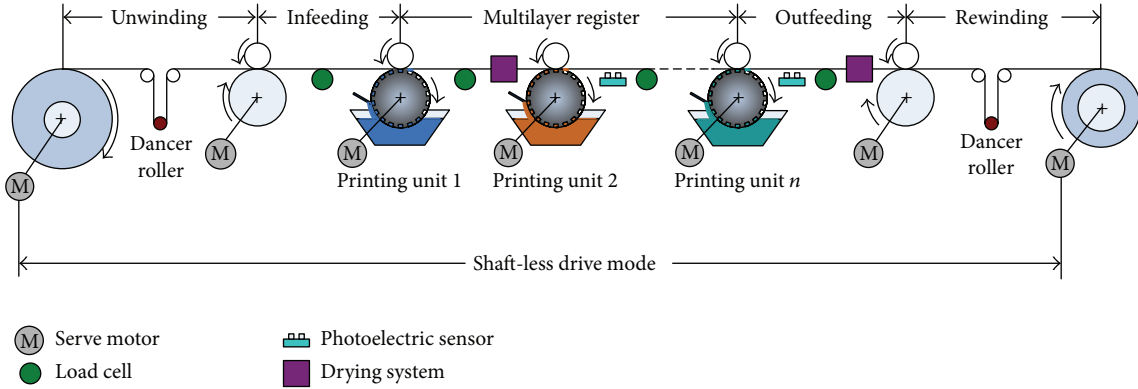


FIGURE 1: Schematic diagram of a gravure printed electronic equipment.

without the loss of accuracy of print registration. In [9], Lee et al. proposed a register strategy based on PID to investigate the dominant factor affecting register error and minimize it.

Some new control methods have been applied to register control system in the recent years. A nonlinear control law is designed with the Lyapunov stability theorem such that the register errors converge to zero in [10], and the method was confirmed to have better performance than the method proposed in [4]. A decentralized memoryless state feedback control law is proposed in [11] where the input delays are converted into state delays using dynamic feedback. In [12], a control strategy based on sliding mode variable structure was proposed for multilayer register system. According to the model established in [4], Chen et al. [13] proposed a decoupling and disturbance rejection control strategy which combines extended state observer with feedforward control for register system. Kim et al. designed register control strategy considering time difference between measurement and actuation for roll-to-roll gravure-offset printing equipment in [14] and then, they [15] proposed a register control method based on a statistical approach and signal processing technology. Although most of these methods resulted in acceptable control performance for traditional printing products, such as newspapers, magazines, and leaflets, printed electronic products require much higher register accuracy. Therefore, to obtain better print quality, it is necessary to present a decoupling control strategy that could effectively deal with the strong coupling, strong interference, time delay, and uncertain nature of multilayer register system. The synthesis control strategy based on active disturbance rejection control (ADRC) is an ideal candidate for multilayer register system. Because the essence of ADRC is that both the internal unmodeled coupling dynamics and the external disturbances can be estimated and compensated in real time [16–18], ADRC has been successfully applied in many fields [19–23]. Although initial evaluations of the application of ADRC for the regulation of register errors were performed in [3, 24], design difficulty of the proposed methods increases rapidly with the increase of printing layers in register system.

The objective of this research is to design a decoupling control strategy based on feedforward control and ADRC for the multilayer register system of gravure printed

electronic equipment. First, a nonlinear mathematical model of the four-layer register system is constructed and a linear model of the nonlinear model is derived in detail based on perturbation method. Next, according to the linear model, a decoupling control strategy is designed based on feedforward control and ADRC for the multilayer register system. Last, to test the effectiveness of the proposed decoupling strategy, simulations and analysis compared with PID and proposed controllers are carried out.

2. Mathematical Model

2.1. Multilayer Register System. The schematic diagram of a R2R gravure printed electronic equipment is shown in Figure 1, which is composed of an unwinding unit, an infeeding unit, a multilayer register system, an outfeeding unit, and a rewinding unit, and n stands for the total number of printing units. Shaftless drive mode has been used in the equipment; that is, all of the driving shafts are driven by independent servomotors. Control of the equipment is basically composed of tension control which is applied to the unwinding, infeeding, outfeeding, and rewinding units and register control which is applied to the multilayer register system. The printing cylinder of printing unit 1 maintains a constant angular velocity, and the angular velocity of other printing cylinders is adjusted according to register errors measured by photoelectric sensors. Load cells are installed at idle rollers in the middle of continuous process for tension pickup. Two passive dancer rollers are used to reduce tension fluctuations and measure the tension signals simultaneously in the unwinding and rewinding units.

Figure 2(a) shows the gravure schematic, and Figure 2(b) shows the schematic diagram of four-layer register system which can meet the needs of many printed electronic products, such as thin film transistors (as shown in Figure 2(b)), solar cells, and RFID tags. Register is the process of aligning successive printed patterns to form a complex multilayer image. Register control is critical because if the successively printed layers are not properly aligned then the functional capabilities of the printed electronic devices are reduced or lost. However, as shown in Figure 2(b), the multilayer register system has a cumulative effect in the process of

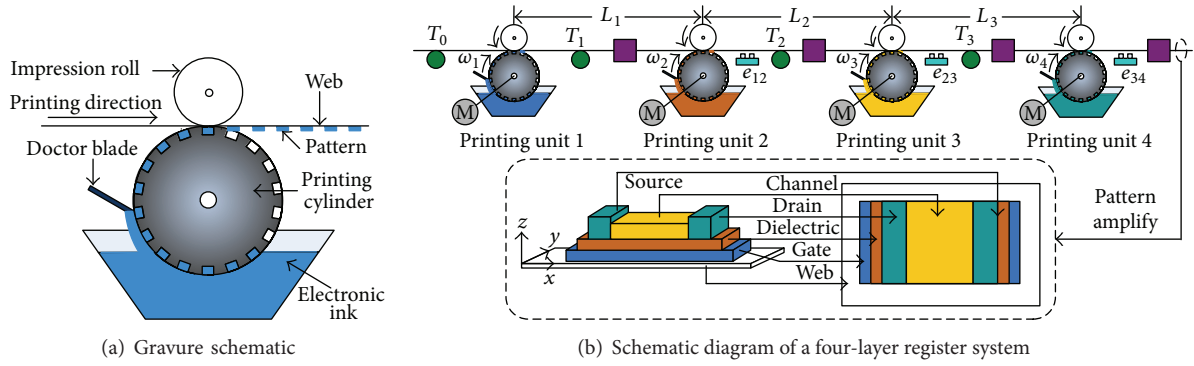


FIGURE 2: Schematic diagram of the gravure and four-layer register system.

printing; namely, the adjustment of register error in upstream printing section will affect all register errors in downstream printing sections, which makes the register system a significant nonlinear, strong coupling, and time-delay system. Furthermore, the drying systems bring a large number of unknown disturbances to the register control system. Hence, to achieve good microscale register accuracy, it is a key technology that a decoupling control strategy is designed to solve the nonlinear, strong coupling, strong interference, and uncertain problems of the register system.

2.2. Register System Model. The machine directional register error of a moving web is defined in two adjacent printing cylinders as the relative difference of the distance between the previous pattern printed by the upstream printing cylinder and the later printed one in the downstream printing cylinder. According to [25], we can get the nonlinear system model of the register error between i th and $(i + 1)$ th printing units as follows:

$$\begin{aligned} AE \frac{de_{i(i+1)}(t)}{dt} = & AE (R_{i+1}\omega_{i+1}(t) - R_i\omega_i(t - t_{Ti})) \\ & - T_i(t) R_i\omega_i(t) \\ & + T_{i-1}(t - t_{Ti}) R_i\omega_i(t - t_{Ti}), \end{aligned} \quad (1)$$

where t_{Ti} is transmission time (also known as time delay) and is defined by

$$t_{Ti} = \frac{L_i}{R_i\omega_i} \approx \frac{L_i}{R_i\omega^*}. \quad (2)$$

It is assumed that the nominal span lengths within adjacent printing units are typically same and there are no manufacturing errors in the register system. Thus, we can obtain (3) for the n -layer register system as follows:

$$\begin{aligned} R_1 = R_2 = \dots = R_i = \dots = R_n = R \\ L_1 = L_2 = \dots = L_i = \dots = L_n = L \\ t_{T1} = t_{T2} = \dots = t_{Ti} = \dots = t_{Tn} = t_T. \end{aligned} \quad (3)$$

Combining (1) and (3), (1) can be represented as follows:

$$\begin{aligned} \frac{de_{i(i+1)}(t)}{dt} = & R\omega_{i+1}(t) - \frac{R}{AE}T_i(t)\omega_i(t) - R\omega_i(t - t_T) \\ & + \frac{R}{AE}T_{i-1}(t - t_T)\omega_i(t - t_T). \end{aligned} \quad (4)$$

According to (4), Figure 2(b), and the working principle of multilayer register in gravure printing, the four-layer register system model can be expressed as follows:

$$\begin{aligned} \frac{de_{12}(t)}{dt} = & R\omega_2(t) - \frac{R}{AE}T_1(t)\omega_1(t) - R\omega_1(t - t_T) \\ & + \frac{R}{AE}T_0(t - t_T)\omega_1(t - t_T) \\ \frac{de_{23}(t)}{dt} = & R\omega_3(t) - \frac{R}{AE}T_2(t)\omega_2(t) - R\omega_2(t - t_T) \\ & + \frac{R}{AE}T_1(t - t_T)\omega_2(t - t_T) \\ \frac{de_{34}(t)}{dt} = & R\omega_4(t) - \frac{R}{AE}T_3(t)\omega_3(t) - R\omega_3(t - t_T) \\ & + \frac{R}{AE}T_2(t - t_T)\omega_3(t - t_T), \end{aligned} \quad (5)$$

where $\omega_2(t)$, $\omega_3(t)$, and $\omega_4(t)$ are the input signals of the register system and $e_{12}(t)$, $e_{23}(t)$, and $e_{34}(t)$ are the output signals of the register system.

Equation (5) shows that the four-layer register system is a multi-input multioutput, strong coupling, time-delay, and nonlinear system. The nonlinear model can be linearized using the perturbation method for the controller design. According to the perturbation method, all the variables in (5) are expressed using the steady-state values and the variable values, as described by the following equation:

$$\begin{aligned} e_{i(i+1)}(t) = & e^* + \Delta e_{i(i+1)}(t) \\ \omega_i(t) = & \omega^* + \Delta\omega_i(t) \\ T_i(t) = & T^* + \Delta T_i(t). \end{aligned} \quad (6)$$

Substituting (6) into (5) and ignoring high order small quantity, (5) can be rewritten as follows:

$$\begin{aligned}
\frac{d\Delta e_{12}(t)}{dt} &= R\Delta\omega_2(t) - \frac{RT^*}{AE}\Delta\omega_1(t) \\
&\quad + R\left(\frac{T^*}{AE} - 1\right)\Delta\omega_1(t - t_T) \\
&\quad + \frac{R\omega^*}{AE}[\Delta T_0(t - t_T) - \Delta T_1(t)] \\
\frac{d\Delta e_{23}(t)}{dt} &= R\Delta\omega_3(t) - \frac{RT^*}{AE}\Delta\omega_2(t) \\
&\quad + R\left(\frac{T^*}{AE} - 1\right)\Delta\omega_2(t - t_T) \\
&\quad + \frac{R\omega^*}{AE}[\Delta T_1(t - t_T) - \Delta T_2(t)] \\
\frac{d\Delta e_{34}(t)}{dt} &= R\Delta\omega_4(t) - \frac{RT^*}{AE}\Delta\omega_3(t) \\
&\quad + R\left(\frac{T^*}{AE} - 1\right)\Delta\omega_3(t - t_T) \\
&\quad + \frac{R\omega^*}{AE}[\Delta T_2(t - t_T) - \Delta T_3(t)].
\end{aligned} \tag{7}$$

Considering $T^* \ll AE$ and omitting the notation “ Δ ” to improve the readability, we can obtain the linearized model of the four-layer register system as follows:

$$\begin{aligned}
\frac{de_{12}(t)}{dt} &= R\omega_2(t) - \frac{RT^*}{AE}\omega_1(t) - R\omega_1(t - t_T) \\
&\quad + \frac{R\omega^*}{AE}[T_0(t - t_T) - T_1(t)] \\
\frac{de_{23}(t)}{dt} &= R\omega_3(t) - \frac{RT^*}{AE}\omega_2(t) + R\omega_2(t - t_T) \\
&\quad + \frac{R\omega^*}{AE}[T_1(t - t_T) - T_2(t)] \\
\frac{de_{34}(t)}{dt} &= R\omega_4(t) - \frac{RT^*}{AE}\omega_3(t) + R\omega_3(t - t_T) \\
&\quad + \frac{R\omega^*}{AE}[T_2(t - t_T) - T_3(t)].
\end{aligned} \tag{8}$$

With Laplace transform, the transfer functions of the four-layer register system can be got:

$$\begin{aligned}
E_{12}(s) &= G_A(s)W_2(s) + G_B(s)W_1(s) + G_C(s)T_0(s) \\
&\quad + G_D(s)T_1(s) \\
E_{23}(s) &= G_A(s)W_3(s) + G_B(s)W_2(s) + G_C(s)T_1(s) \\
&\quad + G_D(s)T_2(s) \\
E_{34}(s) &= G_A(s)W_4(s) + G_B(s)W_3(s) + G_C(s)T_2(s) \\
&\quad + G_D(s)T_3(s),
\end{aligned} \tag{9}$$

where $G_A(s)$, $G_B(s)$, $G_C(s)$, and $G_D(s)$ are expressed as

$$\begin{aligned}
G_A(s) &= \frac{R}{s} \\
G_B(s) &= -\frac{R}{s}\left(\frac{T^*}{AE} + e^{-t_T s}\right) \\
G_C(s) &= \frac{R\omega^*}{AEs}e^{-t_T s} \\
G_D(s) &= -\frac{R\omega^*}{AEs}.
\end{aligned} \tag{10}$$

According to (9), we can obtain the linear model of the adjacent two-layer register error between i th and $(i + 1)$ th printing unit as follows:

$$\begin{aligned}
E_{i(i+1)}(s) &= G_A(s)W_{i+1}(s) + G_B(s)W_i(s) \\
&\quad + G_C(s)T_{i-1}(s) + G_D(s)T_i(s).
\end{aligned} \tag{11}$$

As shown in (11), the register error $E_{i(i+1)}(s)$ is the combined result of multiple factors including $W_i(s)$, $W_{i+1}(s)$, $T_{i-1}(s)$, and $T_i(s)$. In shaftless drive mode, $W_{i+1}(s)$ is the control variable of two-layer register system whose corresponding transfer function $G_A(s)$ is the characteristics of register system on which the controller design is based. $W_i(s)$ is the coupling interference of the angular velocity from upstream printing unit i . $T_{i-1}(s)$ and $T_i(s)$ are the coupling interference of the web tension.

3. Design Decoupling Control Strategy

According to (11), an integrated decoupling control strategy based on feedforward control and ADRC is proposed for two-layer register system in Figure 3.

Figure 3 shows that the decoupling control strategy consists of a feedforward controller composed of $C_{W_i}(s)$, $C_{T_{i-1}}(s)$, and $C_{T_i}(s)$ and an ADRC controller. $C_{W_i}(s)$, $C_{T_{i-1}}(s)$, and $C_{T_i}(s)$ compensate the register errors caused by the variations of W_i , T_{i-1} , and T_i , respectively. The ADRC controller adjusts inputs $e_{ri(i+1)}$ of the register system and actively estimates and compensates the unmodeled coupling dynamics and disturbances in real time.

3.1. Design Feedforward Controller. As shown in Figure 2, the angular velocity of printing cylinders and the tension of the web can be measured directly by encoders installed at servomotors and load cells, respectively. Therefore, additive feedforward controller can alleviate the register errors caused by upstream modeled interferences through preadjustment.

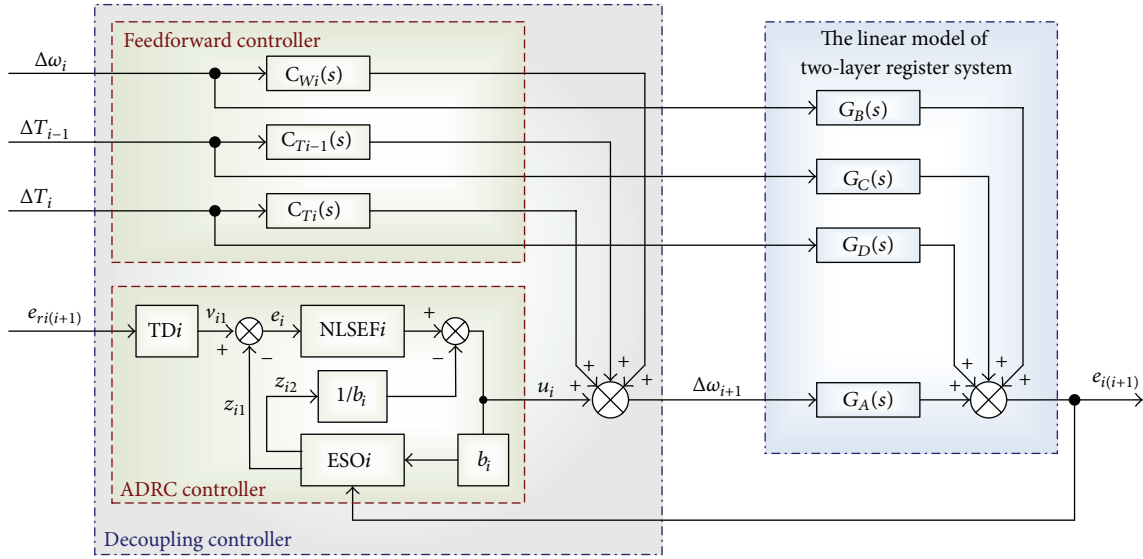


FIGURE 3: Block diagram of the integrated decoupling control strategy.

According to Figure 3 and the superposition theorem of linear system, the output of the two-layer register system can be written as

$$\begin{aligned}
 E_{i(i+1)}(s) = & \frac{G_A(s) C_i(s)}{1 + G_A(s) C_i(s)} E_{ri(i+1)}(s) \\
 & + \frac{G_B(s) + C_{Wi}(s) G_A(s)}{1 + G_A(s) C_i(s)} W_i(s) \\
 & + \frac{G_C(s) + C_{Ti-1}(s) G_A(s)}{1 + G_A(s) C_i(s)} T_{i-1}(s) \\
 & + \frac{G_D(s) + C_{Ti}(s) G_A(s)}{1 + G_A(s) C_i(s)} T_i(s).
 \end{aligned} \quad (12)$$

The feedforward controller can be designed based on invariance principle for canceling out the register errors caused by the variations of W_i , T_{i-1} , and T_i . We can obtain (13) as follows:

$$\begin{aligned}
 G_B(s) + C_{Wi}(s) G_A(s) &= 0 \\
 G_C(s) + C_{Ti-1}(s) G_A(s) &= 0 \\
 G_D(s) + C_{Ti}(s) G_A(s) &= 0.
 \end{aligned} \quad (13)$$

Hence, the feedforward controller (namely, $C_{Wi}(s)$, $C_{Ti-1}(s)$, and $C_{Ti}(s)$) can be designed as follows:

$$\begin{aligned}
 C_{Wi}(s) &= -\frac{G_B(s)}{G_A(s)} = \frac{T^*}{AE} + e^{-t_T s} \\
 C_{Ti-1}(s) &= -\frac{G_C(s)}{G_A(s)} = -\frac{\omega^*}{AE} e^{-t_T s} \\
 C_{Ti}(s) &= -\frac{G_D(s)}{G_A(s)} = \frac{\omega^*}{AE}.
 \end{aligned} \quad (14)$$

3.2. Design ADRC Controller. Because (11) shows that the two-layer register system is the first-order system, one first-order ADRC controller is needed for the decoupling control strategy. As shown in Figure 3, the ADRC controller consists of a tracking differentiator (TD), an extended state observer (ESO), and a nonlinear states error feedback (NLSEF).

The TD is a nonlinear component in which a tracking signal and an approximately differential signal of the system input can be acquired according to the system input signal, even for a nondifferentiable or noncontinuous input signal. Figure 3 shows that v_{i1} is tracking the signal of reference input $e_{ri(i+1)}$. According to [17–19], the discrete forms of the TD are expressed as follows:

$$fh_i(n) = fhan(v_{i1}(n) - e_{ri(i+1)}(n), v_{i2}(n), r_i, h)$$

$$v_{i1}(n+1) = v_{i1}(n) + hv_{i2}(n) \quad (15)$$

$$v_{i2}(n+1) = v_{i2}(n) + hf h_i(n),$$

where n is the natural number ($n = 0, 1, 2, 3, \dots$), r_i is the velocity factor, and h is the sampling step. According to [18, 21, 26], $fhan(x_1, x_2, r, h)$ is a nonlinear function that guarantees the fastest convergence from v_{i1} to $e_{ri(i+1)}$ without any overshoot and is defined as follows:

$$d = rh;$$

$$d_0 = hd$$

$$y = x_1 + hx_2;$$

$$a_0 = (d^2 + 8r|y|)^{1/2}$$

$$a = \begin{cases} x_2 + \frac{a_0 - d}{2} \text{sign}(y), & |y| > d_0 \\ x_2 + \frac{y}{h}, & |y| \leq d_0 \end{cases}$$

$$\text{fhan}(x_1, x_2, r, h) = - \begin{cases} r \text{sign}(a), & |a| > d \\ r \frac{a}{d}, & |a| \leq d. \end{cases} \quad (16)$$

The ESO is the core of ADRC which can not only track the system output variables and their differentiated signals but also actively estimate unmodeled coupling dynamics and disturbances in real time. Figure 3 shows that z_{i1} and z_{i2} track output $e_{i(i+1)}$ and estimated value of the unmodeled coupling dynamics and disturbances in the register system, respectively. According to [17, 18], the discrete forms of the second-order ESO i are obtained as follows:

$$q_i(n) = z_{i1}(n) - e_{i(i+1)}(n)$$

$$z_{i1}(n+1) = z_{i1}(n) + h(z_{i2}(n) - \beta_{i1}q_i(n) + b_i u_i(n)) \quad (17)$$

$$z_{i2}(n+1) = z_{i2}(n) + h(-\beta_{i2} \text{fal}(q_i(n), 0.5, h)),$$

where β_{i1} and β_{i2} are the ESO gains and b_i is the compensation factor. The $\text{fal}(e, \alpha, \delta)$ is a nonlinear function defined as follows:

$$\text{fal}(e, \alpha, \delta) = \begin{cases} \frac{e}{\delta^{1-\alpha}}, & |e| \leq \delta \\ |e|^\alpha \text{sign}(e), & |e| > \delta. \end{cases} \quad (18)$$

The NLSEF is a nonlinear combination of the resulting difference e_i caused by the v_{i1} and z_{i1} generated by TD and ESO, respectively. The control law of the ADRC can actively compensate for the unmodeled coupling dynamics and disturbances which are estimated by ESO in real time. According to [17, 18], we can obtain the discrete forms of the NLSEF i as follows:

$$e_i(n+1) = v_{i1}(n+1) - z_{i1}(n+1)$$

$$u_i(n+1) = k_{pi} \text{fal}(e_i(n+1), 0.5, \delta) - \frac{z_{i2}(n+1)}{b_i}, \quad (19)$$

where δ is the interval length of the linear segment and k_{pi} is the proportionality coefficient.

Combining (15), (17), and (19), the discrete algorithm of the ADRC i is expressed as

$$fh_i(n) = \text{fhan}(v_{i1}(n) - e_{ri(i+1)}(n), v_{i2}(n), r_i, h)$$

$$v_{i1}(n+1) = v_{i1}(n) + h v_{i2}(n)$$

$$v_{i2}(n+1) = v_{i2}(n) + h f h_i(n)$$

$$q_i(n) = z_{i1}(n) - e_{i(i+1)}(n)$$

$$z_{i1}(n+1) = z_{i1}(n) + h(z_{i2}(n) - \beta_{i1}q_i(n) + b_i u_i(n))$$

$$z_{i2}(n+1) = z_{i2}(n) + h(-\beta_{i2} \text{fal}(q_i(n), 0.5, h))$$

$$e_i(n+1) = v_{i1}(n+1) - z_{i1}(n+1)$$

$$u_i(n+1) = k_{pi} \text{fal}(e_i(n+1), 0.5, \delta) - \frac{z_{i2}(n+1)}{b_i}. \quad (20)$$

In actual printing process, the reference input of the register system is zero, scilicet $e_{ri(i+1)} = 0$. Consequently, the discrete algorithm of the ADRC can also be represented as follows:

$$q_i(n) = z_{i1}(n) - e_{i(i+1)}(n)$$

$$z_{i1}(n+1) = z_{i1}(n) + h(z_{i2}(n) - \beta_{i1}q_i(n) + b_i u_i(n))$$

$$z_{i2}(n+1) = z_{i2}(n) + h(-\beta_{i2} \text{fal}(q_i(n), 0.5, h)) \quad (21)$$

$$e_i(n+1) = -z_{i1}(n+1)$$

$$u_i(n+1) = k_{pi} \text{fal}(e_i(n+1), 0.5, \delta) - \frac{z_{i2}(n+1)}{b_i}.$$

As shown in Figure 3, output $\Delta\omega_{i+1}$ of the decoupling control strategy is composed of the ADRC controller's output u_i and the feedforward controller's outputs.

4. Simulation and Analysis

The comparative simulation of the four-layer register system between proposed decoupling control strategy and PID and ADRC control strategies is performed to investigate the performance of the proposed decoupling control strategy. The structure of the decoupling control strategy for four-layer register system is shown in Figure 4. The decoupling controller i ($i = 1, 2, 3$) of the two-layer register system in Figure 4 is shown in Figure 3. Figures 5(a) and 5(b) show the structures of the PID and ADRC control strategies, respectively, for four-layer register system.

The simulation adopts a fixed-step size mode and the fixed-step size is 10 ms (namely, the sampling step $h = 10$ ms) in MATLAB. The parameters of the register system used in the simulation are summarized in Table 1. On the basis of the same mathematical model and parameters, all parameters of ADRC and PID controllers are adjusted under the condition of $\omega^* = 1000$ rad/min, and the parameters are not changed with the change of the simulation conditions. The adjustment principle and procedure of ADRC controller parameters have been introduced in [27–29]. According to these literatures and our experiences, the adjustment procedure of the ADRC controller parameters is as follows.

Step 1. ESO parameter β_{i1} is equal to the reciprocal of the sampling step h . Thus, we can obtain $\beta_{i1} = 100$.

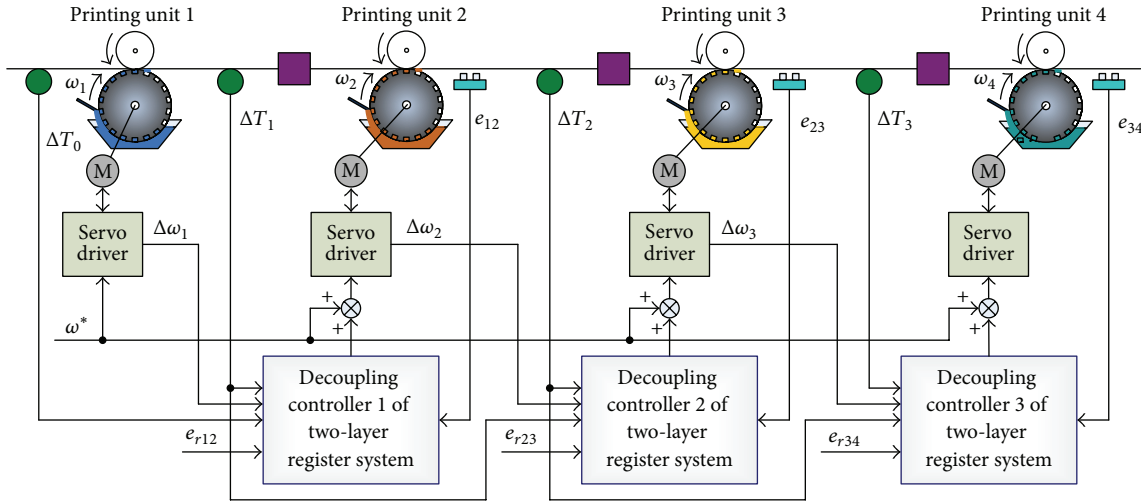


FIGURE 4: Structure of the decoupling control strategy for four-layer register system.

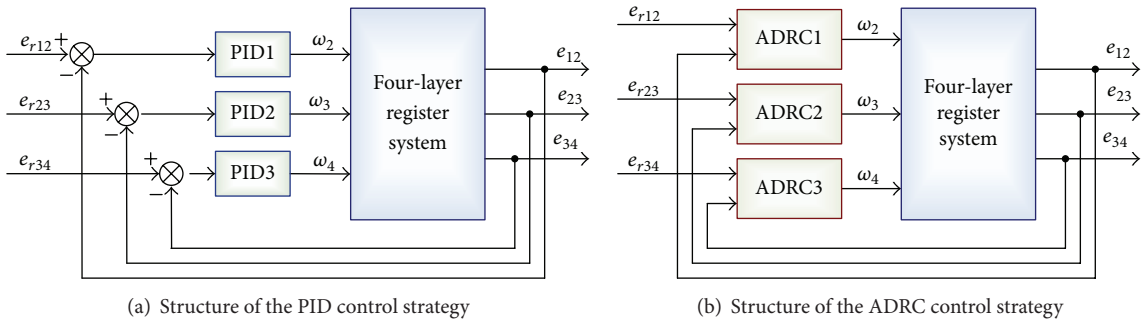


FIGURE 5: Structures of the PID and ADRC control strategies for four-layer register system.

TABLE 1: System parameters in simulation.

| Parameters | Value | Units |
|------------|--------------------|--------------|
| L | 6.28 | m |
| R | 0.2 | m |
| T_0 | 100 | N |
| A | 2×10^{-5} | m^2 |
| E | 2.1×10^9 | Pa |

Step 2. The ESO parameter β_{i2} is greater than β_{i1} . Under the open-loop condition, β_{i2} is adjusted to make z_{i1} trace $e_{ri(i+1)}$ with no vibration and β_{i2} is as big as possible under no vibration condition of the ESO output z_{i2} .

Step 3. The TD parameter r_i is adjusted to make v_{i1} and v_{i2} quickly trace system reference input $e_{ri(i+1)}$ and differentiated signal of $e_{ri(i+1)}$, respectively, in the open-loop condition.

Step 4. Under the closed-loop condition, the NLSEF parameter k_{ip} is adjusted to make the output $e_{i(i+1)}$ stable within reference input $e_{ri(i+1)}$ with no vibration.

The adjusted parameters of the PID and ADRC controllers are listed in Table 2.

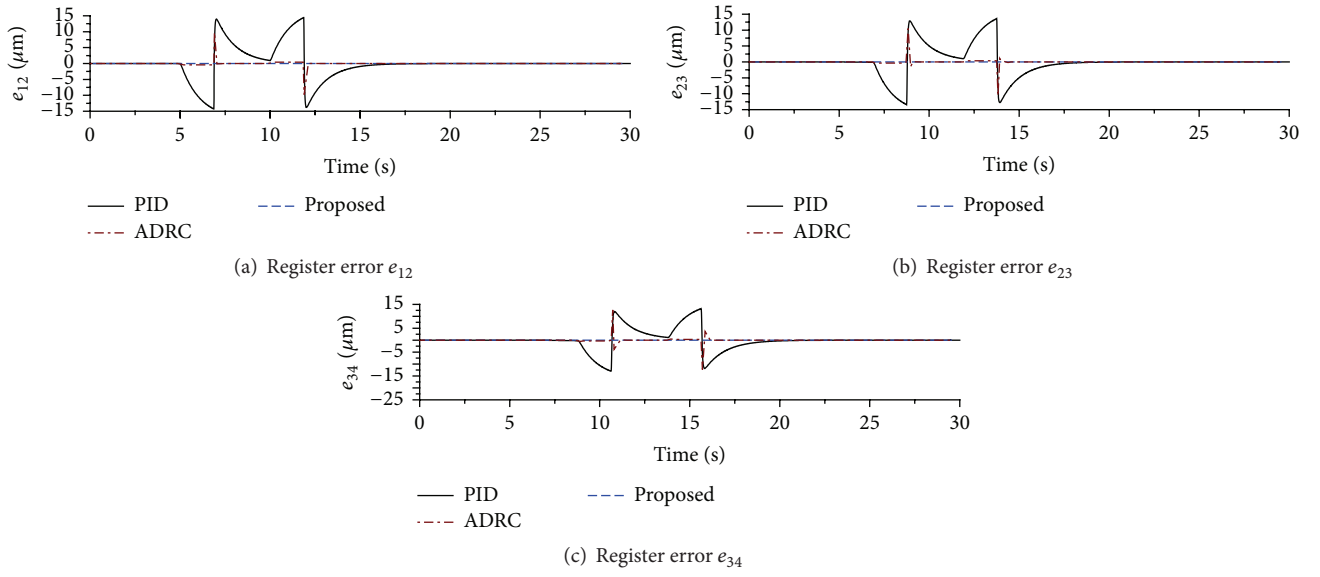
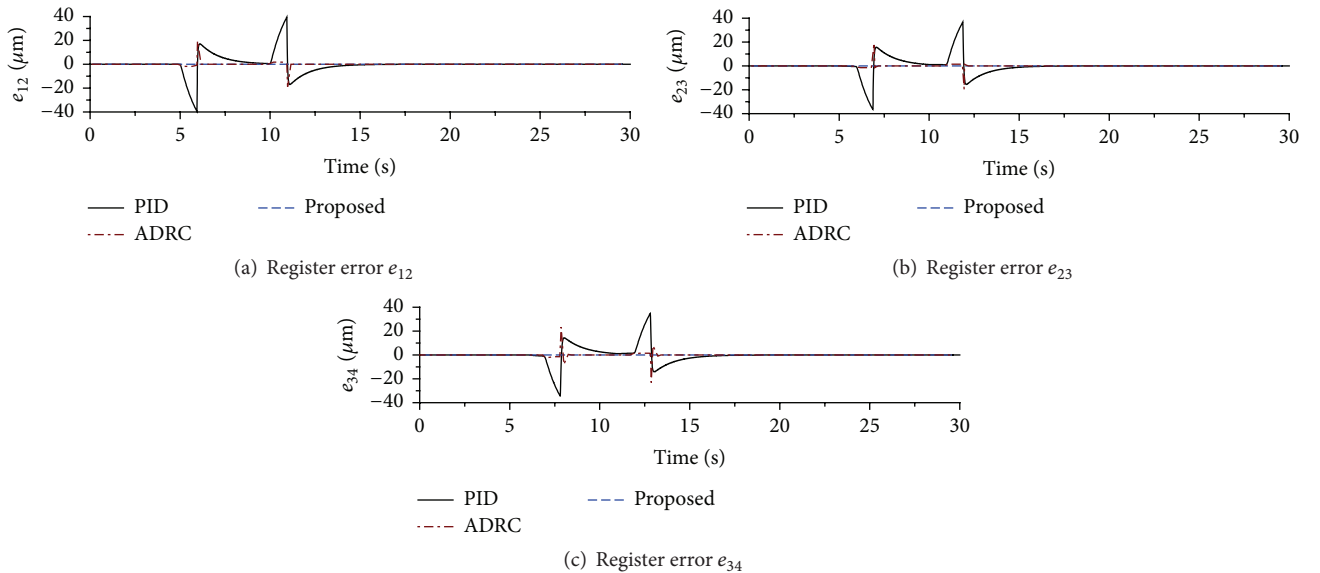
4.1. Performance against Tension Interference. $T_0(t)$ has a step change from 100 N to 130 N at 5 s and a step change from 130 N to 100 N at 10 s to investigate the performance against tension coupling interference of the proposed decoupling control strategy. The simulation behaviors of the PID, ADRC, and proposed decoupling control strategies are shown in Figures 6, 7, and 8.

Figures 6 and 7 show that, under the tension interference of $T_0(t)$, the register errors in PID and ADRC control strategies increase gradually with the increase of $\omega_1(t)$. As shown in Figure 8, under the same interference, the register errors in the proposed control strategy present the same trend as those in the PID and ADRC control strategies. However, compared with PID and ADRC control strategies, the range and duration of the register errors under the proposed control strategy are much smaller in the same simulation conditions, as shown in Figures 6 and 7. For example, when ω^* is equal to 2000 rad/min, the ranges of $e_1(t)$ fluctuation are 39.5 μm and 18.32 μm in the PID and ADRC control strategies, respectively, but under the proposed control strategy, the range of $e_1(t)$ fluctuation is only 38.6 nm.

The simulation results indicate that the feedforward and ADRC controllers can effectively compensate the register errors caused by the variations of $T_0(t)$; namely, the proposed decoupling control strategy has better performance against

TABLE 2: Controller parameters in simulation.

| Control strategy | Controller | Controller parameters |
|-----------------------------|------------|--|
| PID | PID1 | $k_{1p} = 70, k_{1i} = 30, k_{1d} = 1.2$ |
| | PID2 | $k_{2p} = 75, k_{2i} = 32, k_{2d} = 1.3$ |
| | PID3 | $k_{3p} = 80, k_{3i} = 35, k_{3d} = 1.3$ |
| ADRC | ADRC1 | $\beta_{11} = 100, \beta_{12} = 830, k_{1p} = 1.95, r_1 = 750$ |
| | ADRC2 | $\beta_{21} = 100, \beta_{22} = 840, k_{2p} = 3.86, r_1 = 750$ |
| | ADRC3 | $\beta_{31} = 100, \beta_{32} = 854, k_{3p} = 4.75, r_1 = 750$ |
| Proposed decoupling control | ADRC1 | $\beta_{11} = 100, \beta_{12} = 890, k_{1p} = 1.35, r_1 = 750$ |
| | ADRC2 | $\beta_{21} = 100, \beta_{22} = 930, k_{2p} = 3.26, r_1 = 750$ |
| | ADRC3 | $\beta_{31} = 100, \beta_{32} = 956, k_{3p} = 4.35, r_1 = 750$ |

FIGURE 6: Performance against tension interference for $\omega^* = 1000$ rad/min.FIGURE 7: Performance against tension interference for $\omega^* = 2000$ rad/min.

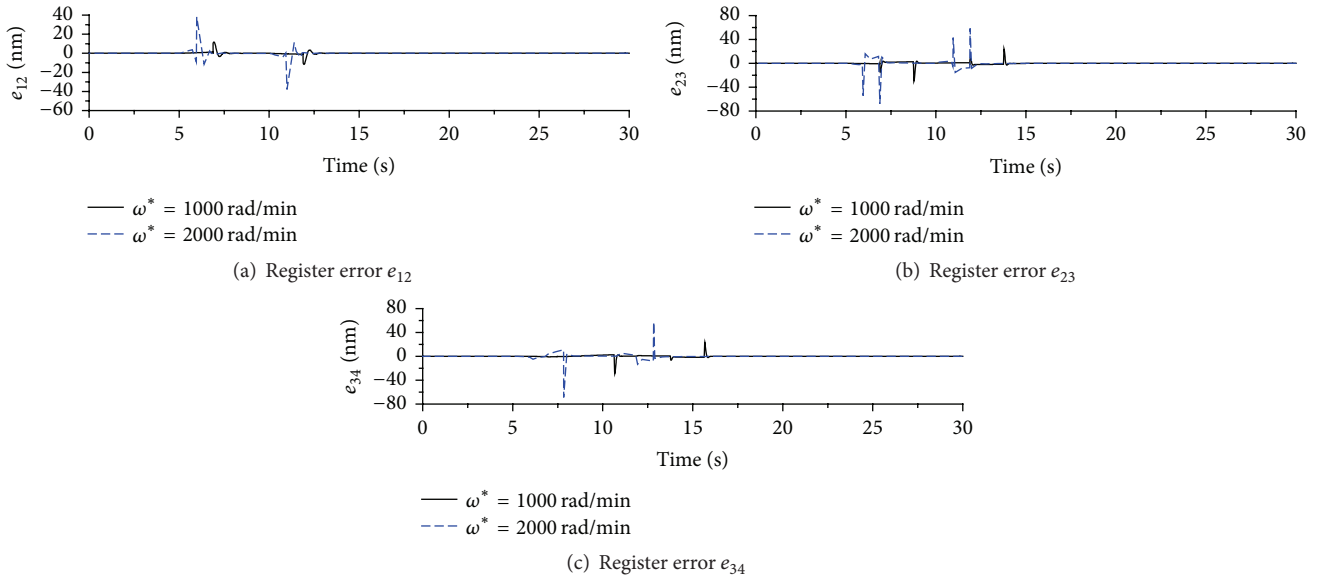
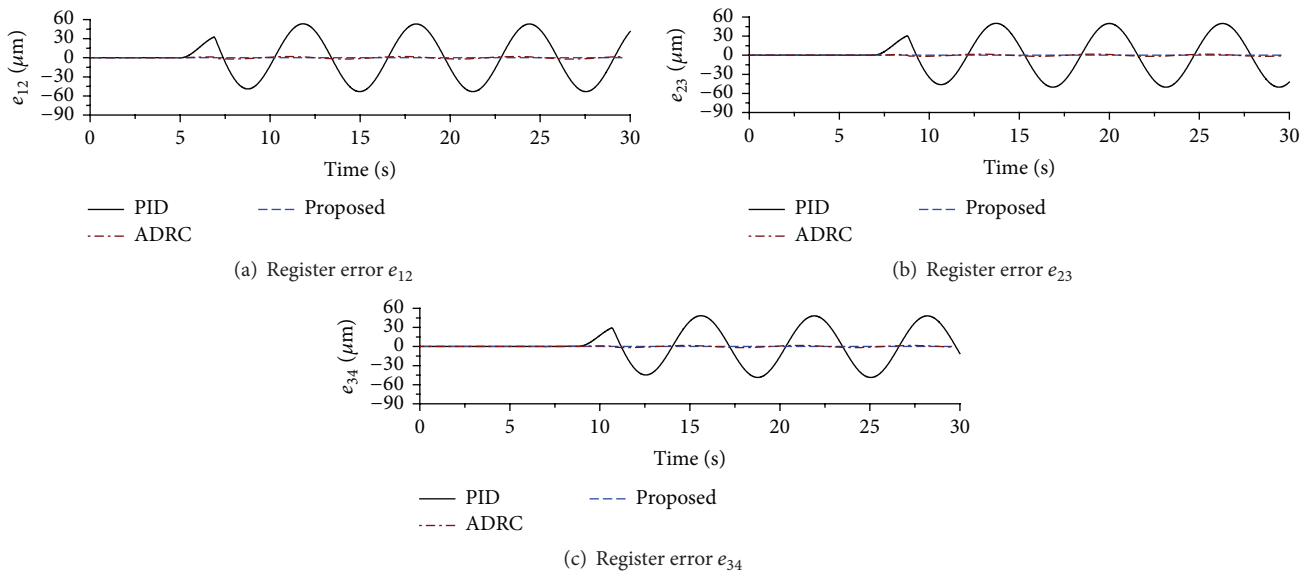


FIGURE 8: Response curves of the proposed decoupling control strategy.

FIGURE 9: Performance against speed interference for $\omega^* = 1000$ rad/min.

tension coupling interferences than the PID and ADRC control strategies.

4.2. Performance against Speed Interference. A sinusoidal interference of $\omega_1(t)$ is set at 5 s with amplitude 1 rad/min and frequency 1 rad/s to demonstrate the ability against speed coupling interference of the proposed decoupling control strategy. Figures 9 and 10 show the comparative performance of the PID, ADRC, and proposed decoupling control strategies. Figures 11 and 12 illustrate the behaviors of the ADRC and proposed decoupling control strategies, respectively.

Figures 9–12 illustrate that the fluctuation of register errors caused by speed interference of $\omega_1(t)$ has the same frequency with the interference in the PID, ADRC, and

proposed control strategies. Unfortunately, the range of register errors under the PID control strategy is much greater than that under the ADRC and proposed control strategies in the same simulation condition, as shown in Figures 9 and 10. Compared with ADRC control strategy, the range of the register errors under the proposed control strategy is much smaller in the same simulation conditions, as shown in Figures 11 and 12. For instance, when ω^* is equal to 1000 rad/min, the amplitude of $e_1(t)$ is only 8.3 nm in the proposed control strategy, but it is 53.2 μm in the PID control strategy and 1.96 μm in the ADRC control strategy.

The simulation results show that because the feedforward and ADRC controllers can obviously alleviate the register errors caused by the interference of $\omega_1(t)$, the proposed

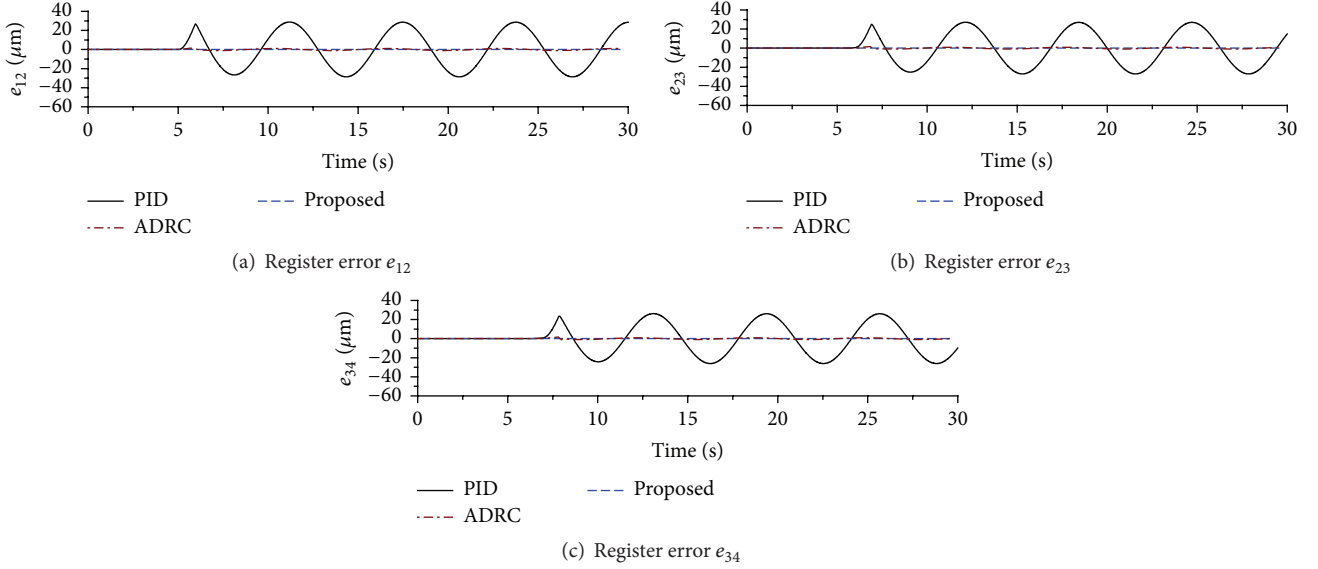
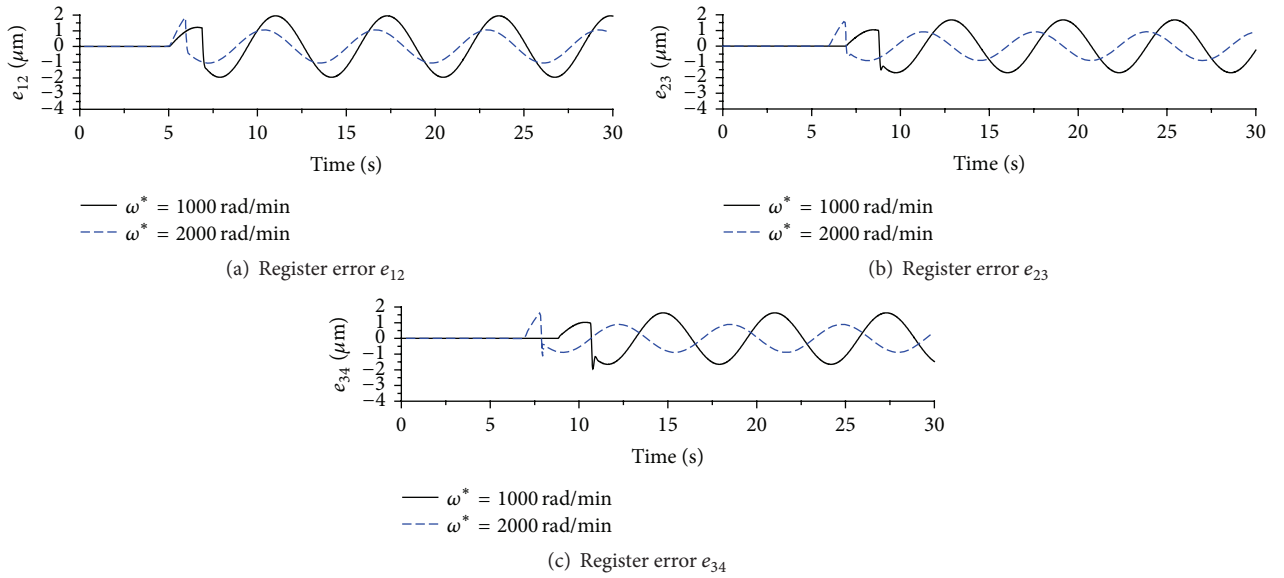
FIGURE 10: Performance against speed interference for $\omega^* = 2000$ rad/min.

FIGURE 11: Response curves of the ADRC control strategy.

decoupling control strategy has better ability against speed coupling interferences than the PID and ADRC control strategies.

4.3. Performance against Web Characteristic Change. The elastic modulus of the web material decreases to 80% in order to establish the performance against characteristic change of web for the proposed decoupling control strategy. With the step change of $T_0(t)$ from 100 N to 130 N at 5 s and from 130 N to 100 N at 10 s, Figures 13, 14, and 15 illustrate the simulation performance of the PID, ADRC, and proposed decoupling control strategies, respectively, when ω^* is equal to 2000 rad/min.

Figures 13 and 14 indicate that, under the PID and ADRC control strategies, the register errors increase gradually with

a decrease in E . For example, the range of $e_1(t)$ fluctuation increases from $39.3 \mu\text{m}$ to $50.1 \mu\text{m}$ in the PID control strategy and from $18.32 \mu\text{m}$ to $22.31 \mu\text{m}$ in the ADRC control strategy. Figure 15 shows that, with a decrease in E , the register errors also increase gradually in the proposed decoupling control strategy. For instance, the range of $e_1(t)$ is 38.6 nm to 46.2 nm when $E = 2.1 \times 10^9 \text{ Pa}$ and $E = 1.68 \times 10^9 \text{ Pa}$, respectively. However, with the same simulation condition, the increasing ranges of the PID and ADRC control strategies are 27.5% and 21.8%, respectively, which are greater than the increasing range 19.7% of register errors under the proposed control strategy.

The simulation results illustrate that because the ADRC controllers can actively estimate and compensate the register errors caused by characteristic change of web, the ADRC and

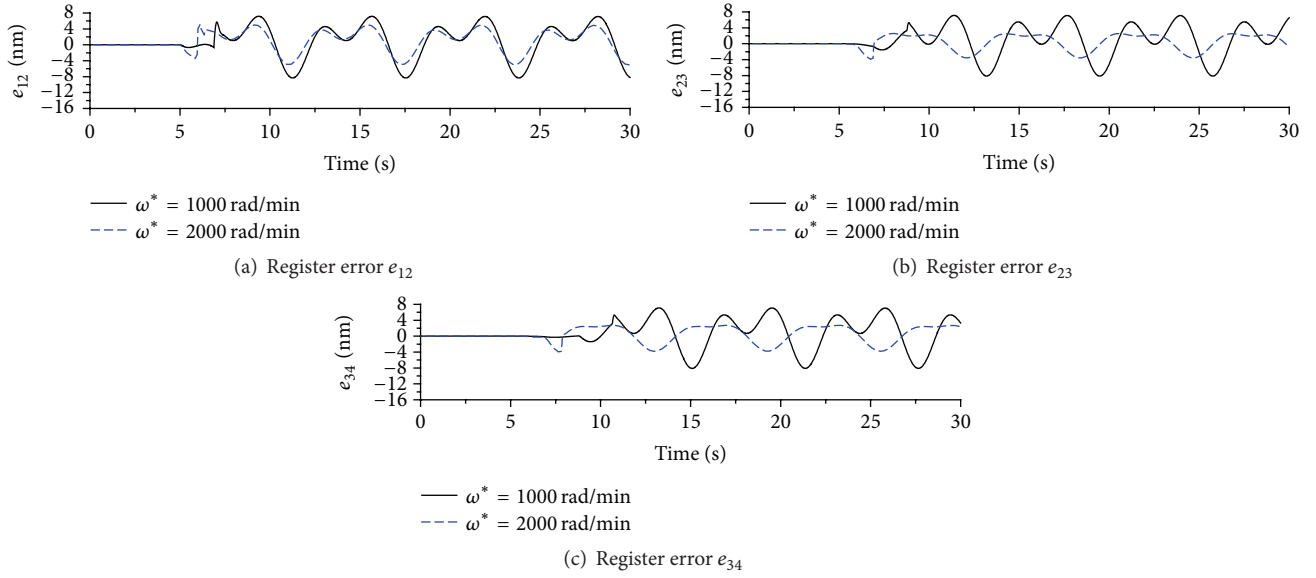


FIGURE 12: Response curves of the proposed decoupling control strategy.

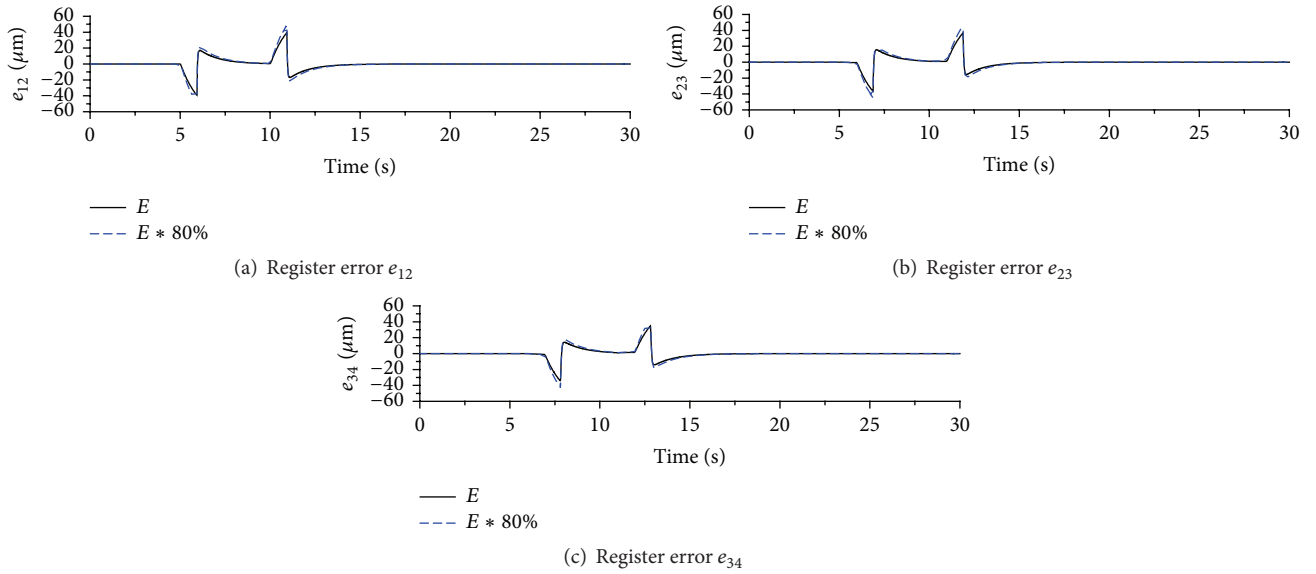


FIGURE 13: Response curves of the PID control strategy.

proposed control strategies have better capability against web characteristic changes than the PID control strategy.

5. Conclusions

In gravure printed electronic equipment, register accuracy is the most important index for the quality of multilayer register system. Therefore, in order to improve the register accuracy of multilayer register system, this paper proposes an innovative decoupling control synthesis strategy based on feedforward control and ADRC for the design of a register decoupling controller for the multilayer register system. The strategy is unique in which it uses feedforward controllers to compensate the register errors caused by the modeled

interferences and uses ADRC controllers to adjust the inputs of the register system and actively estimate and compensate the register errors caused by the unmodeled disturbances in real time, which makes the accuracy of the register controller greatly improve.

The simulation results illustrate that the proposed decoupling control strategy not only can effectively compensate the register errors caused by the variations of $T_0(t)$ and $\omega_1(t)$ (namely, modeled interferences) but also can obviously alleviate the register errors caused by the change of E (namely, unmodeled disturbance). The stability of the ADRC controller for nonlinear system has been proved in [30–32]. In this paper, although the stability of the proposed decoupling control strategy is not strictly proved by stability criterion

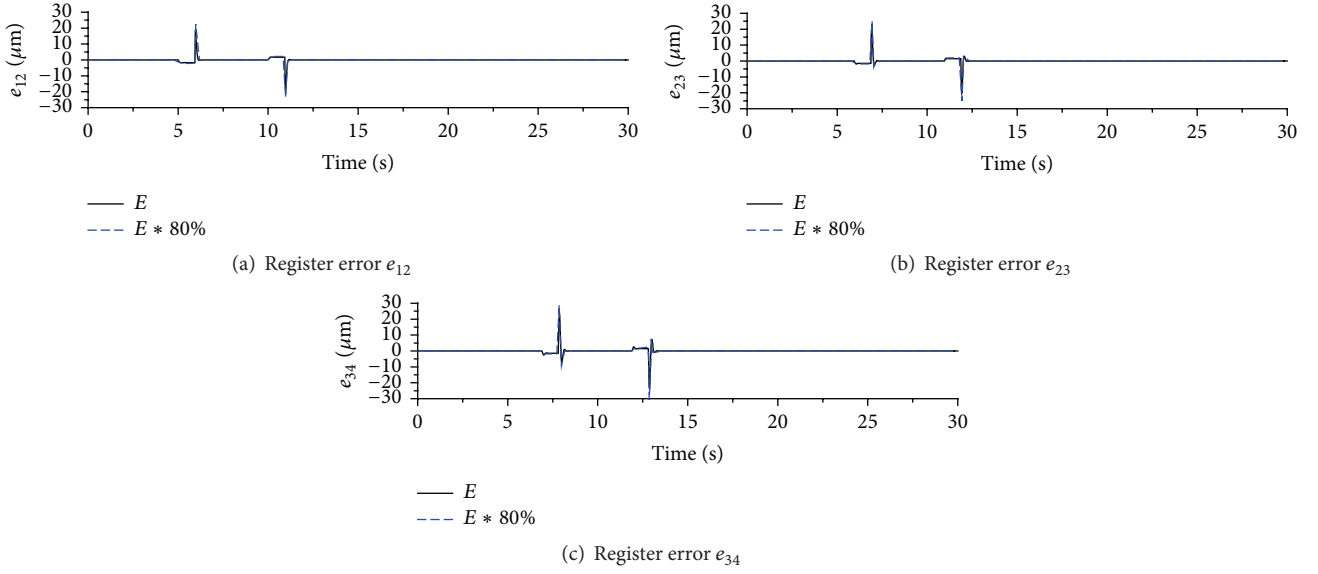


FIGURE 14: Response curves of the ADRC control strategy.

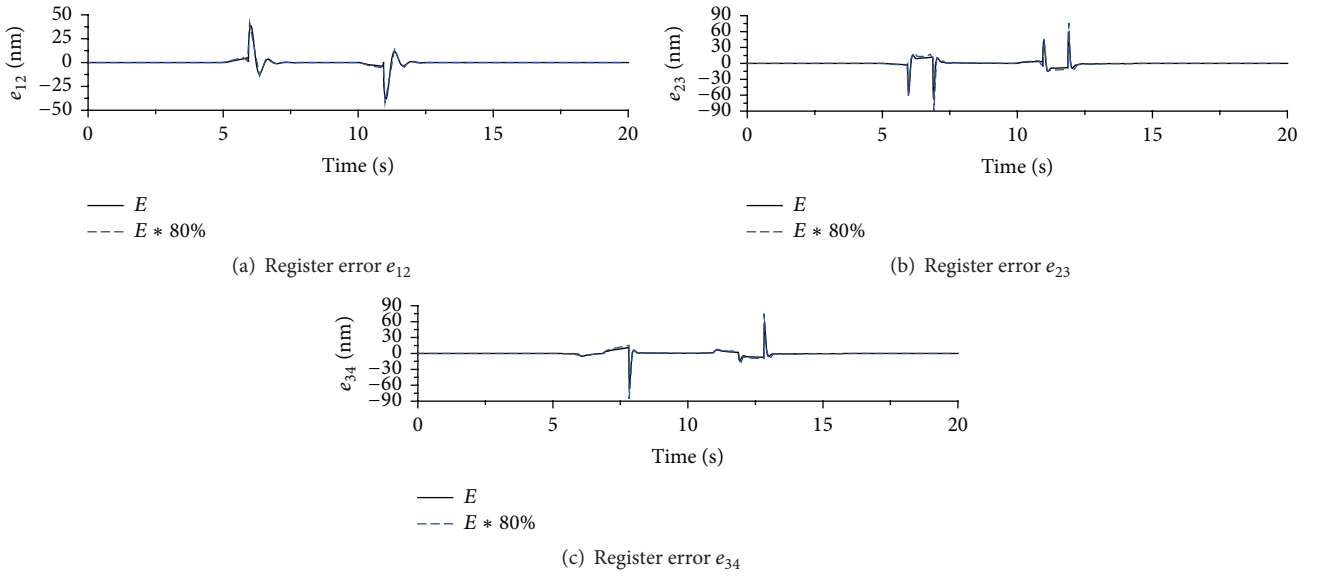


FIGURE 15: Response curves of the proposed decoupling control strategy.

for four-layer register system, the simulation results show that, with the disappearance of transient disturbances (for instance the interference of $T_0(t)$ in simulation), the outputs of the four-layer register system can return to their original equilibrium state rapidly. In other words, the proposed decoupling control strategy is stable for the four-layer register system. Therefore, this study demonstrates that the proposed strategy is a promising solution for solving the problem of the multilayer register system in R2R gravure printed electronic equipment.

Nomenclature

$e_{i(i+1)}$: Register error between i th and $(i + 1)$ th printing units (m)

e^* : Steady-state value of the $e_{i(i+1)}$ (m)
 $\Delta e_{i(i+1)}$: Variable value of the $e_{i(i+1)}$ (m)
 $e_{ri(i+1)}$: Reference inputs of the $e_{i(i+1)}$ (m)
 $E_{i(i+1)}(s)$: Image function of the $e_{i(i+1)}(t)$ (m)
 ω_i : Angular velocity of the printing cylinder i (rad/min)
 ω^* : Steady-state value of the ω_i (rad/min)
 $\Delta \omega_i$: Variable value of the ω_i (rad/min)
 $W_i(s)$: Image function of the $\omega_i(t)$ (rad/min)
 R_i : Radius of the printing cylinder i
 T_0 : Web tension of the infedding unit (N)
 T_i : Web tension in the i th span (N)
 T^* : Steady-state value of the T_i (N)
 ΔT_i : Variable value of the T_i (N)
 $T_i(s)$: Image function of the $T_i(t)$ (N)

- L_i : Nominal span length of the web in the i th span (m)
 t_{Ti} : Transmission time of the web from i th to $(i + 1)$ th printing units (s)
 E : Modulus of elasticity of the web material (Pa)
 A : Cross-sectional area of the web (m^2).

Competing Interests

The authors declare that there is no conflict of interests regarding the publication of this paper.

Acknowledgments

This project is supported by the National Natural Science Foundation of China (Grant nos. 51505376 and 51305341) and by the Natural Science Basic Research Plan in Shaanxi Province of China (Grant no. 2016JQ5038).

References

- [1] M. Jung, J. Kim, H. Koo, W. Lee, V. Subramanian, and G. Cho, "Roll-to-roll gravure with nanomaterials for printing smart packaging," *Journal of Nanoscience and Nanotechnology*, vol. 14, no. 2, pp. 1303–1317, 2014.
- [2] H.-K. Kang, C.-W. Lee, and K.-H. Shin, "Novel modeling of correlation between two-dimensional registers in large-area multilayered roll-to-roll printed electronics," *Japanese Journal of Applied Physics*, vol. 50, no. 1, Article ID 016701, 2011.
- [3] S. Liu, X. Mei, J. Li, K. He, and Q. Wen, "Design feedforward active disturbance rejection control controller for multi-color register system," *Journal of Mechanical Engineering*, vol. 51, no. 5, pp. 143–150, 2015.
- [4] T. Yoshida, S. Takagi, Y. Muto, and T. Shen, "Modeling and register control of sectional drive gravure printing press," *Transactions of the Japan Society of Mechanical Engineers, Part C*, vol. 74, no. 6, pp. 1438–1444, 2008.
- [5] M. Zhou, Z. Chen, Y. Zheng, and L. Zou, "Model based PD control during the speed-up phase in roll-to-roll web register systems," in *Proceedings of the 33rd Chinese Control Conference (CCC '14)*, pp. 5139–5143, Nanjing, China, July 2014.
- [6] J. Li, X. Mei, T. Tao, and S. Liu, "Research on the register system modelling and control of gravure printing press," *Proceedings of the Institution of Mechanical Engineers, Part C: Journal of Mechanical Engineering Science*, vol. 226, no. 3, pp. 626–635, 2012.
- [7] H. Kang, C. Lee, and K. Shin, "Modeling and compensation of the machine directional register in roll-to-roll printing," *Control Engineering Practice*, vol. 21, no. 5, pp. 645–654, 2013.
- [8] Z. Chen, J. He, Y. Zheng, T. Song, and Z. Deng, "An optimized feedforward decoupling PD register control method of Roll-to-Roll web printing systems," *IEEE Transactions on Automation Science and Engineering*, vol. 13, no. 1, pp. 274–283, 2016.
- [9] J. Lee, J. Seong, J. Park, S. Park, D. Lee, and K.-H. Shin, "Register control algorithm for high resolution multilayer printing in the roll-to-roll process," *Mechanical Systems and Signal Processing*, vol. 60, pp. 706–714, 2015.
- [10] T. Yoshida, S. Takagi, Y. Muto, and T. Shen, "Register control of roto gravure printing press. Application of nonlinear control theory to sectional drive printing press," *Electronics and Communications in Japan*, vol. 94, no. 1, pp. 17–24, 2011.
- [11] A. Seshadri and P. R. Pagilla, "Decentralized control of print registration in roll-to-roll printing presses," in *Proceedings of the ASME Dynamic Systems and Control Conference (DSCC '13)*, pp. 1–10, Palo Alto, Calif, USA, October 2013.
- [12] M. Yang and S. Zhang, "Simulation and research of register control system based on sliding mode variable structure," in *Proceedings of the 25th Chinese Control and Decision Conference (CCDC '13)*, pp. 514–519, Guiyang, China, May 2013.
- [13] Y.-J. Chen, Z.-H. Chen, and Z.-H. Deng, "Active disturbance rejection and decoupling control of gravure press register system," *Control Theory and Applications*, vol. 31, no. 6, pp. 814–820, 2014.
- [14] C. H. Kim, H.-I. You, and S.-H. Lee, "Register control of roll-to-roll gravure-offset printing equipment considering time difference between measurement and actuation," *Proceedings of the Institution of Mechanical Engineers, Part C: Journal of Mechanical Engineering Science*, vol. 226, no. 11, pp. 2726–2738, 2012.
- [15] C. Kim, H. You, and J. Jo, "Register control of roll-to-roll printing system based on statistical approach," *Japanese Journal of Applied Physics*, vol. 52, no. 5, pp. 1–5, 2013.
- [16] Z. Gao, "Active disturbance rejection control: a paradigm shift in feedback control system design," in *Proceedings of the American Control Conference*, pp. 2399–2405, Minneapolis, Minn, USA, June 2006.
- [17] J. Han, *Active Disturbance Rejection Control Technique*, National Defence Industry Press, Beijing, China, 2008.
- [18] J. Han, "From PID to active disturbance rejection control," *IEEE Transactions on Industrial Electronics*, vol. 56, no. 3, pp. 900–906, 2009.
- [19] S. Liu, X. Mei, F. Kong, and K. He, "A decoupling control algorithm for unwinding tension system based on active disturbance rejection control," *Mathematical Problems in Engineering*, vol. 2013, Article ID 439797, 18 pages, 2013.
- [20] Q. Zheng and Z. Gao, "Predictive active disturbance rejection control for processes with time delay," *ISA Transactions*, vol. 53, no. 4, pp. 873–881, 2014.
- [21] D. Li, C. Li, Z. Gao, and Q. Jin, "On active disturbance rejection in temperature regulation of the proton exchange membrane fuel cells," *Journal of Power Sources*, vol. 283, pp. 452–463, 2015.
- [22] G. Liang, W. Li, and Z. Li, "Control of superheated steam temperature in large-capacity generation units based on active disturbance rejection method and distributed control system," *Control Engineering Practice*, vol. 21, no. 3, pp. 268–285, 2013.
- [23] L. Sun, D. Li, K. Hu, K. Y. Lee, and F. Pan, "On tuning and practical implementation of active disturbance rejection controller: a case study from a regenerative heater in a 1000 MW power plant," *Industrial & Engineering Chemistry Research*, vol. 55, no. 23, pp. 6686–6695, 2016.
- [24] S.-H. Liu, X.-S. Mei, K. He, and J. Li, "Active disturbance rejection decoupling control for multi-color register system in gravure printing machine," *Control Theory and Applications*, vol. 31, no. 11, pp. 1574–1579, 2014.
- [25] S. Liu, X. Mei, J. Li, and L. Ma, "Machine directional register system modeling for shaft-less drive gravure printing machines," *Mathematical Problems in Engineering*, vol. 2013, Article ID 251636, 10 pages, 2013.

- [26] D. Li, Z. Li, Z. Gao, and Q. Jin, "Active disturbance rejection-based high-precision temperature control of a semibatch emulsion polymerization reactor," *Industrial and Engineering Chemistry Research*, vol. 53, no. 8, pp. 3210–3221, 2014.
- [27] X. Chen, D. Li, Z. Gao, and C. Wang, "Tuning method for second-order active disturbance rejection control," in *Proceedings of the 30th Chinese Control Conference (CCC '11)*, pp. 6322–6327, July 2011.
- [28] S. Liu, X. Mei, F. Kong, and J. Shen, "Tension controller design for unwinding tension system based on active disturbance rejection control," in *Proceedings of the 9th IEEE International Conference on Mechatronics and Automation (ICMA '12)*, pp. 1798–1803, Chengdu, China, August 2012.
- [29] W. Xue and Y. Huang, "On parameters tuning and capability of sampled-data ADRC for nonlinear coupled uncertain systems," in *Proceedings of the 32nd Chinese Control Conference*, pp. 317–321, Xi'an, China, October 2013.
- [30] Q. Zheng, L. Q. Gao, and Z. Gao, "On stability analysis of active disturbance rejection control for nonlinear time-varying plants with unknown dynamics," in *Proceedings of the 46th IEEE Conference on Decision and Control (CDC '07)*, pp. 3501–3506, IEEE, New Orleans, La, USA, December 2007.
- [31] J. Li, Y. Xia, X. Qi, Z. Gao, K. Chang, and F. Pu, "Absolute stability analysis of non-linear active disturbance rejection control for single-input-single-output systems via the circle criterion method," *IET Control Theory & Applications*, vol. 9, no. 15, pp. 2320–2329, 2015.
- [32] J. Li, X. Qi, Y. Xia et al., "On asymptotic stability for nonlinear ADRC based control system with application to the ball-beam problem," in *Proceedings of the 2016 American Control Conference*, pp. 4725–4730, Boston, Mass, USA, July 2016.

Research Article

Multiple Model-Based Synchronization Approaches for Time Delayed Slaving Data in a Space Launch Vehicle Tracking System

Haryong Song and Yongtae Choi

Flight Safety Technology Team, Korea Aerospace Research Institute, 169-84 Gwahangno, Yuseong-gu, Daejeon 305-806, Republic of Korea

Correspondence should be addressed to Haryong Song; hrsong@kari.re.kr

Received 19 May 2016; Revised 13 July 2016; Accepted 19 July 2016

Academic Editor: Quanmin Zhu

Copyright © 2016 H. Song and Y. Choi. This is an open access article distributed under the Creative Commons Attribution License, which permits unrestricted use, distribution, and reproduction in any medium, provided the original work is properly cited.

Due to the inherent characteristics of the flight mission of a space launch vehicle (SLV), which is required to fly over very large distances and have very high fault tolerances, in general, SLV tracking systems (TSs) comprise multiple heterogeneous sensors such as radars, GPS, INS, and electrooptical targeting systems installed over widespread areas. To track an SLV without interruption and to hand over the measurement coverage between TSs properly, the mission control system (MCS) transfers slaving data to each TS through mission networks. When serious network delays occur, however, the slaving data from the MCS can lead to the failure of the TS. To address this problem, in this paper, we propose multiple model-based synchronization (MMS) approaches, which take advantage of the multiple motion models of an SLV. Cubic spline extrapolation, prediction through an α - β - γ filter, and a single model Kalman filter are presented as benchmark approaches. We demonstrate the synchronization accuracy and effectiveness of the proposed MMS approaches using the Monte Carlo simulation with the nominal trajectory data of Korea Space Launch Vehicle-I.

1. Introduction

The range safety system (RSS) [1] for the flight mission of a space launch vehicle (SLV) consists of multiple heterogeneous tracking systems (TSs) with mission control systems (MCSs). Critical launch mission details such as time-space-position information (TSPI), launch mission status data, that is, quick look message (QLM), and flight safety information can be acquired from the RSS. Tracking an extensive mission trajectory of an SLV requires widespread multiple TSs so that the RSS covers the entire trajectory of the SLV flight mission. Generally, multiple TSs are spread out over different sites and they automatically hand over observation coverage according to the flight of the SLV. In this circumstance, one of the most important roles of the RSS is to distribute slaving data to each TS for continuous tracking of the SLV. If a critical network delay results in time delayed slaving data to be sent to the TSs, the MCS will not receive accurate SLV tracking data. This problem can lead to significant difficulties for the SLV mission progress and analysis. Therefore, the motivation of

this research is to enhance slaving data accuracy by compensating for possible network time delays. The basic solution to this problem is simple (linear or nonlinear) extrapolation of the filtered data. In this case, extrapolation methods simply propagate the TSPI data without regard to the system dynamics of the SLV. On the other hand, a Kalman filter (KF) and its prediction capability [2, 3] can reflect the system dynamics of the SLV, which results in better synchronization performance. However, since a KF only utilizes a single dynamic model, in general, the tracking performance of a KF for a maneuvering target is inferior to multiple model estimators [4]. In addition, due to stage separation, the flight phase of an SLV is separated into two parts, the propelled flight phase (PFP) and the coasting flight phase (CFP). Hence, the dynamic model of an SLV can be described using multiple models so that the multiple flight phases are properly accounted for. To adaptively select one of the multiple dynamic models according to the flight phase of the SLV, multiple model estimators (MME) such as an interacting multiple model (IMM) [5] and a multiple model adaptive estimator (MMAE) [6] could significantly

improve SLV tracking when a network delay results in delayed slaving data transmission.

In the past several decades, considerable research has been undertaken in the field of launch vehicle tracking based on multiple dynamic models; researchers have shown interest in various applications such as the tracking of reentry vehicles, short-range projectiles, and sounding rockets [7–13]. A reentry vehicle tracking problem known as highly nonlinear dynamics was conducted using a modified IMM, with a different algorithm cycle compared with an ordinary IMM with multiple modes of diverse ballistic coefficients [7]. Short-range ballistic munitions or projectiles with multiple models such as spin-stabilized and fin-stabilized models were implemented using an IMM [8, 9]. Both research alternatives can be applied in the impact point prediction of projectiles. Tactical ballistic missile tracking was carried out using an IMM estimator with three modes [10]. The first mode was a constant axial force model for the boosting and reentry phases. The second mode was a ballistic acceleration model that incorporated the gravitational, Coriolis, and centripetal forces for the exoatmospheric phase. The final mode was a standard autocorrelated acceleration Singer's model for malfunction motions of missiles such as reentry tumbling. A multiple IMM algorithm with an unbiased mixing approach for multiple modes of thrusting or for ballistic projectiles was presented [11, 12]. A sounding rocket with multiple modes of propelled flight or free fall flight was tracked using a multiple model adaptive estimation approach [14].

In this paper, multiple model-based synchronization (MMS) approaches are proposed to synchronize the time delayed slaving data of the RSS. The proposed approaches can be expressed via two distinct multiple models, a nonlinear model and a linear model. The nonlinear model considers comprehensive factors such as thrust, gravity, drag coefficient, Mach number, and air density [10–13]. Although the nonlinear model precisely describes the motion of the SLV, it requires complex information concerning the SLV specifications to be collected in advance. In contrast, in the case of the linear dynamic model, a simple constant velocity (CV) or constant acceleration (CA) model with multiple hypotheses, which takes advantage of Singer's model [16, 17], can be utilized [14]. To describe the motion of the SLV, the motion modes of both models are separated into two parts, PFP and CFP. We propose a slaving data synchronization approach for the RSS based on MME so that the MCS can adaptively find an appropriate dynamic model at an arbitrary time index, where time delay has occurred. The performance of slaving data synchronization is compared to various benchmark methods such as cubic spline extrapolation, prediction through an α - β - γ filter, and a single model KF to demonstrate the effectiveness of the proposed algorithm.

The remainder of the paper is organized as follows. Section 2 presents a statement of the problem for delayed slaving data in RSS. In Section 3, conventional synchronization approaches are illustrated. In Section 4, two proposed MME-based synchronization approaches are derived. Section 5 presents simulation settings and results; the comparison between different types of synchronization approaches is

depicted as an aspect of RMS error of the state vector. Finally, in Section 6, the conclusions of this paper are presented.

2. Problem Statement for Delayed Slaving Data in RSS

The transmission of slaving data from the MCS to multiple TSs facilitates seamless tracking of the SLV in a sparsely located multiple TS environment. If a data transmission delay problem occurs, it can cause an SLV tracking failure. As depicted in Figure 1, the antennas of TSs are pointing at the SLV by controlling their attitude according to slaving data from the MCS. In this situation, a slight time delay in slaving data can give rise to large differences between the antenna beam and the SLV due to the fast movement of the SLV. To solve this problem, we propose MMS approaches. Hence, the goal of this paper is to find a synchronized state $\hat{X}_{k+s}^{\text{sync}}$ at time $k+s$ (where s is a known delay) based on delayed slaving data \hat{X}_k^{delay} at time k such that

$$\hat{X}_{k+s}^{\text{sync}} = f^p \left(s, \hat{X}_k^{\text{delay}} \right), \quad X = [x \ y \ z]^T, \quad (1)$$

where f^p is a linear or nonlinear propagation function and $X = [x \ y \ z]^T$ is a slaving state vector that is composed of x -axis, y -axis, and z -axis positions but is not limited to the position components.

3. Conventional Synchronization Approaches for Slaving Data

3.1. Synchronization Using Cubic Spline Extrapolation [18, 19].

Let us assume a synchronized slaving state vector to be an unknown function of the delayed slaving state vector whose values are known only until time k . We then define a cubic spline extrapolation function $f_n^{\text{ep}}(k+s)$, where $n = x, y, z$ at a specific synchronization time $k+s$ that is extrapolated based on the known function $f_n(k)$ that has a real value, with $N+1$ points, where $k_0 \leq k \leq k_N$.

We approximate $f_n^{\text{ep}}(k+s)$ as a three-order polynomial based on the interval $[k_i, k_{i+1}]$, where $i = 0, \dots, N-1$. Then $f_n^{\text{ep}}(k+s)$ can be defined as follows:

$$\begin{aligned} f_n^{\text{ep}}(k+s) &= \{f_n(k), k \in [k_i, k_{i+1}], i = 0, \dots, N-1\}, \\ f_n(k) &= a_{n,i}k^3 + b_{n,i}k^2 + c_{n,i}k + d_{n,i}, \end{aligned} \quad (2)$$

where $a_{n,i}$, $b_{n,i}$, $c_{n,i}$, and $d_{n,i}$ are unknown coefficients. To find the unknown coefficients, we make the assumption that $f_n(k)$ should be continuous in $[k_0, k_N]$. Therefore, the following equation containing unknown coefficients $a_{n,i}$, $b_{n,i}$, $c_{n,i}$, and $d_{n,i}$ is obtained:

$$\begin{aligned} f_{n,i}(k_i) &= f_{n,i+1}(k_i) \\ f'_{n,i}(k_i) &= f'_{n,i+1}(k_i), \end{aligned}$$

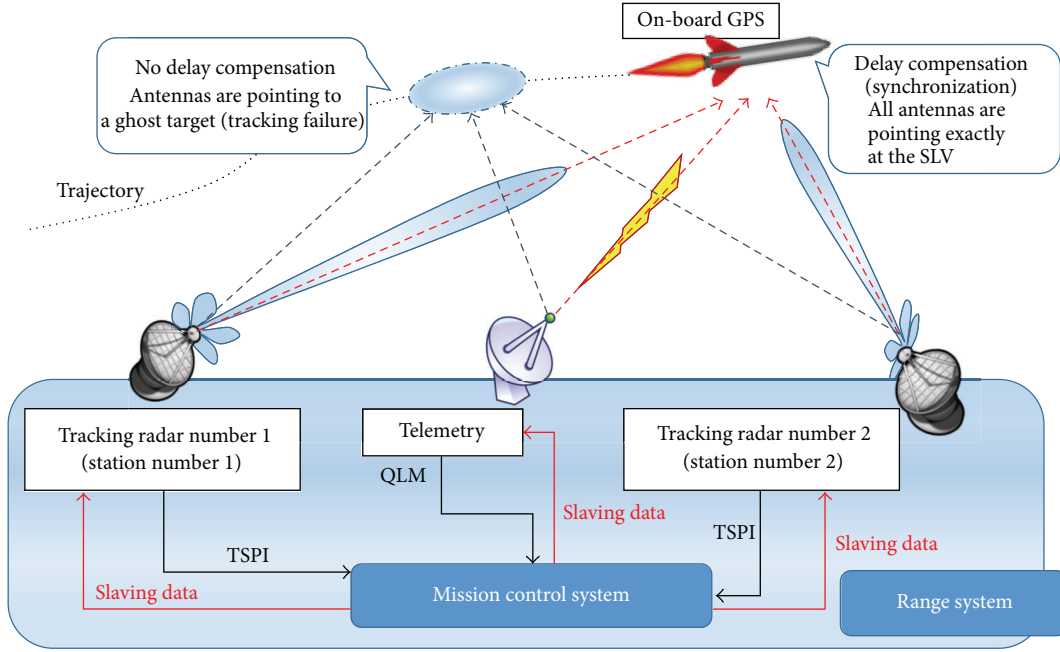


FIGURE 1: Illustration of problem statement for delayed slaving data in RSS.

$$f''_{n,i}(k_i) = f''_{n,i+1}(k_i) \\ n = x, y, z, i = 1, \dots, N-1. \quad (3)$$

On combining (2) and (3), the cubic polynomials $f_n^{\text{ep}}(k+s)$ are reconstructed by solving the linear equations obtained. Once we find the coefficients $a_{n,i}$, $b_{n,i}$, $c_{n,i}$, and $d_{n,i}$, where $i = 0, \dots, N-1$, we can evaluate $f_n^{\text{ep}}(k+s)$, where s is an arbitrary lead-time for future points in $[x_0, x_{N+s}]$.

3.2. Synchronization Using an α - β - γ Filter. When the state estimation covariance for a time invariant system converges under suitable conditions to a steady-state value, explicit expressions of the steady-state covariance and filter gain can be obtained. The resulting steady-state filters for noisy kinematic models are known as α - β and α - β - γ filters [20]. In this paper, a combined α - β - γ filter using both an expanding memory polynomial filter (EMF) and a fading memory polynomial filter (FMF) was used [21, 22]. At first, the EMF is represented as follows:

$$p_{n,k}^E = p_{n,k-1}^E + \Delta t v_{n,k-1}^E + \frac{\Delta t^2}{2} a_{n,k-1}^E \\ + \frac{3(3k^2 + 3k + 2)}{(k+3)(k+2)(k+1)} \epsilon_{n,k}^E, \\ v_{n,k}^E = v_{n,k-1}^E + \Delta t a_{n,k-1}^E \\ + \frac{1}{\Delta t} \frac{18(2k+1)}{(k+3)(k+2)(k+1)} \epsilon_{n,k}^E,$$

$$a_{n,k}^E = a_{n,k-1}^E + \frac{1}{\Delta t^2} \frac{60}{(k+3)(k+2)(k+1)} \epsilon_{n,k}^E, \\ \epsilon_{n,k}^E = y_{n,k} - p_{n,k-1}^E - \Delta t v_{n,k-1}^E - \frac{\Delta t^2}{2} a_{n,k-1}^E, \quad (4)$$

where Δt is the sampling time and $p_{n,k}^E$, $v_{n,k}^E$, and $a_{n,k}^E$ are the position, velocity, and acceleration estimates of the EMF, respectively. In addition, the variance reduction factor (VRF) [22] of the EMF, that is, VRF^E , can be represented as

$$\text{VRF}^E = \frac{9k^2 + 27k + 24}{k(k+1)(k-1)}. \quad (5)$$

On the other hand, the FMF and its VRF (VRF^F) can be written as follows:

$$p_{n,k}^F = p_{n,k-1}^F + \Delta t v_{n,k-1}^F + \frac{\Delta t^2}{2} a_{n,k-1}^F + (1-\lambda^3) \epsilon_{n,k}^F, \\ v_{n,k}^F = v_{n,k-1}^F + \Delta t a_{n,k-1}^F + \frac{3}{2\Delta t} (1-\lambda)^2 (1+\lambda) \epsilon_{n,k}^F, \\ a_{n,k}^F = a_{n,k-1}^F + \frac{1}{\Delta t^2} (1-\lambda)^3 \epsilon_{n,k}^F, \quad (6) \\ \epsilon_{n,k}^F = y_{n,k} - p_{n,k-1}^F - \Delta t v_{n,k-1}^F - \frac{\Delta t^2}{2} a_{n,k-1}^F, \\ \text{VRF}^F = \frac{1-\lambda}{(1+\lambda)^5} (19 + 24\lambda + 16\lambda^2 + 6\lambda^3 + \lambda^4),$$

where $0 < \lambda < 1$. Both filters are conducted in parallel but only one of them is selected as a final estimate by comparing

the VRFs. During the early tracking phase, the EMF is selected as the final estimate; however, at a certain time, where VRF^F is larger than VRF^E , FMF is selected as the final estimate:

$$\begin{aligned} \widehat{X}_{n,k}^{\alpha\beta\gamma} &= f_n \widehat{X}_{n,k-1}^{\alpha\beta\gamma} + K \left[y_k - H^{\alpha\beta\gamma} \widehat{X}_{n,k-1}^{\alpha\beta\gamma} \right], \\ \begin{bmatrix} p_{n,k} \\ v_{n,k} \\ a_{n,k} \end{bmatrix} &= \begin{bmatrix} 1 & \Delta t & \frac{\Delta t^2}{2} \\ 0 & 1 & \Delta t \\ 0 & 0 & 1 \end{bmatrix} \begin{bmatrix} p_{n,k-1} \\ v_{n,k-1} \\ a_{n,k-1} \end{bmatrix} \\ &+ \begin{bmatrix} \alpha \\ \frac{\beta}{\Delta t} \\ \frac{\gamma}{\Delta t^2} \end{bmatrix} \begin{bmatrix} y_k - H^{\alpha\beta\gamma} \begin{bmatrix} p_{n,k-1} \\ v_{n,k-1} \\ a_{n,k-1} \end{bmatrix} \end{bmatrix}, \\ \text{where } X_{n,k}^{\alpha\beta\gamma} &= [p_{n,k} \ v_{n,k} \ a_{n,k}]^T, \ H^{\alpha\beta\gamma} = [1 \ 0 \ 0], \end{aligned} \quad (7)$$

$$\text{VRF}^E \geq \text{VRF}^F \longrightarrow$$

$$p_{n,k} = p_{n,k}^E,$$

$$v_{n,k} = v_{n,k}^E,$$

$$a_{n,k} = a_{n,k}^E,$$

$$\text{VRF}^F > \text{VRF}^E \longrightarrow$$

$$p_{n,k} = p_{n,k}^F,$$

$$v_{n,k} = v_{n,k}^F,$$

$$a_{n,k} = a_{n,k}^F.$$

Finally, synchronization using an α - β - γ filter is completed by linear propagation using the system matrix f_n such that

$$\widehat{X}_{n,k+s}^{\alpha\beta\gamma} = \left(\prod_{L=1}^s f_n \right) \cdot \widehat{X}_{n,k}^{\alpha\beta\gamma}. \quad (8)$$

3.3. Kalman Predictor. The motion of the SLV is simply depicted as a discretized Wiener process acceleration model [20]:

$$X_{k+1} = FX_k + w_k, \quad (9)$$

where the state vector $X_k \in \mathfrak{R}^9$ consists of the position, velocity, and acceleration components along x -axis, y -axis, and z -axis, respectively; that is, $X_k = [x_{p,k} \ x_{v,k} \ x_{a,k} \ y_{p,k} \ y_{v,k} \ y_{a,k} \ z_{p,k} \ z_{v,k} \ z_{a,k}]^T$. The system

matrix and covariance matrix of the system noise w_k are represented as (10) and (11), respectively:

$$f_{n=x,y,z} = \begin{bmatrix} 1 & \Delta t & \frac{\Delta t^2}{2} \\ 0 & 1 & \Delta t \\ 0 & 0 & 1 \end{bmatrix}, \quad (10)$$

$$F = \begin{bmatrix} f_x & \mathbf{0}_3 & \mathbf{0}_3 \\ \mathbf{0}_3 & f_y & \mathbf{0}_3 \\ \mathbf{0}_3 & \mathbf{0}_3 & f_z \end{bmatrix},$$

$$E[w_k w_l^T] = Q \delta_{k-l},$$

$$q_{L=x,y,z} = \begin{bmatrix} \frac{\Delta t^5}{20} & \frac{\Delta t^4}{8} & \frac{\Delta t^2}{6} \\ \frac{\Delta t^4}{8} & \frac{\Delta t^3}{3} & \frac{\Delta t^2}{2} \\ \frac{\Delta t^3}{6} & \frac{\Delta t^2}{2} & \Delta t \end{bmatrix}, \quad (11)$$

$$Q = \begin{bmatrix} q_x & \mathbf{0}_3 & \mathbf{0}_3 \\ \mathbf{0}_3 & q_y & \mathbf{0}_3 \\ \mathbf{0}_3 & \mathbf{0}_3 & q_z \end{bmatrix}.$$

A radar measurement for the SLV gives the spherical coordinate observations such that

$$Z_k = h(X_k) + v_{s,k},$$

$$Z_k \in \mathfrak{R}^3, \ v_{s,k} \in \mathfrak{R}^3,$$

$$Z_k = \begin{bmatrix} r_k \\ \varphi_k \\ \theta_k \end{bmatrix} = \begin{bmatrix} \sqrt{x_{p,k}^2 + y_{p,k}^2 + z_{p,k}^2} \\ \tan^{-1} \left(\frac{y_{p,k}}{x_{p,k}} \right) \\ \tan^{-1} \left(\frac{y_{p,k}}{\sqrt{x_{p,k}^2 + y_{p,k}^2}} \right) \end{bmatrix} + \begin{bmatrix} v_r \\ v_\varphi \\ v_\theta \end{bmatrix}, \quad (12)$$

where $v_{s,k} \sim \mathbb{N}(0, R_{s,k})$ and $R_{s,k} = \text{diag}(\sigma_r^2, \sigma_\varphi^2, \sigma_\theta^2)$. Using a 3D debiased converted measurement [23], we can transform the original nonlinear equations (12) into their linear form as

$$\mathbf{z}_k = HX_k + v_k, \quad v_k \in \mathfrak{R}^3,$$

$$\mathbf{z}_k = \begin{bmatrix} x_k \\ y_k \\ z_k \end{bmatrix} = \begin{bmatrix} 1 & \mathbf{0}_{1 \times 5} & \mathbf{0}_{1 \times 3} \\ \mathbf{0}_{1 \times 3} & 1 & \mathbf{0}_{1 \times 5} \\ \mathbf{0}_{1 \times 5} & 1 & \mathbf{0}_{1 \times 2} \end{bmatrix} X_k + \begin{bmatrix} v_{x,k} \\ v_{y,k} \\ v_{z,k} \end{bmatrix}. \quad (13)$$

Here, $v_{c,k}$ is the converted measurement noise expressed in terms of Cartesian coordinates; that is, $v_k \sim \mathbb{N}(0, R_k)$:

$$R_k = \begin{bmatrix} R_{xx,k} & R_{xy,k} & R_{xz,k} \\ R_{yx,k} & R_{yy,k} & R_{yz,k} \\ R_{zx,k} & R_{zy,k} & R_{zz,k} \end{bmatrix}. \quad (14)$$

Prediction or fixed-lead prediction in mean square means the synchronization of the slaving data is the estimation of the state at a future time $k+s$, where $s > 0$ beyond the observation interval; that is, based on data up to an earlier time [20, 24],

$$\widehat{X}_{k+s|k} = E(X_{k+s|k} | Z_k), \quad Z_k = \{z_0, \dots, z_k\}. \quad (15)$$

The optimal predictor or synchronized state $\widehat{X}_{k+s|k} \triangleq \widehat{X}_{k+s|k}^{\text{KP}}$ and its error covariance $P_{k+s|k} \triangleq P_{k+s|k}^{\text{KP}}$ are given by the Kalman predictor equations [2, 24]:

$$\begin{aligned} \widehat{X}_{k+s|k}^{\text{KP}} &= F_{k+s-1} \widehat{X}_{k+s-1|k}^{\text{KP}} = \dots = \Phi_{k+s,k} \widehat{X}_{k|k}^{\text{KP}}, \\ \widehat{X}_{k|k}^{\text{KP}} &\triangleq \widehat{X}_{k|k}^{\text{KF}}, \\ P_{k+s|k}^{\text{KP}} &= F_{k+s-1} P_{k+s-1|k}^{\text{KP}} F_{k+s-1}^T + Q_{k+s-1} \\ &= \Phi_{k+s,k} P_{k|k}^{\text{KP}} \Phi_{k+s,k}^T \\ &\quad + \sum_{j=0}^{s-1} \Phi_{k+s,k+j+1} Q_{k+j} \Phi_{k+s,k+j+1}^T, \quad P_{k|k}^{\text{KP}} \triangleq P_{k|k}^{\text{KF}}, \\ \Phi_{k+s,k} &= F_{k+s-1} F_{k+s-2} \dots F_k, \\ \Phi_{k,k} &= I_n, \end{aligned} \quad (16)$$

$k > 1,$

where $\widehat{X}_{k|k}^{\text{KF}}$ and $P_{k|k}^{\text{KF}}$ are the KF estimate and covariance, respectively.

4. Proposed MME-Based Synchronization Approaches

4.1. Synchronization Using an IMM with Singer's Linear Model. Singer [16] described 2D manned maneuvering targets in range-bearing coordinates. This model can be adapted to the SLV kinematics in 3D Cartesian coordinates with multiple flight phases:

$$\begin{aligned} \begin{bmatrix} \dot{p}_n \\ \dot{v}_n \\ \dot{a}_n \end{bmatrix} &= F \begin{bmatrix} p_n \\ v_n \\ a_n \end{bmatrix} + G w_n, \\ F &= \begin{bmatrix} 0 & 1 & 0 \\ 0 & 0 & 1 \\ 0 & 0 & -\alpha_n \end{bmatrix}, \\ G &= \begin{bmatrix} 0 \\ 0 \\ 0 \end{bmatrix}, \end{aligned} \quad (17)$$

where $w_n \in \mathcal{R}^{3 \times 1}$ is a white noise process along the Cartesian axis $n = x, y, z$. The parameter $\beta = 1/\alpha_n$ is the maneuver correlation time constant, and σ_{an}^2 is the acceleration variance describing maneuver intensity. In a steady state,

$$\sigma_{w_n}^2 = 2\alpha_n \sigma_{an}^2. \quad (18)$$

To describe SLV kinematics, the model must cope with crucial nonzero mean acceleration maneuvers during the propelled phase. In addition, after each stage's engine burns out, a multiple model approach is applied to the coasting flight; that is, one model describes PFP, whereas the other depicts the CFP. Empirically tuned, independent probability density functions (PDFs) represented by TUM describe the accelerations of the SLV in the local coordinate frame. Figure 2 shows the means and variances of the acceleration processes of the SLV in this paper. The discrete-time model with state transition matrix $\Psi_n(\alpha_n, \Delta t)$ is as follows:

$$\begin{aligned} \begin{bmatrix} p_{n,k+1} \\ v_{n,k+1} \\ a_{n,k+1} \end{bmatrix} &= \Psi_n(\alpha_n, \Delta t) \begin{bmatrix} p_{n,k} \\ v_{n,k} \\ a_{n,k} \end{bmatrix} + w_{n,k}, \\ \Psi_n(\alpha_n, \Delta t) &= e^{F\Delta t} \begin{bmatrix} 1 & \Delta t & (\alpha_n \Delta t - 1 + e^{-\alpha_n \Delta t}) \\ 0 & 1 & \frac{(1 - e^{-\alpha_n \Delta t})}{\alpha_n} \\ 0 & 0 & e^{-\alpha_n \Delta t} \end{bmatrix}, \\ w_{n,k} &= \int_{k\Delta t}^{(k+1)\Delta t} e^{F[(k+1)\Delta t - r]} G w_n dr. \end{aligned} \quad (19)$$

In the case of the PFP, $w_{n,k}$ is a nonzero mean white noise sequence caused by the nonzero mean acceleration μ_{an} seen in Figure 2. A nonzero mean white noise sequence for the PFP should be considered in the target kinematics when implementing the state propagation stage in the KF. Thus, the deterministic input $u_{n,k}$ caused by $w_{n,k}$ along x -axis, y -axis, and z -axis is derived as follows:

$$\begin{aligned} u_{x,k} &= E[w_{x,k}] = E \left\{ \int_{k\Delta t}^{(k+1)\Delta t} e^{F[(k+1)\Delta t - r]} G w_x dr \right\} \\ &\approx E \left\{ \int_{k\Delta t}^{(k+1)\Delta t} \begin{bmatrix} e^{-\alpha_x[(k+1)\Delta t - r]} \\ 0 \\ 0 \end{bmatrix} w_x dr \right\}, \\ u_{x,k} &= \frac{\mu_{ax}}{\alpha_n \begin{bmatrix} 1 - e^{-\alpha_x \Delta t} \\ 0 \\ 0 \end{bmatrix}}. \end{aligned} \quad (20)$$

y -axis and z -axis can be derived in the same manner as shown in (20). The maneuver excitation covariance [10], which represents the uncertainty of the SLV kinematics model, is

$$\begin{aligned} Q_{n,k}(\alpha_n, \Delta t) &= E \{ (w_{n,k} - E[w_{n,k}]) (w_{n,k} - E[w_{n,k}])^T \} \\ &= 2\alpha_n \sigma_{an}^2 \begin{bmatrix} q_{11} & q_{12} & q_{13} \\ q_{12} & q_{22} & q_{23} \\ q_{13} & q_{23} & q_{33} \end{bmatrix}. \end{aligned} \quad (21)$$

The specific components of q_{11}, \dots, q_{33} are illustrated in [25]. In addition, the measurement matrix H_L for Singer's model can be depicted as

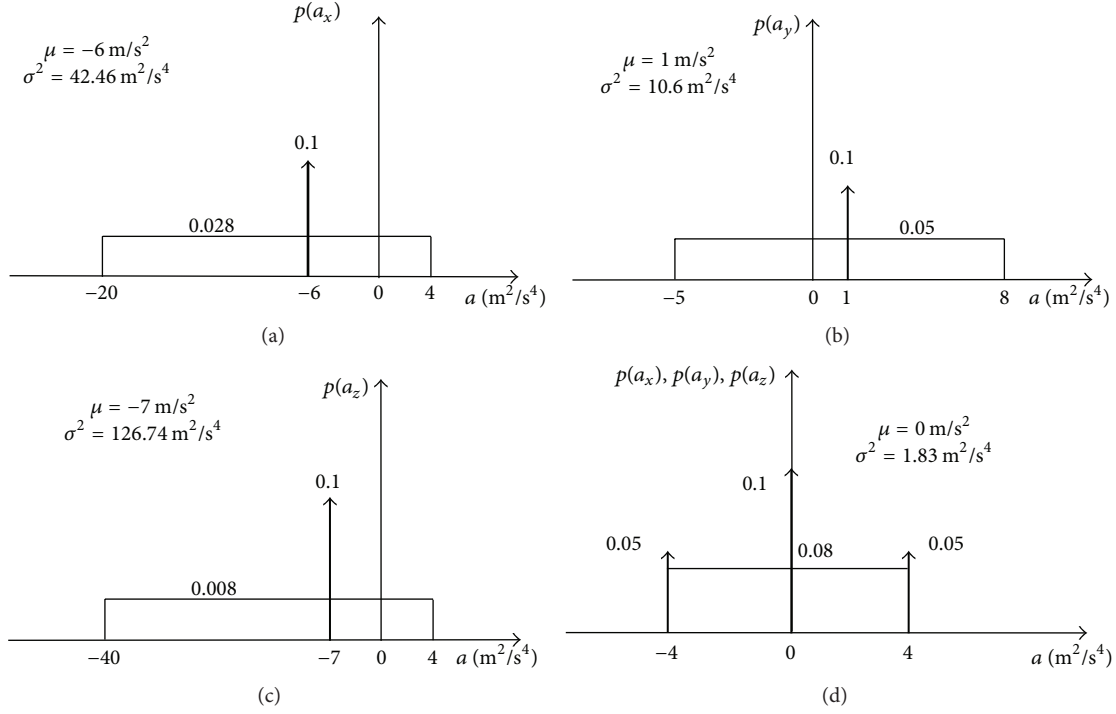


FIGURE 2: Nonzero mean acceleration PDF in the PFP model (a) along x -axis, (b) along y -axis, and (c) along z -axis. Zero mean acceleration PDF in the CFP Model (d) along x -axis, y -axis, and z -axis.

$$z_{L,k} = H_L \mathbf{x}_{L,k} + v_k, \quad H_L = \begin{bmatrix} 1 & 0 & 0 \\ 0 & \mathbf{0}_{3 \times 2} & 1 & \mathbf{0}_{3 \times 2} & 0 & \mathbf{0}_{3 \times 2} \\ 0 & 0 & 0 & 1 & 0 & 0 \end{bmatrix}, \quad \mathbf{x}_{L,k} = [x_k \quad \dot{x}_k \quad \ddot{x}_k \quad y_k \quad \dot{y}_k \quad \ddot{y}_k \quad z_k \quad \dot{z}_k \quad \ddot{z}_k]^T, \quad (22)$$

where v_k is measurement noise (as shown in (14)) with error covariance.

4.1.1. IMM with Singer's Linear Model. From (19)–(22) in Section 4.1, we can rewrite the Markov jump linear systems, where the i th model of the finite multiple model set $\mathfrak{M} = \{m^{(1)}, \dots, m^{(M)}\}$ obeys the following equations:

$$\begin{aligned} \mathbf{x}_{L,k+1} &= \Psi_k^{(i)} \mathbf{x}_{L,k} + w_k^{(i)}, \\ z_{L,k} &= H_L \mathbf{x}_{L,k} + v_k, \end{aligned} \quad (23)$$

where

$$\begin{aligned} \text{cov}(w_k^{(i)}) &= Q_k^{(i)}, \\ \text{cov}(v_k) &= R_k, \\ \Psi_k^{(i)} &= \text{diag}(\Psi_{x,k}(\alpha_x^{(i)}, \Delta t), \Psi_{y,k}(\alpha_y^{(i)}, \Delta t), \\ &\quad \Psi_{z,k}(\alpha_z^{(i)}, \Delta t)), \end{aligned}$$

$$\begin{aligned} Q_k^{(i)} &= \text{diag}(Q_{x,k}(\alpha_x^{(i)}, \Delta t), Q_{y,k}(\alpha_y^{(i)}, \Delta t), \\ &\quad Q_{z,k}(\alpha_z^{(i)}, \Delta t)). \end{aligned} \quad (24)$$

Here, σ_{an}^2 for the SLV can be represented by TUM as in Figure 2. The PDFs of Figures 2(a)–2(d) are experimentally sampled from the nominal acceleration profile of the SLV. The superscript (i) denotes quantities pertinent to model $m^{(i)}$ in \mathfrak{M} , and the jumps of the system mode are assumed to have transition probabilities:

$$\Pr\{m_{k+1}^{(j)} | m_k^{(i)}\} \triangleq \pi_{ij}, \quad (25)$$

where $m_k^{(i)}$ denotes the event in which model $m^{(i)}$ matches the system mode in effect at time k . In our application, $M = 2$, and $m^{(1)}$ and $m^{(2)}$ are the propelled and coasting modes, respectively.

Finally, complete recursion of the IMM with mode matched KF for the SLV tracking is summarized as follows:

- (i) Model-conditioned reinitialization (for $i = 1, 2, \dots, M$):

- (a) predicted mode probability: $\mu_{L,k|k-1}^{(i)} \triangleq \Pr\{m_k^{(i)} | z_{L,k-1}\} = \sum_j \pi_{ji} \mu_{L,k-1}^{(j)}$,
 (b) mixing weight: $\mu_{L,k-1}^{ji} \triangleq \Pr\{m_{k-1}^{(j)} | m_k^{(i)}, z_{L,k-1}\} = \sum_j \pi_{ji} \mu_{L,k-1}^{(j)} / \mu_{L,k-1}^{(i)}$,
 (c) mixing estimate and covariance:

$$\begin{aligned} \bar{\mathbf{x}}_{L,k-1|k-1}^{(i)} &\triangleq E[\mathbf{x}_{L,k-1|k-1} | m_k^{(i)}, z_{L,k-1}] \\ &= \sum_j \bar{\mathbf{x}}_{L,k-1|k-1}^{(j)} \mu_{L,k-1}^{ji}, \\ \bar{P}_{L,k-1|k-1}^{(i)} &= \sum_j \left[P_{L,k-1|k-1}^{(j)} + (\bar{\mathbf{x}}_{L,k-1|k-1}^{(i)} - \bar{\mathbf{x}}_{L,k-1|k-1}^{(j)}) \right. \\ &\quad \cdot (\bar{\mathbf{x}}_{L,k-1|k-1}^{(i)} - \bar{\mathbf{x}}_{L,k-1|k-1}^{(j)})^T \left. \right] \mu_{L,k-1}^{ji}. \end{aligned} \quad (26)$$

(ii) Model-conditioned filtering (for $i = 1, 2, \dots, M$):

(a) predicted estimate and covariance:

$$\begin{aligned} \hat{\mathbf{x}}_{L,k|k-1}^{(i)} &= \Psi_{k-1}^{(i)} \bar{\mathbf{x}}_{L,k-1|k-1}^{(i)} + \mathbf{u}_{k-1}^{(i)}, \\ \text{where } \mathbf{u}_{k-1}^{(1)} &= \begin{bmatrix} u_{x,k-1}^T & u_{y,k-1}^T & u_{z,k-1}^T \end{bmatrix}^T, \mathbf{u}_{k-1}^{(2)} = \mathbf{0}_{3 \times 1}, \end{aligned} \quad (27)$$

$$P_{L,k|k-1}^{(i)} = \Psi_{k-1}^{(i)} \bar{P}_{L,k-1|k-1}^{(i)} \Psi_{k-1}^{(i)T} + Q_{k-1}^{(i)},$$

(b) measurement residual: $\tilde{z}_{L,k}^{(i)} = z_{L,k} - H_L \hat{\mathbf{x}}_{L,k|k-1}^{(i)} - \nu_k$,

(c) residual covariance: $S_{L,k}^{(i)} = H_L P_{L,k|k-1}^{(i)} H_L^T - R_k$,

(d) filter gain: $K_{L,k}^{(i)} = P_{L,k|k-1}^{(i)} H_L^T (S_{L,k}^{(i)})^{-1}$,

(e) update of state and covariance: $\hat{\mathbf{x}}_{L,k|k}^{(i)} = \hat{\mathbf{x}}_{L,k|k-1}^{(i)} + K_{L,k}^{(i)} \tilde{z}_{L,k}^{(i)}$, $P_{L,k|k}^{(i)} = P_{L,k|k-1}^{(i)} - K_{L,k}^{(i)} S_{L,k}^{(i)} K_{L,k}^{(i)T}$.

(iii) Mode probability update (for $i = 1, 2, \dots, M$):

- (a) mode likelihood: $\Lambda_{L,k}^{(i)} \triangleq p[z_{L,k}^{(i)} | m_k^{(i)}, Z_{L,k-1}] \stackrel{\text{assume}}{=} \mathcal{N}(z_{L,k}^{(i)}; 0, S_{L,k}^{(i)})$,
 (b) mode probability: $\mu_{L,k}^{(i)} = \mu_{L,k|k-1}^{(i)} \Lambda_{L,k}^{(i)} / (\sum_j \mu_{L,k|k-1}^{(j)} \Lambda_{L,k}^{(j)})$.

(iv) Combination (for $i = 1, 2, \dots, M$):

$$\begin{aligned} \hat{\mathbf{x}}_{L,k|k} &= \sum_i \hat{\mathbf{x}}_{L,k|k}^{(i)} \mu_{L,k}^{(i)}, \\ \bar{P}_{L,k|k}^{(i)} &= \sum_i \left[P_{L,k|k}^{(i)} + (\hat{\mathbf{x}}_{L,k|k}^{(i)} - \hat{\mathbf{x}}_{L,k|k}) (\hat{\mathbf{x}}_{L,k|k}^{(i)} - \hat{\mathbf{x}}_{L,k|k})^T \right] \mu_{L,k}^{(i)}. \end{aligned} \quad (28)$$

Singer's MMS of time delayed slaving data is completed by propagating the combined estimate based on the current mode's dynamic model such that

$$\begin{aligned} \hat{\mathbf{x}}_{L,k+s|k}^{\text{sync}} &= \Phi_{k+s,k}^{\text{sync}} \hat{\mathbf{x}}_{L,k|k}, \\ \Phi_{k+s,k}^{\text{sync}} &= F_{k+s-1}^{\text{sync}} F_{k+s-2}^{\text{sync}} \cdots F_k^{\text{sync}}, \\ \Phi_{k,k}^{\text{sync}} &= I_n, \end{aligned} \quad (29)$$

$k > 1,$

where $F_{k+s-1}^{\text{sync}}, F_{k+s-2}^{\text{sync}}, \dots, F_k^{\text{sync}}$ are system matrices depending on a flight phase mode at current time k .

4.2. Synchronization Using an IMM with a Nonlinear Ballistic Model. For a nonlinear ballistic model, the state vector for the propelled mode is denoted as

$$\mathbf{x}_t = [x_t \ y_t \ z_t \ \dot{x}_t \ \dot{y}_t \ \dot{z}_t \ \xi_t \ \tau_t]^T, \quad (30)$$

where ξ_t is the drag coefficient and τ_t is the thrust. Generally, the drag coefficient varies significantly with the Mach number regime: subsonic, transonic, and supersonic. Therefore, we take advantage of the dynamic model considering a Mach number-dependent multiplier [11, 12] such that

$$\begin{bmatrix} \ddot{x} \\ \ddot{y} \\ \ddot{z} \end{bmatrix} = \underbrace{\frac{\tau}{V} \begin{bmatrix} \dot{x} \\ \dot{y} \\ \dot{z} \end{bmatrix}}_{\text{thrust term}} + \underbrace{\xi \xi_m D \begin{bmatrix} \dot{x} \\ \dot{y} \\ \dot{z} \end{bmatrix}}_{\text{drag term}} + \underbrace{g \begin{bmatrix} 0 \\ 0 \\ 1 \end{bmatrix}}_{\text{gravity term}} + \tilde{\omega}_1, \quad (31)$$

$$\dot{\xi} = \tilde{\omega}_2,$$

$$\dot{\tau} = \tilde{\omega}_3.$$

The first term on the right side of (31) represents the thrust (m^2/s) of the SLV in x , y , and z directions. Two distinct multiple modes of a nonlinear SLV model can be separated by the existence of thrust. In other words, the existence of thrust signifies propelled flight mode, whereas zero thrust signifies coasting flight mode. V is the magnitude of the velocity $\mathbf{v} = [\dot{x} \ \dot{y} \ \dot{z}]^T$, that is, the SLV speed (m/s). The second part of (31) is the drag term, which is related to velocity and altitude; that is, $D = -\rho(z)V/2$, where $\rho(z) = \rho_0 e^{-cz}$ is the air density (kg/m^3) at an altitude z (m) and c is the air density constant (m^{-1}) [9]. ξ is the drag coefficient and ξ_m is the Mach number-dependent drag coefficient multiplier, which is approximated by the cubic spline curve shown in Figure 3. In this paper, for the drag characteristics of the SLV, which are applied in the subsequent simulation section, drag coefficients of the Saturn V launch vehicle [15] are used. The third part of (31) is a gravity term. Gravity g is the standard acceleration due to gravity at sea level, which is assumed to be constant throughout the trajectory, with a value of 9.812 m/s^2 . $\tilde{\omega}_1$, $\tilde{\omega}_2$, and $\tilde{\omega}_3$ are assumed to be continuous time zero mean white Gaussian noises. The drag coefficient and thrust acceleration are represented as Wiener processes with a slow variation [11, 12].

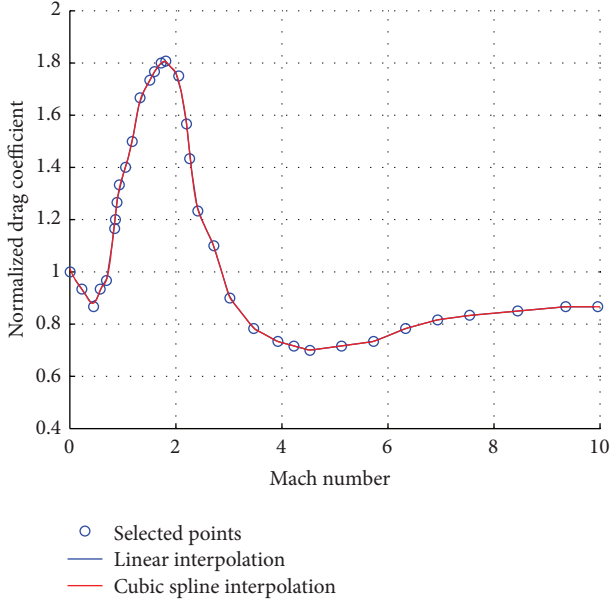


FIGURE 3: Normalized drag coefficient [15].

We can modify the dynamic equations (30) and (31) as a compact form such that

$$\dot{\mathbf{x}}_t = f[\mathbf{x}_t] + \tilde{\omega}_t, \quad (32)$$

where

$$f[\mathbf{x}_t] = \begin{bmatrix} \dot{x}_t \\ \dot{y}_t \\ \dot{z}_t \\ \tau \frac{\dot{x}_t}{V_t} + \xi_t D_t \dot{x}_t \\ \tau \frac{\dot{y}_t}{V_t} + \xi_t D_t \dot{y}_t \\ \tau \frac{\dot{z}_t}{V_t} + \xi_t D_t \dot{z}_t - g \end{bmatrix}, \quad (33)$$

$$\tilde{\omega}_t = [\tilde{\omega}_{1,t} \quad \tilde{\omega}_{2,t} \quad \tilde{\omega}_{3,t}]^T.$$

The state vector equation (33) is discretized by a second-order Taylor expansion [26]. Then, (33) can be written as

a discretized continuous time system with white process noise such that

$$\mathbf{x}_{k+1} = \mathbf{x}_k + f[\mathbf{x}_k] \Delta t + A_k f[\mathbf{x}_k] \frac{\Delta t^2}{2} + \omega_k, \quad (34)$$

where A_k is the Jacobian of (33) evaluated at \mathbf{x}_k [26] and ω_k is the discretized continuous time process noise for the sampling interval Δt . The corresponding covariance matrix of the discretized process noise is

$$Q = \begin{bmatrix} Q_1 q_v & \mathbf{0}_{6 \times 1} & \mathbf{0}_{6 \times 1} \\ \mathbf{0}_{1 \times 6} & \Delta t q_\xi & 0 \\ \mathbf{0}_{1 \times 6} & 0 & \Delta t q_\tau \end{bmatrix}, \quad (35)$$

$$Q_1 = \begin{bmatrix} \frac{\Delta t^3}{3} I_3 & \frac{\Delta t^2}{2} I_3 \\ \frac{\Delta t^2}{2} I_3 & \Delta t I_3 \end{bmatrix},$$

where I_3 is the 3×3 identity matrix and the continuous time process noise intensities q_v , q_ξ , and q_τ are the corresponding power spectral densities.

The measurement matrix H_{NL} for the nonlinear ballistic multiple model can be depicted as

$$z_{NL,k} = H_{NL} \mathbf{x}_{NL,k} + \nu_k, \quad (36)$$

$$H_{NL} = [I_3 \quad \mathbf{0}], \quad \mathbf{x}_{NL,k} = [x_k \quad y_k \quad z_k \quad \dot{x}_k \quad \dot{y}_k \quad \dot{z}_k \quad \xi_k \quad \tau_k]^T,$$

where ν_k is measurement noise with error covariance $R_k \delta_{k-j} = E[\nu_k \nu_j^T]$, that is, (14).

An IMM algorithm for nonlinear dynamics with different sizes of the mode state vector is summarized as follows [25]:

(v) Model-conditioned reinitialization (for $i = 1, 2, \dots, M$):

- (a) predicted mode probability: $\mu_{NL,k|k-1}^{(i)} \triangleq \Pr\{m_k^{(i)} | z_{NL,k-1}\} = \sum_j \pi_{ji} \mu_{NL,k-1}^{(j)}$,
- (b) mixing weight:

$$\mu_{NL,k-1}^{ji} \triangleq \Pr\{m_{k-1}^{(j)} | m_k^{(i)}, z_{NL,k-1}\} = \frac{\sum_j \pi_{ji} \mu_{NL,k-1}^{(j)}}{\mu_{NL,k-1}^{(i)}}, \quad (37)$$

(c) unbiased mixing estimate and covariance:

$$\bar{\mathbf{x}}_{NL,k-1|k-1}^{(i)} \triangleq E[\mathbf{x}_{NL,k-1|k-1} | m_k^{(i)}, z_{NL,k-1}] = \sum_j \hat{\chi}_{NL,k-1|k-1}^{(j)} \mu_{NL,k-1}^{ji},$$

$$\text{where } \hat{\chi}_{NL,k-1|k-1}^{(1)} \triangleq \hat{\mathbf{x}}_{NL,k-1|k-1}^{(1)}, \quad \hat{\chi}_{NL,k-1|k-1}^{(2)} \triangleq [\hat{\mathbf{x}}_{NL,k-1|k-1}^{(2)T}, \tau_{k-1}]^T, \quad (38)$$

$$\bar{P}_{NL,k-1|k-1}^{(i)} = \sum_j \left[P_{NL,k-1|k-1}^{(i)} + (\bar{\mathbf{x}}_{NL,k-1|k-1}^{(i)} - \hat{\chi}_{NL,k-1|k-1}^{(j)}) (\bar{\mathbf{x}}_{NL,k-1|k-1}^{(i)} - \hat{\chi}_{NL,k-1|k-1}^{(j)})^T \right] \mu_{NL,k-1}^{ji}.$$

(vi) Model-conditioned filtering (for $i = 1, 2, \dots, M$):

(a) predicted estimate and covariance:

$$\begin{aligned}\hat{\mathbf{x}}_{\text{NL},k|k-1}^{(i)} &= \hat{\mathbf{x}}_{\text{NL},k-1|k-1}^{(i)} + f \left[\hat{\mathbf{x}}_{\text{NL},k-1|k-1}^{(i)} \right] \Delta t \\ &\quad + \hat{A}_{\text{NL},k-1}^{(i)} f \left[\hat{\mathbf{x}}_{\text{NL},k-1|k-1}^{(i)} \right] \frac{\Delta t^2}{2}, \\ \hat{A}_k^{(i)} &= \left. \frac{\partial f}{\partial \mathbf{x}} \right|_{\mathbf{x}=\hat{\mathbf{x}}_k^{(i)}},\end{aligned}\quad (39)$$

$$P_{\text{NL},k|k-1}^{(i)} = \Omega_{k-1}^{(i)} \bar{P}_{\text{NL},k-1|k-1}^{(i)} \Omega_{k-1}^{(i)T} + Q_{k-1},$$

$$\Omega_{k-1}^{(i)} = I + \hat{A}_{\text{NL},k-1}^{(i)},$$

(b) measurement residual: $\tilde{z}_{\text{NL},k}^{(i)} = z_{\text{NL},k} - H_{\text{NL}} \hat{\mathbf{x}}_{\text{NL},k|k-1}^{(i)} - \nu_k,$

(c) residual covariance: $S_{\text{NL},k}^{(i)} = H_{\text{NL}} P_{\text{NL},k|k-1}^{(i)} H_{\text{NL}}^T - R_k,$

(d) filter gain: $K_{\text{NL},k}^{(i)} = P_{\text{NL},k|k-1}^{(i)} H_{\text{NL}}^T (S_{\text{NL},k}^{(i)})^{-1},$

(e) update of state and covariance:

$$\begin{aligned}\hat{\mathbf{x}}_{\text{NL},k|k}^{(i)} &= \hat{\mathbf{x}}_{\text{NL},k|k-1}^{(i)} + K_{\text{NL},k}^{(i)} \tilde{z}_{\text{NL},k}^{(i)}, \\ P_{\text{NL},k|k}^{(i)} &= P_{\text{NL},k|k-1}^{(i)} - K_{\text{NL},k}^{(i)} S_{\text{NL},k}^{(i)} K_{\text{NL},k}^{(i)T}.\end{aligned}\quad (40)$$

(vii) Mode probability update (for $i = 1, 2, \dots, M$):

(a) mode likelihood:

$$\begin{aligned}\Lambda_{\text{NL},k}^{(i)} &\triangleq p \left[z_{\text{NL},k}^{(i)} \mid m_k^{(i)}, Z_{\text{NL},k-1} \right] \\ &\stackrel{\text{assume}}{=} \mathbb{N} \left(z_{\text{NL},k}^{(i)}; 0, S_{\text{NL},k}^{(i)} \right),\end{aligned}\quad (41)$$

(b) mode probability: $\mu_{\text{NL},k}^{(i)} = \mu_{\text{NL},k|k-1}^{(i)} \Lambda_{\text{NL},k}^{(i)} / (\sum_j \mu_{\text{NL},k|k-1}^{(j)} \Lambda_{\text{NL},k}^{(j)}).$

(viii) Combination (for $i = 1, 2, \dots, M$):

$$\begin{aligned}\hat{\mathbf{x}}_{\text{NL},k|k} &= \sum_i \hat{\mathbf{x}}_{\text{NL},k|k}^{(i)} \mu_{\text{NL},k}^{(i)}, \\ \hat{P}_{\text{NL},k|k}^{(i)} &= \sum_i \left[P_{\text{NL},k|k}^{(i)} \right. \\ &\quad \left. + \left(\hat{\mathbf{x}}_{\text{NL},k|k} - \hat{\mathbf{x}}_{\text{NL},k|k}^{(i)} \right) \left(\hat{\mathbf{x}}_{\text{NL},k|k} - \hat{\mathbf{x}}_{\text{NL},k|k}^{(i)} \right)^T \right] \mu_{\text{NL},k}^{(i)}.\end{aligned}\quad (42)$$

The nonlinear MMS of time delayed slaving data is completed by propagating the combined estimate based on the current mode's estimated vector such that

$$\begin{aligned}\hat{\mathbf{x}}_{\text{NL},k+s|k} &= \hat{\mathbf{x}}_{\text{NL},k|k} + f \left[\hat{\mathbf{x}}_{\text{NL},k|k} \right] \cdot s + \hat{A}_{\text{NL},k} f \left[\hat{\mathbf{x}}_{\text{NL},k|k} \right] \\ &\quad \cdot \frac{s^2}{2},\end{aligned}\quad (43)$$

where s is a lead-time for synchronization ($s = n \cdot \Delta t$). If the SLV is in the PFP ($\mu_{\text{NL},k}^{(1)} > \mu_{\text{NL},k}^{(2)}$), the current state estimate includes the thrust term; that is, the state vector $\mathbf{x}_{\text{NL},k} = [x_k \ y_k \ z_k \ \dot{x}_k \ \dot{y}_k \ \dot{z}_k \ \xi_k \ \tau_k]^T$. If the SLV is not in the PFP, the state vector does not include the thrust term ($\tau_k = 0$).

5. Simulation Results

To demonstrate the performance of the proposed synchronization approaches for delayed slaving data, we simulated the SLV tracking problem based on the nominal flight trajectory of the Korea Space Launch Vehicle-I (KSLV-I). In the simulation, the radar measurement noise intensities of (12) are selected as $\sigma_r = 15$ m, $\sigma_\phi = 0.01$ deg, and $\sigma_\theta = 0.01$ deg. The nominal flight sequence of KSLV-I is as follows. First, the payload fairing separates during the first stage flight at 215.4 s. After the first stage engine shutdown at 228.7 s, the upper stage separates from the first stage and enters the CFP. The second stage continues in the CFP until the kick motor ignition at 395 s, and the vehicle then enters the PFP. At the end of kick motor combustion (452.7 s), the upper stage enters the target orbit in CFP as in the previous separation. Finally, the satellite is inserted into the target orbit after it separates from the upper stage during CFP at 540 s. Since delayed slaving data from the MCS to the TSs can occur in both the PFP and CFP, synchronization simulations are conducted at arbitrary points of the flight phases. Figure 4 shows the synchronization error of the delayed slaving data with respect to the benchmark and the proposed approaches for delays of $s = 0.1, 0.2, \dots, 1$ s. Figures 4(a)–4(c) illustrate synchronization errors, where delayed slaving data occurred at 155 s, which is the first stage of PFP, and Figures 4(d)–4(f) show synchronization errors, where delayed slaving data occurred at 280 s, which is the first stage of CFP. As shown in Figures 4(a)–4(c), the extrapolation and α - β - γ filter-based approach cannot find the proper synchronized slaving data. The synchronization errors of these approaches exponentially increase according to increasing delay s ; in particular, the error of the extrapolation approaches an out-of-figure bound (2500 m). On the other hand, the Kalman prediction and the proposed approaches have stable synchronization errors even if the delay time s is larger. Furthermore, we can observe that the errors in the synchronization approach of the Kalman prediction are relatively larger than the proposed approaches, especially in the PFP. As explained in the flight sequence of KSLV-I, in general, the motion of the SLV is described by multiple dynamics (in our case PFP and CFP) rather than single dynamics. However, the dynamic model of the KF and prediction capability used in this paper is the constant acceleration (CA) model. This means that the filter is optimized with respect to CA motion, which is actually not occurring in our application. This is why the performance of the Kalman prediction-based synchronization is worse than the proposed approaches. Nonetheless, we can see that the y -axis synchronization errors shown in Figures 4(b) and 4(e) are small. This result is observed because the y -axis motion of KSLV-I in a local coordinate is relatively smaller than the other axis motion, and the CA model approximately expresses this

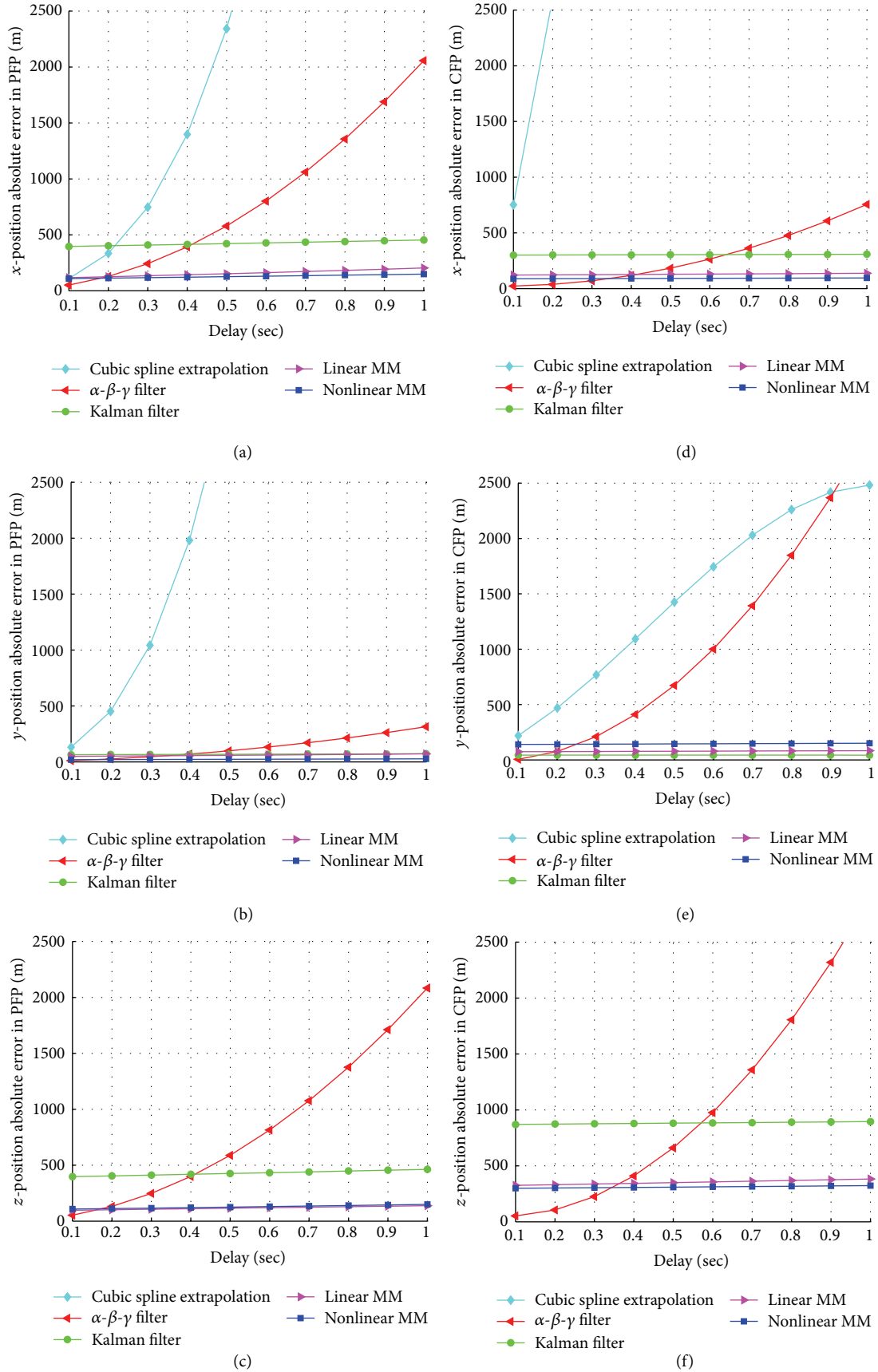


FIGURE 4: Synchronization errors at PFP and CFP.

small motion. A single KF prediction model cannot exactly describe the motion of both PFP and CFP, whereas the proposed multiple model-based approaches work well. As shown in Figure 4, regardless of the delay s , the proposed multiple model-based approaches find synchronized position vectors. In the comparison of synchronization performance between linear IMM and nonlinear IMM synchronization, the nonlinear IMM-based synchronization approach shows the best performance, except for y -axis, where CA motion is dominant. In addition, the difference between the proposed multiple model-based approaches is very small as shown in Figure 4, but the complexities of the algorithms for real-time applications are quite dissimilar. Hence, the operator may adaptively select one of the proposed approaches according to one's environment.

6. Conclusions

In this paper, we investigated the time synchronization approaches of delayed slaving data in the RSS for SLV tracking. One of the most important roles of the RSS is to distribute slaving data to each TS for continuous tracking of the SLV. If there is a critical network delay resulting in time delayed slaving data being sent to each TS, the MCS will not receive accurate SLV tracking data. This problem can give rise to significant difficulties for the SLV mission progress and analysis. To overcome this problem, we proposed MMS approaches which take advantage of the multiple motion models of an SLV. The linear IMM-based synchronization approach was developed using Singer's model with ternary uniform mixtures and the nonlinear IMM-based synchronization approach was derived from a nonlinear ballistic model with a drag coefficient. For verification of the proposed algorithms, SLV tracking simulations using KSLV-I and the radar measurement data generated from nominal trajectory were conducted. To demonstrate the superiority of time synchronization performance in these simulations, we compared the proposed algorithm with benchmark approaches for absolute error between the nominal trajectory data and the synchronized slaving data; the simulation results demonstrated that the proposed MMS approaches performed competitively.

Competing Interests

The authors declare that there are no competing interests regarding the publication of this paper.

References

- [1] R. Varaprasad and V. Seshagiri Rao, "Range safety real-time system for satellite launch vehicle missions-testing methodologies," *Defence Science Journal*, vol. 56, no. 5, pp. 693–700, 2006.
- [2] H. R. Song, M. G. Jeon, T. S. Choi, and V. Shin, "Two fusion predictors for discrete-time linear systems with different types of observations," *International Journal of Control, Automation and Systems*, vol. 7, no. 4, pp. 651–658, 2009.
- [3] H. Song, V. Shin, and M. Jeon, "Mobile node localization using fusion prediction-based interacting multiple model in cricket sensor network," *IEEE Transactions on Industrial Electronics*, vol. 59, no. 11, pp. 4349–4359, 2012.
- [4] T. Kirubarajan and Y. Bar-Shalom, "Kalman filter versus IMM estimator: when do we need the latter?" *IEEE Transactions on Aerospace and Electronic Systems*, vol. 39, no. 4, pp. 1452–1457, 2003.
- [5] E. Mazor, A. Averbuch, Y. Bar-Shalom, and J. Dayan, "Interacting multiple model methods in target tracking: a survey," *IEEE Transactions on Aerospace and Electronic Systems*, vol. 34, no. 1, pp. 103–123, 1998.
- [6] P. D. Hanlon and P. S. Maybeck, "Multiple-model adaptive estimation using a residual correlation Kalman filter bank," *IEEE Transactions on Aerospace and Electronic Systems*, vol. 36, no. 2, pp. 393–406, 2000.
- [7] S.-J. Shin, "Re-entry vehicle tracking with a new multiple model estimation applicable to highly non-linear dynamics," *IET Radar, Sonar & Navigation*, vol. 9, no. 5, pp. 581–588, 2015.
- [8] S. Conover, J. Kerce, G. Brown, L. Ehrman, and D. Hardiman, "Impact point prediction of small ballistic munitions with an interacting multiple model estimator," in *Acquisition, Tracking, Pointing, and Laser Systems Technologies XXI*, vol. 6569 of *Proceedings of SPIE*, Orlando, Fla, USA, 2007.
- [9] V. C. Ravindra, Y. Bar-Shalom, and P. Willett, "Projectile identification and impact point prediction," *IEEE Transactions on Aerospace and Electronic Systems*, vol. 46, no. 4, pp. 2004–2021, 2010.
- [10] W. J. Farrell III, "Interacting multiple model filter for tactical ballistic missile tracking," *IEEE Transactions on Aerospace and Electronic Systems*, vol. 44, no. 2, pp. 418–426, 2008.
- [11] T. Yuan, Y. Bar-Shalom, P. Willett, E. Mozeson, S. Pollak, and D. Hardiman, "A multiple IMM estimation approach with unbiased mixing for thrusting projectiles," *IEEE Transactions on Aerospace and Electronic Systems*, vol. 48, no. 4, pp. 3250–3267, 2012.
- [12] T. Yuan, Y. Bar-Shalom, P. Willett, and D. Hardiman, "Impact point prediction for thrusting projectiles in the presence of wind," *IEEE Transactions on Aerospace and Electronic Systems*, vol. 50, no. 1, pp. 102–119, 2014.
- [13] X. Li and V. Jilkov, "Survey of maneuvering target tracking. part II: motion models of ballistic and space targets," *IEEE Transactions on Aerospace and Electronic Systems*, vol. 46, no. 1, pp. 96–119, 2010.
- [14] J. Cesar Bolzani de Campos Ferreira and J. Waldmann, "Covariance intersection-based sensor fusion for sounding rocket tracking and impact area prediction," *Control Engineering Practice*, vol. 15, no. 4, pp. 389–409, 2007.
- [15] <http://www.braeunig.us/apollo/saturnV.htm>.
- [16] R. A. Singer, "Estimating optimal tracking filter performance for manned maneuvering targets," *IEEE Transactions on Aerospace and Electronic Systems*, vol. 6, no. 4, pp. 473–483, 1970.
- [17] R. A. Singer and K. W. Behnke, "Real-time tracking filter evaluation and selection for tactical applications," *IEEE Transactions on Aerospace and Electronic Systems*, vol. AES-7, no. 1, pp. 100–110, 1971.
- [18] W. Press, B. Flannery, S. Teukolsky, and W. Vetterling, *Numerical Recipes in FORTRAN: The Art of Scientific Computing*, Cambridge University, New York, NY, USA, 2nd edition, 1992.
- [19] S. Dyer and J. Dyer, "Cubic-spline interpolation: part I," *IEEE Instrumentation & Measurement Magazine*, pp. 44–46, 2001.
- [20] Y. Bar-Shalom, X. Li, and T. Kirubarajan, *Estimation with Applications to Tracking and Navigation*, John Wiley & Sons, New York, NY, USA, 2001.

- [21] N. Morrison, *Introduction to Sequential Smoothing and Prediction*, McGraw-Hill, 1969.
- [22] E. Brookner, *Tracking and Kalman Filtering Made Easy*, John Wiley & Sons, 1998.
- [23] P. Suchomski, "Explicit expressions for debiased statistics of 3D converted measurements," *IEEE Transactions on Aerospace and Electronic Systems*, vol. 35, no. 1, pp. 368–370, 1999.
- [24] H. R. Song, I. Y. Song, and V. Shin, "Multisensory prediction fusion of nonlinear functions of the state vector in discrete-time systems," *International Journal of Distributed Sensor Networks*, vol. 2015, Article ID 249857, 13 pages, 2015.
- [25] H. Song and Y. Han, "Comparison of space launch vehicle tracking using different types of multiple models," in *Proceedings of the International Conference on Information Fusion*, pp. 1–8, Heidelberg, Germany, July 2016.
- [26] R. K. Mehra, "A comparison of several nonlinear filters for reentry vehicle tracking," *IEEE Transactions on Automatic Control*, vol. 16, no. 4, pp. 307–319, 1971.

Research Article

An Expert PI Controller with Dead Time Compensation of Monitor AGC in Hot Strip Mill

Fei Zhang,^{1,2} Shengyue Zong,¹ Xiang Wang,³ and Xiaohuai Ren⁴

¹Engineering Research Institute, University of Science and Technology Beijing, Beijing 100083, China

²School of Electrical, Computer & Telecommunications Engineering, University of Wollongong, Wollongong, NSW 2522, Australia

³Material Industry & Development Department, Aerospace Research Institute of Material & Processing Technology, Beijing 100076, China

⁴Research and Design Institute of USTB Co., Ltd., Beijing 100083, China

Correspondence should be addressed to Fei Zhang; zhfeicn@gmail.com

Received 19 May 2016; Revised 6 July 2016; Accepted 12 July 2016

Academic Editor: Magdi S. Mahmoud

Copyright © 2016 Fei Zhang et al. This is an open access article distributed under the Creative Commons Attribution License, which permits unrestricted use, distribution, and reproduction in any medium, provided the original work is properly cited.

Hot strip rolling production is a high-speed process which requires high-speed control and communication system, but because of the long distance between the delivery stand of the finishing mill and the gauge meter, dead time occurs when strip is transported from the site of the actuator to another location where the gauge meter takes its reading, which seriously affects the thickness control effect. According to the process model which is developed based on the measured data, a filtered Smith predictor is applied to predict the thickness deviation of the finishing mill. At the same time, an expert PI controller based on feature information is proposed for the strip thinning during looper rising and coiler biting period and the strip thickening during the tension loss period of the strip tail end. As a result, the thickness accuracy has been improved by about 1.06% at a steady rolling speed and about 1.23% in acceleration and deceleration.

1. Introduction

Figure 1 shows the outline of a typical 1700 mm hot strip mill (HSM). Its purpose is to process cast steel slabs into steel strip. Hot rolling can achieve large dimensional changes in a single step; the slabs, of up to 35 t weight, are typically 250 mm thick and 10 m long, and the rolled strips are typically 2 mm thick and 1250 m long. This reduction in thickness is achieved by passing the piece through a series of rolling mill stands. Typically, at the first stand, the roughing mill (RM), the thickness of the hot slab (1240°C) is reduced by making several passes, forward and reverse, through the mill. At the end of this roughing process the piece will be 35 mm thick and 70 m long and its temperature will have dropped to 1050°C. Further reduction in thickness takes place in the six or seven close-coupled rolling finishing stands. The strip elongation is so great that the piece can straddle a region from the finishing mill (FM) approach tables to the coiler. During this part of the process, pieces normally have a final rolling temperature of 870°C followed by coiling at 600°C [1].

Thickness precision is one of the most important quality indexes in strip rolling process [2, 3]. Monitor automatic gauge control (AGC) based on hydraulic roll gap control system is widely used in modern strip rolling mills [4–7]. In monitor AGC system, gauge meter is used to measure strip gauge derivation, which is installed at the delivery side of the finishing mill. The strip thickness can be controlled by adjusting the roll gap. Because of restriction of mill structure and requirement of maintenance, the install location of gauge meter is far from the mill. As shown in Figure 2, the rolling mill produces steel strip at a speed of v , and gauge meter measures the strip thickness h . By comparing h with thickness reference h_0 , thickness deviation Δh is obtained. Then the gap correction value of monitor AGC ΔS_M is calculated. At the same time, the gap correction value of other types of AGC ΔS_X is calculated too. ΔS_M and ΔS_X are subsequently added to the gap set value S_0 to get the target gap S_r . At last, hydraulic cylinders are used to modify the gap between a pair of working rolls that squeeze the material into the desired

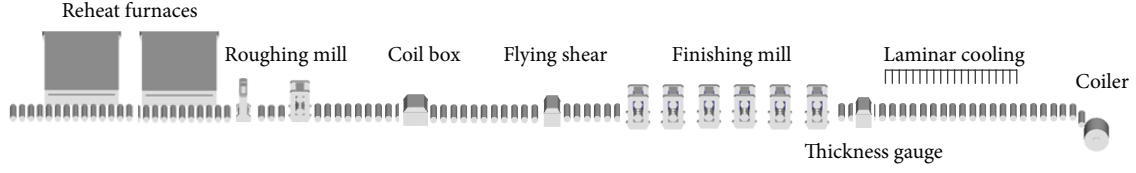


FIGURE 1: A typical hot strip mill layout.

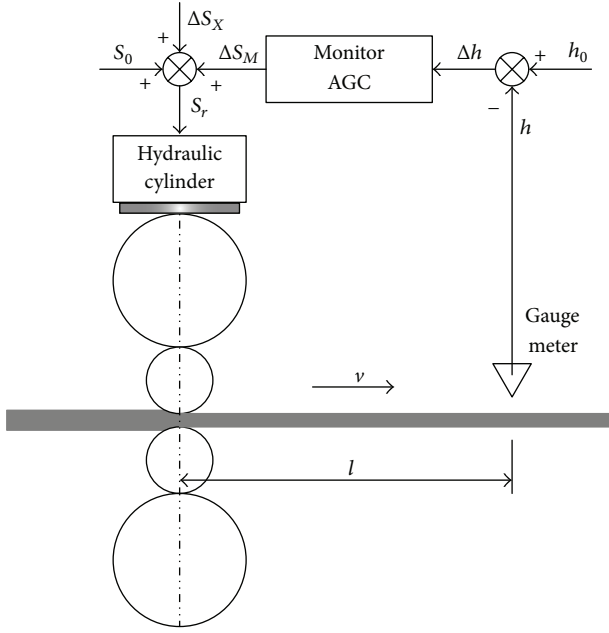


FIGURE 2: Simplified schematic diagram of monitor AGC.

thickness. The dead time τ in this process is caused by the distance l between the rolls and the gauge meter

$$\tau = \frac{l}{v}. \quad (1)$$

During that interval, the process does not respond to the controller's activity at all, and any attempt to manipulate the process variable before the dead time has elapsed inevitably fails.

According to control theory, the time delay in any feedback system reduces system stability and deteriorates dynamic characteristics, especially for the case of $\tau/T \geq 0.5$, where T is the time constant [8]. Because the inertia time constant T of the hydraulic system is generally less than 50 ms, the value of τ/T of the delivery stand is greater than 0.5 and those of the upstream stands are much greater.

Plants with a long time delay can often not be controlled effectively using a simple PID (Proportional, Integral, and Derivative) controller. The main reason for this is that the additional phase lag contributed by the time delay tends to destabilize the closed-loop system. The stability problem can be solved by decreasing the controller gain. However, in this case the response obtained is very sluggish [8, 9].

The Smith predictor (SP), shown in Figure 3, is well known as an effective dead time compensator for a stable process with long time delay [10]. The widespread application of the SP has been hindered by two problems. First, it is difficult to tune manually, because the practicing engineer is not very familiar with process modeling and it is a time-consuming manual task. Second, the predictor is sensitive to process parameter variations, as in any other advanced control technique. Hence the need for retuning the SP is more frequent than that for the PID controller [11, 12].

2. Filtered Smith Predictor (FSP)

The well-known SP is a dead time compensator (DTC) widely used in the industry in which a dead time nominal process model is used. Nevertheless, the main drawback of this algorithm is that dead time errors can destabilize the system. A robust solution is the FSP, in which a filter is included to attenuate the oscillation caused by delay mismatches [13]. The proposed controller is shown in Figure 4. It can be seen that the structure is the same as in the SP with an additional filter $F_r(s)$. Because of its characteristics, the FSP can be used to compute a controller taking into account the robustness, coping with unstable plants, improving the disturbance rejection properties, and decoupling the set-point and disturbance responses [14]. Therefore, all the drawbacks of the SP are considered in the design, using only one structure and, as will be shown, a unified design procedure.

In the structure $P_m(s) = G_m(s)e^{-\tau_m s}$ is a process model, $G_m(s)$ is the dead time-free model and $G_c(s)$ is the primary controller. In the nominal case ($P(s) = P_m(s)$) the closed-loop transfer function for set-point changes is the same for the SP and FSP:

$$H_r(s) = \frac{Y(s)}{R(s)} = \frac{G_c(s)P_m(s)}{1 + G_c(s)G_m(s)}. \quad (2)$$

Note that the delay is eliminated from the characteristic equation and $F_r(s)$ does not affect $H_r(s)$. Assume that the real plant differs from the nominal case ($P_m(s) \neq P(s)$) and consider a family of plants $P(s) = G_p(s)e^{-\tau_p s}$ such that $P(s) = P_m(s)[1 + \delta P(s)] = P_m(s) + \Delta P(s)$, and its characteristic equation is given by

$$1 + G_c(s)G_m(s) + G_c(s)G_m(s)P_m(s)\delta P(s) = 0. \quad (3)$$

The condition for closed-loop SP robustness is that, for all frequencies and all plants in the family, the distance between

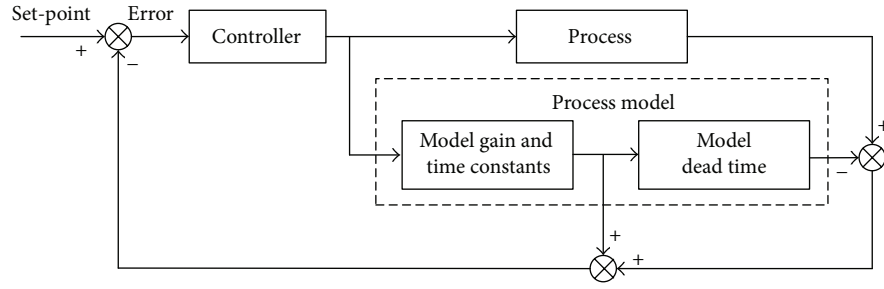


FIGURE 3: Smith predictor control scheme.

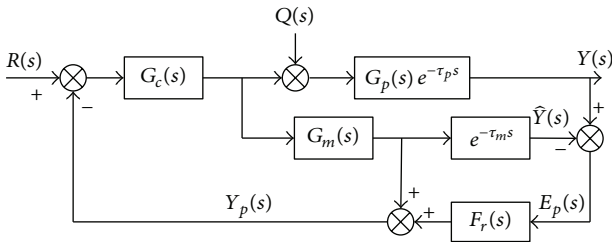


FIGURE 4: Structure of FSP.

$G_c(s)G_m(s)$ and the -1 point in the Nyquist diagram ($|1 + G_c(s)G_m(s)|$ is greater than $|G_c(s)\Delta P(s)|$). Thus, for the SP,

$$\overline{\delta P}(s) < dP_{SP}(s) = \frac{|1 + G_c(s)G_m(s)|}{|G_c(s)G_m(s)|}, \quad (4)$$

$$s = j\omega, \quad \forall \omega > 0,$$

where j is the imaginary unit and ω is the frequency, and $\overline{\delta P}(\omega)$ is the multiplicative norm-bound uncertainty [15, 16].

Therefore, when the closed-loop transfer equation (2) is defined, $dP_{SP}(s)$ is also fixed and if $G_c(s)$ is chosen for a high performance then robustness will be poor. Thus, if $G_c(s)$ is not appropriately chosen, small uncertainties may destabilize the system.

The characteristic equation for $P(s)$ is then

$$1 + G_c(s)G_m(s) + G_c(s)G_m(s)P_m(s)F_r(s)\delta P(s) = 0. \quad (5)$$

Considering that the nominal system is stable, the robust stability condition for the FSP is

$$\overline{\delta P}(s) < dP_{FSP}(s) = \frac{|1 + G_c(s)G_m(s)|}{|G_c(s)G_m(s)F_r(s)|}, \quad (6)$$

$$s = j\omega, \quad \forall \omega > 0.$$

If $F_r(s)$ is a low-pass filter, it can be used to improve the robustness of the system at the desired region of frequency [14]. Although $F_r(s)$ does not affect $H_r(s)$, it modifies the disturbance rejection response defined by

$$H_q(s) = \frac{Y(s)}{Q(s)} = P_m(s) \left[1 - \frac{G_c(s)P_m(s)F_r(s)}{1 + G_c(s)G_m(s)} \right]. \quad (7)$$

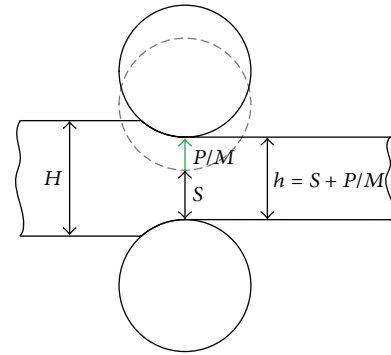


FIGURE 5: Roll force modeling principles.

Thus $F_r(s)$ must be tuned for a compromise between robustness and disturbance rejection performance.

Note that only $Y(s)/Q(s)$ and $dP(\omega)$ are modified by the inclusion of the filter. That is, the filter $F_r(s)$ can be used to improve the robustness or the disturbance rejection capabilities of the system without affecting the nominal set-point response. Furthermore, $F_r(s)$ can be tuned to obtain an internal stable system when controlling unstable plants. Therefore, the proposed controller has enough degrees of freedom to obtain compromise between robustness and a desired set-point and disturbance rejection responses.

3. FSP for Monitor AGC

A typical and basic modeling task is that associated with setting up the roll gaps in a mill. The large deformation force P required to reduce the strip thickness from entry thickness H to exit thickness h causes the stand frame holding the rolls to stretch and mill rolls to bend and flatten. The result is the exit thickness as a function of force P . In simplified form this can be expressed as [1]

$$h = S + f(P), \quad (8)$$

where S is the unloaded roll gap and the term $f(P)$ is the mill stretch.

As shown in Figure 5, the normally used simplified thickness model of gauge meter equation or spring equation has the following form [17]:

$$h = S + \frac{P}{M}, \quad (9)$$

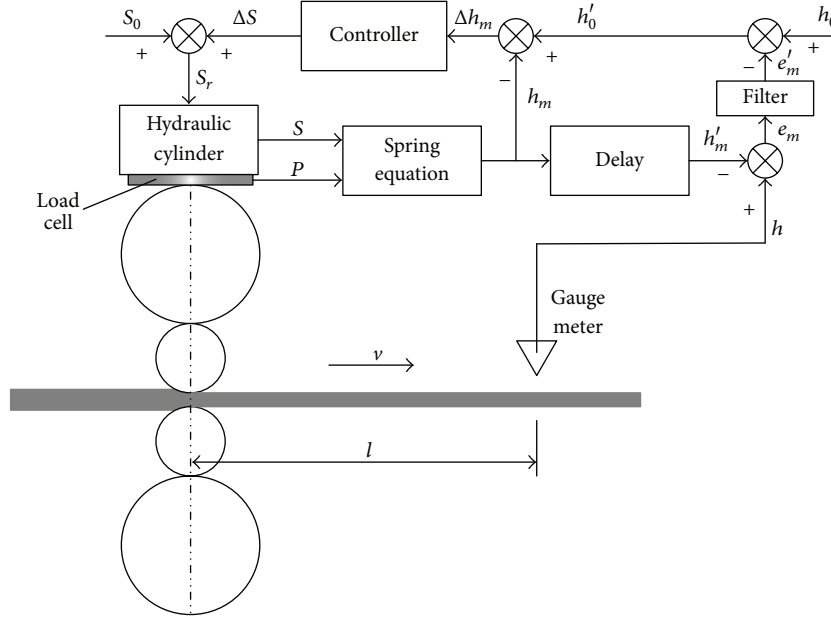


FIGURE 6: Monitor AGC system with SP.

where M is the mill modulus or stiffness coefficient and P/M is the approximate value of mill stretch.

Because of the inaccuracy of empirical formula and the measurement error, there is a deviation of the calculated thickness from the actual thickness. The delayed calculated thickness is compared with the measured thickness and the deviation e_m of the two is obtained to correct the deviation and improve the model accuracy. The monitor AGC system with SP is shown in Figure 6, where h_m is the calculated thickness and h'_m is the delayed calculated thickness.

As can be seen in Figure 6, the thickness deviation Δh_m can be calculated by the following formula:

$$\Delta h_m = (h'_m - h_m) - (h - h_0) = (h_m e^{-\tau s} - h_m) - \Delta h. \quad (10)$$

If the roll gap S_i remains unchanged, we have [7]

$$\Delta h_i = \frac{Q_i}{Q_i + M_i} \Delta H_i, \quad i = 1, 2, \dots, 6, \quad (11)$$

where i refers to stand F_i , Δh_i and ΔH_i are the exit thickness and the entry thickness of stand F_i , respectively, M_i is the stiffness coefficient of stand F_i , and Q_i is the plastics coefficient of the rolled material in stand F_i .

Because the material flows passing through different stands are equal, the exit thickness of stand $F(i-1)$ is equal to the entry thickness of stand F_i with the dead time τ_{i-1} , which means that

$$H_i = h_{i-1} e^{-\tau_{i-1} s}, \quad i = 2, 3, \dots, 6 \quad (12)$$

or

$$\Delta H_i = \Delta h_{i-1} e^{-\tau_{i-1} s}, \quad i = 2, 3, \dots, 6. \quad (13)$$

Substituting (12) in (10) we get

$$\Delta h_i = \frac{Q_i}{Q_i + M_i} \Delta h_{i-1} e^{-\tau_{i-1} s}, \quad i = 2, 3, \dots, 6. \quad (14)$$

If the thickness deviation Δh_m is relatively large, it will overload the delivery stand of the finishing mill and affect the crown and flatness of the strip, so Smith's method monitor AGC correction is distributed to upstream stand AGC to prevent the load unbalance [7]. At the same time, because the first few stands are too far to get good control effect, monitor AGC is only implemented to the last three stands of the finishing mill, as shown in Figure 7, where Δh_m is the exit thickness deviation to be eliminated; k_i ($i = 4, 5, 6$) are the distribution coefficients of stand F_i and meet the condition of $0 < k_4 < k_5 < k_6 = 1$; M_i and Q_i ($i = 4, 5, 6$) are the stiffness coefficients and plastic coefficients of stand F_i ; τ_4 , τ_5 , and τ_6 are the dead time when material is transported from F_4 to F_5 , F_5 to F_6 , and F_6 to gauge meter, respectively; Δh_{mi} ($i = 4, 5, 6$) are the thickness deviation to be eliminated by stand F_i and its upstream stands; $\Delta h'_{mi}$ ($i = 4, 5$) are the thickness modification of stand $F(i+1)$ influenced by thickness modification before stand $F(i+1)$; Δh_{Mi} ($i = 4, 5, 6$) are the thickness deviation to be eliminated only by stand F_i ; ΔS_{Mi} and ΔS_{Xi} ($i = 4, 5, 6$) are the gap correction value of monitor AGC and other types of AGC of stand F_i ; S_{0i} and S_{ri} are the gap set value and gap target value of stand F_i ; M represents the motor of looper.

As shown in Figure 7, the thickness deviation to be eliminated only by stand F_i can be calculated from

$$\Delta h_{Mi} = \begin{cases} k_i \Delta h_m, & i = 4 \\ \Delta h_{mi} - \frac{Q_i}{Q_i + M_i} k_{i-1} \Delta h_m e^{-\tau_{i-1} s}, & i = 5, 6. \end{cases} \quad (15)$$

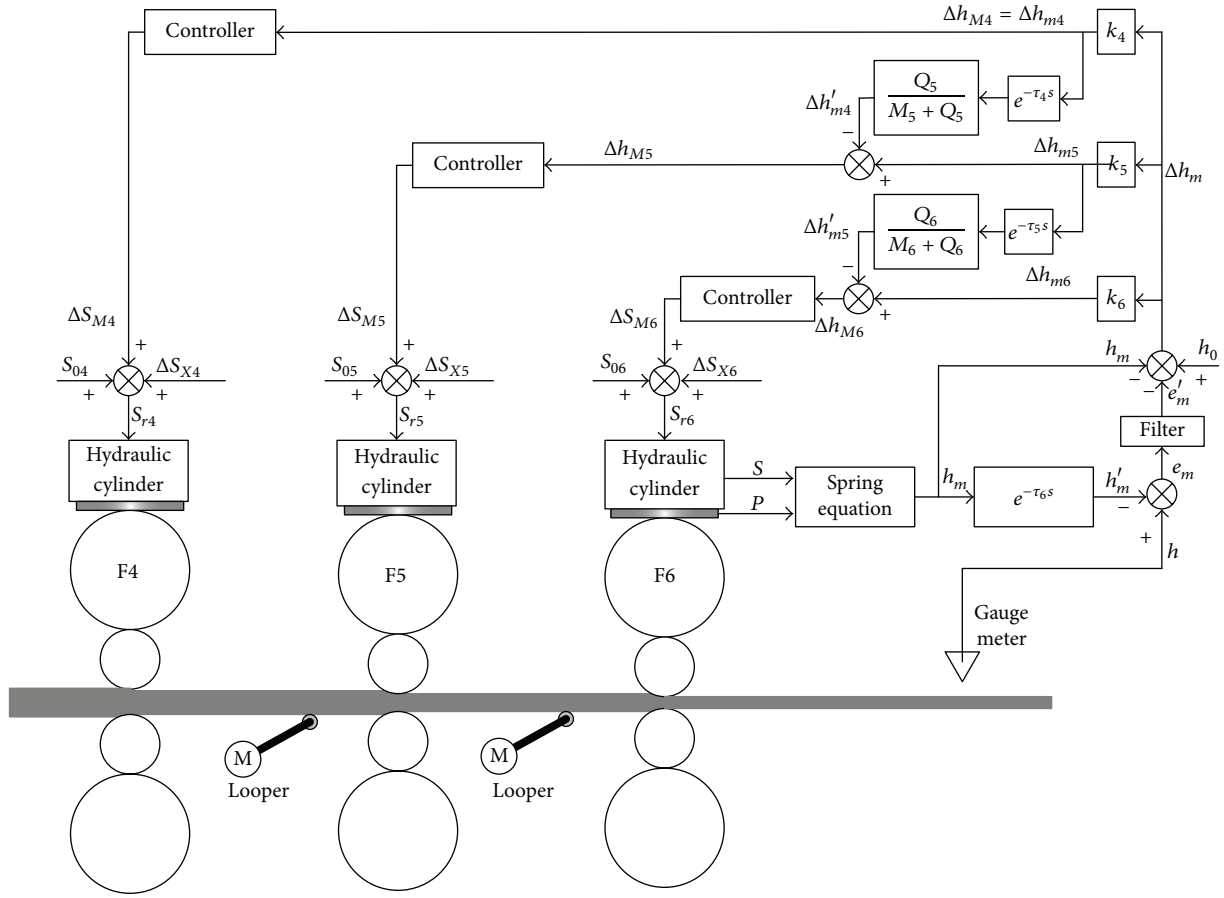


FIGURE 7: Schematic diagram of the complete monitor AGC system.

4. Expert PI Controller Design

The Proportional-Integral (PI) controller is adopted as the primary controller in monitor AGC. PI parameters k_p and k_i are expected to be modified appropriately based on the current status of the system to obtain a good dynamic performance in the actual control process. But the control algorithm purely based on the mathematical model is difficult to meet the requirements of the control system and get the satisfactory dynamic performance, especially in the case of parameter variations and load disturbances. The expert system adjusting control output based on feature information is proposed for the strip thinning during looper rising and coiler biting period and the strip thickening during the tension loss period of the strip tail end, as shown in Figure 8.

The expert PI controller is shown in Figure 9. The input basic information of the expert controller includes $\varphi_1 = \{\text{Thickness set value}\}$, $\varphi_2 = \{\text{Thickness deviation } e\}$, $\varphi_3 = \{\text{Width set value}\}$, $\varphi_4 = \{\text{Speed mode}\}$, $\varphi_5 = \{\text{Looper rising period}\}$, $\varphi_6 = \{\text{Coiler biting period}\}$, $\varphi_7 = \{\text{Tension loss period of the strip tail end}\}$, and $\varphi_8 = \{\text{Steel grade}\}$.

The main expert knowledge in the knowledge base is as follows:

- (1) k_p and k_i are 0.6 and 0.15, respectively, when the thickness set value is less than 2.0 mm, 0.8 and 0.2

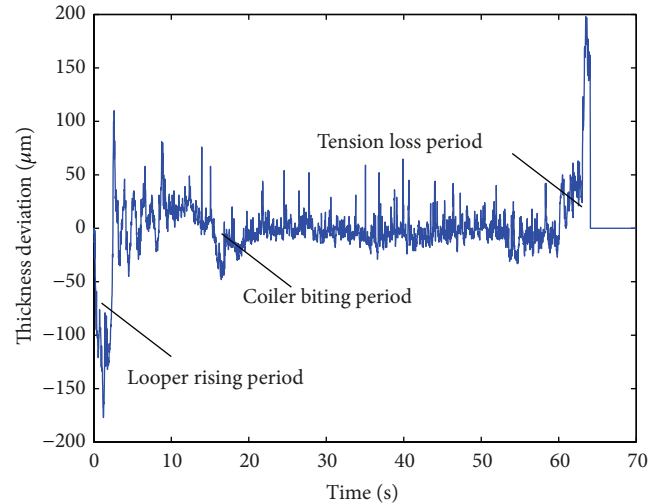


FIGURE 8: Thickness deviation of the old monitor AGC system.

when the value is 2.0 to 5.0 mm, and 1.1 and 0.22 when the value is greater than 5.0 mm;

- (2) k_p and k_i decrease 0.1 and 0.02, respectively, when the width set value is greater than 1450 mm;
- (3) k_p decreases 0.2 and k_i increases 0.04 during speed-up rolling;

TABLE 1: Thickness comparison at a steady rolling speed.

| Category | h_0/mm | Ratio in corresponding range/% | | | | |
|------------|-----------------|----------------------------------|----------------------------------|----------------------------------|----------------------------------|-----------------------------------|
| | | $ \Delta h \leq 20 \mu\text{m}$ | $ \Delta h \leq 30 \mu\text{m}$ | $ \Delta h \leq 40 \mu\text{m}$ | $ \Delta h \leq 50 \mu\text{m}$ | $ \Delta h \leq 100 \mu\text{m}$ |
| New system | 3.00 | 93.10 | 96.54 | 98.18 | 98.88 | 99.90 |
| | 4.00 | 90.33 | 93.98 | 96.70 | 98.08 | 99.79 |
| | 5.00 | 89.03 | 95.38 | 96.83 | 97.93 | 99.74 |
| | 6.00 | 85.46 | 93.82 | 96.02 | 97.04 | 99.58 |
| Old system | 3.00 | 90.89 | 96.07 | 97.62 | 98.05 | 99.89 |
| | 4.00 | 88.49 | 92.78 | 95.23 | 96.52 | 99.36 |
| | 5.00 | 87.80 | 94.75 | 95.42 | 96.89 | 99.54 |
| | 6.00 | 83.08 | 91.77 | 95.04 | 96.56 | 99.47 |

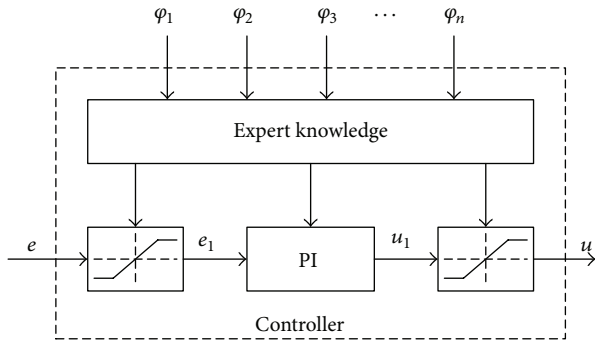


FIGURE 9: Expert PI controller.

- (4) k_p and k_i increase 0.3 and 0.04, respectively, when SPCC steel is being rolled;
- (5) e_1 decreases $100 \mu\text{m}$ and $30 \mu\text{m}$ on the basis of e during looper rising period and coiler biting period, respectively;
- (6) e_1 gradually increases on the basis of e during tension loss period of the strip tail end;
- (7) u reaches the preset maximum (or minimum) when e is greater than $150 \mu\text{m}$ (or less than $-150 \mu\text{m}$);
- (8) k_p increases 0.2 and k_i decreases 0.02 when the absolute value of e is greater than $100 \mu\text{m}$ and less than or equal to $150 \mu\text{m}$;

(9) k_p decreases 0.2 and k_i increases 0.02 when the absolute value of e is greater than $10 \mu\text{m}$ and less than or equal to $50 \mu\text{m}$;

(10) k_p is 0 and k_i increases 0.04 when the absolute value of e is less than $10 \mu\text{m}$.

5. Application Results

The monitor AGC tactics have been applied to the thickness control of a 1700 mm HSM and achieved good control effect. The control quality and the robustness of the system are very good, which proves the rationality of the system control principle. The system overcomes the subjective phenomenon of the instability of the manual operation, reduces the labor intensity of the operator, and improves the quality of the steel strip. Figure 10 is a measurement by X-ray gauge meter to the delivery thickness curve when the new monitor AGC system is working. As can be seen in Figure 8, the new AGC system achieves better thickness performance than the old AGC system.

We have collected statistics data for 2 months and conclude from the data analysis that the average thickness qualified rate of the AGC system with new monitor algorithm is generally higher than that of the AGC system with old algorithm. The application results of some main specifications are shown in Tables 1 and 2, where h_0 is the target thickness and Δh is the thickness deviation. Taking the steel strip with $h_0 = 4.0 \text{ mm}$ as an example, the ratio σ in corresponding range $|\Delta h| \leq 30 \mu\text{m}$ at a steady rolling speed is calculated as follows:

$$\sigma = \frac{\text{Length of the strip rolled at a steady rolling speed with } |\Delta h| \leq 30 \mu\text{m}}{\text{Total length of the strip rolled at a steady rolling speed}}. \quad (16)$$

It can be calculated from Tables 1 and 2 that the average ratio of the new system and the old system is 94.76% and 95.82% at a steady rolling speed and 94.27% and 93.04% in acceleration and deceleration. As an important indicator, the ratio in corresponding range is generally used to represent the thickness precision. Therefore, it can be said that the thickness accuracy has been improved by about 1.06% at

a steady rolling speed and about 1.23% in acceleration and deceleration.

6. Conclusion

This paper has presented a monitor AGC algorithm of expert PI controller with FSP which is suitable for the control of

TABLE 2: Thickness comparison in acceleration and deceleration.

| Category | h_0/mm | Ratio in corresponding range/% | | | | |
|------------|-----------------|----------------------------------|----------------------------------|----------------------------------|----------------------------------|-----------------------------------|
| | | $ \Delta h \leq 20 \mu\text{m}$ | $ \Delta h \leq 30 \mu\text{m}$ | $ \Delta h \leq 40 \mu\text{m}$ | $ \Delta h \leq 50 \mu\text{m}$ | $ \Delta h \leq 100 \mu\text{m}$ |
| New system | 3.00 | 90.81 | 94.90 | 97.25 | 98.54 | 99.56 |
| | 4.00 | 87.90 | 91.26 | 94.86 | 97.51 | 99.79 |
| | 5.00 | 84.80 | 93.93 | 95.36 | 97.33 | 99.74 |
| | 6.00 | 79.89 | 91.62 | 94.66 | 96.19 | 99.58 |
| Old system | 3.00 | 87.44 | 94.52 | 97.05 | 97.44 | 99.89 |
| | 4.00 | 85.63 | 90.33 | 93.51 | 95.57 | 99.36 |
| | 5.00 | 83.17 | 94.08 | 93.46 | 96.01 | 99.54 |
| | 6.00 | 77.29 | 88.50 | 93.01 | 95.59 | 99.47 |

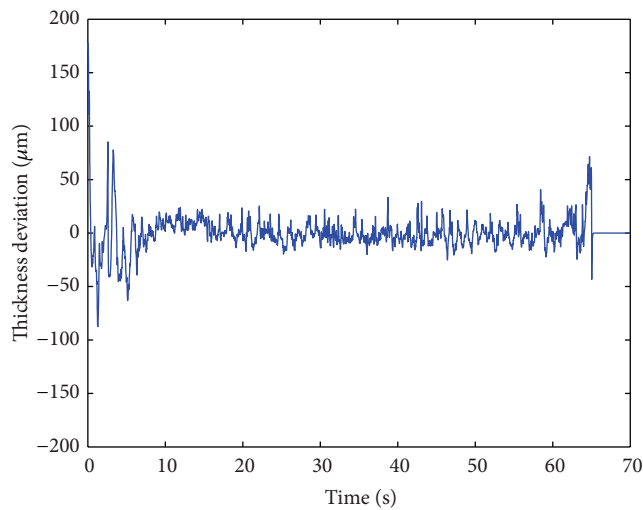


FIGURE 10: Thickness deviation of the new monitor AGC system.

processes with long dead time. Compared with a conventional algorithm it has the advantage of obtaining real-time thickness and improving robustness. Moreover, the discrete model of FSP control strategy is easy to implement and tune.

The disadvantage of new monitor AGC system is that the greater thickness deviation correction in downstream stands of FM causes the greater variation in strip shape quality resulting in excessive burden to the bending control system of work roll during thickness deviation correction, so the process automation system should adopt more accurate models and perform more exact setup calculations to overcome it.

Competing Interests

The authors declare that there are no competing interests regarding the publication of this paper.

Acknowledgments

This work is partially supported by the Fundamental Research Funds for the Central Universities (FRF-TP-15-061A3), National Natural Science Funds of China (51404021), and Beijing Municipal Natural Science Foundation (3154035).

References

- [1] P. J. Reeve, A. F. MacAlister, and T. S. Bilkhu, "Control, automation and the hot rolling of steel," *Philosophical Transactions of the Royal Society A: Mathematical, Physical and Engineering Sciences*, vol. 357, no. 1756, pp. 1549–1571, 1999.
- [2] H.-Y. Zhang, J. Sun, D.-H. Zhang, S.-Z. Chen, and X. Zhang, "Improved Smith prediction monitoring AGC system based on feedback-assisted iterative learning control," *Journal of Central South University*, vol. 21, no. 9, pp. 3492–3497, 2014.
- [3] Z. Fei, X. Xiaofei, W. Binbin, and R. Xiaohuai, "Virtual gauging system for hot strip mill," *Sensors and Transducers*, vol. 172, no. 6, pp. 105–110, 2014.
- [4] H. Dyja, J. Markowski, and D. Stoiński, "Asymmetry of the roll gap as a factor improving work of the hydraulic gauge control in the plate rolling mill," *Journal of Materials Processing Technology*, vol. 60, no. 1–4, pp. 73–80, 1996.
- [5] S. Khosravi, A. Afshar, and F. Barazandeh, "Design of a novel fuzzy adaptive PI controller for monitor hydraulic AGC system of cold rolling mill," in *Proceedings of the 2nd International Conference on Instrumentation Control and Automation (ICA '11)*, pp. 53–58, IEEE, Bandung, Indonesia, November 2011.
- [6] W. Y. Chien, H. H. Cheng, C. S. Yi, and M. C. Chang, "A strategy to monitor AGC in consideration of rolling force distribution," *China Steel Technical Report* 26, 2013.
- [7] D. Li, J.-C. Liu, S.-B. Tan, X. Yu, and C.-J. Zhang, "A new monitor-AGC system in hot continues rolling," in *Proceedings of the 33rd Chinese Control Conference (CCC '14)*, pp. 6319–6323, Nanjing, China, July 2014.
- [8] D. Zhang, H. Zhang, T. Sun, and X. Li, "Monitor automatic gauge control strategy with a Smith predictor for steel strip rolling," *Journal of University of Science and Technology Beijing*, vol. 15, no. 6, pp. 827–832, 2008.
- [9] I. Kaya, "Autotuning of a new PI-PD smith predictor based on time domain specifications," *ISA Transactions*, vol. 42, no. 4, pp. 559–575, 2003.
- [10] O. J. M. Smith, "Closed control of loops with dead time," *Chemical Engineering Progress*, no. 53, pp. 217–219, 1957.
- [11] J. Sun, D.-H. Zhang, X. Li, J. Zhang, and D.-S. Du, "Smith prediction monitor AGC system based on fuzzy self-tuning pid control," *Journal of Iron and Steel Research International*, vol. 17, no. 2, pp. 22–26, 2010.
- [12] C.-C. Hang, Q.-G. Wang, and L.-S. Cao, "Self-tuning Smith predictors for processes with long dead time," *International Journal of Adaptive Control and Signal Processing*, vol. 9, no. 3, pp. 255–270, 1995.

- [13] J. E. Normey-Rico and E. F. Camacho, *Control of Dead-Time Processes*, Springer, London, UK, 2007.
- [14] J. E. Normey-Rico and E. F. Camacho, "Unified approach for robust dead-time compensator design," *Journal of Process Control*, vol. 19, no. 1, pp. 38–47, 2009.
- [15] M. Morari and E. Zafriou, *Robust Process Control*, Prentice Hall, Englewood Cliffs, NJ, USA, 1989.
- [16] L. Roca, J. L. Guzman, J. E. Normey-Rico, M. Berenguel, and L. Yebra, "Filtered Smith predictor with feedback linearization and constraints handling applied to a solar collector field," *Solar Energy*, vol. 85, no. 5, pp. 1056–1067, 2011.
- [17] F. Zhang, Y. Zhang, J. Hou, and B. Wang, "Thickness control strategies of plate rolling mill," *International Journal of Innovative Computing, Information and Control*, vol. 11, no. 4, pp. 1227–1237, 2015.

Research Article

Novel Robust Exponential Stability of Markovian Jumping Impulsive Delayed Neural Networks of Neutral-Type with Stochastic Perturbation

Yang Fang,¹ Kelin Li,^{1,2} and Yunqi Yan³

¹School of Science, Sichuan University of Science & Engineering, Sichuan 643000, China

²Institute of Nonlinear Physical Science, Sichuan University of Science & Engineering, Sichuan 643000, China

³College of Mechanical Engineering, Sichuan University of Science & Engineering, Sichuan 643000, China

Correspondence should be addressed to Yang Fang; fyang22@163.com

Received 28 January 2016; Revised 12 April 2016; Accepted 19 May 2016

Academic Editor: Olfa Boubaker

Copyright © 2016 Yang Fang et al. This is an open access article distributed under the Creative Commons Attribution License, which permits unrestricted use, distribution, and reproduction in any medium, provided the original work is properly cited.

The robust exponential stability problem for a class of uncertain impulsive stochastic neural networks of neutral-type with Markovian parameters and mixed time-varying delays is investigated. By constructing a proper exponential-type Lyapunov-Krasovskii functional and employing Jensen integral inequality, free-weight matrix method, some novel delay-dependent stability criteria that ensure the robust exponential stability in mean square of the trivial solution of the considered networks are established in the form of linear matrix inequalities (LMIs). The proposed results do not require the derivatives of discrete and distributed time-varying delays to be 0 or smaller than 1. Moreover, the main contribution of the proposed approach compared with related methods lies in the use of three types of impulses. Finally, two numerical examples are worked out to verify the effectiveness and less conservativeness of our theoretical results over existing literature.

1. Introduction

Up to now, the stability analysis of neural networks is an important research field in modern cybernetic area, since most of the successful applications of neural networks significantly depend on the stability of the equilibrium point of neural networks. Many papers related to this problem have been published in the literature; see [1] for a survey.

During implementation of artificial neural networks, time-varying delays [2–4] are unavoidable due to finite switching speeds of the amplifiers, and the neural signal propagation is often distributed in a certain time period with the presence of an amount of parallel pathways with a variety of axon sizes and lengths. Therefore, it is necessary to consider mixed time-varying delays (discrete time-varying delay and distributed time-varying delay) to design the neural networks models. There are many works focusing on the mixed time-varying delays [5–8], among which delay-dependent criteria are generally less conservative than delay-independent ones when the sizes of time-delays are small, and the maximum

allowable delay bound is the main performance index of delay-dependent stability analysis [9]. In addition, as a special type of time delayed neural networks, neutral-type neural networks precisely describe that the past state of the networks will affect the current state. Therefore, the problems of stability and synchronization for such a class of neural networks have been studied in many references; see [10–22].

It is well known that the other three sources which may lead to instability and poor performances in neural networks are stochastic perturbation, impulsive perturbations, and parametric uncertainties. Most of this viewpoint is attributable to the following three reasons: (1) A neural network can be stabilized or destabilized by certain stochastic inputs [23–26]. (2) In the real world, many evolutionary processes are characterized by abrupt changes at time. These changes are called impulsive phenomena, which have been found in various fields, such as physics, optimal control, and biological mathematics [27]. (3) The effects of parametric uncertainties cannot be ignored in many applications [28–30]. Hence, stochastic perturbation, impulsive perturbations,

and parametric uncertainties also should be taken into consideration when dealing with the stability issue of neural networks.

On the other hand, Markovian jumping systems [31] can be seen as a special class of hybrid systems with two different states, which involve both time-evolving and event-driven mechanisms. So such systems would be used to model the abrupt phenomena such as random failures and repairs of the components, changes in the interconnections of subsystems, and sudden environment changes. Thus, many relevant analysis results for Markovian jumping neural networks with impulses have been reported; see [32–38] and the references therein.

Recently, by using the concept of the minimum impulsive interval, Bao and Cao [11], Zhang et al. [12], and Gao et al. [13] derived some sufficient conditions to ensure exponential stability in mean square for neutral-type impulsive stochastic neural networks with Markovian jumping parameters and mixed time delays. However, in [11–13], the authors ignored parametric uncertainties. And in these three papers, the derivatives of time-varying delays need to be zero or smaller than one. So far, there are few results on the study of robust exponential stability of neutral-type impulsive stochastic neural networks with Markovian jumping parameters, mixed time-varying delays, and parametric uncertainties. More importantly, the impulses can be divided into three types to discuss the following: the impulses are stabilizing; the impulses are neutral-type (i.e., they are neither helpful for stability of neural networks nor destabilizing); and the impulses are destabilizing. Some interesting results for analyzing and synthesizing impulsive nonlinear systems that divide impulses into three types can be seen in [39–46]. In [39–41, 43], the authors studied the stability problem of impulsive neural networks with discrete time-varying delay by using the Lyapunov-Razumikhin method; several criteria for global exponential stability of the discrete-time or continuous-time neural networks are established in terms of matrix inequalities. In [42, 44–46], combining the impulsive comparison theory and triangle inequality, some important results about three-type impulses for different neural networks have been obtained. However, distributed time-varying delay has not been taken into account in all abovementioned references; how to deal with the stability problem of Markovian jumping impulsive stochastic neural networks with mixed delays is also a meaningful direction. Motivated by above discussion, based on the concepts of three-type impulses, this paper focuses on the robust exponential stability in mean square of impulsive stochastic neural networks with Markovian jumping parameters, mixed time-varying delays, and parametric uncertainties. By constructing a proper exponential-type Lyapunov-Krasovskii functional, linear matrix inequality (LMI) technique, Jensen integral inequality and free-weight matrix method, several novel sufficient conditions in terms of linear matrix inequalities (LMIs) are derived to guarantee the robust exponential stability in mean square of the trivial solution of the considered model. Compared with references [11–13], the constructed model renders more practical factors since the parametric uncertainties have been taken into account, and the derivatives of discrete and

distributed time-varying delays need to be 0 or smaller than 1. Moreover, the main contribution of the proposed approach compared with related methods lies in the use of three types of impulses.

The organization of this paper is as follows. In Section 2, the robust exponential stability problem of impulsive stochastic neural networks with Markovian jumping parameters, mixed time-varying delays, and parametric uncertainties is described and some necessary definitions and lemmas are given. Some new robust exponential stability criteria are obtained in Section 3. In Section 4, two illustrative examples are given to show the effectiveness and less conservatism of the proposed method. Finally, conclusions are given in Section 5.

Notation. Let \mathbb{R} denote the set of real numbers, let \mathbb{R}^+ denote the set of all nonnegative real numbers, let \mathbb{R}^n and $\mathbb{R}^{n \times m}$ denote the n -dimensional and $n \times m$ dimensional real spaces equipped with the Euclidean norm, and let $\|\cdot\|$ refer to the Euclidean vector norm and the induced matrix norm. \mathbb{N}^+ denotes the set of positive integers. For any matrix $X \in \mathbb{R}^{n \times n}$, $X > 0$ denotes that X is a symmetric and positive definite matrix. If X_1, X_2 are symmetric matrices, then $X_1 \leq X_2$ means that $X_1 - X_2$ is a negative semidefinite matrix. X^T and X^{-1} mean the transpose of X and the inverse of a square matrix. I denotes the identity matrix with appropriate dimensions. Let $\tau > 0$ and $C([-\tau, 0]; \mathbb{R}^n)$ denote the family of all continuous \mathbb{R}^n -valued functions $\xi(\theta)$ on $[-\tau, 0]$ with the norm $\|\xi\| = \sup_{-\tau \leq \theta \leq 0} \|\xi(\theta)\|$. Let $\omega(t) = [\omega_1(t), \omega_2(t), \dots, \omega_n(t)]^T$ be an n -dimensional Brownian motion defined on a complete probability space $(\Omega, \mathcal{F}, \mathcal{P})$ with a natural filtration $\{\mathcal{F}_t\}_{t \geq 0}$ (i.e., $\mathcal{F}_t = \sigma\{\omega(s) : 0 \leq s \leq t\}$), which satisfies $E d\omega(t) = 0$ and $E[d\omega(t)]^2 = dt$. $L^p_{\mathcal{F}_t}([-\tau, 0]; \mathbb{R}^n)$ ($t \geq 0$) denote the family of all \mathcal{F}_t measurable bounded $C([-\tau, 0]; \mathbb{R}^n)$ -valued random variables $\xi = \{\xi(\theta) : -\tau \leq \theta \leq 0\}$ such that $\int_{-\tau}^0 E|\xi(s)|^p ds < \infty$, where $E\{\cdot\}$ stands for the correspondent expectation operator with respect to the given probability measure \mathcal{P} . The notation $*$ always denotes the symmetric block in one symmetric matrix. Matrix dimensions, if not explicitly stated, are assumed to be compatible for operations.

2. Model Description and Preliminaries

Let $\{r(t), t \geq 0\}$ be a right continuous Markov chain in a complete probability space $(\Omega, \mathcal{F}, \mathcal{P})$ taking values in a finite state space $S = \{1, 2, \dots, N\}$ with generator $\Pi = (\pi_{ij})_{N \times N}$ given by

$$\begin{aligned} \mathcal{P}\{r(t + \Delta t) = j \mid r(t) = i\} \\ = \begin{cases} \pi_{ij}\Delta t + o(\Delta t), & \text{if } i \neq j, \\ 1 + \pi_{ii}\Delta t + o(\Delta t), & \text{if } i = j, \end{cases} \end{aligned} \quad (1)$$

where $\Delta t > 0$ and $\lim_{\Delta t \rightarrow 0} (o(\Delta t)/\Delta t) = 0$. Here $\pi_{ij} \geq 0$ ($i \neq j$) is the transition rate from mode i to mode j while $\pi_{ii} = -\sum_{j \neq i} \pi_{ij}$ is the transition rate from mode i to mode i .

Consider a class of impulsive stochastic neural networks of neural-type with Markovian jumping parameters, mixed time-varying delays, and parametric uncertainties, which can be presented by the following impulsive integrodifferential equation:

$$\begin{aligned} d[u(t) - D(r(t))u(t - \tau_3(t))] &= \left[-C(r(t))u(t) \right. \\ &+ (A(r(t)) + \Delta A(r(t)))f(u(t)) \\ &+ (B(r(t)) + \Delta B(r(t)))f(u(t - \tau_1(t))) \\ &+ (E(r(t)) + \Delta E(r(t))) \int_{t-\tau_2(t)}^t f(u(s))ds + J \Big] dt \quad (2) \\ &+ \sigma(t, r(t), u(t), u(t - \tau_1(t)), u(t - \tau_2(t)), \\ &u(t - \tau_3(t)))d\omega(t), \quad t \neq t_k, \\ \mathcal{D}u(t_k^+) &= W_k(r(t))\mathcal{D}u(t_k^-), \quad t = t_k, \quad k \in \mathbb{N}^+, \end{aligned}$$

for $t > 0$, where $u(t) = (u_1(t), u_2(t), \dots, u_n(t))^T \in \mathbb{R}^n$ is the state vector associated with n neurons at time t . In the continuous part of system (2), $C(r(t)) = \text{diag}\{c_1(r(t)), c_2(r(t)), \dots, c_n(r(t))\}$ is a diagonal matrix with positive entries $c_i(r(t)) > 0$ ($i = 1, 2, \dots, n$); the matrices $A(r(t)) = (a_{ij}(r(t)))_{n \times n}$, $B(r(t)) = (b_{ij}(r(t)))_{n \times n}$, and $E(r(t)) = (e_{ij}(r(t)))_{n \times n}$ are the connection weight matrix, the discrete time-varying delay connection weight matrix, and the distributed-delay connection weight matrix, respectively; $\Delta A(r(t))$, $\Delta B(r(t))$, and $\Delta E(r(t))$ are the time-varying parametric uncertainties; $f(u(t)) = (f_1(u_1(t)), f_2(u_2(t)), \dots, f_n(u_n(t)))^T \in \mathbb{R}^n$ is the nonlinear neuron activation function which describes the behavior in which the neurons respond to each other; $J = [J_1, J_2, \dots, J_n]^T \in \mathbb{R}^n$ is a constant external input vector; $\tau_1(t)$, $\tau_2(t)$, and $\tau_3(t)$ are, namely, the discrete time-varying delay, distributed time-varying delay, and neutral time-varying delay, which satisfy $0 \leq h_1 \leq \tau_1(t) \leq h_2$, $\dot{\tau}_1(t) \leq \mu_1$, $0 \leq \tau_2(t) \leq \tau_2$, $\dot{\tau}_2(t) \leq \mu_2$, $0 \leq \tau_3(t) \leq \tau_3$, and $\dot{\tau}_3(t) \leq \mu_3$; the noise perturbation (or the diffusion coefficient) $\sigma(t, r(t), u(t), u(t - \tau_1(t)), u(t - \tau_2(t)), u(t - \tau_3(t))) : \mathbb{R}^+ \times S \times \mathbb{R}^n \times \mathbb{R}^n \times \mathbb{R}^n \rightarrow \mathbb{R}^{n \times n}$ is a Borel measurable function. In the discrete part of system (2), $\mathcal{D}u(t_k^+) = W_k(r(t))\mathcal{D}u(t_k^-)$, $k \in \mathbb{N}^+$ is the impulse at the moment of time t_k of an operator defined as $\mathcal{D}u(t) = u(t) - D(r(t))u(t - \tau_3(t))$; $W_k(r(t)) \in \mathbb{R}^{n \times n}$ is the impulse gain matrix at the moment of time t_k ; the discrete instant set $\{t_k\}$ satisfies $0 = t_0 < t_1 < t_2 < \dots < t_k < \dots$, $\lim_{k \rightarrow \infty} t_k = \infty$; $\mathcal{D}u(t_k^-)$ and $\mathcal{D}u(t_k^+)$ are the left-hand and right-hand limits of operator $\mathcal{D}u(t)$ at t_k , respectively; as usual, we always assume that $\mathcal{D}u(t_k^+) = \mathcal{D}u(t_k)$.

Remark 1. In the continuous part of system (2), the evolution of state vector $u(t)$ is driven by the evolution of the operator $\mathcal{D}u(t) = u(t) - D(r(t))u(t - \tau_3(t))$. Consequently, we consider state jumping of the operator $\mathcal{D}u(t)$ at impulsive time in the discrete part of system (2). In system (2) of [13], $\dot{\omega}(t)$ has been used to build the main model, which is wrong since Brown motion is nowhere differentiable with probability 1 [47].

For convenience, we denote $r(t) = i$, $i \in S$; then the matrices $D(r(t))$, $C(r(t))$, $A(r(t))$, $B(r(t))$, $E(r(t))$, $\Delta A(r(t))$, $\Delta B(r(t))$, and $\Delta E(r(t))$ will be written as D_i , C_i , A_i , B_i , E_i , ΔA_i , ΔB_i , and ΔE_i , respectively. Therefore, system (2) can be rewritten as follows:

$$\begin{aligned} d[u(t) - D_i u(t - \tau_3(t))] &= \left[-C_i u(t) + (A_i + \Delta A_i) \right. \\ &\cdot f(u(t)) + (B_i + \Delta B_i) f(u(t - \tau_1(t))) \\ &+ (E_i + \Delta E_i) \int_{t-\tau_2(t)}^t f(u(s))ds + J \Big] dt + \sigma(t, i, \\ &u(t), u(t - \tau_1(t)), u(t - \tau_2(t)), u(t - \tau_3(t)))d\omega(t), \\ &t \neq t_k, \\ \mathcal{D}u(t_k^+) &= W_{ik} \mathcal{D}u(t_k^-), \quad t = t_k, \quad k \in \mathbb{N}^+. \end{aligned} \quad (3)$$

The initial condition of system (3) is given in the following form:

$$\begin{aligned} u(s) &= \varphi(s), \quad s \in [-\tau, 0], \\ r(0) &= i_0, \\ \tau &= \max\{h_2 + \tau_3, \tau_2 + \tau_3\}, \end{aligned} \quad (4)$$

for any $\varphi(s) \in L^2_{\mathcal{F}_0}([-\tau, 0]; \mathbb{R}^n)$.

To prove our main results, the following hypotheses are needed:

- (H1) All the eigenvalues of matrix D_i , $i \in S$, are inside the unit circle, which guarantees the stability of difference system $u(t) - D_i u(t - \tau_3(t)) = 0$.
- (H2) Each neuron activation function f_j is continuous [48], and there exist scalars l_j^- and l_j^+ such that

$$l_j^- \leq \frac{f_j(a) - f_j(b)}{a - b} \leq l_j^+, \quad (5)$$

for any $a, b \in \mathbb{R}$, $a \neq b$, $j = 1, 2, \dots, n$, where l_j^+ and l_j^- can be positive, negative, or zero. And we set

$$\begin{aligned} L_1 &= \text{diag}(l_1^-, l_2^-, \dots, l_n^-), \\ L_2 &= \text{diag}(l_1^+, l_2^+, \dots, l_n^+). \end{aligned} \quad (6)$$

- (H3) The noise matrix $\sigma(t, i, \cdot, \cdot, \cdot, \cdot)$ is local Lipschitz continuous and satisfies the linear growth condition as well, and $\sigma(0, i, 0, 0, 0, 0) = 0$. Moreover, there exist positive definite matrices H_{1i} , H_{2i} , H_{3i} , and H_{4i} ($i \in S$) such that

$$\begin{aligned} \text{trace}[\sigma^T(t, i, z_1, z_2, z_3, z_4) \sigma(t, i, z_1, z_2, z_3, z_4)] \\ \leq z_1^T H_{1i} z_1 + z_2^T H_{2i} z_2 + z_3^T H_{3i} z_3 + z_4^T H_{4i} z_4, \end{aligned} \quad (7)$$

for all $z_1, z_2, z_3, z_4 \in \mathbb{R}^n$, $t \in \mathbb{R}^+$, and $i \in S$.

(H4) The time-varying admissible parametric uncertainties $\Delta A_i(t)$, $\Delta B_i(t)$, $\Delta E_i(t)$, $i \in S$, are in terms of

$$[\Delta A_i(t) \ \Delta B_i(t) \ \Delta E_i(t)] = Z_i F_i(t) [H_i \ J_i \ K_i], \quad (8)$$

where Z_i , H_i , J_i , and K_i are known real constant matrices with appropriate dimensions and $F_i(t)$ is the uncertain time-varying matrix-valued function satisfying

$$F_i^T(t) F_i(t) \leq I, \quad \forall t \geq 0. \quad (9)$$

In this paper, we always assume that some conditions are satisfied so that system (3) has a unique equilibrium point. Let $u^* = (u_1^*, u_2^*, \dots, u_n^*) \in \mathbb{R}^n$ be the equilibrium point of system (3). For simplicity, we can shift the equilibrium u^* to the origin by letting $x(t) = u(t) - u^*$. Then system (3) can be transformed into the following one:

$$\begin{aligned} d[x(t) - D_i x(t - \tau_3(t))] &= [-C_i x(t) + (A_i + \Delta A_i) \\ &\cdot g(x(t)) + (B_i + \Delta B_i) g(x(t - \tau_1(t))) \\ &+ (E_i + \Delta E_i) \int_{t-\tau_2(t)}^t g(x(s)) ds] dt + \sigma(t, i, x(t), \\ &x(t - \tau_1(t)), x(t - \tau_2(t)), x(t - \tau_3(t))) d\omega(t), \\ &t \neq t_k, \end{aligned} \quad (10)$$

$$\mathcal{D}x(t_k^+) = W_{ik} \mathcal{D}x(t_k^-), \quad t = t_k, \quad k \in N^+,$$

where $g(x(\cdot)) = f(u(\cdot) + u^*) - f(u^*)$. The initial condition of system (10) is given in terms of

$$\begin{aligned} x(s) &= \psi(s) = \varphi(s) - u^*, \quad s \in [-\tau, 0], \\ r(0) &= i_0, \\ \tau &= \max\{h_2 + \tau_3, \tau_2 + \tau_3\}. \end{aligned} \quad (11)$$

Noting that $g(0) = 0$ and $\sigma(0, i, 0, 0, 0, 0) = 0$, we know that the trivial solution of system (10) exists. Thus, the stability problem of u^* of system (3) converts to the stability problem of the trivial solution of system (10). On the other hand, from hypothesis (H1), we get

$$I_j^- \leq \frac{g_j(a) - g_j(b)}{a - b} \leq I_j^+, \quad (12)$$

for any $a, b \in \mathbb{R}$, $a \neq b$, $j = 1, 2, \dots, n$.

Next, let $x(t; \xi)$ denote the state trajectory from the initial data $x(\theta) = \xi(\theta)$ on $-\tau \leq \theta \leq 0$ in $L^2_{\mathcal{F}_0}([-\tau, 0]; \mathbb{R}^n)$. Based on above discussion, system (10) has a trivial solution $x(t; 0) \equiv 0$ corresponding to the initial condition $\xi = 0$. For simplicity, we write $x(t; \xi) = x(t)$.

The following definition and lemmas are useful for developing our main results.

Definition 2 (see [49]). The trivial solution of system (10) is said to be exponentially stable in mean square if for every $\xi \in L^2_{\mathcal{F}_0}([-\tau, 0]; \mathbb{R}^n)$, there exist constants $\gamma > 0$ and $\mathcal{M} > 0$ such that the following inequality holds:

$$E \|x(t; \xi)\|^2 \leq \mathcal{M} e^{-\gamma t} \sup_{-\tau \leq \theta \leq 0} E \|\xi(\theta)\|^2, \quad (13)$$

where γ is called the exponential convergence rate.

Lemma 3 (Jensen integral inequality; see Gu [50]). For any constant matrix $M > 0$, any scalars s_1 and s_2 with $s_1 < s_2$, and a vector function $\eta(t) : [a, b] \rightarrow \mathbb{R}$ such that the integrals concerned are well defined, then the following inequality holds:

$$\begin{aligned} &\left(\int_{s_1}^{s_2} \eta(s) ds \right)^T M \left(\int_{s_1}^{s_2} \eta(s) ds \right) \\ &\leq (s_2 - s_1) \int_{s_1}^{s_2} \eta(s)^T M \eta(s) ds. \end{aligned} \quad (14)$$

Lemma 4 (Wang et al. [51]). For given matrices E , F , and G with $F^T F \leq I$ and scalar $\varepsilon > 0$, the following inequality holds:

$$GFE + E^T F^T G^T \leq \varepsilon GG^T + \varepsilon^{-1} E^T E. \quad (15)$$

Remark 5. Some inequalities have been widely used to derive less conservative conditions to analyze and synthesize problems of time-delay systems, for example, Gronwall-Bellman inequality [52], Halanay inequality [53], Jensen integral inequality, Wirtinger integral [54], and reciprocally convex approach [55] in which Jensen integral inequality is the most used, and Lemma 4 also holds if $s_1 = s_2$.

Remark 6. Similar to [8], we further investigate the substantial influence of the three-type impulses for the exponential stability issue of stochastic neural networks of neutral-type with both Markovian jump parameters and mixed time delays.

3. Main Results

In this section, the robust exponential stability in mean square of the trivial solution for system (10) is studied under hypotheses (H1) to (H4).

Before proceeding, by using the model transformation technique, we rewritten system (10) as

$$\begin{aligned} d[x(t) - D_i x(t - \tau_3(t))] &= z(t) dt + \sigma(t) d\omega(t), \\ &t \neq t_k, \quad k \in \mathbb{N}^+, \end{aligned} \quad (16)$$

where

$$\begin{aligned} z(t) &= -C_i x(t) + (A_i + \Delta A_i) g(x(t)) + (B_i + \Delta B_i) \\ &\cdot g(x(t - \tau_1(t))) + (E_i + \Delta E_i) \int_{t-\tau_2(t)}^t g(x(s)) ds, \\ \sigma(t) &= \sigma(t, i, x(t), x(t - \tau_1(t)), x(t - \tau_2(t)), \\ &x(t - \tau_3(t))). \end{aligned} \quad (17)$$

Theorem 7. Assume that hypotheses (H1)–(H4) hold. For given scalars h_1, h_2, τ_2, τ_3 , and μ_1, μ_2, μ_3 , the trivial solution of system (10) is robustly exponentially stable in mean square if there exist positive scalars $\lambda_i, \alpha_i \geq -1$ ($\alpha_i \neq 0$), $\alpha = \max\{1 + \alpha_i\}$ ($i \in S$), $\kappa_1, \kappa_2, \gamma$, positive definite matrices P_i ($i \in S$), $Q_1, Q_2, Q_3, Q_4, Q_5, Q_6$, positive diagonal matrices R_i, S_i ($i \in S$), and any real matrices N_q ($q = 1, 2, \dots, 10$) of appropriate dimensions such that

$$P_i \leq \lambda_i I, \quad (18)$$

$$W_{ik}^T P_l W_{ik} - P_i \leq \alpha_i P_i \quad [\text{here } r(t_k) = l], \quad (19)$$

$$\Phi_i = \begin{bmatrix} \Phi'_i & \Gamma_{1i} & \Gamma_{2i} \\ * & -\kappa_1 I & 0 \\ * & * & -\kappa_2 I \end{bmatrix} < 0, \quad (20)$$

where

$$\Phi'_i = (\phi'_{imn})_{13 \times 13},$$

$$m = 1, 2, \dots, 13, \quad n = 1, 2, \dots, 13,$$

$$\Gamma_{1i} = \begin{bmatrix} P_i Z_i \\ 0_{12n \times n} \end{bmatrix},$$

$$\Gamma_{2i} = \begin{bmatrix} D_i^T P_i Z_i \\ 0_{12n \times n} \end{bmatrix},$$

$$\begin{aligned} \phi'_{i1,1} = & -P_i C_i - C_i^T P_i + \gamma P_i + \lambda_i H_{1i} + \sum_{j=1}^N \pi_{ij} P_j \\ & + e^{-\gamma h_2} Q_1 + \sum_{j=2}^3 e^{-\gamma \tau_j} Q_j \\ & + \frac{h_2 - h_1}{\gamma} (e^{\gamma h_2} - e^{\gamma h_1}) Q_5 \\ & + \frac{\tau_3}{\gamma} (e^{\gamma \tau_3} - 1) Q_6 - 2L_1 R_i L_2 + N_1 + N_1^T \\ & + N_6 + N_6^T, \end{aligned}$$

$$\phi'_{i1,2} = -N_1 + N_2^T,$$

$$\phi'_{i1,3} = -N_6 + N_7^T,$$

$$\begin{aligned} \phi'_{i1,4} = & - \left(\sum_j^N \pi_{ij} P_j \right) D_i - \gamma P_i D_i + C_i^T P_i D_i - N_1 D_i \\ & - N_6 D_i + N_3^T + N_8^T, \end{aligned}$$

$$\phi'_{i1,5} = N_1 D_i + N_4^T,$$

$$\phi'_{i1,6} = N_6 D_i + N_9^T,$$

$$\phi'_{i1,7} = P_i A_i + (L_1 + L_2) R_i,$$

$$\phi'_{i1,8} = P_i B_i,$$

$$\phi'_{i1,9} = P_i E_i,$$

$$\phi'_{i1,10} = -N_1 + N_5^T,$$

$$\phi'_{i1,11} = -N_6 + N_{10}^T,$$

$$\begin{aligned} \phi'_{i2,2} = & \lambda_i H_{2i} - (1 - \mu_1) h(\mu_1) Q_1 - 2L_1 S_i L_2 - N_2 \\ & - N_2^T, \end{aligned}$$

$$\phi'_{i2,4} = -N_2 D_i - N_3^T,$$

$$\phi'_{i2,5} = N_2 D_i - N_4^T,$$

$$\phi'_{i2,8} = (L_1 + L_2) S_i,$$

$$\phi'_{i2,10} = -N_2 - N_5^T,$$

$$\phi'_{i3,3} = \lambda_i H_{3i} - (1 - \mu_2) h(\mu_2) Q_2 - N_7 - N_7^T,$$

$$\phi'_{i3,4} = -N_7 D_i - N_8^T,$$

$$\phi'_{i3,6} = N_7 D_i - N_9^T,$$

$$\phi'_{i3,11} = -N_7 - N_{10}^T,$$

$$\begin{aligned} \phi'_{i4,4} = & \gamma D_i^T P_i D_i + D_i^T \left(\sum_{j=1}^N \pi_{ij} P_j \right) D_i + \lambda_i H_{4i} \\ & - (1 - \mu_3) h(\mu_3) Q_3 - N_3 D_i - D_i^T N_3^T \\ & - N_8 D_i - D_i^T N_8^T, \end{aligned}$$

$$\phi'_{i4,5} = N_3 D_i - D_i^T N_4^T,$$

$$\phi'_{i4,6} = N_8 D_i - D_i^T N_9^T,$$

$$\phi'_{i4,7} = -D_i^T P_i A_i,$$

$$\phi'_{i4,8} = -D_i^T P_i B_i,$$

$$\phi'_{i4,9} = -D_i^T P_i E_i,$$

$$\phi'_{i4,10} = -N_3 - D_i^T N_5^T,$$

$$\phi'_{i4,11} = -N_8 - D_i^T N_{10}^T,$$

$$\phi'_{i5,5} = N_4 D_i + D_i^T N_4^T,$$

$$\phi'_{i5,10} = -N_4 + D_i^T N_5^T,$$

$$\phi'_{i6,6} = N_9 D_i + D_i^T N_9^T,$$

$$\phi'_{i6,11} = -N_9 + D_i^T N_{10}^T,$$

$$\phi'_{i7,7} = \frac{\tau}{\gamma} (e^{\gamma \tau} - 1) Q_4 - 2R_i + \kappa_1 H_i^T H_i + \kappa_2 H_i^T H_i,$$

$$\begin{aligned}
\phi'_{i8,8} &= -2S_i + \kappa_1 J_i^T J_i + \kappa_2 J_i^T J_i, \\
\phi'_{i9,9} &= -Q_4 + \kappa_1 K_i^T K_i + \kappa_2 K_i^T K_i, \\
\phi'_{i10,10} &= -N_5 - N_5^T, \\
\phi'_{i11,11} &= -N_{10} - N_{10}^T, \\
\phi'_{i12,12} &= -Q_5, \\
\phi'_{i13,13} &= -Q_6,
\end{aligned} \tag{21}$$

and the function $h(u) \in \mathbb{R}^+$, $u \in \mathbb{R}$, is defined as

$$h(u) = \begin{cases} 1, & u > 1, \\ e^{-2\gamma\tau}, & u \leq 1 \end{cases} \tag{22}$$

and for $\alpha_i > 0$, $-\gamma + \ln \alpha / \inf\{t_k - t_{k-1}\} < 0$, $k \in \mathbb{N}^+$, other elements of Φ'_i are all equal to 0.

Proof. Let $x_t = x(t + s)$, $s \in [-\tau, 0]$. As discussed in [56–59], $\{x_t, r(t), t \geq 0\}$ is a $C([- \tau, 0]; \mathbb{R}^n) \times S$ -valued Markov process. Construct the following stochastic Lyapunov-Krasovskii functional candidate for system (10):

$$V(t, i, x_t) = V_1(t, i, x_t) + V_2(t, i, x_t) + V_3(t, i, x_t), \tag{23}$$

where

$$\begin{aligned}
V_1(t, i, x_t) &= e^{\gamma t} (x(t) - D_i x(t - \tau_3(t)))^T \\
&\quad \cdot P_i(x(t) - D_i x(t - \tau_3(t))), \\
V_2(t, i, x_t) &= \int_{t-\tau_1(t)}^t e^{\gamma(s-h_2)} x^T(s) Q_1 x(s) ds \\
&\quad + \int_{t-\tau_2(t)}^t e^{\gamma(s-\tau_2)} x^T(s) Q_2 x(s) ds \\
&\quad + \int_{t-\tau_3(t)}^t e^{\gamma(s-\tau_3)} x^T(s) Q_3 x(s) ds, \\
V_3(t, i, x_t) &= \tau \int_{-\tau}^0 \int_{t+\beta}^t e^{\gamma(s-\beta)} g^T(x(s)) Q_4 g(x(s)) ds d\beta \\
&\quad + (h_2 - h_1) \int_{-h_2}^{-h_1} \int_{t+\beta}^t e^{\gamma(s-\beta)} x^T(s) Q_5 x(s) ds d\beta \\
&\quad + \tau_3 \int_{-\tau_3}^0 \int_{t+\beta}^t e^{\gamma(s-\beta)} x^T(s) Q_6 x(s) ds d\beta.
\end{aligned} \tag{24}$$

For $t \in [t_{k-1}, t_k]$, $k \in \mathbb{N}^+$, denote \mathfrak{L} to be the weak infinitesimal operator of the random process $x_t = x(t + s)$, $s \in [-\tau, 0]$; then along the trajectory of system (10) we have

$$\begin{aligned}
\mathfrak{L}V(t, i, x_t) &= \mathfrak{L}V_1(t, i, x_t) + \mathfrak{L}V_2(t, i, x_t) \\
&\quad + \mathfrak{L}V_3(t, i, x_t),
\end{aligned} \tag{25}$$

where

$$\begin{aligned}
\mathfrak{L}V_1(t, i, x_t) &= \gamma e^{\gamma t} (x(t) - D_i x(t - \tau_3(t)))^T P_i(x(t) \\
&\quad - D_i x(t - \tau_3(t))) + 2e^{\gamma t} (x(t) \\
&\quad - D_i x(t - \tau_3(t)))^T P_i \left[-C_i x(t) \right. \\
&\quad + (A_i + \Delta A_i) g(x(t)) \\
&\quad + (B_i + \Delta B_i) g(x(t - \tau_1(t))) \\
&\quad + (E_i + \Delta E_i) \int_{t-\tau_2(t)}^t g(x(s)) ds \left. \right] \\
&\quad + e^{\gamma t} \text{trace} [\sigma^T(t) P_i \sigma(t)] + e^{\gamma t} (x(t) \\
&\quad - D_i x(t - \tau_3(t)))^T \left(\sum_{j=1}^N \pi_{ij} P_j \right) (x(t) \\
&\quad - D_i x(t - \tau_3(t))), \\
\mathfrak{L}V_2(t, i, x_t) &= e^{\gamma(t-h_2)} x^T(t) Q_1 x(t) - (1 - \dot{\tau}_1(t)) \\
&\quad \cdot e^{\gamma(t-\tau_1(t)-h_2)} x^T(t - \tau_1(t)) Q_1 x(t - \tau_1(t)) \\
&\quad + e^{\gamma(t-\tau_2)} x^T(t) Q_2 x(t) - (1 - \dot{\tau}_2(t)) \\
&\quad \cdot e^{\gamma(t-\tau_2(t)-\tau_2)} x^T(t - \tau_2(t)) Q_2 x(t - \tau_2(t)) \\
&\quad + e^{\gamma(t-\tau_3)} x^T(t) Q_3 x(t) - (1 - \dot{\tau}_3(t)) \\
&\quad \cdot e^{\gamma(t-\tau_3(t)-\tau_3)} x^T(t - \tau_3(t)) Q_3 x(t - \tau_3(t)), \\
\mathfrak{L}V_3(t, i, x_t) &= \tau \int_{-\tau}^0 e^{\gamma(t-\beta)} g^T(x(t)) Q_4 g(x(t)) d\beta \\
&\quad - \tau \int_{-\tau}^0 e^{\gamma t} g^T(x(t + \beta)) Q_4 g(x(t + \beta)) d\beta \\
&\quad + (h_2 - h_1) \int_{-h_2}^{-h_1} e^{\gamma(t-\beta)} x^T(t) Q_5 x(t) d\beta - (h_2 \\
&\quad - h_1) \int_{-h_2}^{-h_1} e^{\gamma t} x^T(t + \beta) Q_5 x(t + \beta) d\beta \\
&\quad + \tau_3 \int_{-\tau_3}^0 e^{\gamma(t-\beta)} x^T(t) Q_6 x(t) d\beta \\
&\quad - \tau_3 \int_{-\tau_3}^0 e^{\gamma t} x^T(t + \beta) Q_6 x(t + \beta) d\beta = \frac{\tau}{\gamma} (e^{\gamma\tau} \\
&\quad - 1) e^{\gamma t} g^T(x(t)) Q_4 g(x(t)) \\
&\quad - \tau e^{\gamma t} \int_{t-\tau}^t g^T(x(s)) Q_4 g(x(s)) ds \\
&\quad + \frac{h_2 - h_1}{\gamma} (e^{\gamma h_2} - e^{\gamma h_1}) e^{\gamma t} x^T(t) Q_5 x(t) - (h_2
\end{aligned} \tag{26}$$

$$\begin{aligned}
& -h_1) e^{\gamma t} \int_{t-h_2}^{t-h_1} x^T(s) Q_5 x(s) ds + \frac{\tau_3}{\gamma} (e^{\gamma \tau_3} - 1) \\
& \cdot e^{\gamma t} x^T(t) Q_6 x(t) - \tau_3 e^{\gamma t} \int_{t-\tau_3}^t x^T(s) Q_6 x(s) ds \\
& \leq \frac{\tau}{\gamma} (e^{\gamma \tau} - 1) e^{\gamma t} g^T(x(t)) Q_4 g(x(t)) - \tau_2(t) \\
& \cdot e^{\gamma t} \int_{t-\tau_2(t)}^t g^T(x(s)) Q_4 g(x(s)) ds \\
& + \frac{h_2 - h_1}{\gamma} (e^{\gamma h_2} - e^{\gamma h_1}) e^{\gamma t} x^T(t) Q_5 x(t) - (h_2 \\
& - h_1) e^{\gamma t} \int_{t-h_2}^{t-h_1} x^T(s) Q_5 x(s) ds + \frac{\tau_3}{\gamma} (e^{\gamma \tau_3} - 1) \\
& \cdot e^{\gamma t} x^T(t) Q_6 x(t) - \tau_3 e^{\gamma t} \int_{t-\tau_3}^t x^T(s) Q_6 x(s) ds.
\end{aligned}$$

(28)

$$\begin{aligned}
& \cdot Q_4 \left[\int_{t-\tau_2(t)}^t g(x(s)) ds \right] \\
& + \frac{h_2 - h_1}{\gamma} (e^{\gamma h_2} - e^{\gamma h_1}) e^{\gamma t} x^T(t) \\
& \cdot Q_5 x(t) - e^{\gamma t} \left[\int_{t-h_2}^{t-h_1} x(s) ds \right]^T \\
& \cdot Q_5 \left[\int_{t-h_2}^{t-h_1} x(s) ds \right] + \frac{\tau_3}{\gamma} (e^{\gamma \tau_3} - 1) \\
& \cdot e^{\gamma t} x^T(t) Q_6 x(t) \\
& - e^{\gamma t} \left[\int_{t-\tau_3}^t x(s) ds \right]^T \\
& \cdot Q_6 \left[\int_{t-\tau_3}^t x(s) ds \right].
\end{aligned}$$

(31)

From hypotheses (H3) and (18), we have

$$\begin{aligned}
& \text{trace} [\sigma^T(t) P_i \sigma(t)] \leq \lambda_i \text{trace} [\sigma^T(t) \sigma(t)] \\
& \leq \lambda_i \left(x^T(t) H_{1i} x(t) \right. \\
& + x^T(t - \tau_1(t)) H_{2i} x(t - \tau_1(t)) \\
& + x^T(t - \tau_2(t)) H_{3i} x(t - \tau_2(t)) \\
& \left. + x^T(t - \tau_3(t)) H_{4i} x(t - \tau_3(t)) \right).
\end{aligned}$$

(29)

Note that inequality (31) still holds if $\tau_2(t) = 0$ and $h_2 = h_1$ since

$$\begin{aligned}
& \int_{t-\tau_2(t)}^t g^T(x(s)) Q_4 g(x(s)) ds \\
& = \left[\int_{t-\tau_2(t)}^t g(x(s)) ds \right]^T Q_4 \left[\int_{t-\tau_2(t)}^t g(x(s)) ds \right] \\
& = 0, \\
& \int_{t-h_2}^{t-h_1} x^T(s) Q_5 x(s) ds \left[\int_{t-h_2}^{t-h_1} x(s) ds \right]^T \\
& \cdot Q_5 \left[\int_{t-h_2}^{t-h_1} x(s) ds \right] = 0, \\
& \int_{t-\tau_3}^t x^T(s) Q_6 x(s) ds = \left[\int_{t-\tau_3}^t x(s) ds \right]^T \\
& \cdot Q_6 \left[\int_{t-\tau_3}^t x(s) ds \right] = 0.
\end{aligned}$$

(32)

Combining (20) and (27) together yields

$$\begin{aligned}
& \mathfrak{L}V_2(t, i, x_t) \\
& \leq e^{\gamma t} \left(x^T(t) (e^{-\gamma h_2} Q_1 + e^{-\gamma \tau_2} Q_2 + e^{-\gamma \tau_3} Q_3) x(t) \right. \\
& - (1 - \mu_1) h(\mu_1) x^T(t - \tau_1(t)) Q_1 x(t - \tau_1(t)) \\
& - (1 - \mu_2) h(\mu_2) x^T(t - \tau_2(t)) Q_2 x(t - \tau_2(t)) \\
& \left. - (1 - \mu_3) h(\mu_3) x^T(t - \tau_3(t)) Q_3 x(t - \tau_3(t)) \right).
\end{aligned}$$

(30)

If $\tau_2(t) > 0$, $h_2 > h_1$, based on (28) and Lemma 3, it is easy to derive that

$$\begin{aligned}
& \mathfrak{L}V_3(t, i, x_t) \leq \frac{\tau}{\gamma} (e^{\gamma \tau} - 1) e^{\gamma t} g^T(x(t)) Q_4 g(x(t)) \\
& - e^{\gamma t} \left[\int_{t-\tau_2(t)}^t g(x(s)) ds \right]^T
\end{aligned}$$

On the other hand, by hypothesis (H2), one can get that there exist positive diagonal matrices $R_i = \text{diag}\{r_{1i}, r_{2i}, \dots, r_{ni}\}$, $S_i = \text{diag}\{s_{1i}, s_{2i}, \dots, s_{ni}\}$, $i \in S$, such that the following inequalities hold

$$\begin{aligned}
& 0 \leq 2e^{\gamma t} \sum_{j=1}^n r_{ji} \left(g_j(x_j(t)) - l_j^- x_j(t) \right) \left(l_j^+ x_j(t) \right. \\
& \left. - g_j(x_j(t)) \right) = 2e^{\gamma t} \left(x^T(t) (L_1 + L_2) R_i g(x(t)) \right. \\
& \left. - x^T(t) L_1 R_i L_2 x(t) - g^T(x(t)) R_i g(x(t)) \right),
\end{aligned}$$

$$\begin{aligned}
0 &\leq 2e^{\gamma t} \sum_{j=1}^n s_{ji} \left(g_j(x_j(t - \tau_1(t))) - l_j^- x_j(t - \tau_1(t)) \right) \\
&\quad \cdot \left(l_j^+ x_j(t - \tau_1(t)) - g_j(x_j(t - \tau_1(t))) \right) \\
&= 2e^{\gamma t} \left(x^T(t - \tau_1(t)) (L_1 + L_2) S_i g(x(t - \tau_1(t))) \right. \\
&\quad - x^T(t - \tau_1(t)) L_1 S_i L_2 x(t - \tau_1(t)) \\
&\quad \left. - g^T(x(t - \tau_1(t))) S_i g(x(t - \tau_1(t))) \right). \tag{33}
\end{aligned}$$

Moreover, by utilizing the well-known Newton-Leibniz formulae and (16), it can be deduced that for any matrices N_q , $q = 1, 2, \dots, 10$, with appropriate dimensions, the following equalities also hold

$$\begin{aligned}
0 &= 2e^{\gamma t} \left[x^T(t) N_1 + x^T(t - \tau_1(t)) N_2 \right. \\
&\quad + x^T(t - \tau_3(t)) N_3 \\
&\quad + x^T(t - \tau_1(t) - \tau_3(t - \tau_1(t))) N_4 \\
&\quad \left. + \left(\int_{t-\tau_1(t)}^t z(s) ds \right)^T N_5 \right] \\
&\quad \cdot \left[(x(t) - D_i x(t - \tau_3(t))) \right. \\
&\quad - (x(t - \tau_1(t)) - D_i x(t - \tau_1(t) - \tau_3(t - \tau_1(t)))) \\
&\quad \left. - \int_{t-\tau_1(t)}^t z(s) ds - \int_{t-\tau_1(t)}^t \sigma(s) d\omega(s) \right], \tag{34} \\
0 &= 2e^{\gamma t} \left[x^T(t) N_6 + x^T(t - \tau_2(t)) N_7 \right. \\
&\quad + x^T(t - \tau_3(t)) N_8 \\
&\quad + x^T(t - \tau_2(t) - \tau_3(t - \tau_2(t))) N_9 \\
&\quad \left. + \left(\int_{t-\tau_2(t)}^t z(s) ds \right)^T N_{10} \right] \\
&\quad \cdot \left[(x(t) - D_i x(t - \tau_3(t))) \right. \\
&\quad - (x(t - \tau_2(t)) - D_i x(t - \tau_2(t) - \tau_3(t - \tau_2(t)))) \\
&\quad \left. - \int_{t-\tau_2(t)}^t z(s) ds - \int_{t-\tau_2(t)}^t \sigma(s) d\omega(s) \right].
\end{aligned}$$

Considering hypothesis (H4), substituting (26)–(34) and $Ed\omega(t) = 0$ into (25) yields that for $t \in [t_{k-1}, t_k)$, $k \in \mathbb{N}^+$,

$$E\mathfrak{L}V(t, i, x_t) \leq e^{\gamma t} E\chi^T(t) \Phi_i'' \chi(t), \tag{35}$$

where

$$\begin{aligned}
\chi^T(t) &= \begin{bmatrix} x^T(t) & x^T(t - \tau_1(t)) & x^T(t - \tau_2(t)) & x^T(t - \tau_3(t)) \\ & x^T(t - \tau_1(t) - \tau_3(t - \tau_1(t))) \\ & x^T(t - \tau_2(t) - \tau_3(t - \tau_2(t))) & g^T(x(t)) \\ & g^T(x(t - \tau_1(t))) & \left(\int_{t-\tau_2(t)}^t g(x(s)) ds \right)^T \\ & \left(\int_{t-\tau_1(t)}^t z(s) ds \right)^T & \left(\int_{t-\tau_2(t)}^t z(s) ds \right)^T \\ & \left(\int_{t-h_1}^{t-h_2} x(s) ds \right)^T & \left(\int_{t-\tau_3}^t x(s) ds \right)^T \end{bmatrix}^T, \\
\Phi_i'' &= \Phi_i' \Big|_{\kappa_1=0, \kappa_2=0} + \begin{bmatrix} P_i Z_i \\ 0_{12n \times n} \end{bmatrix} F_i(t) \begin{bmatrix} 0_{6n \times n} \\ H_i^T \\ J_i^T \\ K_i^T \\ 0_{4n \times n} \end{bmatrix}^T \\
&\quad + \begin{bmatrix} 0_{6n \times n} \\ H_i^T \\ J_i^T \\ K_i^T \\ 0_{4n \times n} \end{bmatrix} F_i^T(t) \begin{bmatrix} P_i Z_i \\ 0_{12n \times n} \end{bmatrix}^T \\
&\quad - \begin{bmatrix} D_i^T P_i Z_i \\ 0_{12n \times n} \end{bmatrix} F_i(t) \begin{bmatrix} 0_{6n \times n} \\ H_i^T \\ J_i^T \\ K_i^T \\ 0_{4n \times n} \end{bmatrix}^T \\
&\quad - \begin{bmatrix} 0_{6n \times n} \\ H_i^T \\ J_i^T \\ K_i^T \\ 0_{4n \times n} \end{bmatrix} F_i^T(t) \begin{bmatrix} D_i^T P_i Z_i \\ 0_{12n \times n} \end{bmatrix}^T. \tag{36}
\end{aligned}$$

Combining Lemma 4 and (35) together yields that there exist two positive scalars κ_1 and κ_2 such that

$$\begin{aligned}
\Phi_i'' &\leq \Xi_i \\
&= \Phi_i' \Big|_{\kappa_1 > 0, \kappa_2 > 0} + \kappa_1^{-1} \begin{bmatrix} P_i Z_i \\ 0_{12n \times n} \end{bmatrix} \begin{bmatrix} P_i Z_i \\ 0_{12n \times n} \end{bmatrix}^T \\
&\quad + \kappa_2^{-1} \begin{bmatrix} D_i^T P_i Z_i \\ 0_{12n \times n} \end{bmatrix} \begin{bmatrix} D_i^T P_i Z_i \\ 0_{12n \times n} \end{bmatrix}^T. \tag{37}
\end{aligned}$$

Applying the Schur complement equivalence [60] to (20) yields $\Xi_i < 0$. Therefore, $\Phi_i'' < 0$, which means

$$E\mathfrak{L}V(t, i, x_t) \leq 0, \quad t \in [t_{k-1}, t_k), \quad k \in \mathbb{N}^+. \tag{38}$$

For $t = t_k, k \in \mathbb{N}^+$, according to (19) and (23) and $Ed\omega(t) = 0$, we have

$$\begin{aligned} EV(t_k, l, x_{t_k}) &= EV(t_k^-, i, x_{t_k^-}) \\ &\quad + Ee^{\gamma t_k} \mathcal{D}x^T(t_k^-) (W_{ik}^T P_l W_{ik} - P_i) \mathcal{D}x(t_k^-) \\ &\leq EV(t_k^-, i, x_{t_k^-}) + \alpha_i EV_1(t_k^-, i, x_{t_k^-}); \end{aligned} \quad (39)$$

if $-1 \leq \alpha_i < 0$, then

$$EV(t_k, l, x_{t_k}) \leq EV(t_k^-, i, x_{t_k^-}); \quad (40)$$

if $\alpha_i > 0$, then

$$\begin{aligned} EV(t_k, l, x_{t_k}) &\leq (1 + \alpha_i) EV(t_k^-, i, x_{t_k^-}) \\ &\leq \alpha EV(t_k^-, i, x_{t_k^-}). \end{aligned} \quad (41)$$

So, from inequalities (38) and (40), for all $i \in S, t \geq 0$, it is true through the mathematical induction that

$$EV(t, i, x_t) \leq EV(0, r(0), x_0), \quad -1 \leq \alpha_i < 0. \quad (42)$$

Similarly, based on inequalities (38) and (41), for all $i \in S, t \in [t_{k-1}, t_k), k \in \mathbb{N}^+$, it is true through the mathematical induction that

$$\begin{aligned} EV(t, i, x_t) &\leq \alpha^{k-1} EV(0, r(0), x_0) \\ &= EV(0, r(0), x_0) e^{(k-1) \ln \alpha} \\ &\leq EV(0, r(0), x_0) e^{(t_{k-1} / \inf\{t_k - t_{k-1}\}) \ln \alpha} \\ &\leq EV(0, r(0), x_0) e^{(\ln \alpha / \inf\{t_k - t_{k-1}\}) t}, \\ &\quad \alpha_i > 0. \end{aligned} \quad (43)$$

From (23), (42), and (43), the following inequalities are, namely, hold

$$\begin{aligned} E(\mathcal{D}x(t))^T (\mathcal{D}x(t)) &\leq \frac{EV(0, r(0), x_0)}{\min_{i \in S} \lambda_{\min}(P_i)} e^{-\gamma t}, \\ &\quad -1 \leq \alpha_i < 0, \quad t \geq 0, \end{aligned} \quad (44)$$

$$\begin{aligned} E(\mathcal{D}x(t))^T (\mathcal{D}x(t)) &\leq \frac{EV(0, r(0), x_0)}{\min_{i \in S} \lambda_{\min}(P_i)} e^{(-\gamma + \ln \alpha / \inf\{t_k - t_{k-1}\}) t}, \\ &\quad \alpha_i > 0, \quad t \in [t_{k-1}, t_k), \quad k \in \mathbb{N}^+. \end{aligned} \quad (45)$$

On the other hand, defined $L = \text{diag}\{l_1, l_2, \dots, l_n\}$ within $l_j = \max\{|l_j^-|, |l_j^+|\}$, $j = 1, 2, \dots, n$, from Lemma 4; it is easy to obtain that there exists a positive scalar ϵ such that

$$\begin{aligned} EV(0, r(0), x_0) &= E(x(0) - D_i x(0 - \tau_3(0)))^T \\ &\quad \cdot P_{r(0)}(x(0) - D_i x(0 - \tau_3(0))) \\ &\quad + \int_{-\tau_1(0)}^0 Ee^{\gamma(s-h_2)} x^T(s) Q_1 x(s) ds \\ &\quad + \sum_{j=2}^3 \int_{-\tau_j(0)}^0 Ee^{\gamma(s-\tau_j)} x^T(s) Q_j x(s) ds \\ &\quad + \tau \int_{-\tau}^0 \int_{\beta}^0 Ee^{\gamma(s-\beta)} g^T(x(s)) Q_4 g(x(s)) ds d\beta \\ &\quad + (h_2 - h_1) \int_{-h_2}^{-h_1} \int_{\beta}^0 Ee^{\gamma(s-\beta)} x^T(s) Q_5 x(s) ds d\beta \\ &\quad + \tau_3 \int_{-\tau_3}^0 \int_{\beta}^0 Ee^{\gamma(s-\beta)} x^T(s) Q_6 x(s) ds d\beta \leq (1 \\ &\quad + \epsilon) x^T(0) P_{r(0)} x(0) + (1 + \epsilon^{-1}) x^T(-\tau_3(0)) \\ &\quad \cdot D_i^T P_{r(0)} D_i x(-\tau_3(0)) \\ &\quad + \left(\lambda_{\max}(Q_1) e^{-\gamma h_2} \int_{-h_2}^0 e^{\gamma s} ds \right. \\ &\quad + \sum_{j=2}^3 \lambda_{\max}(Q_j) e^{-\gamma \tau_j} \int_{-\tau_j}^0 e^{\gamma s} ds \\ &\quad + \tau \lambda_{\max}(L^T Q_4 L) \int_{-\tau}^0 \int_{\beta}^0 e^{\gamma(s-\beta)} ds d\beta \\ &\quad + (h_2 - h_1) \lambda_{\max}(Q_5) \int_{-h_2}^{-h_1} \int_{\beta}^0 e^{\gamma(s-\beta)} ds d\beta \\ &\quad \left. + \tau_3 \lambda_{\max}(Q_6) \int_{-\tau_3}^0 \int_{\beta}^0 e^{\gamma(s-\beta)} ds d\beta \right) \\ &\quad \cdot \sup_{-\tau \leq \theta \leq 0} E \|\xi(\theta)\|^2 \\ &\leq \left\{ [(1 + \epsilon) + (1 + \epsilon^{-1}) \|D_i^T\| \|D_i\|] \max_{i \in S} \lambda_i \right. \\ &\quad + \lambda_{\max}(Q_1) \frac{e^{-\gamma h_2}}{\gamma} (1 - e^{-\gamma h_2}) \\ &\quad + \sum_{j=2}^3 \lambda_{\max}(Q_j) \frac{e^{-\gamma \tau_j}}{\gamma} (1 - e^{-\gamma \tau_j}) \\ &\quad \left. + \frac{\tau \lambda_{\max}(L^T Q_4 L)}{\gamma} \left(\frac{e^{\gamma \tau} - 1}{\gamma} - \tau \right) \right\} \end{aligned}$$

$$\begin{aligned}
& + \frac{(h_2 - h_1) \lambda_{\max}(Q_5)}{\gamma} \left(\frac{e^{\gamma h_2} - e^{\gamma h_1}}{\gamma} - (h_2 - h_1) \right) \\
& + \frac{\tau_3 \lambda_{\max}(Q_6)}{\gamma} \left(\frac{e^{\gamma \tau_3} - 1}{\gamma} - \tau_3 \right) \left\{ \sup_{-\tau \leq \theta \leq 0} E \|\xi(\theta)\|^2 \right\} \\
& = \mathcal{M}_1 \sup_{-\tau \leq \theta \leq 0} E \|\xi(\theta)\|^2,
\end{aligned} \tag{46}$$

where

$$\begin{aligned}
\mathcal{M}_1 & = \left[(1 + \epsilon) + (1 + \epsilon^{-1}) \|D_i^T\| \|D_i\| \right] \max_{i \in \mathcal{S}} \lambda_i \\
& + \lambda_{\max}(Q_1) \frac{e^{-\gamma h_2}}{\gamma} (1 - e^{-\gamma h_2}) \\
& + \sum_{j=2}^3 \lambda_{\max}(Q_j) \frac{e^{-\gamma \tau_j}}{\gamma} (1 - e^{-\gamma \tau_j}) \\
& + \frac{\tau \lambda_{\max}(L^T Q_4 L)}{\gamma} \left(\frac{e^{\gamma \tau} - 1}{\gamma} - \tau \right) \\
& + \frac{(h_2 - h_1) \lambda_{\max}(Q_5)}{\gamma} \left(\frac{e^{\gamma h_2} - e^{\gamma h_1}}{\gamma} - (h_2 - h_1) \right) \\
& + \frac{\tau_3 \lambda_{\max}(Q_6)}{\gamma} \left(\frac{e^{\gamma \tau_3} - 1}{\gamma} - \tau_3 \right).
\end{aligned} \tag{47}$$

In addition, one can see that

$$\begin{aligned}
Ex^T(t) x(t) & = E \left\{ (\mathcal{D}x(t) + D_i x(t - \tau_3(t)))^T \right. \\
& \cdot (\mathcal{D}x(t) + D_i x(t - \tau_3(t))) \left. \right\} = E \left\{ (\mathcal{D}x(t))^T \right. \\
& \cdot (\mathcal{D}x(t)) + 2(\mathcal{D}x(t))^T D_i x(t - \tau_3(t)) \\
& + x^T(t - \tau_3(t)) D_i^T D_i x(t - \tau_3(t)) \left. \right\} \\
& = E(\mathcal{D}x(t))^T (\mathcal{D}x(t)) + 2E(\mathcal{D}x(t))^T D_i x(t - \tau_3(t)) \\
& + x^T(t - \tau_3(t)) D_i^T D_i x(t - \tau_3(t)).
\end{aligned} \tag{48}$$

By utilizing Lemma 4 and (48), a positive scalar ϵ can be found, such that

$$\begin{aligned}
Ex^T(t) x(t) & \leq (1 + \epsilon) E(\mathcal{D}x(t))^T (\mathcal{D}x(t)) \\
& + (1 + \epsilon^{-1}) \lambda_{\max}(D_i^T D_i) Ex^T(t - \tau_3(t)) \\
& \cdot x(t - \tau_3(t)),
\end{aligned} \tag{49}$$

$$(1 + \epsilon^{-1}) \lambda_{\max}(D_i^T D_i) e^{\gamma \tau_3} < 1. \tag{50}$$

If $-1 \leq \alpha_i < 0$, by using (44) and (49), for any $t^* \geq 0$, we can get the following result by the same derivation in [22]:

$$\begin{aligned}
\sup_{0 \leq t \leq t^*} \{E[x^T(t) x(t)] e^{\gamma t}\} & \leq \frac{(1 + \epsilon) EV(0, r(0), x_0)}{\min_{i \in \mathcal{S}} \lambda_{\min}(P_i)} \\
& + (1 + \epsilon^{-1}) \lambda_{\max}(D_i^T D_i) e^{\gamma \tau_3} \\
& \cdot \sup_{0 \leq t \leq t^*} \{E[x^T(t - \tau_3(t)) x(t - \tau_3(t))] e^{\gamma(t - \tau_3(t))}\} \\
& \leq \frac{(1 + \epsilon) EV(0, r(0), x_0)}{\min_{i \in \mathcal{S}} \lambda_{\min}(P_i)} + (1 + \epsilon^{-1}) \\
& \cdot \lambda_{\max}(D_i^T D_i) e^{\gamma \tau_3} \left[\sup_{-\tau_3(t) \leq \theta < 0} E \|\xi(\theta)\|^2 \right. \\
& + \sup_{0 \leq t \leq t^*} \{E[x^T(t) x(t)] e^{\gamma t}\} \left. \right] \\
& \cdot \lambda_{\max}(D_i^T D_i) e^{\gamma \tau_3} \left[\sup_{-\tau \leq \theta \leq 0} E \|\xi(\theta)\|^2 \right. \\
& + \sup_{0 \leq t \leq t^*} \{E[x^T(t) x(t)] e^{\gamma t}\} \left. \right] \\
& + \frac{(1 + \epsilon) EV(0, r(0), x_0)}{\min_{i \in \mathcal{S}} \lambda_{\min}(P_i)}.
\end{aligned} \tag{51}$$

Because (46) and (50) hold, we have

$$\sup_{0 \leq t \leq t^*} \{E[x^T(t) x(t)] e^{\gamma t}\} \leq \mathcal{M} \sup_{-\tau \leq \theta \leq 0} E \|\xi(\theta)\|^2, \tag{52}$$

where

$$\begin{aligned}
\mathcal{M} & = \frac{((1 + \epsilon) M_1 / \min_{i \in \mathcal{S}} \lambda_{\min}(P_i) + (1 + \epsilon^{-1}) \lambda_{\max}(D_i^T D_i) e^{\gamma \tau_3})}{(1 - (1 + \epsilon^{-1}) \lambda_{\max}(D_i^T D_i) e^{\gamma \tau_3})}.
\end{aligned} \tag{53}$$

Letting $t^* \rightarrow \infty$ yields

$$\sup_{t \in [0, \infty)} \{E[x^T(t) x(t)] e^{\gamma t}\} \leq \mathcal{M} \sup_{-\tau \leq \theta \leq 0} E \|\xi(\theta)\|^2. \tag{54}$$

Obviously, for $-1 \leq \alpha_i < 0$, $t \geq 0$,

$$Ex^T(t) x(t) \leq \mathcal{M} e^{-\gamma t} \sup_{-\tau \leq \theta \leq 0} E \|\xi(\theta)\|^2. \tag{55}$$

Next, along the same line of (55), it can be deduced that for $\alpha_i > 0$, $t \in [t_{k-1}, t_k]$, $k \in \mathbb{N}^+$,

$$\begin{aligned}
Ex^T(t) x(t) & \leq \mathcal{M}' e^{(-\gamma + \ln \alpha / \inf\{t_k - t_{k-1}\})t} \sup_{-\tau \leq \theta \leq 0} E \|\xi(\theta)\|^2,
\end{aligned} \tag{56}$$

where

$$\mathcal{M}' = \frac{\left((1 + \varepsilon) M_1 / \min_{i \in S} \lambda_{\min}(P_i) + (1 + \varepsilon^{-1}) \lambda_{\max}(D_i^T D_i) e^{(\gamma - \ln \alpha / \inf\{t_k - t_{k-1}\})\tau_3}\right)}{(1 - (1 + \varepsilon^{-1}) \lambda_{\max}(D_i^T D_i) e^{(\gamma - \ln \alpha / \inf\{t_k - t_{k-1}\})\tau_3})}. \quad (57)$$

Hence, for $\alpha_i \geq -1$ ($\alpha_i \neq 0$), by Definition 2 and (55) and (56), it can be seen that the trivial solution of system (10) is robustly exponentially stable in mean square. Moreover, the exponential convergence rate is

$$\begin{aligned} \gamma, \quad & \text{if } -1 \leq \alpha_i < 0, \\ \gamma - \frac{\ln \alpha}{\inf\{t_k - t_{k-1}\}}, \quad & \text{if } \alpha_i > 0. \end{aligned} \quad (58)$$

This completes the proof of Theorem 7. \square

Remark 8. In fact, exponential convergence rate of the trivial solution of system (10) is the inherent essence. The constructed exponential-type Lyapunov-Krasovskii functional in the proof of Theorem 7 is aimed at estimating a closely approximate exponential convergence rate of the trivial solution of system (10) mathematically.

Remark 9. When $-1 \leq \alpha_i < 0$, the impulses are stabilizing; when $\alpha_i > 0$, the impulses are destabilizing; and when $W_{ik} = I$, the impulses are neutral-type (i.e., they are neither helpful for stability of system (10) nor destabilizing). $\alpha_i \neq 0$ is necessary since the Markovian jumping would occur at the impulsive time instants; that is, P_i is changing with the mode's change, and there always exist scalars $\alpha_i > 0$ such that $P_i \leq (1 + \alpha_i)P_i$. To the best of authors' knowledge, there is no result about dividing the impulses into three types for robust global exponential stability for impulsive stochastic neural networks of neutral-type with Markovian parameters, mixed time delays, and parametric uncertainties. Moreover, because the stability analysis for the case of neutral-type impulses is similar to that of destabilizing impulses, the robust exponential stability in mean square of system (10) has been classified into two categories: $-1 \leq \alpha_i < 0$ and $\alpha_i > 0$.

Remark 10. As shown in (58), the effects of the three types of impulses for the exponential convergence rate of the trivial solution of system (10) have been explicitly presented, which further verifies the characteristics of the different impulses.

When system (10) is without parametric uncertainties, by constructing the same Lyapunov-Krasovskii functional, from Theorem 7, the following corollary can be deduced to guarantee the exponential stability in mean square of the trivial solution of system (10).

Corollary 11. Assume that hypotheses (H1)–(H3) hold. For given scalars h_1, h_2, τ_2, τ_3 , and μ_1, μ_2, μ_3 , the trivial solution of system (10) is exponentially stable in mean square if there exist positive scalars $\lambda_i, \alpha_i \geq -1$ ($\alpha_i \neq 0$), $\alpha = \max\{1 + \alpha_i\}$ ($i \in S$), γ , positive definite matrices P_i ($i \in S$), $Q_1, Q_2, Q_3, Q_4, Q_5, Q_6$,

positive diagonal matrices R_i, S_i ($i \in S$), and any real matrices N_q ($q = 1, 2, \dots, 10$) of appropriate dimensions such that

$$\begin{aligned} P_i &\leq \lambda_i I, \\ W_{ik}^T P_l W_{ik} - P_i &\leq \alpha_i P_i \quad [\text{here } r(t_k) = l], \\ \Phi'_i &< 0, \end{aligned} \quad (59)$$

where

$$\begin{aligned} \Phi'_i &= (\phi'_{imn})_{13 \times 13}, \\ m &= 1, 2, \dots, 13, \quad n = 1, 2, \dots, 13, \\ \phi'_{i1,1} &= -P_i C_i - C_i^T P_i + \gamma P_i + \lambda_i H_{1i} + \sum_{j=1}^N \pi_{ij} P_j \\ &\quad + e^{-\gamma h_2} Q_1 + \sum_{j=2}^3 e^{-\gamma \tau_j} Q_j \\ &\quad + \frac{h_2 - h_1}{\gamma} (e^{\gamma h_2} - e^{\gamma h_1}) Q_5 \\ &\quad + \frac{\tau_3}{\gamma} (e^{\gamma \tau_3} - 1) Q_6 - 2L_1 R_i L_2 + N_1 + N_1^T \\ &\quad + N_6 + N_6^T, \\ \phi'_{i1,2} &= -N_1 + N_2^T, \\ \phi'_{i1,3} &= -N_6 + N_7^T, \\ \phi'_{i1,4} &= -\left(\sum_j^N \pi_{ij} P_j\right) D_i - \gamma P_i D_i + C_i^T P_i D_i - N_1 D_i \\ &\quad - N_6 D_i + N_3^T + N_8^T, \\ \phi'_{i1,5} &= N_1 D_i + N_4^T, \\ \phi'_{i1,6} &= N_6 D_i + N_9^T, \\ \phi'_{i1,7} &= P_i A_i + (L_1 + L_2) R_i, \\ \phi'_{i1,8} &= P_i B_i, \\ \phi'_{i1,9} &= P_i E_i, \\ \phi'_{i1,10} &= -N_1 + N_5^T, \\ \phi'_{i1,11} &= -N_6 + N_{10}^T, \end{aligned}$$

$$\begin{aligned}\phi'_{i2,2} &= \lambda_i H_{2i} - (1 - \mu_1) h(\mu_1) Q_1 - 2L_1 S_i L_2 - N_2 \\ &\quad - N_2^T,\end{aligned}$$

$$\phi'_{i2,4} = -N_2 D_i - N_3^T,$$

$$\phi'_{i2,5} = N_2 D_i - N_4^T,$$

$$\phi'_{i2,8} = (L_1 + L_2) S_i,$$

$$\phi'_{i2,10} = -N_2 - N_5^T,$$

$$\phi'_{i3,3} = \lambda_i H_{3i} - (1 - \mu_2) h(\mu_2) Q_2 - N_7 - N_7^T,$$

$$\phi'_{i3,4} = -N_7 D_i - N_8^T,$$

$$\phi'_{i3,6} = N_7 D_i - N_9^T,$$

$$\phi'_{i3,11} = -N_7 - N_{10}^T,$$

$$\begin{aligned}\phi'_{i4,4} &= \gamma D_i^T P_i D_i + D_i^T \left(\sum_{j=1}^N \pi_{ij} P_j \right) D_i + \lambda_i H_{4i} \\ &\quad - (1 - \mu_3) h(\mu_3) Q_3 - N_3 D_i - D_i^T N_3^T \\ &\quad - N_8 D_i - D_i^T N_8^T,\end{aligned}$$

$$\phi'_{i4,5} = N_3 D_i - D_i^T N_4^T,$$

$$\phi'_{i4,6} = N_8 D_i - D_i^T N_9^T,$$

$$\phi'_{i4,7} = -D_i^T P_i A_i,$$

$$\phi'_{i4,8} = -D_i^T P_i B_i,$$

$$\phi'_{i4,9} = -D_i^T P_i E_i,$$

$$\phi'_{i4,10} = -N_3 - D_i^T N_5^T,$$

$$\phi'_{i4,11} = -N_8 - D_i^T N_{10}^T,$$

$$\phi'_{i5,5} = N_4 D_i + D_i^T N_4^T,$$

$$\phi'_{i5,10} = -N_4 + D_i^T N_5^T,$$

$$\phi'_{i6,6} = N_9 D_i + D_i^T N_9^T,$$

$$\phi'_{i6,11} = -N_9 + D_i^T N_{10}^T,$$

$$\phi'_{i7,7} = \frac{\tau}{\gamma} (e^{\gamma\tau} - 1) Q_4 - 2R_i,$$

$$\phi'_{i8,8} = -2S_i,$$

$$\phi'_{i9,9} = -Q_4,$$

$$\phi'_{i10,10} = -N_5 - N_5^T,$$

$$\phi'_{i11,11} = -N_{10} - N_{10}^T,$$

$$\phi'_{i12,12} = -Q_5,$$

$$\phi'_{i13,13} = -Q_6,$$

(60)

and the function $h(u) \in \mathbb{R}^+$, $u \in \mathbb{R}$, is defined as

$$h(u) = \begin{cases} 1, & u > 1, \\ e^{-2\gamma\tau}, & u \leq 1. \end{cases} \quad (61)$$

And for $\alpha_i > 0$, $-\gamma + \ln \alpha / \inf\{t_k - t_{k-1}\} < 0$, $k \in \mathbb{N}^+$, other elements of Φ'_i are all equal to 0.

When system (10) is without Markovian jumping parameters, parametric uncertainties, distributed time-varying delay, impulses, and stochastic perturbation, then system (10) can be written as

$$\begin{aligned}d[x(t) - Dx(t - \tau_3(t))] \\ = [-Cx(t) + Ag(x(t)) + Bg(x(t - \tau_1(t)))] dt.\end{aligned} \quad (62)$$

Construct a Lyapunov-Krasovskii functional as follows:

$$\begin{aligned}V(t, x(t)) &= e^{\gamma t} (x(t) - Dx(t - \tau_3(t)))^T \\ &\quad \cdot P(x(t) - Dx(t - \tau_3(t))) \\ &\quad + \int_{t-\tau_1(t)}^t e^{\gamma(s-h_2)} x^T(s) Q_1 x(s) ds \\ &\quad + \int_{t-\tau_3(t)}^t e^{\gamma(s-\tau_3)} x^T(s) Q_2 x(s) ds + (h_2 - h_1) \\ &\quad \cdot \int_{-h_2}^{-h_1} \int_{t+\beta}^t e^{\gamma(s-\beta)} x^T(s) Q_3 x(s) ds d\beta \\ &\quad + \tau_3 \int_{-\tau_3}^0 \int_{t+\beta}^t e^{\gamma(s-\beta)} x^T(s) Q_4 x(s) ds d\beta.\end{aligned} \quad (63)$$

From Theorem 7, the following corollary can be deduced to guarantee the exponential stability of the trivial solution of system (62).

Corollary 12. Assume that hypotheses (H1)-(H2) hold. For given scalars h_1 , h_2 , τ_3 , and μ_1 , μ_3 , the trivial solution of system (62) is exponentially stable if there exist positive scalar γ , positive definite matrices P , Q_1 , Q_2 , Q_3 , Q_4 , positive diagonal matrices R , S , and any real matrices N_q ($q = 1, 2, \dots, 5$) of appropriate dimensions such that

$$\Phi' < 0, \quad (64)$$

where

$$\begin{aligned}
 \Phi' &= (\phi'_{imm})_{9 \times 9}, \quad m = 1, 2, \dots, 9, \quad n = 1, 2, \dots, 9, \\
 \phi'_{1,1} &= -PC - C^T P + \gamma P + e^{-\gamma h_2} Q_1 + e^{-\gamma \tau_3} Q_2 \\
 &\quad + \frac{h_2 - h_1}{\gamma} (e^{\gamma h_2} - e^{\gamma h_1}) Q_3 \\
 &\quad + \frac{\tau_3}{\gamma} (e^{\gamma \tau_3} - 1) Q_4 - 2L_1 R L_2 + N_1 + N_1^T, \\
 \phi'_{1,2} &= -N_1 + N_2^T, \\
 \phi'_{1,3} &= -\gamma P D + C^T P D - N_1 D + N_3^T, \\
 \phi'_{1,4} &= N_1 D + N_4^T, \\
 \phi'_{1,5} &= P A + (L_1 + L_2) R, \\
 \phi'_{1,6} &= P B, \\
 \phi'_{1,7} &= -N_1 + N_5^T, \\
 \phi'_{2,2} &= -(1 - \mu_1) h(\mu_1) Q_1 - 2L_1 S L_2 - N_2 - N_2^T, \\
 \phi'_{2,3} &= -N_2 D - N_3^T, \\
 \phi'_{2,4} &= N_2 D - N_4^T, \\
 \phi'_{2,6} &= (L_1 + L_2) S, \\
 \phi'_{2,7} &= -N_2 - N_5^T, \\
 \phi'_{3,3} &= \gamma D^T P D - (1 - \mu_3) h(\mu_3) Q_2 - N_3 D - D^T N_3^T, \\
 \phi'_{3,4} &= N_3 D - D^T N_4^T, \\
 \phi'_{3,5} &= -D^T P A, \\
 \phi'_{3,6} &= -D^T P B, \\
 \phi'_{3,7} &= -N_3 - D^T N_5^T, \\
 \phi'_{4,4} &= N_4 D + D^T N_4^T, \\
 \phi'_{4,7} &= -N_4 + D^T N_5^T, \\
 \phi'_{5,5} &= -2R, \\
 \phi'_{6,6} &= -2S, \\
 \phi'_{7,7} &= -N_5 - N_5^T, \\
 \phi'_{8,8} &= -Q_3, \\
 \phi'_{9,9} &= -Q_4,
 \end{aligned} \tag{65}$$

and the function $h(u) \in \mathbb{R}^+$, $u \in \mathbb{R}$, is defined as

$$h(u) = \begin{cases} 1, & u > 1, \\ e^{-2\gamma\tau}, & u \leq 1. \end{cases} \tag{66}$$

And other elements of Φ' are all equal to 0.

4. Numerical Results

In this section, two numerical examples are presented to illustrate the effectiveness of the obtained results.

Example 13 (see [13]). Let the state space of Markov chain $\{r(t), t \geq 0\}$ be $S = \{1, 2\}$ with generator

$$\Pi = \begin{bmatrix} -0.45 & 0.45 \\ 0.5 & -0.5 \end{bmatrix}. \tag{67}$$

Consider 2D delayed impulsive stochastic neural networks of neutral-type (10) with Markovian switching and parametric uncertainties:

$$\begin{aligned}
 C_1 &= \begin{pmatrix} 2.9 & 0 \\ 0 & 2.8 \end{pmatrix}, \\
 C_2 &= \begin{pmatrix} 2.5 & 0 \\ 0 & 2.6 \end{pmatrix}, \\
 A_1 &= \begin{pmatrix} 0.2 & 0.18 \\ 0.3 & 0.19 \end{pmatrix}, \\
 A_2 &= \begin{pmatrix} 0.3 & 0 \\ 0.4 & 0 \end{pmatrix}, \\
 B_1 &= \begin{pmatrix} 0.8 & 0.2 \\ 0.2 & 0.3 \end{pmatrix}, \\
 B_2 &= \begin{pmatrix} 2.5 & 1.5 \\ 1 & 2.5 \end{pmatrix}, \\
 D_1 &= \begin{pmatrix} 0.2 & 0 \\ 0 & 0.2 \end{pmatrix}, \\
 D_2 &= \begin{pmatrix} 0.3 & 0 \\ 0 & 0.3 \end{pmatrix}, \\
 E_1 &= \begin{pmatrix} 4 & 0.04 \\ 0.14 & 4 \end{pmatrix}, \\
 E_2 &= \begin{pmatrix} 4 & 1.5 \\ 1 & 4 \end{pmatrix}, \\
 Z_1 &= \begin{pmatrix} 0.1 & -0.2 \\ 0.7 & 0.2 \end{pmatrix}, \\
 Z_2 &= \begin{pmatrix} -0.1 & -0.2 \\ -0.1 & 0.2 \end{pmatrix}, \\
 H_1 &= \begin{pmatrix} -0.3 & 0.1 \\ -0.2 & 0.1 \end{pmatrix}, \\
 H_2 &= \begin{pmatrix} 0.3 & -0.4 \\ 0.7 & -0.1 \end{pmatrix},
 \end{aligned}$$

$$J_1 = \begin{pmatrix} -0.5 & -0.4 \\ 0.2 & -0.2 \end{pmatrix},$$

$$J_2 = \begin{pmatrix} -0.1 & -0.4 \\ 0.4 & 0.3 \end{pmatrix},$$

$$K_1 = \begin{pmatrix} -0.2 & 0.2 \\ 0.1 & 0.8 \end{pmatrix},$$

$$K_2 = \begin{pmatrix} 0.1 & 0.3 \\ -0.4 & -0.3 \end{pmatrix},$$

$$F_1(t) = \begin{pmatrix} \sin(t) & 0 \\ 0 & \cos(t) \end{pmatrix},$$

$$F_2(t) = \begin{pmatrix} \cos(t) & 0 \\ 0 & \sin(t) \end{pmatrix},$$

$$g(x(t)) = \tanh(x(t)),$$

$$\tau_1(t) = 0.6 + 0.6 \sin(2t),$$

$$\tau_2(t) = 0.25 + 0.25 \cos(4t),$$

$$\tau_3(t) = 1.5 + 1.5 \cos(t),$$

$$\sigma_1(t) = \sigma_2(t)$$

$$\begin{aligned} &= \begin{pmatrix} 0.3x_1(t) & 0 \\ 0 & 0.2x_2(t - \tau_1(t)) \end{pmatrix} \\ &+ \begin{pmatrix} 0.3x_2(t) & 0 \\ 0 & 0.2x_2(t - \tau_2(t)) \end{pmatrix} \\ &+ \begin{pmatrix} 0.3x_1(t - \tau_2(t)) & 0 \\ 0 & 0.2x_2(t - \tau_3(t)) \end{pmatrix}. \end{aligned} \quad (68)$$

Then system (10) satisfies hypotheses (H1)–(H3) with

$$h_1 = 0,$$

$$h_2 = 1.2,$$

$$\tau_2 = 0.5,$$

$$\tau_3 = 3,$$

$$\mu_1 = 1.2,$$

$$\mu_2 = 1,$$

$$\mu_3 = 1.5,$$

$$\tau = 4.2,$$

$$H_{11} = H_{12} = 0.18I,$$

$$H_{21} = H_{22} = 0.08I,$$

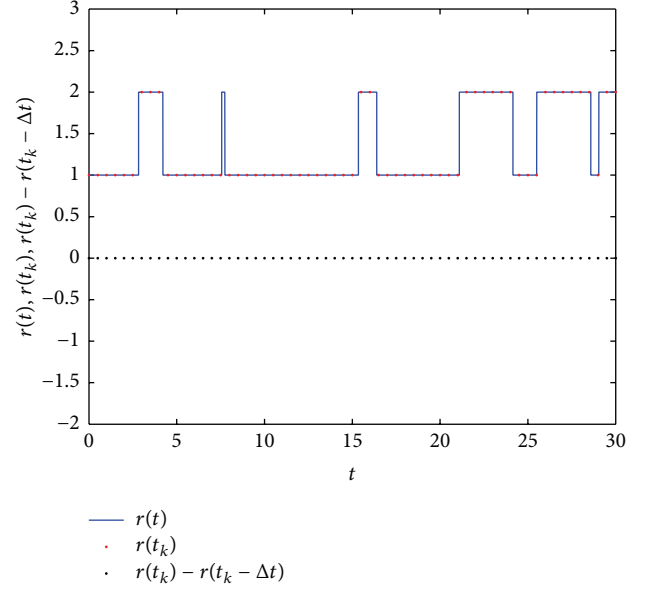


FIGURE 1: The 2-state Markov chain with $t_k = 0.5 + t_{k-1}$, $k \in \mathbb{N}^+$, $\Delta t = 0.001$ in Example 13.

$$H_{31} = H_{32} = 0.18I,$$

$$H_{41} = H_{42} = 0.08I,$$

$$L_1 = 0,$$

$$L_2 = I,$$

$$L = I.$$

(69)

Case of the Stabilizing Impulses. Study the following impulsive gain matrices:

$$W_{1k} = \begin{pmatrix} 0.9 & 0 \\ 0 & 0.9 \end{pmatrix},$$

$$W_{2k} = \begin{pmatrix} 0.9 & 0 \\ 0 & 0.9 \end{pmatrix}, \quad (70)$$

$$k \in \mathbb{N}^+.$$

By choosing $\alpha_1 = -0.1$, $\alpha_2 = -0.1$, then the impulses are the stabilizing impulses. We set $t_k = 0.5 + t_{k-1}$, $k \in \mathbb{N}^+$, $\Delta t = 0.001$. The 2-state Markov chain with $r(0) = 1$ is shown in Figure 1, among which the right continuous Markov chain $\{r(t), t \geq 0\}$ is denoted by the solid blue line, and the Markov chain of the impulsive time instants $\{r(t_k), k \in \mathbb{N}^+\}$ is denoted by the red point, and the black point is used to judge whether the Markovian jumping occurs at the impulsive time instants, that is, $r(t_k) - r(t_k - \Delta t)$. From Figure 1, we can conclude that the Markovian jumping does not occur at the impulsive time instants when $t_k = 0.5 + t_{k-1}$, $k \in \mathbb{N}^+$, $\Delta t = 0.001$.

By using the LMI toolbox in MATLAB, we search the maximum exponential convergence rate which is 5.4297

subject to the LMIs (18)–(20). Let $\gamma = 0.5$; we can obtain the following feasible solutions to the LMIs (18)–(20) in Theorem 7:

$$P_1 = \begin{pmatrix} 0.0019 & -0.0001 \\ -0.0001 & 0.0010 \end{pmatrix},$$

$$P_2 = \begin{pmatrix} 0.0018 & -0.0010 \\ -0.0010 & 0.0023 \end{pmatrix},$$

$$Q_1 = \begin{pmatrix} 0.0229 & -0.0002 \\ -0.0002 & 0.0214 \end{pmatrix},$$

$$Q_2 = \begin{pmatrix} 0.0192 & -0.0002 \\ -0.0002 & 0.0177 \end{pmatrix},$$

$$Q_3 = \begin{pmatrix} 0.0089 & 0 \\ 0 & 0.0091 \end{pmatrix},$$

$$Q_4 = \begin{pmatrix} 0.0020 & 0.0001 \\ 0.0001 & 0.0027 \end{pmatrix},$$

$$Q_5 = \begin{pmatrix} 0.0231 & -0.0003 \\ -0.0003 & 0.0213 \end{pmatrix},$$

$$Q_6 = \begin{pmatrix} 0.0023 & 0 \\ 0 & 0.0021 \end{pmatrix},$$

$$R_1 = \begin{pmatrix} 0.1752 & 0 \\ 0 & 0.1752 \end{pmatrix},$$

$$R_2 = \begin{pmatrix} 0.1703 & 0 \\ 0 & 0.1703 \end{pmatrix},$$

$$S_1 = \begin{pmatrix} 0.1399 & 0 \\ 0 & 0.1399 \end{pmatrix},$$

$$S_2 = \begin{pmatrix} 0.1356 & 0 \\ 0 & 0.1356 \end{pmatrix},$$

$$N_1 = \begin{pmatrix} -0.2415 & -0.0016 \\ -0.0016 & -0.2542 \end{pmatrix},$$

$$N_2 = \begin{pmatrix} 0.2773 & 0.0014 \\ 0.0014 & 0.2885 \end{pmatrix},$$

$$N_3 = \begin{pmatrix} 0.0934 & 0.0005 \\ 0.0005 & 0.0965 \end{pmatrix},$$

$$N_4 = \begin{pmatrix} -0.0946 & -0.0002 \\ -0.0002 & -0.0968 \end{pmatrix},$$

$$N_5 = \begin{pmatrix} 0.2595 & 0.0006 \\ 0.0006 & 0.2638 \end{pmatrix},$$

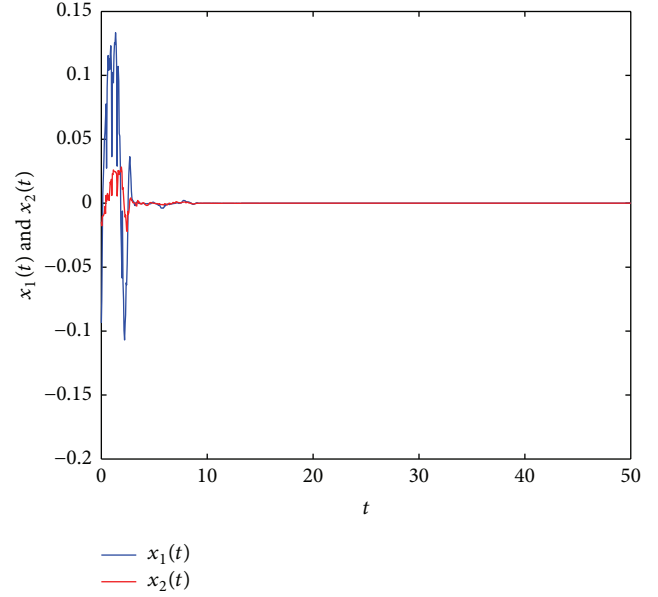


FIGURE 2: The dynamic behavior of system (10) with the stabilizing impulses, with the initial condition of every state uniformly randomly selected from $[-0.1; 0.1]$, $s \in [-4.2, 0]$ in Example 13.

$$N_6 = \begin{pmatrix} -0.2368 & -0.0016 \\ -0.0016 & -0.2497 \end{pmatrix},$$

$$N_7 = \begin{pmatrix} 0.2395 & 0.0015 \\ 0.0015 & 0.2517 \end{pmatrix},$$

$$N_8 = \begin{pmatrix} 0.0923 & 0.0007 \\ 0.0007 & 0.0964 \end{pmatrix},$$

$$N_9 = \begin{pmatrix} -0.0947 & -0.0003 \\ -0.0003 & -0.0974 \end{pmatrix},$$

$$N_{10} = \begin{pmatrix} 0.2581 & 0.0007 \\ 0.0007 & 0.2635 \end{pmatrix},$$

$$\lambda_1 = 0.0677,$$

$$\lambda_2 = 0.0816,$$

$$\kappa_1 = 0.0015,$$

$$\kappa_2 = 0.0015.$$

(71)

Set the simulation step size $h = 0.05$ and $r(0) = 1$, $\Delta t = 0.001$. The dynamic behavior of system (10) with the stabilizing impulses in Example 13 is presented in Figure 2, with the initial condition of every state uniformly randomly selected from $[-0.1; 0.1]$, $s \in [-4.2, 0]$. Therefore, it can be verified that system (10) with the stabilizing impulses is robustly exponentially stable in mean square with exponential convergence rate 0.5.

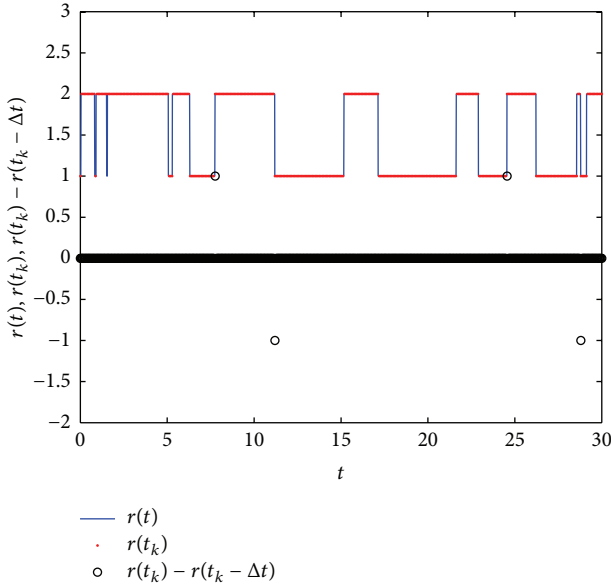


FIGURE 3: The 2-state Markov chain with $t_k = 0.08 + t_{k-1}$, $k \in \mathbb{N}^+$, $\Delta t = 0.01$ in Example 13.

Case of the Destabilizing Impulses. Study the following impulsive gain matrices:

$$\begin{aligned} W_{1k} &= \begin{pmatrix} 1.08 & 0 \\ 0 & 1.08 \end{pmatrix}, \\ W_{2k} &= \begin{pmatrix} 1.08 & 0 \\ 0 & 1.08 \end{pmatrix}, \end{aligned} \quad (72)$$

$k \in \mathbb{N}^+.$

By choosing $\alpha_1 = 0.5$, $\alpha_2 = 0.5$, then the impulses are the destabilizing impulses. In order to find the maximum exponential convergence rate, we first assume that the Markovian jumping may occur at the impulsive time instants. By using the LMI toolbox in MATLAB, we search the maximum exponential convergence rate which is 5.4020 subject to the LMIs (18)–(20), and $\inf\{t_k - t_{k-1}\} > \ln(1.5)/5.4020 = 0.0751$. Then set $t_k = 0.08 + t_{k-1}$, $k \in \mathbb{N}^+$, $\Delta t = 0.01$. The 2-state Markov chain with $r(0) = 1$ is shown in Figure 3, among which the right continuous Markov chain $\{r(t), t \geq 0\}$ is denoted by the solid blue line, and the Markov chain of the impulsive time instants $\{r(t_k), k \in \mathbb{N}^+\}$ is denoted by the red point, and the black circle is used to judge whether the Markovian jumping occurs at the impulsive time instants, that is, $r(t_k) - r(t_k - \Delta t)$. From Figure 3, we can conclude that the Markovian jumping would occur at the impulsive time instants when $t_k = 0.08 + t_{k-1}$, $k \in \mathbb{N}^+$, $\Delta t = 0.01$, which further verify the correctness of the assumption.

Set the simulation step size $h = 0.04$ and $r(0) = 1$, $\Delta t = 0.01$. The dynamic behavior of system (10) with the destabilizing impulses in Example 13 is presented in Figure 4, with the initial condition of every state uniformly randomly selected from $[-0.1; 0.1]$, $s \in [-4.2, 0]$. Therefore, it can be verified that system (10) with the destabilizing impulses is robustly exponentially stable in mean square.

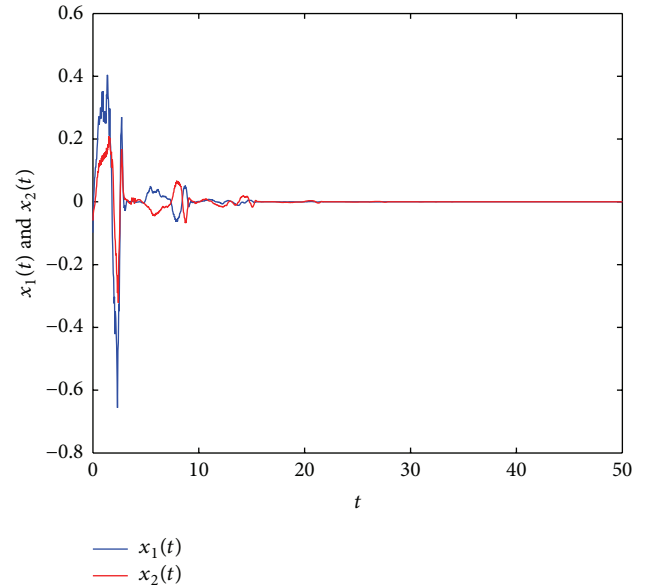


FIGURE 4: The dynamic behavior of system (10) with the destabilizing impulses, with the initial condition of every state uniformly randomly selected from $[-0.1; 0.1]$, $s \in [-4.2, 0]$ in Example 13.

Case of the Neural-Type Impulses. Study the following impulsive gain matrices:

$$\begin{aligned} W_{1k} &= \begin{pmatrix} 1 & 0 \\ 0 & 1 \end{pmatrix}, \\ W_{2k} &= \begin{pmatrix} 1 & 0 \\ 0 & 1 \end{pmatrix}, \end{aligned} \quad (73)$$

$k \in \mathbb{N}^+.$

By choosing $\alpha_1 = 1$, $\alpha_2 = 1$, then the impulses are the neutral-type impulses. In order to find the maximum exponential convergence rate, we first assume that the Markovian jumping may occur at the impulsive time instants. By using the LMI toolbox in MATLAB, we search the maximum exponential convergence rate which is 5.4039 subject to the LMIs (19)–(20), and $\inf\{t_k - t_{k-1}\} > \ln(2)/5.4039 = 0.1283$. Then we set $t_k = 0.15 + t_{k-1}$, $k \in \mathbb{N}^+$, $\Delta t = 0.01$. The 2-state Markov chain with $r(0) = 1$ is shown in Figure 5, among which the right continuous Markov chain $\{r(t), t \geq 0\}$ is denoted by the solid blue line, and the Markov chain of the impulsive time instants $\{r(t_k), k \in \mathbb{N}^+\}$ is denoted by the red point, and the black circle is used to judge whether the Markovian jumping occurs at the impulsive time instants, that is, $r(t_k) - r(t_k - \Delta t)$. From Figure 5, we can conclude that the Markovian jumping would occur at the impulsive time instants when $t_k = 0.15 + t_{k-1}$, $k \in \mathbb{N}^+$, $\Delta t = 0.01$, which further verify the correctness of the assumption.

Set the simulation step size $h = 0.05$ and $r(0) = 1$, $\Delta t = 0.01$. The dynamic behavior of system (10) with the neutral-type impulses in Example 13 is presented in Figure 6, with the initial condition of every state uniformly randomly selected from $[-0.1; 0.1]$, $s \in [-4.2, 0]$. Therefore, it can be

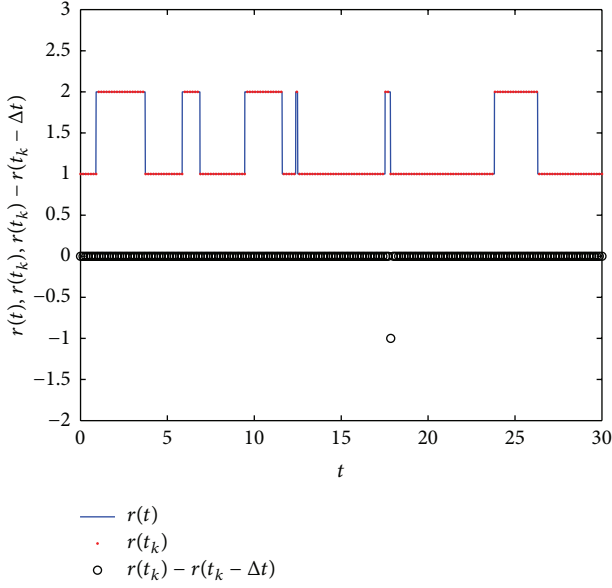


FIGURE 5: The 2-state Markov chain with $t_k = 0.15 + t_{k-1}$, $k \in \mathbb{N}^+$, $\Delta t = 0.01$ in Example 13.

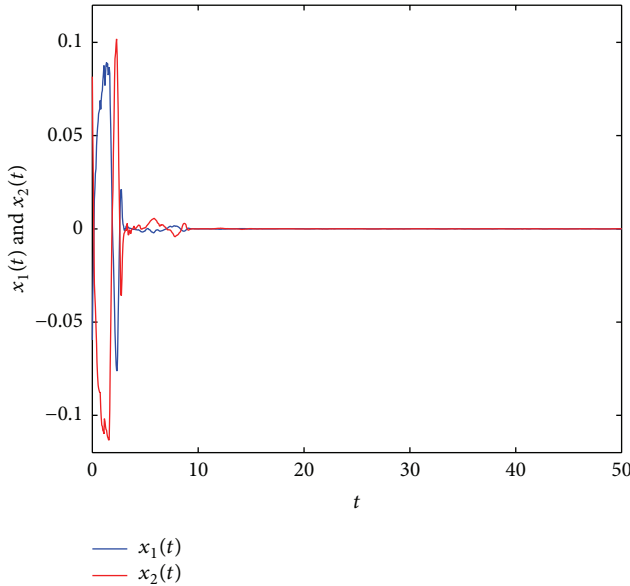


FIGURE 6: The dynamic behavior of system (10) with the neutral-type impulses, with the initial condition of every state uniformly randomly selected from $[-0.1; 0.1]$, $s \in [-4.2, 0]$ in Example 13.

verified that system (10) with the neutral-type impulses is robustly exponentially stable in mean square.

Example 14 (see [16]). Consider 2D delayed neural networks of neutral-type (62):

$$C = \begin{pmatrix} 5 & 0 \\ 0 & 5 \end{pmatrix},$$

$$A = \begin{pmatrix} 1 & 1 \\ 1 & -1 \end{pmatrix},$$

TABLE 1: The maximum allowable delay bound (MADB) h_2 for different values of γ .

| Methods | γ | 0.2000 | 1.3800 |
|-------------------|----------|---------|---------|
| Example 1 in [16] | h_2 | 22.2000 | 1.0000 |
| Corollary 12 | h_2 | 88.1009 | 15.6047 |

$$B = \begin{pmatrix} 1 & 1 \\ 1 & -1 \end{pmatrix},$$

$$D = \begin{pmatrix} -0.5 & 0 \\ 0 & -0.5 \end{pmatrix},$$

$$g(x(t)) = (0.25 \tanh(x_1(t)), 0.25 \tanh(x_2(t)))^T,$$

$$\tau_1(t) = 0.5\tau' + 0.5\tau' \cos\left(\frac{1}{\tau'}t\right), \quad \tau' > 0,$$

$$\tau_3(t) = 1.$$

(74)

Then system (64) satisfies hypotheses (H1)-(H2) with

$$h_1 = 0,$$

$$h_2 = \tau',$$

$$\tau_3 = 1,$$

$$\mu_1 = 0.5,$$

$$\mu_3 = 0,$$

$$\tau = \tau' + 1,$$

$$L_1 = 0,$$

$$L_2 = \text{diag}(0.25, 0.25),$$

$$L = \text{diag}(0.25, 0.25).$$

(75)

By using the LMI toolbox in MATLAB, we search for the fact that the LMI (64) in Corollary 12 is feasible for any $\gamma \leq 12.5883$ and $\tau' \leq 2.0000$. A comparison of the maximum upper delay bound (MADB) h_2 for different values of γ that guarantee the exponential stability of system (62) is made in Table 1 from which we can see that for this system of Example 14, the results in this paper are less conservative than that in [16].

5. Conclusion

In this paper, delay-dependent robust exponential stability criteria for a class of uncertain impulsive stochastic neural networks of neutral-type with Markovian parameters and mixed time-varying delays have been derived by the use of the Lyapunov-Krasovskii functional method, Jensen integral inequality, free-weight matrix method, and the LMI framework. The proposed results do not require the derivatives of discrete and distributed time-varying delays to be 0 or smaller than 1. Moreover, the main contribution of the

proposed approach compared with related methods lies in the use of three types of impulses. Finally, two numerical examples are worked out to demonstrate the effectiveness and less conservativeness of our theoretical results over existing literature. One of our future research directions is to apply the proposed method to study the synchronization problem for Markovian jumping chaotic delayed neural networks of neutral-type via impulsive control.

Competing Interests

The authors declare that there is no conflict of interests regarding the publication of this paper.

Acknowledgments

This work was supported by the Opening Project of Sichuan Province University Key Laboratory of Bridge Non-Destruction Detecting and Engineering Computing under Grant no. 2014QZJ01 and Grant no. 2015QYJ01 and National Natural Science Foundation of China under Grant 61573010 and Grant 11501391.

References

- [1] H. Zhang, Z. Wang, and D. Liu, "A comprehensive review of stability analysis of continuous-time recurrent neural networks," *IEEE Transactions on Neural Networks and Learning Systems*, vol. 25, no. 7, pp. 1229–1262, 2014.
- [2] J. Cao, R. Rakkiyappan, K. Maheswari et al., "Exponential H_∞ filtering analysis for discrete-time switched neural networks with random delays using sojourn probabilities," *Science China Technological Sciences*, vol. 59, no. 3, pp. 387–402, 2016.
- [3] R. Rakkiyappan, S. Dharani, and J. Cao, "Synchronization of neural networks with control packet loss and time-varying delay via stochastic sampled-data controller," *IEEE Transactions on Neural Networks and Learning Systems*, vol. 26, no. 12, pp. 3215–3226, 2015.
- [4] J. Cao, R. Sivasamy, and R. Rakkiyappan, "Sampled-data H_∞ synchronization of chaotic Lur'e systems with time delay," *Circuits Systems & Signal Process*, vol. 35, pp. 811–835, 2016.
- [5] Q. Zhu, J. Cao, and R. Rakkiyappan, "Exponential input-to-state stability of stochastic Cohen-Grossberg neural networks with mixed delays," *Nonlinear Dynamics*, vol. 79, no. 2, pp. 1085–1098, 2015.
- [6] Q. Zhu, R. Rakkiyappan, and A. Chandrasekar, "Stochastic stability of Markovian jump BAM neural networks with leakage delays and impulse control," *Neurocomputing*, vol. 136, pp. 136–151, 2014.
- [7] Q. Zhu and J. Cao, "Exponential stability of stochastic neural networks with both Markovian jump parameters and mixed time delays," *IEEE Transactions on Systems, Man, and Cybernetics Part B: Cybernetics*, vol. 41, no. 2, pp. 341–353, 2011.
- [8] Q. Zhu and J. Cao, "Stability analysis for stochastic neural networks of neutral type with both Markovian jump parameters and mixed time delays," *Neurocomputing*, vol. 73, no. 13–15, pp. 2671–2680, 2010.
- [9] O. M. Kwon, J. H. Park, S. M. Lee, and E. J. Cha, "Analysis on delay-dependent stability for neural networks with time-varying delays," *Neurocomputing*, vol. 103, no. 2, pp. 114–120, 2013.
- [10] G. Zhang, X. Lin, and X. Zhang, "Exponential stabilization of neutral-type neural networks with mixed interval time-varying delays by intermittent control: a CCL approach," *Circuits, Systems, and Signal Processing*, vol. 33, no. 2, pp. 371–391, 2014.
- [11] H. Bao and J. Cao, "Stochastic global exponential stability for neutral-type impulsive neural networks with mixed time-delays and Markovian jumping parameters," *Communications in Nonlinear Science and Numerical Simulation*, vol. 16, no. 9, pp. 3786–3791, 2011.
- [12] H. Zhang, M. Dong, Y. Wang, and N. Sun, "Stochastic stability analysis of neutral-type impulsive neural networks with mixed time-varying delays and Markovian jumping," *Neurocomputing*, vol. 73, no. 13–15, pp. 2689–2695, 2010.
- [13] Y. Gao, W. Zhou, C. Ji, D. Tong, and J. Fang, "Globally exponential stability of stochastic neutral-type delayed neural networks with impulsive perturbations and Markovian switching," *Nonlinear Dynamics*, vol. 70, no. 3, pp. 2107–2116, 2012.
- [14] C.-D. Zheng, Y. Gu, W. Liang, and Z. Wang, "Novel delay-dependent stability criteria for switched Hopfield neural networks of neutral type," *Neurocomputing*, vol. 158, pp. 117–126, 2015.
- [15] J. Xia, J. H. Park, and H. Zeng, "Improved delay-dependent robust stability analysis for neutral-type uncertain neural networks with Markovian jumping parameters and time-varying delays," *Neurocomputing*, vol. 149, pp. 1198–1205, 2015.
- [16] C.-H. Lien, K.-W. Yu, Y.-F. Lin, Y.-J. Chung, and L.-Y. Chung, "Global exponential stability for uncertain delayed neural networks of neutral type with mixed time delays," *IEEE Transactions on Systems, Man, and Cybernetics, Part B: Cybernetics*, vol. 38, no. 3, pp. 709–720, 2008.
- [17] H. Zhang, Z. Liu, and G.-B. Huang, "Novel delay-dependent robust stability analysis for switched neutral-type neural networks with time-varying delays via SC technique," *IEEE Transactions on Systems, Man, and Cybernetics, Part B: Cybernetics*, vol. 40, no. 6, pp. 1480–1491, 2010.
- [18] S. Lakshmanan, J. H. Park, H. Y. Jung, O. M. Kwon, and R. Rakkiyappan, "A delay partitioning approach to delay-dependent stability analysis for neutral type neural networks with discrete and distributed delays," *Neurocomputing*, vol. 111, no. 6, pp. 81–89, 2013.
- [19] W. Zhou, Q. Zhu, P. Shi, H. Su, J. Fang, and L. Zhou, "Adaptive synchronization for neutral-type neural networks with stochastic perturbation and Markovian switching parameters," *IEEE Transactions on Cybernetics*, vol. 44, no. 12, pp. 2848–2860, 2014.
- [20] Q. Zhu, W. Zhou, L. Zhou, M. Wu, and D. Tong, "Mode-dependent projective synchronization for neutral-type neural networks with distributed time-delays," *Neurocomputing*, vol. 140, pp. 97–103, 2014.
- [21] X. Li, "Global robust stability for stochastic interval neural networks with continuously distributed delays of neutral type," *Applied Mathematics and Computation*, vol. 215, no. 12, pp. 4370–4384, 2010.
- [22] Y. Zhang, D.-W. Gu, and S. Xu, "Global exponential adaptive synchronization of complex dynamical networks with neutral-type neural network nodes and stochastic disturbances," *IEEE Transactions on Circuits and Systems I: Regular Papers*, vol. 60, no. 10, pp. 2709–2718, 2013.
- [23] F. Deng, Q. Luo, and X. Mao, "Stochastic stabilization of hybrid differential equations," *Automatica*, vol. 48, no. 9, pp. 2321–2328, 2012.

- [24] X. Mao, G. G. Yin, and C. Yuan, "Stabilization and destabilization of hybrid systems of stochastic differential equations," *Automatica*, vol. 43, no. 2, pp. 264–273, 2007.
- [25] S. Blythe, X. Mao, and X. Liao, "Stability of stochastic delay neural networks," *Journal of the Franklin Institute*, vol. 338, no. 4, pp. 481–495, 2001.
- [26] Q. Zhu and J. Cao, "Mean-square exponential input-to-state stability of stochastic delayed neural networks," *Neurocomputing*, vol. 131, pp. 157–163, 2014.
- [27] V. Lakshmikantham, D. D. Bainov, and P. S. Simeonov, *Theory of Impulsive Differential Equations*, World Scientific, Singapore, 1989.
- [28] H. Zhang, T. Ma, G.-B. Huang, and Z. Wang, "Robust global exponential synchronization of uncertain chaotic delayed neural networks via dual-stage impulsive control," *IEEE Transactions on Systems, Man, and Cybernetics, Part B: Cybernetics*, vol. 40, no. 3, pp. 831–844, 2010.
- [29] H. Li, B. Chen, Q. Zhou, and S. Fang, "Robust exponential stability for uncertain stochastic neural networks with discrete and distributed time-varying delays," *Physics Letters A*, vol. 372, no. 19, pp. 3385–3394, 2008.
- [30] T. Huang, C. Li, S. Duan, and J. A. Starzyk, "Robust exponential stability of uncertain delayed neural networks with stochastic perturbation and impulse effects," *IEEE Transactions on Neural Networks and Learning Systems*, vol. 23, no. 6, pp. 866–875, 2012.
- [31] N. N. Krasovskii and A. Lidskii, "Analytical design of controllers in systems with random attributes. I. Statement of the problem, method of solving," *Automation and Remote Control*, vol. 22, pp. 1021–1025, 1961.
- [32] C.-D. Zheng, Y. Wang, and Z. Wang, "New stability results of neutral-type neural networks with continuously distributed delays and impulses," *International Journal of Computer Mathematics*, vol. 91, no. 9, pp. 1880–1896, 2014.
- [33] Q. Zhu and J. Cao, "Stability of Markovian jump neural networks with impulse control and time varying delays," *Nonlinear Analysis: Real World Applications*, vol. 13, no. 5, pp. 2259–2270, 2012.
- [34] C.-D. Zheng, Y. Wang, and Z. Wang, "Stability analysis of stochastic fuzzy Markovian jumping neural networks with leakage delay under impulsive perturbations," *Journal of the Franklin Institute*, vol. 351, no. 3, pp. 1728–1755, 2014.
- [35] M. Dong, H. Zhang, and Y. Wang, "Dynamics analysis of impulsive stochastic Cohen-Grossberg neural networks with Markovian jumping and mixed time delays," *Neurocomputing*, vol. 72, no. 7–9, pp. 1999–2004, 2009.
- [36] R. Rakkiyappan and P. Balasubramaniam, "Dynamic analysis of Markovian jumping impulsive stochastic Cohen-Grossberg neural networks with discrete interval and distributed time-varying delays," *Nonlinear Analysis: Hybrid Systems*, vol. 3, no. 4, pp. 408–417, 2009.
- [37] H. Jiang and J. Liu, "Dynamics analysis of impulsive stochastic high-order BAM neural networks with Markovian jumping and mixed delays," *International Journal of Biomathematics*, vol. 4, no. 2, pp. 149–170, 2011.
- [38] Q. Zhu and J. Cao, "Stability analysis of Markovian jump stochastic BAM Neural networks with impulse control and mixed time delays," *IEEE Transactions on Neural Networks and Learning Systems*, vol. 23, no. 3, pp. 467–479, 2012.
- [39] S.-L. Wu, K.-L. Li, and J.-S. Zhang, "Exponential stability of discrete-time neural networks with delay and impulses," *Applied Mathematics and Computation*, vol. 218, no. 12, pp. 6972–6986, 2012.
- [40] S. L. Wu, K.-L. Li, and T. Z. Huang, "Exponential stability of static neural networks with time delay and impulses," *IET Control Theory & Applications*, vol. 5, no. 8, pp. 943–951, 2011.
- [41] S.-L. Wu, K.-L. Li, and T.-Z. Huang, "Global exponential stability of static neural networks with delay and impulses: discrete-time case," *Communications in Nonlinear Science and Numerical Simulation*, vol. 17, no. 10, pp. 3947–3960, 2012.
- [42] J. Lu, D. W. C. Ho, and J. Cao, "A unified synchronization criterion for impulsive dynamical networks," *Automatica*, vol. 46, no. 7, pp. 1215–1221, 2010.
- [43] W.-H. Chen and W. X. Zheng, "Global exponential stability of impulsive neural networks with variable delay: an LMI approach," *IEEE Transactions on Circuits and Systems I: Regular Papers*, vol. 56, no. 6, pp. 1248–1259, 2009.
- [44] W. Zhang, Y. Tang, X. Wu, and J.-A. Fang, "Synchronization of nonlinear dynamical networks with heterogeneous impulses," *IEEE Transactions on Circuits and Systems I: Regular Papers*, vol. 61, no. 4, pp. 1220–1228, 2014.
- [45] W. Zhang, Y. Tang, J.-A. Fang, and X. Wu, "Stability of delayed neural networks with time-varying impulses," *Neural Networks*, vol. 36, pp. 59–63, 2012.
- [46] W. K. Wong, W. Zhang, Y. Tang, and X. Wu, "Stochastic synchronization of complex networks with mixed impulses," *IEEE Transactions on Circuits and Systems I: Regular Papers*, vol. 60, no. 10, pp. 2657–2667, 2013.
- [47] D. J. Higham, "An algorithmic introduction to numerical simulation of stochastic differential equations," *SIAM Review*, vol. 43, no. 3, pp. 525–546, 2001.
- [48] H. K. Khalil, *Nonlinear Systems*, Prentice Hall, Upper Saddle River, NJ, USA, 1996.
- [49] Q. Zhu and J. Cao, "Robust exponential stability of markovian jump impulsive stochastic Cohen-Grossberg neural networks with mixed time delays," *IEEE Transactions on Neural Networks*, vol. 21, no. 8, pp. 1314–1325, 2010.
- [50] K. Gu, "An integral inequality in the stability problem of time-delay systems," in *Proceedings of the 39th IEEE Conference on Decision and Control*, pp. 2805–2810, Sydney, Australia, December 2000.
- [51] Y. Wang, L. Xie, and C. E. de Souza, "Robust control of a class of uncertain nonlinear systems," *Systems and Control Letters*, vol. 19, no. 2, pp. 139–149, 1992.
- [52] T. H. Gronwall, "Note on the derivatives with respect to a parameter of the solutions of a system of differential equations," *Annals of Mathematics*, vol. 20, no. 4, pp. 292–296, 1919.
- [53] A. Halanay and J. A. Yorke, "Some new results and problems in the theory of differential-delay equations," *SIAM Review*, vol. 13, pp. 55–80, 1971.
- [54] A. Seuret and F. Gouaisbaut, "Wirtinger-based integral inequality: application to time-delay systems," *Automatica*, vol. 49, no. 9, pp. 2860–2866, 2013.
- [55] P. G. Park, J. W. Ko, and C. Jeong, "Reciprocally convex approach to stability of systems with time-varying delays," *Automatica*, vol. 47, no. 1, pp. 235–238, 2011.
- [56] Z. Wang, Y. Liu, and X. Liu, "Exponential stabilization of a class of stochastic system with markovian jump parameters and mode-dependent mixed time-delays," *IEEE Transactions on Automatic Control*, vol. 55, no. 7, pp. 1656–1662, 2010.
- [57] H. Huang, T. Huang, and X. Chen, "A mode-dependent approach to state estimation of recurrent neural networks with Markovian jumping parameters and mixed delays," *Neural Networks*, vol. 46, pp. 50–61, 2013.

- [58] X. Yang, J. Cao, and J. Lu, "Synchronization of randomly coupled neural networks with markovian jumping and time-delay," *IEEE Transactions on Circuits and Systems I: Regular Papers*, vol. 60, no. 2, pp. 363–376, 2013.
- [59] A. V. Skorohod, *Asymptotic Methods in the Theory of Stochastic Differential Equations*, American Mathematical Society, 2009.
- [60] S. Boyd, L. El Ghaoui, E. Feron et al., *Linear Matrix Inequalities in System and Control Theory*, SIAM, Philadelphia, Pa, USA, 1994.